The microbial diversity and function of Arctic supraglacial biomes.

Stefanie Lutz

Submitted in accordance with the requirements for the degree of Doctor of Philosophy

The University of Leeds
School of Earth & Environment

December 2015

Declaration

The candidate confirms that the work submitted is her own, except where work which has formed part of jointly authored publications has been included. The contribution of the candidate and the other authors to this work has been explicitly indicated below. The candidate confirms that appropriate credit has been given within the thesis where reference has been made to the work of others.

The work in **Chapter 4** of the thesis has appeared in publication as follows:

Lutz, S., Anesio, A. M., Villar, S. E. J. & Benning, L. G. (2014) Variations of algal communities cause darkening of a Greenland glacier. *FEMS Microbiology Ecology*, 89(2), 402-414.

Field work was carried out by SL, LGB and AMA. All analyses, data interpretation, writing and production of figures and tables were completed by SL. SEJV carried out the Raman spectroscopic analyses. Manuscript was written by SL and discussions with all co-authors helped improve it.

The work in **Chapter 5** of the thesis has appeared in publication as follows:

Lutz, S., Anesio, A. M., Edwards, A. & Benning, L. G. (2015) Microbial diversity on Icelandic glaciers and ice caps. *Frontiers in Microbiology*, 6, 307.

Field work was carried out by SL and LGB. All analyses, data interpretation, writing and production of figures and tables were completed by SL. All DNA work was carried out by SL at Aberystwyth University. Manuscript was written by SL and discussions with all co-authors helped improve it.

The work in **Chapter 6** of the thesis has appeared in publication as follows:

Lutz, S., Anesio, A. M., Field, K. & Benning, L. G. (2015) Integrated 'omics', targeted metabolite and single-cell analyses of Arctic snow algae functionality and adaptability. *Frontiers in Microbiology, 6, 1323.*

Field work was carried out by SL and LGB. All analyses, data interpretation, writing and production of figures and tables were completed by SL. Metabolomics work was carried out by SL at the University of Sheffield under supervision of KF. Manuscript was written by SL and discussions with all co-authors helped to improve it.

The work in **Chapter 7** of the thesis reproduces a manuscript in review with *Nature Communications* (since 09.09.2015):

Lutz, S., Anesio, A. M., Raiswell, R., Edwards, A., Newton, R. J., Gill, F. & Benning, L. G. (in review) Algae Melt Arctic Glaciers: The Biogeography and Function of Snow Microbiomes.

Field work was carried out by SL, AMA and LGB. All analyses, data interpretation, writing and production of figures and tables were completed by SL. All DNA work was carried out by SL at Aberystwyth University. CNP work was carried out by SL under supervision of RJN. Fatty acid analyses were carried out by SL under supervision of FG. Albedo model was developed by RR with data provided by SL. Manuscript was written by SL and discussions with all co-authors helped to improve it.

The work in **Chapter 8** of the thesis reproduces a manuscript in the final stages of preparation for submission to *the ISME Journal*:

Lutz, S., Anesio, A. M., Edwards, A, Newton, R. J. & Benning, L. G. (in prep) Linking microbial diversity and functionality of Arctic glacial surface habitats.

Field work was carried out by SL, AMA and LGB. All analyses, data interpretation, writing and production of figures and tables were completed by SL. All DNA work was carried out by SL at Aberystwyth University. CNP work was carried out by SL under supervision of RJN. Manuscript was written by SL and discussions with all co-authors helped to improve it.

Acknowledgements

I would like to thank Liane G. Benning for always being immensely supportive and encouraging, for giving me endless opportunities to gain new experiences and enlarge my knowledge and for her endless optimism.

Special thanks to Alexandre M. Anesio for great support, his always encouraging words and for many hilarious moments in the field that I will never forget.

I would like to thank the whole Cohen geochemistry group for a great time and a lot of fun. Massive thanks goes also to our IT guys who are absolute heroes.

I am grateful to SEE and a Vice Chancellor Fellowhsip Contribution to LGB for funding my PhD and the following societies for additional grants awarded during my PhD: National Geographic, the European Association for Geochemistry, the Society for General Microbiology, the Royal Geographical Society, and the European Astrobiology Network Association.

I am very grateful for my family, who has always supported me, no matter what I decided to do. Without them I would not be who I am today.

I am also very grateful to Aleš, Andrea and all my friends for distracting me from work with climbing, caving, squash (thanks Ekbal!), coffee and tea breaks (thanks James!), after-work G&T (thanks again James!), and Catan (thanks Andy, Pieter, Adam!).

Abstract

The main aim of this research project was to improve our understanding of the diversity, function and ecology of glacial microbiomes. Snow and ice algae are critical players in supraglacial habitats and form extensive blooms in spring and summer. Here I present results on the diversity and the function of snow and ice algae on 21 glaciers in 4 Arctic settings: Greenland, Iceland, Svalbard and Sweden. For the first time, I have evaluated the full microbial community composition (*i.e.*, algae, bacteria, archaea) in the main supraglacial habitats, namely green snow, red snow, biofilms, dirty ice, and cryoconite holes. I have cross-correlated these data with metabolic analyses (*i.e.*, metabolomics, pigments, fatty acids) and critical physico-chemical parameters.

I found that snow and ice algae were the first communities to appear after the onset of melting and they showed positive net photosynthetic rates indicating accumulation of organic matter. Furthermore, for the first time I have described these communities in Iceland. My data reveal that red pigmented snow algae are cosmopolitan, and independent of location specific geochemical and mineralogical factors. Only six taxa made up >99% of the algal communities: two uncultured *Chlamydomonadaceae*, C*hloromonas polyptera*, *Chloromonas nivalis*, *Chloromonas alpina* and *Raphidonema sempervirens*. In contrast, the composition of green snow varied between the studied locations with higher relative abundance of *Raphidonema sempervirens* and *Microglena sp.* in Svalbard, and *Chloromonas polyptera* in Sweden. Furthermore, I show that green and red snow are not successive stages but two independent phenomena with different adaptation strategies.

In all sites, bacteria were mostly represented by the phyla *Bacteriodetes*, *Proteobacteria* and *Cyanobacteria.* The bacterial community composition varied between the different habitats on the phylum level, whereas on the class level they also showed strong biogeography. Archaea showed overall low species diversity.

The synthesis of pigments and fatty acids in snow and ice algae were mainly driven by nitrogen and less so by phosphorus limitation. This is especially important for pigments which cause a darkening of glacial surfaces. I show that snow and ice algae dramatically decrease surface albedo which will eventully result in higher melting rates of glaciers.

List of contents

List of figures

List of tables

List of abbreviations

ANOVA	Analysis of Variance
C:N:P	Carbon:Nitrogen:Phosphorus ratio
CCA	Canonical Correspondence Analysis
Chl	Chlorophyll
DNA	Deoxyribonucleic Acid
DOC	Dissolved Organic Carbon
FTIR	Fourier-Transform Infrared
GC-MS	Gas Chromatrography Mass Spectrometry
GrIS	Greenland Ice Sheet
IC	Ion Chromatography
ICP-MS	Inductively Coupled Plasma Mass Spectrometry
HPLC	High-Pressure Liquid Chromatography
MUFA	Monounsaturated Fatty Acids
PAR	Photosynthetic Active Radiation
PCA	Principal Component Analysis
PCR	Polymerase Chain Reaction
pri. Car	primary Carotenoids
PUFA	Polyunsaturated Fatty Acids
sec. Car	secondary Carotenoids
SFA	Saturated Fatty Acids
SEM	Scanning Electron Microscopy
TEM	Transmission Electron Microscopy
rRNA	ribosomal Ribonucleic Acid
UV	Ultraviolet irradiation
VIS	Visible light irradiation
XRD	X-ray Diffraction

Chapter 1: Introduction

1.1 Background

Glaciers are important components of the Earth's climate and water system. They contribute to global sea level rise and are the largest freshwater reservoir (70%) (Shiklomanov, 1993). Physical and chemical aspects of glaciers have been studied intensively; however, the field of glacial microbiology is still in its infancy. Snow and ice habitats have only recently been recognised as a biome despite being dominated by microorganisms of all three domains of life that play crucial roles in biogeochemical processes both on a local and global scale (Anesio & Laybourn-Parry, 2012; Hodson et al, 2008). The presence of liquid water during the melt season in summer allows the habitability of glacial surfaces and a variety of distinct microbial habitats can be found including the snowpack, bare ice, and cryoconite holes.

So far, most attention has been paid to cryoconite holes that are dominated by bacterial species and that form when dust melts into the glacial surfaces and become filled with meltwater (Hodson et al, 2008).

However, these habitats cover only 1-10% of glacial surfaces (Anesio et al, 2009) whereas the largest proportion (>90%) is covered by snow throughout the year and increasingly by bare ice as the melt season progresses. Snow and ice algae have been suggested to cover large parts of these surfaces; yet, despite their high abundance very little is known about their importance in carbon and nutrient cycling.

First described by the ancient Greek Aristotle (Gentz-Werner, 2007), snow algae have been known for a long time and they have been studied in many cryospheric settings including Svalbard (Leya et al, 2004; Müller et al, 2001; Stibal et al, 2007), Alaska (Takeuchi, 2002), Greenland (Yallop et al, 2012), the Himalayans (Yoshimura et al, 2006), the Rocky Mountains (Thomas & Duval, 1995), Antarctica (Fujii et al, 2010; Remias et al, 2013) and the European Alps (Remias et al, 2005). The majority of the 'true' snow algae belong to the C*hlamydomonadaceae* (*Chlorophyta*), yet most descriptions are not based on phylogenetic analyses but on microscopic identifications. Dramatic morphological

changes in their life cycles make species identification by microscopy very challenging and susceptible to misassignments. Therefore the most described taxa *Chlamydomonas nivalis* and *Chloromonas nivalis* are actually polyphyletic and have to be treated as collective taxa (Leya et al, 2004).

Snow algae have evolved specialised cryophilic adaptations that are crucial for thriving in high light environments that can be found on glacial surfaces in summer. These include the accumulation of secondary carotenoids to shield the photosystem from excessive irradiation and formation of robust spores with thick cell walls (Remias et al, 2010). In spring, when the snow becomes waterlogged, extensive snow algal blooms can be found. Depending on the nature of the pigments these blooms cause “green snow” (chlorophylls) or “red snow” (carotenoids, all shades of red from orange to pink; Remias et al, 2005). This colouration of the snow causes a darkening of glacial surfaces. An effect on surface albedo and in turn melting processes has been suggested before (Thomas and Duval, 1995; Yallop et al., 2012; Takeuchi, 2013). However, a quantitative link for these processes is still lacking.

The filamentous ice algae that dominate the bare ice surfaces have only recently been described more in detail (Remias et al, 2012a; Remias et al, 2009; Yallop et al, 2012), but a diversity and functional characterisation is so far still lacking. When the snow pack disappears “clean ice” (white ice without visual presence of particles and low algal abundance) becomes colonised by filamentous algae which produce the brownish pigment purpurogallin carboxylic acid-6-O-b-D-glucopyranoside (Remias et al, 2012b). This pigmentation together with accumulated mineral debris turn the ice surface into “dirty ice”. Ice algae belong to the *Zygnematophyceae* and the most described species are *Ancylonema nordenskiöldii* and *Mesotaenium berggrenii* (Remias et al, 2012a; Remias et al, 2009).

Many studies have addressed various aspects of snow algal and (in lesser extend) ice algal ecology and physiology (Hoham & Duval, 2001; Kol, 1968; Leya et al, 2004; Remias et al, 2012a; Takeuchi, 2002) and targeted individual metabolic groups including pigments (Leya et al, 2009; Remias et al, 2005; Remias et al, 2012b) and fatty acids (Spijkerman et al, 2012). However, large-scale studies integrating microbial diversity and function and interglacial comparisons are lacking. Therefore snow and ice algal species and their functioning still remain

cryptic and we know very little about the complexity of the biological inventory in snow and ice environments.

Understanding snow and ice algal functios will not only help to get a better understanding of the communities themselves but also of the environment they live in and the potential changes this environment may undergo particularly regarding climate change. Furthermore, studying snow algae and the processes by which they sustain life in such harsh settings can also help us quantify how life might survive (or has survived) on planetary bodies aside from Earth (e.g., Mars or icy moons, e.g., Europa and Enceladus). Finally, this data will complement other disciplines of glaciology towards a joint effort to improve our understanding of the response of glacial systems in a warming climate, in particular with respect to the microbial darkening of glacial surfaces leading to higher melt rates of glaciers. Considering global warming, active cell growths will increase in terms of extent and duration creating a positive feedback mechanism reducing albedo and accelerating melting even further.

1.2 Research hypotheses

The main aim of this research project was to improve our understanding of the diversity, function and ecology of glacial microbiomes. To achieve this, a multi-year (3 years) as well a large spatial sampling campaign of many individual glaciers and snow fields across the Arctic was pursued using a combined multi-disciplinary field and laboratory approach at the interface of microbiology, molecular biology bioinformatics and geochemistry.

The specific hypotheses I tested were the following:

1) Snow and ice algae are important primary colonisers and producers on glacial surfaces. (→ Chapter 4)
2) Snow algae are present and abundant in Iceland where not a single description of snow algae exists so far. (→ Chapter 5)
3) Green and red snow are successive stages. (→ Chapters 6 and 8)
4) The microbial community composition varies over time and space (→ Chapters 4, 5, 7 and 8)

5) The physico- and geochemical environment influences the community composition and their metabolic functions. (→ Chapters 5-8)
6) Algal functionality (e.g., pigments) varies over time and space. (Chapters 4, 7 and 8)
7) The algal activity has a significant effect on their environment, in particular on the decrease of surface albedo. (→ Chapters 4-7)

1.3 Thesis outline

The thesis consists of 11 chapters. Chapter 1 includes the introduction, background and research objectives. Chapter 2 describes the state of the art in our current knowledge (literature review). All methodologies are described in detail in chapter 3. This is followed by 5 results chapters that constitute of 3 published papers, 1 manuscript in review and 1 manuscript in preprartion for submission. Results from the entire thesis are discussed in chapter 9 and summarised as the main conclusions in chapter 10. Finally, an outlook for future work is given in chapter 11.

References

Anesio, A. M., Hodson, A. J., Fritz, A., Psenner, R. & Sattler, B. (2009) High microbial activity on glaciers: importance to the global carbon cycle. *Global Change Biology*, 15(4), 955-960.

Anesio, A. M. & Laybourn-Parry, J. (2012) Glaciers and ice sheets as a biome. *Trends in Ecology & Evolution*, 27(4), 219-225.

Fujii, M., Takano, Y., Kojima, H., Hoshino, T., Tanaka, R. & Fukui, M. (2010) Microbial community structure, pigment composition, and nitrogen source of red snow in Antarctica. *Microbial Ecology*, 59(3), 466-475.

Gentz-Werner, P. (2007) *Roter Schnee: oder Die Suche nach dem färbenden Prinzip*. Berlin: Akademie Verlag.

Hodson, A., Anesio, A. M., Tranter, M., Fountain, A., Osborn, M., Priscu, J., Laybourn-Parry, J. & Sattler, B. (2008) Glacial ecosystems. *Ecological Monographs*, 78(1), 41-67.

Hoham, R. & Duval, B. (2001) Microbial ecology of snow and freshwater ice with emphasis on snow algae. Cambridge University Press: Cambridge.

Kol, E. (1968) *Kryobiologie; Biologie und Limnologie des Schnees und Eises*, *24*E. Schweizerbart.

Leya, T., Müller, T., Ling, H. U. & Fuhr, G. (2004) Snow algae from north-western Spitsbergen (Svalbard). *The coastal ecosystem of Kongsfjorden, Svalbard. Synopsis of biological research performed at the Koldewey Station in the years 1991-2003*.

Leya, T., Rahn, A., Lütz, C. & Remias, D. (2009) Response of arctic snow and permafrost algae to high light and nitrogen stress by changes in pigment composition and applied aspects for biotechnology. *FEMS microbiology ecology*, 67(3), 432-443.

Müller, T., Leya, T. & Fuhr, G. (2001) Persistent snow algal fields in Spitsbergen: field observations and a hypothesis about the annual cell circulation. *Arctic, Antarctic, and Alpine Research*, 42-51.

Remias, D., Holzinger, A., Aigner, S. & Lütz, C. (2012a) Ecophysiology and ultrastructure of Ancylonema nordenskiöldii (Zygnematales, Streptophyta), causing brown ice on glaciers in Svalbard (high arctic). *Polar Biology*, 1-10.

Remias, D., Holzinger, A. & Lütz, C. (2009) Physiology, ultrastructure and habitat of the ice alga Mesotaenium berggrenii (Zygnemaphyceae, Chlorophyta) from glaciers in the European Alps. *Phycologia*, 48(4), 302-312.

Remias, D., Karsten, U., Lütz, C. & Leya, T. (2010) Physiological and morphological processes in the Alpine snow alga Chloromonas nivalis (Chlorophyceae) during cyst formation. *Protoplasma*, 243(1-4), 73-86.

Remias, D., Lütz-Meindl, U. & Lütz, C. (2005) Photosynthesis, pigments and ultrastructure of the alpine snow alga Chlamydomonas nivalis. *European Journal of Phycology*, 40(3), 259-268.

Remias, D., Schwaiger, S., Aigner, S., Leya, T., Stuppner, H. & Lütz, C. (2012b) Characterization of an UV-and VIS-absorbing, purpurogallin-derived secondary pigment new to algae and highly abundant in Mesotaenium berggrenii (Zygnematophyceae, Chlorophyta), an extremophyte living on glaciers. *FEMS microbiology ecology*, 79(3), 638-648.

Remias, D., Wastian, H., Lütz, C. & Leya, T. (2013) Insights into the biology and phylogeny of Chloromonas polyptera (Chlorophyta), an alga causing orange snow in Maritime Antarctica. *Antarctic Science*, 25(05), 648-656.

Shiklomanov, I. (1993) World Fresh Water Resources. In: Gleick PH, ed. *Water crisis: A guide to world fresh water resources*. New York: Oxford University Press.

Spijkerman, E., Wacker, A., Weithoff, G. & Leya, T. (2012) Elemental and fatty acid composition of snow algae in Arctic habitats. *Frontiers in microbiology*, 3, 380.

Stibal, M., Elster, J., Šabacká, M. & Kaštovská, K. (2007) Seasonal and diel changes in photosynthetic activity of the snow alga Chlamydomonas nivalis (Chlorophyceae) from Svalbard determined by pulse amplitude modulation fluorometry. *FEMS microbiology ecology*, 59(2), 265-273.

Takeuchi, N. (2002) The altitudinal distribution of snow algae on an Alaska glacier (Gulkana Glacier in the Alaska Range). *Hydrological Processes*, 15(18), 3447-3459.

Thomas, W. H. & Duval, B. (1995) Sierra Nevada, California, USA, snow algae: snow albedo changes, algal-bacterial interrelationships, and ultraviolet radiation effects. *Arctic and alpine research*, 27(4), 389-399.

Yallop, M. L., Anesio, A. M., Perkins, R. G., Cook, J., Telling, J., Fagan, D., MacFarlane, J., Stibal, M., Barker, G. & Bellas, C. (2012) Photophysiology and albedo-changing potential of the ice algal community on the surface of the Greenland ice sheet. *The ISME journal*, *6*(12), 2302-2313.

Yoshimura, Y., Kohshima, S., Takeuchi, N., Seko, K. & Fujita, K. (2006) Snow algae in a Himalayan ice core: new environmental markers for ice-core analyses and their correlation with summer mass balance. *Annals of Glaciology*, 43(1), 148-153.

Chapter 2: Literature review

2.1 Introduction

The cryosphere covers about 10 % of Earth's surface and has only recently been recognised as a biome (Anesio & Laybourn-Parry, 2011). Although lower in cell numbers and diversity than more temperate environments, many microorganisms (both autotrophs and heterotrophs) survive and even thrive in snow and ice. Glacial surfaces are usually thought to be very homogenous, yet they are composed of a range of distinct microbial habitats (i.e., snow fields, bare ice, cryoconites; Anesio & Laybourn-Parry, 2011). A good overview of glacial habitats is given in Hodson et al. (2008). Conditions for the habitability of glacial surface environments are still not well understood and are dependent on many abiotic environmental factors (e.g., nutrients, light irradiation) as well as life's survival strategies (e.g., pigments, cyst formation) to overcome harsh conditions.

2.2 Stress factors of snow and ice environments

Below I will briefly introduce some of the stress factors that can be found on glacial surfaces:

2.2.1 Temperature

Temperature is one of the key factors controlling cold environments by regulating water availability and therefore nutrient transport and availability and cellular processes. During the summer months snow and ice surfaces show a more or less constant temperature of 0°C allowing vegetational periods. During the rest of the year liquid water is unavailable. Chemical reactions rates drop exponentially with decreasing temperatures (Siddiqui et al, 2004). Cold temperatures slow down the hydrolysis and oxidation of organic material and the weathering of inorganic debris what makes ice and snow to cryogenic vaults preserving biosignatures.

2.2.2 Water

Most of the year low temperatures do not allow the presence of liquid water. In summer repetitive freeze-thaw cycles can occur which represent ongoing osmotic stress for biological cells (Kirst, 1990). During freezing cells have to fight intracellular ice crystal formation, which can lead to cell rupture and dehydration.

2.2.3 Nutrients

Nutrients can range from literally nothing to local hotspots when liquid water is only available in the intercrystalline space and ions become highly concentrated. Main sources for nutrients are the surrounding bedrock depending on its nutrient content and release that is controlled by the weathering rate, aeolian dust, anthropogenic aerosols and biological debris. Nutrient availability can reach high concentrations when animal populations are close by (e.g., birds, polar bears). Optimal macro-nutrient concentration are often described using the Redfield ratio (C:N:P 106:16:1) (Gruber & Deutsch, 2014; Redfield, 1963). Although established for marine communities, the study of the Redfield ratio has been extended to other environments and its consistency and the underlying biological mechanisms still remain unknown.

2.2.4 Light irradiation

The ozone layer absorbs all UV-C (100-280 nm) radiation, however not all UV-B, (280-350 nm) which is therefore the most harmful light irradiation for cells in natural environments on Earth. Cell damage can occur either directly to DNA or proteins or by indirect effects caused by the production of reactive oxygen species (Vincent & Neale, 2000). Less harmful, but still damaging is UV-A irradiation (315-400 nm), which is not absorbed by DNA (absorption maximum 260 nm) or proteins (absorption maximum 280 nm), but can induce secondary photoreactions or photosensitizing reactions (Hargreaves et al, 2007). Since UV radiation negatively affects DNA and protein functios, it causes damage in nearly all cellular processes.

The closer to the poles the more concentrated is solar radiation resulting in very short vegetative time periods with continuous (24 h) irradiation for photosynthetic organisms. Irradiation between snow crystals is much higher than above the snow surface because of local reflections at snow crystals. However, it is decreasing logarithmically with snow depth (Gorton et al, 2001).

Biflagellates of the snow algae *Chlamydomonas nivalis* have shown to be greatly affected by UV-B irradiation in lab studies and showed a high impairment of mobility (Häder & Häder, 1989). UV radiation also inhibited photosynthesis of green snow (*Chloromonas sp.*) by about 85% and red snow (*Chlamydomonas nivalis*) only by 25% (Thomas & Duval, 1995).

2.3 Snow fields

Snow fields are dominated by the unicellular snow algae taxa *Chlamydomonas* and *Chloromonas* belonging to the *Chlorophyceae* (*Chlorophyta*). In summer they can cause macroscopically visible colouration of the snow, which can be green, yellow, orange, brown, pink or red. This phenomenon has been known for a long time and has already been described by the Ancient Greek Aristotle (Gentz-Werner, 2007). Yet, only in the 19th century due to the development of microscopy scientists were able to link this to biological processes namely snow algae blooms and the taxon *Chlamydomonas nivalis* was named by Wille (1903). Since then a large number of snow algal species has been described and wrongly classified as *Chlamydomonas nivalis*. Kol (1968) was the first to state that this taxon has to be regarded as a collective name and that it is not the only species that causes the colouring. An overview about the taxonomy is given by Ettl (1983). The same applies for the taxon *Chloromonas nivalis* that cannot be regarded as one species either. Populations earlier described as *Chloromonas nivalis* are different species which was revealed by genetic analyses (Leya, 2004). *Chlamydomonas nivalis* and *Chloromonas nivalis* are polyphyletic and therefore the species richness in snow habitats is much higher than previously expected.

Snow algae are true cosmopolitans and have been described in many places such as Svalbard (Leya, 2004; Leya et al, 2000; Müller et al, 1998; Müller et al, 2001b), the Alps (Lütz-Meindl & Lütz, 2006), Antarctica (Fujii et al, 2010), the Giant Mountains in the Czech Republic (Kvíderová, 2012), the Rocky Mountains in the

USA (Williams et al, 2003), the Sierra Nevada in Spain (Thomas & Duval, 1995), the Atlas Mountains in Morocco (Duval et al, 1999), the Himalayans (Yoshimura et al, 2006), and Alaska (Takeuchi, 2013). A first overview on snow algal ecology was given by Hoham et al. (2001).

True snow algae are psychrophiles with a temperature optimum below 15°C, maximum temperature around 20°C and the preferred growth temperature around 0°C. Many cryophilic adaptation strategies can only be found in truly psychrophilic snow algae (Hoham & Duval, 2001).

The colour of the snow depends of the algal species, their life stage and their abundance. Green snow is caused by young green algal cells with chlorophyll being the dominant pigment. Red snow (from now on used to summarise yellow, orange, brown, pink and red variations) is caused by mature green algae with a higher content of secondary carotenoids. Due to the colouring of the snow caused by intracellular pigments the snow albedo is heavily decreased, which can lead to increased melting (Thomas & Duval, 1995).

Bacterial abundances and production rates were found to be higher in red snow containing algae compared to white snow with low snow algal numbers (Thomas & Duval, 1995), which suggests that snow algae are an important source of organic matter.

Parameters controlling snow algal distribution are far from being fully understood. Stibal et al. (2007) concluded that ecosystem chemistry may play a minor role in comparison to physical processes (e.g., slope). Mueller et al. (1998) found no correlation between nutrient content of melt water and snow algal distribution. Snow algal cells can also be transported over large distances by wind or birds. Transport to higher mountain regions is of special importance for induction of algal blooms in the following year (Müller et al, 2001b).

Only recently snow algal parasites, namely chytrids, have been identified and they seem to influence nutrient release and therefore snow food-web dynamics (Naff et al, 2013).

The photosynthetic performance also depends on metrological conditions since snow flurries will cover algal cells and suppress photosynthesis (Jones, 1999).

2.3.1 Life cycle of *Chlamydomonas nivalis*

An overview of the hypothetical life cycle of *Chlamydomonas* is given in Figure 2.1. Most of the year cells remain dormant in the ice or soil as cysts. At the onset of melting in late spring/early summer *Chlamydomonas* cysts are re-activated. Young flagellates emerge from the mother cell and actively swim upwards to the snow surface until they reach adequate conditions for photosynthesis. They reproduce vegetatively and/or sexually and form new populations. Once conditions become harsher (e.g., high irradiation in summer) flagellates transform into robust non-motile cysts accompanied by intracellular rearrangements, such as accumulation of carotenoids (to shield chloroplast), enhanced lipid production (less cytoplasmatic water content), and reinforcement of the cell wall. During the ongoing snow melt cysts accumulate at the snow surface where they are still photosynthetically active (but not dividing) until they get covered again by snow in autumn (Remias et al, 2010). In this life stage cysts can survive for decades. Once conditions become more favourable germination is induced and cysts release several flagellated daughter cells (typically four to eight).

Although algal cells can survive in resting stages for decades, induced free radicals and singlet oxygen species can accumulate over time (Buma et al, 1995) and damage proteins (Chauhan et al, 1998) and pigments (Rajagopal et al, 2000).

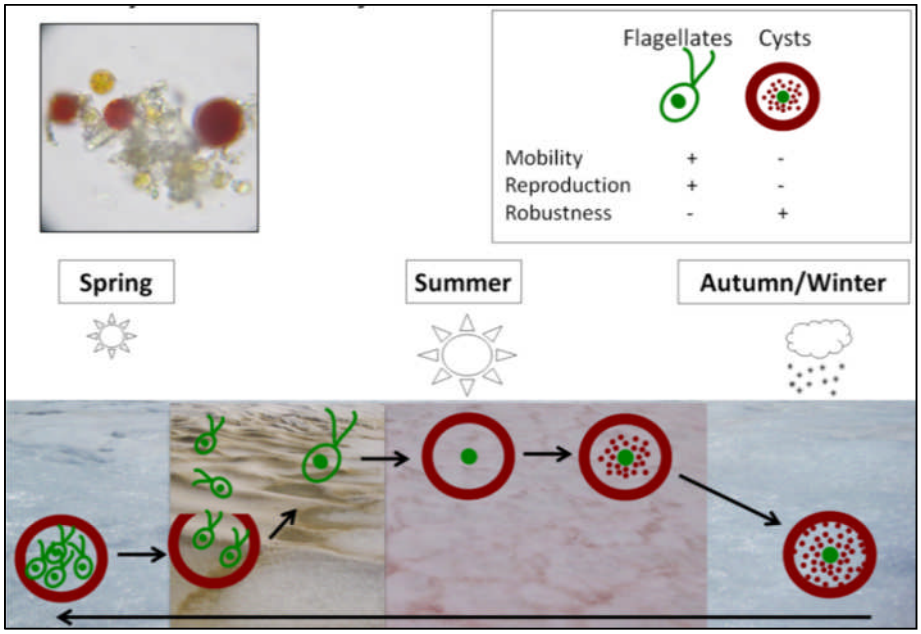

Figure 2.1: Hypothetical life cycle of *Chlamydomonas nivalis*.

2.3.2 Ecophysiological adaptation strategies

2.3.2.1 Adjustment of macromolecular and macro-nutrient stochiometry

Carbon is abundant in all macromolecules. In contrast, nitrogen and phosphorus are absent in lipids and carbohydrates, which can become the major macromolecular compounds of cells under nutrient-limiting conditions (Geider & La Roche, 2002). The Redfield ratio of C:N:P 106:16:1 has been described to be optimal for algal exponential growth and incorporation of macronutrients into reproductive biomolecules including phosphate-rich ribosomes (Klausmeier et al, 2004; Sterner & Elser, 2002). When nitrogen or phosphorus become limiting, carbon incorporation is preferentially stored as starch or lipids in response to a high C:N cellular ratio (James et al, 2011). In most environments phosphorus limitation is reached before nitrogen limitation (Penuelas et al, 2013). However, low N:P ratios have also been observed in phytoplankton which can show low N:P ratios during blooms since fast-growing cells require phosphorus for ribosomes. When resources become limiting, cells shift their metabolism to a nitrogen-rich light and nutrient acquisition metabolism, which leads to higher N:P ratios (Mills & Arrigo, 2010). Geider and La Roche (2002) also showed in laboratory studies with marine

microalgae that the idea of a fixed Redfield ratio may not be valid. Particulate C:N is higher than 6.6 and N:P lower than 16 during nutrient-replete growth. Particulate N:P is much lower than 16 due to the accumulation of inorganic P storage products.

Proteins are a major reservoir for excess nitrogen and more than 70% of cellular nitrogen can be stored in them (Rhee, 1978). Glycoproteins are also major component of snow algal cell walls and they increase during cyst formation.

Accumulation of lipids has been found to accompany nitrogen limitation in cryophilic green algae (Pichrtová et al, 2014). During nitrogen limiting conditions, the metabolism is shifted to the production of nitrogen-free metabolites including lipids. Triacylglycerol (TGA) neutral lipids are often synthesized in response to high light or nutrient deprivation (James et al, 2011).

2.3.2.2 Lipids and fatty acids

Low temperatures typically lead to a reduction in membrane fluidity and ultimately to a loss of function. Membrane fluidity is controlled by the lipid composition. At low temperatures organisms produce more unsaturated and methyl-branched fatty acids. Steric constraints are introduced that change the packing order or reduce membrane interactions (Chintalapati et al, 2004).

Lipids play an important role in snow algal survival. Worsening conditions induce lipid formation, which results in the reduction of cytoplasmatic water content and volume counteracting intracellular freezing at subzero temperatures. Lipid bodies are also the storage location of photoprotective secondary carotenoids. Under nitrogen-deficiency the metabolism is directed towards nitrogen-free metabolites such as fatty acids and lipids (Leya et al, 2009).

Fatty acids play an essential role as structural elements of membranes and as storage compounds (Thompson Jr, 1996). The relative composition of fatty acids depends on environmental factors including temperature, light irradiation, and nutrient availability (Piorreck et al, 1984; Roessler, 1990), but can also vary between species (Spijkerman et al, 2012). Organisms adapted to lower temperatures usually contain a higher ratio of polyunsaturated fatty acids (PUFAs)

to saturated fatty acids (SFAs). Unsaturated FAs are incorporated into membranes to maintain their fluidity, flexibility and functionality under cold conditions. In general the total amount of fatty acids is higher in nutrient limited cultures (Rodolfi et al, 2008). A higher content of lipids also decreases the cytoplasmatic water content and therefore reduces intracellular freezing. Piorreck et al. (1984) found a positive correlation between nitrogen concentrations and fatty acid production of lab cultures of green algae and they showed that a high production of polyunsaturated fatty acids (PUFA) occurred at high N concentrations, whereas at lower concentrations there was a shift towards a higher relative abundance of C16:0 and C18:1.

Cysts from western Spitsbergen (Spijkerman et al, 2012) were found to contain 75-85% UFAs (45-55% PUFAs, 25-40% MUFAs) with MUFA C18:1n-9 being the most abundant FA (followed by C16:0, C16:4, C18:2n-6, C18:3n-3). Lab cultures exposed to high light settings and nitrogen starvation increased their content in C18:1n-9 in contrast to non-starving cultures at lower light settings. One explanation may be a metabolism shifted towards nitrogen free non-protein compounds under nitrogen deficiency.

Bidigare et al (1992) found large difference in FA content between green and red snow algae cells from Antarctica (Bidigare et al, 1993). Rezanka et al. (2008) found *Chloromonas brevispina* cysts from the Bhemian Forest in the Czech Republic containing mainly PUFAs (75% of total FA content) and production of unusual medium-chained PUFAs.

Fatty acids are also often linked to pigments and astaxanthin has been shown to be associated with higher amounts of C18:1 (Řezanka et al, 2008). Pigments are stored in cytoplasmatic lipid droplets around the nucleus and chloroplast, which results in their shading (Boussiba, 2000; Remias et al, 2005).

2.3.2.3 Biological pigments

Biological pigments, also known as biochromes, are substances produced by living organisms for various purposes including photosynthesis, signalling or protection (e.g., camouflage).

Chlorophyll is ubiquitous among photosynthetic organisms and critical in photosynthesis since it allows the absorption of energy from light. It most strongly absorbs in the blue and red portion of the electromagnetic spectrum. In green algae and vascular plants two forms of chlorophyll are known, namely Chl a and b. The biosynthesis of chlorophyll occurs within chloroplasts. The chlorophyll molecule consists of a cyclic tetrapyrrole with centrally chelated Mg^{2+} and a C_{20} phytol tail (Figure 2.2). Chl b is increasingly produced in low light settings to extend the absorption spectrum of Chl a optimising light uptake. Therefore higher amounts of Chl b can often be found in young snow algal cells, whereby mature cells that havebeen exposed to higher amounts of light often contatin a decreased amount of Chl b.

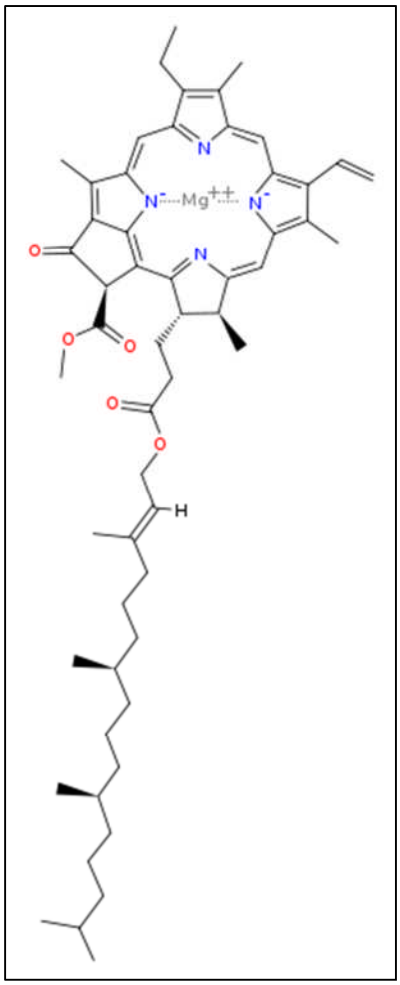

Figure 2.2: Structure of chlorophyll a. Source: Wikipedia (16.07.2015).

Carotenoids can be synthesized by all photosynthetic organisms and are also present in non-photosynthetic prokaryotes, archaea and fungi. Animals are usually not capable to synthesize caretoinds, but can obtain and employ them in their metabolism. Recently aphids have been reported to produce their own carotenoids from carotenoid biosynthesis genes that are likely derived from fungi via horizontal gene transfer and have been incorporated in their genome (Moran & Jarvik, 2010). All carotenoids are tetraterpenoids and contain 40 carbon molecules (Figure 2.3). They strongly absorb in the blue portion of the electromagnetic spectrum. Primary carotenoids (e.g., lutein, β-carotene) are directly involved in the photosynthetic apparatus in contrast to secondary carotenoids (e.g., canthaxanthin, astaxanthin). They are split into two classes, carotenes exclusively consist of hydrogen and carbon atoms, xanthophylls also contain one or more oxygen functions. Carotenoids are usually synthesized and confined in plastids. However, under unfavourable conditions, an extraplastidal carotenoid accumulation can occur in green algae such as *Chlamydomonas nivalis* and *Haematococcus pluvialis.* The protective effect is enhanced by the concentration of carotenoids in cytoplasmatic lipid droplets around the nucleus and chloroplast, which results in their shading (Boussiba, 2000; Remias et al, 2005).

Carotenoids play an important role in many biological functions including light harvesting, stabilisation of the pigment-protein complexes, metabolic storage, regulation of membrane fluidity and stability, and probably most important photoprotection. The latter one can occur via absorption of excessive photosynthetic energy, shading the chloroplast against high irradiation or as a pool of antioxidative compounds. Due to the presence of conjugated polyene chains, they are unstable in the presence of light, heat or oxygen (Řezanka et al, 2008).

Carotenoid biosynthesis is triggered by a number of unfavourable environmental factors such as high light conditions, N-deficiency, as well as depletion in P, S, K and Fe, and oxidative stress.

Remias et al. (2010) showed that *Chlamydomonas nivalis* cells can survive elevated levels of UV-B irradiation (1.43 W m^{-2}) for a short time period. This is accompanied by a decrease in photosynthetic activity and an increased production of primary carotenoids.

Due to their broad pigmentation snow algae can tolerate an extremely broad range of light intensities and qualities.

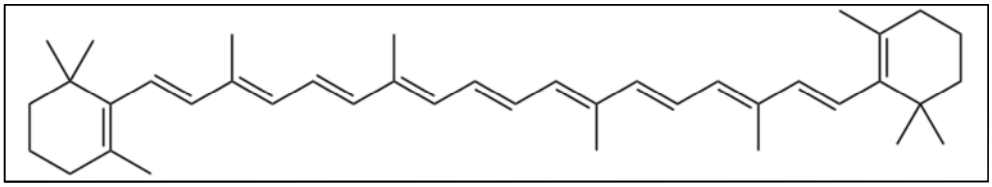

Figure 2.3: Molecular structure of β-carotene. Source: Wikipedia (16.07.0215).

The xanthophyll cycle (Figure 2.4) enzymatically removes epoxy groups from xantophylls to create de-epoxidated xantophylls. Under high light conditions violaxanthin is rapidly converted to antheraxanthin and zeaxanthin by de-epoxidation. This non-photochemical quenching mechanism reduces the amount of energy which reaches the photosynthetic reaction centres and therefore prevents photoinhibition. High amounts of violaxanthin indicate low-light adapted thylakoids which can be due to either low light settings or the shading effect of an increased amount of other secondary carotenoids. The de-epoxidation state can be calculated with the formula:

$$(Ant+Zea)/(Vio+Ant+Zea)$$

In snow algal species with no or low secondary carotenoid metabolism excessive energy is directed towards the xanthophyll cycle and dissipated as heat through non-photochemical quenching (Szyszka et al, 2007).

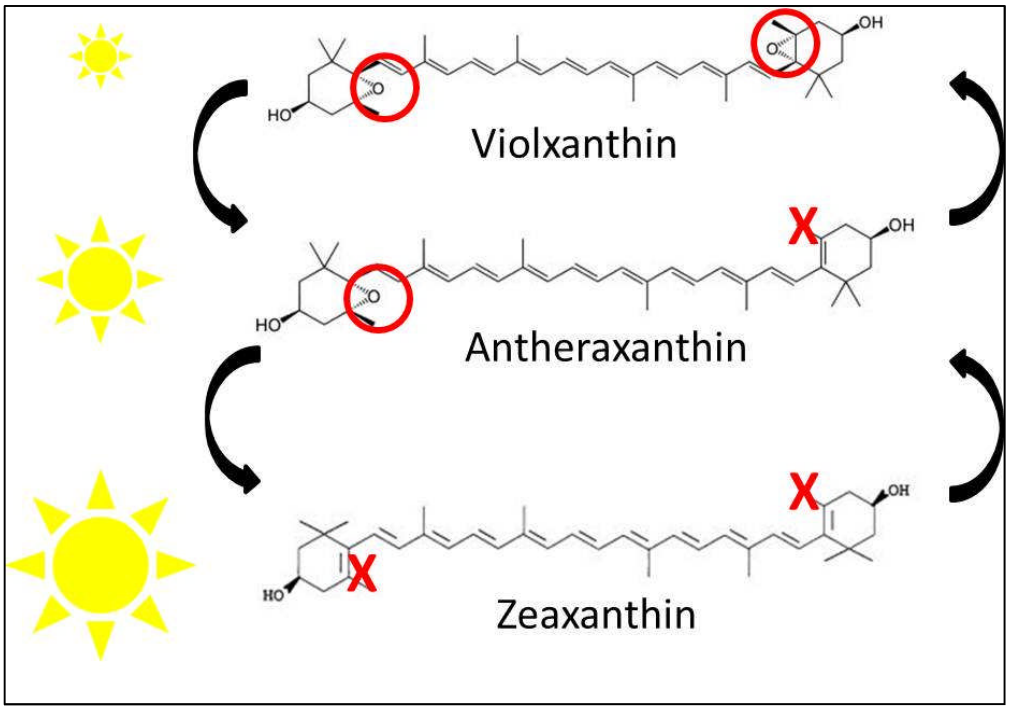

Figure 2.4: The xantophyll cycle.

Astaxanthin (Figure 2.5) is a xanthophyll with high absorption capacities in the VIS range. However, it is localised in extraplastidal lipid bodies and therefore only indirectly involved in photoprotection by shielding the chloroplast from excessive irradiation that would otherwise be damaging to the photosynthetic activity.

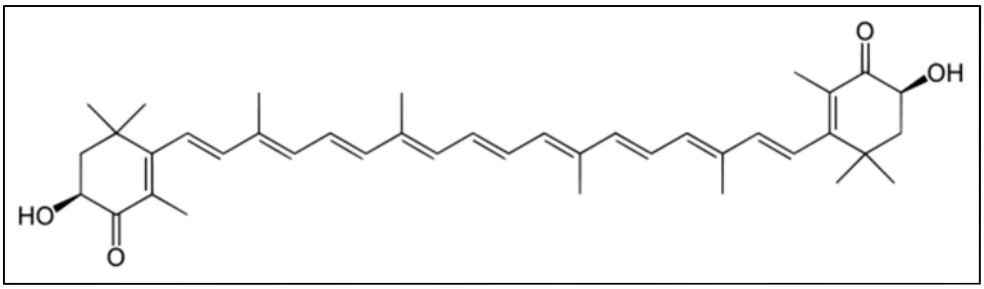

Figure 2.5: Molecular structure of astaxanthin. Source: Wikipedia (16.07.0215).

Astaxanthin is often esterified with fatty acids and sugars. Řezanka et al. (2008) identified more than 100 different molecular species of astaxanthin diglucoside

diesters. The absorption spectrum of astaxanthin remains unchanged regardless of esterification or glycosylation.

In *Chlamydomonas nivalis* astaxanthin seems to be the main pigment which causes the deep red colouration of *C. nivalis* populated snow. In major hypnoblast the astaxanthin content can be about 20 times higher than Chl a. Remias et al. (2005) suggest it being responsible for the high photostability without photoinhibition at the snow surface. The cis-isomer (13-Z) of astaxanthin is known to provide enhanced protection also in the UV-A region (Remias & Lutz, 2007). In contrast, *Chloromonas nivalis* cell usually contain less astaxanthin and therefore appear to be less red. The compensation of excessive irradiation probably occurs mainly via the xanthophyll cycle (higher de-epoxidised pigments) at the chloroplast level (Remias et al, 2010).

2.3.2.4 Thickening of cell wall/cyst formation

Cyst formation is accompanied by thickening of the cell wall to prevent cell death by desiccation, UV penetration, and grazing by predators. Additional mucilage layers have a similar effect and improve adherence to substrate after snow melt (Müller et al, 1998).

Some cells are found with inorganic and organic particles covering the cell walls (Lütz-Meindl & Lütz, 2006), mostly seen for *Chlamydomonas* species. For *Chloromonas* species this is not known (personal communication Daniel Remias).

2.3.2.5 Mycosporine-like amino acids (MAA)

Mycosporine-like amino acids are a family of more than 20 small secondary metabolites which are produced by organisms living in high light exposure settings. They act as sunscreen compounds by absorbing UV in the 310-365 nm spectrum. Although known to be widespread in prokaryotic and eukaryotic organisms, several studies have reported the absence of MAA’s in red cysts (Reisser & Houben, 2001; Remias et al, 2010; Sommaruga & Garcia-Pichel, 1999), which

likely use other protective strategies including pigments and thickening of the cell wall (see above).

2.3.2.6 Phenolics

Phenolics are water-soluble compounds with antioxidative functions scavenging singlet oxygen and free radicals in biological systems. Remias et al. (2010) found no phenolics *in Chloromonas nivalis*. In a lab experiment Duval et al. (1999) found a 5-12% increase in total phenolics after UV-A exposure of 7 days and a 12-24% increase after exposure to UV-C.

2.4 Supraglacial ice

2.4.1 Bare glacial ice

The filamentous ice algae that dominate the bare ice surfaces have only recently been described more in detail (Remias et al, 2012a; Remias et al, 2009; Yallop et al, 2012).

Ice algae belong to the *Zygnematophyceae* and the most described species are *Ancylonema nordenskiöldii* Berggren 1871 and *Mesotaenium berggrenii* Lagerheim. Ice algal mass blooms cause a grey colouration of the ice and they show cosmopolitan occurrence in many permanently frozen alpine and polar settings (Kol, 1968; Remias et al, 2012a; Remias et al, 2009; Takeuchi et al, 2006; Uetake et al, 2010; Yallop et al, 2012). The metabolic season is limited to a short period in summer when liquid water is available. Due to the lack of any flagellated stage, the glacial ice algae are restricted to the ice surface and cannot actively move upwards into the snow layers. In contrast to snow algae, they are able to persist harsh conditions with relatively thin and less rigid cell walls and without formation of cysts (Remias et al, 2009). *Mesotaenium berggrenii* cells exposed to -25ºC could be revived and show that they are well adapted to overwintering in a frozen state (Ling & Seppelt, 1990).

Raphidonema sempervirens can be abundant on glacial ice surfaces as well. However, it is a typical permafrost algae and not a true snow algal species.

Laboratory experiments (Leya et al, 2009) also demonstrated that *Raphidonema sempervirens* does not share one of the main cryophilic properties of true snow algae, *i.e.*, the production of secondary carotenoids (*e.g.*, astaxanthin). Yet, in culture and under optimal conditions *Raphidonema sempervirens* is able to produce significant amounts of primary carotenoids, *i.e*. xantophylls (Leya et al, 2009). Furthermore, Stibal and Elster (2005) have suggested that *Raphidonema sempervirens* is likely introduced onto glacial surfaces by wind rather than through *in-situ* propagation. Thus, it remains unclear whether this species is a critical player in the ecology of glaciers.

.

Figure 2.6: Filamentous ice algae *Ancylonema nordenskiöldii* (Source: Yallop et al., 2012). Scale bar = 10 µm

2.4.2 Ecophysiological adaptation strategies

Ancylonema nordenskilöldii and *Mesotaenium berggrenii* accumulate a hydrophilic brownish vascuolar pigment with a tannin nature, which was identified by Remias et al. (2012b) as purpurogallin carboxylic acid-6-O-b-D-glucopyranoside, whereas secondary carotenoids seem to be absent (Remias et al, 2009). The brownish pigment has a broad absorption range in the visible as well as the UV-A and UV-B range and therefore plays an important role in shielding the chloroplast and avoid photoinhibition. The same pigmentation can be found in algal cells thriving in less UV irradiated settings, suggesting that this compound may additionally act as an antimicrobial agent against grazers apart from the photoprotective role (Remias et al, 2012b).

Due to their dark pigmentation and their wide occurrence glacial ice algae play an important role in reducing the albedo of bare ice fields during summer and thus in increasing glacial melting (Yallop et al., 2012).

2.4.3 Cryoconites

First described and named by the Swedish explorer A. E. Nordenskjöld during his Greenland expedition 1870, cryoconites are derived from 'cryo' meaning ice and 'conite' meaning dust (Nordenskjöld, 1875). Among glacial surface habitats, cryoconite holes (cyanobacteria dominated water-filled holes formed by the preferential melt of organic and inorganic dark particles) have been by far the more extensively studied habitats (Cameron et al, 2012; Edwards et al, 2014).

Cryoconites form from solar-heated organic and inorganic debris that melts into the ice by absorbing more radiation than the surrounding ice due to the lower albedo. Small individual holes can coalesce into larger holes or can become connected by meltwater channels. There are three types of cryoconites: cryoconite holes, stream cryoconites and dispersed cryoconite granules. They can be found in the ablation zones of glaciers (Porazinska et al, 2004).

They are unique environments filled with liquid water and seeded by material from the local environment. Nutrient and microbe input can be either wind-blown, via melt or rain water or direct lateral input through englacial piping (Kaštovská et al, 2005)

They can cover up to 10% of a glacier's surface and contain highly diverse microbial communities including viruses, bacteria (mainly cyanobacteria and proteobacteria), algae (mainly *Chlorophyceae*), fungi, and even ciliates, copepods, insects, tardigrades, nematodes, and rotifers (Anesio et al, 2009; Anesio et al, 2007; Christner et al, 2003; Edwards et al, 2010; Hodson et al, 2007; Müller et al, 2001a).

Anesio et al. (2007) found that in cryoconite holes photosynthesis exceeds respiration and they have the potential to fix up to 64 Gg of carbon per year, which is important in the context of a globally changing climate. Despite the low temperatures, microbial activity in cryoconite sediments can be exceptionally high (Säwström et al, 2002) and approximate more temperate and nutrient rich regions (Anesio et al, 2007). This makes them hot spots for biogeochemical cycling

(Hodson et al, 2007; Telling et al, 2011). Cyanobacteria and heterotrophic bacteria are the main nutrient cyclers (Kaštovská et al, 2005; Margesin et al, 2002). This is even enhanced by their viral-induced lysis and subsequent release of nutrients (Anesio et al, 2007).

In winter, the top of cryoconite holes is usually frozen, but they still absorb more solar energy than the surrounding due to the underlying dark sediment, which may allow the existence of liquid water. In summer, they are open to the atmosphere, allowing an exchange of gases, nutrient and microbes (Hodson et al, 2007). The chemistry and microbiology of individual cryoconites are often very distinct from other cryoconites due to hydraulic isolation from glacial melt water (Tranter et al, 2004).

2.5 Englacial and subglacial ice

Englacial and subglacial environments are characterised by extreme conditions including high pressure, low temperature, darkness and acidity (Price, 2000; 2007) and are dominated by chemoautotrophic and heterotrophic bacteria. Since metabolic rates in englacial ecosystems are likely to be very low, these ecosystems play a minor role in the overall glacial biogeochemical nutrient cycling since all nutrients and energy are likely to be expended in repair of molecular damage only (Price, 2007). At the rock-ice interface metabolic rates are likely to be slightly higher due to weathering of minerals (Sharp et al, 1999).

2.6 Bacteria

So far, more studies have been published targeting bacteria than algae. These mostly targeted relatively fresh spring snow (Larose et al 2009) or clean summer snow (Cameron et al 2014). *Proteobacteria* and *Bacteriodetes* are commonly found in polar snow (Møller et al, 2013) and are able to rapidly exploit organic matter (Abell & Bowman, 2005; Riemann & Winding, 2001). *Bacteriodetes* are known to be able to degrade complex organic structure and are often associated with high organic environments (Battin et al, 2001; Kirchman, 2002; Pereira, 2010).

For example, a high abundance of *Proteobacteria* was found in snow in Greenland (Cameron et al., 2014), in snow and ice in China (Segawa et al., 2014), in spring snow in Svalbard (Larose et al., 2009), in snow, slush and surface ice in Svalbard (Hell et al., 2013), and in cryoconite holes in the Alps and Svalbard (Edwards et al., 2013; Edwards et al., 2014). Furthermore, in previous studies *Bacteroidetes* also showed a higher relative abundance in cryoconite holes (Edwards et al., 2013; Edwards et al., 2014).

2.7 Archaea

Currently, only very few studies have documented the presence of archaea in glacial environments. They have been found in a glacial stream in Austria (Battin et al, 2001), in subglacial sediments in Canada (Boyd et al, 2011) and in cryoconite holes in Antarctica (Cameron et al, 2012) and Svalbard (Zarsky et al, 2013). These studies offer a consensus that the apparent diversity of Archaea on glacier surfaces is low with *Nitrososphaerales* (*Thaumarchaeota*) and *Methanosarcinales (Euryarchaeota)* being the main archaeal taxa present. *Nitrosphaerales* are important ammonia-oxidizers (Stieglmeier et al, 2014; Tourna et al, 2011; Zarsky et al, 2013), whereas *Methanobacteriales* are anaerobic methanogens. Cameron et al. (2012) found a limited number of taxa affiliated with *Thaumarchaeaota* and *Methanobacteriaceae* restricted to Antarctic cryoconite and Cameron et al. (2014) reported similar low archaeal diversity in 4 snow samples collected between 1.6 to 9.5 km from the margin of the Greenland Ice Sheet.

2.8 Genomics of glacial environments

Complete genomes from the psychrophilic bacteria *Sulfotalea psychrophila* (Rabus et al, 2004), *Colwellia psychrerythraea* 34H (Methé et al, 2005) and *Pseudoalteromonas haloplanktis* TAC125 (Médigue et al, 2005) have been sequenced. Draft genomes of the two archaea *Methanococcoides burtonii* and *Methanogenium frigidum* (Saunders et al, 2003) are also available. Recently the first genome of a psychrotolerant eukaryote, the unicellular green algae *Cocomyxa subellipsoidea* C-169, has been sequenced. With emerging massive parallel

sequencing, more genomes will probably follow. Although mesophilic, *Chlamydomonas reinhardtii* is genetically closely related to snow algae species and its full genome is also available (Merchant et al, 2007).

Metagenomics (Handelsman et al, 1998) is a genomics approach including the complete microbial gene pool of a specific environment and has been proposed to be the most accurate quantitative approach for microbial community description (Von Mering et al, 2007). So far, studies have only focussed on prokaryotic (i.e., bacteria, archaea) glacial metagenomes (Choudhari et al, 2013; Edwards et al, 2013; Møller et al, 2013; Simon et al, 2009) or targeted only specific eukaryotic genes (e.g., 18S rRNA; Darcy et al, 2011; Hoham et al, 2002).

2.9 Applications/Significance

2.9.1 Carbon and nutrient export

The cryosphere covers about 10% of the Earth's surface and glaciers are the largest reservoir of freshwater. With temperatures rising globally, melting rates of glaciers have gone up affecting freshwater availability and sealevel rise. Climate-warming is predicted to have a large impact on glacial runoff with high importance for organic carbon fluxes from glacial surface to downstream ecosystems including deglaciated soils, lakes or coastal waters (Foreman et al, 2007; Hodson et al, 2008; Hood et al, 2015; Schütte et al, 2009; Telling et al, 2011; Wynn et al, 2007). The contribution of DOC from mountain glaciers is higher than from the Greenland and Antarctic ice sheets (Hood et al, 2015).

Whether glacial environments act as source or sink for CO_2 is still not understood. Due to large-scale microbial activity on glaciers and ice sheets their interiors seem to function as sinks for CO_2 due to photosynthetic fixation of CO_2 into organic matter, whereas exteriors seem to release more CO_2 by heterotrophic respiration (Stibal et al, 2012). Williams et al. (2003) also suggests that snow fields inhabited by snow algae also may be a global sink for CO_2.

Castello and Rogers (2005) found that $1x10^{17} – 10^{21}$ viable microbes are liberated each year by global glacial melting events with the potential to feed downstream communities.

2.9.2 Surface albedo

As part of their life cycle and as a mechanism of protection from high irradiation, snow algal species produce red pigments (carotenoids). Through this protective reaction, algal blooms colour snow and ice surfaces and cause a darkening of glacial surfaces which in turn leads to a decrease in surface albedo (Takeuchi, 2013; Thomas & Duval, 1995; Yallop et al, 2012). Such a decrease of albedo may speed up melting processes even further.

2.9.3 Analogous extraterrestrial environments

Glacial systems on Earth represent good analogues for other icy environments in our solar system, such as the Martian polar ice caps (McKay & Stoker, 1989), the Jovian moon Europa, and the Saturnian moon Enceladus. Understanding microbial survival strategies on Earth helps us to guide the search for life elsewhere.

Cryophilic microbes were suggested as one of four Earth analogues for Mars (Rothschild, 1990). The likelihood of the presence of prokaryotes over eukaryotes is more likely, yet snow and ice algae have evolved numerous cryophilic adaptation mechanisms although they are young on an evolutionary scale and therefore are worth to study.

2.9.4 Biotechnology

Cryophiles are a fertile ground for biosprospecting (de Pascale et al, 2012; Siddiqui & Cavicchioli, 2006) and cold-adapted proteins and lipids have found widespread use in biotechnological applications such as industrial processes at low temperatures, enzymology, food industry and medicine (Feller et al, 1996; Fendrihan & Negoiţă, 2012; Margesin & Schinner, 1994). In contrast to mesohphiles, cold-adapted enzymes of cryophiles are active and very efficient at a low temperature range (~ 0-20°C) which is economically beneficial since no heating system is necessary and processes can be run at lower temperature (*i.e.*, cold-adapted proteases, amylases, cellulases and lipases are used in laundry and cryophiles in waste water treatment and remediation of soils at ambient temperatures; Margesin & Schinner, 1994). Lower temperatures also reduce the risk of microbial contamination since mesophiles have their growth optimum at

higher temperature and cold-adapted enzymes can be inactivated by a gentle heat treatment (Margesin & Schinner, 1994).

The algal pigment astaxanthin is also an important food supplement for farmed salmonids (e.g., salmon and trout) to impart colouration. In natural habitats salmonids obtain carotenoids from natural sources, but in fish farms this is not provided and they would be whitish and unattractive for consumers. At the moment *Haematococcus*, a mesophilic green algae, is the main industrial astaxanthin producer if cultured under light and nutrient stress (Lorenz & Cysewski, 2000).

Due to of its powerful antioxidant properties it is also used in medical products such as sunscreens to protect human skin from damaging UV irradiation (González et al, 2008).

References

Abell, G. & Bowman, J. P. (2005) Colonization and community dynamics of class Flavobacteria on diatom detritus in experimental mesocosms based on Southern Ocean seawater. *FEMS Microbiology Ecology*, 53(3), 379-391.

Anesio, A. M., Hodson, A. J., Fritz, A., Psenner, R. & Sattler, B. (2009) High microbial activity on glaciers: importance to the global carbon cycle. *Global Change Biology*, 15(4), 955-960.

Anesio, A. M. & Laybourn-Parry, J. (2011) Glaciers and ice sheets as a biome. *Trends in Ecoogy & Evoution*, 27, 219–225.

Anesio, A. M., Mindl, B., Laybourn-Parry, J. & Sattler, B. (2007) Virus dynamics in cryoconite holes on a high Arctic glacier (Svalbard). *Journal of Geophysical Research*, 112(4), G04S31.

Battin, T. J., Wille, A., Sattler, B. & Psenner, R. (2001) Phylogenetic and functional heterogeneity of sediment biofilms along environmental gradients in a glacial stream. *Applied and Environmental Microbiology*, 67(2), 799-807.

Bidigare, R., Ondrusek, M., Kennicutt, M., Iturriaga, R., Harvey, H., Hoham, R. & Macko, S. (1993) Evidence for a photoprotective function for secondary carotenoids of snow algae. *Journal of Phycology*, 29(4), 427-434.

Boussiba, S. (2000) Carotenogenesis in the green alga *Haematococcus pluvialis*: cellular physiology and stress response. *Physiologia Plantarum*, 108(2), 111-117.

Boyd, E. S., Lange, R. K., Mitchell, A. C., Havig, J. R., Hamilton, T. L., Lafrenière, M. J., Shock, E. L., Peters, J. W. & Skidmore, M. (2011) Diversity, abundance, and potential activity of nitrifying and nitrate-reducing microbial assemblages in a subglacial ecosystem. *Applied and Environmental Microbiology*, 77(14), 4778-4787.

Buma, A. G., Hannen, E. J., Roza, L., Veldhuis, M. J. & Gieskes, W. W. (1995) Monitoring ultraviolet-B-induced DNA damage in individual diatiom cells by immunofluorescent thymine dimer detection. *Journal of Phycology*, 31(2), 314-321.

Cameron, K. A., Hodson, A. J. & Osborn, A. M. (2012) Structure and diversity of bacterial, eukaryotic and archaeal communities in glacial cryoconite holes from the Arctic and the Antarctic. *FEMS Microbiology Ecology*, 82(2), 254-267.

Castello, J. D. & Rogers, S. O. (2005) *Life in ancient ice.* Princeton University Press: Princeton.

Chauhan, S., Pandey, R. & Singhal, G. S. (1998) Ultraviolet-B induced changes in ultrastructure and D1/D2 proteins in cyanobacteria *Synechococcus* sp. PCC 7942. *Photosynthetica*, 35(2), 161-167.

Chintalapati, S., Kiran, M. & Shivaji, S. (2004) Role of membrane lipid fatty acids in cold adaptation. *Cellular and Molecular Biology (Noisy-le-Grand, France)*, 50(5), 631.

Choudhari, S., Smith, S., Owens, S., Gilbert, J. A., Shain, D. H., Dial, R. J. & Grigoriev, A. (2013) Metagenome sequencing of prokaryotic microbiota collected from Byron Glacier, Alaska. *Genome Announcements*, 1(2).

Christner, B. C., Kvitko, B. H. & Reeve, J. N. (2003) Molecular identification of bacteria and eukarya inhabiting an Antarctic cryoconite hole. *Extremophiles*, 7(3), 177-183.

Darcy, J. L., Lynch, R. C., King, A. J., Robeson, M. S. & Schmidt, S. K. (2011) Global distribution of *Polaromonas* phylotypes-evidence for a highly successful dispersal capacity. *PloS one*, 6(8), e23742.

de Pascale, D., De Santi, C., Fu, J. & Landfald, B. (2012) The microbial diversity of Polar environments is a fertile ground for bioprospecting. *Marine genomics*, 8, 15-22.

Duval, B., Shetty, K. & Thomas, W. H. (1999) Phenolic compounds and antioxidant properties in the snow alga *Chlamydomonas nivalis* after exposure to UV light. *Journal of Applied Phycology*, 11(6), 559-566.

Edwards, A., Anesio, A. M., Rassner, S. M., Sattler, B., Hubbard, B., Perkins, W. T., Young, M. & Griffith, G. W. (2010) Possible interactions between bacterial diversity, microbial activity and supraglacial hydrology of cryoconite holes in Svalbard. *The ISME Journal*, 5(1), 150-160.

Edwards, A., Mur, L. A., Girdwood, S. E., Anesio, A. M., Stibal, M., Rassner, S. M., Hell, K., Pachebat, J. A., Post, B. & Bussell, J. S. (2014) Coupled cryoconite ecosystem structure–function relationships are revealed by comparing bacterial communities in alpine and Arctic glaciers. *FEMS Microbiology Ecology*, 89, 222–237.

Edwards, A., Pachebat, J. A., Swain, M., Hegarty, M., Hodson, A. J., Irvine-Fynn, T. D., Rassner, S. M. & Sattler, B. (2013) A metagenomic snapshot of taxonomic

and functional diversity in an alpine glacier cryoconite ecosystem. *Environmental Research Letters*, 8(3), 035003.

Ettl, H. (1983) Chlorophyta 1. Phytomonadina.

Feller, G., Narinx, E., Arpigny, J. L., Aittaleb, M., Baise, E., Genicot, S. & Gerday, C. (1996) Enzymes from psychrophilic organisms. *FEMS Microbiology Reviews*, 18(2-3), 189-202.

Fendrihan, S. & Negoiţă, T. G. (2012) Psychrophilic microorganisms as important source for biotechnological processes. *Adaption of Microbial Life to Environmental Extremes*, 133-172. Springer:Vienna.

Foreman, C. M., Sattler, B., Mikucki, J. A., Porazinska, D. L. & Priscu, J. C. (2007) Metabolic activity and diversity of cryoconites in the Taylor Valley, Antarctica. *Journal of Geophysical Research*, 112(G4), G04S32.

Fujii, M., Takano, Y., Kojima, H., Hoshino, T., Tanaka, R. & Fukui, M. (2010) Microbial community structure, pigment composition, and nitrogen source of red snow in Antarctica. *Microbial Ecology*, 59(3), 466-475.

Geider, R. & La Roche, J. (2002) Redfield revisited: variability of C: N: P in marine microalgae and its biochemical basis. *European Journal of Phycology*, 37(1), 1-17.

Gentz-Werner, P. (2007) *Roter Schnee: oder Die Suche nach dem färbenden Prinzip*. Berlin: Akademie Verlag.

González, S., Fernández-Lorente, M. & Gilaberte-Calzada, Y. (2008) The latest on skin photoprotection. *Clinics in Dermatology*, 26(6), 614-626.

Gorton, H. L., Williams, W. E. & Vogelmann, T. C. (2001) The Light Environment and Cellular Optics of the Snow Alga *Chlamydomonas nivalis* (Bauer) Wille. *Photochemistry and Photobiology*, 73(6), 611-620.

Gruber, N. & Deutsch, C. A. (2014) Redfield's evolving legacy. *Nature Geoscience*, 7(12), 853-855.

Häder, D.-P. & Häder, M. A. (1989) Effects of solar UV-B irradiation on photomovement and motility in photosynthetic and colorless flagellates. *Environmental and experimental botany*, 29(2), 273-282.

Handelsman, J., Rondon, M. R., Brady, S. F., Clardy, J. & Goodman, R. M. (1998) Molecular biological access to the chemistry of unknown soil microbes: a new frontier for natural products. *Chemistry & Biology*, 5(10), R245-R249.

Hargreaves, A., Taiwo, F., Duggan, O., Kirk, S. & Ahmad, S. (2007) Near-ultraviolet photolysis of β-phenylpyruvic acid generates free radicals and results in DNA damage. *Journal of Photochemistry and Photobiology B: Biology*, 89(2), 110-116.

Hodson, A., Anesio, A. M., Ng, F., Watson, R., Quirk, J., Irvine-Fynn, T., Dye, A., Clark, C., McCloy, P. & Kohler, J. (2007) A glacier respires: quantifying the

distribution and respiration CO2 flux of cryoconite across an entire Arctic supraglacial ecosystem. *Journal of Geophysical Research*, 112(G4), G04S36.

Hodson, A., Anesio, A. M., Tranter, M., Fountain, A., Osborn, M., Priscu, J., Laybourn-Parry, J. & Sattler, B. (2008) Glacial ecosystems. *Ecological Monographs,* 78(1), 41-67.

Hoham, R. & Duval, B. (2001) Microbial ecology of snow and freshwater ice with emphasis on snow algae. Cambridge University Press: Cambridge.

Hoham, R. W., Bonome, T. A., Martin, C. W. & Leebens-Mack, J. H. (2002) A combined 18S rDNA and rbcL phylogenetic analysis of *Chloromonas* and *Chlamydomonas* (*Chlorophyceae*, *Volvocales*) emphazising snow and other cold-temperature habitats. *Journal of Phycology*, 38(5), 1051-1064.

Hood, E., Battin, T. J., Fellman, J., O'Neel, S. & Spencer, R. G. (2015) Storage and release of organic carbon from glaciers and ice sheets. *Nature Geoscience*, 8(2), 91-96.

James, G. O., Hocart, C. H., Hillier, W., Chen, H., Kordbacheh, F., Price, G. D. & Djordjevic, M. A. (2011) Fatty acid profiling of *Chlamydomonas reinhardtii* under nitrogen deprivation. *Bioresource Technology*, 102(3), 3343-3351.

Jones, H. (1999) The ecology of snow-covered systems: a brief overview of nutrient cycling and life in the cold. *Hydrological Processes*, 13(14-15), 2135-2147.

Kaštovská, K., Elster, J., Stibal, M. & Šantrůčková, H. (2005) Microbial assemblages in soil microbial succession after glacial retreat in Svalbard (high Arctic). *Microbial Ecology*, 50(3), 396-407.

Kirchman, D. L. (2002) The ecology of Cytophaga–Flavobacteria in aquatic environments. *FEMS Microbiology Ecology*, 39(2), 91-100.

Kirst, G. (1990) Salinity tolerance of eukaryotic marine algae. *Annual Review of Plant Biology*, 41(1), 21-53.

Klausmeier, C. A., Litchman, E., Daufresne, T. & Levin, S. A. (2004) Optimal nitrogen-to-phosphorus stoichiometry of phytoplankton. *Nature*, 429(6988), 171-174.

Kol, E. (1968) *Kryobiologie; Biologie und Limnologie des Schnees und Eises*, *24*E. Schweizerbart.

Kvíderová, J. (2012) Research on cryosestic communities in Svalbard: the snow algae of temporary snowfields in Petuniabukta, Central Svalbard. *Czech Polar Reports*, 2, 8-19.

Leya, T. (2004) *Feldstudien und genetische Untersuchungen zur Kryophilie der Schneealgen Nordwestspitzbergens.* Aachen: Shaker.

Leya, T., Müller, T., Ling, H. & Fuhr, G. (2000) Taxonomy and biophysical properties of cryophilic microalgae and their environmental factors in Northwest Spitsbergen, Svalbard, *57th Eastern Snow Conference, Syracuse, New York, USA*.

Leya, T., Rahn, A., Lütz, C. & Remias, D. (2009) Response of arctic snow and permafrost algae to high light and nitrogen stress by changes in pigment composition and applied aspects for biotechnology. *FEMS Microbiology Ecology*, 67(3), 432-443.

Ling, H. & Seppelt, R. (1990) Snow algae of the Windmill Islands, continental Antarctica. *Mesotaenium berggrenii* (*Zygnematales, Chlorophyta*) the alga of grey snow. *Antarctic Science*, 2(02), 143-148.

Lorenz, R. T. & Cysewski, G. R. (2000) Commercial potential for *Haematococcus microalgae* as a natural source of astaxanthin. *Trends in Biotechnology*, 18(4), 160-167.

Lütz-Meindl, U. & Lütz, C. (2006) Analysis of element accumulation in cell wall attached and intracellular particles of snow algae by EELS and ESI. *Micron*, 37(5), 452-458.

Margesin, R. & Schinner, F. (1994) Properties of cold-adapted microorganisms and their potential role in biotechnology. *Journal of Biotechnology*, 33(1), 1-14.

Margesin, R., Zacke, G. & Schinner, F. (2002) Characterization of heterotrophic microorganisms in alpine glacier cryoconite. *Arctic, Antarctic, and Alpine Research*, 34(1), 88-93.

McKay, C. P. & Stoker, C. R. (1989) The early environment and its evolution on Mars: implication for life. *Reviews of Geophysics*, 27(2), 189-214.

Médigue, C., Krin, E., Pascal, G., Barbe, V., Bernsel, A., Bertin, P. N., Cheung, F., Cruveiller, S., D'Amico, S. & Duilio, A. (2005) Coping with cold: the genome of the versatile marine Antarctica bacterium *Pseudoalteromonas haloplanktis* TAC125. *Genome Research*, 15(10), 1325-1335.

Merchant, S. S., Prochnik, S. E., Vallon, O., Harris, E. H., Karpowicz, S. J., Witman, G. B., Terry, A., Salamov, A., Fritz-Laylin, L. K. & Maréchal-Drouard, L. (2007) The *Chlamydomonas* genome reveals the evolution of key animal and plant functions. *Science*, 318(5848), 245-250.

Methé, B. A., Nelson, K. E., Deming, J. W., Momen, B., Melamud, E., Zhang, X., Moult, J., Madupu, R., Nelson, W. C. & Dodson, R. J. (2005) The psychrophilic lifestyle as revealed by the genome sequence of *Colwellia psychrerythraea* 34H through genomic and proteomic analyses. *Proceedings of the National Academy of Sciences of the United States of America*, 102(31), 10913-10918.

Mills, M. M. & Arrigo, K. R. (2010) Magnitude of oceanic nitrogen fixation influenced by the nutrient uptake ratio of phytoplankton. *Nature Geoscience*, 3(6), 412-416.

Møller, A. K., Søborg, D. A., Al-Soud, W. A., Sørensen, S. J. & Kroer, N. (2013) Bacterial community structure in High-Arctic snow and freshwater as revealed by pyrosequencing of 16S rRNA genes and cultivation. *Polar Research*, 32.

Moran, N. A. & Jarvik, T. (2010) Lateral transfer of genes from fungi underlies carotenoid production in aphids. *Science*, 328(5978), 624-627.

Müller, D. R., Vincent, W. F., Pollard, W. H. & Fritsen, C. H. (2001a) Glacial cryoconite ecosystems: a bipolar comparison of algal communities and habitats. *Nova Hedwigia Beiheft*, 123, 173-198.

Müller, T., Bleiss, W., Martin, C. D., Rogaschewski, S. & Fuhr, G. (1998) Snow algae from northwest Svalbard: their identification, distribution, pigment and nutrient content. *Polar Biology*, 20(1), 14-32.

Müller, T., Leya, T. & Fuhr, G. (2001b) Persistent snow algal fields in Spitsbergen: field observations and a hypothesis about the annual cell circulation. *Arctic, Antarctic, and Alpine Research*, 42-51.

Naff, C., Darcy, J. & Schmidt, S. (2013) Phylogeny and biogeography of an uncultured clade of Snow Chytrids. *Environmental Microbiology*, *5*(10), 2672-2680.

Nordenskjöld, N. (1875) Cryoconite found 1870, July 19th-25th, on the inland ice, east of Auleitsivik Fjord, Disco Bay, Greenland. *Geological Magazine, Decade*, 2(2), 157-162.

Penuelas, J., Poulter, B., Sardans, J., Ciais, P., van der Velde, M., Bopp, L., Boucher, O., Godderis, Y., Hinsinger, P. & Llusia, J. (2013) Human-induced nitrogen–phosphorus imbalances alter natural and managed ecosystems across the globe. *Nature Communications*, 4, 2934.

Pereira, P. R. G. (2010) *Marine Bacteroidetes: distribution patterns and role in the degradation of organic matter*. Bremen.

Pichrtová, M., Kulichová, J. & Holzinger, A. (2014) Nitrogen Limitation and Slow Drying Induce Desiccation Tolerance in Conjugating Green Algae (*Zygnematophyceae, Streptophyta*) from Polar Habitats. *PloS one*, 9(11), e113137.

Piorreck, M., Baasch, K.-H. & Pohl, P. (1984) Biomass production, total protein, chlorophylls, lipids and fatty acids of freshwater green and blue-green algae under different nitrogen regimes. *Phytochemistry*, 23(2), 207-216.

Porazinska, D., Fountain, A., Nylen, T., Tranter, M., Virginia, R. & Wall, D. (2004) The biodiversity and biogeochemistry of cryoconite holes from McMurdo Dry Valley glaciers, Antarctica. *Arctic, Antarctic, and Alpine Research*, 36(1), 84-91.

Price, P. B. (2000) A habitat for psychrophiles in deep Antarctic ice. *Proceedings of the National Academy of Sciences*, 97(3), 1247-1251.

Price, P. B. (2007) Microbial life in glacial ice and implications for a cold origin of life. *FEMS Microbiology Ecology*, 59(2), 217-231.

Rabus, R., Ruepp, A., Frickey, T., Rattei, T., Fartmann, B., Stark, M., Bauer, M., Zibat, A., Lombardot, T. & Becker, I. (2004) The genome of *Desulfotalea psychrophila*, a sulfate-reducing bacterium from permanently cold Arctic sediments. *Environmental Microbiology*, 6(9), 887-902.

Rajagopal, S., Murthy, S. & Mohanty, P. (2000) Effect of ultraviolet-B radiation on intact cells of the cyanobacterium Spirulina platensis: characterization of the

alterations in the thylakoid membranes. *Journal of Photochemistry and Photobiology B: Biology*, 54(1), 61-66.

Redfield, A. C. (1963) The influence of organisms on the composition of sea water. *The sea*, 26-77.

Reisser, W. & Houben, P. (2001) Different strategies of aeroterrestrial algae in reacting to increased levels of UV-B and ozone. *Nova Hedwigia Beiheft*, 123, 291-296.

Remias, D., Albert, A. & Lütz, C. (2010) Effects of realistically simulated, elevated UV irradiation on photosynthesis and pigment composition of the alpine snow alga *Chlamydomonas nivalis* and the arctic soil alga *Tetracystis* sp.(*Chlorophyceae*). *Photosynthetica*, 48(2), 269-277.

Remias, D., Holzinger, A., Aigner, S. & Lütz, C. (2012a) Ecophysiology and ultrastructure of *Ancylonema nordenskiöldii* (*Zygnematales*, *Streptophyta*), causing brown ice on glaciers in Svalbard (high arctic). *Polar Biology*, 1-10.

Remias, D., Holzinger, A. & Lütz, C. (2009) Physiology, ultrastructure and habitat of the ice alga *Mesotaenium berggrenii* (*Zygnemaphyceae*, *Chlorophyta*) from glaciers in the European Alps. *Phycologia*, 48(4), 302-312.

Remias, D., Lütz-Meindl, U. & Lütz, C. (2005) Photosynthesis, pigments and ultrastructure of the alpine snow alga *Chlamydomonas nivalis*. *European Journal of Phycology*, 40(3), 259-268.

Remias, D. & Lutz, C. (2007) Characterisation of esterified secondary carotenoids and of their isomers in green algae: a HPLC approach. *Algological Studies*, 124(1), 85-94.

Remias, D., Schwaiger, S., Aigner, S., Leya, T., Stuppner, H. & Lütz, C. (2012b) Characterization of an UV-and VIS-absorbing, purpurogallin-derived secondary pigment new to algae and highly abundant in Mesotaenium berggrenii (*Zygnematophyceae*, *Chlorophyta*), an extremophyte living on glaciers. *FEMS Microbiology Ecology*, *79*(3), 638-648.

Řezanka, T., Nedbalová, L., Sigler, K. & Cepák, V. (2008) Identification of astaxanthin diglucoside diesters from snow alga *Chlamydomonas nivalis* by liquid chromatography–atmospheric pressure chemical ionization mass spectrometry. *Phytochemistry*, 69(2), 479-490.

Rhee, G.-Y. (1978) Effects of N: P atomic ratios and nitrate limitation on algal growth, cell composition, and nitrate uptake 1. *Limnology and oceanography*, 23(1), 10-25.

Riemann, L. & Winding, A. (2001) Community dynamics of free-living and particle-associated bacterial assemblages during a freshwater phytoplankton bloom. *Microbial Ecology*, 42(3), 274-285.

Rodolfi, L., Chini Zittelli, G., Bassi, N., Padovani, G., Biondi, N., Bonini, G. & Tredici, M. R. (2008) Microalgae for oil: Strain selection, induction of lipid synthesis and outdoor mass cultivation in a low-cost photobioreactor. *Biotechnology and Bioengineering*, 102(1), 100-112.

Roessler, P. G. (1990) Environmental control of glycerolipid metabolism in microalgae: commercial implications and future research directions. *Journal of Phycology*, 26(3), 393-399.

Rothschild, L. J. (1990) Earth analogs for Martian life. Microbes in evaporites, a new model system for life on Mars. *Icarus*, 88(1), 246-260.

Saunders, N. F., Thomas, T., Curmi, P. M., Mattick, J. S., Kuczek, E., Slade, R., Davis, J., Franzmann, P. D., Boone, D. & Rusterholtz, K. (2003) Mechanisms of thermal adaptation revealed from the genomes of the Antarctic Archaea *Methanogenium frigidum* and *Methanococcoides burtonii*. *Genome Research*, 13(7), 1580-1588.

Säwström, C., Mumford, P., Marshall, W., Hodson, A. & Laybourn-Parry, J. (2002) The microbial communities and primary productivity of cryoconite holes in an Arctic glacier (Svalbard 79 N). *Polar Biology*, 25(8), 591-596.

Schütte, U. M., Abdo, Z., Bent, S. J., Williams, C. J., Schneider, G. M., Solheim, B. & Forney, L. J. (2009) Bacterial succession in a glacier foreland of the High Arctic. *The ISME Journal*, 3(11), 1258-1268.

Sharp, M., Parkes, J., Cragg, B., Fairchild, I. J., Lamb, H. & Tranter, M. (1999) Widespread bacterial populations at glacier beds and their relationship to rock weathering and carbon cycling. *Geology*, 27(2), 107-110.

Siddiqui, K. S., Bokhari, S. A., Afzal, A. J. & Singh, S. (2004) A novel thermodynamic relationship based on Kramers theory for studying enzyme kinetics under high viscosity. *IUBMB life*, 56(7), 403-407.

Siddiqui, K. S. & Cavicchioli, R. (2006) Cold-adapted enzymes. *Annual Reviews in Biochemistry*, 75, 403-433.

Simon, C., Wiezer, A., Strittmatter, A. W. & Daniel, R. (2009) Phylogenetic diversity and metabolic potential revealed in a glacier ice metagenome. *Applied and Environmental Microbiology*, 75(23), 7519-7526.

Sommaruga, R. & Garcia-Pichel, F. (1999) UV-absorbing mycosporine-like compounds in planktonic and benthic organisms from a high-mountain lake. *Archiv für Hydrobiologie*, 144(3), 255-269.

Spijkerman, E., Wacker, A., Weithoff, G. & Leya, T. (2012) Elemental and fatty acid composition of snow algae in Arctic habitats. *Frontiers in Microbiology*, 3, 380.

Sterner, R. W. & Elser, J. J. (2002) *Ecological stoichiometry: the biology of elements from molecules to the biosphere.* Princeton University Press: Princeton.

Stibal, M. & Elster, J. (2005) Growth and morphology variation as a response to changing environmental factors in two Arctic species of *Raphidonema* (*Trebouxiophyceae*) from snow and soil. *Polar Biology*, 28(7), 558-567.

Stibal, M., Elster, J., Šabacká, M. & Kaštovská, K. (2007) Seasonal and diel changes in photosynthetic activity of the snow alga *Chlamydomonas nivalis*

(*Chlorophyceae*) from Svalbard determined by pulse amplitude modulation fluorometry. *FEMS Microbiology Ecology*, 59(2), 265-273.

Stibal, M., Šabacká, M. & Žárský, J. (2012) Biological processes on glacier and ice sheet surfaces. *Nature Geoscience*, 5(11), 771-774.

Stieglmeier, M., Klingl, A., Alves, R. J., Simon, K.-M. R., Melcher, M., Leisch, N. & Schleper, C. (2014) *Nitrososphaera viennensis* sp. nov., an aerobic and mesophilic ammonia-oxidizing archaeon from soil and member of the archaeal phylum Thaumarchaeota. *International Journal of Systematic and Evolutionary Microbiology*, ijs. 0.063172-0.

Szyszka, B., Ivanov, A. G. & Hüner, N. (2007) Psychrophily is associated with differential energy partitioning, photosystem stoichiometry and polypeptide phosphorylation in *Chlamydomonas raudensis*. *Biochimica et Biophysica Acta (BBA)-Bioenergetics*, 1767(6), 789-800.

Takeuchi, N. (2013) Seasonal and altitudinal variations in snow algal communities on an Alaskan glacier (Gulkana glacier in the Alaska range). *Environmental Research Letters*, 8(3), 035002.

Takeuchi, N., Uetake, J., Fujita, K., Aizen, V. B. & Nikitin, S. D. (2006) A snow algal community on Akkem glacier in the Russian Altai mountains. *Annals of Glaciology*, 43(1), 378-384.

Telling, J., Anesio, A. M., Tranter, M., Irvine-Fynn, T., Hodson, A., Butler, C. & Wadham, J. (2011) Nitrogen fixation on Arctic glaciers, Svalbard. *Journal of Geophysical Research*, 116(G3), G03039.

Thomas, W. H. & Duval, B. (1995) Sierra Nevada, California, USA, snow algae: snow albedo changes, algal-bacterial interrelationships, and ultraviolet radiation effects. *Arctic and Alpine Research*, 27(4), 389-399.

Thompson Jr, G. A. (1996) Lipids and membrane function in green algae. *Biochimica et Biophysica Acta (BBA)-Lipids and Lipid Metabolism*, 1302(1), 17-45.

Tourna, M., Stieglmeier, M., Spang, A., Könneke, M., Schintlmeister, A., Urich, T., Engel, M., Schloter, M., Wagner, M. & Richter, A. (2011) *Nitrososphaera viennensis*, an ammonia oxidizing archaeon from soil. *Proceedings of the National Academy of Sciences*, 108(20), 8420-8425.

Tranter, M., Fountain, A. G., Fritsen, C. H., Berry Lyons, W., Priscu, J. C., Statham, P. J. & Welch, K. A. (2004) Extreme hydrochemical conditions in natural microcosms entombed within Antarctic ice. *Hydrological Processes*, 18(2), 379-387.

Uetake, J., Naganuma, T., Hebsgaard, M. B., Kanda, H. & Kohshima, S. (2010) Communities of algae and cyanobacteria on glaciers in west Greenland. *Polar Science*, 4(1), 71-80.

Vincent, W. F. & Neale, P. J. (2000) Mechanisms of UV damage to aquatic organisms. *The effects of UV radiation in the marine environment*, 10, 72-100.

Von Mering, C., Hugenholtz, P., Raes, J., Tringe, S., Doerks, T., Jensen, L., Ward, N. & Bork, P. (2007) Quantitative phylogenetic assessment of microbial communities in diverse environments. *Science*, 315(5815), 1126-1130.

Wille, N. (1903) *Algologische Notizen IX-XIV*.

Williams, W. E., Gorton, H. L. & Vogelmann, T. C. (2003) Surface gas-exchange processes of snow algae. *Proceedings of the National Academy of Sciences*, 100(2), 562-566.

Wynn, P. M., Hodson, A. J., Heaton, T. H. & Chenery, S. (2007) Nitrate production beneath a High Arctic glacier, Svalbard. *Chemical Geology*, 244(1), 88-102.

Yallop, M. L., Anesio, A. M., Perkins, R. G., Cook, J., Telling, J., Fagan, D., MacFarlane, J., Stibal, M., Barker, G. & Bellas, C. (2012) Photophysiology and albedo-changing potential of the ice algal community on the surface of the Greenland ice sheet. *The ISME Journal*, *6*(12), 2302-2313.

Yoshimura, Y., Kohshima, S., Takeuchi, N., Seko, K. & Fujita, K. (2006) Snow algae in a Himalayan ice core: new environmental markers for ice-core analyses and their correlation with summer mass balance. *Annals of Glaciology*, 43(1), 148-153.

Zarsky, J. D., Stibal, M., Hodson, A., Sattler, B., Schostag, M., Hansen, L. H., Jacobsen, C. S. & Psenner, R. (2013) Large cryoconite aggregates on a Svalbard glacier support a diverse microbial community including ammonia-oxidizing archaea. *Environmental Research Letters*, 8(3), 035044.

Chapter 3: Methodology

3.1 Field sites

21 glaciers were sampled in the 4 Arctic settings Svalbard, Arctic Sweden, Greenland and Iceland (Figure 3.1). 179 sites were sampled for various analyses that are described below and in the results chapters. These field sites were chosen in order to get a good representation of varying geographical parameters including low *vs.* high latitude, low *vs.* high elevation and maritime *vs.* continental.

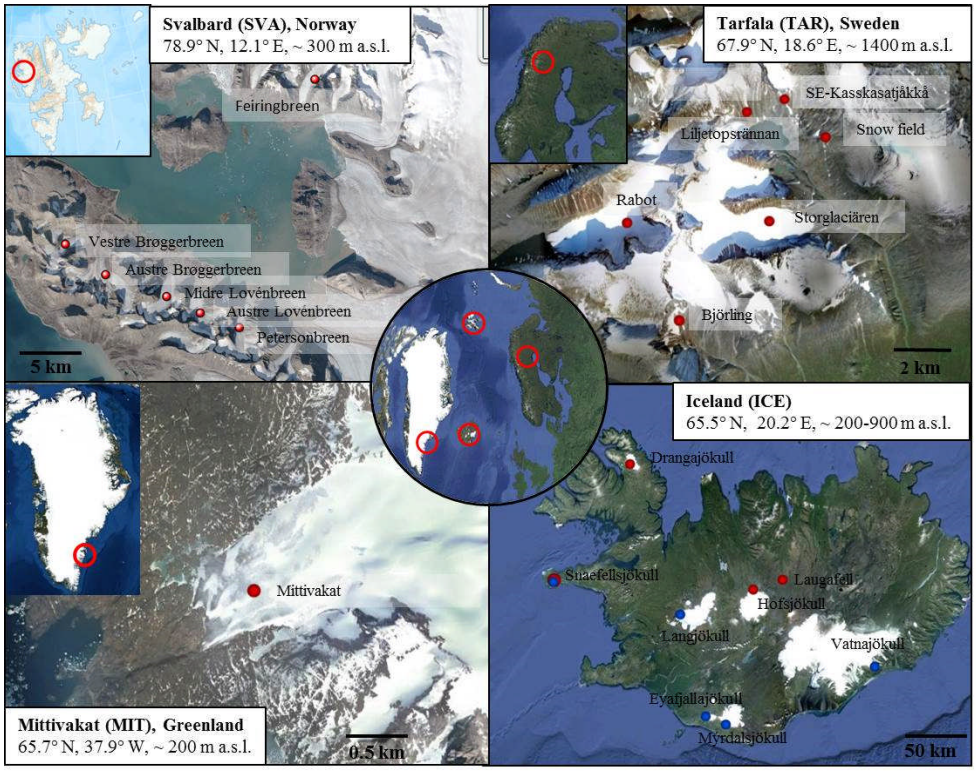

Figure 3.1: Map of the different field sites in Svalbard, Arctic Sweden, Greenland and Iceland. Dots represent various sampling events.

3.2 Field measurements

At each sampling point and prior to sampling, the snow temperature (upper few cm), pH and conductivity were measured *in-situ* using a daily-calibrated multi-meter (Hanna instruments, HI 98129). For all snow and runoff samples, pH and conductivity were measured after allowing the multi-meter to equilibrate in the upper 2-3 cm of the sampling site. For ice samples this was achieved by melting a

few ice chips prior to measurements. Furthermore, at each site, irradiation was measured using a radiometer with specific sensors for photosynthetic active radiation (PAR) and ultraviolet radiation (UV-A and UV-B, SolarLight PMA2100). Albedo was calculated by taking the ratio of reflected to incident radiation (400-700 nm range) and measuring the values always in the same position to the sun. Measurements were carried out with the sensors held at 30 cm above the snow surface (field of view 160º, effective measurement area 0.5 m^2) and by first pointing the sensor upwards (incident radiation) and then towards the snow/ice surface (reflected radiation). Five measurements for incident and reflected radiation were acquired each. The error of the measurement (standard deviation) was below 10 %.

During the field season in Greenland in order to evaluate community activity and the proportion of autotrophy *vs.* heterotrophy, respiration experiments were carried out by measuring O_2 concentrations over time. For this a large volume of various samples were collected in sterile sampling bags and slowly (~ 3-4 h) melted on-site. For each sample type (see below), melted but homogenous subsamples were transferred into 50 mL glass bottles that had been rinsed multiple times with the respective sample. The bottles were completely filled up, initial (time zero) O_2 concentrations measured and subsequently air-tightly sealed with ground glass stoppers. O_2 concentrations were measured using an O_2 meter (Hach HQ30d). Per sample three bottles were wrapped in light impermeable white plastic to measure net community O_2 respiration, while three bottles each were left unwrapped to measure O_2 production and respiration. The bottles were left for up to two days on the glacial surface and final O_2 concentrations were measured after 24 or 48 h. Net O_2 production was calculated by the difference between wrapped and unwrapped bottles. At each measurement point the temperature was simultaneously measured using the O_2 meter and temperature corrections were applied.

3.3 Field sampling strategy

Based on visual observations several distinct microbial glacial surface habitats that were considered to be highly representative of the whole glacial surface were defined as follows: clean snow (white snow with no visual presence of particles), green snow (light to dark green colouration, often deep penetration of the snowpack), red snow (red colouration with all shades from orange to pink with

variable densities of particles and only within the surface layer), biofilms (wet snow at snow-ice melting interfaces), clean ice (white ice with no visual presence of particles), grey ice (light grey to dark grey colouration and variable densities of particles), cryoconite holes (1-50 cm large rounded or elongated and variably deep holes filled with sediment), and glacial runoff (melt rivers and channels). In each of these habitats (except for glacial runoff where only one sample was collected) various samples were collected for microbial, mineralogical and geochemical analyses.

3.4 Field sample preservation and handling

Samples for inorganic aqueous analyses were collected either in sterile 50 mL centrifuge tubes or sterile sample bags. The snow/ice samples were melted at room temperature over a ~ 6 hour period and all samples were filtered through single use 0.2 µM cellulose-acetate syringe filters. For cation analyses by inductively coupled plasma mass spectrometry (ICP-MS), samples were directly filtered into acid-washed (HCl) and pre-acidified (Aristar grade HNO_3) Nalgene HDPE bottles, while for anion analyses by ion chromatography (IC), samples were stored un-acidified in 15 mL centrifuge tubes.

For dissolved organic carbon (DOC) and organic particulate analysis, samples were collected in 250 mL glass jars that had been ashed at 450 °C. for > 4 h. After melting at room temperature these samples were filtered through ashed 0.7 µm glass fibre filters (GFF) directly into pre-acidified (100µl Aristar grade HCl) 40 mL, amber glass vials with Teflon® seals (Supelco). The filters containing particulates were folded into quarters and preserved cold and in ashed aluminium foil for pigment and fatty acid analyses.

From these samples particulates for X-ray diffraction (XRD), Fourier transform infrared spectroscopy (FTIR) and Raman analyses were also collected by filtration through 0.2 µm polycarbonate filters. For imaging and cell counts using light microscopy (LM) as well as for scanning and transmission electron microscopy (SEM, TEM) melted but unconcentrated samples were preserved in 2.5% glutaraldehyde. Samples were returned to Leeds either frozen in liquid nitrogen in a cryo-shipper or in an ice-box at ~ 4 ˚C.

3.5 Aqueous organic (DOC) and inorganic analyses

Anions (NO_2^-, NO_3^-, Cl^-, SO_4^{2-}) were analysed in filtered samples by ion chromatography (IC) on a Dionex DX 600 system with an autosampler, an IonPac AS16 analytical column with an AG16 guard column, an eluent gradient of 0-15 mM KOH and an ED50 conductivity detector. Injection volume was 25 µL and flow rate was set to 0.35 mL min^{-1}. For NO_2^- analysis the UV detector was set to 211 nm. The precision of the analysis was 5% and the limits of detection (LOD) were the following: NO_3^- = 96 ppb, Cl^- = 72 ppb, SO_4^{2-} = 121 ppb.

Major, minor and trace elements were measured by inductively coupled plasma mass spectrometry (ICP-MS) on an Agilent 7500ce with collision cell Octopole Reaction System (ORS) technology (ICP-MS facility, University of Portsmouth). The precision of the analysis was 3% and LODs were the following: Al, Ba, Co, Cr, Cu, Fe, Mg, Ni, Si, Sr, Zn = 0.1 ppb; Bi, Cd, Mn, Pb = 0.01 ppb; Ca, Na = 1 ppb; K,P,S = 10 ppb**.**

Dissolved organic carbon (DOC) was analysed on a Shimadzu TOC analyser (University of Plymouth). The precision of the analysis was 5%. PO_4 was analysed by segmented flow-injection analyses (AutoAnalyser3, Seal Analytical). The precision of the analysis was 3%.

Carbohydrates were determined by Ion Chromatography on a Dionex ICS-3000 system (Sunnyvale, USA). The carbohydrates fucose, rhamnose, arabinose, galactose, glucose, xylose/mannose, fructose/sucrose, ribose and lactose were separated isocratically on a CarboPac PA20 column (3×150mm), after passing through a CarboPac PA20 guard column (3x30 mm). Fructose/sucrose and xylose/mannose are co-eluting and hence were reported together. The precision was 3%.

3.6 Total carbon, total nitrogen, total sulphur, total phosphate and carbon and nitrogen isotopes

Particulates in the samples were analysed for $\delta^{15}N$ and $\delta^{13}C$ by a Vario Pyro Cube elemental analyser (Elementar Inc) coupled to an Isoprime mass spectrometer. Samples were combusted in tin capsules at 1150 °C and gases were separated using temperature controlled adsorption/desorption columns. Carbon analyses were calibrated with in-house C4-sucrose and urea standards assigned values of -

11.93‰ and -46.83‰ respectively via calibration with the international standards LSVEC (-46.479‰), CH7 (-31.83‰), CH6 (-10.45‰), and CO-1 (+2.48‰). Nitrogen isotope values were calibrated using the international standards USGS-25 and USGS-26 with assigned values of -30.4‰ and +53.7‰ respectively. Total carbon (TC), total nitrogen (TN), and total sulphur (TS) were derived from the thermal conductivity detector in the elemental analyser and calibrated using a sulphanilamide standard. Particulate phosphorus was extracted by ashing of the samples at 550°C for 2 h and incubating in 1 M HCl for 16 h according to extraction step V in Ruttenberg et al (2009).

3.7 Mineralogy

The mineralogical composition of each sample was determined by X-ray diffraction (XRD) with dried and ground samples analysed on a Bruker D8 Advance diffractometer. XRD spectra were recorded from 2-75°2Θ using a copper diffraction source and a run time of 12 min per sample. Spectra were analysed in DIFFRAC.EVA (Bruker, V.3.0).

3.8 Imaging

Cell morphologies and organic and inorganic debris distributions were imaged by light microscopy and scanning and transmission electron microscopy (LM, SEM and TEM). For SEM imaging of cell morphologies and distribution of organic and inorganic debris an ethanol exchange series (30, 50, 70, 90, 100%; 30 min per step) was prepared on samples that had been preserved in 2.5 % glutaraldehyde. A droplet of the fixed and exchanged sample was dispersed on an Al stub, air-dried and coated with 3 nm of Pt. Images were acquired on a Phillips Environmental Scanning Electron Microscope (E-SEM) at an accelerating voltage of 10 kV and a working distance of 10-12 mm and a LEO 1530 Field-Emission Gun SEM (FEG-SEM) at an accelerating voltage of 3 kV and working distance of 3-4 mm. For TEM, microtomed sections of the fixed and ethanol exchanged samples were prepared and resulting grids were imaged on a JEOL 1200-TEM at an accelerating voltage of 80 keV.

3.9 Fourier transform infrared spectroscopy

3.9.1 Bulk analyses

Functional groups distributions were determined on bulk, dried samples by Fourier transform infrared (FTIR) using an A2 Technology Microlab Portable mid-IR spectrometer with a Diamond internal reflection cell (DATR), with spectra acquired in the mid-infrared range (650- 4000 cm^{-1}). From the bulk spectra, the peak area ratios of the main functional groups representing the lipids (CH_2 and CH_3 stretching modes between 3050 and 2800 cm^{-1}), and proteins (amide I and II bands at 1700-1500 cm^{-1}) to those of the carbohydrates (C-O-C, C-O-P, P-O-P ring vibrations between 1204-815 cm^{-1}) were evaluated in Omnic (Thermos Scientific, V.5.1).

3. 9.2 Single cell analyses (Synchroton radiation)

Micro-analyses were carried out at the Multimode infrared imaging and micro-spectroscopy (MIRIAM) beamline, B22 at the Diamond Light Source (UK). Individual snow algal cells that were thawed and deposited on ZnSe windows were imaged and analyses in transmission mode by Fourier transform infrared (FTIR) spectroscopy. A Bruker FTIR spectrometer interlinked with the synchrotron-light (Benning et al., 2004) and a microscope was used to collect images and spectra via a broadband MCT detector, a x36 objective and a x36 condenser. We collected data either using a 20 µm x 20 µm aperture or a 6 µm x 6 µm aperture. Spectra were acquired over the mid-infrared range between 4000 and 650 cm^{-1} and at each point / pixel 512 spectra were co-added. All data were processed in Opus (V7.2). Functional group values for individual cells were derived from peak areas under the CH_2-CH_3-CH lipid/protein bands (~ 3100 – 2800 cm^{-1}), the C-O of the ester lipid band (~ 1720 cm^{-1}), the main protein bands (1700-1600 cm^{-1} for amide 1) and 1600 – 1500 cm^{-1} for amide 2) and the carbohydrate bands (between 1200 – 930 cm^{-1}). Area ratios for total proteins (1700-1500 cm^{-1}) over C-H lipids (3050-2800 cm^{-1}) and proteins (1700-1500 cm^{-1}) over C-O ester lipids (1850-1700 cm^{-1}) were calculated. We quantified the functional groups in 4 green and 12 red single cells and collected on each cell between 12 and 64 single spectra. It is worth noting that

we analysed single spherical cells in transmission mode and thus all spectra represent average intensities through the spheres.

3.10 Raman spectroscopy

Raman analyses were performed on a Renishaw InVia Raman spectrometer with two lasers at 514 nm and 785 nm excitation wavelengths, an attached microscope with a 50x magnification objective and a resolution of 4 cm^{-1}. Raman spectra were collected on singe algal cells or individual mineral grains with the aim of cross-confirming organic compound specificity and mineral composition.

3.11 Pigment analysis

To determine the carotenoid and chlorophyll contents in the samples, high pressure liquid chromatography (HPLC) and a modified carotenoid/chlorophyll specific extraction protocol (Remias & Lutz, 2007) were used. Cells were disrupted by shock freezing in liquid nitrogen for 10 min followed by grinding using a Teflon® mortar and pestle. The resulting powder was re-suspended in 1 mL of dimethylformamide (DMF) and 1.0 mm glass beads and horizontally shaken on a laboratory shaker (MoBio Vortex Genie 2) at maximum speed (3000 rpm) for 10 min followed by centrifugation for 5 min at 10 000 rpm. The supernatant was separated from the debris by filtering through a 0.45 µm Teflon® filter and the filtrate was mixed with methanol (25 vol %). Extracted samples were analysed immediately on an Agilent Technologies 1200 Infinity HPLC instrument with a gradient pump, an autosampler, a variable wavelength detector and ODS Hypersil column (250x4.6 mm; 5 um particle size). Two solvents were used: solvent A consisted of a mixture of acetonitrile/water/methanol/hexane/tris buffer at ratios of 80:7:3:1:1 while solvent B was a mix of methanol and hexane at a ratio of 5:1. The HPLC was run at a flow rate of 1 mL min^{-1} and with an injection volume of 25 µL. Spectra were recorded from 200 to 800 nm and chromatograms were quantified at 450 nm for carotenoids and 660 nm for chlorophyll a and b. Run time was 60 min and the protocol required a 15 minute run with 100% of solvent A followed by a linear gradient from 100 % solvent A to 100% solvent B between 32 and 45 min

and finally with 15 minutes of column re-equilibration through a 5 min linear gradient from solvent B back to 100% solvent to A, followed by a further column conditioning with 100 % solvent A for 10 min. The following commercially available standards were used for peak identification and calculation of the peak area: chlorophyll a, chlorophyll b (Sigma), violaxanthin, neoxanthin, antheraxanthin, lutein, β-carotene, trans-astaxanthin, and cis-astaxanthin (Carotenature). The precision of the analysis was 5%.

3.12 Fatty acids analysis

Fatty acids were extracted according to the method described by Wacker & Martin-Creuzberg (2007). Briefly, 20 ng of internal standard (tricosanoic acid methyl ester) were added to each sample, before ultrasonic extraction using dichloromethane:methanol (2:1 v:v), followed by centrifugation to remove particulates and evaporation of solvent from the supernatant. Fatty acids were transesterified by adding methanolic HCl to the dried extract and heating at 60˚ C for 20 minutes. After cooling, fatty acid methyl esters were extracted in isohexane, solvent was removed under nitrogen and the sample resuspended in isohexane for analysis

Analysis of fatty acid methyl esters was carried out using a Trace 1300 gas chromatograph with flame ionisation detector (Thermo Scientific, Hemel Hempstead, UK), equipped with a non-polar-fused silica capillary column (CPSil-5CB, 50m x 0.32mm x 0.12 mm, Agilent Technologies, USA). Samples (1µl) were injected in splitless mode, with the injector maintained at 200˚C. Carrier gas was helium, with a constant flow rate of 1.5 ml/min. The following temperature programme was used: initial temperature 40 °C, rising to 140 °C at 20 °C min^{-1}, then rising to 240 °C at 4 ° min^{-1}, holding at 240 °C for 5 min. Fatty acid methyl esters were identified by comparison of retention time with those of reference compounds (Supelco, USA) and by gas chromatography/mass spectrometry. Gas chromatography/mass spectrometry was carried out using the gas chromatograph and column previously described, with identical operating conditions, coupled to an ISQ mass spectrometer (Thermo Scientific, Hemel Hempstead, UK). The transfer line and the ion source were maintained at 300˚C. The emission current

was set to 50mA and the electron energy to 70 eV. The analyser was set to scan at m/z 50–650 with a scan cycle time of 0.6 s. The precision of the analysis was 5%.

3.13 DNA analyses

Total DNA was extracted using the PowerSoil® DNA Isolation kit (MoBio Laboratories). 16S rRNA genes were amplified using bacterial primers 27F (5'-AGAGTTTGATCMTGGCTCAG) and 357R (5'-CTGCTGCCTYCCGTA) (tagged with the Ion Torrent adapter sequences and MID barcode) spanning the V1-V2 hypervariable regions. 18S rRNA genes were amplified using the eukaryotic primers 528F (5′-GCGGTAATTCCAGCTCCAA) and 706R (5'-AATCCRAGAATTTCACCTCT) (Cheung et al., 2010) (tagged with the Ion Torrent adapter sequences and MID barcode) spanning the V4-V5 hypervariable region. Polymerase chain reactions (PCR) were performed using Platinum® PCR SuperMix High Fidelity according to manufacturer's protocols. Initial denaturation at 95 ºC for 5 min was followed by 30 cycles of denaturation at 95 ºC for 30 s, annealing at 60 ºC for 30 s and elongation at 72 ºC for 30 s. Final elongation was at 72 ºC for 7 min. Archaeal 16S rRNA genes were amplified following a nested PCR approach. The first PCR reaction was carried out using primers 20F (5'-TCCGGTTGATCCYGCCRG) and 915R (5′–GTGCTCCCCCGCCAATTCCT). Initial denaturation at 95 ºC for 5 min was followed by 35 cycles of denaturation at 95 ºC for 30 s, annealing at 62 ºC for 30 s and elongation at 72 ºC for 180 s. Final elongation was at 72 ºC for 10 min. The PCR product was used as template for the second PCR reaction with primers 21F (5'-TCCGGTTGATCCYGCCGG) and 519R (5'- GWATTACCGCGGCKGCTG) (tagged with the Ion Torrent adapter sequences and MID barcode) spanning the V1-V2 hypervariable region. Initial denaturation at 95 ºC for 5 min was followed by 30 cycles of denaturation at 95 ºC for 30 s, annealing at 60 ºC for 30 s and elongation at 72 ºC for 30 s. Final elongation was at 72 ºC for 7 min. All PCRs were carried out in triplicates to reduce amplification bias and in reaction volumes of 1 x 25 µl and 2 x 12.5 µl. All pre-amplification steps were done in a laminar flow hood with DNA-free certified plastic ware and filter tips. The pooled amplicons were purified with AMPure XP beads (Agencourt©) with a bead to DNA ratio of 0.6 to remove nucleotides, salts and primers and analyzed on the Agilent 2100 Bioanalyser (Agilent Technologies)

with the High Sensitivity DNA kit (Agilent Technologies) and quality, size and concentration were determined. Sequencing was performed on an Ion Torrent Personal Genome Machine using the Ion Xpress™ Template Kit and the Ion 314™ or Ion 316™ chips following manufacturer's protocols. The raw sequence data was processed in QIIME (Caporaso et al., 2010). Barcodes and adapter sequences were removed from each sequence. Filtering of sequences was performed using an average cutoff of Q20 over a 350 bp range. Reads shorter than 200 bp were removed. OTUs were picked *de novo* using a threshold of 99%, 97% and 95% identity. Taxonomic identities were assigned for representative sequences of each OTU using the reference databases Greengenes for bacteria and archaea. The Silva database (DeSantis et al., 2006; extended with additional 223 sequences of cryophilic algae kindly provided by Dr. Thomas Leya from the CCCryo - Culture Collection of Cryophilic Algae, Fraunhofer IZI-BB) was used for eukaryotes. Data were aligned using PyNAST and a 0.80 confidence threshold. Singletons were excluded from the analysis. Bacterial sequences matching plant plastids were removed from the data set prior to further analysis. Eukaryotic sequences matching *Chloroplastida* were pulled out of the data set and stored in a separate OTU table. In order to focus upon algal diversity, sequences matching *Embryophyta* (e.g., moss, fern) were removed from the data set. For archaea, sequences matching bacteria were removed. For diversity analyses samples were rarefied to the smallest sequence number and Shannon indices were calculated in QIIME. A matrix of each OTU table representing relative abundance was imported into Past3 (Hammer et al., 2012) for multivariate statistical analyses (principal component analysis, PCA). Representative sequences of the major algal species found in all samples were imported into Geneious (7.1.3., Biomatters) for phylogenetic tree building based on neighbor-joining.

Metagenome libraries were constructed using the Ion Plus Fragment Library ™ and the Ion Xpress Barcode Adapter ™ kits according to manufacturer's instructions. The libraries were analysed on the Agilent 2100 Bioanalyser (Agilent Technologies) with the High Sensitivity DNA kit (Agilent Technologies) and quality, size and concentration were determined. Sequencing was performed on an Ion Torrent Personal Genome Machine using the Ion Xpress™ Template Kit and the Ion 314™ chip following manufacturer's protocols. The raw sequence data was processed in QIIME (Caporaso et al, 2010). Barcodes and adapter sequences were removed from each sequence. Filtering of sequences was performed using an average cutoff of Q20 over a 350 bp range and a minimum read length of 200 bp.

Sequence reads were assigned to protein references sequences in the IMG database using blat.

3.14 Metabolomics

Samples were centrifuged at 20,000 rpm to pellet algal cells. Pellets were ground to a powder in liquid nitrogen. Biphasic extractions of algal metabolites were prepared as per the methods of Overy et al. (2005) in 750 µl of a sterile methanol:chloroform:water/6:2.5:1 mix for 60 minutes on ice. 400 µl of sterile water were added and extracts were vortexed and centrifuged at 12,000 rpm for 2 min to produce biphasic extractions. 200 µl of the aqueous/polar phase of each metabolite extract was diluted with 200 µl of methanol and 400 µl 0.1% formic acid and analysed by direct injection ToF-LC-MS (QStar Elite System, Applied Biosystems, Massachusetts, USA). Broad range spectra for mass numbers 50-1000 Da were collected over 240 cycles (each cycle lasting 0.9998 s) in positive ion mode using the following instrument settings: resolution of 4000, GS1 at 27.0, CUR at 20.0, and IS of 3500.0. Source temperature was 100°C and cone gas flow rate was maintained at 10 µl min^{-1}. Samples were run in triplicate and the resulting spectra combined using the Analyst QS 2.0 (Applied Biosystems, Massachusetts, USA) software. Mass numbers (or mass to charge ratios, *m*/z) were rounded into 0.01 Da bins and the relative abundance (Total Ion Count - %TIC) for each mass number within that bin summed (Overy et al., 2005;Field and Lake, 2011). All data processing was carried out using in-house software (Burrell & Cameron, unpublished) based upon the binning procedures of Overy et al.(2005).

Metabolic profiles were compared using the OPLS-DA method and the Simca-P multivariate data analysis software (Umetrics, Sweden) using binned mass numbers as the primary variable and sample type as the observational variable. Discriminatory *m/z* values with an R^2 close to 1.0 were assigned identities and metabolic pathways using the online database Biocyc (http://biocyc.org/) and the Kyoto Encyclopedia of Genes and Genomes (KEGG, http://genome.jp/kegg/), using the *Chlamydomonas reinhardtii* reference library wherever possible.

3.15 Statistical analyses

Principal component analyses (PCA), canonical correspondence analyses (CCA) and Pearson correlations were carried out in PAST v3.06 (Hammer et al, 2012) and one-way analysis of variance (ANOVA) was done in SPSS v19 (IBM).

PCA is a multi-variate statistical procedure to identify patterns in a data set and elucidate the components causing variance in the data. It is especially useful in data of high dimension since dimensions can be collapsed without losing (too much) information. The principal components are the directions where there is most variance. Directions are represented by eigenvectors and the amount of variance, *i.e.*, how much the data is spread out, is represented by its eigenvalue. Eigenvectors are vectors of a square matrix that do not change their directions under the associated linear transformation. The number of eigenvectors and eigenvalues correspond to the number of dimensions in the data set. Principal component analysis aims to find a new coordinate system with the largest variance for the data set in order to visualise patterns. In order to do so the two eigenvectors with the highest eigenvalues are chosen to re-frame the data set with a new x and y axis.

CCA is a method to compare two multi-variate data sets (*e.g.*, the composition of a microbial community and environmental factors) and to elucidate relationships between them. It uses two matrices, the response matrix (*e.g.*, community composition) and the explanatory matrix (*e.g.*, environmental factors) and aims to find a new ordination to incorporate both data sets. Canonical in contrast to regular correspondence analysis uses multiple regression on the environmental matrix for optimization and only variables that can be 'explained' by the environmental matrix are included in the final results, *i.e.*, if there is a correlation of the explanatory variables to the final ordination. The significance of these correlations is calculated by permutation. Permutation is the process of re-arranging elements within a data matrix and for each permutation a test statistic is calculated to create a null distribution. Statistical significance is asserted, if the value for the non-permuted data is sufficiently different from those in the null distribution.

The Pearson correlation measures the linear dependence between two variables. It is calculated by the covariance of the two variables divided by the product of their standard deviation. The coefficient ranges from +1 (total positive correlation), over 0 (no correlation) to -1 (total negative correlation). Covariance is a measure

for the strength of the correlation between variables, *i.e.*, how much they change (or do not change) together. The standard deviations represent the amount of variation in a set of data values, *i.e.*, their spread.

ANOVA is a statistical test to analyse the differences among group means and therefore represents a t-test for more than two groups. It compares the amount of variation between groups with the amount of variation within groups. The null hypothesis assumes that all groups are random. One-way ANOVA examines the influence of two different categorical independent variables on one continuous dependent variable, whereas two-way ANOVA also assesses if there are any interactions between the two independent variables. If there is a significant overall difference between groups, this is followed up by a *post hoc* test, *e.g.*, Tukey's test, to determine where the difference has occurred between the groups.

The significance of statistical hypotheses is determined by the p-value. A significance level (α, traditionally 5% or 1%) is chosen before the test is performed. If p is equal or smaller than α, it suggests that the data is inconsistent with the null hypothesis and therefore that hypothesis needs to be rejected. The null hypothesis assumes no relationship between two phenomena and therefore a p-value below α suggests significance of the relationship. Although very widely used by biologists the p-value has received a lot of criticism including the arbitrary choice of significance level and its usage has even been suggested to be banned (Leek & Peng, 2015).

References

Caporaso, J. G., Kuczynski, J., Stombaugh, J., Bittinger, K., Bushman, F. D., Costello, E. K., Fierer, N., Pena, A. G., Goodrich, J. K. & Gordon, J. I. (2010) QIIME allows analysis of high-throughput community sequencing data. *Nature methods*, 7(5), 335-336.

Hammer, O., Harper, D. & Ryan, P. (2012) PAST: paleontological statistics software package for education and data analysis. Paleontol Electron 4 (art. 4): 9.

Leek, J. T. & Peng, R. D. (2015) Statistics: P values are just the tip of the iceberg. *Nature*, 520(7549), 612-612.

Overy, S., Walker, H., Malone, S., Howard, T., Baxter, C., Sweetlove, L., Hill, S. & Quick, W. (2005) Application of metabolite profiling to the identification of traits in a population of tomato introgression lines. *Journal of Experimental Botany*, 56(410), 287-296.

Remias, D. & Lutz, C. (2007) Characterisation of esterified secondary carotenoids and of their isomers in green algae: a HPLC approach. *Algological Studies*, 124(1), 85-94.

Ruttenberg, K., Ogawa, N., Tamburini, F., Briggs, R., Colasacco, N. & Joyce, E. (2009) Improved, high-throughput approach for phosphorus speciation in natural sediments via the SEDEX sequential extraction method. *Limnology and Oceanography: Methods*, 7(5), 319-333.

Wacker, A. & Martin-Creuzburg, D. (2007) Allocation of essential lipids in Daphnia magna during exposure to poor food quality. *Functional Ecology*, 21(4), 738-747.

Chapter 4: Variations of algal communities cause darkening of a Greenland glacier.

Lutz, S., Anesio, A. M., Villar, S. E. J. & Benning, L. G.

Published in *FEMS microbiology ecology*, 89(2), 402-414 (2014)

Abstract

We have assessed the microbial ecology on the surface of Mittivakkat glacier in SE-Greenland during the exceptional high melting season in July 2012 when the so far most extreme melting rate for the Greenland Ice Sheet has been recorded. By employing a complementary and multi-disciplinary field sampling and analytical approach we quantified the dramatic changes in the different microbial surface habitats (green snow, red snow, biofilms, grey ice, cryoconite holes). The observed clear change in dominant algal community and their rapidly changing cryo-organic adaptation inventory was linked to the high melting rate. The changes in carbon and nutrient fluxes between different microbial pools (from snow to ice, cryoconite holes and glacial forefronts) revealed that snow and ice algae dominate the net primary production at the onset of melting and that they have the potential to support the cryoconite hole communities as carbon and nutrient sources. A large proportion of algal cells is retained on the glacial surface and temporal and spatial changes in pigmentation contribute to the darkening of the snow and ice surfaces. This implies that the fast, melt-induced algal growth has a high albedo reduction potential, and this may lead to a positive feedback speeding up melting processes.

4.1 Introduction

The cryosphere covers about 10 % of Earth's surface and has only recently been recognised as a biome (Anesio & Laybourn-Parry, 2012). Although lower in cell numbers than more temperate environments, many microorganisms (both autotrophs and heterotrophs) survive and even thrive in/on snow and ice. Glacial surfaces are usually assumed to be rather homogenous in terms of their microbiology, but they are composed of a range of distinct microbial habitats that include snow, bare ice, and cryoconites (Anesio & Laybourn-Parry, 2012). Importantly, on snow and ice surfaces various studies have shown that primary productivity is limited usually by light and nutrient availability (Remias et al., 2005, Stibal et al., 2007, Leya et al., 2009, Yallop et al., 2012, Takeuchi,2013).

Algal blooms colouring snow and ice surfaces are abundant on glacial surfaces and have been known for a long time (first reported by the ancient Greek Aristotle (Gentz-Werner, 2007)) and they have been described from many cryospheric

settings (Thomas & Duval, 1995, Leya et al., 2000, Müller et al., 2001, Williams et al., 2003, Leya et al., 2004, Takeuchi et al., 2006, Lütz et al., 2009, Duval et al., 2010, Fujii et al., 2010). In order to adapt to the harsh conditions on snow and ice surfaces (e.g., high irradiation, low nutrient concentrations) algae are equipped with a suite of protective biomolecules, i.e., pigments (Müller et al., 1998, Remias et al., 2005). Dominant species on snow fields belong to the unicellular *Chlamydomonaceae*, with the most prominent representative being *Chlamydomonas nivalis*, a species that needs to be treated as a collective taxon (Leya 2004). Green snow is assumed to be caused by young, trophic stages of snow algae, whereby more mature and carotenoid-rich resting stages result in all shades of red snow. The physiology, morphologies and ecological traits of snow algal communities have been described in various studies (Hoham & Duval, 2001, Leya et al., 2004, Remias et al., 2005, Remias et al., 2013).

Ice algae on the other hand have only recently been described and, so far, seem to have a less complex life cycle, where they thrive on bare glacial ice as immotile (often chained up) cells and only rarely form spores (Remias et al. 2012a, Yallop et al. 2012). Their pigmentation has recently been identified as the brownish pigment purpurogallin carboxylic acid-6-O-b-D-glucopyranoside (Remias et al., 2012b), which causes a less distinct grey colouration of the ice surface. Ice algae belong to the *Zygnematophyceae* and the most described species are *Ancylonema nordenskiöldii* and *Mesotaenium bergrenii*.

In addition to snow and ice, cryoconite holes - cyanobacteria dominated water-filled holes - covering about 1-10% of glacial surfaces are also known as hotspots for nutrient cycling. Compared to snow and ice, cryoconite holes have been by far the more extensively studied ice surface habitats (e.g., Stibal et al., 2008, Hodson et al., 2010, Telling et al., 2011, Anesio & Laybourn-Parry, 2012).

In most of the studies discussed above, single surface glacial habitats (e.g., either snow, or ice or cryoconite holes) and in most cases only individual species or adaptation strategies have been addressed. However, integrating microbial ecological traits of all habitats and adaptations on a full glacial scale is lacking. Here, we present results from a comprehensive and complementary study of the microbial ecology of Mittivakkat glacier in south-east Greenland, a glacier whose biology has not been investigated yet. Our field work period (July 2012) was characterised by extremely high temperatures and an anomalous, stagnant ridge of

warm air over Greenland, which caused the most extreme melting event of the Greenland Ice Sheet (GrIS) in the last 150 years (Nghiem et al., 2012). During the summer of 2012, the Mittivakkat glacier experienced its fourth largest mass loss year since 1995 (Hanna et al., 2012, Mernild et al., 2012, Tedesco et al., 2013), most probably speeding up physical and microbial processes. To our knowledge this is the first report detailing the entire microbial ecology of a glacial surface ecosystem, and also addressing the fast temporal and spatial changes in algal communities and the adaptive inventories of the various algal species and linking these to the resulting effects on the changes in physical properties of the glacier.

4.2 Methods

4.2.1 Field site

Mittivakkat glacier (MIT), located in south-east Greenland just below the Arctic Circle (65.6 °N; 37.8 W) is a polythermal glacier with low mean annual temperatures of -1.7 °C (Cappelen et al., 2011). MIT is located on Ammassalik Island and is an independent glacier separated from the Greenland Ice Sheet. The bottom of the glacier is located at 128 m. a.s.l, the terminus at 180 m a.s.l. and its summit at 880 m a.s.l. The surrounding bedrock consists mainly of gneisses and gabbro-anorthosite intrusions (Escher et al., 1976). Between the 6th and 23rd of July 2012, we carried out an in-depth snow, ice and melt water sampling campaign that was complemented by a series of in situ metabolic and irradiation measurements over an area of ~ 1 km² (Figure 4.1) of MIT. We aimed at characterizing the changes in the glacial ecology during a single melting season. This was particularly pertinent due to the extremely high melting rates in the summer of 2012 (Mernild et al., 2012, Hanna et al., 2013). Hanna et al (2013) carried out a detailed mass balance study in the 2 weeks following our field campaign on Mittivakkat glacier. They have shown that the glacier experienced its fourth largest mass loss since 1995 during summer of 2012. In the 3 weeks prior to their detailed measurements our monitoring of the surface changes of MIT showed a move of the snow line up from ~ 128 to ~ 250 m a.s.l. During our campaign and based on visual observations we surveyed and defined several distinct microbial glacial surface habitats that are considered to be highly representative of the whole glacial surface: clean snow (white snow with no visual presence of particles), green

snow (light to dark green and depth pervasive distribution of colour), red snow (variably dense light pink to dark red pigmentation that was usually only forming a thin covering on white snow), biofilms (wet snow at snow-ice melting interfaces), clean ice (white ice with no visual presence of particles), grey ice (light grey to dark grey ice covered with dark particles), cryoconite holes (1-50 cm large usually rounded or elongated and variably deep holes filled with sediment), and glacial runoff (melt rivers and channels). In each of these habitats (except for glacial runoff where only one sample was collected) we collected various samples for microbial, mineralogical and geochemical analyses. Throughout the field campaign we collected a total of 24 samples which represented different habitats that developed with time at various sites (Figure 4.1 and Table 4.1). A true time resolved sampling could not be carried out since the snow-melt was fast and the aspect of sampling spots varied substantially even within 24 h. Below we only briefly describe the main field and laboratory approaches, and the full details are given in the Supporting Information (SI).

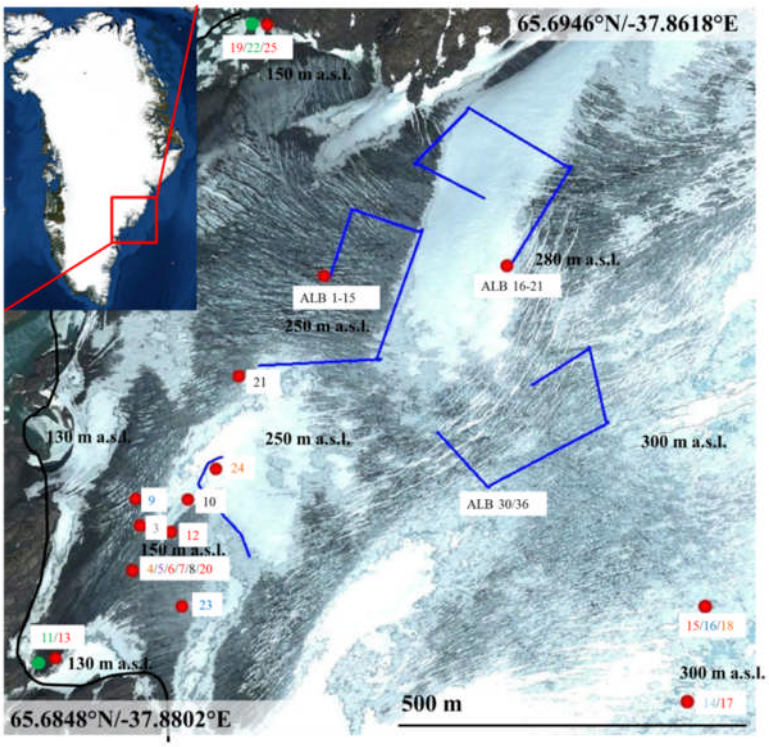

Figure 4.1: Mittivakkat Glacier in SE-Greenland showing the distribution of our sampling and measurement sites; blue lines represent albedo survey traverses (ALB). Black line delineates the bottom of the glacier. Numbers and colours correspond to the sample numbers MIT-2 - MIT-25 (grey = white snow, green = green snow, red = red snow, light blue = clean ice, dark blue = grey ice, brown = biofilms, black = cryoconite holes, purple = runoff. Image source: Google Earth (August 2012)

Table 4.1: Coordinates, sample habitat categorization and field measurements for each sampling site on Mittivakkat glacier (MIT-2-MIT-25).

Sample no.	Sample description	Collection date July 2012	GPS location [24 H, UTM]	Elevation [m]	pH	Temp. [°C]	Cond. [uM]	PAR [W/m²]	UV-A [W/m²]	UV-B [W/m²]	Albedo [%]
MIT-2	Clean Snow #1	9th									
MIT-3	Clean Snow #2	9th	0551579 E, 7285535 N	190	7.05	1.7	0	346	40.2	1.14	83
MIT-4	Biofilm #1	10th	0551567 E, 7285460 N	155	6.39	0	0	131	17.8	0.72	
MIT-5	Surface Runoff	10th	0551567 E, 7285460 N	155	5.59	0	0	195	27.0	1.01	
MIT-6	Red Snow #1	10th	0551567 E, 7285460 N	155	5.31	0	0	191	24.4	1.02	
MIT-7	Red Snow #2	10th	0551567 E, 7285460 N	155	5.67	0	2	204	28.1	1.13	
MIT-8	Cryoconite hole #1	10th	0551567 E, 7285460 N	155							
MIT-9	Grey Ice #1	12th	0551571 E, 7285579 N	196				276	35.3	1.39	
MIT-10	Cryconite hole #2	12th	0551659 E, 7285580 N	196	5.84	0	0	275	34.4	1.34	
MIT-11	Green Snow #1	12th	0551435 E, 7285308 N	128	5.49	0	0	182	20.3	0.61	39
MIT-12	Red Snow #3	12th	0551631 E, 7285526 N	204	5.73	0	0	318	38.1	1.37	
MIT-13	Red Snow #4	12th	0551435 E, 7285308 N	128	5.83	0.2	0	182	20.3	0.61	
MIT-14	Clean Ice #1	14th	0552441 E, 7285291 N	294				356	41.0	2.13	63
MIT-15	Red Snow #5	14th	0552463 E, 7285438 N	299	5.73	0	0				
MIT-16	Grey Ice #2	14th	0552463 E, 7285438 N	299	5.46	0	0				39
MIT-17	Red Snow #6	14th	0552441 E, 7285291 N	294	5.48	0	0	356	41.0	2.13	57
MIT-18	Biofilm #2	14th	0552463 E, 7285438 N	299	5.62	0	0				23
MIT-19	Red Snow #7	17th	0551778 E, 7286368 N	150	4.68	0.7	0	345	46.2	1.54	39
MIT-20	Red Snow #8	10th	0551567 E, 7285460 N	155	5.31	0	0	191	24.4	1.02	
MIT-21	Cryoconite hole #3	17th	0551741 E, 7285782 N	233	6.35	0.1	0				27
MIT-22	Green Snow #2	17th	0551778 E, 7286368 N	150	5.02	0	0	345	46.2	1.54	48

MIT-23	Grey Ice #3	19th	0551651 E, 7285404 N	195					38
MIT-24	Biofilm #3	19th	0551705 E, 7285631 N	204	5.75	0	0		20
MIT-25	Red Snow #9	17th	0551778 E, 7286368 N	150					

4.2.2 Field measurements

A total of 24 samples – labelled MIT-2 to MIT-25 – was collected (MIT-1 represents a blank sample that we processed in the same way like all other samples). In order to obtain a good spatial and temporal representation of the glacial surface habitats, 2 clean snow, 2 green snow, 9 red snow, 3 biofilm, 1 clean ice, 3 grey ice, 3 cryoconite holes and 1 runoff sample were randomly collected over the full monitoring area of 1 km2. Due to the extremely fast snow melting rates (Hanna et al., 2013) re-sampling of the same habitat at the exact same site was not feasible for the snow or ice habitats. Even from one day to another melting changed most habitats dramatically and often led to the transformation of one habitat into another (e.g., clean snow → red snow or red snow/ biofilm → grey ice). Thus a time resolved sampling of the same habitat on the same site was not possible and samples were collected at different sites tacking into account the habitat definitions described above.

At each sampling point prior to sampling, the snow temperature (upper few cm), pH and conductivity were measured in-situ using a multi-meter (Hanna instruments, HI 98129). In all snow habitats and the runoff, pH and conductivity measurements were done after allowing the multi-meter to equilibrate in the upper 2-3 cm of the respective habitat. For the clean and grey ice habitats this was achieved by melting a few ice chips on site and measuring the values with the multi-meter. Furthermore, at each site (as well as during a large survey, see below), irradiation was measured with a radiometer with specific PAR, UVA and UVB sensors (SolarLight PMA2100). Albedo was calculated by taking the ratio of reflected to incident radiation (400-700 nm range) and measuring the values always in the same position to the sun. There was no cloud cover during the whole field campaign. Measurements were carried out with the sensors held at 30 cm above the snow surface (field of view 160º, effective measurement area 0.5 m2) and by first pointing the sensor upwards (incident radiation) and then towards the snow/ice surface (reflected radiation). Five measurements for incident and reflected radiation were acquired each. The error of the measurement (standard deviation) was below 10 %. The rate of snow-melt was monitored over an area of 80 m² with tagged poles inserted into the snow and down to the ice layer, with measurements taken every 1-2 days (at site MIT-3). Snow, ice and water samples were collected either in sterile 50 mL centrifuge tubes (for all inorganic analyses) or in 250 mL ashed

glass jars (for organic analyses). All samples were kept cold (in packed snow) and processed within 24 hours (see below). In order to evaluate the bulk community activity and the proportion of autochthonous carbon production and consumption, measurements of changes in O2 concentrations over 24 to 48 h in light and dark bottles were conducted at three sites (MIT 3/11/13). At the end of each field day, 1 ml of untreated snow, ice, biofilm and cryoconite samples was imaged using a portable light microscope (100 and 400 x magnification) and snow (spherical cells) and ice algal (desmids) cells were counted on a hemocytometer. A minimum of 150 cells or 300 µl of sample was counted. All samples were counted in duplicates.

4.2.3 Aqueous and solid phase analyses.

All samples were processed within 24 h of sampling in order to preserve solutions and solids for various analyses. Full details of the various sample handling stages are given in the SI. Processed and preserved samples were returned to the UK either cold or frozen. Aqueous samples were analysed for anion and cation compositions using ion chromatography (IC) and for trace metals using inductive coupled plasma mass spectrometry (ICP-MS). Microbial and inorganic debris were imaged using light, scanning electron and transmission electron microscopy (LM, SEM and TEM, respectively). Functional group distribution and mineralogy were characterized using vibrational spectroscopy (Fourier transform infrared, FTIR, and Raman) and X-ray diffraction (XRD) methods with the FTIR focussing on the ratios of lipids and proteins to carbohydrates, the XRD on the mineral characterization and the Raman on the major differences in organic compounds and the cross-confirmation of mineralogical characteristics. For the characterization of the chlorophyll to carotenoid ratios in the snow algae samples, high pressure liquid chromatography (HPLC) was used on extracted snow algal pigments and data are presented as ratios of carotenoids to chlorophyll a (Chl a). Full details for all methods are provided in the SI.

4.3 Results

4.3.1 Physical change of the glacial surface and change in algal communities

At the beginning of the field season (6th of July), the glacier was fully snow-covered and no particles were macroscopically visible on the snow. After a couple of days (8th of July), concomitant with a dramatic ambient air temperature increase (~ 5º C over a few days, based on temperature loggers of the Department of Geosciences and Natural Resource Management, University of Copenhagen), which induced the onset of intense melting, two green snow patches (covering each ~ 20 m2 and reaching down to almost the bare ice layer, i.e., 20-40 cm) formed at the bottom of the glacier (~ 130 m a.s.l., Figure 4.1 and 4.2a). Within the following two days (10th of July), thin layers of red snow (Figure 4.1, 4.2a and 4.2b top right) developed in patches initially close to the green snow. Gradually within the next two weeks of observation (10th to 23rd of July), numerous and fast changing light to dark red snow patches formed on the snow covered glacier. The distribution of these red snow patches progressed upwards with the snow line from the bottom of the glacier to increasingly higher levels (from 128 m a.s.l. to ~ 350 m a.s.l.) (Figure 4.1 and 4.2a). Following the onset of melting, we estimated that, at various times during our sampling season, between 5 and 50% of the 1 km² surveyed area was covered by a thin layer (often < 1-2 mm thick) of red snow. This estimate was based on our observations during the albedo surveys (totalling 700 measurements of albedo) as well as visual estimates during the initial and end field site surveys. It is worth mentioning that the distribution of these red snow patches (and indeed of most snow or ice habitats) was highly patchy and both temporally and spatially heterogeneous not just in distribution but also in terms of patch size, with patches as small as 0.5 m^2 or as large as 30 m^2. However, once melting of the snow occurred, small water pools formed at snow-ice interfaces. We defined as the biofilm habitat the intermediate surface environment between snow and ice habitats dominated by brownish-blackish film like aggregates (Figure 4.2b bottom left and 4.2c). These were characterized by extremely high microbial contents and photosynthetic activity (Figure 4.2b bottom left, Figure 4.3) but also likely by the presence of high concentrations of inorganic impurities (dust, black carbon, etc.) that accumulated due to the melting snow. On areas where all snow had melted, the bare ice surface was either extremely clean (clean ice habitat, mostly in areas of slightly higher topography) or it became covered with greyish mottled particles

(grey ice habitat) and variably sized cryoconite holes. At the end of the field season (25th of July) we estimate (based on the 1km^2 survey area) that ~ 70-90 % of the glacier < 350 m a.s.l. was snow free and dominated by grey ice interspersed with cryoconite holes. At the end of our field observations on Mittivakkat glacier clean snow without any visually distinctive microbial presence could only be found above 350 m a.s.l.

These melt-driven spatial and temporal changes in the macroscopic aspect of the glacier surfaces were accompanied by a clear change in the algal community, distribution and abundance (Figure 4.2; Table 4.2). The algal species that dominated each observed habitat differed in shape, colouring and density and each habitat dramatically changed in occurrence and spatial distribution of microorganisms as the melt season progressed. Species identification by light microscopy showed that spherical, chlorophyll-rich green and carotenoid-rich red snow algae cells were predominantly represented by resting cysts of the unicellular snow algae *Chlamydomonas nivalis*, while ice algae were represented either by the filamentous *Ancylonema nordenskiöldii* (predominantly chains) or by the unicellular *Mesotaenium berggrenii* (Figure 4.2b). Both algal types (snow and ice algae) were found in snow and ice samples, but were dominant in their respective habitats. The biofilms, which formed at the snow – ice interface were characterized by a broad range of snow to ice algae ratios (Table 4.2) and showed the highest concentrations of mineral/organic debris (algae and bacteria) and the overall density of snow and ice algal cells in these samples was far higher compared to other algal samples.

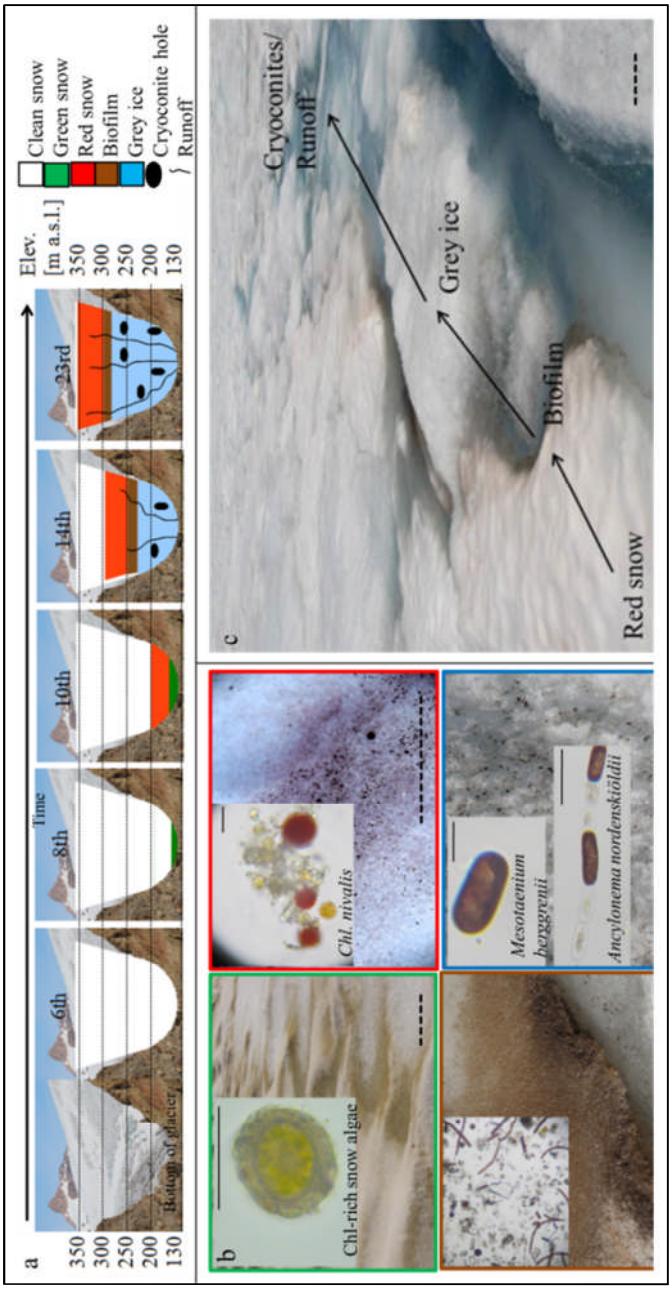

Figure 4.2: Schematic representation of the changes in the spatial (elevation) and temporal (time from left to right) distribution in microbial habitats during the field season. (a and c) show the microbial habitats and (b) showing various algal communities observed on glacier; (b top left image) shows the green snow sample MIT-22 with the corresponding chlorophyll-rich green algae; (b top right image) shows sample MIT-19 and the spherical yellow and red snow algae *Chlamydomonas nivalis*; (b bottom left image) shows a biofilm (sample MIT-4) likely producing O_2 bubbles and its corresponding mixed community of spherical snow algae and filamentous ice algae and (b bottom right image) shows a grey ice sample (MIT-9) with the corresponding ice algal strains. (c) shows the transition between habitats in a relatively small area. Solid scale bar: 10 µm, dotted scale bar: 10 cm. Approximate elevation lines were added in (a) as a guide to the eye only; in (a) snow and ice habitats are represented by the different colours, while cryoconite holes and the runoff are represented by the graphical symbols in the legend at right.

Table 4.2: Cell counts from the on-site light microscopic measurements showing the ranges that characterised the snow (spherical cells) and ice algae (filamentous cells) in each habitat (see also Figure 4.2).

Category	Sample no.	Snow algae [cells ml^{-1}]	Ice algae [cells ml^{-1}]	Ratio snow/ice algae
Green snow (n=1)	MIT-22	4245	ND	ND
Red snow	MIT-6	8580	ND	ND
(n=8)	MIT-7	25800	26210	1 : 1
	MIT-12	12900	232	56 1
	MIT-13	11900	190	63 : 1
	MIT-15	27000	13886	2 : 1
	MIT-17	1770	6076	1 : 3
	MIT-19	5900	ND	ND
	MIT-20	52000	8664	6 : 1
Average		18231	9210	2 : 1
Grey ice	MIT-9	409	5306	1 : 13
(n=3)	MIT-16	6920	19991	1: 3
	MIT-23	1843	7057	1 : 4
Average		3057	10785	1 : 4
Biofilm	MIT.4	1860	60	31 : 1
(n=3)	MIT-18	12400	52600	1 : 4
	MIT-24	48000	368000	1 : 8
Average		20753	140220	1 : 7
Cryoconite	MIT-8	9150	16950	1 : 2
Holes	MIT-10	480	20	24 : 1
(n=3)	MIT-21	270	ND	ND
		3300	8485	1:3
Runoff (n=1)	MIT-5	1.43	0.28	5 : 1

ND = not detected

4.3.2 Field measurements

The snow melting progressed fast during our field season. We measured surface melting rates of 5 cm of snow per day, which over the monitored 1 km^2 area equates to 0.05 km^3 of snow loss per day. Despite this, the snow and ice temperature at each collection site varied only over a narrow range from 0 to 1.7 °C. The pH varied from slightly acid (4.7-5.8) for algal sites to near neutral (5.8-6.4) for biofilms and cryoconite holes to neutral (7.05) for clean snow. The pH of the runoff fell within the slightly acidic pH range (5.6). Photosynthetic active radiation (PAR) measurements at the sampling sites ranged from 131-356 W m-2, UV-A from 17.8-46.2 W m-2 and UV-B from 0.61-2.13 W m-2, while albedo at the sampling sites and during the albedo survey (averages in Table 4.3 and all measurements in Table A.1) clearly changed from habitat to habitat. The difference in albedo from the clean (75%) to red snow (~25 %) and to biofilms (20 %) is attributed here to a clear link to increased pigmentation and mineral contents (see below). However, a quantitative evaluation of the relative contribution of other impurities such as inorganic dust, other organic matter, black carbon and other changes in physical parameters of snow and ice (i.e., grain size, water contents) were not specifically quantified in this study and still require further investigations.

The measured net rates (i.e., the difference between gross photosynthesis and community respiration) of the red snow, biofilm and grey ice samples all showed positive trends with the highest values measured for the biofilm sample (Figure 4.3). Cryoconite holes were the only habitat with negative values or net photosynthesis in balance. These results suggest an accumulation of organic matter in all glacial habitats, except for the cryoconite holes, which at this time in the melting season seem to be primarily a location for net consumption of organic matter. Part of this net consumption is also likely derived from organic matter produced in the red and green snow or the grey ice habitats.

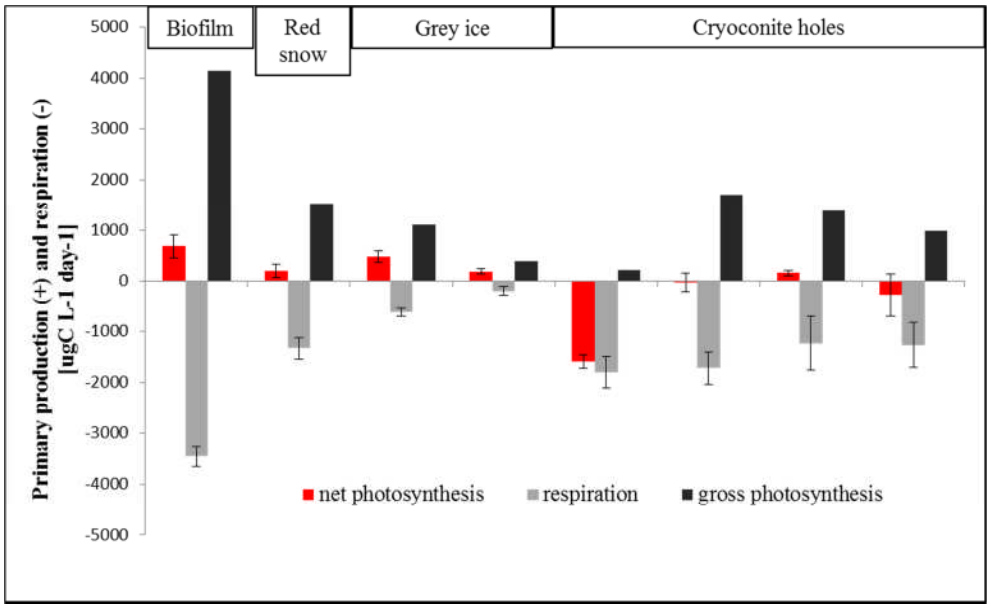

Figure 4.3: Microbial activity determined as net photosynthesis rates for all measured sample types: biofilm, cryoconites (4 sample sets), ice algae from the grey ice (2 sample sets) and red snow algae; each bar represents the average of three individual measurements with the error bars shown.

Table 4.3: Average albedo measurements (in %) for habitats identified on Mittivakkat and comparisons with literature data from the few other glacial settings where similar habitats were evaluated.

Category	This study	Other studies
Clean snow	75 ± 5	89.3 ± 1.8 (fresh)[a]
		58.0 ± 5.5 (older) [a]
Clean ice	58 ± 8	59 ± 1[b]
Red snow	49 ± 8	45.5 ± 1.7% - 51.0 ± 6.6 [a]
Green snow	44 ± 4	
Grey ice	35 ± 10	35 ± 1[b]
Runoff	30 ± 4	
Cryoconite holes	23 ± 15	
Biofilm	20 ± 4	

[a]Thomas and Duval, 1995; [b] Yallop et al., 2012;

4.3.3 Inorganic aqueous and solid analysis

Aqueous analysis (Table A.2) revealed at all sites and for all cations and anions concentration values that were mostly low (< ppm) No major differences between sites regardless of microbial presence or absence were observed. Samples contained not just biological components, but also dust debris and the prevailing minerals in each sample, determined by XRD, were quartz, plagioclase, smectite, mica, amphibole and chlorite. These are all minerals that are low in nutrients (e.g., low in P, K, Mg), and are extremely slowly weathered, thus representing poor sources of nutrients for the prevailing microbial communities. Most of these minerals were confirmed through Raman analyses which also identified the presence of black carbon, as well as traces of haematite, limonite and microcline in some samples (Table A.3).

4.3.4 Electron microscopy

Within each algae type, electron imaging revealed large variations in morphological characteristics (Figure A.2 and A.3). For snow algae we found a range of morphologies including fairly smooth cells with no or few nipples, cells with uniformly distributed nipples, cells with wave-like surface patterns, shrivelled cells (likely due to sample drying and instrument vacuum) and cells with mucilage sheets.

4.3.5 Organic inventory and functional group distributions

Unfortunately due to a sample processing error the DOC/DIC values could not be used and thus the dissolved carbon fluxes between different communities and off the glacier are not available. However, from the vibrational spectroscopic data we can gain an insight into the changes in prevailing organic compounds in the different algal habitats. The peak area ratios derived from the bulk FTIR data revealed an increasing trend of higher protein/carbohydrate and lipid/carbohydrate ratios from green snow over grey ice and biofilms to red snow (Figure 4.4). A series of organic compounds representing among others specific carotenoid C-C bands and chlorophyll bands were clearly identified at the single-cell level by Raman spectroscopy. However, an unambiguous assignment to specific

carotenoids could not be carried out, as peak positions even for the same carotenoid band varied from cell to cell even within the same class of cell (see SI text and Table A.4). In addition, it has been recently shown that even small variation in conformation in the carotenoids can affect band positions dramatically (de Oliveira et al., 2010).

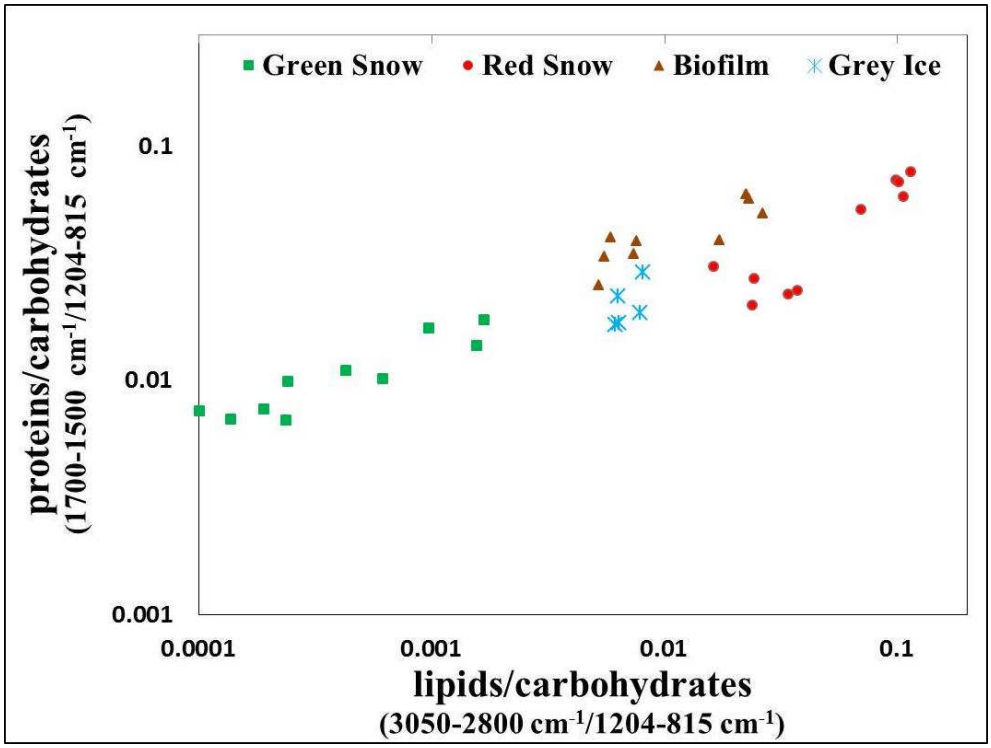

Figure 4.4: Ratios of functional groups of protein, lipids and carbohydrates of the different habitats.

4.3.6 Pigment composition

Chlorophyll and carotenoid contents were analysed for all collected samples but only quantified for snow samples since the used method is optimised for these samples. In all snow algae samples chlorophyll a and b and the primary carotenoids neoxanthin, lutein, β-carotene, violaxanthin, zeaxanthin and antheraxanthin were identified in the HPLC traces. The only secondary carotenoid identified was astaxanthin and its fatty acid ester derivatives (Bidigare et al., 1993). The ratios of chlorophyll a to primary and secondary carotenoids and their spatial and temporal variations on Mittivakkat glacier are shown in Table 4.4 and Figure 4.5. It is worth noting that samples collected at the onset of melting and snow colonisation (MIT-

6/7/11/19/20/22), as well as samples collected higher up the glacier (latest melting onset, MIT-15/17) are characterized by higher chlorophyll and primary carotenoid contents, whereas samples collected about a week later (MIT-25, ALB-22/23/24) contained a much large proportion of secondary carotenoids (Fig 5a and 5b). Among these specifically astaxanthin, as well as an increasing esterification resulting in astaxanthin mono and di esters, was evident. Furthermore, in these latter collected samples the trans-configuration of astaxanthin was prevalent over the cis-configuration (Table 4.4). However, interestingly in the green snow sample MIT-11, collected at the beginning of the melting, only traces of astaxanthin were present, whereas the second green snow sample MIT-22, collected a few days later at a different location (Figure 4.1), already contained higher amounts of astaxanthin. Despite the large variance in contents and nature of carotenoids among the different red snow samples, no trend could be established for the xantophyll cycle pigments. Pigment analysis of the clean snow samples resulted in only small peaks for chlorophyll and none for carotenoids (not quantified).

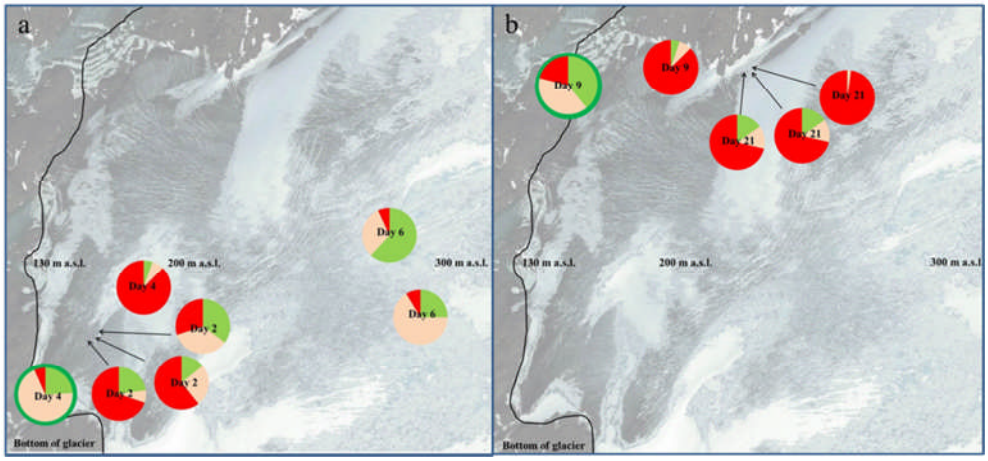

Figure 4.5: Overview of pigment ratios in snow algae on Mittivakkat glaciers and spatial (a) and temporal (b) differences. Green portions of each pie chart represents Chlorophyll *a* and *b* contents (Chl's), light red primary (pri. Car) and dark red secondary (sec. Car) carotenoids; the two pie charts with dark green rings represent the two green snow samples, all others are red snow samples.

Table 4.4: Chlorophyll and carotenoid analyses for green and red snow samples shown as area ratios normalized to chlorophyll a. Note that the red sample set also includes samples that were collected during the albedo survey (ALB samples); for these samples only coordinates, albedo and pigment data is available; shown in grey are total chlorophylls and total primary and secondary carotenoids.

chl a = 1	Neo	Vio	trans-Ast	cis-Ast	Ant	Lut	Zea	Chl b	trans-Ast mono esters	cis-Ast mono esters	trans-Ast di esters	cis-Ast di esters	all Ast	Chloro-phylls	Primary carotenoids	Secondary carotenoids
Green snow																
MIT-11	0.00	0.00	0.00	0.00	0.00	3.56	0.00	0.24	0.34	0.00	0.00	0.00	0.34	1.24	3.56	0.34
MIT-22	0.48	0.00	0.00	0.00	0.00	1.11	0.00	1.37	1.09	0.19	0.00	0.00	1.28	2.37	2.41	1.28
Red snow																
MIT-6	0.09	0.05	1.05	0.11	0.03	0.86	0.31	0.19	1.83	0.64			3.63	1.19	0.39	3.63
MIT-7	0.05	0.11	3.99	0.67	0.05	1.43	0.57	0.26	0.55	0.21			5.42	1.26	2.26	5.42
MIT-12	0.14	0.16	2.37	0.41	0.28	0.71	0.22	0.15	6.30	3.52	4.60	1.68	18.88	1.15	1.51	18.88
MIT-15	0.01	0.05	0.08	0.00	0.03	0.40	0.05	0.17	0.03	0.02			0.13	1.17	0.59	0.13
MIT-17	0.04	0.43	0.37	0.00	0.45	1.70	0.69	0.30	0.08	0.00			0.45	1.30	3.44	0.45
MIT-19	0.04	0.04	0.20	0.04	0.00	0.60	0.06	0.21	0.27	0.17			0.68	1.21	0.76	0.68
MIT-20	0.10	0.09	0.75	0.12	0.04	0.98	0.17	0.39	0.23	0.09			1.19	1.39	1.39	1.19
MIT-25	0.04	0.02	0.84	0.13	0.00	0.66	0.28	0.15	9.26	5.11	2.55	1.55	19.44	1.15	1.66	19.44
ALB-22	0.05	0.08	0.18	0.03	0.01	0.69	0.09	0.22	1.89	0.64	2.95		5.69	1.22	1.07	5.69
ALB-23	0.07	0.13	0.34	0.00	0.00	1.16	0.35	0.19	5.39	3.79	17.26	16.24	43.02	1.19	2.01	43.02
ALB-24	0.40	0.23	2.57	0.21	0.00	5.66	0.00	0.24	45.62	41.74	131.63	224.65	446.42	1.24	8.60	446.42

4.4 Discussion

During the extremely fast 2012 melting season on Mittivakkat glacier (Hanna et al., 2013) our data revealed that snow and ice algae covered a substantial area of the glacial surface and that they had a potential strong influence on both local and downstream physical and biological glacial surface processes. Snow and ice algae are important primary colonisers and carbon producers in the low-nutrient snow and ice fields and due to their coloration they have a major impact on snow and ice albedo with reductions down to 20 % compared to albedo of fresh snow of 75%. Albedo values often also contain contributions from other non-algal impurities (mineral dust, black carbon, etc), and these contributions need to be further investigated. However, this was beyond the scope of this paper.

With respect to cell transfer between habitats and although the microbial biomass in cryoconite holes is dominated by heterotrophic bacteria and cyanobacteria (Säwström et al., 2002, Christner et al., 2003, Edwards et al., 2010), our cell counts show that algal cells are washed into cryoconite holes, becoming an important organic matter source for the prevalent community. Cryoconite holes, in turn, are a dominant habitat after the snow melt in the ablation zone of glaciers and can be self-sustainable and regarded as hot spots for nutrient cycling. However, we hypothesise that both snow and ice algal communities have an important role in supporting cryoconite communities.

4.4.1 Change in life signals

We have shown that snow and ice algae exhibit very different life cycles and cytostructural adaptation strategies (Figure 4.4). Green snow, which is dominated by chlorophyll-rich snow algae cells showed lowest protein and lipid content in relation to carbohydrates. On the other hand, the more mature red algal stage is characterised by incorporation of large amount of storage compounds such as lipid bodies in which pigments are stored (Remias et al., 2005). Late stage spore formation is also accompanied by thickening of the cell walls, mainly composed of glycoproteins, which are also the main compound of mucilage sheets in the spores (Siddiqui & Cavicchioli, 2006). In contrast, ice algae species have thin cell walls and seem not to require equivalent biomolecular protection, which would explain

the lower relative lipid and protein content found in the ice habitats by our study. This could also be due to a shorter and less complex life cycle of ice algae, which still remains unknown. Since biofilms are a mixture of snow and ice algae, they showed intermediate levels of lipid and proteins. Whether the intermediate ratios also indicate better protection from harsh conditions (e.g., high irradiation) due to the protective water layer and a better nutrient supply due to the adhering matrix, still needs to be further investigated.

Although snow algae pigmentation has been extensively studied (Müller et al., 1998, Remias et al., 2005, Leya et al., 2009, Remias et al., 2010, Remias et al., 2013), the trigger and the process and mechanisms leading to pigment production are not fully understood. Our results show that on a single glacier and even over a short time period there is a great heterogeneity in pigment compositions, both in space (Figure 4.5a) and time (Figure 4.5b). This fact needs to be taken into account when pigment contents are described at a specific sampling site and time and when comparisons with other locations are made. Snow samples collected a week apart from almost the same location showed much higher secondary carotenoid contents relative to the initial samples, while esterified astaxanthin was only found in samples collected 2 weeks after melting initiation (Table 4.4 and Figure 4.5). Although biological processes are known to occur very slowly at 0 degrees, snow algae seem to adapt quickly to changing conditions with a broad range of pigment ratios (i.e., chlorophylls and carotenoids). Carotenoids play an important role in photo-protection by absorbing excessive photosynthetic energy, shading the chloroplast against high irradiation or as a pool of antioxidative compounds (Grossman et al., 2004). Although various carotenoid pigments were identified in our samples (Table 4.4 and Figure 4.5), and despite a good peak separation in the HPLC chromatograms, none of the xantophylls (carotenoids with oxygen functional groups) violaxanthin, zeaxanthin and antheraxanthin were found in the two green snow samples (MIT-11, MIT-22), and only a minor component of these xantophylls was found in the red snow samples. In addition, since we targeted the main snow algae pigments in our analyses we did not find the main ice algae pigment (purpurogallin carboxylic acid-6-O-b-D-glucopyranoside), which was recently identified by Remias et al (2012b). Remias et al. (2012a) showed that the ice alga *Ancylonema nordenskiöldii* has abundant secondary pigments. However we did not detect any secondary carotenoids in our ice algal samples. This could be because the samples were collected at the beginning of the melting season and ice

algae may not have been exposed long enough to excessive irradiation in order to produce secondary carotenoids.

4.4.2 Nutrient cycling on the glacier and delivery to downstream ecosystems

Glaciers are usually considered as important nutrient deliverers for downstream ecosystems such as deglaciated soils, lakes or coastal waters (Foreman et al., 2007, Hood et al., 2009, Stibal et al., 2012). We showed here that throughout the 3 weeks of our field season, nutrients were not in excess on Mittivakkat glacier. In our observation period, nutrient concentrations in all collected and analysed snow, ice and water samples (MIT-2 – MIT-25) were overall low and this is also represented in the low nutrient values in our runoff sample (MIT-5) suggesting low nutrient export. This also indicates that any mineral dust delivered nutrients were either not bioavailable or that any delivered dust was immediately consumed by the fast growing snow and ice algae. Thus, fast nutrient re-cycling followed by nutrient retention in the microbial biomass dominated the processes observed on Mittivakkat glacier. In addition, cell counts of our runoff sample (and the lack of cells in the clean snow and ice) indicate that only very few algal cells were transported off the glacier (Table 4.2). Microscopy revealed that algal cells were transferred from one microbial pool to another – i.e., from the snow to the ice and from the snow and ice to the cryoconite holes. Thus we hypothesise that carbon loss in form of algal cell removal is negligible on glaciers, but that snow and ice algae act as carbon sources for the bacterial communities in the later active cryoconite holes (Irvine-Fynn et al., 2012). Although information on organic carbon contents or export is lacking for this glacier, the high cell and nutrient retention (Tables 4.2 and A.2) imply a similar trend for particulate organic carbon (POC). Cell retention is also strongly supported by the FTIR and microscopy evidence (Figures 4.5 and A.2) which showed high contents of ‘sticky’ extracellular polymeric substances (primarily carbohydrates). This was specifically true for the biofilms growing at the snow-ice interface and in the red snow algae that colonised the highest reaches of the glacier. However, dissolved organic carbon (DOC) is likely to be exported off the glacier (Hood et al., 2009).

4.4.3 Cell retention and effect on albedo

On Mittivakkat glacier we found that the growth of snow and ice algae is the dominant process immediately upon melting onset and most snow fields transgress through a red snow to grey ice stage. The extent of the snow and ice algae coverage is also linked to the amount of stagnant water, which in turn, is strongly influenced by slope and runoff rates (Stibal et al., 2012). The clear positive net photosynthetic rates (i.e., assumed here as an indicative of the accumulation of organic matter) in the snow and ice samples compared to the cryoconite hole samples collected at the same time show that snow and ice algae dominate the primary production at the onset of melting. Here, we demonstrate that the growth and retention of cells at the surface of snow and ice have a strong influence on albedo. Depending on the complexity of the produced pigments (which in turn is linked to cell maturity) as well as cell density, both the green and red snow algae can reduce the albedo to values as low as 40% which is comparable to values reported by Thomas et al (1995). Interestingly the rather ephemeral biofilms at the snow ice interface reduced albedo values down to ~ 20% (Table 4.3) which is comparable to albedo values for cryoconites (Takeuchi & Li, 2008, Takeuchi, 2009). The effect and role of ice algae on albedo, despite their high spatial coverage once most snow has melted, is the least well known. Our values for the grey ice were comparable to those reported by Yallop et al (2012) and reached 35%. Yallop et al (2012) and Cook et al. (2012) have suggested that ice algae may fix up to eleven times more carbon than cryoconites holes (based on dry weight of sediment). Combining the contribution of the early-season dominating snow algae and the late season dominating ice algae not just on albedo but also on primary productivity and carbon fluxes, leads us to suggest that they are major players in the ecology of glaciers and ice sheets and potentially strong impact on adjacent ecosystems. A decreased albedo may have positive feedbacks on the algal community with higher and longer melting events further enhancing algal growth and most likely even extending their period of metabolic activity. However, higher cell numbers will most likely be constrained by nutrient availability, which we show to be very low in our study. Nitrogen depletion is known to trigger secondary carotenoid production what in return could be responsible for the dark red colouration of snow fields (Remias et al., 2005, Leya et al., 2009) reducing albedo to a greater extent. During the time of observation, the development of pigmentation was not the sole cause of the observed darkening of the glacial surface although we hypothesise here it was likely the most dramatic. Takeuchi (2009, 2013) also found that the

change in spectral reflectance on an Alaskan glacier is not only due to the physical properties of the glacial surface, but also due to biological processes. However, previous studies have shown that the age of snow, which affects water content and grain size, and especially aggregation of allochtonous dust particles (e.g., dark inorganic and black carbon) (Wientjes et al., 2011) can also play important roles. Our observations indicate that dust probably played a minor role on the measured snow fields, whereas the accumulation and aggregation of allochtonous materials on the bare exposed ice surface is more important. However, the relative contribution of algal pigmentation vs. dust to the grey colouration of the bare grey ice remains unknown and needs further investigation.

Acknowledgments

The authors would like to thank the anonymous reviewers for their comments that helped to improve the manuscript. The research leading to these results has received funding from INTERACT (grant agreement No 262693), under the European Union's Seventh Framework Programme and an University of Leeds School of Earth and Environment grant to SL and LGB. We acknowledge Dr. S. Allshorn from the Cohen Laboratories at the School of Earth and Environment, University of Leeds for help with IC measurements, Dr. Gary Fones from the University of Portsmouth for the ICP-MS measurements and the Department of Geosciences and Natural Resource Management at the University of Copenhagen for provision of temperature data. The authors state no conflict of interest.

References

Anesio, A. M. & Laybourn-Parry, J. (2012) Glaciers and ice sheets as a biome. *Trends in ecology & evolution*, 27(4), 219-225.

Bidigare, R., Ondrusek, M., Kennicutt, M., Iturriaga, R., Harvey, H., Hoham, R. & Macko, S. (1993) Evidence for a photoprotective function for secondary carotenoids of snow algae. *Journal of Phycology*, 29(4), 427-434.

Cappelen, J., Laursen, E. V., Jørgensen, P. V. & Kern-Hansen, C. (2011) DMI monthly Climate Data Collection 1768-2010, Denmark, The Faroe Islands and Greenland. *Technical Report 06-09*.

Christner, B. C., Kvitko, B. H. & Reeve, J. N. (2003) Molecular identification of bacteria and eukarya inhabiting an Antarctic cryoconite hole. *Extremophiles*, 7(3), 177-183.

Cook, J., Hodson, A., Anesio, A., Hanna, E., Yallop, M., Stibal, M., Telling, J. & Huybrechts, P. (2012) An improved estimate of microbially mediated carbon fluxes from the Greenland ice sheet. *Journal of Glaciology*, 58(212), 1098-1108.

de Oliveira, V. E., Castro, H. V., Edwards, H. G. & de Oliveira, L. F. C. (2010) Carotenes and carotenoids in natural biological samples: a Raman spectroscopic analysis. *Journal of Raman Spectroscopy*, 41(6), 642-650.

Duval, B., Duval, E. & Hoham, R. W. (2010) Snow algae of the Sierra Nevada, Spain, and high Atlas mountains of Morocco. *International Microbiology*, 2(1), 39-42.

Edwards, A., Anesio, A. M., Rassner, S. M., Sattler, B., Hubbard, B., Perkins, W. T., Young, M. & Griffith, G. W. (2010) Possible interactions between bacterial diversity, microbial activity and supraglacial hydrology of cryoconite holes in Svalbard. *The ISME journal*, 5(1), 150-160.

Escher, A., Watt, W. S. (1976) *Geology of Greenland.* Geological Survey of Greenland.

Foreman, C. M., Sattler, B., Mikucki, J. A., Porazinska, D. L. & Priscu, J. C. (2007) Metabolic activity and diversity of cryoconites in the Taylor Valley, Antarctica. *Journal of Geophysical Research*, 112(G4), G04S32.

Fujii, M., Takano, Y., Kojima, H., Hoshino, T., Tanaka, R. & Fukui, M. (2010) Microbial community structure, pigment composition, and nitrogen source of red snow in Antarctica. *Microbial ecology*, 59(3), 466-475.

Grossman, A. R., Lohr, M. & Im, C. S. (2004) Chlamydomonas reinhardtii in the landscape of pigments. *Annu. Rev. Genet.*, 38, 119-173.

Hanna, E., Fettweis, X., Mernild, S. H., Cappelen, J., Ribergaard, M. H., Shuman, C. A., Steffen, K., Wood, L. & Mote, T. L. (2014) Atmospheric and oceanic climate forcing of the exceptional Greenland ice sheet surface melt in summer 2012. *International Journal of Climatology*, 34(4), 1022-1037.

Hanna, E., Mernild, S. H., Cappelen, J. & Steffen, K. (2012) Recent warming in Greenland in a long-term instrumental (1881–2012) climatic context: I. Evaluation of surface air temperature records. *Environmental Research Letters*, 7(4), 045404.

Hodson, A., Cameron, K., Boggild, C., Irvine-Fynn, T., Langford, H., Pearce, D. & Banwart, S. (2010) The structure, biological activity and biogeochemistry of cryoconite aggregates upon an Arctic valley glacier: Longyearbreen, Svalbard. *Journal of Glaciology*, 56(196), 349-362.

Hoham, R. & Duval, B. (2001) Microbial ecology of snow and freshwater ice with emphasis on snow algae. Cambridge University Press: Cambridge.

Hood, E., Fellman, J., Spencer, R. G., Hernes, P. J., Edwards, R., D'Amore, D. & Scott, D. (2009) Glaciers as a source of ancient and labile organic matter to the marine environment. *Nature*, 462(7276), 1044-1047.

Irvine-Fynn, T., Edwards, A., Newton, S., Langford, H., Rassner, S., Telling, J., Anesio, A. & Hodson, A. (2012) Microbial cell budgets of an Arctic glacier surface quantified using flow cytometry. *Environmental microbiology*, 14(11), 2998-3012.

Leya, T., Müller, T., Ling, H. & Fuhr, G. (2000) Taxonomy and biophysical properties of cryophilic microalgae and their environmental factors in Northwest Spitsbergen, Svalbard, *57th Eastern Snow Conference, Syracuse, New York, USA*.

Leya, T., Müller, T., Ling, H. U. & Fuhr, G. (2004) Snow algae from north-western Spitsbergen (Svalbard). *The coastal ecosystem of Kongsfjorden, Svalbard. Synopsis of biological research performed at the Koldewey Station in the years 1991-2003*.

Lütz, C., Remias, D. & Holzinger, A. (2009) Comparative Ultrastructure of Snow- and Ice-Algae from Polar and Alpine Habitats.

Mernild, S. H., Knudsen, N. T. & Hanna, E. (2012) Mittivakkat Gletscher, the longest-observed mountain glacier in Greenland, experiences its fourth largest mass loss year since 1995. Available at: http://www.eu-interact.org/fileadmin/user_upload/pdf/Mittivakkat_Gletscher_2012_press_release.pdf.

Müller, T., Bleiß, W., Martin, C.-D., Rogaschewski, S. & Fuhr, G. (1998) Snow algae from northwest Svalbard: their identification, distribution, pigment and nutrient content. *Polar Biology*, 20(1), 14-32.

Nghiem, S., Hall, D., Mote, T., Tedesco, M., Albert, M., Keegan, K., Shuman, C., DiGirolamo, N. & Neumann, G. (2012) The extreme melt across the Greenland ice sheet in 2012. *Geophysical Research Letters*, 39(20).

Remias, D., Albert, A. & Lütz, C. (2010) Effects of realistically simulated, elevated UV irradiation on photosynthesis and pigment composition of the alpine snow alga Chlamydomonas nivalis and the arctic soil alga Tetracystis sp.(Chlorophyceae). *Photosynthetica*, 48(2), 269-277.

Remias, D., Holzinger, A., Aigner, S. & Lütz, C. (2012a) Ecophysiology and ultrastructure of Ancylonema nordenskiöldii (Zygnematales, Streptophyta), causing brown ice on glaciers in Svalbard (high arctic). *Polar Biology*, 35(6), 899-908.

Remias, D., Lütz-Meindl, U. & Lütz, C. (2005) Photosynthesis, pigments and ultrastructure of the alpine snow alga Chlamydomonas nivalis. *European Journal of Phycology*, 40(3), 259-268.

Remias, D., Schwaiger, S., Aigner, S., Leya, T., Stuppner, H. & Lütz, C. (2012b) Characterization of an UV-and VIS-absorbing, purpurogallin-derived secondary pigment new to algae and highly abundant in Mesotaenium berggrenii (Zygnematophyceae, Chlorophyta), an extremophyte living on glaciers. *FEMS microbiology ecology*, *79*(3), 638-648.

Remias, D., Wastian, H., Lütz, C. & Leya, T. (2013) Insights into the biology and phylogeny of Chloromonas polyptera (Chlorophyta), an alga causing orange snow in Maritime Antarctica. *Antarctic Science*, 25(05), 648-656.

Säwström, C., Mumford, P., Marshall, W., Hodson, A. & Laybourn-Parry, J. (2002) The microbial communities and primary productivity of cryoconite holes in an Arctic glacier (Svalbard 79 N). *Polar Biology*, 25(8), 591-596.

Siddiqui, K. S. & Cavicchioli, R. (2006) Cold-adapted enzymes. *Annu. Rev. Biochem.*, 75, 403-433.

Stibal, M., Elster, J., Šabacká, M. & Kaštovská, K. (2007) Seasonal and diel changes in photosynthetic activity of the snow alga Chlamydomonas nivalis (Chlorophyceae) from Svalbard determined by pulse amplitude modulation fluorometry. *FEMS microbiology ecology*, 59(2), 265-273.

Stibal, M., Šabacká, M. & Žárský, J. (2012) Biological processes on glacier and ice sheet surfaces. *Nature Geoscience*, 5(11), 771-774.

Stibal, M., Tranter, M., Benning, L. G. & Řehák, J. (2008) Microbial primary production on an Arctic glacier is insignificant in comparison with allochthonous organic carbon input. *Environmental microbiology*, 10(8), 2172-2178.

Takeuchi, N. (2009) Temporal and spatial variations in spectral reflectance and characteristics of surface dust on Gulkana Glacier, Alaska Range. *Journal of Glaciology*, 55(192), 701-709.

Takeuchi, N. (2013) Seasonal and altitudinal variations in snow algal communities on an Alaskan glacier (Gulkana glacier in the Alaska range). *Environmental Research Letters*, 8(3), 035002.

Takeuchi, N. & Li, Z. (2008) Characteristics of surface dust on Ürümqi glacier No. 1 in the Tien Shan mountains, China. *Arctic, Antarctic, and Alpine Research*, 40(4), 744-750.

Takeuchi, N., Uetake, J., Fujita, K., Aizen, V. B. & Nikitin, S. D. (2006) A snow algal community on Akkem glacier in the Russian Altai mountains. *Annals of Glaciology*, 43(1), 378-384.

Tedesco, M., Fettweis, X., Mote, T., Wahr, J., Alexander, P., Box, J. & Wouters, B. (2013) Evidence and analysis of 2012 Greenland records from spaceborne observations, a regional climate model and reanalysis data. *Cryosphere Discussions (The)*, 6.

Telling, J., Anesio, A. M., Tranter, M., Irvine-Fynn, T., Hodson, A., Butler, C. & Wadham, J. (2011) Nitrogen fixation on Arctic glaciers, Svalbard. *Journal of Geophysical Research*, 116(G3), G03039.

Thomas, W. H. & Duval, B. (1995) Sierra Nevada, California, USA, snow algae: snow albedo changes, algal-bacterial interrelationships, and ultraviolet radiation effects. *Arctic and alpine research*, 27(4), 389-399.

Wientjes, I., Van de Wal, R., Reichart, G.-J., Sluijs, A. & Oerlemans, J. (2011) Dust from the dark region in the western ablation zone of the Greenland ice sheet. *The Cryosphere, Volume 5, Issue 3, 2011, pp. 589-601*, 5, 589-601.

Williams, W. E., Gorton, H. L. & Vogelmann, T. C. (2003) Surface gas-exchange processes of snow algae. *Proceedings of the National Academy of Sciences*, 100(2), 562-566.

Yallop, M. L., Anesio, A. M., Perkins, R. G., Cook, J., Telling, J., Fagan, D., MacFarlane, J., Stibal, M., Barker, G. & Bellas, C. (2012) Photophysiology and albedo-changing potential of the ice algal community on the surface of the Greenland ice sheet. *The ISME journal*, *6*(12), 2302-2313.

Chapter 5: Microbial diversity on Icelandic glaciers and ice caps.

Lutz, S., Anesio, A. M., Edwards, A. & Benning, L. G.

Published in *Frontiers in microbiology*, 6, 307 (2015)

Abstract

Algae are important primary colonizers of snow and glacial ice, but hitherto little is known about their ecology on Iceland's glaciers and ice caps. Due do the close proximity of active volcanoes delivering large amounts of ash and dust, they are special ecosystems. This study provides the first investigation of the presence and diversity of microbial communities on all major Icelandic glaciers and ice caps over a three year period. Using high-throughput sequencing of the small subunit ribosomal RNA genes (16S and 18S), we assessed the snow community structure and complemented these analyses with a comprehensive suite of physical-, geo- and biochemical characterizations of the aqueous and solid components contained in snow and ice samples. Our data reveal that a limited number of snow algal taxa (*Chloromonas polyptera*, *Raphidonema sempervirens* and two uncultured *Chlamydomonadaceae)* support a rich community comprising of other micro-eukaryotes, bacteria and archaea. *Proteobacteria* and *Bacteroidetes* were the dominant bacterial phyla. Archaea were also detected in sites where snow algae dominated and they mainly belong to the *Nitrososphaerales*, which are known as important ammonia oxidizers. Multivariate analyses indicated no relationships between nutrient data and microbial community structure. However, the aqueous geochemical simulations suggest that the microbial communities were not nutrient limited because of the equilibrium of snow with the nutrient-rich and fast dissolving volcanic ash. Increasing algal secondary carotenoid contents in the last stages of the melt seasons have previously been associated with a decrease in surface albedo, which in turn could potentially have an impact on the melt rates of Icelandic glaciers.

5.1 Introduction

Glaciers and ice sheets cover about 10% of the Earth's surface and are the largest freshwater reservoir. They are a critical component of the Earth's climate system and with temperatures rising globally, melting rates are increasing affecting freshwater availability and sea level rise (Meier et al., 2007). Glacial surfaces have not been considered to harbour much life until recently (Hodson et al., 2008; Anesio and Laybourn-Parry, 2012). They are considered an extreme environment

yet they contain species of all three domains of life including bacteria, archaea, fungi, protozoa and even invertebrates (Anesio and Laybourn-Parry, 2012). Among glacial surface habitats, cryoconite holes (cyanobacteria dominated water-filled holes formed by the preferential melt of organic and inorganic dark particles) have been by far the more extensively studied habitats (Cameron et al., 2012; Edwards et al., 2014). However, the largest proportion (>90%) of glacial surfaces is covered by snow and increasingly by bare ice towards the end of the melting season. Snow algae (*Chlorophyta*) are the most prolific and colourfully striking microbial species colonizing snow and ice surfaces. First described by the ancient Greek Aristotle (Gentz-Werner, 2007), snow algae have been known for a long time and they have been studied in many polar and alpine cryospheric settings including Greenland (Lutz et al., 2014), Svalbard (Müller et al., 2001; Leya et al., 2004), the European Alps (Remias et al., 2005), the Rocky Mountains (Thomas and Duval, 1995), Antarctica (Fujii et al., 2010; Remias et al., 2013)), Alaska (Takeuchi, 2013) and the Himalayans (Yoshimura et al., 2006). We have recently shown that they are important primary colonizers and net primary producers supporting other snow and ice microbial communities as carbon and nutrient sources (Lutz et al., 2014). As part of their life cycle and as a mechanism of protection from high irradiation, snow algal species produce red pigments (carotenoids). Through this protective reaction, algal blooms colour snow and ice surfaces and cause a darkening of glacial surfaces which in turn leads to a decrease in surface albedo (Thomas and Duval, 1995; Yallop et al., 2012; Takeuchi, 2013; Lutz et al., 2014; Benning et al., 2014). Such a decrease of albedo may speed up melting processes even further. This is of special interest in Iceland where glaciers have been shown to be retreating very fast (Staines et al., 2014) and where albedo is also affected by the presence of volcanic dust and ash on snow and ice surfaces.

Currently, not a single description of snow algae from any of the glaciers or ice caps in Iceland is available in the literature and no Icelandic snow algal species are available in cryogenic culture collections. Thus, we do not know if they are present, and if so, if they are abundant or what their bio-geographical distribution or ecological role might be. This is despite the fact that anecdotal evidence from scientists working on Iceland's glaciers and ice caps (e.g., personal communication from Glaciology Prof. Magnús Tumi Guðmundsson, University of Iceland) suggests that occasionally in the late summer 'reddish snow' patches can be observed. Icelandic glaciers represent a special case of glacial ecosystems due to

their vicinity to active volcanoes and thus constant input of fresh ash through dust or eruptions. The very abundant dark ash that covers most snow and ice fields on Iceland's glaciers and ice caps in the summer melting season is most likely also the reason why so far coloured snow algae have not been described. The darkness of volcanic ash contributes to the darkening of Icelandic glacial surfaces and their faster melting (Guðmundsson et al., 2005, Möller et al., 2014). Possibly, this effect also extends the active growth season of snow algae due to earlier and prolonged availability of liquid water. The highly soluble volcanic ash (Ritter, 2007; Jones and Gislason, 2008) is an important source of essential nutrients (e.g., N, P, Fe) and thus could be a good substrate for snow algal growth, which may further enhance the negative effect on surface albedo.

With this study we aimed to identify the presence of snow and ice algae on Icelandic glacial surfaces. Furthermore, we wanted to detail their associated microbial communities, and finally place the communities on all major Icelandic glaciers and ice caps in the context of variations in biogeography and physico-chemical parameters of snow and ice.

5.2 Materials and methods

5.2.1 Field site, sampling and measurements

A total of 33 snow and 1 ice samples (labelled with "ICE" for Iceland, followed by the collection year and sample number: ICE-12_1-7, ICE-13_1-24 and ICE-14_1-3; Table 5.1) was collected from 7 glaciers and 1 ice cap in Iceland (see Table 5.1 for details). Snow fields in the terminus areas of the western glacier Snaefellsjökull, the northern glacier Drangajökull, the central glacier Hofsjökull, as well as a large permanent snow field near Laugafell in the Central Highlands were sampled at the end of July in 2012. In early June 2013 we sampled the terminus areas of the southern glaciers Vatnajökull, Eyafjallajökull, Mýrdalsjökull and Solheimajökull and the western glaciers Snaefellsjökull and Langjökull. Finally, we sampled 3 snow fields that covered fresh lava fields from the 2010 eruption of Eyafjallajökull at the end of August in 2014 in order to also assess how and if fresh microbial colonization had occurred. It is worth noting that in 2012 and 2014 melting had been very advanced leading to thin snow covers on the termini of all

glaciers and smaller permanent snow fields. However, microbial colonization was well developed at all sites. In contrast, the samples in 2013 were collected in early June, when melting had just been initiated and thick snow packs were still present at all sites and microbial colonization was less prominent or widely distributed. Nevertheless, at each site, regardless of years and stage of the melting season, we collected where possible two adjacent samples: one clean snow sample (no macroscopically visible particles) and one red snow sample (with visible particles). The exceptions were Solheimajökull, sampled in 2013, where snow patches were only present at the edges of deep crevasses and thus only bare, grey ice was sampled and Eyafjallajökull sampled from 2014, where only red snow and no 'clean' snow could be found at the late stage in the melt season. It is important to note that all samples that are labelled 'red snow' or 'grey ice' in Table 5.1 always contained high loads of volcanic ash or dust debris, while the samples termed 'clean snow' did not contain ash, dust or any macroscopically visible biomass and filtering of the clean snow did not result in enough biomass for genomic or other analyses of the particulates.

At each sampling point prior to sample collection, snow temperature, pH and conductivity were measured in the field using a daily calibrated multi-meter (Hanna instruments, HI 98129). Irradiation was measured using a radiometer with specific PAR, UV-A and UV-B sensors (SolarLight, PMA2100). Surface albedo was calculated by taking the ratio of reflected to incident radiation (400-700 nm range) as previously described (Lutz et al. 2014). Snow samples were collected either in sterile 50 mL centrifuge tubes (red snow) or large sterile *Whirl-Pak*® bags (clean snow) and in 250 mL pre-ashed (*450°C* >4 hours) glass jars for all organic analyses. The snow samples were slowly melted at room temperature over a ~ 6 hour period. All samples were processed (filtered, acidified, etc.) within max 6-8 hours post collection in order to preserve them for various analyses in the home laboratory. All DNA and filtered organic samples were flash-frozen in liquid nitrogen and returned to Leeds in a cryo-shipper after which they were stored at -80˚C until further processing. All processed inorganic samples were stored cold (4˚C, in the dark) until analysed.

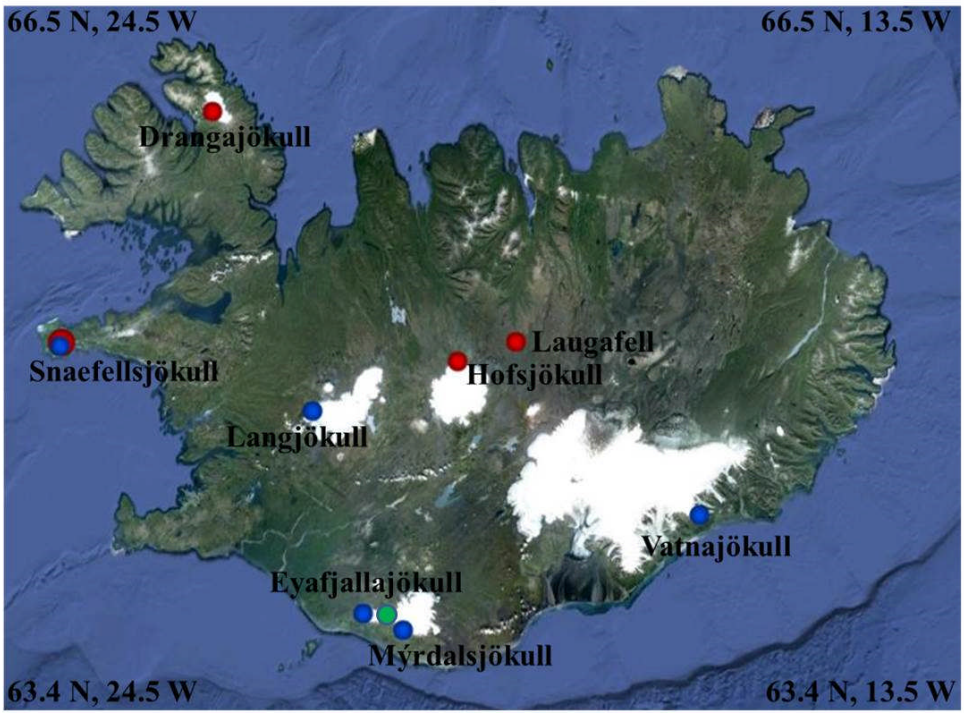

Figure 5.1: Map showing the 2012 (red dots), 2013 (blue dots) and 2014 (green dot) sampling sites (further details see Table 5.1). Image Source Google Earth (June 2013).

Table 5.1: Overview of samples, locations, coordinates and field measurements.

Sample label	Glacier	Sample description	Collection date	GPS location [UTM]	Elevation [m]	pH	Snow temp. [°C]	PAR [W/m²]	UV-A [W/m²]	UV-B [W/m²]	Albedo [%]
ICE-12_1	Snaefellsjökull	Red snow	26/07/2012	27W 0371148 E, 7190818 N	695						
ICE-12_2	Drangajökull	Red snow	27/07/2012	27W 0442009 E, 7334293 N	230	5.27	0.3				
ICE-12_3	Drangajökull	Red snow	27/07/2012	27W 0442125 E, 7334250 N	196	6.15	0				
ICE-12_4	Laugafell snow field	Red snow	29/07/2013	27W 0632892 E, 7222179 N	908	4.96		237	21.2	1.24	42
ICE-12_5	Laugafell snow field	Clean snow	29/07/2013	27W 0632892 E, 7222179 N	908	5.68	0.1	254			39
ICE-12_6	Hofsjökull	Red snow	29/07/2013	27W 0600998 E, 7206978 N	906	6.44	0.5	104			
ICE-12_7	Hofsjökull	Red snow	29/07/2013	27W 0600998 E, 7206978 N	906	6.47	0	98			19
ICE-13_1	Snaefellsjökull	Red snow	02/06/2013	27W 0372788 E, 7188065 N	461	5.46	0	100	20.8	0.61	64
ICE-13_2	Snaefellsjökull	Red snow	02/06/2013	27W 0372427E, 7188287 N	366	5.07	0.2				
ICE-13_3	Eyjafjallajökull	Clean snow	07/06/2013	27V 0563957 E, 7056674 N	1156	5.59	0.1	356			78
ICE-13_4	Eyjafjallajökull	Red snow	07/06/2013	27V 0563563 E, 7056695 N	1121	5.10	0.2	316			73
ICE-13_5	Eyjafjallajökull	Red snow	07/06/2013	27V 0559557 E, 7056046 N	736	5.50	0	94			33
ICE-13_6	Eyjafjallajökull	Red snow	07/06/2013	27V 0559557 E, 7056046 N	736	5.55	0	89			65
ICE-13_7	Mýrdalsjökull	Clean snow	07/06/2013	27V 0587893 E, 7049973 N	925	5.20	1	245			89
ICE-13_8	Mýrdalsjökull	Red snow	07/06/2013	27V 0588165 E, 7049601 N	923	5.86	1	150	18.6	0.42	72
ICE-13_9	Mýrdalsjökull	Red snow	07/06/2013	27V 0588165 E, 7049601 N	923	5.96	0	118			55
ICE-13_10	Solheimajökull	Grey ice	07/06/2013	27V 0582585 E, 7046897 N	244			127			42
ICE-13_11	Vatnajökull	Clean snow	08/06/2013	28W 0459058 E, 7125767 N	767	5.98	0	173			80
ICE-13_12	Vatnajökull	Grey ice	08/06/2013	28W 0459058 E, 7125451 N	695			136	19	0.06	18
ICE-13_13	Vatnajökull	Red snow	08/06/2013	28W 0459058 E, 7125451 N	695	7.08	0	137			27

ICE-13_14	Vatnajökull	Red snow	08/06/2013	28W 0459058 E, 7125451 N	695	6.04	0	148			42
ICE-13_15	Vatnajökull	Red snow	08/06/2013	28W 0459058 E, 7125451 N	695	5.83	0	151			47
ICE-13_16	Langjökull	Red snow	10/06/2013	27W 0521378 E, 7168876 N	812	6.53	0	52	6.42	0.21	60
ICE-13_17	Langjökull	Clean snow	10/06/2013	27W 0521378 E, 7168876 N	812	6.26	0	54			67
ICE-13_18	Langjökull	Red snow	10/06/2013	27W 0521378 E, 7168876 N	812	5.93	0	88			43
ICE-13_19	Langjökull	Red snow	10/06/2013	27W 0521378 E, 7168876 N	812	5.89	0	96			47
ICE-13_21	Snaefellsjökull	Red snow	12/06/2013	27W 0370323 E, 7188655 N	705	5.31	0	117			57
ICE-13_22	Snaefellsjökull	Clean snow	12/06/2013	27W 0370323 E, 7188655 N	705	5.84	0	122			71
ICE-13_23	Snaefellsjökull	Red snow	12/06/2013	27W 0370323 E, 7188655 N	705	6.19	0	170			73
ICE-13_24	Snaefellsjökull	Red snow	12/06/2013	27W 0370323 E, 7188655 N	705	5.96	0	195			51
ICE-14_1	Eyjafjallajökull	Red snow	28/08/2014	27V 0577039 E, 7057638 N	1004	7.73	0				
ICE-14_1	Eyjafjallajökull	Red snow	28/08/2014	27V 0577174 E, 7057468 N	1024	7.78	0				
ICE_14_3	Eyjafjallajökull	Red snow	28/08/2014	27V 0577101 E, 7057803 N	1010	7.91	0				

Conductivity in all samples was 0 µS/cm.

5.2.2 Bio- and geochemical analyses

Several of the methods used to analyse solutions and solid samples described below are equivalent to the methods employed and explained in detail in Lutz et al. (2014). Here we briefly summarize all standard aqueous and solid analyses and explain in detail those methods that are new compared to our previous work. For anion analysis by ion chromatography (IC, Dionex, 5% precision) and cation analysis by inductively coupled plasma mass spectrometry (ICP-MS, Agilent, 3% precision), samples were filtered through 0.2 µM cellulose-acetate filters into either pre-acidified (Aristar grade HNO_3) Nalgene HDPE bottles (cations) or into un-acidified 15 mL centrifuge tubes (anions). For dissolved organic carbon (DOC), PO_4 and organic particulate analysis, samples collected in ashed glass jars were filtered through ashed 0.7 µm glass fibre filters (GFF) directly into pre-acidified (Aristar grade HCl) vials using glass syringes and metal filter holders. PO_4 was analysed by segmented flow-injection analyses (AutoAnalyser3, Seal Analytical, 5% precision), while dissolved organic carbon (DOC) was analysed on a total organic carbon analyser (TOC, Shimadzu TOC-V, 3% precision). The GFF filters containing particulates were preserved in pre-ashed aluminium foil for pigment and fatty acid analyses. Pigment compositions (chlorophylls and carotenoids) were analysed using high-pressure liquid chromatography (HPLC, Agilent 1220 Infinity, 5% precision) after extraction in dimethylformamide and quantified using pigment standards (chlorophylls: Sigma, carotenoids: Carotenature). Fatty acids were extracted in dichloromethane:methanol (2:1, v:v) in two steps and extracts were combined, followed by transesterification in 3 M methanolic HCl for 20 min at 65 ^{o}C and three consecutive extractions in isohexane. Tricosanoic acid methyl ester (Sigma) was used as an internal standard and a 37 component FAME mix (Supelco) as external standard. The extracts were separated by gas chromatography (Thermo Scientific, Trace1300, 5% precision), spectra were recorded on a mass spectrometer (ISQ Single Quadrupole) and quantified on a flame ionization detector (FID). Particulates were also collected on 0.2 µm polycarbonate filters for mineralogical analysis by X-ray diffraction (XRD, D8 Bruker). Total carbon (TC), nitrogen (TN) and sulphur (TS) and nitrogen isotopes were analysed by pyrolysis at 1500 ˚C (Vario Pyro Cube, Elementar Inc) followed by mass spectrometry (Isoprime Mass Spectrometer, 0.1% precision). For imaging by light microscopy (LM, Leica DM750) unconcentrated samples were preserved in 2.5% glutaraldehyde and images recorded through a 63x objective. The

hydrogeochemical modelling software *PHREEQC* (Parkhurst, 1995, using the LLNL database) was used to determine the saturation indexes for our aqueous solutions.

5.2.3 DNA sequencing

All samples contained low amounts of biomass and therefore red snow samples from the same glacier and same collection year were pooled in order to obtain a sufficient quantity of DNA for sequencing (Table 5.6). Total DNA was extracted using the PowerSoil® DNA Isolation kit (MoBio Laboratories). 16S rRNA genes were amplified using bacterial primers 27F (5'-AGAGTTTGATCMTGGCTCAG) and 357R (5'-CTGCTGCCTYCCGTA) (tagged with the Ion Torrent adapter sequences and MID barcode) spanning the V1-V2 hypervariable regions. 18S rRNA genes were amplified using the eukaryotic primers 528F (5′-GCGGTAATTCCAGCTCCAA) and 706R (5'-AATCCRAGAATTTCACCTCT) (Cheung et al., 2010) (tagged with the Ion Torrent adapter sequences and MID barcode) spanning the V4-V5 hypervariable region. Polymerase chain reactions (PCR) were performed using Platinum® PCR SuperMix High Fidelity according to manufacturer's protocols. Initial denaturation at 95 ºC for 5 min was followed by 30 cycles of denaturation at 95 ºC for 30 s, annealing at 60 ºC for 30 s and elongation at 72 ºC for 30 s. Final elongation was at 72 ºC for 7 min. Archaeal 16S rRNA genes were amplified following a nested PCR approach. The first PCR reaction was carried out using primers 20F and 915R. Initial denaturation at 95 ºC for 5 min was followed by 35 cycles of denaturation at 95 ºC for 30 s, annealing at 62 ºC for 30 s and elongation at 72 ºC for 180 s. Final elongation was at 72 ºC for 10 min. The PCR product was used as template for the second PCR reaction with primers 21F (5'-TCCGGTTGATCCYGCCGG) and 519R (5'-GWATTACCGCGGCKGCTG) (tagged with the Ion Torrent adapter sequences and MID barcode) spanning the V1-V2 hypervariable region. Initial denaturation at 95 ºC for 5 min was followed by 30 cycles of denaturation at 95 ºC for 30 s, annealing at 60 ºC for 30 s and elongation at 72 ºC for 30 s. Final elongation was at 72 ºC for 7 min. All PCRs were carried out in triplicates to reduce amplification bias and in reaction volumes of 1 x 25 µl and 2 x 12.5 µl. All pre-amplification steps were done in a laminar flow hood with DNA-free certified plastic ware and filter tips. The pooled amplicons were purified with AMPure XP beads

(Agencourt©) with a bead to DNA ratio of 0.6 to remove nucleotides, salts and primers and analyzed on the Agilent 2100 Bioanalyser (Agilent Technologies) with the High Sensitivity DNA kit (Agilent Technologies) and quality, size and concentration were determined. Sequencing was performed on an Ion Torrent Personal Genome Machine using the Ion Xpress™ Template Kit and the Ion 314™ chip following manufacturer's protocols. The only exceptions were the archaeal amplicons of samples ICE-14_1, ICE-14_2 and ICE-14_3 which were sequenced on an Ion 316™ chip. The raw sequence data was processed in QIIME (Caporaso et al., 2010). Barcodes and adapter sequences were removed from each sequence. Filtering of sequences was performed using an average cutoff of Q20 over a 350 bp range. Reads shorter than 200 bp were removed. OTUs were picked *de novo* using a threshold of 99%, 97% and 95% identity. Taxonomic identities were assigned for representative sequences of each OTU using the reference databases Greengenes for bacteria and archaea. The Silva database (DeSantis et al., 2006; extended with additional 223 sequences of cryophilic algae kindly provided by Dr. Thomas Leya from the CCCryo - Culture Collection of Cryophilic Algae, Fraunhofer IZI-BB) was used for eukaryotes. Data were aligned using PyNAST and a 0.80 confidence threshold. Singletons were excluded from the analysis. For bacterial sequence matching, plant plastids were removed from the data set prior to further analysis. For eukaryotic sequence matching *Chloroplastida* were pulled out of the data set and stored in a separate OTU table. In order to focus upon algal diversity, sequences matching *Embryophyta* (e.g., moss, fern) were removed from the data set. For archaea, sequences matching bacteria were removed. Finally, for diversity analyses samples were rarefied to the smallest sequence number and Shannon indices were calculated in QIIME. A matrix of each OTU table representing relative abundance was imported into Past3 (Hammer et al., 2012) for multivariate statistical analyses (principal component analysis, PCA). Representative sequences of the major algal species found in all samples were imported into Geneious (7.1.3., Biomatters) for phylogenetic tree building based on neighbor-joining. Sequences have been deposited to the European Nucleotide Archive (ENA) under accession number PRJEB8832.

5.3 Results

5.3.1 Physico-, geochemical and biochemical analyses

Snow temperatures at each collection site varied only over a narrow range between 0 and 1.0 °C (Table 5.1). The pH was slightly acidic for most sites and there were no clear differences between red algal (4.96 – 6.53) or clean snow (5.20 – 6.26) sites. Only the samples collected in 2014 from snow fields on fresh volcanic lava and that had high contents of fresh volcanic ash inputs from the 2010 Eyafjallajökull eruption showed a more alkaline pH (7.73-7.91). This is not surprising since fresh volcanic glass is highly reactive and buffers any waters in contact with it to a pH between 7.5 and 8 (Oelkers and Gislason, 2001, Gislason and Oelkers, 2003). The albedo values differed from clean snow (76% ± 8) to sites with algal growth (56% ± 14; Table 5.1). Aqueous geochemical analysis (Table 5.2) revealed low values (< ppm) for all cations and anions in our samples. Geochemical modelling confirmed that our solutions were undersaturated with respect to most solid phases except for Fe oxides (goethite, hematite) and Al-hydroxides (boehmite, diaspore, gibbsite, Table B.7). However, values for dissolved organic carbon (DOC) varied dramatically and ranged from 15 to 200 µM (Table 5.2). The total carbon contents (TC, in % of total dry filtered particulate weight) were below 2% in all sites with one exception (ICE-13_1, Snaefellsjökull) where a TC content of 7.6% was found (Table 5.3). In all analysed samples the total nitrogen contents were below 0.3% and total sulphur below 0.1%. There were no large variations in N and S among the sample sites. Carbon to nitrogen (C/N) ratios varied over a broad range from 1.7 (ICE-13_8, Mýrdalsjökull) to 28.5 (ICE-13_1, Snaefellsjökull). Nitrogen isotopes were overall negative and ranged from -11.2 to -4.2 ‰.

Table 5.2: Combined organic (DOC) and inorganic aqueous chemical data for the samples collected in 2012 and 2013.

Sample ID	DOC [µM C]	$PO4_3^-$ [nM P]	$NO_3^{-\#}$	$SO_4^{2-\#}$	$Cl^{-\#}$	Al*	Ba*	Ca*	Cr*	Cu*	Fe*	K*	Mg*	Mn*	Na*	Ni*	Pb*	S*	Si*	Sr*	Zn*
ICE-12_1			<	171	243	3	1	15	<	<	5	14	10	1	124	<	<		76	<	2
ICE-12_2			<	<	135	560	7	200	2	1	337	55	131	5	214	1	<		626	2	22
ICE-12_3			<	<	114	17	7	22	1	1	17	38	11	<	99	<	<		40	<	25
ICE-12_4			<	181	275	4	13	26	<	<	3	44	13	1	234	<	<		483	<	30
ICE-12_5			99	<	125	6	13	41	<	<	6	34	4	<	57	<	<		24	<	31
ICE-12_6			<	<	100	12	11	21	7	1	40	33	15	2	98	3	<		264	<	40
ICE-12_7			<	<	275	101	22	166	<	1	84	73	113	5	231	<	<		734	1	30
ICE-13_1	94	117.9	371	127	255	1.4	<	45.3	<	<	4.6	<	15.1	1.4	209	<	<	<	63.3	0.49	1.6
ICE-13_2	200	89.2	<	<	176	1.4	<	37.3	<	<	5.1	<	10.4	1.3	132	<	<	<	72.5	0.38	2
ICE-13_3		92.7	<	<	147	0.59	<	4.8	<	<	8.9	<	2.8	0.24	89.3	<	<	<	10.1	<	0.28
ICE-13_4	82	119.8	<	<	363	1.7	<	18.4	<	<	1.3	29.8	11.8	0.84	245	<	<	<	36.9	0.26	0.19
ICE-13_5	33	84.9	<	127	377	6.4	<	86.6	<	<	12.9	32.3	46.4	4.9	266	<	<	<	193	0.68	0.22
ICE-13_6	86	78.6	<	<	275	1.7	<	19.2	<	<	3.2	28.5	13.5	1	145	<	<	<	54.3	0.27	0.24
ICE-13_7		43.5	<	128	539	0.68	<	1.1	<	<	0.3	<	0.8	0.05	3.3	<	<	<	10.8	<	2.3
ICE-13_8	58	172.0	<	<	488	4.7	<	94.5	<	<	9.1	28.7	34.2	0.95	398	<	<	<	94.5	0.43	0.22
ICE-13_9	15	296.3	<	<	156	14.7	<	132	<	<	29.7	30.8	54.5	2.2	156	<	<	<	330	0.57	<
ICE-13_10			<	145	95	1.9	<	20.1	<	<	2.1	15.4	7.5	0.72	126	<	<	20.5	21.1	0.14	1.6
ICE-13_11	201	74.7	100	<	0	0.51	<	5.9	<	<	0.4	<	2.2	0.06	41.2	<	<	<	20.2	<	1.1
ICE-13_12	92	230.4	<	<	0	11.4	0.14	89.2	6.2	0.18	14.5	<	30.8	3.1	76.1	<	0.02	<	63.4	0.57	1.8
ICE-13_13	50	89.3	<	<	274	0.98	<	31	<	<	1.1	<	9.9	0.44	198	<	<	<	20.3	0.17	0.7
ICE-13_14	37	308.5	<	<	371	4.6	<	84.2	<	<	8.8	43.1	53.9	2.6	188	<	<	<	306	0.45	0.22

ICE-13_15	33	262.7	<	<	100	5.8	<	48	<	<	11.9	<	28.9	1.4	98.7	<	<	<	185	0.23	<
ICE-13_16	54	53.9	3499	<	0	1.2	<	12.8	<	<	3.1	<	5.4	0.57	47	<	<	<	35.8	0.12	0.96
ICE-13_17	26	448.9	225	<	72	1.4	<	<	<	<	1.1	16.4	0.8	0.05	67.8	<	<	<	10.5	<	0.89
ICE-13_18	149	78.3	<	<	79	8.3	<	20.6	<	0.39	2.1	17.6	6.5	0.36	70.5	<	<	<	69.8	0.21	0.76
ICE-13_19	41	62.8	<	<	486	8.1	<	24.5	<	0.32	2.1	<	7.8	0.33	385	<	0.56	<	64.7	0.23	1
ICE-13_21	58	54.5	<	<	718	2.1	<	26	<	<	9.1	18.6	14.4	0.95	523	<	0.03	<	18.8	0.26	3.6
ICE-13_22	103	85.8	<	<	881	1.1	<	12.5	<	<	1.3	<	18.7	0.08	658	<	0.02	18.8	10.1	0.18	0.61
ICE-13_23	59	30.2	456	<	742	0.52	<	3.9	0.27	<	2.3	12.5	2.5	0.1	577	<	<	<	23.2	<	0.29
ICE-13_24	58	145.8	468	145	611	1.8	<	7.9	<	<	7.7	<	11.4	1	386	<	<	16.4	38.3	0.19	0.12

All values except DOC and PO_4^{3-} are given in ppb; NO^{3-}, SO_4^{2-} and Cl^- all determined by IC, all others analyzed by ICP-MS; limit of detection (LOD) for IC: NO_3^- = 96 ppb, Cl^- = 72 ppb, SO_4^{2-} = 121 ppb, LOD's for ICP-MS: Al, Ba, Co, Cr, Cu, Fe, Mg, Ni, Si, Sr, Zn = 0.1 ppb; Bi, Cd, Mn, Pb = 0.01 ppb; Ca, Na = 1 ppb; K,P,S = 10 ppb; no value indicates no measurement available for the respective sample; note Co was < LOD in all samples and Co was < LOD in all samples except in ICE-13_19 (0.07).

Table 5.3: Total carbon ($TC_{(s)}$), total nitrogen ($TN_{(s)}$) and total sulfur ($TS_{(s)}$) (all based on % of dry weight of sample) as well as the nitrogen isotope values from the analyzed particulates in the 2012 and 2013 collected red snow and grey ice samples that contained enough particulate material for analyses; listed are also the solid $C/N_{(s)}$ ratio calculated from TC and TN values.

Sample ID	Glacier	$TC_{(s)}$ [%]	$TN_{(s)}$ [%]	$TS_{(s)}$ [%]	$C/N_{(s)}$	$d^{15}N_{(s)}$ [‰]
ICE-12_7	Hofsjökull	0.64	0.12	0.05	5.4	-11.2
ICE-13_1	Snaefellsjökull	7.62	0.27	0.09	28.5	
ICE-13_2	Snaefellsjökull	1.69	0.08	0.08	20.7	
ICE-13_4	Eyafjallajökull	0.08	0.01	0.02	6.4	
ICE-13_5	Eyafjallajökull	1.27	0.07	0.09	18.4	-4.2
ICE-13_6	Eyafjallajökull	0.64	0.03	0.07	19.0	-7.0
ICE-13_8	Mýrdalsjökull	0.02	0.01	0.04	1.7	
ICE-13_9	Mýrdalsjökull	0.06	0.01	0.06	4.3	
ICE-13_10	Solheimajökull	0.25	0.01	0.08	19.4	
ICE-13_12	Vatnajökull	0.19	0.03	0.09	7.4	-6.2
ICE-13_14	Vatnajökull	0.09	0.02	0.05	3.6	-7.5
ICE-13_15	Vatnajökull	0.07	0.01	0.05	6.3	
ICE-13_16	Langjökull	0.22	0.02	0.05	10.0	-5.7
ICE-13_18	Langjökull	0.30	0.04	0.03	8.3	
ICE-13_21	Snaefellsjökull	1.20	0.10	0.08	12.2	-4.6
ICE-13_24	Snaefellsjökull	1.08	0.10	0.07	10.7	-3.9

The fatty acid distribution was similar in all analysed snow samples and characterized by predominance of saturated C16 and C18 fatty acids (up to 100%; Tables 5.5 and B.1). The most abundant unsaturated fatty acids were C16:1, C18:1, C18:2, C18:3. Among these C18:1 was the most prominent fatty acid and the highest proportion of unsaturated fatty acids was found on Drangajökull and Hofsjökull (63-80%), the two glaciers sampled late in the 2012 season. Pigment analysis revealed that chlorophylls (Chl a and Chl b) made up the largest proportion in all samples with a range of 31 to 100 % of total pigments, followed by secondary carotenoids (between 0% and 69%) and primary carotenoids (violaxanthin, zeaxanthin, lutein, β-carotene; up to 8%). Samples in 2012 and 2014 were collected later in the melting season and thus not surprisingly showed higher secondary carotenoids contents (up to 69%). The only secondary carotenoid identified was astaxanthin and the trans-configuration of astaxanthin was prevalent over the cis-configuration and astaxanthin mono esters could also be identified.

The mineralogical analysis of the particulates revealed that the dominant minerals in all samples were quartz, plagioclase (albite, anorthite) and pyroxene with some contributions from clays, basaltic glass and hematite (Figure B.1). Hematite was one of the main supersaturated mineral phases in our solutions as shown by the geochemical modeling (Table B.7). This bulk mineralogical composition varied little among all collected samples and matches the typical mineralogy of the fresh ash (Jones and Gislasson ,2008) and dust from the prime rocks in Iceland, which can be basaltic to rhyolitic (Jakobsson et al., 2008).

Table 5.4: Pigment composition of red snow samples that contained enough particulate material for analysis. Individual pigments were quantified in ug/L and reported as total chlorophylls, total primary carotenoids and total secondary carotenoids in % of total pigments.

Sample ID	Glacier	Chl a [µg/L]	Chl b [µg/L]	Vio [µg/L]	Zea [µg/L]	Lut [µg/L]	β-Car [µg/L]	trans-Ast [µg/L]	cis-Ast mono esters [µg/L]	trans-Ast mono esters [µg/L]	Total chlorophylls [%]	Total primary carotenoids [%]	Total secondary carotenoids [%]
ICE-12_1	Snaefellsjökull	10528	1739			552		980		142	88	4	8
ICE-12_3	Drangajökull	4673	12207		34			580	545		94	0	6
ICE-12_4	Laugafell		5816								100	0	0
ICE-12_7	Hofsjökull		8306					502			94	0	6
ICE-13_5	Eyjafjallajökull	3079				255				4	92	8	0
ICE-13_8	Mýrdalsjökull	2504									100	0	0
ICE-13_15	Vatnajökull	8123	40	67							99	1	0
ICE-13_16	Langjökull	8280								1	100	0	0
ICE-13_21	Snaefellsjökull	20120		18		250				240	98	1	1
ICE-13_23	Snaefellsjökull	16016		13		257	13			338	96	2	2
ICE-14_1	Eyjafjallajökull	62	34							157	31	0	69
ICE-14_2	Eyjafjallajökull	87	46							28	78	0	22
ICE-14_3	Eyjafjallajökull	138	69							31	83	0	17

Table 5.5: Fatty acid composition of the red snow samples collected in 2012 and 2013. Fatty acid compounds are reported as percentage of total fatty acids. Most prominent fatty acids (full table see SI) are reported as well as total saturated (SFA), total monounsaturated (MUFA), total polyunsaturated (PUFA), total unsaturated (UFA) fatty acids and the ratios of saturated to unsaturated fatty acids.

Compound	Glacier	C16:0	C16:1	C18:0	C18:1	C18:2	C18:3	SFA	MUFA	PUFA	UFA	Ratio SFA/UFA
ICE-12_2	Drangajökull	20	8	0	58	7	7	20	67	13	80	0.2
ICE-12_3	Drangajökull	18	8	10	52	5	4	31	60	9	69	0.4
ICE-12_5	Laugafell	16	3	57	18	0	0	73	20	0	20	3.6
ICE-12_6	Hofsjökull	18	2	18	53	5	3	37	55	7	63	0.6
ICE-12_7	Hofsjökull	14	4	3	43	27	0	22	48	31	78	0.3
ICE-13_1	Snaefellsjökull	16	16	17	13	6	3	40	29	9	39	1.0
ICE-13_2	Snaefellsjökull	19	12	12	14	11	6	39	26	17	43	0.9
ICE-13_4	Eyafjallajökull	94	0	0	6	0	0	94	6	0	6	16.0
ICE-13_5	Eyafjallajökull	25	8	16	9	12	12	52	17	27	44	1.2
ICE-13_6	Eyafjallajökull	21	2	12	13	10	14	41	15	29	44	0.9
ICE-13_8	Mýrdalsjökull	42	0	56	0	0	0	100	0	0	0	
ICE-13_9	Mýrdalsjökull	38	0	38	16	9	0	75	16	9	25	3.1
ICE-13_12	Vatnajökull	22	5	12	20	6	16	40	25	35	60	0.7
ICE-13_14	Vatnajökull	26	5	11	0	14	29	49	5	44	50	0.98
ICE-13_15	Vatnajökull	26	0	17	16	4	5	60	16	9	25	2.4
ICE-13_16	Langjökull	24	2	10	15	14	15	45	18	36	53	0.8
ICE-13_18	Langjökull	25	4	30	16	9	6	65	20	15	35	1.9
ICE-13_19	Langjökull	33	2	49	5	3	3	88	7	6	12	7.0
ICE-13_21	Snaefellsjökull	27	3	9	21	7	16	44	22	29	51	0.9
ICE-13_24	Snaefellsjökull	28	2	12	16	7	7	61	17	14	31	2.0

5.3.2 Species composition

The presence of snow algae was confirmed in all collected samples by light microscopy (Figure 5.2). Samples from 2012, collected in the late melt season showed overall more red pigmentation, whereas in 2013 samples (collected at the beginning of the melt season) contained more green and yellow pigmented cells (Figure 5.2 and Table 5.4).

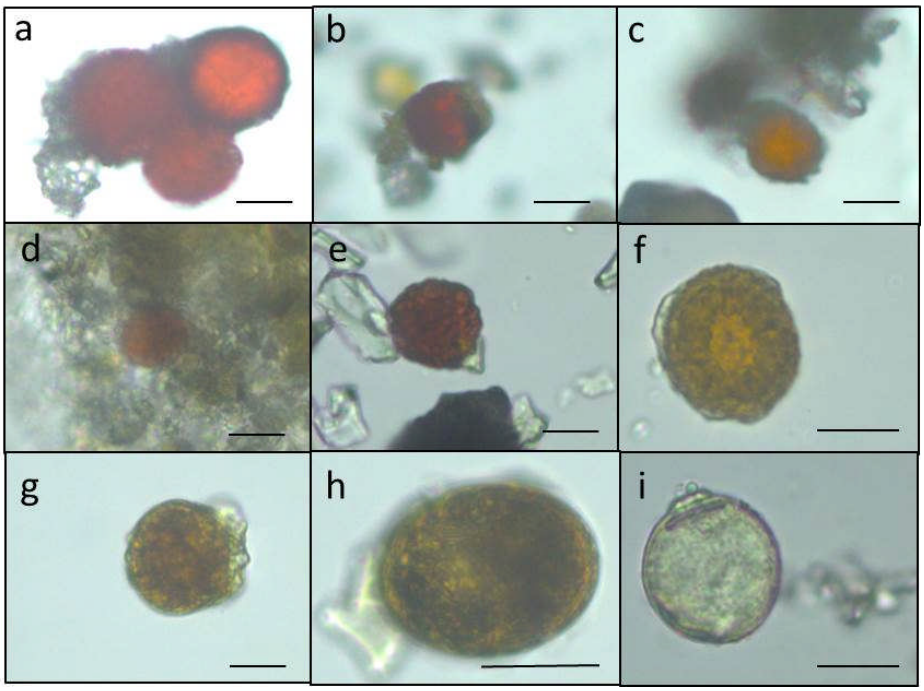

Figure 5.2: Light microscopy images of snow algae from the different sampling sites revealing the more red pigmented algae collected in 2012 compared to the less red pigmented algae sampled in 2013. (a) Drangajökull (ICE-12_3), (b) Laugafell (ICE-12_4), (c) Hofsjökull (ICE-12_6), (d) Snaefellsjökull (ICE-13_2), (e) Eyafjallajökull (ICE-13_5), (f) Mýrdalsjökull (ICE-13_8), (g) Vatnajökull (ICE-13_14), (h) Langjökull (ICE-13_16), (i) Snaefellsjökull (ICE-13_21).

Since algal species identification by microscopy can be deceiving due to various morphological changes during their life stages, targeted DNA sequencing was carried out to reveal algal species composition as well as the full microbial diversity (other micro-eukaryotes, bacteria, archaea) associated with snow algal sites. From all sequences that were amplified with the 18S rRNA primers, a total of 108,790 sequences (12 samples in total; Table 5.6) passed the QIIME quality pipeline (quality score > 20) corresponding to 2,811 operational taxonomic units that clustered at 97% sequence identity.

Table 5.6: Number of sequences (seqs) for the pooled red snow samples for each glacier and the respective Shannon diversity index (H').

		Eukaryotes					Bacteria				Archaea		
Glacier	**Pooled samples**	**Raw seqs**	**Seqs after QC**	**H' euk**	**Seqs assigned to algae**	**H' algae**	**Raw seqs**	**Seqs after QC**	**Seqs assigned to bac**	**H' bac**	**Raw seqs**	**Seqs after QC**	**Seqs assigned to arch**
Drangajökull	ICE-12_2/3	5474	2013	5.55	714	4.50	6383	2333	513	5.13	9206	1443	4*
Laugafell	ICE-12_4	1908	597	6.02	89	4.47	2533	818	120	5.27	18323	6294	540
Hofsjökull	ICE-12_6/7	6523	2168	5.61	792	3.88	3105	1336	339	5.38	18956	623	33
Vatnajökull	ICE-13_13/14/15	9948	3438	5.02	66	4.51	2689	770	14	5.06	4034	646	210
Langjökull	ICE-13_16/18	318	104	5.65	340	4.26	2398	913	111	5.29	5675	643	334
Langjökull	ICE-13_19	7273	3065	4.99	38	4.26	6541	2153	444	5.14	14680	4129	77
Snaefellsjökull	ICE-13_21/23/24	5123	1588	5.51	41	4.04	5850	2032	486	3.97	9800	3072	338
Eyafjallajökull	ICE-13_4/5/6	2391	1072	5.14	37	4.21	12075	2897	55	5.27	10862	2268	0*
Mýrdalsjökull	ICE-13_8/9	2479	809	5.14	8	n.d.	406	97	2*	n.d.	14760	5426	3*
Eyafjallajökull	ICE-14_1	34082	23959	5.11	3357	1.74	3842	1884	938	4.53	85138	66535	65727
Eyafjallajökull	ICE-14_2	8716	6962	3.75	3307	1.07	3875	2145	1158	4.64	841	809	558
Eyafjallajökull	ICE-14_3	24555	17196	4.96	4460	1.81	13230	6843	3390	4.59	28203	22350	21572

*removed from analysis due to low sequence numbers, n.d.=not determined due to low sequence numbers

Clustering of OTUs at 99%, 97% or 95% sequence similarity resulted in differences for OTUs counts (Table B.2), however not for taxa assignments and relative abundance of taxa (Tables B.3, and B.4 and B.5) and therefore a 97% similarity was chosen to be most representative for all further analyses. OTUs aligned and assigned to our extended Silva database (see methods) on all phylogenetic levels revealed differences between the eight sampling sites. *Chloroplastida* (green algae) and *Fungi* made up the largest proportion of eukaryotic sequences followed by *Alveolata* (Figure 5.3). All samples collected in 2013 (except Vatnajökull) showed a much higher abundance of sequences assigned to *Fungi* (67.0-94.9% of total sequences as opposed to 4.5-29.8% of total sequences in 2012, except Laugafell), with the most abundant class represented by the *Microbotryomycetes* (*Basidomycota*) (see full OTU tables in the Supplementary Information (SI) files). Samples collected in 2012 and 2014 (except Eyafjallajökull, ICE-14_1) showed a higher abundance of C*hloroplastida* (35.4-60.6%; compared to fungi: 6.6-53.5%) and also the presence of *Stramenopiles* (e.g., *Chrysophyceae;* Eyafjallajökull sampled in 2014), *Rhizaria* (e.g., *Cercozoa*; Drangajökull and Hofsjökull sampled in 2012) and *Alveolata* (e.g., *Ciliophora*; Laugafell sampled in 2012 and Eyafjallajökull in 2014). Shannon indices (Table 5.6) for all eukaryotes varied over a broad range from H' = 3.75 (Eyafjallajökull, ICE-14_2) to H' = 6.02 (Laugafell)

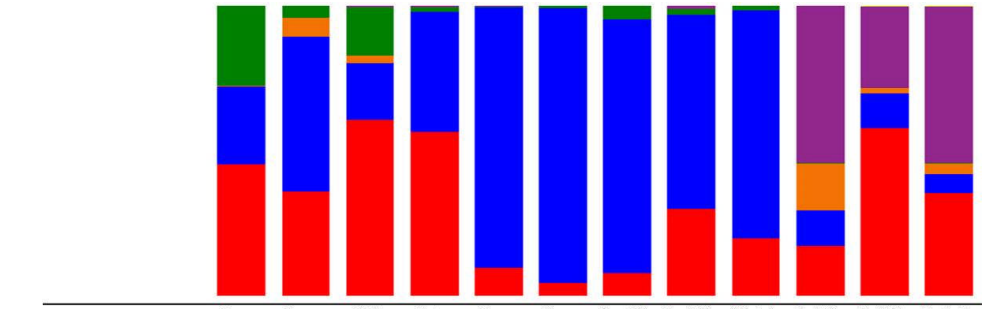

Taxon	Dranga-jökull ICE-2 2/.3	Lauga-fell ICE-12 4	Hofs-jökull ICE-12 6/7	Vatna-jökull ICE-13 13/14/15	Lang-jökull ICE-13 16/18	Lang-jökull ICE-13 19	Snaefells-jökull ICE-13 21/23/24	Eyafjalla-jökull ICE-13 4/5/6	Mýrdals-jökull ICE-13 8/9	Eyafjalla-jökull ICE-14 1	Eyafjalla-jökull ICE-14 2	Eyafjalla-jökull ICE-14 3
Archaeplastida; Chloroplastida	45.3	35.9	60.6	56.6	9.7	4.5	7.8	29.8	19.7	17.3	57.9	35.4
Opisthokonta; Fungi	27.0	53.5	19.7	41.4	89.9	94.9	87.4	67.0	78.7	12.1	12.0	6.6
SAR; Alveolata	0.1	6.3	2.6	0.0	0.0	0.0	0.0	0.0	0.0	16.3	1.8	3.7
SAR; Rhizaria	27.6	4.2	16.5	1.5	0.2	0.7	4.8	2.0	1.6	0.0	0.0	0.0
SAR; Stramenopiles	0.0	0.0	0.6	0.6	0.2	0.0	0.0	1.1	0.0	54.3	28.1	53.9

Figure 5.3: Distribution of 97% clustered OTUs aligned and assigned to eukaryotes. Values are the relative abundance of the taxa in percentage of total sequences and figure shows taxa with OTUs of a minimum total observation count of 0.1%. It is important to note that values are rounded to one digit; therefore the abundance of a taxon with a value of 0.0 in one sample can range between 0.00 and 0.04%. A full OTU table can be found in the SI.

In order to investigate algal relative abundance all sequences corresponding to *Chloroplastida* were filtered from the main OTU table (Figure 5.4) with 567 OTUs remaining. Sequences matching *Embryophyta* showed low abundance with <7% for all samples with Vatnajökull being the exception and a value of 22% of total eukaryotic sequences. All sequences matching *Embryophyta* were removed from further analyses. The most abundant genera of algae belong to the *Chlamydomonadaceae* with *Chloromonas polyptera* being the dominant taxon. Two uncultured *Chlamydomonadaceae* species were also highly abundant and based on their 18S rRNA sequences they shared the highest sequence similarity (89-93% similarity) with other *Chloromonas* species found in our samples (Figure B.2). The *Trebouxiaceae* were represented by *Raphidonema sempervirens* as the dominant taxon. Other *Chloromonas* species with intermediate abundance (up to 16.7%) were *Chr. nivalis*, *Chr. alpina* and *Chr. tughillensis*. Relative abundance of *Chlamydomonas*, *Ancylonema* and *Mesotaenium*, that are typically described on glacial surfaces worldwide, was very low (< 0.1 %). In the Langjökull sample we also found a high number of sequences matching *Prototheca cutis*, a newly discovered pathogenic algae (Satoh et al., 2010), that may be derived from sledge dog feces that was abundant close to our sampling site. Full OTU tables can be found in the SI files. Shannon indices (Table 5.6) for algal species did not reveal large differences between sites (H’ = 3.88-4.51). The exceptions were the three samples collected from Eyafjallajökull in 2014, which showed a much lower diversity in the algae species (H’ = 1.07-1.81). The PCA analysis of the algal species (Figure 5.5) revealed taxonomic distance between sampling sites, however, separation was not caused by increasing geographic distance or collection time.

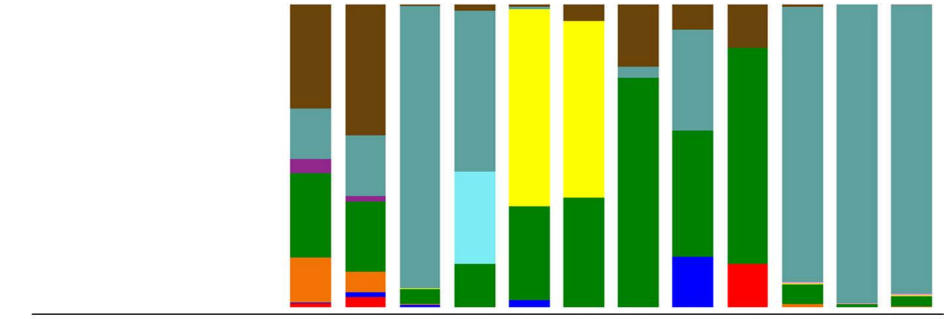

Taxon	Dranga-jökull ICE-12 2/3	Lauga-fell ICE-12 4	Hofs-jökull ICE-12 6/7	Vatna-jökull ICE-13 13/14/15	Lang-jökull ICE-13 16/18	Lang-jökull ICE-13 19	Snaefells-jökull ICE-13 21/23/24	Eyafjalla-jökull ICE-13 4/5/6	Mýrdals-jökull ICE-13 8/9	Eyafjalla-jökull ICE-14 1	Eyafjalla-jökull ICE-14 2	Eyafjalla-jökull ICE-14 3
Chlorophyceae; uncultured Chlamydomonadaceae (1)	1.4	3.3	0.0	0.0	0.0	0.0	0.0	0.0	14.3	0.0	0.0	0.0
Chlorophyceae; Chloromonas cf. alpina CCCryo 033-99	0.2	1.7	0.8	0.0	2.2	0.0	0.0	16.7	0.0	0.1	0.0	0.1
Chlorophyceae; Chloromonas nivalis CCCryo 005-99	14.9	6.7	0.2	0.0	0.0	0.0	0.0	0.0	0.0	1.0	0.0	0.0
Chlorophyceae; Chloromonas polyptera	27.8	23.3	5.1	14.3	31.1	36.1	75.9	41.7	71.4	6.5	0.9	3.6
Chlorophyceae; Chloromonas tughillensis	4.6	1.7	0.0	0.0	0.0	0.0	0.0	0.0	0.0	0.0	0.0	0.0
Trebouxiophyceae; Prototheca cutis	0.0	0.0	0.2	0.0	65.2	58.3	0.0	0.0	0.0	0.1	0.1	0.2
Trebouxiophyceae; uncultured	0.0	0.0	0.0	30.6	0.0	0.0	0.0	0.0	0.0	0.0	0.0	0.0
Trebouxiophyceae; Raphidonema nivale	0.0	0.0	0.0	0.0	0.0	0.0	0.0	0.0	0.0	0.5	0.4	0.5
Trebouxiophyceae; Raphidonema sempervirens	16.6	20.0	93.3	53.1	0.7	0.0	3.4	33.3	0.0	90.9	98.5	95.4
Chlorophyceae; uncultured Chlamydomonadaceae (2)	34.5	43.3	0.5	2.0	0.7	5.6	20.7	8.3	14.3	0.8	0.1	0.0
Chlorophyceae; uncultured Chlamydomonadaceae (3)	0.0	0.0	0.0	0.0	0.0	0.0	0.0	0.0	0.0	0.1	0.0	0.2

Figure 5.4: Distribution of 97% clustered OTUs aligned and assigned to known algal species. Values are the relative abundance of the taxa in percentage of total sequences and figure shows taxa with OTUs of a minimum total observation count of 0.05%. It is important to note that values are rounded to one digit; therefore the abundance of a taxon with a value of 0.0 in one sample can range between 0.00 and 0.04%.A full OTU table can be found in the SI.

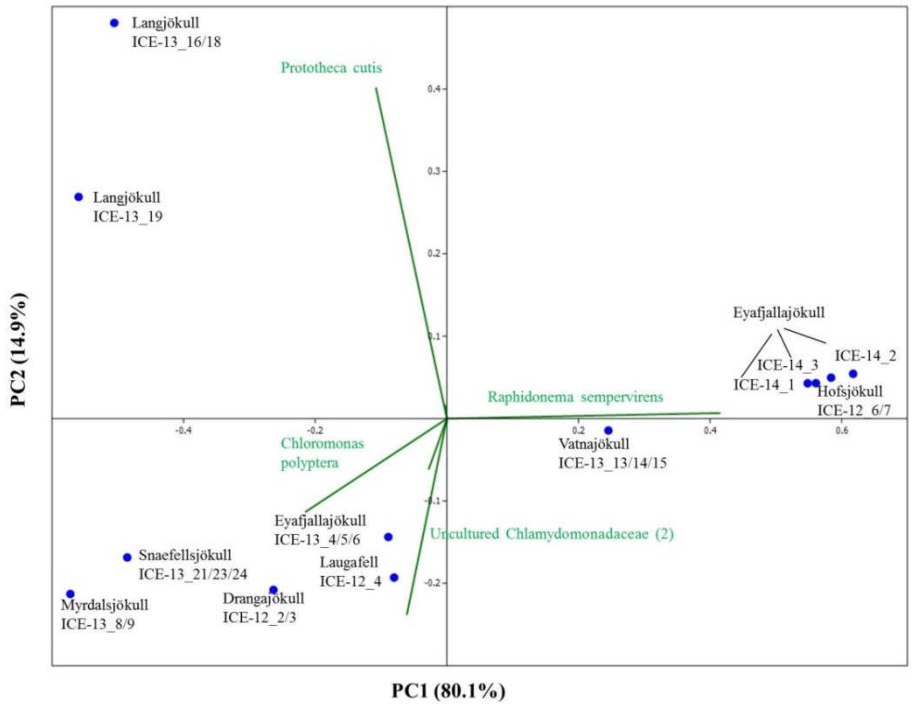

Figure 5.5: Principal component analysis of algal species revealing taxonomic distance between sampling sites and species causing separation. However, taxonomic distance cannot be explained by increasing geographic distance or collection time.

Bacterial primer amplification resulted in 24,221 sequences (12 samples in total) passing the QIIME quality pipeline corresponding to 1,733 operational taxonomic units clustered at 97% sequence identity. Again similar values were derived when the relative abundance of taxa for OTUs were clustered at different similarities of 99%, 97% and 95% (Table B.5). OTUs aligned and assigned to the Greengenes database revealed differences between the eight sampling sites. The most abundant bacterial phyla were *Proteobacteria*, *Bacteriodetes* and *Cyanobacteria* (see Figure 5.6). Within the *Proteobacteria*, *Betaproteobacteria* were most abundant followed by *Alphaproteobacteria*. *Betaproteobacteria* were present in high abundance on Snaefellsjökull (95.1%) in 2012, Langjökull in 2013 (80.3 and 71.9%) and Eyafjallajökull in 2014 (28.7-65.4%). In contrast, *Alphaproteobacteria* were most abundant on Vatnajökull (49.5%) and Eyafjallajökull in 2013 (42.6%), and Drangajökull (42.0 %) in 2012. Within the *Bacteriodetes*, the *Sphingobacteria* and *Saprospirae* were the most abundant representative classes in the samples collected in 2012 and 2014. *Sphingobacteria* showed higher relative abundance on Hofsjökull (32.2%) and on Drangajökull (18.8%) whereas *Saprospirae* were more present on Hofsjökull (38.4%), in the three samples collected from Eyafjallajökull in 2014 (28.0-45.5%), Laugafell (28.5%) and Drangajökull 24.1%). *Cyanobacteria* (*Nostocophycideae* and *Oscillatoriophycideae*) were strongly represented only on Eyafjallajökull (74.0%), Vatnajökull (56.4%) and Langjökull (24.4%) collected in 2013. The Shannon indices for most bacterial samples (Table 5.6) varied over a narrow range (H’ = 5.13 – 5.38) and showed the same trend as for algae with similar values for all glaciers. Exceptions were again the three samples collected from Eyafjallajökull in 2014 (4.52-4.64) and the pooled Snaefellsjökull sample collected in 2013, which had the lowest bacterial diversity index among all bacterial samples (H’ = 3.97). PCA analysis (Figure 5.7) showed samples collected in 2012 and 2014 clustering together due to higher relative abundance of *Bacteriodetes* (*Sphingobacteria, Saprospirae*), whereas samples collected in 2013 clustered together due to higher proportions of *Betaproteobacteria* and *Cyanobacteria* (*Nostocophicidae, Oscillatoriophycideae*).

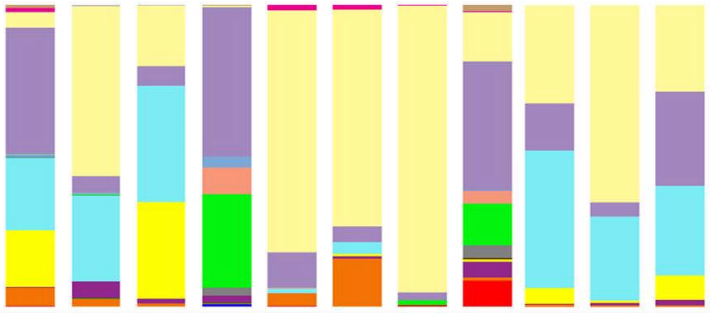

Taxon	Dranga-jökull ICE-12 2/3	Lauga-fell ICE-12 4	Hofs-jökull ICE-12 6/7	Vatna-jökull ICE-13 13/14/15	Lang-jökull ICE-13 16/18	Lang-jökull ICE-13 19	Snaefells-jökull ICE-13 21/23/24	Eyafjalla-jökull ICE-13 4/5/6	Eyafjalla-jökull ICE-14 1	Eyafjalla-jökull ICE-14 2	Eyafjalla-jökull ICE-14 3
Acidobacteria; Acidobacteriia	0.4%	0.0%	0.1%	0.0%	0.2%	0.0%	0.5%	8.6%	0.0%	0.0%	0.0%
Acidobacteria; Solibacteres	0.0%	0.0%	0.0%	0.7%	0.0%	0.0%	0.0%	0.0%	0.0%	0.0%	0.0%
Actinobacteria; Actinobacteria	6.0%	2.6%	0.9%	0.3%	4.1%	15.9%	0.0%	1.0%	0.8%	0.5%	0.6%
Actinobacteria; Thermoleophilia	0.0%	0.2%	0.0%	0.3%	0.0%	0.1%	0.0%	0.0%	0.0%	0.0%	0.0%
Bacteroidetes; Cytophagia	0.1%	5.4%	1.4%	2.3%	0.0%	0.7%	0.1%	5.4%	0.1%	0.7%	1.7%
Bacteroidetes; Sphingobacteriia	18.8%	0.0%	32.2%	0.0%	0.2%	0.7%	0.0%	0.6%	5.3%	0.8%	8.1%
Bacteroidetes; Saprospirae	24.1%	28.5%	38.4%	0.0%	1.4%	3.8%	0.0%	0.2%	45.5%	28.0%	29.7%
Chlorobi; Ignavibacteria	0.0%	0.0%	0.0%	0.0%	0.0%	0.0%	0.0%	0.0%	0.0%	0.0%	0.0%
Chlorobi; SJA-28	0.5%	0.0%	0.0%	0.0%	0.0%	0.0%	0.0%	0.0%	0.0%	0.0%	0.0%
Chloroflexi; Ktedonobacteria	0.0%	0.0%	0.0%	0.0%	0.0%	0.0%	0.0%	0.5%	0.0%	0.0%	0.0%
Cyanobacteria;	0.0%	0.0%	0.0%	2.7%	0.0%	0.0%	0.0%	4.1%	0.0%	0.0%	0.0%
Cyanobacteria; Nostocophycideae	0.0%	0.2%	0.0%	30.8%	0.0%	0.0%	1.5%	13.7%	0.0%	0.0%	0.0%
Cyanobacteria; Oscillatoriophycideae	0.0%	0.0%	0.0%	9.0%	0.5%	0.0%	0.0%	4.3%	0.0%	0.0%	0.0%
Cyanobacteria; Synechococcophycideae	0.5%	0.5%	0.0%	3.7%	0.0%	0.0%	0.0%	0.3%	0.0%	0.0%	0.0%
Firmicutes; Bacilli	0.0%	0.0%	0.0%	0.0%	0.0%	0.1%	0.0%	0.0%	0.0%	0.0%	0.0%
Gemmatimonadetes; Gemmatimonadetes	0.1%	0.5%	0.0%	0.0%	0.0%	0.1%	0.0%	0.0%	0.0%	0.0%	0.0%
Proteobacteria; Alphaproteobacteria	42.0%	5.4%	6.6%	49.5%	11.6%	5.1%	2.7%	42.6%	15.6%	4.5%	31.2%
Proteobacteria; Betaproteobacteria	4.9%	56.2%	20.1%	0.3%	80.3%	71.9%	95.1%	16.2%	32.6%	65.4%	28.7%
Proteobacteria; Deltaproteobacteria	0.4%	0.5%	0.1%	0.0%	0.0%	0.0%	0.0%	0.2%	0.0%	0.0%	0.0%
Proteobacteria; Gammaproteobacteria	1.3%	0.0%	0.1%	0.0%	1.8%	1.6%	0.1%	0.3%	0.0%	0.1%	0.1%
Spirochaetes; Spirochaetes	0.0%	0.0%	0.0%	0.0%	0.0%	0.0%	0.0%	0.0%	0.0%	0.0%	0.0%
WPS-2	0.9%	0.0%	0.0%	0.3%	0.0%	0.0%	0.1%	2.1%	0.0%	0.0%	0.0%

Figure 5.6: Distribution of 97% clustered OTUs aligned and assigned to known bacterial species. Values are the relative abundance of the taxa in percentage of total sequences and figure shows taxa with >0.01% abundance. It is important to note that values are rounded to one digit; therefore the abundance of a taxon with a value of 0.0 in one sample can range between 0.00 and 0.04%. A full OTU table can be found in the SI.

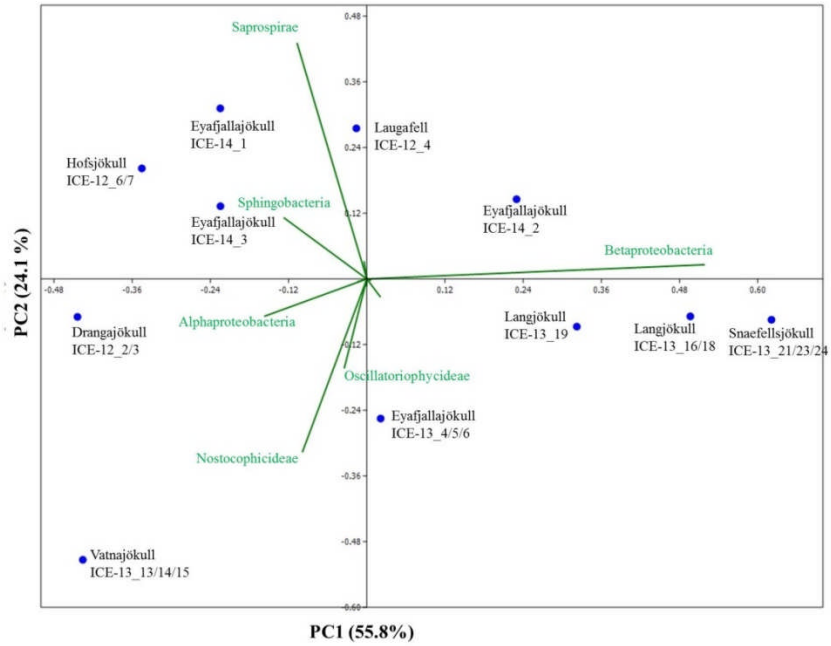

Figure 5.7: Principal component analysis of bacterial species revealing taxonomic distance between sampling sites and species causing separation. Samples collected in 2012 and 2014 cluster together due to a higher relative abundance of *Bacteriodetes* (*Sphingobacteria, Saprospirae*), whereas samples collected in 2013 contain higher proportions of *Betaproteobacteria* and *Cyanobacteria* (*Nostocophicidae, Oscillatoriophycideae*).

Achaea were detected in most snow samples. For samples collected in 2013 and 2014 ~ 80% of all sequences could not be assigned to archaeal species after passing the QIIME quality pipeline and were removed from the analysis. Samples with only very few sequences left (n < 10) were completely removed from the analysis and only six samples were further analyzed. For samples collected in 2014 and sequenced on a #316v2 chip (see methods), we gained 114,182 raw sequences and 89,694 sequences passed the QIIME quality pipeline. For both sequencing runs and independent from the large variation in sequence numbers, the most striking feature is that the archaeal species diversity is very low and dominated by 1-2 species only. The dominant phyla (>98% of all sequences) on most glaciers (Laugafell, Vatnajökull, Langjökull, Snaefellsjökull) belong to the *Nitrososphaerales* (*Thaumarchaeota*). Only on Hofsjökull (ICE-12_6/7) *Methanosarcinales* (*Euryarchaeota*) were found in higher abundance (71.6%) than *Nitrososphaerales*, and in one of the 2014 Eyafjallajökull samples (ICE-14_2) the *Cenarchaeales* (*Thaumarchaeota*) were found to make up 18.1% of the abundance besides the dominant *Nitrososphaerales*.

Table 5.7: Distribution of 97% clustered OTUs aligned and assigned to archaea in analyzed red snow samples, revealing a dominance of the two phyla *Nitrososphaerales* (*Thaumarchaeota*) and *Methanosarcinales (Euryarchaeota).* It is important to note that values are rounded to one digit; therefore the abundance of a taxon with a value of 0.0 in one sample can range between 0.00 and 0.04%.

Taxon	Lauga-fell ICE-12 4/5	Hofs-jökull ICE-12 6/7	Vatna-jökull ICE-13 11-15	Lang-jökull ICE-13 16-18	Lang-jökull ICE-13 19	Snaefells-jökull ICE-13 21-24	Eyafjalla-jökull ICE-14 1	Eyafjalla-jökull ICE-14 2	Eyafjalla-jökull ICE-14 3
Crenarchaeota; MBGA	0.0	0.0	0.0	0.0	0.0	0.2	0.0	0.0	0.0
Crenarchaeota; Thaumarchaeota; Cenarchaeales; Cenarchaeaceae	2.8	0.7	7.7	0.3	1.1	4.2	0.0	0.0	0.0
Crenarchaeota; Thaumarchaeota; Cenarchaeales; SAGMA-X	0.0	0.0	0.0	0.0	0.5	0.0	0.0	18.1	0.0
Crenarchaeota; Thaumarchaeota; Nitrososphaerales; Nitrososphaeraceae	**96.5**	**27.6**	**92.0**	**99.7**	**98.1**	**95.6**	**100.0**	**78.6**	**99.9**
Euryarchaeota; Methanobacteria; Methanobacteriales; MSBL1	0.0	0.0	0.0	0.0	0.0	0.0	0.0	0.0	0.0
Euryarchaeota; Methanomicrobia; Methanosarcinales; Methanosarcinaceae	**0.0**	**71.6**	**0.0**	**0.0**	**0.0**	**0.0**	**0.0**	**3.2**	**0.0**

5.4 Discussion

5.4.1 Microbial diversity

To our knowledge, this is the first time that microbial diversity in general and snow algae in particular have been described on Icelandic glaciers and ice caps.

5.4.1.1 Eukaryotic communities

Snow algae were present and abundant on all studied glaciers and ice caps. The algal species diversity was in all cases very low and only four phylotypes with highest sequence similarity to *Chloromonas polyptera*, *Raphidonema sempervirens* and two uncultured *Chlamydomonadaceae* comprised >95% of the total sequences in all our samples. This is in agreement with Leya (2004) who also described low algal diversity, with 2-3 species making up >95% of the snow algal community, on glaciers in Svalbard. It is worth noting however, that all available 18S rRNA gene data targeting snow algae are based on culture-dependent studies and clone libraries entailing a high degree of bias and a limited sequencing depth respectively. Therefore a direct comparison with the few previous studies that targeted snow algae communities (e.g., Leya et al. 2004; Remias et al. 2013) is difficult although all suggest low diversity. Furthermore, it is also well known that snow algae can dramatically change their morphologies during their life cycles (Müller et al., 2001). This makes classifications and inter-study comparisons based on microscopy very challenging and over the course of the last decades many snow algal species have been re-classified in some cases even several times (personal communication from Dr. Thomas Leya). For this reason, the most notable snow algal taxon *Chlamydomonas nivalis* needs to be treated as a collective taxon and not as a single species (Leya et al., 2004).

The most dominant species in our samples, *Chloromonas polyptera* has so far only been described from coastal Antarctic snow fields in the vicinity of penguin rockeries where this species has been identified based on microscopy and clone library sequencing of the 18S rRNA gene (Remias et al., 2013). This taxon is known to share many cryophilic strategies with the more famous snow algae species *Chloromonas nivalis* (Remias et al., 2013). These strategies include the formation of cyst stages and accumulation of the protective carotenoid astaxanthin.

The two uncultured *Chlamydomonadaceae* species (labelled as *Chlamydomonadaceae* 1 and *Chlamydomonadaceae* 2 in Figure 5.4) are abundant in the Alps and are also known for the formation of cyst stages (personal communication Thomas Leya). However, not much is known about their physiology, since culturing efforts have not been successful so far. Based on their 18S rRNA they show the highest sequence similarity (89-93% similarity) with other *Chloromonas* species found in our samples (Figure B.2).

The second most abundant species *Raphidonema sempervirens* (Figure 5.4) is better known as a typical permafrost algae and is not a true snow algae species. Laboratory experiments (Leya et al., 2009) also demonstrated that *Raphidonema sempervirens* does not share one of the main cryophilic properties of true snow algae, i.e., the production of secondary carotenoids (e.g., astaxanthin). Yet, in culture and under optimal conditions *Raphidonema sempervirens* is able to produce significant amounts of primary carotenoids (xanthophylls; Leya et al., 2009). In our samples, we only detected relatively minor amounts of the xanthophylls violaxantin and lutein (Table 5.4) besides chlorophyll and the secondary carotenoid astaxantin. However, analyses of natural snow algae samples revealed that pigment distributions are most often highly variable and dependent on sampling time and location. For example, in Lutz et al. (2014) we have shown that the pigment composition on a single glacier dramatically changed during a two week melting season. Furthermore, Stibal and Elster (2005) have suggested that *Raphidonema sempervirens* is likely introduced onto glacial surfaces by wind rather than through *in-situ* propagation. Thus, despite its high abundance in some of our samples (e.g., 93.3 % in Hofsjökull in 2012 and 90.9-98.5% in Eyafjallajökull in 2014) it remains unclear whether this species plays an active role in the ecology of Icelandic glaciers and elsewhere.

All samples collected early in the melt season in 2013 (except Vatnajökull) showed a much higher relative abundance of sequences assigned to *Fungi* (67.0-94.9% of total sequences), with the most abundant class represented by the *Microbotryomycetes* (*Basidomycota*), in comparison to *Chloroplastida* (4.5-29.8%). The higher relative abundance of fungi in our samples could be due to the earlier sampling time (beginning of June in 2013 compared to end of July in 2012 and end of August in 2014) and thus before the onset of melting, which initiates the bloom of snow algal communities. In contrast, samples collected in 2012 and 2014 showed a higher relative abundance of *Chloroplastida* (35.4-60.6%; fungi: 6.6-

53.5%). They also confirmed the presence of *Stramenopiles* (e.g., *Chrysophyceae*; Eyafjallajökull 2014 samples), *Rhizaria* (e.g., *Cercozoa*; Drangajökull and Hofsjökull 2012 samples) and *Alveolata* (e.g., *Ciliophora*; Laugafell and Eyafjallajökull in 2014), which were only found in considerable abundances where snow algal sequences were also abundant. Their presence may support the importance of snow algal communities as primary colonizers, producers of organic carbon and nutrient sources for other microbial communities.

5.4.1.2 Bacterial communities

A comparison with previous bacterial studies of snow is easier since more 16S rRNA gene studies have been published so far. However, these mostly targeted relatively fresh spring snow (Larose et al 2009) or clean summer snow (Cameron et al 2014). In our study, we targeted bacteria in summer snow that were associated with snow algal communities. Yet, considering that algal diversity is limited to very few taxa, we could not find a match between bacterial and algal species composition (Figures 5.5 and 5.7). Likewise for algae, bacterial species compositions from samples collected late in the melt season (August 2012 and 2014) compared to early in the season (June 2013) suggest a likely seasonal effect. Specifically, *Betaproteobacteria* were more abundant in sequence data from earlier in the melt season (2013 samples) whereas *Bacteroidetes* were more abundant later in the season (2012 and 2014 samples). In other studies a high relative abundance of *Proteobacteria* and *Bacteroidetes* has often been found in snow and ice samples not associated with algal blooms. For example, a high abundance of *Proteobacteria* was found in snow in Greenland (Cameron et al., 2014), in snow and ice in China (Segawa et al., 2014), in spring snow in Svalbard (Larose et al., 2009), in snow, slush and surface ice in Svalbard (Hell et al., 2013), and in cryoconite holes in the Alps and Svalbard (Edwards et al., 2013; Edwards et al., 2014). Furthermore, in previous studies *Bacteroidetes* also showed a higher relative abundance in cryoconite holes (Edwards et al., 2013; Edwards et al., 2014).

5.4.1.3 Archaeal communities

We were also able to confirm the presence of archaea in our samples. Currently, only very few studies have documented the presence of archaea in glacial environments. They have been found in a glacial stream in Austria (Battin et al.,

2001), in subglacial sediments in Canada (Boyd et al., 2011) and in cryoconite holes in Antarctica (Cameron et al., 2012) and Svalbard (Zarsky et al., 2013). Our study revealed a very limited diversity, with *Nitrososphaerales* (*Thaumarchaeota*) and *Methanosarcinales (Euryarchaeota)* being the only archaeal taxa present (Table 5.7), consistent with the earlier studies. Cameron et al. (2012) similarly found a limited number of taxa affiliated with *Thaumarchaeaota* and *Methanobacteriaceae* restricted to Antarctic cryoconite. Cameron et al. (2014) reported similar low archaeal diversity in 4 snow samples collected between 1.6 to 9.5 km from the margin of the Greenland Ice Sheet. Therefore, when taken into consideration jointly, these studies offer a consensus that the apparent diversity of Archaea on glacier surfaces is low. *Nitrososphaerales* may play an important role in nitrogen cycling contributing towards ammonia oxidation and nitrification (Tourna et al., 2011; Zarsky et al., 2013; Stieglmeier et al., 2014). However, in order to fully explore such links further detailed analyses are needed.

5.4.2 Environmental parameters

In order to investigate the environmental parameters controlling snow algal species distribution we analysed a large suite of physical and chemical parameters in all collected snow samples. We quantified aqueous nutrient and trace metal contents as well as particulate nutrient abundances. Our geochemical modelling (Table B.7) showed that nutrients and trace metals varied over a narrow range, and were in equilibrium with the nutrient-rich and fast dissolving ubiquitously present volcanic ash (Dagsson-Waldhauserova et al., 2015) which likely supports snow algal communities to thrive. However, we could not establish any relevant differences between sites of red and clean snow. Spijkerman et al. (2012) also could not find a relation between dissolved and particulate nutrients in red snow samples in Svalbard.

Nitrogen is often the most important nutrient for microbial growth. Particulate $d^{15}N$ results showed throughout negative values ranging from -11.2 to -3.9 ‰ suggesting an atmospheric nitrogen source for all samples. This indicates that the source of nitrogen is very similar for all glaciers and not a selecting factor for snow algal and bacterial distribution. Other studies have identified faecal pellets from bird colonies as the main primary source, which would lead to more recycled nitrogen and thus more positive nitrogen isotopic values (Fuji et al., 2010). Analysis of the

particulate carbon to nitrogen ratios (C/N) revealed nitrogen limiting conditions (C/N > 6.6, Redfield ratio) for Langjökull, Snaefellsjökull and Eyafjallajökull and non-limiting conditions (C/N < 6.6) for Hofsjökull, Mýrdalsjökull and Vatnajökull. Although in this study particulate carbon was analysed as total carbon (TC), the largest proportion is likely to be organic carbon since no carbonates were found in the XRD analysis and overall carbonates are highly unlikely in basaltic rocks. Nevertheless, overall the total carbon and nitrogen contents and C/N ratios in our solid samples are similar to most values measured in other glacial communities such as snow algae in Svalbard (C/N: 16-33; Spijkerman et al., 2012), in cryoconite holes on a Himalayan Glacier (C: 2.7%, N: 0.27%, C/N: 10; Takeuchi et al., 2001) and in cryoconite holes in Svalbard (C: up to 4%, N: up to 0.4%, C/N 12.5; Stibal et al., 2006).

We could not identify patterns for any of the analysed environmental parameters to explain differences in species composition between glaciers. However, we may not have captured all parameters and there may be trends for overall biomass. Furthermore, the extend of melting and stage in the melt season at the time of collection may play a more important role and needs to be investigated in future studies.

5.4.3 Metabolic inventory

Snow algae have evolved a well-adapted physiology and metabolism in order to thrive in glacial environments (Remias et al., 2005, Leya et al., 2009). Fatty acids play an essential role as structural elements of their membranes and as storage compounds (Thompson Jr., 1996). The relative composition of fatty acids depends on environmental factors such as temperature, irradiation and nutrient availability (Piorreck et al., 1984; Roessler, 1990), but also varies between species (Spijkerman et al., 2012). In our samples we found mainly the two common saturated C16 and C18 fatty acids, but also unsaturated C16 and C18 compounds. Temperature is one of the main factors that affect the fatty acid composition, with a general trend towards increasing unsaturation with decreasing temperatures. However, in this study, temperature effects can be neglected since measured snow temperatures varied by less than 1˚C (Table 5.1). Therefore, we contend differences in fatty acid abundance more likely originate from varying nutrient concentrations. Piorreck et al. (1984) found a positive correlation between nitrogen concentrations and fatty

acid production of lab cultures of green algae and they showed that a high production of polyunsaturated fatty acids (PUFA) occurred at high N concentrations, whereas at lower concentrations there was a shift towards a higher relative abundance of C16:0 and C18:1. Spijkerman et al. (2012) also reported an increase in C18:1 production of lab cultures with decreasing nitrogen concentrations. One explanation may be a metabolism shifted towards nitrogen free non-protein compounds with nitrogen deficiencies.

Fatty acids are also often linked to pigments and astaxanthin has been shown to be associated with higher amounts of C18:1 fatty acids (Řezanka et al., 2008). The same trend could be found in our samples with higher astaxanthin contents in samples collected in 2012 towards the end of the melt season and also the highest relative abundance of C18:1. Astaxanthin is one of the main pigments causing an intensive red coloration of snow algal cells. Samples collected in 2012 showed overall more red pigmentation, potentially due to the collection date being towards the end of the melt season and longer exposure periods to stress (e.g., irradiation), whereas in 2013 samples were collected earlier in the season and showed more green and yellow pigmented cells (see Figure 5.2 and Table 5.4). Astaxanthin was primarily found in samples collected in the 2012 and 2014 field campaigns, which were carried out later in the melt season after longer periods of higher irradiation. This also matches our findings in Greenland where we followed pigment development over a three-week period and found increasing amounts of astaxanthin while the melting progressed (Lutz et al., 2014). In their samples from Antarctica, Remias et al. (2013) found much higher secondary carotenoid contents (51%) for *Chloromonas polyptera*, which was also one of the dominant species in our study. The lower secondary carotenoid content in our samples that were dominated by *Chloromonas polyptera* could be due to lower stress levels in Iceland (e.g., less excessive irradiation) or the high content of *Raphidonema sempervirens* contributing to the total pigment content and which is not known to produce these pigments (Leya et al., 2009). It is important to mention that a contribution of pigmentation derived from *Embryophyta* (mainly Chl a) to the total analysed pigment composition cannot be excluded.

The pigmentation may also be linked to the observed decrease in albedo from clean snow (76% ± 8) to sites where we observed algal colonization (56% ± 14). In Iceland, the most common considered component of albedo change is the volcanic ash and the combination of black ash and coloured algae affect albedo

measurements dramatically. A quantitative evaluation of the algal contribution to the observed decrease in albedo is still lacking and needs to be further investigated. However, the observed reduction in albedo at our algal sampling sites (Table 5.1) matches our previous observations in Greenland using the same approach (Lutz et al., 2014).

In conclusion, we show that snow algae are abundant on all major Icelandic glaciers and ice caps with a rich community comprising of other micro-eukaryotes, bacteria and archaea. Snow algal pigmentation and volcanic ash are causing a reduction of surface albedo, which in turn could potentially have an impact on the melt rates of Icelandic glaciers.

Acknowledgement

The authors would like to thank Dr Susan Girdwood (Aberystwyth University), Dr Christy Waterfall and Ms Jane Coghill (University of Bristol) for help with the DNA sequencing, Dr Rob Newton (University of Leeds) for support with the carbon and nitrogen analyses and Dr Fiona Gill (University of Leeds) for help with the fatty acid analysis. We would like to acknowledge Dr Anthony Stockdale (University of Leeds) for the phosphorus analysis, Neil Bramall (University of Sheffield) for the ICP-MS analysis and Dr Alan Tappin (Plymouth University) for the DOC analysis. Dr Juan Diego Rodriguez-Blanco from the Nano-Science Centre (University of Copenhagen) is thanked for his help with the *PHREEQC* modelling. This work was funded by a University of Leeds grant to SL and LGB, by the Dudley Stamp Memorial Award from the Royal Geographical Society and the President's Fund for Research Visit grant from the Society for General Microbiology granted to SL, the NE/J02399X/1 grant to AMA and the NE/K000942/1 grant to AE.

References

Anesio, A.M., and Laybourn-Parry, J. (2011). Glaciers and ice sheets as a biome. *Trends in ecology & evolution*, 27(4), 219-225.

Battin, T.J., Wille, A., Sattler, B., and Psenner, R. (2001). Phylogenetic and functional heterogeneity of sediment biofilms along environmental gradients in a glacial stream. *Applied and environmental microbiology*, 67, 799-807.

Benning, L.G., Anesio, A.M., Lutz, S., and Tranter, M. (2014). Biological impact on Greenland's albedo. *Nature Geoscience*, 7(10), 691-691.

Boyd, E.S., Lange, R.K., Mitchell, A.C., Havig, J.R., Hamilton, T.L., Lafrenière, M.J., Shock, E.L., Peters, J.W., and Skidmore, M. (2011). Diversity, abundance, and potential activity of nitrifying and nitrate-reducing microbial assemblages in a subglacial ecosystem. *Applied and environmental microbiology*, 77(14), 4778-4787.

Cameron, K.A., Hagedorn, B., Dieser, M., Christner, B.C., Choquette, K., Sletten, R., Crump, B., Kellogg, C., and Junge, K. (2014). Diversity and potential sources of microbiota associated with snow on western portions of the Greenland Ice Sheet. *Environmental microbiology*, *17*(3), 594-609.

Cameron, K.A., Hodson, A.J., and Osborn, A.M. (2012). Structure and diversity of bacterial, eukaryotic and archaeal communities in glacial cryoconite holes from the Arctic and the Antarctic. *FEMS microbiology ecology*, 82, 254-267.

Caporaso, J.G., Kuczynski, J., Stombaugh, J., Bittinger, K., Bushman, F.D., Costello, E.K., Fierer, N., Pena, A.G., Goodrich, J.K., and Gordon, J.I. (2010). QIIME allows analysis of high-throughput community sequencing data. *Nature methods*, 7, 335-336.

Cheung, M.K., Au, C.H., Chu, K.H., Kwan, H.S., and Wong, C.K. (2010). Composition and genetic diversity of picoeukaryotes in subtropical coastal waters as revealed by 454 pyrosequencing. *The ISME journal*, 4, 1053-1059.

Dagsson-Waldhauserova, P., Arnalds, O., Olafsson, H., Hladil, J., Skala, R., Navratil, T., Chadimova, L., and Meinander, O. (2015). Snow–Dust Storm: Unique case study from Iceland, March 6–7, 2013. *Aeolian Research*, 16**,** 69-74.

Desantis, T.Z., Hugenholtz, P., Larsen, N., Rojas, M., Brodie, E.L., Keller, K., Huber, T., Dalevi, D., Hu, P., and Andersen, G.L. (2006). Greengenes, a chimera-checked 16S rRNA gene database and workbench compatible with ARB. *Applied and environmental microbiology*, 72, 5069-5072.

Edwards, A., Mur, L.A., Girdwood, S.E., Anesio, A.M., Stibal, M., Rassner, S.M., Hell, K., Pachebat, J.A., Post, B., and Bussell, J.S. (2014). Coupled cryoconite ecosystem structure–function relationships are revealed by comparing bacterial communities in alpine and Arctic glaciers. *FEMS microbiology ecology*, *89*(2), 222-237.

Edwards, A., Pachebat, J.A., Swain, M., Hegarty, M., Hodson, A.J., Irvine-Fynn, T.D., Rassner, S.M., and Sattler, B. (2013). A metagenomic snapshot of taxonomic and functional diversity in an alpine glacier cryoconite ecosystem. *Environmental Research Letters*, 8, 035003.

Einarsson, O., and Douglas, G. (1994). *Geology of Iceland: rocks and landscape.* Mál og menning.

Fujii, M., Takano, Y., Kojima, H., Hoshino, T., Tanaka, R., and Fukui, M. (2010). Microbial community structure, pigment composition, and nitrogen source of red snow in Antarctica. *Microbial ecology* 59, 466-475.

Gentz-Werner, P. (2007). *Roter Schnee: oder Die Suche nach dem färbenden Prinzip.* Berlin: Akademie Verlag.

Gislason, S.R., and Oelkers, E.H. (2003). Mechanism, rates, and consequences of basaltic glass dissolution: II. An experimental study of the dissolution rates of basaltic glass as a function of pH and temperature. *Geochimica et Cosmochimica Acta* 67, 3817-3832.

Guðmundsson, S., Björnsson, H., Pálsson, F., and Haraldsson, H. (2005). *Energy balance calculations of Brúarjökull during the August 2004 floods in Jökla, N-Vatnajökull, Iceland.* Institute of Earth Sciences, University of Iceland.

Hammer, O., Harper, D., and Ryan, P. (2012). PAST: paleontological statistics software package for education and data analysis. Paleontol Electron 4 (art. 4): 9..

Hell, K., Edwards, A., Zarsky, J., Podmirseg, S.M., Girdwood, S., Pachebat, J.A., Insam, H., and Sattler, B. (2013). The dynamic bacterial communities of a melting High Arctic glacier snowpack. *The ISME journal*, 7, 1814-1826.

Hodson, A., Anesio, A.M., Tranter, M., Fountain, A., Osborn, M., Priscu, J., Laybourn-Parry, J., and Sattler, B. (2008). Glacial ecosystems. *Ecological Monographs* 78, 41-67.

Jakobsson, S.P., Jónasson, K., and Sigurdsson, I.A. (2008). The three igneous rock series of Iceland. *Jökull,* 58, 117-138.

Jones, M.T., and Gislason, S.R. (2008). Rapid releases of metal salts and nutrients following the deposition of volcanic ash into aqueous environments. *Geochimica et Cosmochimica Acta,* 72**,** 3661-3680.

Larose, C., Berger, S., Ferrari, C., Navarro, E., Dommergue, A., Schneider, D., and Vogel, T.M. (2010). Microbial sequences retrieved from environmental samples from seasonal Arctic snow and meltwater from Svalbard, Norway. *Extremophiles,* 14**,** 205-212.

Leya, T. (2004). *Feldstudien und genetische Untersuchungen zur Kryophilie der Schneealgen Nordwestspitzbergens.* Aachen*:* Shaker.

Leya, T., Müller, T., Ling, H. U. & Fuhr, G. (2004) Snow algae from north-western Spitsbergen (Svalbard). *The coastal ecosystem of Kongsfjorden, Svalbard. Synopsis of biological research performed at the Koldewey Station in the years 1991-2003*.

Leya, T., Rahn, A., Lütz, C., and Remias, D. (2009). Response of arctic snow and permafrost algae to high light and nitrogen stress by changes in pigment composition and applied aspects for biotechnology. *FEMS microbiology ecology* 67, 432-443.

Lutz, S., Anesio, A.M., Jorge Villar, S.E., and Benning, L.G. (2014). Variations of algal communities cause darkening of a Greenland glacier. *FEMS microbiology ecology*, *89*(2), 402-414.

Meier, M.F., Dyurgerov, M.B., Rick, U.K., O'neel, S., Pfeffer, W.T., Anderson, R.S., Anderson, S.P., and Glazovsky, A.F. (2007). Glaciers dominate eustatic sea-level rise in the 21st century. *Science*, 317, 1064-1067.

Möller, R., Möller, M., Björnsson, H., Guðmundsson, S., Pálsson, F., Oddsson, B., Kukla, P.A., and Schneider, C. (2014). MODIS-derived albedo changes of Vatnajökull (Iceland) due to tephra deposition from the 2004 Grímsvötn eruption. *International Journal of Applied Earth Observation and Geoinformation* 26, 256-269.

Müller, T., Leya, T., and Fuhr, G. (2001). Persistent snow algal fields in Spitsbergen: field observations and a hypothesis about the annual cell circulation. *Arctic, Antarctic, and Alpine Research*, 33(1), 42-51.

Oelkers, E.H., and Gislason, S.R. (2001). The mechanism, rates and consequences of basaltic glass dissolution: I. An experimental study of the dissolution rates of basaltic glass as a function of aqueous Al, Si and oxalic acid concentration at 25 C and pH= 3 and 11. *Geochimica et Cosmochimica Acta*, 65, 3671-3681.

Parkhurst, D.L. (1995). User's guide to PHREEQC: A computer program for speciation, reaction-path, advective-transport, and inverse geochemical calculations.

Piorreck, M., Baasch, K.-H., and Pohl, P. (1984). Biomass production, total protein, chlorophylls, lipids and fatty acids of freshwater gr,n and blue-green algae under different nitrogen regimes. *Phytochemistry* 23, 207-216.

Remias, D., Lütz-Meindl, U., and Lütz, C. (2005). Photosynthesis, pigments and ultrastructure of the alpine snow alga Chlamydomonas nivalis. *European Journal of Phycology*, 40, 259-268.

Remias, D., Wastian, H., Lütz, C., and Leya, T. (2013). Insights into the biology and phylogeny of Chloromonas polyptera (Chlorophyta), an alga causing orange snow in Maritime Antarctica. *Antarctic Science*, 25(05), 648-656.

Řezanka, T., Nedbalová, L., Sigler, K., and Cepák, V. (2008). Identification of astaxanthin diglucoside diesters from snow alga *Chlamydomonas nivalis* by liquid c hromatography–atmospheric pressure chemical ionization mass spectrometry. *Phytochemistry*, 69, 479-490.

Ritter, E. (2007). Carbon, nitrogen and phosphorus in volcanic soils following afforestation with native birch (Betula pubescens) and introduced larch (Larix sibirica) in Iceland. *Plant and Soil,* 295**,** 239-251.

Roessler, P.G. (1990). Environmental control of glycerolipid metabolism in microalgae: commercial implications and future research directions. *Journal of Phycology*, 26, 393-399.

Segawa, T., Ishii, S., Ohte, N., Akiyoshi, A., Yamada, A., Maruyama, F., Li, Z., Hongoh, Y., and Takeuchi, N. (2014). The nitrogen cycle in cryoconites: naturally occurring nitrification-denitrification granules on a glacier. *Environmental microbiology*, 16, 3250-3262.

Spijkerman, E., Wacker, A., Weithoff, G., and Leya, T. (2012). Elemental and fatty acid composition of snow algae in Arctic habitats. *Frontiers in Microbiology*, 3, 380.

Stibal, M., and Elster, J. (2005). Growth and morphology variation as a response to changing environmental factors in two Arctic species of Raphidonema (Trebouxiophyceae) from snow and soil. *Polar Biology*, 28, 558-567.

Stibal, M., Šabacká, M., and Kaštovská, K. (2006). Microbial communities on glacier surfaces in Svalbard: impact of physical and chemical properties on abundance and structure of cyanobacteria and algae. *Microbial ecology,* 52, 644-654.

Stieglmeier, M., Klingl, A., Alves, R.J., Simon, K.-M.R., Melcher, M., Leisch, N., and Schleper, C. (2014). Nitrososphaera viennensis sp. nov., an aerobic and mesophilic ammonia-oxidizing archaeon from soil and member of the archaeal phylum Thaumarchaeota. *International Journal of Systematic and Evolutionary Microbiology*, ijs. 0.063172-063170.

Takeuchi, N. (2002). Optical characteristics of cryoconite (surface dust) on glaciers: the relationship between light absorbency and the property of organic matter contained in the cryoconite. *Annals of Glaciolog,y* 34, 409-414.

Takeuchi, N. (2013). Seasonal and altitudinal variations in snow algal communities on an Alaskan glacier (Gulkana glacier in the Alaska range). *Environmental Research Letters*, 8(3), 035002.

Takeuchi, N., Kohshima, S., and Seko, K. (2001). Structure, formation, and darkening process of albedo-reducing material (cryoconite) on a Himalayan glacier: a granular algal mat growing on the glacier. *Arctic, Antarctic, and Alpine Research*, 115-122.

Thomas, W.H., and Duval, B. (1995). Sierra Nevada, California, USA, snow algae: snow albedo changes, algal-bacterial interrelationships, and ultraviolet radiation effects. *Arctic and alpine research*, 27(4), 389-399.

Tourna, M., Stieglmeier, M., Spang, A., Könneke, M., Schintlmeister, A., Urich, T., Engel, M., Schloter, M., Wagner, M., and Richter, A. (2011). Nitrososphaera viennensis, an ammonia oxidizing archaeon from soil. *Proceedings of the National Academy of Sciences* 108, 8420-8425.

Yallop, M.L., Anesio, A.M., Perkins, R.G., Cook, J., Telling, J., Fagan, D., Macfarlane, J., Stibal, M., Barker, G., and Bellas, C. (2012). Photophysiology and albedo-changing potential of the ice algal community on the surface of the Greenland ice sheet. *The ISME journal*, 6(12), 2302-2313.

Yoshimura, Y., Kohshima, S., Takeuchi, N., Seko, K., and Fujita, K. (2006). Snow algae in a Himalayan ice core: new environmental markers for ice-core analyses and their correlation with summer mass balance. *Annals of Glaciology,* 43, 148-153.

Zarsky, J.D., Stibal, M., Hodson, A., Sattler, B., Schostag, M., Hansen, L.H., Jacobsen, C.S., and Psenner, R. (2013). Large cryoconite aggregates on a Svalbard

glacier support a diverse microbial community including ammonia-oxidizing archaea. *Environmental Research Letters*, 8(3), 035044.

Chapter 6: Integrated ‘omics’, targeted metabolite and single-cell analyses of Arctic snow algae functionality and adaptability

Lutz, S., Anesio, A. M., Field, K. & Benning, L. G.

Published in *Frontiers in microbiology*, 6, 1323 (2015)

Abstract

Snow algae are poly-extremophilic microalgae and important primary colonisers and producers on glaciers and snow fields. Depending on their pigmentation they cause green or red mass blooms during the melt season. This decreases surface albedo and thus further enhances snow and ice melting. Although the phenomenon of snow algal blooms has been known for a long time, large aspects of their physiology and ecology sill remain cryptic. This study provides the first in-depth and multi-omics investigation of two very striking adjacent green and red snow fields on a glacier in Svalbard. We have assessed the algal community composition of green and red snow including their associated microbiota, *i.e.*, bacteria and archaea, their metabolic profiles (targeted and non-targeted metabolites) on the bulk and single-cell level, and assessed the feedbacks between the algae and their physico-chemical environment including liquid water content, pH, albedo and nutrient availability. We demonstrate that green and red snow clearly vary in their physico-chemical environment, their microbial community composition and their metabolic profiles. For the algae this likely reflects both different stages of their life cycles and their adaptation strategies. Green snow represents a wet, carbon and nutrient rich environment and is dominated by the algae *Microglena* sp. with a metabolic profile that is characterized by key metabolites involved in growth and proliferation. In contrast, the dry and nutrient poor red snow habitat is colonised by various *Chloromonas* species with a high abundance of storage and reserve metabolites likely to face upcoming severe conditions. Combining a multitude of techniques we demonstrate the power of such complementary approaches in elucidating the function and ecology of extremophiles such as green and red snow algal blooms, which play crucial roles in glacial ecosystems.

6.1 Introduction

Snow algae are poly-extremophilic microalgae that thrive on snow fields and glaciers in polar and alpine regions. They are prolific primary colonisers and producers (Lutz et al., 2014) despite being subjected to a multitude of harsh environmental conditions including low temperatures, high irradiation, freeze-thaw cycles, desiccation, low pH and broad variation in the levels of nutrients. They

have evolved specialised cryogenic adaptations including accumulation of secondary carotenoids to shield the photosystem from excessive irradiation and the formation of robust spores with thick cell walls (Remias et al., 2010b). In spring, when the snow starts to melt, extensive snow algal blooms occur. Depending on the nature and composition of the coloured pigments, these blooms cause a green or red (all shades from orange to pink) colouration of the snow. As part of the life cycle and as a mechanism of protection from high irradiation, snow algae can adjust their pigmentation from predominantly chlorophylls ("green snow") to carotenoids ("red snow") (Remias et al., 2005). However, it is still unknown whether all green snow undergoes a transition to red snow or whether red and green snow represent two independent phenomena. The colouration causes a darkening of snow surfaces, which in turn decreases surface albedo and eventually may speed up melting processes (Thomas & Duval, 1995;Yallop et al., 2012;Benning et al., 2014;Lutz et al., 2014;Lutz et al., 2015b).

First described by Aristotle (Gentz-Werner, 2007), snow algae have been known for a long time and they have been studied in many cryospheric settings including Svalbard (Mueller et al., 2001; Leya et al., 2004; Stibal et al., 2007; Lutz et al., 2015b), Iceland (Lutz et al., 2015a), Alaska (Takeuchi, 2002), Greenland (Lutz et al., 2014), the Himalayans (Yoshimura et al., 2006), the Rocky Mountains (Thomas & Duval, 1995), Antarctica (Fujii et al., 2010; Remias et al., 2013) and the European Alps (Remias et al., 2005). Most of the 'true' snow algae belong to the *Chlamydomonadaceae* (*Chlorophyta*). Dramatic morphological changes during their life cycles make an unambiguous species identification by microscopy very challenging and susceptible to misassignments. Therefore, the most described taxa *Chlamydomonas nivalis* and *Chloromonas nivalis* are actually polyphyletic and must be treated as collective taxa (Leya et al., 2004; Matsuzaki et al., 2015).

Many studies have addressed various aspects of snow algal ecology and physiology (Kol, 1968; Hoham and Duval, 2001; Takeuchi, 2002; Leya et al., 2004) and targeted individual metabolic groups including pigments (Remias et al., 2005; Leya et al., 2009) and fatty acids (Spijkerman et al., 2012). However, a detailed snow algal species characterization as well as their functionality remain cryptic. To our knowledge, germination of mature red snow algal spores and the replication of a full snow algal life cycle from trophic stages to spores under controlled laboratory conditions have so far been unsuccessful. Therefore, a better understanding relies

heavily on a comprehensive collection and evaluation of field samples, which in turn are not always clearly interpretable.

Nevertheless, combining various 'omic' and metabolite analyses on such samples may help further elucidate their life cycle. Metabolites are the end product of cellular biochemical processes and therefore the ultimate response of an organism to their environment (Jamers et al., 2009). As such, the complement of metabolites within an organism – its metabolome - may provide insights into potential stress factors in the environment (Viant, 2007). For instance, secondary metabolites, which are small, polar molecules not directly related to growth, development or reproduction, are key to algal survival and thriving. Secondary metabolites are often multifunctional, commonly acting as antioxidants. Such compounds act to either inhibit the generation of reactive oxygen species or to quench them when they do form. This helps to maintain the cell's redox homeostasis (Kutchan & Dixon, 2005; Vickers et al., 2009; Agati et al., 2012; Ramel et al., 2012). Individual groups of metabolites have been targeted in snow algae including pigments (Bidigare et al., 1993; Remias et al., 2005; Leya et al., 2009), fatty acids (Řezanka et al., 2008; Spijkerman et al., 2012) and phenolics (Duval et al., 1999). However, the used targeted metabolic analyses were restricted to a few metabolites and as such do not have the high-throughput capacity of the so-called 'omics' techniques. Despite the increasing power and resolution of these new techniques in recent years, they have not thus far been applied to cryophilic snow algae. One reason could be the lack of appropriate reference genomes as currently, the closest fully sequenced green algal strain is *Chlamydomonas reinhardtii* (Merchant et al., 2007), a model organism for freshwater *Chlorophyta* adapted to mesophilic temperatures and hence not sharing common cryogenic adaptations.

To close this gap we explored in this study the questions whether (a) the formation of green and red snow are linked or independent phenomena, (b) if and how the life stages of red and green snow algae differ and (c) what the potential feedbacks are between the presence of algae and their physico-chemical environment, which is crucial for understanding the potential importance of glacial biomes for the export of metabolites to downstream ecosystems. We targeted specific metabolic groups including pigments, fatty acids and carbohydrates, and complemented these analyses through detailed metagenomics and metabolomics analyses and quantified the functional gene inventory and respective metabolomes of green and red snow communities. These bulk analyses were also complemented by targeted single cell

synchrotron infrared spectroscopic analyses to determine functional groups in individual snow algal cells for the first time. Such targeted or non-targeted techniques inherit their own advantages and challenges. With this contribution we promote the power of a combined application of a multitude of different techniques to help elucidate the snow algal phenomenon in two adjacent very striking green and red snow algae fields on a glacier in Svalbard (Figure 6.1). Understanding snow algal diversity and functioning will not only help us obtain a better understanding of the communities themselves but also help us assess the environment they live in and the potential changes this environment may undergo, particularly in light of the increased melting due to the fast changing Arctic climate.

6.2 Material and Methods

6.2.1 Field Site, Sampling, and Measurements

Two adjacent, very striking green and red snow algae fields were sampled on Feiringbreen in Svalbard on the 8th of August in 2013 (Figure 6.1). The snow fields were found next to a cliff in the close vicinity of bird rookeries. The intensely green coloured snow was very wet and formed a layer of about 10 cm in thickness, whereas the red (nearly pink) colouration was equally striking, but could only be found in the top centimetre of much drier snow. Often the red snow was separated from the green snow by between 1 and up to 30 cm of white, clean snow (without macroscopically visible coloured cells or debris), yet some sections of the red snow were immediately adjacent to the green snow (Figure 6.1).

All sampling and field measurements as well as several of the analytical approaches have previously been described in full (Lutz et al., 2014;Lutz et al., 2015a). Here we only summarize these methods and give full details of newly used methods. In brief, at each sampling site we measured pH, conductivity and temperature with a daily-calibrated meter (Hanna instruments, HI 98129) prior to sampling. Photosynthetic active radiation (PAR) and UV irradiation, as well as surface albedo (400-700 nm range), were measured using a radiometer (SolarLight, PMA2100). Samples were collected in sterile centrifuge tubes or sterile *Whirl-Pak*® bags (Figure 6.1) and in pre-ashed glass jars (450◦C >4 h) for organic

analyses. All samples were slowly melted at room temperature within ~ 6 hours of collection and processed and preserved (e.g., filtered, acidified) for further analyses within ~ 8 hours following collection. Samples for DNA and all metabolite analyses were flash-frozen in liquid nitrogen and stored at -80°C until analysed. All inorganic samples (both filtered aqueous fractions and particulates) were stored cold (4°C) and in the dark.

6.2.2 Aqueous and particulate geochemical characterizations

Aqueous analyses were carried out by Ion Chromatography (IC, Dionex, anions) and by inductively coupled plasma mass spectrometry (ICP-MS, Agilent, cations). We used a total organic carbon analyser (Shimadzu, TOC 5000A) for dissolved organic carbon (DOC) measurements, and a segmented flow-injection analyses (AutoAnalyser3, Seal Analytical) for analyses of dissolved phosphate.

Particulates, separated from solutions through filtration were analysed for total carbon (TC), total nitrogen (TN), total sulphur (TS), as well as $\delta^{15}N$ and $\delta^{13}C$, by pyrolysis at 1500 °C (Vario Pyro Cube, Elementar Inc.) followed by mass spectrometry (Isoprime Mass Spectrometer). Particulate phosphorus was extracted by ashing of the samples at 550°C for 2 h and incubating in 1 M HCl for 16 h according to extraction step V in Ruttenberg et al. (2009). The mineralogy of the particulates was determined by X-ray diffraction (XRD, Bruker D8).

6.2.3 Algal abundance and biomass evaluations

Algal cells were imaged on a Leica DM750 microscope equipped with a 63 x objective and counted with a hemocytometer in triplicates. For cell size analyses, 100 cell diameters per sample were measured in ImageJ. Cell volumes were calculated assuming a perfect spherical shape ($V=4/3*\pi*r^3$) and total algal biomass was calculated using the average cell volume and cell abundance.

6.2.4 Amplicon and metagenome sequencing

Total DNA was extracted using the PowerSoil® DNA Isolation kit (MoBio Laboratories). 16S rRNA genes were amplified using bacterial primers 27F (5'-AGAGTTTGATCMTGGCTCAG) and 357R (5'-CTGCTGCCTYCCGTA) (tagged with the Ion Torrent adapter sequences and MID barcode) spanning the V1-V2 hypervariable regions. 18S rRNA genes were amplified using the eukaryotic primers 528F (5′-GCGGTAATTCCAGCTCCAA) and 706R (5'-AATCCRAGAATTTCACCTCT) (Cheung et al., 2010) (tagged with the Ion Torrent adapter sequences and MID barcode) spanning the V4-V5 hypervariable region. Polymerase chain reactions (PCR) were performed using Platinum® PCR SuperMix High Fidelity according to manufacturer's protocols. Initial denaturation at 95 ºC for 5 min was followed by 30 cycles of denaturation at 95 ºC for 30 s, annealing at 60 ºC for 30 s and elongation at 72 ºC for 30 s. Final elongation was at 72 ºC for 7 min. Archaeal 16S rRNA genes were amplified following a nested PCR approach. The first PCR reaction was carried out using primers 20F and 915R. Initial denaturation at 95 ºC for 5 min was followed by 35 cycles of denaturation at 95 ºC for 30 s, annealing at 62 ºC for 30 s and elongation at 72 ºC for 180 s. Final elongation was at 72 ºC for 10 min. The PCR product was used as template for the second PCR reaction with primers 21F (5'-TCCGGTTGATCCYGCCGG) and 519R (5'- GWATTACCGCGGCKGCTG) (tagged with the Ion Torrent adapter sequences and MID barcode) spanning the V1-V2 hypervariable region. Initial denaturation at 95 ºC for 5 min was followed by 30 cycles of denaturation at 95 ºC for 30 s, annealing at 60 ºC for 30 s and elongation at 72 ºC for 30 s. Final elongation was at 72 ºC for 7 min. All PCRs were carried out in triplicates to reduce amplification bias and in reaction volumes of 1 x 25 µl and 2 x 12.5 µl. All pre-amplification steps were carried out in a laminar flow hood with DNA-free certified plastic ware and filter tips. The pooled amplicons were purified with AMPure XP beads (Agencourt©) with a bead to DNA ratio of 0.6 to remove nucleotides, salts and primers and analyzed on the Agilent 2100 Bioanalyser (Agilent Technologies) with the High Sensitivity DNA kit (Agilent Technologies) and quality, size and concentration were determined. Sequencing was performed on an Ion Torrent Personal Genome Machine using the Ion Xpress™ Template Kit and the Ion 314™ or Ion 316™ chips following manufacturer's protocols. The raw sequence data was processed in QIIME (Caporaso et al., 2010). Barcodes and adapter sequences were removed from each sequence. Filtering of sequences was performed using an average cutoff of Q20 over a 350 bp range. Reads shorter than

200 bp were removed. OTUs were picked *de novo* using a threshold of 97% identity. Taxonomic identities were assigned for representative sequences of each OTU using the reference databases Greengenes for bacteria and archaea. The Silva database (DeSantis et al., 2006; extended with additional 223 sequences of cryophilic algae kindly provided by Dr. Thomas Leya from the CCCryo - Culture Collection of Cryophilic Algae, Fraunhofer IZI-BB) was used for eukaryotes. Data were aligned using PyNAST and a 0.80 confidence threshold. Singletons were excluded from the analysis. Bacterial sequences matching plant plastids were removed from the data set prior to further analysis. Eukaryotic sequences matching *Chloroplastida* were pulled out of the data set and stored in a separate OTU table. In order to focus upon algal diversity, sequences matching *Embryophyta* (e.g., moss, fern) were removed from the data set. For archaea, sequences matching bacteria were removed.

Metagenome libraries were constructed using the Ion Plus Fragment Library™ and the Ion Xpress Barcode Adapter™ kits according to manufacturer's instructions. The libraries were analysed on an Agilent 2100 Bioanalyser (Agilent Technologies) with a High Sensitivity DNA kit (Agilent Technologies) to determine DNA quality, size and concentration. Sequencing was performed on an Ion Torrent Personal Genome Machine using the Ion Xpress™ Template Kit and the Ion 314™ chip following manufacturer's protocols. The raw sequence data was processed in QIIME (Caporaso et al., 2010). Barcodes and adapter sequences were removed from each sequence. Filtering of sequences was performed using an average cut-off of Q20 over a 350 bp range and a minimum read length of 200 bp. Sequence reads were assigned to protein references sequences in the IMG database using *blat* (Kent, 2002). The KEGG Orthology (KO) system was used to derive major functional categories for the annotated genes. Sequences have been deposited to the European Nucleotide Archive (ENA) under accession number PRJEB11474.

6.2.5 Non-targeted metabolome analyses

Samples were centrifuged at 20,000 rpm to pellet algal cells. Pellets were ground to a powder in liquid nitrogen. Biphasic extractions of algal metabolites were prepared as per the methods of Overy et al. (2005) in 750 µl of a sterile methanol:chloroform:water/6:2.5:1 mix for 60 minutes on ice. 400 µl of sterile

water were added and extracts were vortexed and centrifuged at 12,000 rpm for 2 min to produce biphasic extractions. 200 µl of the aqueous/polar phase of each metabolite extract was diluted with 200 µl of methanol and 400 µl 0.1% formic acid and analysed by direct injection ToF-LC-MS (QStar Elite System, Applied Biosystems, Massachusetts, USA). Broad range spectra for mass numbers 50-1000 Da were collected over 240 cycles (each cycle lasting 0.9998 s) in positive ion mode using the following instrument settings: resolution of 4000, GS1 at 27.0, CUR at 20.0, and IS of 3500.0. Source temperature was 100°C and cone gas flow rate was maintained at 10 µl min^{-1}. Samples were run in triplicate and the resulting spectra combined using the Analyst QS 2.0 (Applied Biosystems, Massachusetts, USA) software. Mass numbers (or mass to charge ratios, *m*/z) were rounded into 0.01 Da bins and the relative abundance (Total Ion Count - %TIC) for each mass number within that bin summed (Overy et al., 2005;Field and Lake, 2011). All data processing was carried out using in-house software (Burrell & Cameron, unpublished) based upon the binning procedures of Overy et al.(2005).

Metabolic profiles were compared using the OPLS-DA method and the Simca-P multivariate data analysis software (Umetrics, Sweden) using binned mass numbers as the primary variable and sample type as the observational variable. Discriminatory *m/z* values with an R^2 close to 1.0 were assigned identities and metabolic pathways using the online database Biocyc (http://biocyc.org/) and the Kyoto Encyclopedia of Genes and Genomes (KEGG, http://genome.jp/kegg/), using the *Chlamydomonas reinhardtii* reference library wherever possible.

6.2.6 Targeted bulk metabolite analyses

To determine the bulk carotenoid and chlorophyll contents in the samples, high pressure liquid chromatography (HPLC) and a modified carotenoid/chlorophyll specific extraction protocol (Remias and Lutz, 2007) were used. Cells were disrupted by shock freezing in liquid nitrogen for 10 min followed by grinding using a Teflon® mortar and pestle. The resulting powder was re-suspended in 1 mL of dimethylformamide (DMF) and 1.0 mm glass beads and horizontally shaken on a laboratory shaker (MoBio Vortex Genie 2) at maximum speed (3000 rpm) for 10 min followed by centrifugation for 5 min at 10 000 rpm. The supernatant was separated from the debris by filtering through a 0.45 µm Teflon® filter and the filtrate was mixed with methanol (25 vol %). Extracted samples were analysed

immediately on an Agilent Technologies 1200 Infinity HPLC instrument with a gradient pump, an autosampler, a variable wavelength detector and ODS Hypersil column (250x4.6 mm; 5 um particle size). Two solvents were used: solvent A consisted of a mixture of acetonitrile/water/methanol/hexane/tris buffer at ratios of 80:7:3:1:1, while solvent B was a mix of methanol and hexane at a ratio of 5:1. The HPLC was run at a flow rate of 1 mL min^{-1} and with an injection volume of 25 µL. Spectra were recorded from 200 to 800 nm and chromatograms were quantified at 450 nm for carotenoids and 660 nm for chlorophyll a and b. Run time was 60 min and the protocol required a 15 minute run with 100% of solvent A followed by a linear gradient from 100 % solvent A to 100% solvent B between 32 and 45 min and finally with 15 minutes of column re-equilibration through a 5 min linear gradient from solvent B back to 100% solvent to A, followed by a further column conditioning with 100 % solvent A for 10 min. The following commercially available standards were used for peak identification and pigment quantifications: chlorophyll a, chlorophyll b (Sigma), violaxanthin, neoxanthin, antheraxanthin, lutein, β-carotene, trans-astaxanthin, and cis-astaxanthin (Carotenature).

Fatty acids were extracted from the particulates according to the method described by Wacker & Martin-Creuzberg (Wacker and Martin-Creuzburg, 2007). Briefly, 20 ng of internal standard (tricosanoic acid methyl ester) were added to each sample, before ultrasonic extraction using dichloromethane:methanol (2:1 v:v), followed by centrifugation to remove particulates and evaporation of solvent from the supernatant. Fatty acids were transesterified by adding methanolic HCl to the dried extract and heating at 60˚ C for 20 minutes. After cooling, fatty acid methyl esters were extracted in isohexane, the solvent was removed under nitrogen and the sample resuspended in isohexane for analysis. Analysis of fatty acid methyl esters was carried out using a Trace 1300 gas chromatograph with flame ionisation detector (Thermo Scientific, Hemel Hempstead, UK), equipped with a non-polar-fused silica capillary column (CPSil-5CB, 50m x 0.32mm x 0.12 mm, Agilent Technologies, USA). Samples (1 µl) were injected in splitless mode, with the injector maintained at 200˚C. Carrier gas was helium, and a constant flow rate of 1.5 ml/min was used. The following temperature programme was used: initial temperature 40 °C, rising to 140 °C at 20 °C min^{-1}, then rising to 240 °C at 4 ° min^{-1}, holding at 240 °C for 5 min. Fatty acid methyl esters were identified by comparison of retention times with those of reference compounds (37 Component FAME Mix, Supelco, USA) and by gas chromatography/mass spectrometry. Gas

chromatography/mass spectrometry analyses was carried out using the gas chromatograph and column previously described, with identical operating conditions, but coupled to an ISQ mass spectrometer (Thermo Scientific, Hemel Hempstead, UK). The transfer line and the ion source were maintained at 300˚C. The emission current was set to 50mA and the electron energy to 70 eV. The analyser was set to scan the mass to charge ratios between 50 and 650 with a scan cycle time of 0.6 s.

Carbohydrate contents and concentrations were determined on a Dionex ICS-3000 Ion Chromatography system (Sunnyvale, USA). The carbohydrates fucose, rhamnose, arabinose, galactose, glucose, xylose/mannose, fructose/sucrose, ribose and lactose were separated isocratically on a CarboPac PA20 column (3×150mm), after passing through a CarboPac PA20 guard column (3x30 mm). Fructose/sucrose and xylose/mannose are co-eluting and hence are reported together.

The relative abundance of functional groups corresponding to proteins, lipids and carbohydrates was evaluated on the bulk particulate samples after deposition of a dried sample aliquot on a single pass diamond window of an Attenuated Total Reflection cell of a Fourier transform infrared spectroscope (FTIR, A2 Technology Microlab). For each bulk particulate sample 1064 spectra collected at a resolution of 4 cm^{-1} over the mid infrared region between 650 and 4000 cm^{-1} were co-added.

6.2.7 Single-cell micro-spectroscopy

Micro-analyses were carried out at the Multimode infrared imaging and micro-spectroscopy (MIRIAM) beamline, B22 at the Diamond Light Source (UK). Individual snow algal cells that were thawed and deposited on ZnSe windows were imaged and analysed in transmission mode by Fourier transform infrared (FTIR) spectroscopy. A Bruker FTIR spectrometer interlinked with the synchrotron-light (Benning et al., 2004) and a microscope was used to collect images and spectra via a broadband MCT detector, a x36 objective and a x36 condenser. We collected data either using a 20 µm x 20 µm aperture or a 6 µm x 6 µm aperture. Spectra were acquired over the mid-infrared range between 4000 and 650 cm^{-1} and at each point / pixel 512 spectra were co-added. All data were processed in Opus (V7.2). Functional group values for individual cells were derived from peak areas under

the CH_2-CH_3-CH lipid/protein bands (~ 3100 – 2800 cm-1), the C-O of the ester lipid band (~ 1720 cm^{-1}), the main protein bands (1700-1600 cm^{-1} for amide 1) and 1600 – 1500 cm^{-1} for amide 2) and the carbohydrate bands (between 1200 – 930 cm^{-1}). Area ratios for total proteins (1700-1500 cm^{-1}) over C-H lipids (3050-2800 cm^{-1}) and proteins (1700-1500 cm^{-1}) over C-O ester lipids (1850-1700 cm^{-1}) were calculated. We quantified the functional groups in 4 green and 12 red single cells and collected on each cell between 12 and 64 single spectra. It is worth noting that we analysed single spherical cells in transmission mode and thus all spectra represent average intensities through the spheres.

6.3 Results

6.3.1 Algal biomass

The intense green snow reached a layer thickness of about 10 cm and the snow was very wet, whereas the red snow formed only a thin (~ 1 centimetre) layer on top of much drier snow. In terms of algae the green snow consisted primarily of small, mostly flagellated cells (Figure 6.1) with an average diameter of 11 µm and cell volume of ~ 700 μm^3 (Table 6.1). The variably reddish coloured algal cells in the red snow consisted mainly of spores with an average diameter of 17 µm and cell volume of ~ 2600 μm^3. Algal cell numbers were an order of magnitude higher in green snow ($6x10^6$ mL^{-1}) compared to red snow (2×10^5 mL^{-1}) and overall biomass was an order of magnitude higher in green snow (~450 mm^3 L^{-1}, as opposed to ~50 mm^3 L^{-1}) (Table 6.1).

.

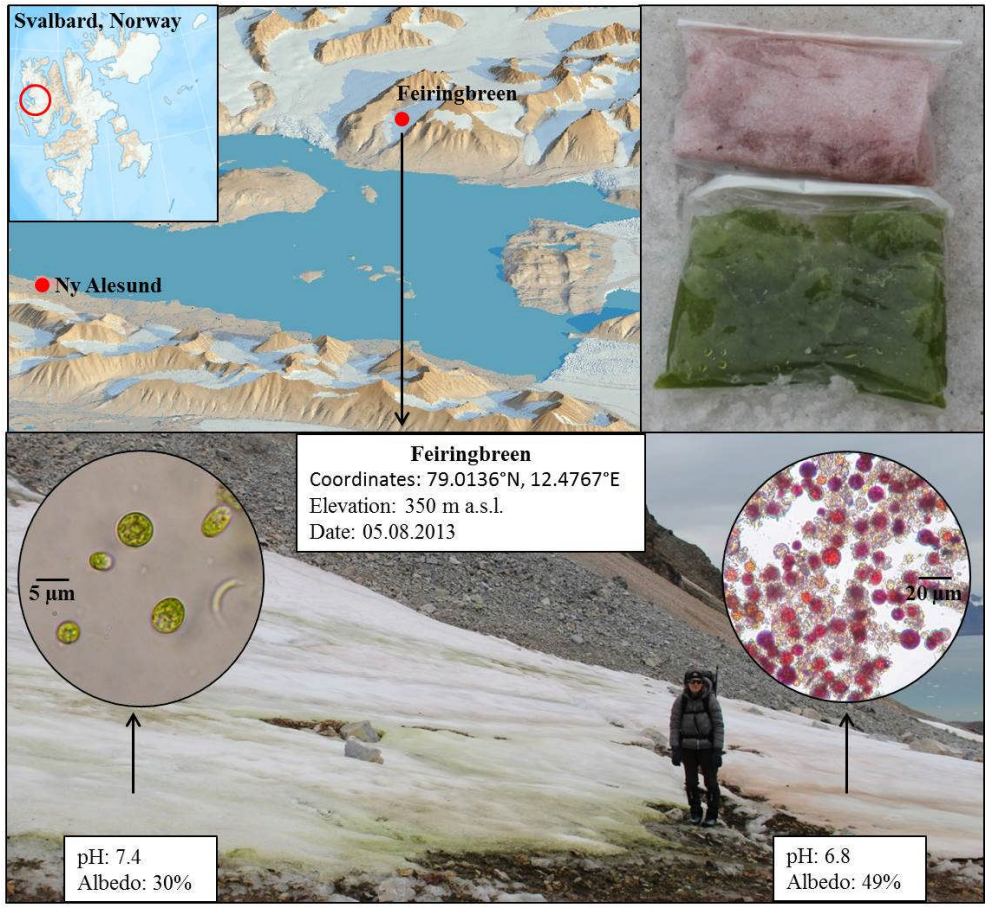

Figure 6.1: Map (top left) showing the sample location on Feiringbreen in Svalbard, bags with sampled green and red snow (top right) and image of the site with superimposed microscopic images of the snow algal cells (bottom). Shown are also coordinates and in field measured pH and albedo values for each snow type

Table 6.1: Cell counts, average cell sizes and overall biomass for green and red snow.

	Green snow	**Red snow**
Cell counts [mL^{-1}]	640,625	20,313
Average cell diameter [um]	11.2 ± 2.5	17.1 ± 2.6
Average cell volume [um^3]	697	2571
Biomass [mm^3 L^{-1}]	446	52

6.3.2 Physico-geochemical characteristics of solutions and particulates

In both red and greed snow patches the temperature (0 ˚C) and conductivity (< 2 $\mu S/cm^2$) were similar but the pH differed by ~ 0.6 pH units with a higher value in the green snow (7.4) compared to red snow (6.8).

In terms of aqueous compositions, most major (e.g., Na, K, Ca, Mn), minor (e.g., Fe, Al) and trace elements (e.g., Co, Cr, Cu, Ni) were between 1 and 3 orders of magnitude higher in concentration in green snow compared to red snow (Table 6.2). DOC and PO_4 were 10 times higher in green snow, whereas NO_3 and SO_4 were high in the green snow but below the limit of detection in red snow. Cl was the only element that was present in red but not in green snow. The concentrations of S analysed by ICP-MS match those of S-SO_4, whereas the concentrations of P (also ICP-MS) were much higher than those analysed by IC as P-PO_4 (Table 6.2).

In the particulates, the total carbon (TC) content per dry weight was similarly high in both samples (green: 35.4%, red: 33.4%) while total nitrogen (TN) was higher in green snow (6.7%, as opposed to 1.9% in red snow). This led to a C/N ratio (Table 6.3) for green snow (5.3) near the optimal Redfield ratio (6.6), whereas the ratio for red snow was much higher (17.7). The C/P ratio for red snow was also 7 times higher (754) than optimal Redfield conditions (106), while the $\delta^{13}C$ value was more negative in red snow (-29.73‰) compared to green snow (-27.67‰).

The prevailing mineralogy in both particulate samples were quartz, calcite, dolomite, chlorite and muscovite corresponding with the prevailing geological units that are surrounding Feiringbreen and that consist primarily of late Palaeozoic (mostly Carboniferous) marbles and mica shists of the Kongsfjorden group (Harland, 1997).

Table 6.2: Organic (DOC) and inorganic aqueous chemical data for green and red snow. DOC and PO4 are in µM, whereas all other compounds are in ppb.

	Green snow	**Red snow**
DOC [µM]	1192	67
PO_4^{3-} [µM]	8.63	0.53
NO_3^-	296	<
SO_4^{2-}	31421	<
Cl^-	<	277
Al	6.2	5.8
Ba	7.2	7.2
Ca	22900	2660
Cd	0.1	0.2
Co	0.8	<
Cr	0.1	<
Cu	1.1	0.2
Fe	10.6	6.3
K	5620	55
Mg	3880	390
Mn	41.0	2.6
Na	720	185
Ni	1.7	0.2
P	1050.0	<
Pb	0.2	0.1
S	11400	49
Si	160	40
Sr	26.0	2.6
Zn	1.5	2.1

NO^{3-}, SO_4^{2-} and Cl^- all determined by IC, all others analysed by ICP-MS; limit of detection (LOC,<) for IC: NO_3^- = 96 ppb, Cl^- = 72 ppb, SO_4^{2-} = 121 ppb, LOD's for ICP-MS: Al, Ba, Co, Cr, Cu, Fe, Mg, Ni, Si, Sr, Zn = 0.1 ppb; Cd, Mn, Pb = 0.01 ppb; Ca, Na = 1 ppb; K,P,S = 10 ppb.

Table 6.3: Total carbon (TC), total nitrogen (TN), total phosphorus (TP) and total sulphur (TS) (all based on % of dry weight of sample), nitrogen and carbon isotope values, and particulate C/N, C/P and N/P ratios calculated from TC, TN and TP values. n.s. = not enough sample for analyses

	Green snow	**Red snow**
Total C [%]	35.39	33.44
Total N [%]	6.73	1.89
Total P [%]	n.s.	0.04
Total S [%]	0.58	0.19
C/N	5.26	17.69
C/P	-	743.82
N/P	-	42.05
δ^{15}N ‰]	n.s.	0.73
δ^{13}C [‰]	-27.67	-29.73

6.3.3 Amplicon and metagenome sequencing

The two samples showed different algal species compositions (Figure 6.2, Table C.1). In the green snow *Microglena sp.* made up 99% of the species composition, whereas in red snow several *Chloromonas* and uncultured *Chlamydomonadaceae* species contributed to a relatively higher species diversity. The most relative abundant species were *Chloromonas nivalis* (48%), an uncultured *Chlamydomonadaceae* (labelled "*2*", 24%), *Chloromonas polyptera* (13%), *Chloromonas cf. alpina* (5%) and *Raphidonema sempervirens* (4%).

For bacteria, *Bacteriodetes* followed by *Proteobacteria* were the most relative abundant phyla in both samples, yet at the class level the bacterial communities were more markedly different (Figure 6.2, Table C.2) with green snow being dominated by *Flavobacteria* (77%), followed by *Betaproteobacteria* (10%), whereas red snow was dominated by *Saprospirae* (87%), followed by *Betaproteobacteria* (9%). It is important to note that *Saprospirae* is an obsolete class and on the family level all sequences were assigned to the *Chitinophagaceae* (Table C.2).

The archaeal species composition was made up by only one taxon in green snow, the *Nitrosophaeraceae* (100%), whereas in red snow *Nitrosophaeraceae* were most abundant (74%), followed by *Cenarchaeaeceae* (26%) (Figure 6.2, Table C.3).

There were no major differences between the two metagenomes in terms of main functional categories for the annotated genes based on KEGG Orthology (KO) (Figure C.1, Table C.4). Genes thought to be involved in carbohydrate metabolism were most abundant (green snow: 12.7%, red snow: 15.2%), followed by amino acid metabolism (green snow: 11.2%, red snow: 9.6%), and energy metabolism (green snow: 8.9%, red snow: 9.2%). Genes involved in carotenoid and fatty acid biosynthesis were below 1% in both samples.

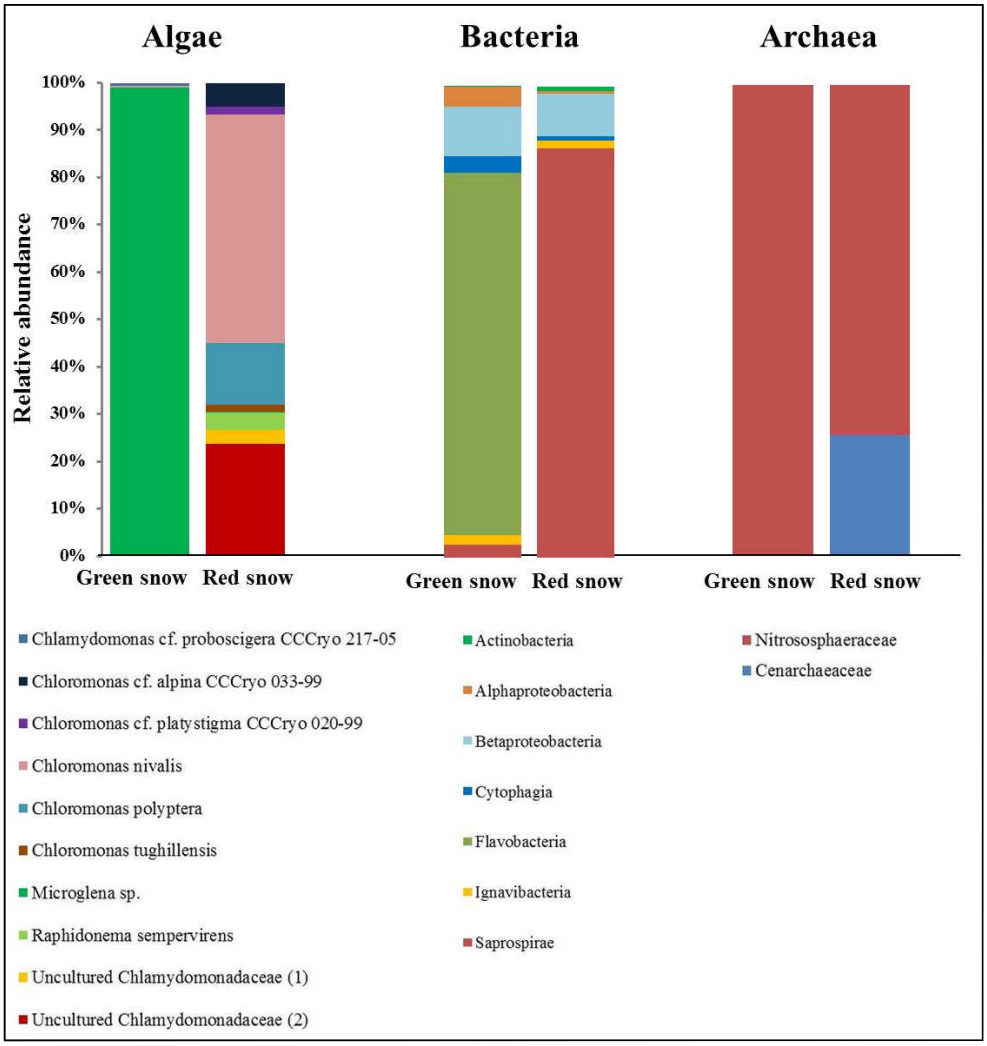

Figure 6.2: Algal (18S rRNA), bacterial (16S rRNA) and archaeal (16S rRNA) community composition of green and red snow, derived from OTU clustering at 97% similarity.

6.3.4 Non-targeted metabolome data

29 mass numbers (*m/z* values) were assigned putative identities and pathways, leading to the identification of 85% of all metabolites in red snow and 56% in green snow (Table 6.4, Figure 6.3). Among these *m/z* 364, corresponds to 5-formamido-1-(5-phospho-D-ribosyl)-imidazole-4-carboxamide, which is a key intermediate compound in several plant secondary metabolite biosynthesis pathways. This compound made up 23.6% of the metabolites in the green snow and was the dominant compound in the red snow (61.2%). Sphinganine 1-phosphate (*m/z* 380), which is part of the sphingolipid metabolic pathway, was the second most relative abundant metabolite in red snow (12.9%), but less represented in green snow (4.5%). Orotidylic acid (*m/z* 365), involved in various metabolic pathways including the uridine monophosphate biosynthesis within the pyrimidine metabolism (Figure C.2), was the third most abundant compound in red snow (3.6%), while in green snow it was just of minor abundance (1.3%) (Table 6.4). In green snow, the mass number *m/z* 276, matching 5-amino-6-D-ribitylaminouracil, a key metabolite involved in several metabolic pathways including riboflavin metabolism (5.7%) was 6 times more abundant compared to red snow (Table 6.4). Similarly, the mass numbers *m/z* 174 likely to be indole-3-acetate, also known as auxin and involved in tryptophan metabolism (9.2%), and *m/z* 202 corresponding to indole-3-pyruvate (3.5%), another tryptophan pathway metabolite (Figure C.3), were also between 2 and 11 times more abundant compared to red snow (Table 6.4).

Metabolites potentially involved in purine metabolism were highest in green (30%) and red snow (63%) (Figure 6.3, Table C.5). Compounds involved in sphingolipid metabolism were the second most abundant in red snow (13%, as opposed to 5% in green snow), whereas tryptophan metabolites were the second most abundant in green snow (13%, as opposed to 3% in red snow; Figure 6.3, Table C.5).

Table 6.4: Main metabolic compounds with mass numbers, their abundance relative to the total metabolites in green and red snow, and candidate metabolites and pathways corresponding to the mass numbers. Underlined candidate metabolites have previously been identified in *Chlamydomonas reinhardtii*.

Mass number (m/z)	Green snow [%]	Red snow [%]	Candidate metabolite	Pathway
114	0.63	0.60	fumarate	purine metabolism
135	1.94	0.09	adenine	purine metabolism
139	0.01	0	carbamyl-phosphate	pyrimidine metabolism
155	0.06	0.03	orotate	pyrimidine metabolism
157	0.07	0.01	dihydro-L-orotate or (S)-dihyrdoorotate	pyrimidine metabolism
159	0.01	<0.01	indole-acetaldehyde	tryptophan metabolism
174	9.18	0.78	indole-3-acetate (auxin)	tryptophan metabolism
175	0.21	0.02	diphosphate	tryptophan and pyrimidine metabolism
180	0	0.01	keto-D-fructose or β-D-fructofuranose	mannitol cycle
182	0.13	0.03	D-sorbitol or D-mannitol	sorbitol biosynthesis or mannitol cycle
202	3.53	1.81	indole-3-pyruvate	tryptophan metabolism
204	0.16	0.46	tryptophan	tryptophan metabolism
246	0.67	0.93	(*RS*)-phospho-3-sulfolactate	coenzyme M biosynthesis I
258	0.10	0.04	β-D-glucose 6-phosphate or β-D-fructofuranose 6-phsosphate	various
260	0.32	0.78	D-mannitol 1-phosphate	mannitol cycle
267	3.84	0.32	adenosine	purine metabolism
276	5.70	0.93	5-amino-6-(D-ribitylamino)uracil	various
322	0	<0.01	uridine-5'-monophosphate	pyrimidine metabolism
336	0	0.01	fructose 1,6-bisphosphate	various
361	0	0.49	guanosine 5'-phosphate	purine metabolism
364	23.57	61.25	5-formamido-1-(5-phospho-D-ribosyl)-imidazole-4-carboxamide	purine metabolism
365	1.34	3.59	orotidine 5'-phosphate (orotidylic acid)	pyrimidine metabolism
380	4.52	12.87	Sphinganine 1-phosphate	sphingolipid metabolism
385	0	<0.01	5-phospho-α-D-ribose 1-diphosphate	pyrimidine and purine metabolism,
440	0.01	0.02	guanosine-diphosphate	purine metabolism
not identified	43.94	14.94		

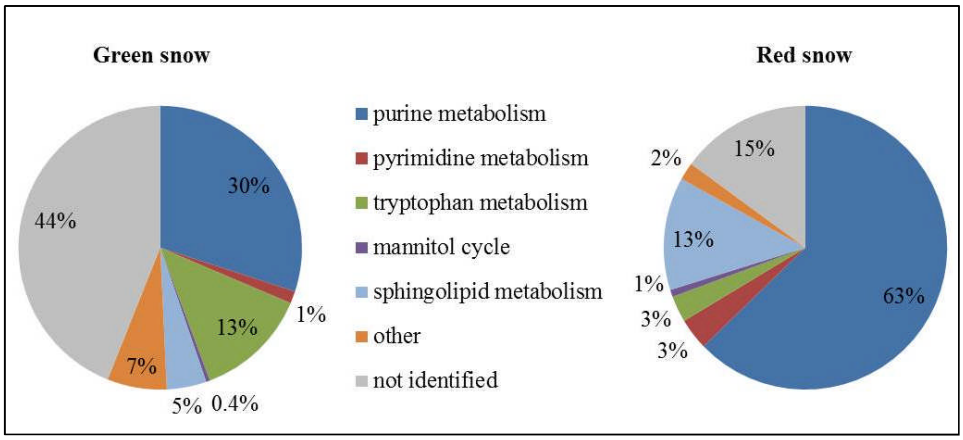

Figure 6.3: Pie charts showing metabolomics data grouped into main metabolic pathways in green and red snow.

6.3.5 Targeted bulk metabolites

Chlorophylls were the most abundant pigments in green snow (71%), followed by primary carotenoids (27%), and only traces of secondary carotenoids (5%). In contrast, the pigment composition in red snow was dominated by secondary carotenoids (92%), with only traces of chlorophylls (4%) and primary carotenoids (4%) (Table 6.5).

Saturated fatty acids (SFA) identified were mainly C16:0 and traces of C18:0, the monounsaturated fatty acids (MUFA) C16:1 and C18:1, and the polyunsaturated fatty acids (PUFA) C16:4, C18:2, C18:3 and C18:4. In the green snow the SFAs (56%) were most abundant, followed by MUFAs (28%), and PUFAs (4%). In contrast, red snow contained a higher proportion of PUFAs (49%), and only about half as much SFAs (28%) than the green snow while the MUFAs (20%) were similar (Table 6.6).

Free carbohydrates were only abundant in high concentration in the green snow with ribose (246 µg L^{-1}), lactose (97 µg L^{-1}, fructose-sucrose (14 µg L^{-1}) and rhamnose (11 µg L^{-1}) being dominant, whereas in red snow most carbohydrate compounds were below 5 µg L^{-1} or below our detection limit (Table 6.7).

The bulk infrared spectroscopy analysis revealed an almost double proportion of proteins in green snow (39%) compared to red snow (20%), yet a slightly increased lipid content in red snow (12%) compared to green snow (7%) (Table 6.8).

Table 6.5: Pigment composition of green and red snow. Individual pigments were quantified in µg/L and also reported as total chlorophylls, total primary carotenoids and total secondary carotenoids in % of total pigments.

	Green snow	Red snow
Chlorophyll a	13372	5187
Chlorophyll b	14792	4105
Neoxanthin	1048	309
Violaxanthin	1830	632
Antheraxanthin	166	0
Lutein	6823	2004
Zeaxanthin	110	17
b-carotene	0	4768
trans-astaxanthin	0	6433
cis-astaxanthin	0	783
trans-astaxanthin mono esters	1055	148475
cis-astaxanthin mono esters	0	20088
total astaxanthin di esters	0	37322
total chlorophylls	71 %	4 %
total primary carotenoids	27 %	4 %
total secondary carotenoids	3 %	92 %

Table 6.6: Fatty acid composition of green and red snow. Fatty acid compounds are reported as percentage of total fatty acids. Individual identified fatty acids are reported as well as total saturated (SFA), total monounsaturated (MUFA) and total polyunsaturated (PUFA) fatty acids.

Compound	Green snow [%]	Red snow [%]
C14:0	0	4
C15:0	0	1
C15 branched	4	0
C16:0	53	20
C16:1	13	6
C16:3	0	3
C16:4	0	13
C18:0	3	3
C18:1	15	14
C18:2	0	7
C18:3	0	21
C18:4	4	5
SFA	56	28
MUFA	28	20
PUFA	4	49

Table 6.7: Free carbohydrate analyses, all compounds in µg L^{-1}.

	Green snow	Red snow
Fucose	<	<
Rhamnose	10.9	1.2
Arabinose	<	<
Galactose	<	2.3
Glucose	<	2.8
Xylose-Mannose	<	<
Fructose-Sucrose	13.7	2.6
Ribose	245.9	3.0
Lactose	97.0	<

Detection limits: Fucose < 0.6 µg L^{-1}, Rhamnose < 0.5 µg L^{-1}, Arabinose < 0.4 µg L^{-1}, Glucose < 0.3 µg L^{-1}, Xylose-Mannose < 0.4 µg L^{-1}, Fructose-Sucrose < 2.4 µg L^{-1}, Ribose < 0.9 µg L^{-1}, Lactose < 6.8 µg L^{-1}.

Table 6.8: Bulk functional group distribution of green and red snow. Main functional groups representing the lipids (CH_2 and CH_3 stretching modes between 3050 and 2800 cm^{-1}), proteins (amide I and II bands at 1700-1500 cm^{-1}) and carbohydrates (C-O-C, C-O-P, P-O-P ring vibrations between 1204-815 cm^{-1}) are reported as percentage of total functional groups.

	Green snow [%]	Red snow [%]
Lipids	7.21	11.41
Proteins	38.72	19.64
Carbohydrates	54.08	68.96

6.3.6 Single-cell functional groups data

From the analysed single cells using synchrotron infrared micro-spectroscopy we evaluated the protein, lipid and ester contributions in 124 spectra collected on single green cells and 324 spectra collected on single red cells (Figure 6.4, Tables 6.9 and 6.10). On average the contributions from amides I and II bands corresponding to protein vibrations dominated the spectra in each green algal cell (Figure 6.4 top spectrum), whereas ester and lipid functional groups were more abundant in single red algal cells (Figure 6.4 bottom spectrum). Ratios of proteins over lipids were on average one order of magnitude higher in green snow algal cells (5.18 ± 0.50) compared to red snow algal cells (0.52 ± 0.42) and proteins over esters were two orders of magnitude higher in green cells (290.56 ± 248.71) compared to red cells (1.76 ± 1.34).

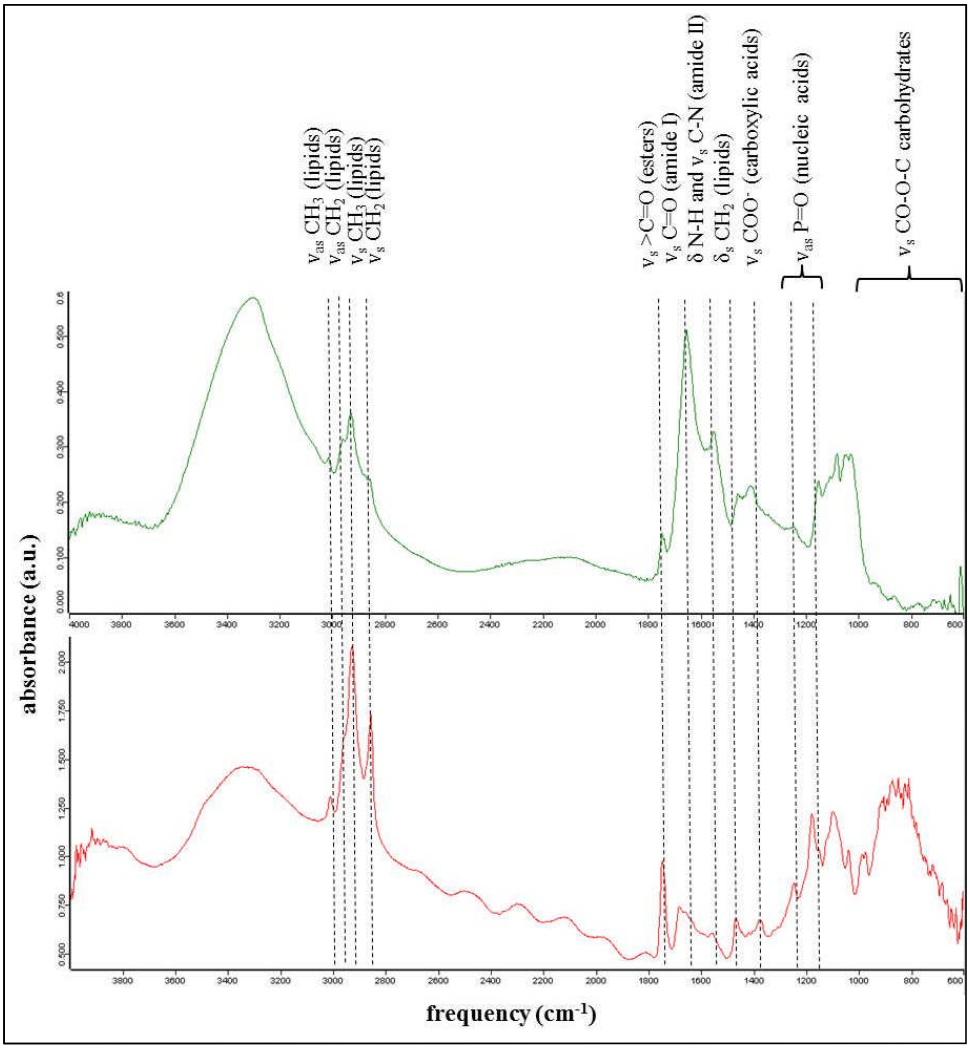

Figure 6.4: Representative synchrotron based infrared spectroscopic spectra of single cells in green (top) and red (bottom) snow. Green cells were characterized by higher amide peaks compared to red cells that showed higher lipids and ester peaks.

Table 6.9: Ratios of functional group areas corresponding to proteins (amides I and II, 1700-1500 cm^{-1}) and lipids (lipids I-IV, 3050-2800 cm^{-1}) of single cells in green and red snow derived from synchrotron radiation infrared spectroscopy. Reported are single point measurements per cell (n), average ratios per cell and standard deviation (StDev) and ranges of ratios.

	Green snow			**Red snow**		
Protein/lipids	Average ± StDev	Range	n	Average ± StDev	Range	n
Single cell 1	1.43 ± 0.30	0.83-3.05	64	1.07 ± 0.40	0.58-2.46	30
Single cell 2	6.42 ± 1.07	5.20-9.20	36	0.08 ± 0.05	0.02-0.18	25
Single cell 3	8.74 ± 1.40	6.73-11.27	12	0.06 ± 0.02	0.01-0.09	16
Single cell 4	4.12 ± 0.56	3.40-5.19	12	0.28 ± 0.12	0.09-0.48	16
Single cell 5				1.18 ± 0.69	0.43-2.58	25
Single cell 6				0.25 ± 0.09	0.11-0.44	25
Single cell 7				0.35 ± 0.16	0.00-0.74	30
Single cell 8				1.07 ± 0.70	0.06-2.20	16
Single cell 9				0.24 ± 0.09	0.12-0.43	16
Single cell 10				0.40 ± 0.15	0.23-0.85	25
Single cell 11				0.94 ± 1.03	0.00-0.56	64
Single cell 12				0.33 ± 0.36	0.00-1.72	36
Average	5.18 ± 0.50			0.52 ± 0.42		

Table 6.10: Ratios of functional groups areas corresponding to proteins (amides I and II, 1700-1500 cm^{-1}) and esters (1850-1700 cm^{-1}) of single cells in green and red snow derived from synchrotron radiation infrared spectroscopy. Reported are single point measurements per cell (n), average ratios per cell and standard deviation (StDev) and ranges of ratios.

	Green snow			**Red snow**		
Protein/esters	Average ± StDev	Range	n	Average ± StDev	Range	n
Single cell 1	93.73 ± 49.86	52.24-374.18	64	3.29 ± 0.90	2.01-6.57	30
Single cell 2	202.36 ± 205.97	85.36-1097.82	36	0.39 ± 0.18	0.09-0.81	25
Single cell 3	211.23 ± 124.00	89.74-499.58	12	0.36 ± 0.10	0.08-0.46	16
Single cell 4	654.92 ± 733.23	162.37-2193.09	12	0.28 ± 0.12	0.61-3.13	16
Single cell 5				1.69 ± 0.91	0.09-0.48	25
Single cell 6				1.40 ± 0.61	0.49-2.59	25
Single cell 7				4.63 ± 3.94	0.04-13.36	30
Single cell 8				1.07 ± 0.70	0.06-2.20	16
Single cell 9				1.24 ± 0.57	0.61-2.53	16
Single cell 10				2.21 ± 0.47	1.31-3.07	25
Single cell 11				3.15 ± 3.14	0.00- 14.41	64
Single cell 12				1.44 ± 1.27	0.00-4.60	36
Average	290.56 ± 248.71			1.76 ± 1.34		

6.4 Discussion

Despite being localized in close proximity to each other, the two adjacent green and red snow fields described above showed large differences in their physico-chemical environment, their community composition and their metabolic profiles.

6.4.1 Physico-chemical environment

Green snow communities are less abundant than red snow communities and have mainly been reported as calcitroph and eurytroph (Kol, 1968) and in favour of relatively high liquid water contents (Fogg, 1967), conditions that are less common for typical snow fields. Such circumstances are usually only found at snow-rock margins (e.g. cliffs) that are often colonized by bird populations, which was also the case in our sampling site on Feiringbreen. The bird rookeries were also evidenced by the much higher nutrient contents (Table 6.2) in the green snow, which was overlaying slightly alkaline carboniferous bedrocks (Figure 6.1).

Previous studies have found a link between pH and snow colouration and this was inferred to be a consequence of the fact that chlorophylls are preferentially synthesised at a higher pH, whereas astaxanthin, the main secondary carotenoid in red snow algae, is favoured at lower pH (5.5-6.0) (Czygan, 1970). Similarly, Remias et al. (2013) found green snow in Antarctica with a pH of ~7.5 and asserted that this was heavily influenced by guano and that the colouration of the snow reached deeper. The green snow in the current study had a higher pH (7.4) than the red snow (6.8) (Figure 6.1), which could be a consequence of carbonate rock buffering through the surrounding bedrocks on which the green snow was found. However, the differing pH could also be the consequence of snow algal activity rather than the cause for their abundance. Such variations in pH could derive from different stages in the snow algal life cycles and their metabolic activities leading to a change in their surrounding environment because the chlorophyll-rich green snow would lead to a net removal of CO_2 through its photosynthetic activity, and thus an increase in pH. This would also match the assertion of Hoham and Duval (2001) who inferred a relationship between pH and the metabolic state of the snow algal life cycle.

The proximity of the sampled site to a cliff with bird colonies and the high water content likely explains the higher DOC and nutrient concentrations in the green snow (Table 6.2). However, the high Ca, K, and Mg concentrations in green snow (Table 6.2) suggest that not all nutrients are derived from bird droppings but that a large proportion likely stem from the dissolution of carbonate or sulfate minerals in the underlying bedrock. This also explains the high SO_4^{2-} concentration in green snow derived most likely from dissolution of gypsum, which is a common mineral or cement in Kongsfjorden rocks (Dineley, 1958) although a contribution from bird droppings reflecting a marine food source could also be the cause. The high nutrient concentrations likely induced competition among species leading to a dominance of the green snow community. The mass bloom of green snow algal cells in a high nutrient environment caused a dramatic decrease in surface albedo (30%, Figure 6.1) and therefore increased the heat retention on the snow surface leading to enhanced melting which further increases the liquid water content. In turn, this may have contributed to higher nutrient concentrations as this may aid mineral or bird dropping dissolution.

The discrepancy between the high concentration of total P and $P\text{-}PO_4$ in green snow suggests a high content of another P species, which is likely to be dissolved organic phosphorus. The high Cl content in red snow but its absence in green snow indicates that the red snow surface layer was affected more or for a longer time by atmospheric inputs (i.e., sea spray) and less so by water-rock interactions with the bedrocks. This matches our observations that the thin layers with red snow algae were not found in contact with the bedrock and the underlying snow was ‘fresher’ i.e., had a shorter deposition residence and metamorphosis time compared to the much wetter green snow.

The high liquid water content in green snow is likely to also act as a protective film against high irradiation. The green flagellates have no thick protective cell walls and are thus much more fragile and sensitive to excessive irradiation. Biflagellates of *Chlamydomonas nivalis* in lab studies have shown to be dramatically affected by UV-B irradiation and showed a high impairment of mobility (Häder & Häder, 1989). UV radiation also inhibits photosynthesis of green snow (*Chloromonas sp.*) by about 85%, compare to an only 25% reduction in red snow (*Chlamydomonas nivalis*) (Thomas & Duval, 1995).

All these factors discussed above suggest that the green and red snow are two independent and not successive phenomena differing in their community composition and life stages. This is also underpinned by the fact that the red snow was much drier and the wet green snow is unlikely to become drier.

The physico-chemical factors including liquid water content, pH and nutrient availability have feedbacks with the snow algae, they likely determine the distribution of the snow algae, yet in turn the snow algae themselves also alter these physical and chemical characteristics after the successful colonisation of the snow. The question remains however if snow algae at a mature red spore stage have a higher selection advantage than for example the green algal cells lacking this stage. This may be the case according to an investigation by Remias et al. (2010a), who reported that flagellated *Chloromonas nivalis* cells can be found only for a short period of time (and thus most likely are often missed in snow algal studies) because these type of cells have only a very short reproductive phase before they enter the process of spore formation. It is thus not surprizing that green snow caused by reproductive cells is often overlooked, because optimal conditions with excess nutrients in snow are not easily maintained, making green snow a rarer and very short-lived phenomenon in nature. This is likely because green flagellated cells are more sensitive to fast changing physico-chemical factors (e.g., water content, pH, nutrients, irradiation) during a melt season. In contrast, the red snow algal spores can cope better with excessive irradiation, desiccation, freeze-thaw cycles and low nutrient concentrations. This may imply that red snow algae cells may be better adapted to long-term colonisation of snow habitats potentially giving them a selective advantage within such dynamic environments, yet to fully elucidate the underpinning mechanisms behind these advantages, more in depth and time-resolved studies in the field are necessary.

6.4.2 Community composition

The green and red snow were also markedly different in their microbial community compositions (Figure 6.2). Green snow was dominated by the snow algae *Microglena sp.* (Figure 6.2, Table C.1), which is likely a polar sub-clade of *Chlamydomonas*. The genus *Microglena* has undergone recent revisions (Demchenko et al., 2012) and shows strong adaptations to low temperatures (Leya,

2013). This species seems to thrive in high-nutrient environments with some shading from solar irradiation based on feedbacks with albedo and water content.

In contrast, the red snow from our sampling site was primarily represented through several *Chloromonas* species and two uncultured *Chlamydomonadaceae* species (Figure 6.2, Table C.1). Both the *Chloromonas* and *Chlamydomonadaceae* species are typical colonisers of red snow (Hoham and Duval, 2001; Leya et al., 2004; Remias et al., 2010b; Remias et al., 2013; Lutz et al., 2015b). These two uncultured *Chlamydomonadaceae* show the highest sequence similarity with other *Chloromonas* species (Lutz et al., 2015a). Despite being well adapted to harsh conditions, they were not abundant in green snow. One explanation could be the more mature life stage. This disfavours fast cell proliferation and may constitute a selective disadvantage compared to *Microglena*, which developed a high biomass in green snow and which may represent a species with a short life span without spore formation. Red snow algal species (*Chloromonas*) seem to be more oligotrophic K-strategists, whereas the green algae *Microglena* represents an r-strategist typical of nutrient rich environments.

In addition, the high algal biomass in both snow patches likely influenced the bacterial community. Although bacterial abundance was not quantified in our study, previous studies have found that bacterial numbers were on average one order of magnitude higher in red snow compared to snow with no visible algal communities colonizing them. Red snow has also been shown to have an at least ten times higher bacterial production rate suggesting a direct transfer of organic carbon from algae to bacteria, fixed through photosynthesis (Thomas and Duval, 1995). *Bacteriodetes* (e.g., *Flavobacterium*) and *Proteobacteria* (e.g., *Polaromonas*, *Rhodoferax*, *Janthinobacterium*), which were most abundant in both studied snow samples (Figure 6.2, Table C.2) are commonly found in Arctic snow (Harding et al., 2011; Møller et al., 2013), and are able to rapidly exploit organic matter (Riemann and Winding, 2001; Abell and Bowman, 2005). *Bacteriodetes* are known to be able to degrade complex organic structure and are often associated with environments of high organic content (Battin et al., 2001; Kirchman, 2002; Thomas et al., 2011). Among the *Bacteriodetes*, the *Flavobacteria* that were most abundant in green snow are often associated with freshwater phytoplankton blooms (Eiler and Bertilsson, 2004; Kolmonen et al., 2004; Eiler and Bertilsson, 2007). *Flavobacterium*, as well as *Saprospira*, that were most abundant in red snow, are also known to be microalgal pathogens (Afi et al., 1996; Salomon and Imai, 2006;

Gachon et al., 2010), which may underpin a potential direct transfer of organic carbon from algae to bacteria.

The archaeal community in both samples was made up by *Nitrosophaeraceae* and *Cenarchaeaceae* (Figure 6.2, Table C.3), which are both known to be important ammonia-oxidizers (Tourna et al., 2011; Zarsky et al., 2013; Stieglmeier et al., 2014), but from our data no further conclusions could be drawn about them.

Although there were large differences in the algal and bacterial community composition between the green and red snow samples, the metagenomes of the two samples revealed few differences in main gene families (Table C.4, Figure C.1) implying that the same functions are covered by different species. However, small differences may not have been revealed due to the limited sequencing depth (Table C.6).

6.4.3 Metabolic profiles

Snow algal cells in the green and red snow analysed in this study were not only different in terms of their community composition, but also in their metabolic profiles (Tables 6.4 and C.5, Figure 6.3). The green snow metabolic profile is more diverse than that of the red snow and is characterized by a more varied complement of metabolites. A large proportion of the green snow metabolites, which are likely predominantly derived from *Microglena*, could not be assigned putative identities. This is in accordance with Bundy et al. (2009), who reported that most environmental metabolic studies fail to identify a large proportion of metabolites. The variation in the metabolic profiles between the two snow samples also likely reflects the different stages in the respective life cycles at which the microbial communities inhabiting the green and red snow were sampled. It is noteworthy that *Microglena* has not been shown to inherit a resting spore stage, whereas this is the case for the *Chloromonas* species that were abundant in red snow (Hoham & Duval, 2001; Remias, 2012).

Nevertheless, metabolites found in the green snow, involved in the tryptophan degradation pathway (e.g., indole-3-pyruvate, indole-3-acetate) were 10 times more abundant compared to red snow (Table 6.4, Figure C.3). The tryptophan degradation pathway results in the production of indole-3-acetate (IAA), otherwise known as auxin. This well-characterized plant hormone has long been known to

enhance growth of green algae such as *Chlorella pyrenoidosa* (Ahmad & Winter, 1968) and the high content of this metabolite supports the hypothesis that the algae in the green snow samples were in a growth stage of development. Alongside IAA, we also observed high concentrations of the pentose sugar ribose and lactose in our green snow samples (Table 6.7). Ribose is a monosaccharide that forms a constituent part of a variety of molecules involved in proliferation (e.g., ATP, RNA), while lactose is a disaccharide that is derived from galactose and glucose with the latter being synthesised during photosynthesis and so is again, indicative of growth and proliferation. Other metabolites that showed higher relative abundance in green snow were adenine and adenosine (mass numbers 135 and 267, Table 6.4), which are known to have an antioxidative, DNA-protective and anti-inflammatory effect on nucleosides (da Rocha Lapa et al., 2012; Hartmann et al., 2015). Overall, the most discriminatory metabolites in the green snow sample suggest a general pattern of growth and proliferation, with intermediates of major biosynthetic pathways for key growth-modulating compounds being particularly abundant (Tables 6.4 and C.5, Figure 6.3).

In the red snow metabolic profiles, we found a high abundance of compounds putatively identified to be involved in purine metabolism (63 %, Tables 6.4 and C.5), which is crucial in the synthesis of the nucleotides guanine and adenine (inosine monophosphate biosynthesis pathway; Table 6.4). Similarly, orotidine 5'-phosphate (Figure C.2), and sphinganine 1-phosphate were both also upregulated in red snow compared to green snow (Table 6.4). Sphinganine 1-phosphate is part of the sphingolipid metabolism, which synthesizes sphingolipids that are believed to inherit a variety of functions including hardening of cell surfaces to protect cells from the harmful environment (Sperling and Heinz, 2003). The upregulation of orotidine 5'-phosphate, which is part of the uridine monophosphate biosynthesis pathway (pyrimidine metabolism) may suggest that red snow algal spores were synthesising ribonucleotides, possibly as storage compounds for overwintering. In this way, there would be a ready source of nitrogen for remobilization (Werner & Witte, 2011) in the spring to facilitate algal proliferation. There are other potential explanations for these observations, such as exposure to RNA-degrading UV radiation or another extreme abiotic condition, however these do not account for the extreme difference in metabolic strategies between red and green snow samples given their close proximity within the field. It may be that the synthesis of

ribonucleotides is associated with increased protein synthesis cells which may also facilitate algal overwintering.

Overall, for psychrotrophic bacteria it has been suggested that a rapid protein turnover, involving upregulation of RNA synthesis and therefore UMP compounds, and the mobilisation/degradation of amino acids during synthesis of new proteins could be an energy-saving mechanism, particularly in low-nutrient environments like the red snow setting (Margesin & Schinner, 1994). Since red snow algal spores do not proliferate during this stage of their life cycle (Remias et al., 2013), energy can be invested in the accumulation of reserve metabolites to face impending severe conditions. This may involve becoming stranded on bare rock or ice after snow melt, which may be associated with higher temperatures, or desiccation stress or burial in deeper snow over winter with freezing and desiccation stress.

The red snow algae cells are nonetheless still photosynthetically active (Thomas & Duval, 1995), and thus they still require protection of their photosystem. This is mainly achieved through the secondary carotenoid synthesis, which made up 92% of the cells pigment content (as opposed to 3% in green snow, Table 6.5). In the red snow sample, the dominant secondary carotenoid astaxanthin was mainly mono- but also di-esterified with fatty acids, thus more lipophilic likely allowing membrane functioning at low temperatures (Remias et al., 2010b). In contrast, in green snow the pigments were mainly chlorophylls and primary carotenoids including violaxanthin, antheraxanthin and zexanthin. These are all part of the xanthophyll cycle, which deviates excessive irradiation via removal of epoxy groups (Demmig-Adams & Adams, 1996). During light stress violaxanthin is converted into antheraxanthin and zeaxanthin (Goss & Jakob, 2010). The higher amount of the epoxidised xanthophyll violaxanthin compared to antheraxanthin and zeaxanthin in the green snow sample suggests relatively lower light stress levels. This could be because of the protective liquid water layer (as discussed above), a rather recent development of this snow algal bloom and hence less exposure to solar irradiation, or the deeper penetration of the snow and therefore a shading effect. In contrast, the drier red snow contained negligible amounts (4 %) of primary carotenoids, and the high content of the secondary carotenoid astaxanthin (Table 6.5) indicates a different light stress response (Lemoine & Schoefs, 2010).

The link between the development of pigments and fatty acids is exemplified in the fact that the polyunsaturated fatty acids (PUFA) were most abundant in red snow, in particular C16:3, C16:4, C18:2 and C18:3, whereas in green snow they were absent (Table 6.6). This matches with the findings of Spijkerman et al (2012) who reported the same fatty acid compounds in red snow algae from western Svalbard and Řezanka et al. (2008) who found that PUFAs accounted for 75% of total fatty acids in *Chloromonas brevisipina* collected from a snow field in the Czech Republic. Fatty acid composition can be affected by temperature, nutrient concentrations and solar radiation (Piorreck et al., 1984). We have recently shown a positive correlation for the abundance of PUFAs, secondary carotenoids and nutrient limitation in red snow algal spores (Lutz et al., 2015b) and this is also well known for other green algae like *Haematococcus pluvialis* when exposed to light or nutrient stress (Lemoine & Schoefs, 2010). The high nutrient availability and the water film that led to lower light stress in the green snow in this study are likely the reason for the absence of polyunsaturated fatty acids but a high abundance of saturated fatty acids.

In contrast, nutrients were limited in red snow and the low dissolved nitrate and phosphate concentrations were also reflected in the high particulate C/N and C/P ratios (Table 6.3). Under nitrogen and phosphorus limiting conditions, the metabolism is directed to N and P free metabolites such as lipids and carbohydrates. These were higher in red snow compared to green snow which contained a higher amount of proteins (Table 6.8). As already mentioned above, lipids are linked to carotenoids and specially astaxanthin since lipids can serve as storage molecules for lipophilic carotenoids during overwintering (Leya, 2013).

These bulk analyses have been verified also at the single cell level through the synchrotron radiation infrared analysis. In single green cells we confirmed the higher relative abundance of protein functional groups compared to the larger abundance of lipid and ester functional groups in all single red cells (Tables 6.9 and 6.10). The esters in the red cells resulted from astaxanthin being esterified with the fatty acids.

The application of multi ‘omic’ approaches, and the combination of targeted *vs.* non-targeted and bulk *vs.* single cell analyses are in still in their infancy when the samples are derived from extreme environments. Specifically, the use of metabolomics in an environmental context is a relatively new technique that

produces a huge amount of data. As such, results stemming from this type of analysis need to be interpreted with caution. However, an advantage of metabolomics is that it can be applied to all species without the knowledge of their genomes (Bundy et al., 2009) and certain metabolites may be very common among plants and algae. Here we have shown that, in combination with targeted metabolic studies, metabolomics is a powerful ecological tool and that the combination of such data with our results from other analyses allows us to be more confident in our data interpretation. Most metabolomics initiatives in recent years have focused on mammalian and in particular human metabolomes (Bundy et al., 2009), therefore more reference organisms need to be studied, under controlled laboratory conditions as well as in the field, and the identification of metabolites needs to be moved forward by targeted metabolic profiling of individual metabolic groups to unravel their functional roles.

Nevertheless, in the first comprehensive study of its kind, we showed that in an extreme natural environment where green and red snow clearly vary in their physico-chemical characteristics, their community composition and their metabolic profiles, these undeniably also reflect different stages of microbial life cycles and adaptation strategies. Our data suggests that green snow and red snow are not successive stages but two independent phenomena with different requirements to their environments. A variety of feedbacks exist between the algal communities and the physico-chemical environment they live in, including liquid water content, pH, albedo and nutrient availability. Those feedbacks are most likely bidirectional, the environment affects algal distribution and function, but the algae also actively alter their environment. The differences in metabolic profiles are explained through growth and proliferation of the algae in the green snow, whereas accumulation and storage of reserve metabolites for upcoming severe conditions in the algae making up the red snow. It is however, only through the power of combining a variety of established and new analytical approaches that we could ultimately elucidate a rather enigmatic environmental phenomena such as green and red snow algal blooms, which have an increased presence and crucial role in the fast melting polar and alpine glacial ecosystems.

Acknowledgments

The authors would like to thank A. Edwards (Aberystwyth University) for help with the DNA sequencing and A. Stockdale (University of Leeds) for the phosphorus analysis. We gratefully acknowledge D. Cameron, J. Lake and the mass spectrometry facilities at the University of Sheffield. We thank the Diamond Light Source for the provision of beamtime under grants SM9197 and SM8989 and gratefully acknowledge the beamline scientists M. Frogley, K. Wehbe and G. Cinque and our colleague Mark Hodson (University of York) for assistance with sample preparation, data acquisition and analysis at Diamond. This work was funded by a University of Leeds grant to SL and LGB as well as by UK Natural Environment Research Council grants NE/J022365/1 to LGB and NE/J02399X/1 to AMA. Financial support for SL's field and lab work through a Young Explorers grant from National Geographic and a President's Fund for Research Visits from the Society for General Microbiology are gratefully acknowledged.

References

Abell, G., and Bowman, J.P. (2005). Colonization and community dynamics of class Flavobacteria on diatom detritus in experimental mesocosms based on Southern Ocean seawater. *FEMS microbiology ecology* 53**,** 379-391.

Afi, L., Metzger, P., Largeau, C., Connan, J., Berkaloff, C., and Rousseau, B. (1996). Bacterial degradation of green microalgae: incubation of Chlorella emersonii and Chlorella vulgaris with Pseudomonas oleovorans and Flavobacterium aquatile. *Organic Geochemistry* 25**,** 117-130.

Agati, G., Azzarello, E., Pollastri, S., and Tattini, M. (2012). Flavonoids as antioxidants in plants: location and functional significance. *Plant Science* 196**,** 67-76.

Ahmad, M.R., and Winter, A. (1968). Studies on the hormonal relationships of algae in pure culture. *Planta* 81**,** 16-27.

Battin, T.J., Wille, A., Sattler, B., and Psenner, R. (2001). Phylogenetic and functional heterogeneity of sediment biofilms along environmental gradients in a glacial stream. *Applied and environmental microbiology* 67**,** 799-807.

Benning, L.G., Anesio, A.M., Lutz, S., and Tranter, M. (2014). Biological impact on Greenland's albedo. *Nature Geoscience*, 7(10), 691-691.

Benning, L.G., Phoenix, V., Yee, N., and Tobin, M. (2004). Molecular characterization of cyanobacterial silicification using synchrotron infrared micro-spectroscopy. *Geochimica et Cosmochimica Acta* 68**,** 729-741.

Bidigare, R., Ondrusek, M., Kennicutt, M., Iturriaga, R., Harvey, H., Hoham, R., and Macko, S. (1993). Evidence for a photoprotective function for secondary carotenoids of snow algae. *Journal of Phycology* 29**,** 427-434.

Bundy, J.G., Davey, M.P., and Viant, M.R. (2009). Environmental metabolomics: a critical review and future perspectives. *Metabolomics* 5**,** 3-21.

Caporaso, J.G., Kuczynski, J., Stombaugh, J., Bittinger, K., Bushman, F.D., Costello, E.K., Fierer, N., Pena, A.G., Goodrich, J.K., and Gordon, J.I. (2010). QIIME allows analysis of high-throughput community sequencing data. *Nature methods* 7**,** 335-336.

Czygan, F.-C. (1970). Blutregen und blutschnee: stickstoffmangel-zellen von Haematococcus pluvialis und Chlamydomonas nivalis. *Archiv für Mikrobiologie* 74**,** 69-76.

Da Rocha Lapa, F., Da Silva, M.D., De Almeida Cabrini, D., and Santos, A.R. (2012). Anti-inflammatory effects of purine nucleosides, adenosine and inosine, in a mouse model of pleurisy: evidence for the role of adenosine A2 receptors. *Purinergic signalling* 8**,** 693-704.

Demchenko, E., Mikhailyuk, T., Coleman, A.W., and Pröschold, T. (2012). Generic and species concepts in Microglena (previously the Chlamydomonas monadina group) revised using an integrative approach. *European Journal of Phycology* 47**,** 264-290.

Demmig-Adams, B., and Adams, W.W. (1996). The role of xanthophyll cycle carotenoids in the protection of photosynthesis. *Trends in Plant science* 1**,** 21-26.

Dineley, D. (1958). A review of the Carboniferous and Permian rocks of the west coast of Vestspitsbergen. *Norsk Geologisk Tidsskrift* 38**,** 197-217.

Duval, B., Shetty, K., and Thomas, W.H. (1999). Phenolic compounds and antioxidant properties in the snow alga Chlamydomonas nivalis after exposure to UV light. *Journal of Applied Phycology* 11**,** 559-566.

Eiler, A., and Bertilsson, S. (2004). Composition of freshwater bacterial communities associated with cyanobacterial blooms in four Swedish lakes. *Environmental microbiology* 6**,** 1228-1243.

Eiler, A., and Bertilsson, S. (2007). Flavobacteria blooms in four eutrophic lakes: linking population dynamics of freshwater bacterioplankton to resource availability. *Applied and environmental microbiology* 73**,** 3511-3518.

Field, K.J., and Lake, J.A. (2011). Environmental metabolomics links genotype to phenotype and predicts genotype abundance in wild plant populations. *Physiologia Plantarum* 142**,** 352-360.

Fogg, G. (1967). Observations on the snow algae of the South Orkney Islands. *Philosophical Transactions of the Royal Society of London B: Biological Sciences* 252**,** 279-287.

Fujii, M., Takano, Y., Kojima, H., Hoshino, T., Tanaka, R., and Fukui, M. (2010). Microbial community structure, pigment composition, and nitrogen source of red snow in Antarctica. *Microbial ecology* 59**,** 466-475.

Gachon, C.M., Sime-Ngando, T., Strittmatter, M., Chambouvet, A., and Kim, G.H. (2010). Algal diseases: spotlight on a black box. *Trends in plant science* 15**,** 633-640.

Gentz-Werner, P. (2007). *Roter Schnee: oder Die Suche nach dem färbenden Prinzip.* Berlin: Akademie Verlag.

Goss, R., and Jakob, T. (2010). Regulation and function of xanthophyll cycle-dependent photoprotection in algae. *Photosynthesis research* 106**,** 103-122.

Häder, D.-P., and Häder, M.A. (1989). Effects of solar UV-B irradiation on photomovement and motility in photosynthetic and colorless flagellates. *Environmental and experimental botany* 29**,** 273-282.

Harding, T., Jungblut, A.D., Lovejoy, C., and Vincent, W.F. (2011). Microbes in high Arctic snow and implications for the cold biosphere. *Applied and environmental microbiology* 77**,** 3234-3243.

Harland, W. (1997). The Geology of Svalbard. Geological Society Memoir 17. The Geological Society: London.

Hartmann, A., Albert, A., and Ganzera, M. (2015). Effects of elevated ultraviolet radiation on primary metabolites in selected alpine algae and cyanobacteria. *Journal of Photochemistry and Photobiology B: Biology* 149**,** 149–155.

Hoham, R., and Duval, B. (2001). Microbial ecology of snow and freshwater ice with emphasis on snow algae. Cambridge University Press: Cambridge.

Jamers, A., Blust, R., and De Coen, W. (2009). Omics in algae: paving the way for a systems biological understanding of algal stress phenomena? *Aquatic Toxicology* 92**,** 114-121.

Kent, W.J. (2002). BLAT—the BLAST-like alignment tool. *Genome Research* 12**,** 656-664.

Kirchman, D.L. (2002). The ecology of Cytophaga–Flavobacteria in aquatic environments. *FEMS microbiology ecology* 39**,** 91-100.

Kol, E. (1968). *Kryobiologie; Biologie und Limnologie des Schnees und Eises.* Stuttgart: Schweizerbart'sche Verlagsbuchhandlung.

Kolmonen, E., Sivonen, K., Rapala, J., and Haukka, K. (2004). Diversity of cyanobacteria and heterotrophic bacteria in cyanobacterial blooms in Lake Joutikas, Finland. *Aquatic Microbial Ecology* 36**,** 201-211.

Kutchan, T., and Dixon, R.A. (2005). Physiology and metabolism: Secondary metabolism: nature's chemical reservoir under deconvolution. *Current opinion in plant biology* 8**,** 227-229.

Lemoine, Y., and Schoefs, B. (2010). Secondary ketocarotenoid astaxanthin biosynthesis in algae: a multifunctional response to stress. *Photosynthesis research* 106**,** 155-177.

Leya, T. (2013). Snow algae: adaptation strategies to survive on snow and ice. *Polyextremophiles*., 401-423. Springer.

Leya, T., Müller, T., Ling, H.U., and Fuhr, G. (2004). Snow algae from north-western Spitsbergen (Svalbard). *The coastal ecosystem of Kongsfjorden, Svalbard. Synopsis of biological research performed at the Koldewey Station in the years 1991-2003***,** 46-54.

Leya, T., Rahn, A., Lütz, C., and Remias, D. (2009). Response of arctic snow and permafrost algae to high light and nitrogen stress by changes in pigment composition and applied aspects for biotechnology. *FEMS microbiology ecology* 67**,** 432-443.

Lutz, S., Anesio, A.M., Edwards, A., and Benning, L.G. (2015a). Microbial diversity on Icelandic glaciers and ice caps. *Frontiers in microbiology* 6**,** 307.

Lutz, S., Anesio, A.M., Raiswell, R., Edwards, A., Newton, R.J., Gill, F., and Benning, L.G. (2015b). Algae Melt Arctic Glaciers: The Biogeography and Function of Snow Microbiomes. *In Review with Nature Communications*.

Lutz, S., Anesio, A.M., Villar, S.E.J., and Benning, L.G. (2014). Variations of algal communities cause darkening of a Greenland glacier. *FEMS microbiology ecology* 89**,** 402-414.

Margesin, R., and Schinner, F. (1994). Properties of cold-adapted microorganisms and their potential role in biotechnology. *Journal of Biotechnology* 33**,** 1-14.

Matsuzaki, R., Kawai-Toyooka, H., Hara, Y., and Nozaki, H. (2015). Revisiting the taxonomic significance of aplanozygote morphologies of two cosmopolitan snow species of the genus Chloromonas (Volvocales, Chlorophyceae). *Phycologia* 54**,** 491-502.

Merchant, S.S., Prochnik, S.E., Vallon, O., Harris, E.H., Karpowicz, S.J., Witman, G.B., Terry, A., Salamov, A., Fritz-Laylin, L.K., and Maréchal-Drouard, L. (2007). The Chlamydomonas genome reveals the evolution of key animal and plant functions. *Science* 318**,** 245-250.

Møller, A.K., Søborg, D.A., Al-Soud, W.A., Sørensen, S.J., and Kroer, N. (2013). Bacterial community structure in High-Arctic snow and freshwater as revealed by pyrosequencing of 16S rRNA genes and cultivation. *Polar Research* 32.

Mueller, D.R., Vincent, W.F., Pollard, W.H., and Fritsen, C.H. (2001). Glacial cryoconite ecosystems: a bipolar comparison of algal communities and habitats. *Nova Hedwigia Beiheft* 123**,** 173-198.

Overy, S., Walker, H., Malone, S., Howard, T., Baxter, C., Sweetlove, L., Hill, S., and Quick, W. (2005). Application of metabolite profiling to the identification of traits in a population of tomato introgression lines. *Journal of Experimental Botany* 56**,** 287-296.

Piorreck, M., Baasch, K.-H., and Pohl, P. (1984). Biomass production, total protein, chlorophylls, lipids and fatty acids of freshwater green and blue-green algae under different nitrogen regimes. *Phytochemistry* 23**,** 207-216.

Ramel, F., Birtic, S., Cuiné, S., Triantaphylidès, C., Ravanat, J.-L., and Havaux, M. (2012). Chemical quenching of singlet oxygen by carotenoids in plants. *Plant Physiology* 158**,** 1267-1278.

Remias, D. (2012). *Cell structure and physiology of alpine snow and ice algae.* Vienna: Springer.

Remias, D., Albert, A., and Lütz, C. (2010a). Effects of realistically simulated, elevated UV irradiation on photosynthesis and pigment composition of the alpine snow alga Chlamydomonas nivalis and the arctic soil alga Tetracystis sp.(Chlorophyceae). *Photosynthetica* 48**,** 269-277.

Remias, D., Karsten, U., Lütz, C., and Leya, T. (2010b). Physiological and morphological processes in the Alpine snow alga Chloromonas nivalis (Chlorophyceae) during cyst formation. *Protoplasma* 243**,** 73-86.

Remias, D., Lütz-Meindl, U., and Lütz, C. (2005). Photosynthesis, pigments and ultrastructure of the alpine snow alga *Chlamydomonas nivalis*. *European Journal of Phycology* 40**,** 259-268.

Remias, D., and Lutz, C. (2007). Characterisation of esterified secondary carotenoids and of their isomers in green algae: a HPLC approach. *Algological Studies* 124**,** 85-94.

Remias, D., Wastian, H., Lütz, C., and Leya, T. (2013). Insights into the biology and phylogeny of Chloromonas polyptera (Chlorophyta), an alga causing orange snow in Maritime Antarctica. *Antarctic Science*, 25(05), 648-656.

Řezanka, T., Nedbalová, L., and Sigler, K. (2008). Unusual medium-chain polyunsaturated fatty acids from the snow alga Chloromonas brevispina. *Microbiological research* 163**,** 373-379.

Riemann, L., and Winding, A. (2001). Community dynamics of free-living and particle-associated bacterial assemblages during a freshwater phytoplankton bloom. *Microbial ecology* 42**,** 274-285.

Ruttenberg, K., Ogawa, N., Tamburini, F., Briggs, R., Colasacco, N., and Joyce, E. (2009). Improved, high-throughput approach for phosphorus speciation in natural sediments via the SEDEX sequential extraction method. *Limnology and Oceanography: Methods* 7**,** 319-333.

Salomon, P., and Imai, I. (2006). Pathogens of harmful microalgae. *Ecology of Harmful Algae*, 271-282. Springer.

Sperling, P., and Heinz, E. (2003). Plant sphingolipids: structural diversity, biosynthesis, first genes and functions. *Biochimica et Biophysica Acta (BBA)-Molecular and Cell Biology of Lipids* 1632**,** 1-15.

Spijkerman, E., Wacker, A., Weithoff, G., and Leya, T. (2012). Elemental and fatty acid composition of snow algae in Arctic habitats. *Frontiers in microbiology* 3, 380.

Stibal, M., Elster, J., Šabacká, M., and Kaštovská, K. (2007). Seasonal and diel changes in photosynthetic activity of the snow alga Chlamydomonas nivalis (Chlorophyceae) from Svalbard determined by pulse amplitude modulation fluorometry. *FEMS microbiology ecology* 59**,** 265-273.

Stieglmeier, M., Klingl, A., Alves, R.J., Simon, K.-M.R., Melcher, M., Leisch, N., and Schleper, C. (2014). Nitrososphaera viennensis sp. nov., an aerobic and mesophilic ammonia-oxidizing archaeon from soil and member of the archaeal phylum Thaumarchaeota. *International Journal of Systematic and Evolutionary Microbiology* 64**,** 2738-2752.

Takeuchi, N. (2002). The altitudinal distribution of snow algae on an Alaska glacier (Gulkana Glacier in the Alaska Range). *Hydrological Processes* 15**,** 3447-3459.

Thomas, F., Hehemann, J.-H., Rebuffet, E., Czjzek, M., and Michel, G. (2011). Environmental and gut bacteroidetes: the food connection. *Frontiers in microbiology* 2, 93.

Thomas, W.H., and Duval, B. (1995). Sierra Nevada, California, USA, snow algae: snow albedo changes, algal-bacterial interrelationships, and ultraviolet radiation effects. *Arctic and alpine research*, 27(4), 389-399.

Tourna, M., Stieglmeier, M., Spang, A., Könneke, M., Schintlmeister, A., Urich, T., Engel, M., Schloter, M., Wagner, M., and Richter, A. (2011). Nitrososphaera viennensis, an ammonia oxidizing archaeon from soil. *Proceedings of the National Academy of Sciences* 108**,** 8420-8425.

Viant, M.R. (2007). Metabolomics of aquatic organisms: the new'omics' on the block. *Marine Ecology Progress Series* 332**,** 301-306.

Vickers, C.E., Gershenzon, J., Lerdau, M.T., and Loreto, F. (2009). A unified mechanism of action for volatile isoprenoids in plant abiotic stress. *Nature Chemical Biology* 5**,** 283-291.

Wacker, A., and Martin-Creuzburg, D. (2007). Allocation of essential lipids in Daphnia magna during exposure to poor food quality. *Functional Ecology* 21**,** 738-747.

Werner, A.K., and Witte, C.-P. (2011). The biochemistry of nitrogen mobilization: purine ring catabolism. *Trends in plant science* 16**,** 381-387.

Yallop, M.L., Anesio, A.M., Perkins, R.G., Cook, J., Telling, J., Fagan, D., Macfarlane, J., Stibal, M., Barker, G., and Bellas, C. (2012). Photophysiology and albedo-changing potential of the ice algal community on the surface of the Greenland ice sheet. *The ISME journal*, 6(12), 2302-2313.

Yoshimura, Y., Kohshima, S., Takeuchi, N., Seko, K., and Fujita, K. (2006). Snow algae in a Himalayan ice core: new environmental markers for ice-core analyses and their correlation with summer mass balance. *Annals of Glaciology* 43**,** 148-153.

Zarsky, J.D., Stibal, M., Hodson, A., Sattler, B., Schostag, M., Hansen, L.H., Jacobsen, C.S., and Psenner, R. (2013). Large cryoconite aggregates on a Svalbard glacier support a diverse microbial community including ammonia-oxidizing archaea. *Environmental Research Letters* 8(3)**,** 035044.

Chapter 7: Algae Melt Arctic Glaciers: The Biogeography and Function of Snow Microbiomes.

Lutz, S., Anesio, A. M., Raiswell, R., Edwards, A., Newton, R.J., Gill, F. & Benning, L. G.

In review with *Nature Communications*.

Abstract

The Arctic is melting at an unprecedented rate and key drivers are changes in snow and ice albedo. Here we show that red snow, a common algal habitat blooming after the onset of melting, plays a crucial role in decreasing albedo. Our data reveal that red snow algae are cosmopolitan, and independent of location specific geochemical and mineralogical factors. The patterns for red snow algae are ubiquitous across the Arctic and their induced reduction in albedo and accelerated melting in turn increase the time and area of exposed bare ice. The uniformity in species composition, pigmentation and albedo reduction allow us to predict that over a single melt season red algae blooms can decrease the integrated snow albedo by up to 13%. In a conservative scenario this could add an additional 35 Gt/yr of melting to the Greenland Ice Sheet alone, yet such a 'bio-albedo' effect has so far not been considered in any climate models.

7.1 Introduction

Glaciers are important components of Earth's climate and hydrologic system. The Arctic is being disproportionately affected by global warming, which in turn provides a strong feedback on the climate system (Pachauri et al, 2014). One of the key parameters in the increase of glacial melt is albedo change (Box et al, 2012). The physical and chemical characteristics of snow and ice have been studied intensively; however, the field of glacial microbiology is still in its infancy. Snow and ice surfaces have been considered barren until recently, yet distinct habitats harbour species of all three domains of life (Anesio & Laybourn-Parry, 2012a). So far, most attention has been paid to cryoconite holes (Edwards et al, 2014; Hodson et al, 2008; Musilova et al, 2015; Stibal et al, 2006), which are dominated by bacteria (Anesio et al, 2009; Edwards et al, 2011). These are however only active once the long lasting snow cover has melted away and their coverage on glaciated areas usually reaches a maximum of 10 % only (Anesio et al, 2009; Anesio & Laybourn-Parry, 2012b; Hodson et al, 2008). In contrast, little is known about the diversity or function of snow algae, nor their global effect on albedo and hence glacial melting. This is despite the fact that coloured snow algal blooms have been

known since Aristotle (Gentz-Werner, 2007), and that they dominate primary production on snow and ice fields (Lutz et al, 2014; Yallop et al, 2012).

For most of the year, the largest proportion of the glacial surfaces in the Arctic is covered by snow, and permanent and seasonal snow can cover up to 35% of the entire Earth's surface (Hell et al, 2013). We have recently shown that on a single glacier snow algae are critical players in snow habitats and the dominating biomass immediately after the onset of melting (Lutz et al, 2014). Snow algae are prolific primary colonisers and producers that can form extensive blooms in spring and summer. Such snow algal blooms can substantially darken the surface of glaciers due to their red pigmentation (secondary carotenoids), which the algae produce as a protection mechanism (e.g., from high levels of irradiation; Remias et al, 2005). We have shown that on an individual glacier in Greenland this phenomenon, known as 'red snow', can reduce the surface albedo locally by up to 20%, which in turn further increases melting rates of snow (Lutz et al, 2014). Previous studies have been unable to generalise this effect due to a lack of information on the distribution and controls on red snow ecology and physiology. These algal studies have so far focussed on describing algae primarily through classical microbiological approaches (e.g., microscopy; Hoham & Duval, 2001; Leya et al, 2004; Takeuchi, 2002) In contrast, in the current study, we have employed high-throughput sequencing to characterize these cryophilic micro-eukaryotes and their associated microbiota, *i.e.*, bacteria and archaea. We evaluated the diversity and functionality of the red snow algal habitat in four geographically well-separated glacial systems across the Arctic comprising of 40 red snow sites on 16 glaciers and snow fields. This way, we have produced the first large scale biogeographical data-set for red snow algae. Knowledge of the global distribution of species and their underlying spatial patterns and processes (*i.e.*, their biogeography) has long been assumed irrelevant for microbial communities. However, recently documented rapid changes in diversity across many ecosystems have led to an increased focus on biogeographical patterns and traits in microorganisms (King et al, 2010; O'Malley, 2007; Ryšánek et al, 2014). Applying universal theories to microorganisms and identifying patterns can help to better understand their ecology and functional roles within an ecosystem, and show how patterns may be altered or themselves alter processes in a changing climate. We cross-correlated the genomic data with geochemical and metabolic measurements and used these parameters to evaluate the environmental forcing factors on microbial community composition

Furthermore, recent snow-albedo models for Greenland (Dumont et al, 2014) suggest that melting accelerates largely due to increased contributions from light-absorbing impurities, with impurities being primarily considered to be anthropogenic or forest fire derived black carbon or Saharan or pro-glacial mineral dust (Doherty et al, 2010; Dumont et al, 2014). However, the contribution of coloured algae to changing albedo and melt rates has not previously been considered (Benning et al, 2014). Therefore, based on our albedo measurements and using a one dimensional moving boundary model, we have calculated the reduction of albedo caused by microbial darkening of glacial surfaces (inferring higher melting rates). This will help improve our understanding of the response of glacial systems to a warming climate.

7.2 Results and Discussion

7.2.1 Cosmopolitan algae but local bacteria

We have assessed the biogeographical patterns for red snow microbiomes across the Arctic and characterised the species composition of red snow in four well-separated and physico-chemically diverse Arctic settings: Svalbard (n=12), Northern Sweden (n=16), Greenland (n=2) and Iceland (n=2). These localities were chosen as they represent different geographical settings including low (67.9˚N) *vs.* high (78.9N) latitude, low (150-400m) *vs.* high (~1200-1400m) elevation, and maritime *vs.* continental settings (Figure 7.1; Table D.1 for full details).

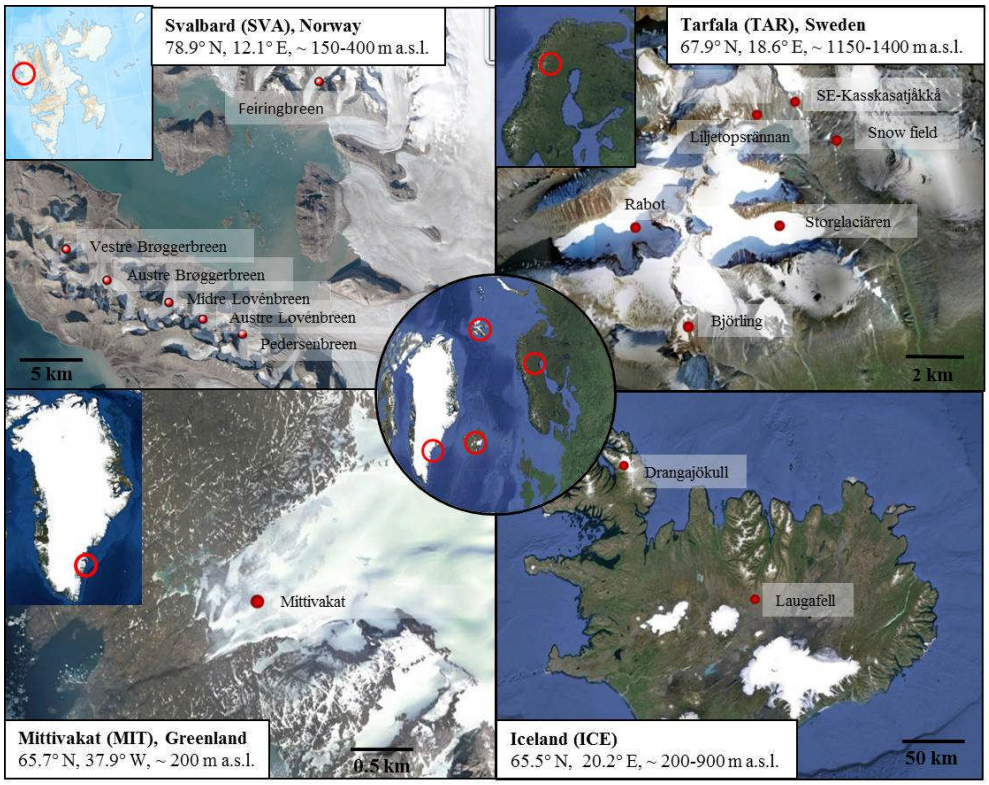

Figure 7.1: Locations of the 16 glaciers and snow fields across the Arctic where 40 sites of red snow were sampled. Red dots represent sampling sites and several sampling events within one site (full details see Table D.1).

In accordance with recent studies of other habitats (e.g., soil, marine; Foissner, 2006; Green & Bohannan, 2006; Martiny et al, 2006), our data show that the bacteria in our red snow samples inherited a strong geographical separation despite their small cell size and therefore high potential for universal distribution. Bacteria were mostly represented by the phyla *Bacteriodetes*, *Proteobacteria* and *Cyanobacteria* (Table D.2). These bacterial phyla have previously been described in snow environments (Cameron et al, 2014; Hell et al, 2013; Larose et al, 2010). However, we found significant differences ($p<0.05$) between locations for the major classes within these phyla (Table 7.1). Samples clustered according to their geographic location (Figure 7.2 A) and the observed differences were derived from large variations in the relative abundance of *Sphingobacteria*, *Saprospirae*, *Alphaproteobacteria*, *Betaproteobacteria* and *Synechococcophycideae*. Among these *Saprospirae*, *Cytophagia*, *Betaproteobacteria* and *Synechococcophycideae* were dominant in Svalbard, *Sphingobacteria* in Northern Sweden, *Sphingobacteria* and *Saprospirae* in Greenland, and *Saprospirae*, *Betaproteobacteria* and *Alphaproteobacteria* in Iceland (Figure 7.2 B; Table D.2).

In contrast, these biogeographic patterns were not observed for the snow algae. Our results demonstrate that the red snow algal community composition and their relative abundance in all studied Arctic sites was highly similar (Figure 7.2 C, D), despite the large distances, physico-chemical characteristics and associated bacterial composition differences between sites. We show that the snow algae are cosmopolitan, which is in contrast to recent molecular studies which suggest that in other terrestrial habitats, and even within a specific habitat, micro-eukaryotes show strong biogeography (Foissner, 2006; Green & Bohannan, 2006; Martiny et al, 2006; Ryšánek et al, 2014). Our data reveal a very low algal diversity. Six taxa make up >99% of the algal communities (Figure 7.2 C, D, Table 7.1 and Table D.4) and all have similar relative abundance values across all samples. The unucultured *Chlamydomonadaceae* (a) was the most abundant species (39-75% Figure 7.2 D), followed by *Chloromonas polyptera* (10-26%), *Chloromonas nivalis* (3-13%), *Chloromonas alpina* (0-1%), the uncultured *Chlamydomonadaceae (b)* and *Raphidonema sempervirens* (1-18%). The small variance in the algal data between sites (Figure 7.2 C) was mainly caused by changes in relative abundance of the uncultured *Chlamydomonadaceae* (a), *Chloromonas polyptera* and *Raphidonema sempervirens*. However, none of the samples clustered according to locations and no significant differences were found between locations for most of the algal species. The exceptions were *Chloromonas nivalis*, which showed a higher relative abundance in samples from Greenland compared to Svalbard, and the uncultured *Chlamydomonadaceae* (a), which had a higher relative abundance in Svalbard compared to Iceland. Similarly, the archaeal community composition revealed no biogeographical patterns and was also characterized by low species diversity. In most samples the main representatives were *Crenarchaeota* with the order *Nitrososphaerales* dominating (up to 100%; Table D.5).

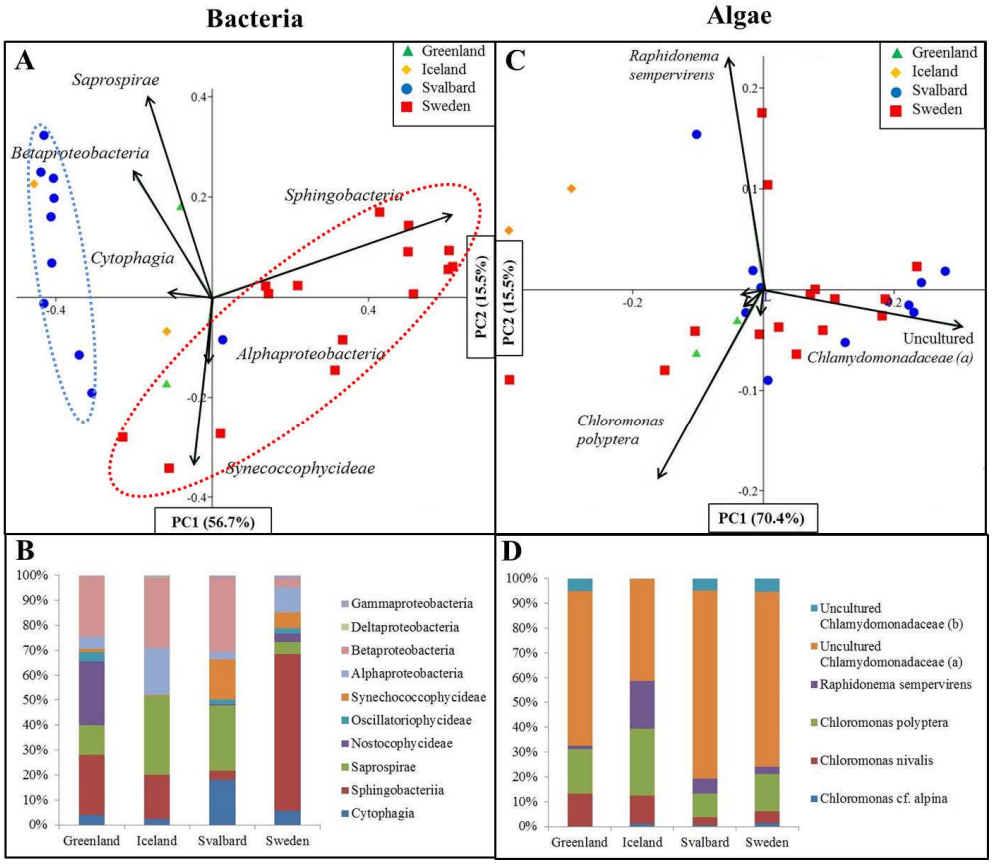

Figure 7.2: PCA of bacterial classes (left) and algal species (right) revealing taxonomic distance between sampling sites and taxa causing separation. Algal species show homogenous community composition across all sites (C), whereas bacteria cluster according to locations, even on the higher taxonomic class level (A, dotted lines have been added to help guide the reader's eye). Bar charts show average communty composition (Table D.2 and D.4 for individual values; Table 7.1 for averages) for each location and confirm similar composition for algae (D) but large differences for bacteria (B).

The homogeneous algal community composition described above was also mirrored in the similar composition of algal cell biomass, fatty acids and pigments with not significant differences between Svalbard and Northern Sweden (Figure 7.3 and Table D.7 to D.9). On average between 10^3 and 10^4 red algal cells mL^{-1} were present in our red snow samples and despite the large variations in environmental parameters, no significant differences were found for cell numbers, cell sizes or total algal biomass (Table 7.1 and Table D.7). Similarly, the fatty acid compositions in all analysed samples were similar with no statistically relevant differences between locations (Tables 7.1 and D.8). On average ~ 45-50% of all fatty acids were made up of polyunsaturated fatty acids (PUFA), while saturated fatty acids (SFA) comprised ~ 30-40% and monounsaturated fatty acids (MUFA)

were the least abundant (~ 10-15%; Figure 7.3, and D.8). The high content of PUFAs likely demonstrates their role as cryo-protectants helping algal cells maintain membrane fluidity and preventing intracellular ice crystal formation (Spijkerman et al, 2012). The production of fatty acids is often linked to pigments (Remias et al, 2005), which play the dominant role in changing the albedo. All samples were characterized by a high content of secondary carotenoids (~70-90%), which are synthesized by the snow algae as a protection mechanism from high levels of irradiation, and with no significant differences between locations. The dominant secondary carotenoid was trans-astaxanthin (Table D.9). The remainder of the analysed pigments were typical primary carotenoids (up to 24%) or chlorophylls *a* and *b* (up to 55 %; Table D.9).

The above documented high algal biomass primarily made up of highly pigmented red algae will invariably affect the amount of light that is reflected from the surface of snow fields. Our measurements (Table D.1) showed a clear decrease in surface albedo compared to algal-free snow sites (Lutz et al, 2015; Lutz et al, 2014) and the measured decrease was similar in all sites independent of the local environment with albedo values of ~0.50 - 0.70 (Table D.1)

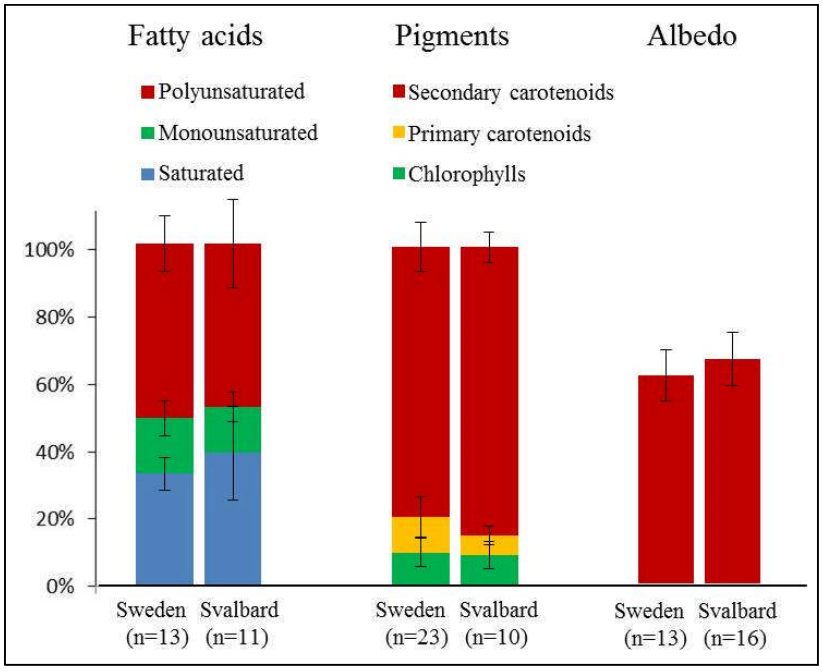

Figure 7.3: Comparison between average fatty acid and pigment compositions with average surface albedo (all in % of total) for all Svalbard and Northern Sweden sites. Error bars are standard deviations (for full details see Tables D.1, D.8, and D.9).

Table 7.1: Statistical analysis of all biological and geochemical results analysed by one-way ANOVA and post-hoc Tukey's test to reveal significant differences between the red snow samples of the sampled geographic locations Svalbard (SVA), Northern Sweden (TAR), Greenland (MIT) and Iceland (ICE). Table shows mean values for each geographic location with respective standard deviations and p-values for the overall significance of the differences between all locations as well as post-hoc pair-wise comparison between two locations (e.g., SVA x TAR). Results with p-values of <0.05 were considered to be significant and are in bold, results with p-values <0.01 were considered to be highly significant and are also underlined.

	All locations	**SVA**	**SVA x TAR**	**TAR**	**TAR x MIT**	**MIT**	**MIT x SVA**	**ICE**	**ICE x SVA**	**ICE x TAR**	**ICE x MIT**
Algae											
***Chloromonas alpina* [%]**	0.858	0.48 ± 0.64	0.870	1.22 ± 3.42	0.938	0.12 ± 0.16	0.998	0.93 ± 1.05	0.996	0.999	0.999
***Chloromonas nivalis* [%]**	**0.010**	3.07± 4.25	0.790	4.56 ± 3.80	0.057	12.99 ± 6.75	**0.022**	10.78 ± 5.81	0.100	0.220	0.952
***Chloromonas polyptera* [%]**	0.190	9.63 ± 6.24	0.601	14.47 ± 12.62	0.970	17.86 ± 7.57	0.715	25.59 ± 3.20	0.191	0.474	0.871
***Raphidonema sempervirens* [%]**	0.095	5.89 ± 11.06	0.758	2.81 ± 5.87	0.994	1.23 ± 1.74	0.878	18.32 ± 2.34	0.215	0.077	0.181
Uncultured *Chlamydomonadaceae* (a) [%]	**0.030**	74.91 ± 14.84	0.590	67.62 ± 16.06	0.961	62.12 ± 1.47	0.685	38.92 ± 6.24	**0.020**	0.075	0.426
Uncultured *Chlamydomonadaceae* (b) [%]	0.322	4.83 ± 3.44	0.998	5.09 ± 3.90	1.000	4.97 ± 0.88	1.000	0 ± 0	0.311	0.254	0.518
Bacteria											
***Bacteriodetes* [%]**											
***Sphingobacteria* [%]**	**<0.001**	3.68 ± 10.29	**<0.001**	60.20 ± 28.56	0.159	23.94 ± 13.15	0.641	9.42 ± 13.31	0.987	0.026	0.913
***Saprospirae* [%]**	**0.023**	24.31 ± 24.15	**0.020**	4.57 ± 6.77	0.933	11.62 ± 1.1	0.725	26.28 ± 3.1	0.998	0.284	0.79
***Cytophagia* [%]**	0.059	16.72 ± 15.5	0.060	5.24 ± 6.90	0.998	3.84 ± 1.4	0.430	2.74 ± 3.78	0.359	0.990	1
***Cyanobacteria* [%]**											
***Nostocophycideae*[%]**	**0.005**	0.64 ± 0.92	0.826	3.39 ± 5.73	**0.006**	25.40 ± 35.07	0.003	0.12 ± 0.17	1.000	0.949	0.021
***Oscillatoriophycideae* [%]**	0.872	1.69 ± 5.09	1.000	1.87 ± 4.00	0.948	3.67 ± 4.76	0.937	0 ± 0	0.959	0.942	0.839
***Synechococcophycideae* [%]**	0.384	15.02 ± 22.40	0.497	6.14 ± 10.04	0.976	1.24 ± 1.75	0.669	0.49 ± 0.03	0.631	0.964	1
***Proteobacteria*[%]**											
***Alphproteobacteria* [%]**	0.144	2.82 ± 3.90	0.489	9.67 ± 14.42	0.946	4.69 ± 4.92	0.997	23.73 ± 25.90	0.133	0.422	0.405
***Betaproteobacteria* [%]**	**0.002**	27.84 ± 18.48	**0.002**	3.36 ± 5.36	0.297	23.99 ± 30.17	0.987	30.57 ± 36.31	0.995	0.108	0.973

Solids (C,N,P,S)											
TC [%]	**0.007**	5.4 ± 4.4	**0.007**	12.4 ± 7.2							
TN [%]	**0.047**	0.3 ± 0.2	**0.047**	0.6 ± 0.4							
TS [%]	**<0.001**	0.12 ± 0.03	**<0.001**	0.07 ± 0.02							
TP [%]	0.153	0.07 ± 0.03	0.153	0.06 ± 0.01							
C/N [ ]	**0.009**	16 ± 3	**0.009**	21 ± 6							
C/P [ ]	**<0.001**	65 ± 31	**<0.001**	186 ± 89							
N/P [ ]	**0.001**	4 ± 2	**0.001**	8 ± 3							
$d^{15}N$ [‰]	0.582	-4.77 ± 2.41	0.582	-4.30 ± 1.84							
$d^{13}C$ [‰]	**0.033**	-27.76 ± 1.52	**0.033**	-25.70 ± 2.02							
Metabolites											
Secondary carotenoids [%]	0.722	80 ± 7	0.722	77 ± 19							
Saturated fatty acids [%]	0.218	32 ± 5	0.218	37 ± 14							
Monounsaturated fatty acids[%]	0.173	16 ± 5	0.173	13 ± 4							
Polyunsaturated fatty acids [%]	0.449	50 ± 8	0.449	46 ± 13							
Biomass											
Cell counts [mL^{-1}]	0.083	43,558 ± 50,308	0.083	12,121 ± 10,552							
Cell volume [μm^3]	0.305	2,044 ± 1,342	0.305	2,859 ± 1,381							
Biomass [$mm^3\ L^{-1}$]	0.263	35 ± 20	0.263	20 ± 15							
Aqueous											
DOC [µM]	**<0.001**	36 ± 13	**<0.001**	189 ± 90							
PO4 [uM]	0.736	0.77 ± 1.71	0.736	0.54 ± 1.08							
NO3 [ppm]	0.399	1008 ± 1986	0.414	236 ± 623	0.996	27 ± 37	0.760	**<0.001**	0.745	0.995	1
SO4 [ppm]	**0.013**	13 ± 46	0.981	17 ± 49	**0.007**	197 ± 278	**0.007**	91 ± 128	0.522	0.549	0.482
Ca [ppb]	0.121	381 ± 588	0.106	45 ± 66	1.000	19 ± 1	0.583	24 ± 3	0.595	1	1
Fe [ppb]	**<0.001**	1.9 ± 1.0	0.983	1.6 ± 1.0	0.175	5.0 ± 1.4	0.256	10 ± 10	**<0.001**	**<0.001**	0.110
K [ppb]	0.395	41 ± 20	0.583	77 ± 92	0.851	121 ± 129	0.492	41 ± 4	1.000	0.913	0.695
Mg [ppb]	0.116	125 ± 206	0.092	7 ± 4	1.000	5 ± 3	0.621	39 ± 36	0.665	1	1
Mn [ppb]	**0.008**	3.7 ± 3.9	**0.005**	0.3 ± 0.3	0.977	1 ± 0	0.470	0.7 ± 1.0	0.378	0.995	0.999

7.2.2 Local environment affects bacteria but not algae

Changes in physico-chemical conditions are known to control variations in microbial diversity in the environment (Fierer & Jackson, 2006; King et al, 2010), yet for snow settings the importance or magnitude of these effects and whether they cause any biogeographical patterning is widely unknown. In order to evaluate the variations among the four chosen geographic locations and their representativeness across the Arctic in terms of differing local snow environments, as well as possible links to varying microbial community structures, we have contrasted the concentrations of essential nutrients, carbon species and trace elements (both dissolved and solid forms; Tables D.10 and D.11).

We found significant differences between the dissolved organic carbon (DOC) and trace metal concentrations between locations (Figure D.1, Tables 7.1 and D.10). DOC was up to five times higher in snow from Northern Sweden compared to Svalbard. Similarly, concentrations of easily leachable elements (Ca, Cl, Mg, Mn, Na, and K) were on average 10 times higher in red snow from Svalbard compared to Northern Sweden (Table D.10), while in Iceland the red snow samples contained up to 100 times higher iron concentrations than any of the other localities. These differences appear to be linked to the higher concentrations of more easily dissolvable mineral phases in Svalbard compared to Northern Sweden, and the higher Fe content in basaltic rocks from Iceland compared to the other sites (Table 7.1). However, none of the essential nutrients (*i.e.*, NO_3, PO_4) showed any statistically relevant differences among locations (Tables 7.1 and D.10).

Mirroring the DOC trend, the total particulate carbon (TC) values as well as the total solid phase carbon to nitrogen (C/N) and carbon to phosphorous (C/P) ratios (Table D.11) were on average 2-3 times higher in Northern Sweden compared to Svalbard, whilst the $\delta^{13}C$ values of bulk organic matter were significantly lower in Svalbard compared to Northern Sweden. In both locations the C/N ratios were below the Redfield ratio but C/P values below Redfield were only present in samples from Northern Sweden (Table D.11). The high TC, DOC and $\delta^{13}C$ values in the snow samples from Northern Sweden likely document a higher amount of allochthonous carbon potentially derived from higher plants and the large amounts of pine pollen blown onto the glaciers and snow fields from the lower parts of the Tarfala valley. However, all red snow samples, regardless of location, were

characterised by similar, predominantly negative organic $\delta^{15}N$ values indicative of an atmospheric source (Table D.11).

We could not find potential links between algal species distribution and geochemical characteristics (Figure D.2). This suggests that the uniform algal species composition was unaffected by and independent of the rather large differences in local geochemical (Table D.10 and D.11) and mineralogical (Table D.12) parameters characterising each site.

In contrast, we found clear links between the bacterial community composition and geochemical parameters, with the most positive correlation found between the carbon species (TC and DOC; Figure D.3) and *Sphingobacteria*. This is not surprising as *Sphingobacteria* are known to be capable of degrading complex organic structures (Thomas et al, 2011) and their abundance in Northern Sweden is consistent with the local high DOC and TC values (Table D.10 and D.11). In all samples and in total contrast to the algae, the bacteria are seemingly subjected to a much higher location specific selection pressure and appeared more affected by the availability of allochthonous carbon and the local geology.

7.2.3 Algal contribution to decreased albedo

The above described ubiquitous distribution, low diversity and similarity in snow algal community compositions and metabolic functions combined with the analogous values measured for the red snow algae induced albedo reduction (Table D.1), allow us to estimate the impact that the red snow algae have on melting rates on snow-covered glacier surfaces compared to snow surfaces free of algae. At the beginning of a melting season all surfaces are covered by dry clean snow. Values for albedo for such snow have been reported in the literature (Box et al, 2012; Dumont et al, 2014; Tedesco et al, 2013) as 0.90±0.05. We compared this literature value for dry clean snow with our data for the changes in albedo with time (Table 7.2), to derive models for the season-long transition from dry clean snow to wet clean snow (0.75±0.05), and to red snow (0.65±0.12) (Table 7.3, Figure 7.4). Using these data and a 100 day melting scenario as a benchmark case we can show that the albedo has a square root dependence on time, analogous to the progress of a freezing front into a liquid (Zhang, 2008). Employing a one-dimensional moving boundary problem applied to our case (Zhang, 2008) is valid under the assumption

that the snow and ice surfaces melt downwards relative to a fixed depth, and that at the same time such a change is accompanied by changes in albedo.

Table 7.2: Values and source of average, minimum and maximum decrease in albedo for dry clean snow, wet clean snow and red snow that were used to develop the albedo model (Figure 7.4).

	Average	**Minimum**	**Maximum**	**Reference**
Dry (winter) clean snow	0.90	0.95	0.85	Dumont et al 2014
Wet clean snow	0.75	0.80	0.70	Lutz et al 2014
Red snow	0.65	0.77	0.53	Lutz et al 2014

Table 7.3: The two models used to assess the effect of red snow algae on the melt rate over a 100 day long melt season (see also Figure 7.4). Model 1 represents a purely physical reduction in albedo values (α) due to melt induced changes in snow crystals shape and size with no input from red algae. Model 2 represents the changes in albedo over the same period but due to the reduction in albedo caused by the presence and bloom of red pigmented snow algae.

	0 d	**25 d**	**50 d**	**100 d**	**Equation**
Model 1: no algae Dry clean snow → Wet clean snow	0.90	0.80	0.75	0.70	$\alpha = 0.8992 - 0.0203t^{0.5}$
Model 2: algae Dry clean snow → Red snow	0.90	0.77	0.65	0.53	$\alpha = 0.9177 - 0.0372t^{0.5}$

Our model shows that the integrated albedo change with time (100 days) is 13% higher in the presence of red algal blooms compared to clean snow that has undergone purely physical albedo change due to melting and change of snow crystal size and structure (Figure 7.4). This for the first time integrated albedo change value compares well with the local albedo of up to 20% previously measured on red algal snow sites on single glaciers or snow fields (Lutz et al, 2014; Thomas & Duval, 1995). The 13% change in integrated albedo is a conservative estimate for the effect of microbial communities during an entire melt season

because with further melting dirty ice and cryoconites will ultimately be exposed, and their albedo values can drop by an additional ~20 % to 0.34±0.15, yet their exposure time is shorter compared to the snow covered period (Lutz et al, 2014).

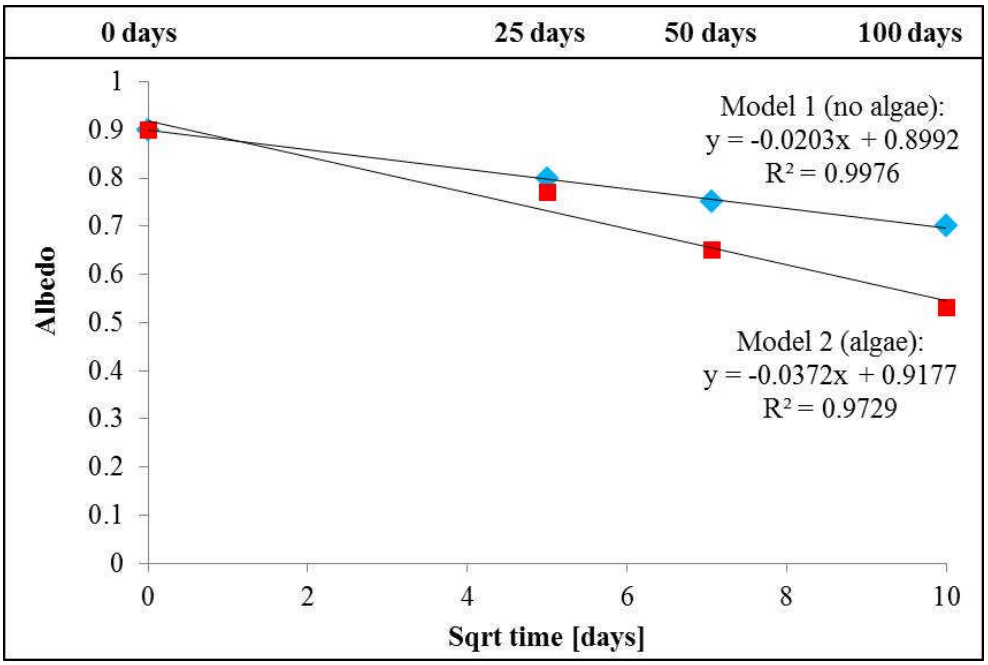

Figure 7.4: Output from the used one dimensional moving boundary model with the derived equations for the changes in albedo over 100 days of melting due to purely physical changes (blue diamonds) and due to the blooming of the red pigmented algae (red squares). For the origin of the used albedo data as well as the values used in our models see Tables 7.2 and 7.3.

To evaluate the larger scale effect of red snow algae induced albedo changes and to predict additional melting caused by snow algal growth we combined our evaluated integrated change (0.13) with values reported by Dumont et al (2014) for the Greenland Ice Sheet (GrIS). They showed that for the whole of the GrIS a change in albedo of 0.01 will lead to a surface mass loss of 27 Gt/yr. A quantitative value for the area of the GrIS covered by snow algae during a melt season is still lacking; however, assuming a coverage of between 10% (conservative estimate) and 100% (extreme estimate) for the GrIS would result in an additional 35 to 350 Gt/yr of melting. Considering global warming and the recent extreme melt event in 2012, when 97% of the entire Greenland Ice Sheet was affected by surface melting (Nghiem et al, 2012), which will re-occur with a high probability and increasing

frequency in the near future (McGrath et al, 2013), and which we infer from our data is one major driver for snow algal growth, this number is likely to tend towards the extreme estimate in the near future.

7.3 Conclusions

We show that snow algae are ubiquitous and show little diversity across the Arctic, despite variations in environmental parameters that significantly impact bacterial community composition. Although we may not have captured all environmental parameters, the patterns we observed occur on all studied glaciers regardless their geochemical and mineralogical compositions. Further investigations are needed to explore the validity of these findings for mid latitudes and the southern hemisphere. However, red snow is a ubiquitous phenomenon in Arctic sites (glaciers and permanent snow fields) and the similarity in snow algal community composition, metabolic function and impact on albedo of snow habitats allows us to upscale our findings and make predictions about the influence of snow algae on melt rates of glaciers across the Arctic. Our model shows that snow algae decrease albedo by 13% over a melt season likely leading to earlier exposure of dirty ice with an even lower surface albedo culminating in a further increase in melt rates. Our work paves the way for a universal model of algal-albedo interaction to be included in future climate models.

7.4 Methods

7.4.1 Field sites

A total of 40 red snow samples was collected from four well separated Arctic locations on 16 glaciers and permanent snow fields: Svalbard (SVA, n=13), Northern Sweden (TAR, n=23), Greenland (MIT, n=2), and Iceland (ICE, n=2) (Figure 7.1; Table D.1). Vestre Brøggerbreen, Midre Lovénbreen, Austre Brøggerbreen, Pedersenbreen, Austre Lovénbreen and Feiringbreen in Svalbard were sampled in July and August 2013, and Storglaciären, Rabot, Liljetopsrännan, SE-Kasskasatjåkkå, Björling and nearby permanent snow fields in Northern Sweden were sampled in July 2013 and July 2014. Mittivakkat glacier in

Greenland and in Iceland the glacier Drangajökull and permanent snow field Laugafell were sampled in July 2012.

7.4.2 Field sampling and measurements

All sampling and field measurements and most analyses have previously been described in full detail (Lutz et al, 2015; Lutz et al, 2014). Here we summarize previously employed methods and give full details of new methods. At each sampling site we measured pH, conductivity and temperature with a daily calibrated meter (Hanna instruments, HI 98129) prior to sampling. Photosynthetic active radiation (PAR) and ultraviolet (UV) radiation, as well as surface albedo (400-700 nm range), were measured using a radiometer (SolarLight, PMA2100) with specific PAR, UV-A and UV-B sensors. Albedo was calculated by taking the ratio of reflected to incident radiation (400-700 nm range) and measuring the values always in the same position to the sun. Measurements were carried out with the sensors held at 30 cm above the snow surface (field of view 160º, effective measurement area 0.5 m^2) and by first pointing the sensor upwards (incident radiation) and then towards the snow/ice surface (reflected radiation). Five measurements for incident and reflected radiation were acquired each. A quantification of the relative contribution of pigments, other light impurities (*i.e.*, mineral dust, black carbon) and snow metamorphism is lacking. However, based on observations in the field, non-organic impurities are likely negligible on red surfaces compared to the pigment disitribution.

Samples were collected in sterile centrifuge tubes or sterile *Whirl-Pak*® bags and in pre-ashed glass jars (450◦C >4 h) for organic analyses. All samples were slowly melted at room temperature within ~ 6 hours and processed and preserved (e.g., filtered, acidified) within ~ 8 hours after collection. Samples for DNA and organic analyses were flash-frozen in liquid nitrogen and stored at -80°C until analysed. All inorganic samples were stored cold (4°C) and in the dark.

7.4.3 Aqueous analyses

Aqueous analyses were carried out by Ion Chromatography (IC, Dionex, anions), by inductively coupled plasma mass spectrometry (ICP-MS, Agilent, cations), on a

total organic carbon analyser (Shimadzu, for dissolved organic carbon contents, DOC) and by segmented flow-injection analyses (AutoAnalyser3, Seal Analytical, dissolved phosphate).

7.4.4 Particulate analyses

Particulates in the samples were analysed for $\delta^{15}N$ and $\delta^{13}C$ by a Vario Pyro Cube elemental analyser (Elementar Inc) coupled to an Isoprime mass spectrometer. Samples were combusted in tin capsules at 1150 °C and gases were separated using temperature controlled adsorption/desorption columns. Carbon analyses were calibrated with in-house C4-sucrose and urea standards assigned values of -11.93‰ and -46.83‰ respectively via calibration with the international standards LSVEC (-46.479‰), CH7 (-31.83‰), CH6 (-10.45‰), and CO-1 (+2.48‰). Nitrogen isotope values were calibrated using the international standards USGS-25 and USGS-26 with assigned values of -30.4‰ and +53.7‰ respectively. Total carbon (TC), total nitrogen (TN), and total sulphur (TS) were derived from the thermal conductivity detector in the elemental analyser and calibrated using a sulphanilamide standard. Particulate phosphorus was extracted by ashing of the samples at 550°C for 2 h and incubating in 1 M HCl for 16 h according to extraction step V in Ruttenberg et al (2009).

7.4.5 Pigment analysis

Carotenoid and chlorophyll contents in the samples were quantified by high pressure liquid chromatography (HPLC) and a modified carotenoid/chlorophyll specific extraction protocol (Remias & Lutz, 2007). Cells were disrupted by shock freezing in liquid nitrogen for 10 min followed by grinding with a Teflon® mortar and pestle. The resulting powder was re-suspended in 1 mL of dimethylformamide (DMF) and 1.0 mm glass beads and horizontally shaken on a laboratory shaker (MoBio Vortex Genie 2) at maximum speed (3000 rpm) for 10 min followed by centrifugation for 5 min at 10 000 rpm. The supernatant was separated from the debris by filtering through a 0.45 µm Teflon® filter and the filtrate was mixed with methanol (25 vol %).

Extracted samples were analysed immediately on an Agilent Technologies 1200 Infinity HPLC instrument with a gradient pump, an autosampler, a variable wavelength detector and ODS Hypersil column (250x4.6 mm; 5 um particle size). Two solvents were used: solvent A consisted of a mixture of acetonitrile/water/methanol/hexane/tris buffer at ratios of 80:7:3:1:1 while solvent B was a mix of methanol and hexane at a ratio of 5:1. The HPLC was run at a flow rate of 1 mL min^{-1} and with an injection volume of 25 µL. Spectra were recorded from 200 to 800 nm and chromatograms were quantified at 450 nm for carotenoids and 660 nm for chlorophyll a and b. Run time was 60 min and the protocol required a 15 minute run with 100% of solvent A followed by a linear gradient from 100 % solvent A to 100% solvent B between 32 and 45 min and finally with 15 minutes of column re-equilibration through a 5 min linear gradient from solvent B back to 100% solvent to A, followed by a further column conditioning with 100 % solvent A for 10 min. The following commercially available standards were used for peak identification: chlorophyll a, chlorophyll b (Sigma), violaxanthin, neoxanthin, antheraxanthin, lutein, β-carotene, trans-astaxanthin, and cis-astaxanthin (Carotenature).

7.4.6 Fatty acids analysis

Fatty acids were extracted according to the method described by Wacker & Martin-Creuzberg (2007). Briefly, 20 ng of internal standard (tricosanoic acid methyl ester) were added to each sample, before ultrasonic extraction using dichloromethane:methanol (2:1 v:v), followed by centrifugation to remove particulates and evaporation of solvent from the supernatant. Fatty acids were transesterified by adding methanolic HCl to the dried extract and heating at 60˚ C for 20 minutes. After cooling, fatty acid methyl esters were extracted in isohexane, solvent was removed under nitrogen and the sample resuspended in isohexane for analysis.

Analysis of fatty acid methyl esters was carried out using a Trace 1300 gas chromatograph with flame ionisation detector (Thermo Scientific, Hemel Hempstead, UK), equipped with a non-polar-fused silica capillary column (CPSil-5CB, 50m x 0.32mm x 0.12 mm, Agilent Technologies, USA). Samples (1 µl) were injected in splitless mode, with the injector maintained at 200˚C. Carrier gas was helium, with a constant flow rate of 1.5 ml/min. The following temperature

programme was used: initial temperature 40 °C, rising to 140 °C at 20 °C min^{-1}, then rising to 240 °C at 4 ° min^{-1}, holding at 240 °C for 5 min. Fatty acid methyl esters were identified by comparison of retention time with those of reference compounds (Supelco, USA) and by gas chromatography/mass spectrometry. Gas chromatography/mass spectrometry was carried out using the gas chromatograph and column previously described, with identical operating conditions, coupled to an ISQ mass spectrometer (Thermo Scientific, Hemel Hempstead, UK). The transfer line and the ion source were maintained at 300˚C. The emission current was set to 50mA and the electron energy to 70 eV. The analyser was set to scan at m/z 50–650 with a scan cycle time of 0.6 s.

7.4.7 DNA sequencing

Total DNA was extracted from pelleted biomass using the PowerSoil® DNA Isolation kit (MoBio Laboratories). 16S rRNA genes were amplified using bacterial primers 27F (5'-AGAGTTTGATCMTGGCTCAG) and 357R (5'-CTGCTGCCTYCCGTA; tagged with the Ion Torrent adapter sequences and MID barcode) spanning the V1-V2 hypervariable regions. 18S rRNA genes were amplified using the eukaryotic primers 528F (5′-GCGGTAATTCCAGCTCCAA) and 706R (5'-AATCCRAGAATTTCACCTCT; tagged with the Ion Torrent adapter sequences and MID barcode; Cheung et al., 2010) spanning the V4-V5 hypervariable region. Polymerase chain reactions (PCR) were performed using Platinum® PCR SuperMix High Fidelity according to manufacturer's protocols. Initial denaturation at 95 ºC for 5 min was followed by 30 cycles of denaturation at 95 ºC for 30 s, annealing at 60 ºC for 30 s and elongation at 72 ºC for 30 s. Final elongation was at 72 ºC for 7 min. Archaeal 16S rRNA genes were amplified following a nested PCR approach. The first PCR reaction was carried out using primers 20F (5'-TCCGGTTGATCCYGCCRG) and 915R (5′–GTGCTCCCCCGCCAATTCCT). Initial denaturation at 95 ºC for 5 min was followed by 35 cycles of denaturation at 95 ºC for 30 s, annealing at 62 ºC for 30 s and elongation at 72 ºC for 180 s. Final elongation was at 72 ºC for 10 min. The PCR product was used as template for the second PCR reaction with primers 21F (5'-TCCGGTTGATCCYGCCGG) and 519R (5'- GWATTACCGCGGCKGCTG) (tagged with the Ion Torrent adapter sequences and MID barcode) spanning the V1-V2 hypervariable region. Initial denaturation at 95 ºC for 5 min was followed

by 30 cycles of denaturation at 95 ºC for 30 s, annealing at 60 ºC for 30 s and elongation at 72 ºC for 30 s. Final elongation was at 72 ºC for 7 min. All PCRs were carried out in triplicates to reduce amplification bias and in reaction volumes of 1 x 25 µl and 2 x 12.5 µl. All pre-amplification steps were done in a laminar flow hood with DNA-free certified plasticware and filter tips. The pooled amplicons were purified with AMPure XP beads (Agencourt©) with a bead to DNA ratio of 0.6 to remove nucleotides, salts and primers and analysed on the Agilent 2100 Bioanalyser (Agilent Technologies) with the High Sensitivity DNA kit (Agilent Technologies) and quality, size and concentration were determined. Sequencing was performed on an Ion Torrent Personal Genome Machine using the Ion Xpress™ Template Kit and the Ion 314™ or Ion 316™ chips following manufacturer's protocols. The raw sequence data was processed in QIIME (Caporaso et al, 2010). Barcodes and adapter sequences were removed from each sequence. Filtering of sequences was performed using an average cutoff of Q20 over the full sequence length (350 bp). Reads shorter than 200 bp were removed. OTUs were picked *de novo* using a threshold of 99%, 97% and 95% identity. Taxonomic identities were assigned for representative sequences of each OTU using the reference databases Greengenes for bacteria and archaea. The Silva database (DeSantis et al., 2006; extended with additional 223 sequences of cryophilic algae kindly provided by Dr. Thomas Leya from the CCCryo - Culture Collection of Cryophilic Algae, Fraunhofer IZI-BB) was used for eukaryotes. Data were aligned using PyNAST and a 0.80 confidence threshold. Singletons were excluded from the analysis. For bacterial sequence matching, plant plastids were removed from the data set prior to further analysis. For eukaryotic sequence matching *Chloroplastida* were pulled out of the data set and stored in a separate OTU table. In order to focus upon algal diversity, sequences matching *Embryophyta* (e.g., moss, fern) were removed from the data set. For archaea, sequences matching bacteria were removed. Finally, for further analyses samples were rarefied to the minimum library size and Shannon indices were calculated in QIIME. A matrix of each OTU table representing relative abundance (raw data) was imported into PAST v3.06 (Hammer et al, 2012) for multivariate statistical analyses (principal component analysis (PCA), canonical correspondence analysis (CCA)) and Pearson correlations. One-way ANOVA was done in SPSS v19 (IBM). Sequences have been deposited to the European Nucleotide Archive (ENA) under accession number PRJEB10548.

7.4.8 Albedo model

Using our mean, minimum and maximum measured albedo values for wet clean snow and red snow and literature data (Dumont et al, 2014) for clean dry snow we developed a simple one-dimensional moving boundary problem model that allows us to predict the effect of red snow algae on albedo. The parameters, equations and boundary conditions used are as follows:

The energy flux equation that links melting to albedo is:

$$Q_M = G(1 - \alpha) + L_{in} - L_{out} + Q_H + Q_L \quad (1)$$

with Q_M = energy flux, G = incoming shortwave radiation, α = albedo, L_{in} = longwave incoming radiation , L_{out} = longwave outgoing radiation, Q_H = sensible heat flux , and Q_L= latent heat flux.

Melt rate (M) is calculated by taking in account the latent heat of melting (L_f):

$$M = Q_M / L_f \quad (2)$$

Table 7.2 shows minimum, maximum and average albedo values for dry clean snow before the onset of melting (Lutz et al, 2014), wet clean snow (no visual presence of algae) at the onset of melting, and red snow (full red snow algal bloom). We used these values to derive two models (Table 7.3) for albedo changes over a 100 day melt season. We compare melting considering a benchmark case of purely physical driven albedo change (i.e., changes in snow crystal sizes and shapes and increasing water content, model 1) with albedo change due to red algal growth (model 2).

The change in melt rate (ΔM) was derived by subtracting the two equations for M_{model1} and M_{model2} (which removes the term $L_{in} - L_{out} + Q_H + Q_L$):

$$\Delta M = M_{model1} - M_{model2} = \Delta (G(1 - \alpha)/L_f) \quad (3)$$

Our benchmark case (model 1) shows albedo (α) changes with time and fits the equation:

$$\alpha = 0.8992 - 0.0203t^{0.5} \quad (4)$$

Consider the transition from clean snow to a surface where the growth of algae produces light red snow after 25 d with an albedo of 0.77 (minimum value), and continued melting produces darker red snow with an albedo of 0.65 (average value)

after 50 days and 0.53 (maximum value) after 100 days (Tables 7.2 and 7.3). The albedo changes with time for this scenario fits the equation:

$$\alpha = 0.9177 - 0.0372t^{0.5} \quad (5)$$

These two equations can be integrated to obtain the cumulative effects of albedo (α) changes with time to give:

$$\int \alpha_{model1}.dt = \int (0.8992 - 0.0203t^{-0.5}).dt = 0.8992t + 0.0203t^{1.5}/1.5$$

$$= 0.8992t + 0.0135t^{1.5} \quad (6)$$

$$\int \alpha_{model2}.dt = \int (0.9177 - 0.0372t^{-0.5}).d$$

$$t = 0.9177t + 0.0372t^{1.5}/1.5 = 0.9177t + 0.0248\,t^{1.5} \quad (7)$$

Subtracting equations (6) and (7) gives $\Delta\alpha = 0.0185t + 0.0113t^{1.5}$ (8)

which represents the albedo changes attributable to algae growth alone. For a melt season of 100 days $\Delta\alpha = 1.85 + 11.27 = 13.12$

In order to assess the error of our analysis, we carried out a sensitivity analysis using the data below (see also Figure D.4):

Dry clean snow (DCS) 0.95-0.90-0.85
Wet clean snow (WCS) 0.80-0.75-0.70
Red snow (RS) 0.77-0.65-0.53

Comparing minimum and average albedo values:

$$\int \alpha_{min}.dt = \int (0.9458 - 0.0186t^{-0.5}).dt = 0.9458t + 0.0186t^{1.5}/1.5 = 0.9458t + 0.0124\,t^{1.5}$$

$$\int \alpha_{average}.dt = \int (0.9049 - 0.0243t^{-0.5}).dt = 0.9049t + 0.0243t^{1.5}/1.5 = 0.9049t + 0.0162t^{1.5}$$

Subtracting gives $\Delta\alpha = 0.0409t - 0.0038t^{1.5}$

So when t = 100, $\Delta\alpha = 4.09 - 0.0038 \times 1000 = 4.09 - 3.8 = 0.29$

Comparing average and maximum values:

$\int \alpha_{average}.dt = \int (0.9049 - 0.0243t^{-0.5}).dt = 0.9049t + 0.0243t^{1.5}/1.5 = 0.9049t + 0.0162t^{1.5}$

$\int \alpha_{max}.dt = \int (0.8641 - 0.0300t^{-0.5}).dt = 0.8641t + 0.0300t^{1.5}/1.5 = 0.8641t + 0.0200\ t^{1.5}$

Subtracting gives $\Delta\alpha = 0.0408t - 0.0038t^{1.5}$

So when t = 100, $\Delta\alpha = 4.08 - 0.0038 \times 1000 = 4.08 - 3.8 = 0.28$

So our sensitivity test is giving a crude range of ~ 0.3 about the mean. Dumont et al (2014) suggested that for the Greenland Ice Sheet (GrIS) M is 27 Gt/yr for each 0.01 change in albedo so this errors equals 0.3 x 0.27/0.01 = 8.1Gt

Acknowledgements The authors would like to thank A. Detheridge (Aberystwyth University), and C. Waterfall and J. Coghill (University of Bristol) for help with the DNA sequencing and A. Stockdale (University of Leeds) for the phosphorus analysis. The research leading to these results was funded by a University of Leeds PhD Scholarship grant to SL and LGB, by a grant from the European Union Seventh Framework Programme INTERACT (grant no 262693) to LGB and by UK Natural Environment Research Council grants NE/J022365/1 to LGB and NE/J02399X/1 to AMA. Financial support for SL's field and lab work through a Young Explorers grant from National Geographic and a President's Fund for Research Visits from the Society for General Microbiology are gratefully acknowledged.

References

Anesio, A. M., Hodson, A. J., Fritz, A., Psenner, R. & Sattler, B. (2009) High microbial activity on glaciers: importance to the global carbon cycle. *Global Change Biology*, 15(4), 955-960.

Anesio, A. M. & Laybourn-Parry, J. (2012a) Glaciers and ice sheets as a biome. *Trends in ecology & evolution*, 27(4), 219-225.

Anesio, A. M. & Laybourn-Parry, J. (2012b) Glaciers and ice sheets as a biome. *Trends in ecology & evolution*, 27(4), 219-225.

Benning, L. G., Anesio, A. M., Lutz, S. & Tranter, M. (2014) Biological impact on Greenland's albedo. *Nature Geoscience*, 7(10), 691-691.

Box, J., Fettweis, X., Stroeve, J., Tedesco, M., Hall, D. & Steffen, K. (2012) Greenland ice sheet albedo feedback: thermodynamics and atmospheric drivers. *The Cryosphere*, 6(4), 821-839.

Cameron, K. A., Hagedorn, B., Dieser, M., Christner, B. C., Choquette, K., Sletten, R., Crump, B., Kellogg, C. & Junge, K. (2014) Diversity and potential sources of microbiota associated with snow on western portions of the Greenland Ice Sheet. *Environmental microbiology*, 17(3), 594-609.

Caporaso, J. G., Kuczynski, J., Stombaugh, J., Bittinger, K., Bushman, F. D., Costello, E. K., Fierer, N., Pena, A. G., Goodrich, J. K. & Gordon, J. I. (2010) QIIME allows analysis of high-throughput community sequencing data. *Nature methods*, 7(5), 335-336.

Doherty, S., Warren, S., Grenfell, T., Clarke, A. & Brandt, R. (2010) Light-absorbing impurities in Arctic snow. *Atmospheric Chemistry and Physics*, 10(23), 11647-11680.

Dumont, M., Brun, E., Picard, G., Michou, M., Libois, Q., Petit, J., Geyer, M., Morin, S. & Josse, B. (2014) Contribution of light-absorbing impurities in snow to Greenland's darkening since 2009. *Nature Geoscience* 7, 509-512.

Edwards, A., Anesio, A. M., Rassner, S. M., Sattler, B., Hubbard, B., Perkins, W. T., Young, M. & Griffith, G. W. (2011) Possible interactions between bacterial diversity, microbial activity and supraglacial hydrology of cryoconite holes in Svalbard. *The ISME journal*, 5(1), 150-160.

Edwards, A., Mur, L. A., Girdwood, S. E., Anesio, A. M., Stibal, M., Rassner, S. M., Hell, K., Pachebat, J. A., Post, B. & Bussell, J. S. (2014) Coupled cryoconite ecosystem structure–function relationships are revealed by comparing bacterial communities in alpine and Arctic glaciers. *FEMS microbiology ecology*, 89(2), 222-237.

Fierer, N. & Jackson, R. B. (2006) The diversity and biogeography of soil bacterial communities. *Proceedings of the National Academy of Sciences of the United States of America*, 103(3), 626-631.

Foissner, W. (2006) Biogeography and dispersal of micro-organisms: a review emphasizing protists. *Acta Protozoologica*, 45(2), 111-136.

Gentz-Werner, P. (2007) *Roter Schnee: oder Die Suche nach dem färbenden Prinzip, 28*. Berlin: Akademie Verlag.

Green, J. & Bohannan, B. J. (2006) Spatial scaling of microbial biodiversity. *Trends in Ecology & Evolution*, 21(9), 501-507.

Hammer, O., Harper, D. & Ryan, P. (2012) PAST: paleontological statistics software package for education and data analysis. *Paleontol Electron*, 4(9).

Hell, K., Edwards, A., Zarsky, J., Podmirseg, S. M., Girdwood, S., Pachebat, J. A., Insam, H. & Sattler, B. (2013) The dynamic bacterial communities of a melting High Arctic glacier snowpack. *The ISME journal*, 7(9), 1814-1826.

Hodson, A., Anesio, A. M., Tranter, M., Fountain, A., Osborn, M., Priscu, J., Laybourn-Parry, J. & Sattler, B. (2008) Glacial ecosystems. *Ecological Monographs*, 78(1), 41-67.

Hoham, R. & Duval, B. (2001) Microbial ecology of snow and freshwater ice with emphasis on snow algae. Cambridge: Cambridge University Press.

King, A. J., Freeman, K. R., McCormick, K. F., Lynch, R. C., Lozupone, C., Knight, R. & Schmidt, S. K. (2010) Biogeography and habitat modelling of high-alpine bacteria. *Nature Communications*, 1, 53.

Larose, C., Berger, S., Ferrari, C., Navarro, E., Dommergue, A., Schneider, D. & Vogel, T. M. (2010) Microbial sequences retrieved from environmental samples from seasonal Arctic snow and meltwater from Svalbard, Norway. *Extremophiles*, 14(2), 205-212.

Leya, T., Müller, T., Ling, H. U. & Fuhr, G. (2004) Snow algae from north-western Spitsbergen (Svalbard). *The coastal ecosystem of Kongsfjorden, Svalbard. Synopsis of biological research performed at the Koldewey Station in the years 1991-2003*, 46-54.

Lutz, S., Anesio, A. M., Edwards, A. & Benning, L. G. (2015) Microbial diversity on Icelandic glaciers and ice caps. *Frontiers in microbiology*, 6, 307.

Lutz, S., Anesio, A. M., Villar, S. E. J. & Benning, L. G. (2014) Variations of algal communities cause darkening of a Greenland glacier. *FEMS microbiology ecology*, 89(2), 402-414.

Martiny, J. B. H., Bohannan, B. J., Brown, J. H., Colwell, R. K., Fuhrman, J. A., Green, J. L., Horner-Devine, M. C., Kane, M., Krumins, J. A. & Kuske, C. R. (2006) Microbial biogeography: putting microorganisms on the map. *Nature Reviews Microbiology*, 4(2), 102-112.

McGrath, D., Colgan, W., Bayou, N., Muto, A. & Steffen, K. (2013) Recent warming at Summit, Greenland: Global context and implications. *Geophysical Research Letters*, 40(10), 2091-2096.

Musilova, M., Tranter, M., Bennett, S. A., Wadham, J. & Anesio, A. M. (2015) Stable microbial community composition on the Greenland Ice Sheet. *Frontiers in microbiology*, 6, 193.

Nghiem, S., Hall, D., Mote, T., Tedesco, M., Albert, M., Keegan, K., Shuman, C., DiGirolamo, N. & Neumann, G. (2012) The extreme melt across the Greenland ice sheet in 2012. *Geophysical Research Letters*, 39(20), L20502.

O'Malley, M. A. (2007) The nineteenth century roots of'everything is everywhere'. *Nature Reviews Microbiology*, 5(8), 647-651.

Pachauri, R. K., Allen, M., Barros, V., Broome, J., Cramer, W., Christ, R., Church, J., Clarke, L., Dahe, Q. & Dasgupta, P. (2014) Climate Change 2014: Synthesis Report. Contribution of Working Groups I, II and III to the Fifth Assessment Report of the Intergovernmental Panel on Climate Change.

Remias, D., Lütz-Meindl, U. & Lütz, C. (2005) Photosynthesis, pigments and ultrastructure of the alpine snow alga Chlamydomonas nivalis. *European Journal of Phycology*, 40(3), 259-268.

Remias, D. & Lutz, C. (2007) Characterisation of esterified secondary carotenoids and of their isomers in green algae: a HPLC approach. *Algological Studies*, 124(1), 85-94.

Ruttenberg, K., Ogawa, N., Tamburini, F., Briggs, R., Colasacco, N. & Joyce, E. (2009) Improved, high-throughput approach for phosphorus speciation in natural sediments via the SEDEX sequential extraction method. *Limnology and Oceanography: Methods*, 7(5), 319-333.

Ryšánek, D., Hrčková, K. & Škaloud, P. (2014) Global ubiquity and local endemism of free living terrestrial protists: phylogeographic assessment of the streptophyte alga Klebsormidium. *Environmental microbiology*, 17(3), 689-698.

Spijkerman, E., Wacker, A., Weithoff, G. & Leya, T. (2012) Elemental and fatty acid composition of snow algae in Arctic habitats. *Frontiers in microbiology*, 3, 380.

Stibal, M., Šabacká, M. & Kaštovská, K. (2006) Microbial communities on glacier surfaces in Svalbard: impact of physical and chemical properties on abundance and structure of cyanobacteria and algae. *Microbial ecology*, 52(4), 644-654.

Takeuchi, N. (2002) The altitudinal distribution of snow algae on an Alaska glacier (Gulkana Glacier in the Alaska Range). *Hydrological Processes*, 15(18), 3447-3459.

Tedesco, M., Fettweis, X., Mote, T., Wahr, J., Alexander, P., Box, J. & Wouters, B. (2013) Evidence and analysis of 2012 Greenland records from spaceborne observations, a regional climate model and reanalysis data. *Cryosphere Discussions (The)*, 6.

Thomas, F., Hehemann, J.-H., Rebuffet, E., Czjzek, M. & Michel, G. (2011) Environmental and gut bacteroidetes: the food connection. *Frontiers in microbiology*, 2, 93.

Thomas, W. H. & Duval, B. (1995) Sierra Nevada, California, USA, snow algae: snow albedo changes, algal-bacterial interrelationships, and ultraviolet radiation effects. *Arctic and alpine research*, 27(4), 389-399.

Wacker, A. & Martin-Creuzburg, D. (2007) Allocation of essential lipids in Daphnia magna during exposure to poor food quality. *Functional Ecology*, 21(4), 738-747.

Yallop, M. L., Anesio, A. M., Perkins, R. G., Cook, J., Telling, J., Fagan, D., MacFarlane, J., Stibal, M., Barker, G. & Bellas, C. (2012) Photophysiology and albedo-changing potential of the ice algal community on the surface of the Greenland ice sheet. *The ISME journal*, 6(12), 2302-2313.

Zhang, Y. (2008) *Geochemical kinetics*. Princeton University Press: Princeton.

Chapter 8: Linking microbial diversity and functionality of Arctic glacial surface habitats.

Lutz, S., Anesio, A. M., Edwards, A, Newton, R. J. & Benning, L. G.

In preparation for submission to the *ISME Journal*.

Abstract

Distinct microbial habitats on glacial surfaces are dominated by snow and ice algae, which are the critical players and the dominant primary colonisers and net producers during a melt season. Here we have for the first time evaluated the role of these algae as part of the full microbial community composition (*i.e.*, algae, bacteria, archaea) in distinct surface habitats and on twelve glaciers and permanent snow fields in Svalbard and the Swedish Arctic. We cross-correlated these data with the analyses of specific metabolites such as fatty acids and pigments, and a full suite of potential critical physico-chemical parameters including major nutrients, and minor and trace metals. We show that correlations between single species, metabolites, and geochemistry can be used to unravel mixed metabolic signals in complex communities, assign them to single species and infer their functionality. Production of the quantified metabolites in snow and ice algae is driven mainly by nitrogen and less so by phosphorus limitation. This is especially important for the synthesis of secondary carotenoids, which cause a darkening of glacial surfaces leading to a decrease in surface albedo and eventually higher melting rates.

8.1 Introduction

The cryosphere covers about 10% of the Earth's surface and glaciers are an important component of the Earth's climate and freshwater system. Snow and ice habitats have recently been recognised as a biome dominated by microorganisms of all three domains of life, playing crucial roles in biogeochemical processes both on a local and global scale (Anesio & Laybourn-Parry, 2012; Hodson et al, 2008; Lutz et al, 2014). The presence of liquid water during the melt season makes glacial surfaces habitable and different microbial communities have been found to dominate the distinct surface habitats. Even on a single glacier these can be comprised of 7 different habitats: clean snow, green snow, red snow, biofilms, clean ice, dirty ice, and cryoconite holes (Lutz et al, 2014).

After the onset of melting, *clean snow* (white snow without visual presence of particles) undergoes a colour change due to snow algal blooming that turns the snow into *green snow* or *red snow*. The dominant species in red snow belong to the

Chlamydomonaceae with *Chlamydomonas* and *Chloromonas* as prominent genera (Leya et al, 2004). Different aspects of snow algae ecology and physiology have been intensively studied in many polar and alpine settings including Svalbard (Leya et al, 2004; Müller et al, 2001), Iceland (Lutz et al, 2015a), Alaska (Takeuchi, 2002), Greenland (Lutz et al, 2014), the Himalayans (Yoshimura et al, 2006), the Rocky Mountains (Thomas & Duval, 1995), Antarctica (Fujii et al, 2010; Remias et al, 2013) and the European Alps (Remias et al, 2005). However, only few studies have addressed snow algal diversity through high-throughput molecular techniques (e.g., Lutz et al, 2015a,b) and no study so far has evaluated the differences or similarities between these habitats on various Arctic glaciers.

When the snow line moves further up the glacier and melting progresses, bare ice becomes exposed. *Clean ice* (white ice without visual presence of particles) becomes colonised by filamentous algae that have only recently been described based on morphological and pigmentation traits (Remias et al, 2012a; Remias et al, 2009; Yallop et al, 2012). The most described species are *Ancylonema nordenskiöldii* and *Mesotaenium berggrenii* and they belong to the *Zygnematophyceae* (Remias et al, 2012a; Remias et al, 2009). They produce the brownish pigment purpurogallin carboxylic acid-6-O-b-D-glucopyranoside (Remias et al, 2012b), which together with accumulated mineral debris turn the ice surfaces into *dirty ice*. At the interface of snow and ice, *biofilms* can develop and these represent an ecotone between the snow and ice habitats.

Although snow and ice habitats dominate the largest proportion of glacial surfaces throughout the melt season, the microbial processes in *cryoconite holes* have been by far the more extensively studied habitats to date (Cameron et al, 2012; Edwards et al, 2014). Cryoconite holes are water-filled holes that form by preferential melt of organic and inorganic dark particles and are dominated by cyanobacterial communities. Although not their preferential habitat, snow and ice algae may eventually end up in cryoconite holes due to melting processes and likely serve as an additional carbon and nutrient source.

Snow and ice algal blooms do not only play a crucial role in carbon and nutrient cycling (Lutz et al 2014), but their pigmentation acts both as a protection from high irradiation but also darkens the surface of glaciers and ice sheets. This is turn leads to a decrease in surface albedo and subsequent further increased melt rates (Benning et al, 2014; Lutz et al, 2014; Takeuchi, 2013; Thomas & Duval, 1995;

Yallop et al, 2012). Yet, knowledge about the microbial diversity or functions in these different habitats is so far lacking.

We evaluated the community structure of the different habitats on twelve glaciers and permanent snow fields in Svalbard and the Swedish Arctic through high-throughput sequencing of the small subunit ribosomal RNA genes (16S and 18S), and combined these with analyses of specific metabolites that are crucial for a cryophilic life style such as fatty acids and pigments (Thompson Jr, 1996), (Boussiba, 2000; Remias et al, 2005). We cross-correlated these data with a full suite of potential critical physico-chemical parameters including major nutrients, trace metals and the prevalent mineralogy.

In this study, we test the hypotheses that (a) our proposed habitat classification defined for a single glacier in Greenland (Lutz et al, 2014) is valid across the Arctic in terms of community structure and function in snow and ice settings, and that (b) snow and ice habitats are affected by biogeographical and geochemical parameters. Finally, we evaluate how the understanding of the controls upon function in contemporary surface habitats can provide insights into past and future glacier surfaces.

8.2 Materials and Methods

A total of 92 samples (10 clean snow, 34 red snow, 15 green snow, 4 biofilm, 7 clean ice, 15 dirty ice, and 7 cryoconite hole sediment samples) were collected across 6 glaciers in Svalbard and 6 glaciers and snow fields in the Swedish Arctic (Tarfala Valley; Figure 8.1, Tables 8.1, 8.2 and E.1). The glaciers in Svalbard (Vestre Brøggerbreen, Midtre Lovénbreen, Austre Brøggerbreen, Pedersenbreen, Austre Lovénbreen and Feiringbreen) were sampled in July and August 2013, and Storglaciären, Rabot, Liljetopsrännan, SE-Kasskasatjåkkå, Björling and nearby permanent snow fields in the Swedish Arctic were sampled in July 2013 and July 2014.

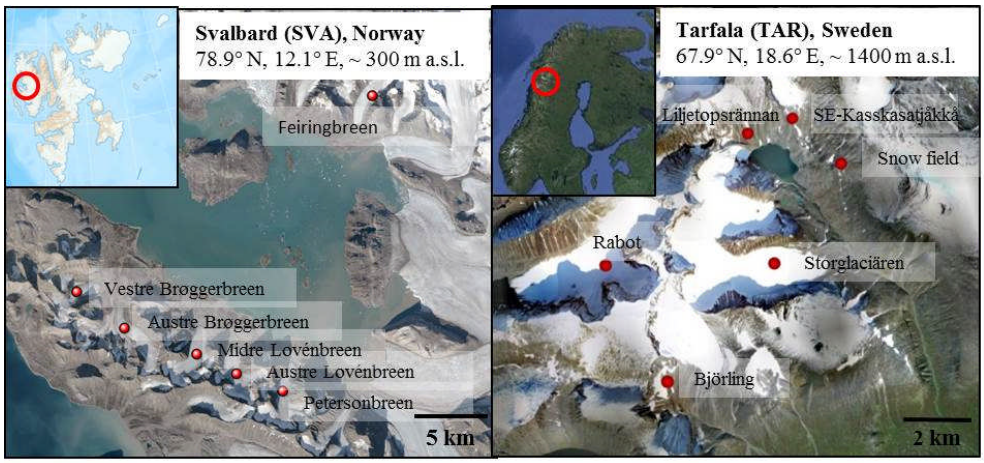

Figure 8.1: Map showing the 2 geographic locations and 12 glaciers and snow fields sampled in Svalbard and Arctic Sweden. At each marked site various habitats were sampled (full details see Table 8.1).

Details of the sampling methods, the field measurements and the majority of the analyses have been described previously (Lutz et al 2014, Lutz et al 2015a) and can be found in the supplementary information. In brief, at each sampling site we measured pH, conductivity and temperature with a daily-calibrated meter (Hanna instruments, HI 98129). PAR, UV irradiation and surface albedo (400-700 nm range) were measured using a radiometer (SolarLight, PMA2100). Next to the field measurement sites, samples were collected either in sterile centrifuge tubes or sterile *Whirl-Pak*® bags (for genomic and inorganic analyses) or in pre-ashed glass jars (450◦C >4 h) for organic analyses. Samples were slowly melted at room temperature and processed for further analyses (*i.e.*, filtered, concentrated, acidified) within ~ 8 hours after collection. Samples for DNA and particulate organic analyses (*i.e.*, pigments, fatty acids) were flash-frozen in liquid nitrogen and stored at -80°C until analysed. All inorganic samples were stored cold (4°C) and in the dark.

Aqueous compounds were analysed by Ion Chromatography (IC, Dionex; anions), by inductively coupled plasma mass spectrometry (ICP-MS, Agilent; cations), while dissolved organic carbon (DOC) was analysed on a total organic carbon analyser (TOC, Shimadzu) and dissolved phosphate by segmented flow-injection analyses (AutoAnalyser3, Seal Analytical).

Samples that contained enough solid particulates were analysed for total carbon (TC), total nitrogen (TN), total sulphur (TS), as well as $\delta^{15}N$ and $\delta^{13}C$, by pyrolysis

at 1500 °C (Vario Pyro Cube, Elementar Inc.) followed by mass spectrometry (Isoprime Mass Spectrometer). Particulate phosphorus was extracted by ashing of the samples at 550°C for 2 h and incubating in 1 M HCl for 16 h according to extraction step V in Ruttenberg et al. (2009) and quantified by segmented flow-injection analyses (AutoAnalyser3, Seal Analytical).

The relative abundance of functional groups corresponding to proteins, lipids and carbohydrates was evaluated by Fourier transform infrared spectroscopy (FTIR, A2 Technology Microlab). Pigments were extracted in dimethylformamide and analysed using high-pressure liquid chromatography (HPLC, Agilent 1220 Infinity). Fatty acids were extracted in dichloromethanol:methanol (2:1, v:v), transesterified in methanolic HCl, followed by extraction in isohexane and analysed by gas chromatography mass spectrometry (GC-MS, Thermo Scientific, Trace1300, ISQ Single Quadrupole).

Of the seven habitats studied, enough particulates for DNA extraction was only available in the green snow, red snow, biofilm, dirty ice and cryoconite hole samples. Total DNA was extracted using the PowerSoil® DNA isolation kit (MoBio Laboratories) and three amplicon libraries were prepared for bacteria, eukaryotes, and archaea. Libraries were sequenced on the Ion Torrent Personal Genome Machine. Raw sequences were processed and OTU tables were constructed in QIIME (Caporaso et al, 2010). Principal component analysis (PCA), canonical correspondence analysis (CCA) and Pearson correlations were carried out in PAST v3.06 (Hammer et al, 2012) and one-way analysis of variance (ANOVA) was done in SPSS v19 (IBM). One-way ANOVA was chosen over two-way ANOVA due to the uneven sampling number for the habitats and locations and to avoid skewness of the statistical analyses. Samples were compared either across habitats within one location or across locations within one habitat by one-way ANOVA.

8.3 Results

8.3.1 Community composition

At all 12 sites were we able to collect samples as per the previously defined habitats (Lutz et al, 2014), namely, clean snow, green snow, red sow, biofilms, clean ice, dirty ice and cryoconite holes comprising of 92 samples (Table E.1). In all sequenced snow and ice samples (n=63) we found a low algal diversity with 9 species making up >99% of the algal communities (3 uncultured *Chlamydomonadaceae*, *Chloromonas polyptera*, *Chloromonas nivalis*, *Chloromonas alpina*, *Microglena sp*., *Raphidonema sempervirens* and *Ancylonema nordenskiöldii*) (Figure 8.2, Table 8.1 for averages and p-values ($p<0.05$ = significant) for differences between habitats; and Table E.2 for full details). Red snow samples (n=27) showed the lowest variation in species composition regardless of their geographic location and all samples were dominated by an uncultured *Chlamydomonadaceae* species (labelled "2"). However, the species composition of green snow (n=14) varied between the two Arctic locations with higher relative abundance of *Microglena sp.* (20x) and *Raphidonema sempervirens* (10x) in Svalbard and *Chloromonas polyptera* (10x) in Sweden. Biofilm samples (n=4) were characterized by higher relative abundance of *Chloromonas polyptera* compared to all other habitats in both Svalbard and Sweden. Dirty ice (n=10) and cryoconite holes (n=7) contained a higher relative abundance of filamentous ice algae with *Raphidonema sempervirens* and *Ancylonema nordenskiöldii* as the dominant taxa and a high similarity in community structure between the two habitats. Cryoconite holes also showed a higher ratio of fungi to algae than snow or ice samples (Table E.3).

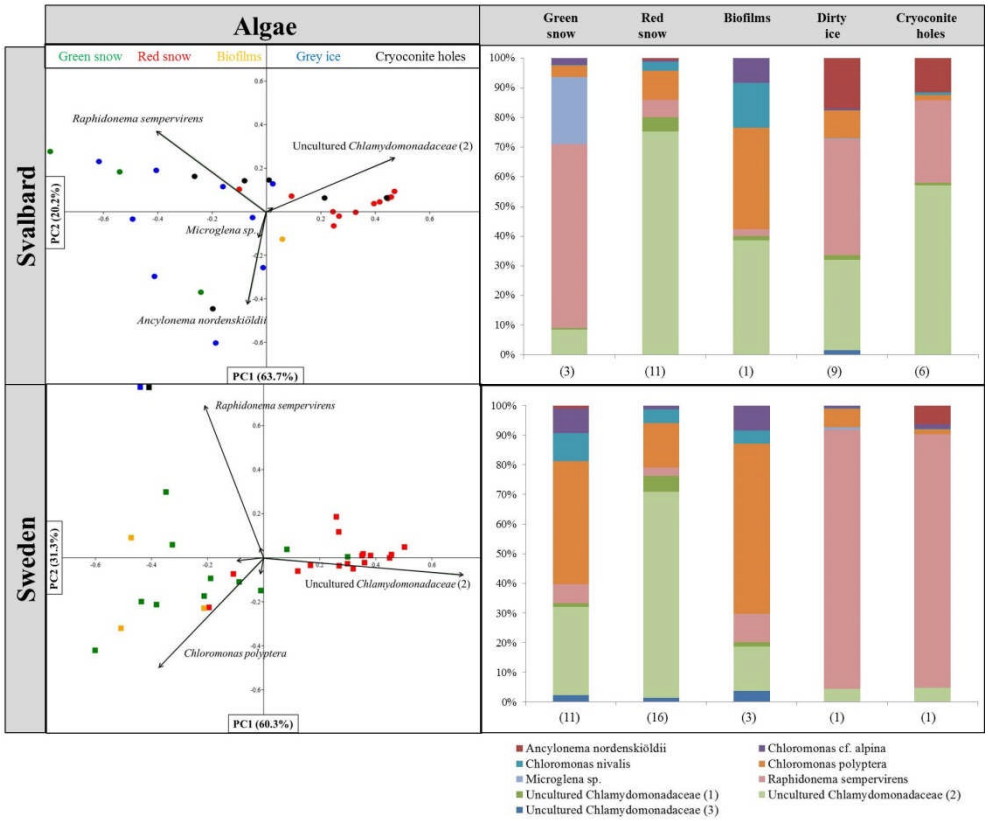

Figure 8.2: Principal component analysis of algal species in the Svalbard and Arctic Sweden samples revealing taxonomic distance between samples and showing the main taxa causing the separations. Samples cluster according to habitats in all locations. Bar charts show average species composition within one habitat and location with the numbers in brackets at the bottom of each chart representing sample numbers per habitat.

Bacteria (Figure 8.3, Table E.4) were mainly represented by the phyla *Proteobacteria*, *Bacteriodetes* and *Cyanobacteria* in both geographic locations with samples more similar within one habitat than in-between habitats. *Bacteriodetes* showed higher relative abundance in snow and transition habitats with highest values for red snow and biofilms and lower abundances in dirty ice and cryoconite holes. *Proteobacteria* were abundant in all habitats, but *Alphaproteobacteria* were particularly more abundant in dirty ice, while *Betaproteobacteria* dominated in green snow. *Cyanobacteria* showed the highest relative abundance in dirty ice and cryoconite holes in Svalbard. Cryoconite holes were the habitats that showed the largest variation between locations with *Cyanobacteria* dominating in Svalbard and *Proteobacteria* in Sweden. Bacterial classes showed larger variations between all locations. Within the *Bacteriodetes*, *Sphingobacteria* were dominating in Sweden, and *Cytophagia*, *Saprospirae* and

Flavobacteria in Svalbard. Within the *Cyanobacteria*, *Synechococcophycideae* were dominant in Svalbard (Table E.4).

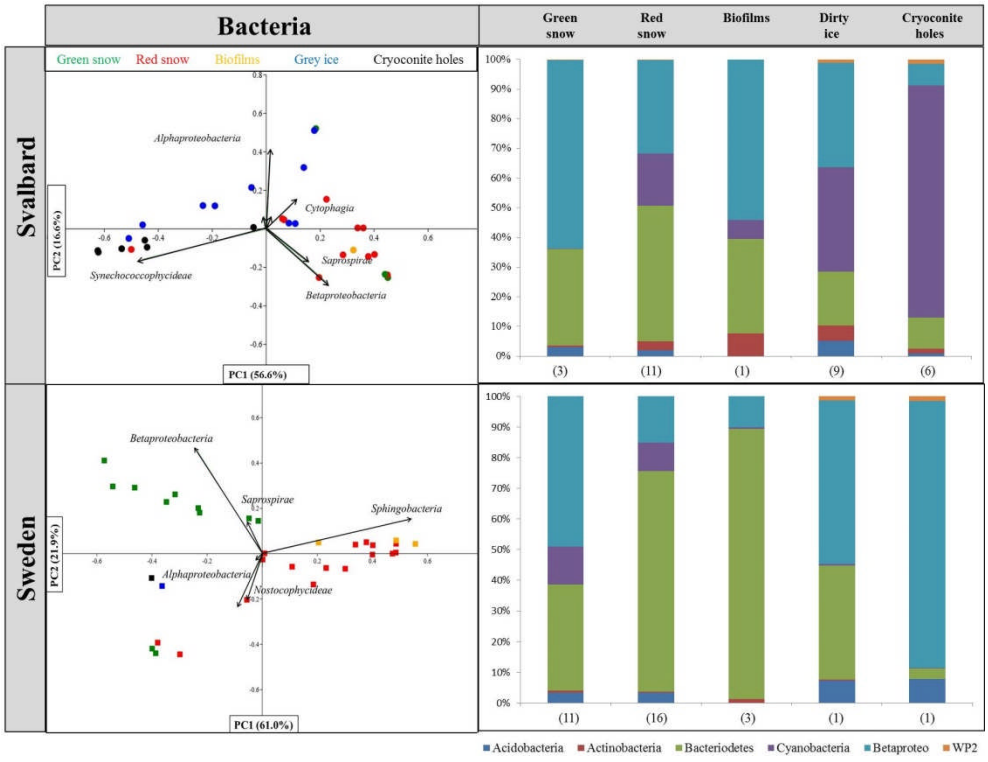

Figure 8.3: Principal component analysis of bacterial phyla in the Svalbard and Arctic Sweden samples revealing taxonomic distance between samples and showing the main taxa causing the separations. Samples cluster according to habitats in all locations. Bar charts show average species composition within one habitat and location with the numbers in brackets at the bottom of each chart representing sample numbers per habitat.

Archaea were detected in all analysed snow, ice and cryoconite samples (n=33). They showed very low diversity and the species composition was mainly made up by two groups, the *Nitrosophaerales* and *Methanobacteriales* (Table E.5).

8.3.2 Aqueous and particulate geochemistry

We evaluated particulate total carbon, nitrogen, phosphorous and sulphur contents (TC, TN< TP, TS), C/N/P ratios, as well as the full suite of dissolved major

nutrients (DOC, PO_4, NO_3), minor and trace metals (e.g., K, Na, Ca, Fe, Mg, Mn), and the bulk mineralogy in each sample.

Most aqueous chemical data showed higher similarities within one location and not habitats (see Tables 8.1 and 8.2 for averages and statistical tests and Table E.7 for full details). DOC values were significantly and on average six times higher in the Swedish Arctic compared to Svalbard. There were no significant differences for other important nutrients including NO_3 and PO_4. Ca, Mg, Mn, Na and Cl were significantly higher in Svalbard compared to Sweden.

For ratios of particular C, N and P we found a range of significant differences with samples clustering according to habitats within one location (Figure E.4). For Svalbard and Sweden, C/N ratios were highest in red snow, followed by biofilms, similar values for dirty ice and cryoconite holes and lowest values in green snow (Table 8.1and E.8). Although the same trend could be observed in both locations, C/N ratios were generally higher in Sweden relative to the samples collected in Svalbard. All samples were above the optimal Redfield ratio for C/N of 6.6:1. We found large differences for C/P ratios. Most samples from Svalbard were below the optimal Redfield ratio of 106:1, while nearly all samples collected from Sweden were above this ratio.

$\delta^{15}N$ values were predominantly negative with no significant trend for habitats or geographic locations (Table E.8). $\delta^{13}C$ values varied over a narrow range and significant trends could only be found for habitats in Svalbard with more negative values for red snow (-27.76‰ ± 1.52) and green snow (-28.21‰ ± 1.51‰) and higher for dirty ice (-26.28‰ ± 0.65) and cryoconite holes (-25.49‰ ± 0.25). There were no significant differences for the different habitats in Sweden and samples showed a larger range compared to Svalbard with values between -30.03‰ and -21.80‰.

The mineralogy slightly varied between the two locations. Quartz, plagioclase, mica and chlorite were present in all sites. In Svalbard we also found pyroxene and muscovite on all studied glaciers with calcite and dolomite on Austre Brøggerbreen and Feiringbreen, and hornblende and biotite in Arctic Sweden.

8.3.3 Metabolites

The relative abundance of functional groups corresponding to lipids, proteins and carbohydrates, clustered according to algal habitats (see Table 8.1 for averages and statistical tests and Table E.9 for full details). Values for proteins and lipids were up to 5% higher in Sweden compared to Svalbard, but the same trends could be observed across the habitats within the respective locations. Concentrations of lipids and proteins were significantly higher in red snow and biofilms, followed by dirty ice and green snow.

The most abundant fatty acids identified were the saturated fatty acids (SFA) C16:0 and C18:0, the monounsaturated fatty acids (MUFA) C16:1 and C18:1, and the polyunsaturated fatty acids (PUFA) C16:4, C18:2, C18:3 and C18:4 (Table 8.1 and E.10). PCA plots revealed clustering of the samples according to habitats and the fatty acids causing separation were C16:4, C18:3 and C18:4 for red snow, while C16:1, C18:1, and C15 branched for green snow, biofilms, dirty ice, and cryoconite holes (Figures 8.4 and E.1). The relative abundance of PUFAs was significantly higher in red snow samples, followed by green snow, dirty ice, biofilms and cryoconite holes. MUFAs also showed significant differences between habitats and were highest in biofilms, followed by green snow, dirty ice, cryoconite holes and lowest in red snow. SFAs showed similar values for all samples and no significant differences between habitats. Dirty ice in Sweden showed 2x higher values of C18:3 and C18:4 compared to Svalbard. Cryoconite holes in Svalbard showed a 2x higher relative abundance of C15 branched fatty acids compared to dirty ice and all other habitats.

The relative abundance of secondary carotenoids (i.e., astaxanthin) varied significantly between habitats and they were highest in red snow, followed by biofilms, green snow, dirty ice and cryoconite holes (Table 8.1 and E.11). Primary carotenoids also varied significantly between habitats and were highest in cryoconite holes, followed by dirty ice, green snow, and were lowest in red snow and biofilms. Chlorophyll concentrations were highest in dirty ice and green snow, followed by cryoconite holes, biofilms and lowest in red snow.

8.3.4 Relationships between community composition, geochemistry and metabolites

We tested for relationships between microbial composition and geochemical parameters of the different glacial surface habitats. All correlations are summarised in Table 8.3. In brief, the two dominant uncultured *Chlamydomonadaceae* (1) and (2) (Figures 8.2 and E.2, Table 8.3) and *Sphingobacteria* (Figure E.3) were positively correlated with C/N ratios, and *Chloromonas polyptera*, *Chloromonas cf. alpina* and *Sphingobacteria* with DOC.

CCA (Figure E.2) and Pearson analyses (Table 8.3) showed a strong positive correlation for the relative abundance of the two uncultured *Chlamydomonadaceae* (1) and (2) with PUFAs, *Chloromonas cf. alpina* with MUFAs and a strong negative correlation for *Raphidonema sempervirens* and PUFAs (Figure 8.4).

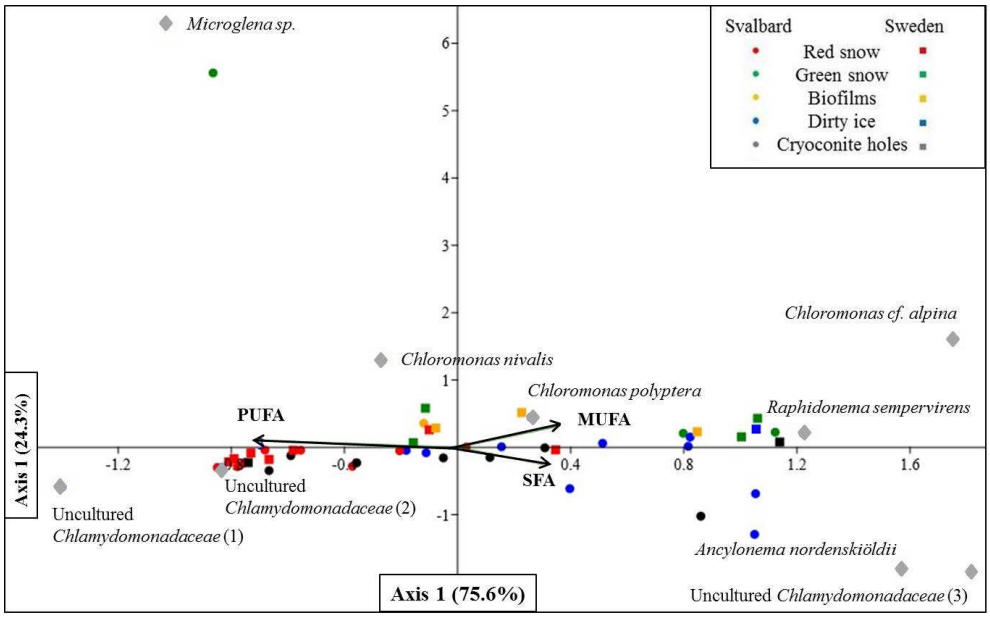

Figure 8.4: CCA analysis showing a positive correlation for the relative abundance of the two uncultured *Chlamydomonadaceae* (1) and (2) with PUFAs, *Chloromonas cf. alpina* with MUFAs and a negative correlation for *Raphidonema sempervirens* and PUFAs.

Secondary carotenoids showed a strong positive correlation (Figure 8.5, Table 8.2) with the two uncultured *Chlamydomonadaceae* (1) and (2) and negative correlation with the uncultured *Chlamydomonadaceae* (3) and *Chloromonas cf. alpina*. *Raphidonema sempervirens* was also positively correlated with primary

carotenoids (Figure 8.5). A positive correlation has been found for *Raphidonema sempervirens* and primary carotenoids and specifically for the pigments Antheraxanthin and Zeaxanthin with *Ancylonema nordenskiöldii*). The uncultured *Chlamydomonadaceae* (2) positively correlated with trans-Astaxanthin.

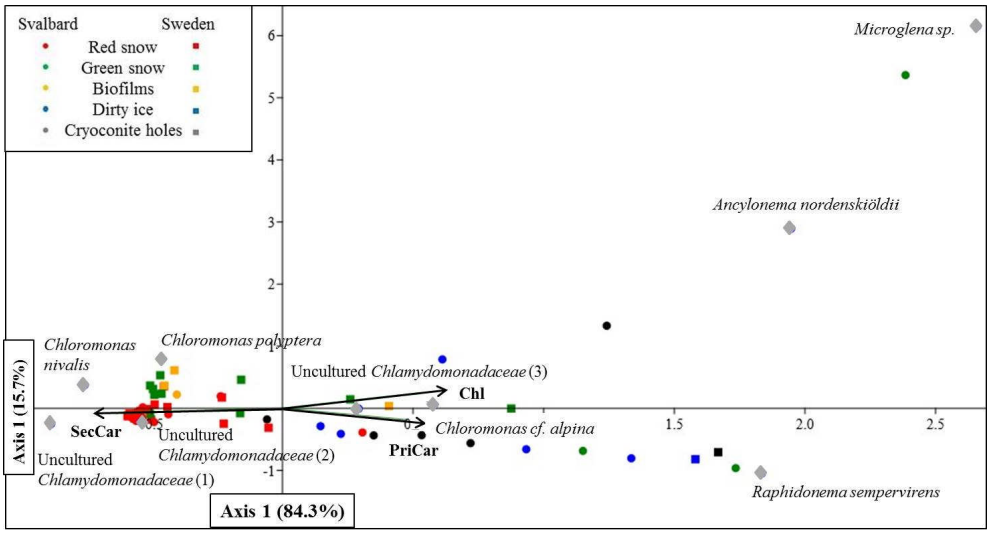

Figure 8.5: CCA analysis showing a positive correlation between the two uncultured *Chlamydomonadaceae* (1) and (2) and negative correlation between the uncultured *Chlamydomonadaceae* (3) and *Chloromonas cf. alpina* and secondary carotenoids. *Raphidonema sempervirens* was also positively correlated with primary carotenoids.

The quantified metabolites correlated with intracellular C/N/P ratios with a positive correlation for increasing C/N ratios and higher content of lipids, secondary carotenoids and PUFAs, and a positive correlation for increasing C/P and N/P ratios and higher lipid, protein and secondary carotenoid contents. The relative abundance of secondary carotenoids also positively correlated with the PUFAs C18:3 and C16:4.

.

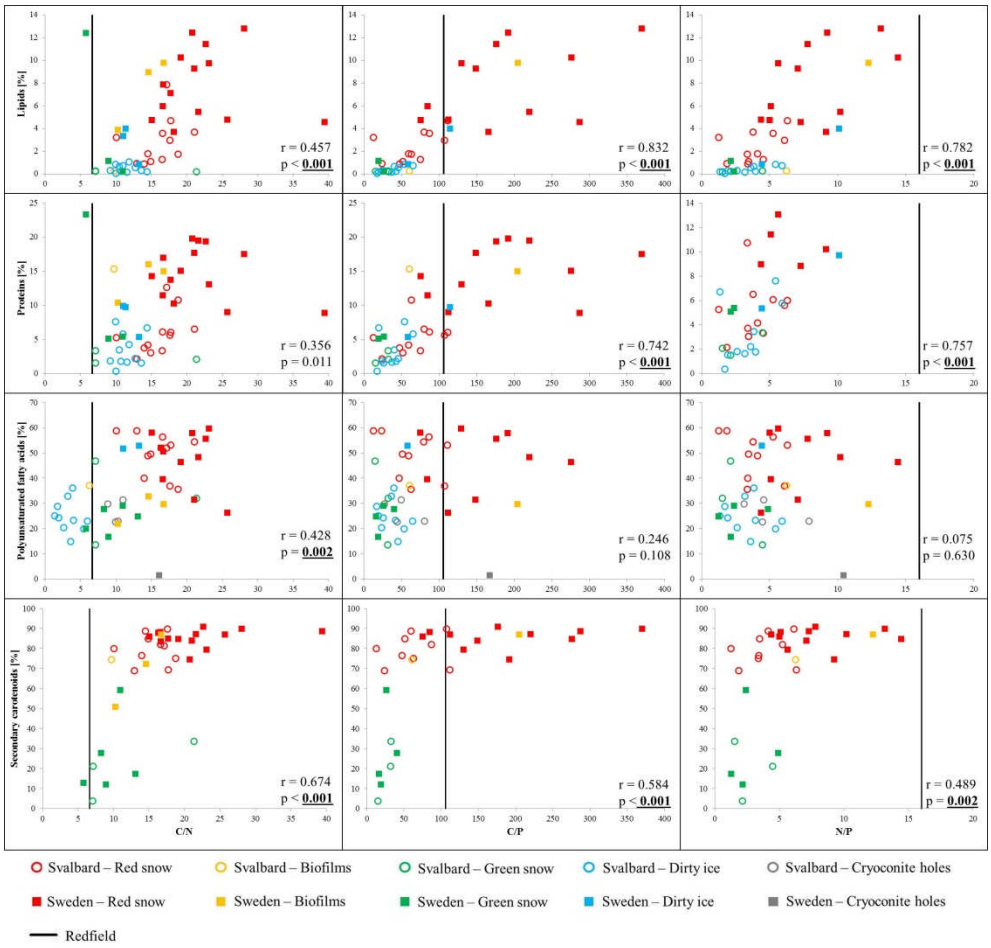

Figure 8.6: Correlations between C/N, C/P and N/P ratios and the relative abundance of analysed metabolites. On average all metabolites correlated positively with the particulate C/N/P ratios. C/N ratios were correlated with higher lipid, secondary carotenoid and PUFA contents; while C/P and N/P ratios were correlated with higher lipid, secondary carotenoid and protein contents. Pearson correlations (r) and p-values (<0.05 is significant) are reported

Table 8.1: Average values, standard deviations and statistical analysis of all biological and geochemical compounds (in % of total), analysed by one-way ANOVA to reveal significant differences between the habitats within one location. Results with p-values of <0.05 were considered to be significant and are in bold, results with p-values <0.01 were considered to be highly significant and are also underlined. n.s. = no sample

	Svalbard p	Green snow	Red snow	Biofilms	Dirty ice	Cryoconite holes	Sweden p	Green snow	Red snow	Biofilms	Dirty ice	Cryoconite holes
Algae												
Ancylonema nordenskiöldii	0.153	0	0.7 ± 2.5	0	16.2 ± 23.9	11.5 ± 20.9	0.429	0.8 ± 2.6	0.0 ± 0.1	0	0	6.2
Chloromonas alpina	**0.024**	2.0 ± 2.4	0.5 ± 0.6	8.3	0.6 ± 0.6	0	**0.023**	7.5 ± 8.8	1.2 ± 3.4	8.2 ± 3.2	0.9	1.5
Chloromonas nivalis	0.093	0.2 ± 0.4	3.1 ± 4.2	15.1	0.1 ± 0.1	0.8 ± 1.1	0.375	8.6 ± 11.3	4.6 ± 3.8	4.2 ± 3.5	0.3	0.2
Chloromonas polyptera	0.169	3.4 ± 4.7	9.6 ± 6.3	33.9	9.0 ± 9.3	1.9 ± 1.4	**<0.001**	37.4 ± 22.8	14.5 ± 12.6	55.6 ± 15.8	6.1	1.5
Microglena sp.	**0.019**	20.2 ± 34.5	0	0	0.3 ± 0.5	0	0.661	0	0.0 ± 0.2	0	0.9	0
Raphidonema sempervirens	**0.002**	55.0± 46.9	5.9 ± 11.1	2.2	37.5 ± 23.2	27.7 ± 18.2	0.455	5.7 ± 10.6	2.8 ± 5.9	9.3 ± 15.8	87.5	83.6
Uncult. *Chlamydomonadaceae* (1)	**<0.001**	7.6 ± 7.6	74.9 ± 14.8	38.2	29.3 ± 17.2	57.0 ± 23.2	**<0.001**	26.8 ± 22.2	67.6 ± 16.0	14.4 ± 15.1	4.3	4.6
Uncult. *Chlamydomonadaceae* (2)	**0.004**	0.5 ± 0.3	4.8 ± 3.4	1.5	1.6 ± 1.5	0.9 ± 0.9	**0.007**	1.2 ± 1.3	5.1 ± 3.9	1.5 ± 1.6	0	0
Bacteria												
Bacteriodetes		32.3 ± 13.6	45.4 ± 27.1	31.9	18.0 ± 13.3	9.7 ± 11.3		34.3 ± 20.5	71.2 ± 27.3	88.0 ± 15.6	24.2 ± 18.5	3.1
Sphingobacteria	0.668	6.6 ± 6.1	3.7 ± 10.3	2.8	4.9 ± 2.8	1.2 ± 0.8	**<0.001**	20.7 ± 17.6	62.9 ± 27.5	85.6 ± 16.5	10.8 ± 0.5	2.5
Saprospirae	**0.058**	15.7 ± 20.8	24.3 ± 24.1	14.2	2.8 ± 2.8	8.3 ± 10.5	0.106	12.1 ± 13.4	4.6 ± 6.7	1.8 ± 1.0	9.3 ±13.1	0
Cytophagia	**0.054**	4.5 ± 3.1	16.7 ± 15.5	9.5	6.7 ± 11.9	0.1 ±0.1	0.202	1.4 ± 1.9	3.7 ± 4.7	0.6 ± 0.4	4.1 ± 5.7	0.6
Cyanobacteria		0.2 ± 0.1	17.4 ± 24.1	6.4	34.7 ± 25.3	71.7 ± 21.2		12.7 ± 25.1	9.7 ± 11.6	0.4 ± 0.6	3.1 ± 3.5	0.2
Nostocophycideae	0.322	0	0.7 ± 0.9	0	0.3 ± 0.8	0.1 ± 0.1	0.472	0.4 ± 0.9	3.4 ± 5.7	0.1 ± 0.1	0	0
Oscillatoriophycideae	0.636	0	1.7 ± 5.1	0	0.1 ± 0.2	0.2 ± 0.1	0.751	3.0 ± 9.0	1.9 ± 4.0	0.1 ± 0.1	0	0
Synechococco-phycideae	**<0.001**	0.2 ± 0.1	15.0 ± 22.4	6.4	34.3 ± 25.5	71.5 ± 21.2	0.357	1.6 ± 1.7	3.9 ± 6.7	0.3 ± 0.5	3.1± 3.5	0.2
Proteobacteria		43.8 ± 36.1	28.6 ± 18.7	47.8	13.4 ± 15.6	2.3 ± 2.9		41.2 ± 22.7	5.2 ± 6.6	6.5 ± 8.0	11.6 ± 8.5	70.2
Alphaproteobacteria	**0.014**	19.5 ± 32.6	2.8 ± 3.9	6.2	21.4 ± 15.6	4.4 ± 3.1	0.697	7.6 ± 8.0	9.7 ± 14.4	3.7 ± 4.7	37.3 ± 2.3	8.1
Betaproteobacteria	**0.003**	43.6 ± 36.1	27.8 ± 18.5	47.8	9.9 ± 10.5	2.1 ±2.9	**0.003**	40.2 ± 22.8	3.3 ± 5.4	6.4 ± 7.8	11.5 ± 8.3	18.7
Fungi [% of total eukaryotes]	**0.001**	21.6 ± 22.4	22.7 ± 10.9	27.5	24.3 ± 13.5	55.4 ± 22.	0.390	36.6 ± 15.1	44.3 ± 22.6	45.2 ± 18.1	38	10.9
Solids (C,N,P,S)												

Total C	0.084	1.8 ± 0.9	5.3 ± 4.5	7.8	2.3 ± 1.8	2.0 ± 1.0	**0.001**	1.4 ± 0.6	12.4 ± 7.2	23.7 ± 5.6	9.6 ± 6.3	10.4
Total N	0.081	0.16 ± 0.04	0.32 ± 0.26	0.81	0.15 ± 0.08	0.20 ± 0.09	**<0.001**	0.16 ± 0.08	0.61 ± 0.42	1.72 ± 0.17	0.85 ± 0.60	0.65
Total P	**0.025**	0.07 ± 0.02	0.07 ± 0.03	0.13	0.05 ± 0.01	0.04 ± 0.01	**0.009**	0.07 ± 0.02	0.06 ± 0.02		0.07 ± 0.01	0.06
Total S	**<0.001**	0.07 ± 0.02	0.11 ± 0.04	0.09	0.06 ± 0.01	0.06 ± 0.00	**<0.001**	0.03 ± 0.01	0.07 ± 0.02	0.16 ± 0.03	0.08 ± 0.04	0.12
C/N	0.764	12 ± 8	16 ± 3	10	29 ± 56	10 ± 1	**<0.001**	9 ± 3	22 ± 6	14 ± 4	12 ± 1	16
C/P	0.705	26 ± 10	63 ± 32	60	59 ± 74	51 ± 23	**0.013**	25 ± 11	186 ± 89		87 ± 40	168
N/P	0.219	3 ± 1	4 ± 2	6	3 ± 2	5 ± 2	**0.019**	3 ± 2	8 ± 3		7 ± 4	10
$\delta^{15}N$	0.106	-3.30 ± 1.50	-4.88 ± 2.50	4.24	-1.67 ± 3.97	-2.15 ± 1.24	0.400	-3.17 ± 3.54	-4.30 ± 1.84	-4.29 ± 0.65	-2.18 ± 0.62	-3.49
$\delta^{13}C$	**0.004**	-31.80 ± 6.30	-27.66 ± 1.61	-27.38	-26.24 ± 0.63	-25.49 ± 0.25	0.056	-26.99 ± 1.15	-25.70 ± 2.02	-28.98 ± 1.38	-25.84 ± 0.06	-25.96
Functional groups												
Carbohydrates	**0.008**	97.5 ± 1.0	91.5 ± 5.0	80.8	96.2 ± 2.6	n.s.	0.146	84.2 ± 17.2	77.1 ± 6.6	79.3 ± 5.1	89.0 ± 4.2	n.s.
Lipids	**0.001**	0.2 ± 0.0	2.7 ± 2.1	3.9	0.4 ± 0.3	n.s.	0.134	4.6 ± 6.8	8.1 ± 3.1	6.6 ± 3.2	2.7 ± 1.6	n.s.
Proteins	0.056	2.3 ± 0.9	5.7 ± 3.3	15.3	3.4 ± 2.4	n.s.	0.207	11.2 ± 10.5	14.7 ± 4.0	14.2 ± 2.6	8.3 ± 2.6	n.s.
Pigments												
Chlorophylls	**0.001**	55 ± 32	10 ± 5	21	66 ±26	53 ± 25	0.310	35 ± 24	14 ± 18	27 ± 18	38 ± 10	n.s.
Primary carotenoids	**0.014**	22 ± 22	11 ± 6	4	21 ± 21	43 ± 24	0.209	16 ± 21	6 ± 5	3 ± 2	51 ± 16	n.s.
Secondary carotenoids	**<0.001**	23 ± 14	80 ± 8	75	14 ± 18	4 ± 6	0.380	49 ± 28	80 ±17	70 ± 18	11 ± 7	n.s.
Fatty acids												
SFA	**0.003**	29 ± 6	32 ± 5	22	42 ± 8	33 ± 5	0.217	39 ± 5	37 ± 14	46 ± 1	34 ± 1	60
MUFA	**0.001**	24 ± 14	16 ± 5	37	20 ± 4	19 ± 3	**<0.001**	35 ± 4	13 ± 4	19 ± 1	13 ± 0	10
PUFA	**<0.001**	30 ± 14	50 ± 8	37	26 ± 7	28 ± 4	**<0.001**	24 ± 5	46 ± 13	28 ± 6	53 ± 1	1
Aqueous geochemistry												
SO4	**0.002**	106.0 ± 76.0	13.3 ± 46.2	0	28.0 ± 65.5	140.7 ± 11.1	0.752	0	18.5 ± 50.6	0	0	141.0
Fe	**0.009**	2.0 ± 1.8	1.9 ± 1.0	4.4	7.8 ± 5.7	5.0 ± 4.6	**<0.001**	5.0 ± 3.4	1.5 ± 1.0	10.0 ± 12.0	120.7 ± 67.0	8.4
K	**0.008**	99.0 ± 22.3	41.3 ± 20.3	120.0	38.5 ± 25.3	70.4 ± 48.9	**<0.001**	48.8 ± 14.7	62.3 ± 74.0	552.0 ± 445.6	43.3 ±38.4	33.0

Table 8.2: Average values and standard deviations for all geochemical compounds that revealed significant ($p<0.05$) differences between Svalbard and Arctic Sweden regardless of the habitats.

	Between locations
DOC [µM]	0.001
Cl [ppb]	<0.001
Ca [ppb]	0.096
Mn [ppb]	0.015
Mn [ppb]	0.027
Na [ppb]	0.001

Table 8.3: Statistical analysis of correlations between biological and geochemical compounds of all analysed samples. Table shows Pearson correlation factors (r) and significance of correlations (p). Correlations with $p < 0.05$ were considered to be significant.

	r	**p**
Algae and geochemistry		
Chloromonas cf. alpina ~ DOC	0.420	0.004
Chloromonas polyptera ~ DOC	0.593	<0.001
Chloromonas polyptera ~ K	0.424	0.002
Raphidonema sempervirens ~ Fe	0.411	0.003
Raphidonema sempervirens ~ Mn	0.402	0.004
Uncultured *Chlamydomonadaceae* (1) ~ C:N	0.337	0.019
Uncultured *Chlamydomonadaceae* (2) ~ C:N	0.456	0.001
Algae and metabolites		
Chloromonas cf. alpina ~ MUFA	0.509	<0.001
Uncultured *Chlamydomonadaceae* (1) ~ PUFA	0.596	<0.001
Uncultured *Chlamydomonadaceae* (2) ~ PUFA	0.593	<0.001
Raphidonema sempervirens ~ PUFA	-0.493	<0.001
Uncultured *Chlamydomonadaceae* (1) ~ Secondary Carotenoids	0.509	<0.001
Uncultured *Chlamydomonadaceae* (2) ~ Secondary Carotenoids	0.544	<0.001
Raphidonema sempervirens ~ Secondary Carotenoids	-0.608	<0.001
Raphidonema sempervirens ~ Primary Carotenoids	0.562	<0.001
Ancylonema nordenskiöldii ~ Antheraxanthin	0.590	0.094
Ancylonema nordenskiöldii ~ Zeaxanthin	0.979	<0.001
Uncultured *Chlamydomonadaceae* (2) ~ trans-Astaxanthin	0.509	0.001
Bacteria and geochemistry		
Sphingobacteria ~ DOC	0.567	<0.001
Sphingobacteria ~ TC	0.431	0.004
Sphingobacteria ~ C:N	0.418	0.003
Sphingobacteria ~ C:P	0.669	<0.001
Sphingobacteria ~ N:P	0.535	<0.001
Sphingobacteria ~ K	0.365	<0.001
Synechococcopycideae ~ SO4	0.398	0.005
Geochemistry and metabolites		
C:N ~ Lipids	0.457	<0.001
C:P ~ Lipids	0.832	<0.001

N:P ~ Lipids	0.782	<0.001
C:N ~ Proteins	0.356	0.011
C:P ~ Proteins	0.742	<0.001
N:P ~ Proteins	0.757	<0.001
C:N ~ Secondary carotenoids	0.428	0.002
C:P ~ Secondary carotenoids	0.246	0.108
N:P ~ Secondary carotenoids	0.630	0.075
C:N ~ PUFA	0.674	<0.001
C:P ~ PUFA	0.584	<0.001
N:P ~ PUFA	0.489	0.002
TC ~ DOC	0.588	<0.001

8.4 Discussion

In this study, we found clear differences for the community structure and function between the different habitats investigated on all studied glaciers. We show that the previously defined habitats on a single glacier in Greenland (Lutz et al 2014) are also applicable for another 12 glaciers and snow fields across the Arctic. With the current study we have for the first time evaluated the full microbial composition in several distinct glacial surface habitats through the use of high-throughput sequencing.

8.4.1 Algal community structure

The composition of red snow was very similar on all studied glaciers, as we have previously shown in a study where we specifically targeted red snow communities on glaciers in Greenland, Iceland, Svalbard and Sweden (Lutz et al, 2015b). In all sites the algal community in red snow was dominated by an uncultured *Chlamydomonadaceae* (2) regardless of variations in any metabolic or geochemical parameter differences between sites (Table E.2).

The algal composition of green snow, as opposed to our findings in red snow, varied strongly between locations with higher relative abundance of *Raphidonema sempervirens* and *Microglena sp*. in Svalbard, and *Chloromonas polyptera* in Sweden. It is important to note that the distribution of green snow on glacial surfaces is by far less important compared to the red snow distribution, which is the dominant snow algal habitat on all glaciers surveyed. In green snow the large

variations in community composition may imply that the green snow community is more sensitive to its physico-chemical environment. *Chloromonas polyptera* and *Chloromonas cf. alpina* seem to thrive in habitats with high water activity, namely green snow and biofilms, which also seem to accumulate a higher mineral content. *Chloromonas polyptera* was also found to be highly abundant in glacial snow in Iceland after heavy rain (Lutz et al., 2015a) and hence wet snow conditions. Both species also seem to prefer environments with more organic carbon and were positively correlated with DOC (Figure E.2 and Table 8.3). However, the variations in community composition of green snow may also be explained by potential different sources for the colonising species. In Svalbard a high concentration of elements likely derived from sea spray input (e.g., SO_4, Cl) or through the weathering of the bedrocks (e.g., Na, Ca, Mg, Table E.7) may indicate a different source for the development of green snow communities.

Surprisingly, the dirty ice habitat did not reveal a high abundance of the previously described ice algae *Ancylonema nordenskiöldii* and *Mesotaenium berggrenii* (Table E.2; Remias et al, 2012a; Remias et al, 2009; Yallop et al, 2012). Only a few samples from Svalbard showed a higher relative abundance of *Ancylonema nordenskiöldii* (up to 65%) and only very few sequences of *Mesotaenium berggrenii* (<0.01%). In our dirty ice samples the dominant algal species (between 10 and 88%) was *Raphidonema sempervirens,* better known as a permafrost algae (Stibal & Elster, 2005), and an uncultured *Chlamydomonadaceae* (2). The latter was most likely transferred to the ice surface from the melting snowpack above the ice as it was the dominant species in the snow. Most algal species identification in snow and ice environments have so far been done by microscopy and only very little sequencing data is available. Therefore there is a potential for misassignments between microscopy and sequencing information. Another reason for the apparent discrepancy between the dominant ice algae in our study and previous investigations could be a potential dominance of external input (*i.e.*, the uncultured *Chlamydomonadaceae* (2) from the melting snowpack, and *Raphidonema sempervirens* from the nearby soil) over *in-situ* thriving of *Ancylonema nordenskiöldii* and *Mesotaenium berggrenii* on dirty ice at the time of sampling.

8.4.2 Bacterial community structure

Overall far more sequencing data on bacteria from various glacial habitats is available in the literature compared to algae (Cameron et al, 2014; Edwards et al, 2011; Hell et al, 2013; Larose et al, 2010; Musilova et al, 2015). However, the data is primarily focussed on bacterial communities in clean snow or cryoconite holes. The transitions between habitats are also reflected in the changing bacterial community. For example, *Bacteriodetes* were dominating in red snow and biofilms in all locations (Figure 8.3 and Table E.4). They are known to play pivotal roles in the degradation of organic matter (Thomas et al, 2011). Cameron et al (2014) found a higher relative abundance of *Proteobacteria* (60%) in their summer snow samples from Greenland and other studies have reported a strong representation of the supraglacial communities including snow, ice and cryoconite holes by *Proteobacteria* (Edwards et al, 2014; Harding et al, 2011; Hell et al, 2013). The high relative abundance of *Bacteriodetes* in the red snow samples as well as their positive correlation with DOC may underpin the importance of red snow algal blooms as carbon source on glacial surfaces.

We found a decline in the relative abundance of *Bacteriodetes* when transitioning from snow to ice. Dirty ice was more dominated by *Proteobacteria* and we found varying compositions for cryoconite holes, which can be considered as the ‘end members’ of supraglacial habitats. The dominating phyla in cryoconite holes were *Cyanobacteria* in Svalbard and *Proteobacteria* in Sweden. There is a large similarity between the community composition of dirty ice and cryoconite holes within one location, which also reflects the transition between those habitats.

Green snow and dirty ice habitats were also dominated by *Proteobacteria*. Among these, *Betaproteobacteria* were dominant in green snow, whereas *Alphaproteobacteria* were dominant in dirty ice. Both habitats seem to be low in organic matter contents (both particulate organic carbon and DOC) compared to red snow, but with different selection pressure on the bacterial class level. *Alphaproteobacteria* have been shown to grow at low carbon and nutrient concentrations (Eiler et al, 2003), which are more typical for ice surfaces. On the other hand, *Betaproteobacteria* often use anaerobic decomposition products of organic-matter, which may be more common in green snow as this mostly forms close to glacial snouts and at the rock interfaces. Green snow is also usually much

'wetter' and more debris rich and has already experienced longer phases of melting.

Within the *Bacteriodetes*, *Sphingobacteria* were only highly abundant in Sweden. They are known to be capable of degrading complex organic structures (Thomas et al, 2011) and were positively correlated with TC and DOC (Figure E.3 and Table 8.3). This could be explained by the vicinity to higher plants and the high abundance of pollen in our samples (Table E.8).

In Svalbard there was a higher relative abundance of species with pathogenic life styles including *Cytophagia, Flavobacteria* and *Saprospirae*, which are known to be microalgal pathogens (Salomon & Imai, 2006). In addition, the fungi *Chytridiomycota* also showed a higher abundance in Svalbard which have been found to be involved in parasitic associations with microalgae (Ibelings et al, 2004). This may imply the presence of important nutrient recycling processes based on non-mutual symbiotic relationships between algae and other community members in Svalbard.

Cyanobacteria were only abundant in dirty ice and cryoconite holes in Svalbard, but not in Sweden. Within the *Synechococcophycidae*, the *Leptolyngbya* were dominant which corroborates the findings of Kaštovská et al. (2005).

8.4.3 Archaeal community structure

Archaea were detected in all analysed samples and showed very low diversity (Table E.5). The species composition was mainly represented by two taxa, the *Nitrosophaerales* and *Methanobacteriales*. *Nitrosphaerales* are important ammonia-oxidizers (Stieglmeier et al, 2014; Tourna et al, 2011; Zarsky et al, 2013), whereas *Methanobacteriales* are anaerobic methanogens. We could not establish any trends for their distribution within the studied habitats.

8.4.4 Community function

Most of our samples showed C/N ratios (Figure E.4, Tables 8.3 and E.8) above the Redfield ratio (C/N/P:106/16/1) which has been described to be optimal for algal exponential growth and incorporation of macronutrients into reproductive

biomolecules including phosphate-rich ribosomes (Klausmeier et al, 2004; Sterner & Elser, 2002). If nitrogen or phosphorus become limiting, carbon incorporation is preferentially stored as starch or lipids leading to a high C/N cellular ratio (James et al, 2011). This matches previous finding confirming nitrogen limitation in snow by algae (Jones & Deblois, 1987; Jones & Tranter, 1989). This is further reflected in the low N/P ratios found across our samples (Figure E.4, Tables 8.3 and E.8). Low N/P ratios have also been observed in phytoplankton during blooms since fast-growing cells require phosphorus for ribosomes (Klausmeier et al, 2004; Sterner & Elser, 2002). In contrast, most of our samples showed low C/P ratios and hence less P limitation. Only red snow samples from Sweden showed high C/P ratios and therefore indicating co-limitation of nitrogen and phosphorus in this particular habitat. However, it cannot be excluded that the high abundance of pollen in Sweden contributed to a higher TC and therefore higher C/N and C/P ratios and also a higher relative abundance of proteins compared to Svalbard.

Lipids were highest in red snow in both Svalbard and Sweden and were positively correlated with C/N ratios (Figure 8.6, Tables 8.3). Accumulation of lipids has been found to be a consequence of nitrogen limitation in cryophilic algae (Pichrtová et al, 2014) since metabolism is shifted to the production of nitrogen-free metabolites during nitrogen limiting conditions. Triacylglycerol (TGA) neutral lipids are often synthesized in response to high light or nutrient deprivation (James et al, 2011). Lipid bodies can also store dissolved astaxanthin which may be a valuable long-term energy source. In addition, C/N ratios in red snow could have also been increased as an effect of the cyst formation of mature snow algal cells and incorporation of nitrogen- and phosphorus-free carotenoids.

The abundance of C,N, and P also positively correlated with the production of important cryophilic biomolecules including fatty acids and pigments (Figure 8.6 and Table 8.3). Algae can change their fatty acid composition in response to changing environmental conditions including temperature, pH and nutrients (James et al, 2011). PUFAs (in particular C16:4 and C18:3) were dominant in red snow in both Sweden and Svalbard and strongly correlated with the presence of the two uncultured *Chlamydomonadaceae* (1) and (2) and high C/N ratios (Figures 8.4, Table 8.3). This is in accordance with laboratory investigations on nitrogen deprived *Chlamydomonas reinhardtii* starch mutants, which produced more MUFAs and also PUFAs including C18:3 compared to nitrogen-sufficient conditions. MUFAs in phospholipids have been found to maintain membrane

fluidity (Bidigare 1993, Leya 2004). They were most abundant in green snow and biofilm samples, the two habitats with the highest water activity and therefore more sensitive to freezing. C15 branched fatty acids are known as biomarker for bacteria (Zelles, 1999) and high abundance in dirty ice and in particular in cryoconite holes is likely due to cyanobacteria.

Secondary carotenoid production was positively correlated with high C/N, C/P and N/P ratios (Figure 8.6, Table 8.3). Our data show that snow and ice algae use different carotenoid synthesis strategies. The main snow algal species showed a strong correlation with secondary carotenoids, whereas there was a negative correlation for the ice algae *Raphidonema sempervirens* and a positive correlation for primary carotenoids (Figure 8.5 and Table 8.3). The second most abundant ice algae *Ancylonema nordenskiöldii* was also positively correlated with the two primary carotenoids Zeaxanthin and Antheraxanthin which may imply that these species are using the xanthophyll cycle instead. This cycle involves the enzymatic removal of epoxy groups from Violaxanthin and Antheraxanthin which results in the de-epoxidised xantophyll Zeaxanthin (Remias, 2012). The production of secondary carotenoids has not been shown yet for ice algae (Leya et al, 2009) and the negative correlation for *Raphidonema sempervirens* and secondary carotenoids as well as with PUFAs that correlate with those indicates the absence of secondary carotenoid production in ice algae.

Nitrogen isotopes did not show any differences between habitats or locations and were predominantly negative suggesting an atmospheric nitrogen source for all samples (Figure E.5, Table E.8). In contrast, carbon isotopes were lower in snow than ice habitats in Svalbard. This could indicate different photosynthetic mechanism and/or more input of allochthonous carbon in the snow samples since the $\delta^{13}C$ values reflect those of vascular plants (Farquhar et al, 1989). No significant variations could be found for Sweden, likely due to the presence of pollen.

Therefore, our study provides indication that production of a range of quantified metabolites in snow and ice algae is driven mainly by the availability of N and less by P but likely also changes the intracellular C/N/P ratios. Correlations between metabolites, geochemistry and single species can be used to unravel mixed metabolic signals in complex communities and assign them to single species and make assumptions about their role in the respective habitat. However, nutrients

stoichiometry may not be the only factor affecting community structure, and other parameters including pH and the physical state of the water may also play an important role.

8.4.5 Implications for the past and future of glacial surfaces

The environment determines the distribution and structure of algal communities, but in return algal blooms also alter their environment after successful colonisation of the different surface glacial habitats. Algal communities exhibit short generation times and are able to adapt their metabolic inventory quickly as response to environmental conditions that change over time and space. Studying their ecological patterns and how these may be altered can give us a valuable outlook into how Arctic glacial and ice sheet surface ecosystems may respond to a changing climate. Climate-warming is predicted to have a large impact on glacial runoff and this will, in turn, also have an effect on organic carbon fluxes from glacial surface to downstream ecosystems (Hood et al, 2015). The contribution of DOC from all mountain glaciers is higher (56% of total DOC export) than from the Greenland and Antarctic ice sheets (Hood et al, 2015). With regard to carbon and nutrient export, snow microbial communities are the prime habitat feeding other supraglacial, subglacial and periglacial habitats (Hodson et al, 2008; Schütte et al, 2009; Telling et al, 2011; Wynn et al, 2007)

Production of the quantified metabolites is driven by availability of major nutrients, which is especially important for production of secondary carotenoids, which in turn can cause a darkening of the glacial surfaces and therefore a decrease in surface albedo. We show that secondary carotenoid production is positively correlated with nitrogen limitation. Considering lower pre-anthropogenic nitrogen levels, this effect may have been even higher in past glaciation events and may have contributed to local heat retention due to lower surface albedos and providing other glacial communities with water in its liquid state, which is crucial for life in general. Possibly, this effect also extends the active growth season of snow algae due to earlier and prolonged availability of liquid water. Furthermore, increasing nitrogen deposition in the future may lead to higher cell numbers eventually reaching limiting conditions and a more widespread darkening effect.

Acknowledgments

The authors would like to thank Andrew Detheridge (Aberystwyth University), and Christy Waterfall and Jane Coghill (University of Bristol) for help with the DNA sequencing. We would like to acknowledge Anthony Stockdale (University of Leeds) for the phosphorus analysis and Fiona Gill for help with the fatty acids analysis. This work was funded by a University of Leeds grant to SL and LGB, by the Young Explorers grant from National Geographic and the President's Fund for Research Visit grant from the Society for General Microbiology granted to SL, the NE/J022365/1 grant to LGB and the NE/J02399X/1 grant to AMA.

References

Anesio, A. M. & Laybourn-Parry, J. (2012) Glaciers and ice sheets as a biome. *Trends in ecology & evolution*, 27(4), 219-225.

Benning, L. G., Anesio, A. M., Lutz, S. & Tranter, M. (2014) Biological impact on Greenland's albedo. *Nature Geoscience*, 7(10), 691-691.

Boussiba, S. (2000) Carotenogenesis in the green alga Haematococcus pluvialis: cellular physiology and stress response. *Physiologia Plantarum*, 108(2), 111-117.

Cameron, K. A., Hagedorn, B., Dieser, M., Christner, B. C., Choquette, K., Sletten, R., Crump, B., Kellogg, C. & Junge, K. (2014) Diversity and potential sources of microbiota associated with snow on western portions of the Greenland Ice Sheet. *Environmental microbiology*, 17(3), 594-609.

Cameron, K. A., Hodson, A. J. & Osborn, A. M. (2012) Structure and diversity of bacterial, eukaryotic and archaeal communities in glacial cryoconite holes from the Arctic and the Antarctic. *FEMS microbiology ecology*, 82(2), 254-267.

Caporaso, J. G., Kuczynski, J., Stombaugh, J., Bittinger, K., Bushman, F. D., Costello, E. K., Fierer, N., Pena, A. G., Goodrich, J. K. & Gordon, J. I. (2010) QIIME allows analysis of high-throughput community sequencing data. *Nature methods*, 7(5), 335-336.

Edwards, A., Anesio, A. M., Rassner, S. M., Sattler, B., Hubbard, B., Perkins, W. T., Young, M. & Griffith, G. W. (2011) Possible interactions between bacterial diversity, microbial activity and supraglacial hydrology of cryoconite holes in Svalbard. *The ISME journal*, 5(1), 150-160.

Edwards, A., Mur, L. A., Girdwood, S. E., Anesio, A. M., Stibal, M., Rassner, S. M., Hell, K., Pachebat, J. A., Post, B. & Bussell, J. S. (2014) Coupled cryoconite

ecosystem structure–function relationships are revealed by comparing bacterial communities in alpine and Arctic glaciers. *FEMS microbiology ecology*, 89(2), 222-237.

Eiler, A., Langenheder, S., Bertilsson, S. & Tranvik, L. J. (2003) Heterotrophic bacterial growth efficiency and community structure at different natural organic carbon concentrations. *Applied and environmental microbiology*, 69(7), 3701-3709.

Farquhar, G. D., Ehleringer, J. R. & Hubick, K. T. (1989) Carbon isotope discrimination and photosynthesis. *Annual review of plant biology*, 40(1), 503-537.

Fujii, M., Takano, Y., Kojima, H., Hoshino, T., Tanaka, R. & Fukui, M. (2010) Microbial community structure, pigment composition, and nitrogen source of red snow in Antarctica. *Microbial ecology*, 59(3), 466-475.

Hammer, O., Harper, D. & Ryan, P. (2012) PAST: paleontological statistics software package for education and data analysis. Paleontol Electron 4 (art. 4): 9.

Harding, T., Jungblut, A. D., Lovejoy, C. & Vincent, W. F. (2011) Microbes in high Arctic snow and implications for the cold biosphere. *Applied and environmental microbiology*, 77(10), 3234-3243.

Hell, K., Edwards, A., Zarsky, J., Podmirseg, S. M., Girdwood, S., Pachebat, J. A., Insam, H. & Sattler, B. (2013) The dynamic bacterial communities of a melting High Arctic glacier snowpack. *The ISME journal*, 7(9), 1814-1826.

Hodson, A., Anesio, A. M., Tranter, M., Fountain, A., Osborn, M., Priscu, J., Laybourn-Parry, J. & Sattler, B. (2008) Glacial ecosystems. *Ecological Monographs*, 78(1), 41-67.

Hood, E., Battin, T. J., Fellman, J., O'Neel, S. & Spencer, R. G. (2015) Storage and release of organic carbon from glaciers and ice sheets. *Nature Geoscience*, 8(2), 91-96.

Ibelings, B. W., De Bruin, A., Kagami, M., Rijkeboer, M., Brehm, M. & Donk, E. V. (2004) Host parasite interactions between freshwater phytoplankton and chytrid fungi (Chytridiomycota). *Journal of Phycology*, 40(3), 437-453.

James, G. O., Hocart, C. H., Hillier, W., Chen, H., Kordbacheh, F., Price, G. D. & Djordjevic, M. A. (2011) Fatty acid profiling of Chlamydomonas reinhardtii under nitrogen deprivation. *Bioresource technology*, 102(3), 3343-3351.

Jones, H. & Deblois, C. (1987) Chemical dynamics of N-containing ionic species in a boreal forest snowcover during the spring melt period. *Hydrological Processes*, 1(3), 271-282.

Jones, H. & Tranter, M. (1989) Interactions Between Meltwater and Organic-Rich Particulate Material in Boreal Forest Snowpacks: Evidence for Both Physico-Chemical and Microbiological Influences.

Kaštovská, K., Elster, J., Stibal, M. & Šantrůčková, H. (2005) Microbial assemblages in soil microbial succession after glacial retreat in Svalbard (high Arctic). *Microbial ecology*, 50(3), 396-407.

Klausmeier, C. A., Litchman, E., Daufresne, T. & Levin, S. A. (2004) Optimal nitrogen-to-phosphorus stoichiometry of phytoplankton. *Nature*, 429(6988), 171-174.

Larose, C., Berger, S., Ferrari, C., Navarro, E., Dommergue, A., Schneider, D. & Vogel, T. M. (2010) Microbial sequences retrieved from environmental samples from seasonal Arctic snow and meltwater from Svalbard, Norway. *Extremophiles*, 14(2), 205-212.

Leya, T., Müller, T., Ling, H. U. & Fuhr, G. (2004) Snow algae from north-western Spitsbergen (Svalbard). *The coastal ecosystem of Kongsfjorden, Svalbard. Synopsis of biological research performed at the Koldewey Station in the years 1991-2003*, 46-54.

Leya, T., Rahn, A., Lütz, C. & Remias, D. (2009) Response of arctic snow and permafrost algae to high light and nitrogen stress by changes in pigment composition and applied aspects for biotechnology. *FEMS microbiology ecology*, 67(3), 432-443.

Lutz, S., Anesio, A. M., Edwards, A. & Benning, L. G. (2015a) Microbial diversity on Icelandic glaciers and ice caps. *Frontiers in microbiology*, 6, 307.

Lutz, S., Anesio, A. M., Raiswell, R., Edwards, A., Newton, R. J., Gill, F. & Benning, L. G. (2015b) Algae Melt Arctic Glaciers: The Biogeography and Function of Snow Microbiomes. *In Review with Nature Communications*.

Lutz, S., Anesio, A. M., Villar, S. E. J. & Benning, L. G. (2014) Variations of algal communities cause darkening of a Greenland glacier. *FEMS microbiology ecology*, 89(2), 402-414.

Müller, T., Leya, T. & Fuhr, G. (2001) Persistent snow algal fields in Spitsbergen: field observations and a hypothesis about the annual cell circulation. *Arctic, Antarctic, and Alpine Research*, 42-51.

Musilova, M., Tranter, M., Bennett, S. A., Wadham, J. & Anesio, A. M. (2015) Stable microbial community composition on the Greenland Ice Sheet. *Frontiers in microbiology*, 6, 193.

Pichrtová, M., Kulichová, J. & Holzinger, A. (2014) Nitrogen Limitation and Slow Drying Induce Desiccation Tolerance in Conjugating Green Algae (Zygnematophyceae, Streptophyta) from Polar Habitats. *PloS one*, 9(11), e113137.

Remias, D. (2012) *Cell structure and physiology of alpine snow and ice algae*. Vienna: Springer.

Remias, D., Holzinger, A., Aigner, S. & Lütz, C. (2012a) Ecophysiology and ultrastructure of Ancylonema nordenskiöldii (Zygnematales, Streptophyta), causing brown ice on glaciers in Svalbard (high arctic). *Polar Biology*, 35(6), 1-10.

Remias, D., Holzinger, A. & Lütz, C. (2009) Physiology, ultrastructure and habitat of the ice alga Mesotaenium berggrenii (Zygnemaphyceae, Chlorophyta) from glaciers in the European Alps. *Phycologia*, 48(4), 302-312.

Remias, D., Lütz-Meindl, U. & Lütz, C. (2005) Photosynthesis, pigments and ultrastructure of the alpine snow alga Chlamydomonas nivalis. *European Journal of Phycology*, 40(3), 259-268.

Remias, D., Schwaiger, S., Aigner, S., Leya, T., Stuppner, H. & Lütz, C. (2012b) Characterization of an UV-and VIS-absorbing, purpurogallin-derived secondary pigment new to algae and highly abundant in Mesotaenium berggrenii (Zygnematophyceae, Chlorophyta), an extremophyte living on glaciers. *FEMS microbiology ecology*, 79(3), 638-648.

Remias, D., Wastian, H., Lütz, C. & Leya, T. (2013) Insights into the biology and phylogeny of Chloromonas polyptera (Chlorophyta), an alga causing orange snow in Maritime Antarctica. *Antarctic Science*, 25(05), 648-656.

Ruttenberg, K., Ogawa, N., Tamburini, F., Briggs, R., Colasacco, N. & Joyce, E. (2009) Improved, high-throughput approach for phosphorus speciation in natural sediments via the SEDEX sequential extraction method. *Limnology and Oceanography: Methods*, 7(5), 319-333.

Salomon, P. & Imai, I. (2006) Pathogens of harmful microalgae, *Ecology of Harmful Algae*Springer, 271-282.

Schütte, U. M., Abdo, Z., Bent, S. J., Williams, C. J., Schneider, G. M., Solheim, B. & Forney, L. J. (2009) Bacterial succession in a glacier foreland of the High Arctic. *The ISME journal*, 3(11), 1258-1268.

Sterner, R. W. & Elser, J. J. (2002) *Ecological stoichiometry: the biology of elements from molecules to the biosphere*Princeton University Press.

Stibal, M. & Elster, J. (2005) Growth and morphology variation as a response to changing environmental factors in two Arctic species of Raphidonema (Trebouxiophyceae) from snow and soil. *Polar Biology*, 28(7), 558-567.

Stieglmeier, M., Klingl, A., Alves, R. J., Simon, K.-M. R., Melcher, M., Leisch, N. & Schleper, C. (2014) Nitrososphaera viennensis sp. nov., an aerobic and mesophilic ammonia-oxidizing archaeon from soil and member of the archaeal phylum Thaumarchaeota. *International Journal of Systematic and Evolutionary Microbiology*, 64, 2738-2752.

Takeuchi, N. (2002) The altitudinal distribution of snow algae on an Alaska glacier (Gulkana Glacier in the Alaska Range). *Hydrological Processes*, 15(18), 3447-3459.

Takeuchi, N. (2013) Seasonal and altitudinal variations in snow algal communities on an Alaskan glacier (Gulkana glacier in the Alaska range). *Environmental Research Letters*, 8(3), 035002.

Telling, J., Anesio, A. M., Tranter, M., Irvine-Fynn, T., Hodson, A., Butler, C. & Wadham, J. (2011) Nitrogen fixation on Arctic glaciers, Svalbard. *Journal of Geophysical Research*, 116(G3), G03039.

Thomas, F., Hehemann, J.-H., Rebuffet, E., Czjzek, M. & Michel, G. (2011) Environmental and gut bacteroidetes: the food connection. *Frontiers in microbiology*, 2, 93.

Thomas, W. H. & Duval, B. (1995) Sierra Nevada, California, USA, snow algae: snow albedo changes, algal-bacterial interrelationships, and ultraviolet radiation effects. *Arctic and alpine research*, 27(4), 389-399.

Thompson Jr, G. A. (1996) Lipids and membrane function in green algae. *Biochimica et Biophysica Acta (BBA)-Lipids and Lipid Metabolism*, 1302(1), 17-45.

Tourna, M., Stieglmeier, M., Spang, A., Könneke, M., Schintlmeister, A., Urich, T., Engel, M., Schloter, M., Wagner, M. & Richter, A. (2011) Nitrososphaera viennensis, an ammonia oxidizing archaeon from soil. *Proceedings of the National Academy of Sciences*, 108(20), 8420-8425.

Wynn, P. M., Hodson, A. J., Heaton, T. H. & Chenery, S. (2007) Nitrate production beneath a High Arctic glacier, Svalbard. *Chemical geology*, 244(1), 88-102.

Yallop, M. L., Anesio, A. M., Perkins, R. G., Cook, J., Telling, J., Fagan, D., MacFarlane, J., Stibal, M., Barker, G. & Bellas, C. (2012) Photophysiology and albedo-changing potential of the ice algal community on the surface of the Greenland ice sheet. *The ISME journal*, 6(12), 2302-2313.

Yoshimura, Y., Kohshima, S., Takeuchi, N., Seko, K. & Fujita, K. (2006) Snow algae in a Himalayan ice core: new environmental markers for ice-core analyses and their correlation with summer mass balance. *Annals of Glaciology*, 43(1), 148-153.

Zarsky, J. D., Stibal, M., Hodson, A., Sattler, B., Schostag, M., Hansen, L. H., Jacobsen, C. S. & Psenner, R. (2013) Large cryoconite aggregates on a Svalbard glacier support a diverse microbial community including ammonia-oxidizing archaea. *Environmental Research Letters*, 8(3), 035044.

Zelles, L. (1999) Fatty acid patterns of phospholipids and lipopolysaccharides in the characterisation of microbial communities in soil: a review. *Biology and Fertility of Soils*, 29(2), 111-129.

Chapter 9: Synthesis discussion

In the following I will bring together and discuss the main findings from chapters 4-8 and contrast those to the proposed research hypotheses (see 1.2):

9.1 Snow and ice algae are important primary colonisers and net producers

On all studied 21 glaciers (Figure 3.1) I could find snow algal blooms, even on the 8 glaciers and snow fields in Iceland where so far no single description of snow algae had existed (see chapter 5). This underpins their important role in these ecosystems.

In chapter 4, I described their development after the onset of melting over a three week period on a single glacier in Greenland and during the exceptional high melting season in July 2012. I found that snow and ice algae were the first communities to appear after the onset of melting and their blooming was the dominant process. I observed a clear change in the dominant algal community with the snow line progressing higher up and most snow fields transgressed through a red snow to grey ice stage (Figure 4.2).

Snow and ice algae are not only important primary colonisers, they are also an important carbon source. The positive net photosynthetic rates (*i.e.*, assumed here as an indicative of the accumulation of organic matter) in the snow and ice samples compared to the cryoconite hole samples (Figure 4.3) collected at the same time showed that snow and ice algae dominate the primary production at the onset of melting. Primary productivity of ice algae has also been reported by Yallop et al (2012) and they have also suggested that ice algae may fix up to eleven times more carbon than cryoconite holes (based on dry weight of sediment). Combining the contribution of the early-season dominating snow algae and the late-season dominating ice algae on primary productivity and thus carbon fluxes, leads me to suggest that they are major players in the ecology of glaciers and ice sheets and potentially strong impact on adjacent ecosystems.

These findings confirm my 1st and 2nd hypotheses:

"Snow and ice algae are important primary colonisers and producers on glacial surfaces."

"Snow algae are present and abundant in Iceland where not a single description of snow algae exists so far."

9.2 Red snow algae are cosmopolitan and independent of location specific factors

In chapter 7, I show that snow algae are cosmopolitan, despite recent molecular studies that suggest that micro-eukaryotes show strong biogeography (Ryšánek et al, 2014) and most microbial taxa do not inherit a cosmopolitan distribution (Foissner, 2006; Green & Bohannan, 2006; Martiny et al, 2006), not even within a specific habitat. I could not find any trends for any of the physico-chemical parameters within the 40 red snow samples from 16 glaciers in Svalbard, Arctic Sweden, Greenland and Iceland. The algal diversity is very low and six taxa made up >99% of the algal communities (Figure 7.2) and all have similar relative abundance values across all samples: two uncultured *Chlamydomonadaceae* (a) with 39-75% and (b) with 0-5% C*hloromonas polyptera* (10-26%), *Chloromonas nivalis* (3-13%), *Chloromonas alpina* (0-1%) and *Raphidonema sempervirens* (1-18%). Although I may not have captured all environmental parameters, the same patterns can be observed on all studied glaciers regardless their geochemical and mineralogical compositions and surface melting is likely a major driver for the algal distribution, which had also been suggested by Stibal et al. (2007).

9.3 Green and red snow are two independent and not successive phenomena

In chapter 6, I show that green and red snow on a glacier in Svalbard do not only vary in their community composition, but also in their physico-chemical environment and metabolic profiles (Figures 6.2 and 6.3). For the algae this likely reflects both different stages of their life cycles and their adaptation strategies. Green snow represents a wet, carbon and nutrient rich environment and is dominated by the algae *Microglena* sp. with a metabolic profile that is

characterized by key metabolites involved in growth and proliferation (e.g., tryptophan degradation pathway). In contrast, the dry and nutrient poor red snow habitat is colonised by various *Chloromonas* species with a high abundance of storage and reserve metabolites likely to face upcoming severe conditions (e.g., upregulation of the uridine monophosphate biosynthesis pathway to synthesize ribonucleotides). My data suggests that green snow and red snow are not successive stages but two independent phenomena with different requirements to their environments.

In chapter 8, the composition of green snow, as opposed to my findings on red snow, varied strongly between the studied locations with higher relative abundance of *Raphidonema sempervirens* and *Microglena sp.* in Svalbard (see chapters 6 and 8), and *Chloromonas polyptera* in Sweden (see chapter 8). It is important to note that the distribution of green snow on glacial surfaces is by far smaller compared to the red snow distribution, which is the dominant snow algal habitat on all glaciers. In green snow the large variations in community composition may imply that the green snow community is more sensitive to its physico-chemical environment. *Chloromonas polyptera* and *Chloromonas cf. alpina* seem to thrive in habitats with high water activity, namely green snow and biofilms, which also seem to accumulate a higher mineral content. *Chloromonas polyptera* was also found to be highly abundant in glacial snow in Iceland after heavy rain (see chapter 5) and hence wet snow conditions. Both species also seem to prefer a high organic environment and were positively correlated with DOC (Table 8.3, Figure E.2). However, the variations in community composition of green snow may also be explained by potential different sources for the colonising species. In Svalbard a high concentration of elements that may be derived from sea spray input (e.g., SO_4, Cl) or through the weathering of basal rocks (e.g., Na, Ca, Mg, Table E.7) has been found and may indicate a different source for the development of green snow communities.

These findings disprove my 3rd hypothesis:

"Green and red snow are successive stages."

9.4 Ice algae community composition seemingly influenced by external snow and soil input

Surprisingly, the grey ice habitat did not reveal a high abundance of the two main described ice algae *Ancylonema nordenskiöldii* and *Mesotaenium berggrenii* (Table E.2; Remias et al, 2012; Remias et al, 2009; Yallop et al, 2012). In my samples the dominant algal species (up to 88%) was *Raphidonema sempervirens*, better known as a permafrost algae (Stibal & Elster, 2005), and the uncultured *Chlamydomonadaceae* that was also most abundant in all red snow samples (see 9.2). The latter was most likely transferred to the ice surface from the melting snowpack above the ice. One reason for the apparent discrepancy between the dominant ice algae in our study and previous investigations could be a potential domination of external input (uncultured *Chlamydomonadaceae* from the snowpack, *Raphidonema sempervirens* from nearby soil) over *in-situ* thriving of *Ancylonema nordenskiöldii* and *Mesotaenium berggrenii* on dirty ice at the time of sampling. Another reason could be a potential for sequencing bias or misassignments between microscopy and sequencing information (see 9.5).

9.5 Possible discrepancies between sequencing and microscopy data

Most algal species identifications have so far been done by microscopy and only very little sequencing data is available. It is well known that algae can dramatically change their morphologies during their life cycles (Müller et al., 2001). This makes classifications and inter-study comparisons based on microscopy very challenging and over the course of the last decades many snow algal species have been re-classified in some cases even several times (personal communication from Dr Thomas Leya). For this reason, the most described snow algal taxa *Chlamydomonas nivalis* and *Chloromonas nivalis* need to be treated as collective taxa and not as single species (Leya et al., 2004). Those taxa were not most abundant in this study, but an uncultured *Chlamydomonadaceae* species that is closely related to other *Chloromonas* species as shown in chapter 5 (Figure B.2). Furthermore the grey ice habitat did not reveal a high abundance of the two main described ice algae *Ancylonema nordenskiöldii* and *Mesotaenium berggrenii* (Remias et al, 2012; Remias et al, 2009; Yallop et al, 2012), but a high abundance

of *Raphidonema sempervirens*. This could be because of similar morphologies and thus difficulties in species assignment by microscopy.

9.6 Bacteria show biogeography and differences between habitats

Overall far more sequencing data on bacteria from various glacial habitats is available in the literature compared to algae (Cameron et al, 2014; Harding et al, 2011; Maccario et al, 2014). In this study, bacteria were mostly represented by the phyla *Bacteriodetes*, *Proteobacteria* and *Cyanobacteria* (Figures 5.6, 7.2, 8.3). These bacterial phyla have previously been described in snow environments (Cameron et al, 2014; Hell et al, 2013; Larose et al, 2010).

The bacterial community composition varied between the different habitats (see chapter 8). *Bacteriodetes* showed the highest relative abundance in red snow and I found a decline in their relative abundance from snow to ice. Dirty ice was more dominated by *Proteobacteria* and I found varying compositions for cryoconite holes which can be seen as the 'end members' of supraglacial habitats. The dominating phyla in cryoconite holes were *Cyanobacteria* in Svalbard and *Proteobacteria* in Sweden. There is a large similarity between the species compositions of dirty ice and cryoconite holes within one location, which reflects the transition between habitats.

In contrast to the algae, the bacteria also showed strong biogeography on the class level and despite of their small cell size and therefore high potential for universal distribution. This is in accordance with recent studies of other microbial habitats (e.g., soil, marine; Foissner, 2006; Green & Bohannan, 2006; Martiny et al, 2006). In chapter 7, I show that there are significant difference ($p<0.05$) for the relative abundance of bacterial classes between locations within the red snow habitat. *Saprospirae*, *Cytophagia*, *Betaproteobacteria* and *Synechococcophycideae* were dominant in Svalbard, *Sphingobacteria* in Northern Sweden, *Sphingobacteria* and *Saprospirae* in Greenland, and *Saprospirae*, *Betaproteobacteria* and *Alphaproteobacteria* in Iceland (Figure 7.2).

9.7 Archaea show low species diversity

Archaea have been detected in all analysed samples and showed very low diversity. Currently, only very few studies have documented the presence of archaea in glacial environments and they offer a consensus that the diversity of archaea on glacial surfaces is low (Battin et al, 2001; Boyd et al, 2011; Cameron et al, 2012; Zarsky et al, 2013).

In my samples, the species composition was mainly represented by three groups, the *Nitrosophaerales, Methanobacteriales* and *Methanosarcinales* (Tables 5.7, D.5, E.5), which matches the results of the above mentioned studies. *Nitrosphaerales* are important ammonia-oxidizers (Stieglmeier et al, 2014; Tourna et al, 2011; Zarsky et al, 2013), whereas *Methanobacteriales* and *Methanosarcinales* are anaerobic methanogens. I could not establish any trends for their distribution within the studied habitats. Some of the samples with a high abundance of methanogens were found close to the glacier snouts and thus could be derived from a subglacial source. However, in order to fully explore such links further detailed analyses are needed.

The findings summarised in 9.2-9.7 confirm mostly my 4th hypothesis. However, they disprove it in particular for the red snow algae and the archaea:

"The microbial community composition varies over time and space"

9.8 Relationships for solid C/N/P ratios but not aqueous geochemistry with community composition and metabolites

In none of the studies (chapter 4-8) I could find trends for the aqueous geochemical parameters and the different habitats, neither could I establish relationships for those with the microbial community structure or the quantified metabolites. DOC was the only aqueous parameter that was significantly higher in the snow and biofilm habitats compared to the ice, which may underpin the importance of snow algal blooms as carbon source to downstream habitats (e.g., ice, soil, the ocean). Yet, the lack of trends could be because of the dynamic nature of glacial surface systems. Single-point measurements may not be representative enough due to the

fast melting in summer. In addition, other parameters including pH and the physical state of the water may also play an important role.

In contrast, I could establish relationships for the solid C/N/P ratios and the microbial community structure and quantified macromolecules and metabolites. Most of my snow and ice samples showed C/N ratios (Figure E.4) above the Redfield ratio (C/N/P:106/16/1) which has been described to be optimal for algal exponential growth and incorporation of macronutrients into reproductive biomolecules including phosphate-rich ribosomes (Klausmeier et al, 2004; Sterner & Elser, 2002). If nitrogen or phosphorus become limiting, carbon incorporation is preferentially stored as starch or lipids leading to a high C/N cellular ratio (James et al, 2011). In contrast, most of my samples showed low C/P ratios. Only red snow samples from Sweden showed high C/P ratios and therefore indicating co-limitation of nitrogen and phosphorus in this particular habitat.

The abundance of C, N, and P also positively correlated with the production of important macromolecules and metabolites including lipids, fatty acids and pigments (Figure 8.6). Lipids were highest in red snow in both Svalbard and Sweden and were positively correlated with C/N ratios (Figure 8.6). Accumulation of lipids has been found to be a consequence of nitrogen limitation in cryophilic algae (Pichrtová et al, 2014) since metabolism is shifted to the production of nitrogen-free metabolites during nitrogen limiting conditions.

PUFAs (in particular C16:4 and C18:3) were dominant in red snow in both Sweden and Svalbard, and strongly correlated with the presence of the mostly abundant uncultured *Chlamydomonadaceae* and high C/N ratios (Figures 8.4). This is in accordance with laboratory investigations on nitrogen deprived *Chlamydomonas reinhardtii* starch mutants, which produced more MUFAs and also PUFAs including C18:3 compared to nitrogen-sufficient conditions. MUFAs in phospholipids have been found to maintain membrane fluidity (Bidigare 1993, Leya 2004). They were most abundant in green snow and biofilm samples, the two habitats with the highest water activity and therefore more sensitive to freezing.

Secondary carotenoid production was positively correlated with high C/N, C/P and N/P ratios (Figure 8.6). My data shows that snow and ice algae use different carotenoids strategies. The main snow algal species showed a strong correlation with secondary carotenoids, whereas there was a negative correlation for the ice algae *Raphidonema sempervirens* and a positive correlation for primary carotenoids (Figure 8.5). The second most abundant ice algae *Ancylonema*

nordenskiöldii was also positively correlated with the two primary carotenoids Zeaxanthin and Antheraxanthin which may imply that these species are using the xantophyll cycle instead. The production of secondary carotenoids has not been shown yet for ice algae (Leya et al, 2009) and the negative correlation for *Raphidonema sempervirens* and secondary carotenoids as well as with PUFAs that correlate with those indicates the absence of secondary carotenoid production in ice algae.

Correlations between metabolites, geochemistry and single species can be used to unravel mixed metabolic signals in complex communities and assign them to single species.

In conclusion, these findings confirm my 5th hypothesis for some of the studied parameters:

"The physico- and geochemical environment influences the community composition and their metabolic functions."

9.9 Metabolite measurements show large heterogeneity at the beginning and no differences towards the end of the melt season.

Although snow algae pigmentation has been extensively studied (Müller *et al.*, 1998, Remias *et al.*, 2005, Leya *et al.*, 2009, Remias *et al.*, 2010, Remias *et al.*, 2013), the trigger and the process and mechanisms leading to pigment production are not fully understood. In chapter 4, I show that on a single glacier and even over a short time period there is a large heterogeneity in pigment compositions, both in space and time (Figure 4.5). This fact needs to be taken into account when pigment contents are described at a specific sampling site and time and when comparisons with other locations are made. Snow samples collected a week apart from almost the same location showed much higher secondary carotenoid contents relative to the initial samples, while esterified astaxanthin was only found in samples collected two weeks after melting initiation. Although biological processes are known to occur very slowly at 0 degrees, snow algae seem to adapt quickly to changing conditions with a broad range of pigment ratios (*i.e.*, chlorophylls and carotenoids).

This matches also my findings in Iceland (see chapter 5), where samples collected in 2012 showed overall more red pigmentation, potentially due to the collection date being towards the end of the melt season and longer exposure periods to stress (e.g., irradiation), whereas in 2013 samples were collected earlier in the season and showed more green and yellow pigmented cells (Figure 5.2). Astaxanthin was primarily found in samples collected in the 2012 and 2014 field campaigns, which were carried out later in the melt season after longer periods of higher irradiation.

At the beginning of the melt season there seem to be large variations in pigment composition, whereas later in the melt season I found no significant differences between the pigment composition of red snow in Svalbard and Northern Sweden (Figure 7.3). In all samples a high content of secondary carotenoids (~70-90%) was reached.

These findings confirm only in part my 6th hypothesis:

"Algal functionality (e.g., pigments) varies over time and space."

9.10 Snow and ice algae decrease surface albedo

In chapter 4, I show in a large albedo study that snow and ice algae dramatically decrease surface albedo. This could be verified in the following chapters (chapters 5-8). Depending on the nature of the produced pigments (chlorophylls *vs.* carotenoids) as well as cell density, both the green and red snow algae can reduce the albedo to values as low as 40% which is comparable to values reported by Thomas et al (1995). The rather ephemeral biofilms at the snow ice interface reduced albedo values even down to ~ 20% which is comparable to albedo values for cryoconites (Takeuchi & Li, 2008, Takeuchi, 2009). My values for the grey ice were comparable to those reported by Yallop et al (2012) and reached 35%. A decreased albedo will likely have positive feedbacks on the algal community, with higher and longer melting events further enhancing algal growth and most likely even extending their period of metabolic activity.

Previous studies have shown that the age of snow, which affects water content and grain size, and especially aggregation of allochtonous dust particles (e.g., dark inorganic and black carbon) (Wientjes *et al.*, 2011) can also play important roles. My observations indicate that dust probably played a minor role on the measured

snow fields, whereas the accumulation and aggregation of allochtonous materials on the bare exposed ice surface is more important. However, the relative contribution of algal pigmentation *vs.* dust to the grey colouration of the bare grey ice remains unknown and needs further investigation (see chapter 11).

The above described ubiquitous red snow algae distribution, low diversity and similarity in snow algal community compositions and metabolic functions (see 9.2 and chapter 7) combined with the analogous values measured for the red snow algae induced albedo reduction (Tables A.1 and D.1), allowed the development of a simple albedo model to estimate the impact that the red snow algae have on melting rates on snow-covered glacier surfaces compared to snow surfaces free of algae. The model shows that the integrated albedo change with time (100 days) is 13% higher in the presence of red algal blooms compared to clean snow that has undergone a purely physical albedo change due to melting and change of snow crystal size and structure. This for the first time integrated albedo change value compares well with the local albedo of up to 20 % previously measured on red snow algal sites (chapter 4).

To evaluate the larger scale effect of red snow algae induced albedo changes and to predict additional melting caused by snow algal growth, the evaluated integrated change (13%) was combined with values reported by Dumont et al. (2014) for the Greenland Ice Sheet (GrIS). They showed that for the whole of the GrIS a change in albedo of 1% will lead to a surface mass loss of 27 Gt/yr. A quantitative value for the area of the GrIS covered by snow algae during a melt season is still lacking; However, assuming a coverage of between 10% (conservative estimate) and 100% (extreme estimate) for the GrIS would result in an additional 35 to 350 Gt/yr of melting. Considering global warming and the recent extreme melt event in 2012, when 97% of the entire Greenland Ice Sheet was affected by surface melting (Nghiem et al, 2012), which is also likely the main driver for algal growth (see 9.2), and which will re-occur with a high probability and increasing frequency in the near future (McGrath et al, 2013), this number is likely to tend towards the extreme estimate in the near future.

In conclusiuon, these findings confirm my 7th hypothesis:

"The algal activity has a significant effect on their environment, in particular on the decrease of surface albedo."

References

Battin, T. J., Wille, A., Sattler, B. & Psenner, R. (2001) Phylogenetic and functional heterogeneity of sediment biofilms along environmental gradients in a glacial stream. *Applied and environmental microbiology*, 67(2), 799-807.

Boyd, E. S., Lange, R. K., Mitchell, A. C., Havig, J. R., Hamilton, T. L., Lafrenière, M. J., Shock, E. L., Peters, J. W. & Skidmore, M. (2011) Diversity, abundance, and potential activity of nitrifying and nitrate-reducing microbial assemblages in a subglacial ecosystem. *Applied and environmental microbiology*, 77(14), 4778-4787.

Cameron, K. A., Hagedorn, B., Dieser, M., Christner, B. C., Choquette, K., Sletten, R., Crump, B., Kellogg, C. & Junge, K. (2014) Diversity and potential sources of microbiota associated with snow on western portions of the Greenland Ice Sheet. *Environmental microbiology*, *17*(3), 594-609.

Cameron, K. A., Hodson, A. J. & Osborn, A. M. (2012) Structure and diversity of bacterial, eukaryotic and archaeal communities in glacial cryoconite holes from the Arctic and the Antarctic. *FEMS microbiology ecology*, 82(2), 254-267.

Dumont, M., Brun, E., Picard, G., Michou, M., Libois, Q., Petit, J., Geyer, M., Morin, S. & Josse, B. (2014) Contribution of light-absorbing impurities in snow to Greenland's darkening since 2009. *Nature Geoscience* 7, 509-512.

Foissner, W. (2006) Biogeography and dispersal of micro-organisms: a review emphasizing protists. *Acta Protozoologica*, 45(2), 111-136.

Green, J. & Bohannan, B. J. (2006) Spatial scaling of microbial biodiversity. *Trends in Ecology & Evolution*, 21(9), 501-507.

Harding, T., Jungblut, A. D., Lovejoy, C. & Vincent, W. F. (2011) Microbes in high Arctic snow and implications for the cold biosphere. *Applied and environmental microbiology*, 77(10), 3234-3243.

Hell, K., Edwards, A., Zarsky, J., Podmirseg, S. M., Girdwood, S., Pachebat, J. A., Insam, H. & Sattler, B. (2013) The dynamic bacterial communities of a melting High Arctic glacier snowpack. *The ISME journal*, 7(9), 1814-1826.

James, G. O., Hocart, C. H., Hillier, W., Chen, H., Kordbacheh, F., Price, G. D. & Djordjevic, M. A. (2011) Fatty acid profiling of Chlamydomonas reinhardtii under nitrogen deprivation. *Bioresource technology*, 102(3), 3343-3351.

Klausmeier, C. A., Litchman, E., Daufresne, T. & Levin, S. A. (2004) Optimal nitrogen-to-phosphorus stoichiometry of phytoplankton. *Nature*, 429(6988), 171-174.

Larose, C., Berger, S., Ferrari, C., Navarro, E., Dommergue, A., Schneider, D. & Vogel, T. M. (2010) Microbial sequences retrieved from environmental samples from seasonal Arctic snow and meltwater from Svalbard, Norway. *Extremophiles*, 14(2), 205-212.

Leya, T., Rahn, A., Lütz, C. & Remias, D. (2009) Response of arctic snow and permafrost algae to high light and nitrogen stress by changes in pigment

composition and applied aspects for biotechnology. *FEMS microbiology ecology*, 67(3), 432-443.

Maccario, L., Vogel, T. M. & Larose, C. (2014) Potential drivers of microbial community structure and function in Arctic spring snow. *Frontiers in microbiology*, 5, 413.

Martiny, J. B. H., Bohannan, B. J., Brown, J. H., Colwell, R. K., Fuhrman, J. A., Green, J. L., Horner-Devine, M. C., Kane, M., Krumins, J. A. & Kuske, C. R. (2006) Microbial biogeography: putting microorganisms on the map. *Nature Reviews Microbiology*, 4(2), 102-112.

McGrath, D., Colgan, W., Bayou, N., Muto, A. & Steffen, K. (2013) Recent warming at Summit, Greenland: Global context and implications. *Geophysical Research Letters*, 40(10), 2091-2096.

Nghiem, S., Hall, D., Mote, T., Tedesco, M., Albert, M., Keegan, K., Shuman, C., DiGirolamo, N. & Neumann, G. (2012) The extreme melt across the Greenland ice sheet in 2012. *Geophysical Research Letters*, 39(20).

Pichrtová, M., Kulichová, J. & Holzinger, A. (2014) Nitrogen Limitation and Slow Drying Induce Desiccation Tolerance in Conjugating Green Algae (Zygnematophyceae, Streptophyta) from Polar Habitats. *PloS one*, 9(11), e113137.

Remias, D., Holzinger, A., Aigner, S. & Lütz, C. (2012) Ecophysiology and ultrastructure of Ancylonema nordenskiöldii (Zygnematales, Streptophyta), causing brown ice on glaciers in Svalbard (high arctic). *Polar Biology*, 35(6), 1-10.

Remias, D., Holzinger, A. & Lütz, C. (2009) Physiology, ultrastructure and habitat of the ice alga Mesotaenium berggrenii (Zygnemaphyceae, Chlorophyta) from glaciers in the European Alps. *Phycologia*, 48(4), 302-312.

Ryšánek, D., Hrčková, K. & Škaloud, P. (2014) Global ubiquity and local endemism of free-living terrestrial protists: phylogeographic assessment of the streptophyte alga Klebsormidium. *Environmental microbiology*, 17(3), 689-698.

Sterner, R. W. & Elser, J. J. (2002) *Ecological stoichiometry: the biology of elements from molecules to the biosphere.* Princeton University Press: Princeton.

Stibal, M. & Elster, J. (2005) Growth and morphology variation as a response to changing environmental factors in two Arctic species of Raphidonema (Trebouxiophyceae) from snow and soil. *Polar Biology*, 28(7), 558-567.

Stibal, M., Elster, J., Šabacká, M. & Kaštovská, K. (2007) Seasonal and diel changes in photosynthetic activity of the snow alga Chlamydomonas nivalis (Chlorophyceae) from Svalbard determined by pulse amplitude modulation fluorometry. *FEMS microbiology ecology*, 59(2), 265-273.

Stieglmeier, M., Klingl, A., Alves, R. J., Simon, K.-M. R., Melcher, M., Leisch, N. & Schleper, C. (2014) Nitrososphaera viennensis sp. nov., an aerobic and mesophilic ammonia-oxidizing archaeon from soil and member of the archaeal phylum Thaumarchaeota. *International Journal of Systematic and Evolutionary Microbiology*, 64, 2738-2752.

Tourna, M., Stieglmeier, M., Spang, A., Könneke, M., Schintlmeister, A., Urich, T., Engel, M., Schloter, M., Wagner, M. & Richter, A. (2011) Nitrososphaera viennensis, an ammonia oxidizing archaeon from soil. *Proceedings of the National Academy of Sciences*, 108(20), 8420-8425.

Yallop, M. L., Anesio, A. M., Perkins, R. G., Cook, J., Telling, J., Fagan, D., MacFarlane, J., Stibal, M., Barker, G. & Bellas, C. (2012) Photophysiology and albedo-changing potential of the ice algal community on the surface of the Greenland ice sheet. *The ISME journal*, 6(12), 2302-2313.

Zarsky, J. D., Stibal, M., Hodson, A., Sattler, B., Schostag, M., Hansen, L. H., Jacobsen, C. S. & Psenner, R. (2013) Large cryoconite aggregates on a Svalbard glacier support a diverse microbial community including ammonia-oxidizing archaea. *Environmental Research Letters*, 8(3), 035044.

Chapter 10: Conclusions

The overall aim of this PhD study was to improve our understanding of the diversity, function, and ecology of Arctic supraglacial biomes, with the emphasis on snow and ice algal communities.

On all studied 21 glaciers in Svalbard, Artic Sweden, Greenland, and for the first time in Iceland, I could find algal blooms, and they are the first communities to appear after the onset of melting. With progressing melting, dramatic changes in the dominant algal communities occur on glacial surfaces and most snow fields transgress through a red snow to grey ice stage. Snow and ice algae are not only important primary colonisers, they also show positive net photosynthetic rates indicating an accumulation of organic matter and are thus an important carbon source.

In the first study of its kind, I have applied high-throughput sequencing to specifically target cryophilic algal communities with their associated microbiome, *i.e.*, bacteria and archaea. I show that red snow algae are cosmopolitan and independent of location specific factors, despite recent molecular studies that suggest that micro-eukaryotes show strong biogeography and most microbial taxa do not inherit a cosmopolitan distribution. The algal diversity is very low and six taxa make up >99% of the algal communities: two uncultured *Chlamydomonadaceae*, C*hloromonas polyptera, Chloromonas nivalis, Chloromonas alpina* and *Raphidonema sempervirens*. The same patterns can be observed on all studied glaciers regardless their geochemical and mineralogical compositions and surface melting is likely one of the main drivers for the algal distribution.

The composition of green snow, as opposed to my findings on red snow, varied strongly between the studied locations with higher relative abundance of *Raphidonema sempervirens* and *Microglena sp.* in Svalbard, and *Chloromonas polyptera* in Sweden. In contrast to previous assumptions, green and red snow are two independent and not successive phenomena with different community compositions, metabolic profiles and physico-chemical environments. Green snow represents a wet, carbon and nutrient rich environment and is characterized by key metabolites involved in growth and proliferation. In contrast, the dry and nutrient

poor red snow habitat shows an upregulation of storage and reserve metabolites likely to face upcoming severe conditions.

The grey ice community seemed to be heavily influenced by external snow and soil input at the time of sampling. The dominant species in my samples were *Raphidonema sempervirens*, better known as a permafrost algae, and the uncultured *Chlamydomonadaceae* that was also most abundant in all red snow samples and that was likely transferred to the ice surface from the melting snowpack above the ice.

The bacterial community composition was mainly represented by *Bacteriodetes*, *Proteobacteria* and *Cyanobacteria. Bacteriodetes* showed the highest relative abundance in red snow and *Proteobacteria in* grey ice. In contrast to the algae, the bacteria also showed strong biogeography on the class level and significant differences for the relative abundance between locations within the red snow habitat.

Archaea have been detected in all analysed samples and showed very low diversity. The species composition was mainly represented by three groups, the *Nitrosophaerales* (ammonia-oxidiser) and *Methanobacteriales* and *Methanosarcinales* (methanogens). Based on the data, I could not establish trends for their distribution within the studied habitats.

None of the quantified aqueous geochemical parameters, except DOC, showed any trends within the different algal habitats. DOC was significantly higher in the snow and biofilm habitats compared to the ice, which may underpin the importance of snow algal blooms as carbon source to downstream habitats (e.g., ice, soil, the ocean). In contrast, I could establish relationships for the solid C/N/P ratios and the microbial community structure and quantified macromolecules and metabolites. Most snow and ice samples showed C/N ratios above the Redfield ratio indicating nitrogen limitation, whereas only red snow samples in Sweden indicated co-limitation of phosphorus. The production of the quantified macromolecules (*i.e.*, lipids) and metabolites (*i.e.*, pigments, fatty acids) correlated mainly with nitrogen and less so with phosphorus limitation. This is especially important for the production of pigments, which in turn can cause a darkening of the glacial surfaces and therefore a decrease in surface albedo. At the beginning of the melt season there seem to be large variations in snow algal pigment composition (*i.e.*, chlorophylls, carotenoids), whereas later in the melt season I found no significant

differences between the pigment composition of red snow in Svalbard and Arctic Sweden. In all samples a high content of secondary carotenoids (~70-90%) was reached.

The snow and ice algal pigmentation dramatically decreases surface albedo with average values of 49% for red snow, 44% for green snow, 35% for grey ice, and even as low as 20% for biofilms. A decreased albedo will likely have positive feedbacks on the algal community, with higher and longer melting events further enhancing algal growth and most likely even extending their period of metabolic activity. A simple albedo model predicted that the integrated albedo change with time over the melt season (100 days) is 13% higher in the presence of red algal blooms compared to clean snow that has undergone a purely physical albedo change due to melting and change of snow crystal size and structure. This could result in an additional 35 (conservative estimate) to 350 (extreme estimate) Gt/yr of melting for the Greenland ice sheet. Considering global warming and more extreme melting events this number is likely to tend towards the extreme estimate in the near future.

In conclusion, the environment determines the distribution and structure of algal communities, but in return algal blooms also alter their environment after successful colonisation of the different surface glacial habitats. Algal communities exhibit short generation times and are able to adapt their metabolic inventory quickly as response to environmental conditions that change over time and space. Studying their ecological patterns and how these may be altered can give us a valuable outlook into how Arctic glacial and ice sheet surface ecosystems may respond to a changing climate

Chapter 11: Outlook

The scope for possible future work is extensive. Due to the nature of field work, the large variety of prevailing environmental parameters and the dramatic physical changes that occur on glacial surfaces during the melt seasons, the diversity and function of glacial microbial communities are still not fully understood. Future studies should thus encompass the following:

1) Whole genome sequencing of reference algal strains

Despite the power of next-generation sequencing techniques and their advances in recent years they have not been applied to cryophilic snow algae. One reason could be the lack of appropriate reference genomes. So far, the closest fully sequenced green algal strain is *Chlamydmonas reinhardtii* (Merchant et al, 2007), a model organism for freshwater *Chlorophyta* but adapted to mesophilic temperatures and hence not sharing common cryogenic adaptations.

The CCCryo culture collection is currently the largest source for pure cryophilic algae that can be used for whole genome sequencing. However, only strains that can be cultivated in the lab are available and therefore important strains may be missed out. This includes one of the uncultured *Chlamydomonadaceae* that was the species with highest relative abundance in all my studies. Single-cell genomics could circumvent this problem. The technologies work well on small-genome organisms such as bacteria, however they are not advanced enough at the moment to be applied on micro-eukaryotes that inherit larger genomes. Multiple targeted amplicon studies could be used instead on those strains that can currently not be cultivated in order to explore their functional potential.

2) Metagenomic studies

Once appropriate reference genomes are available in public databases, extensive metagenomic studies need to be carried out to explore the functional potential of environmental snow and ice communities in order to distinguish between the functional potential of individual groups of organism including algae and bacteria. This will also help to identify their roles in crucial biogeochemical processes (e.g., carbon and nutrient cycling).

Whole single genomes as well as metagenomes will also help to identify genes that have been transferred between organisms (horizontal gene transfer) or genes that can be associated with viral infections.

3) Metatranscriptomics and metabolomics

In order to get a better understanding of algal functioning, time-resolved high-throughput studies are needed. A good approach would be to look at the full spread of organismal response to environmental stress by quantifying rather short-lived transcripts as well as the metabolic end products of the response. Environmental parameters (e.g., nutrients, irradiation) could be varied and monitoring the response of snow and ice algae would help to elucidate their functioning.

4) Algal life cycles

The snow and in particular ice algal life cycles are still not well understood. The contribution of cells that get transported by wind from afar and introduced onto snow and ice surfaces by wind deposition and the in-situ over-wintering in the snowpack and reviving of cells in spring has not been quantified yet. This may also vary between glaciers that experience low or high snow accumulation rates in winter.

5) Albedo components

A quantitative evaluation of the algal contribution to the observed decrease in albedo is still lacking and needs to be further investigated. The contribution of the different components decreasing surface albedo – black carbon, minerals, biology – needs to be quantified. The importance of algal impact also needs to be evaluated for glacier with varying (inorganic) debris cover thicknesses.

6) Impact of global warming on glacial communities

Climate change will alter the selection pressure on cryophilic microorganisms (Pearce, 2008). Snow and ice algae are important primary colonisers and producers and therefore play crucial roles in glacial ecosystems. The adaptation potential of snow and algae to increased melting and irradiation levels is not well understood and we are not able to predict the effect of climate change on these ecosystems. Studying communities in high altitude and hence high irradiation settings (e.g.,

Himalayans, Andes) and comparing the species diversity and metabolic function to communities in low irradiation settings may contribute to a better understanding of their adaptation potential.

References

Merchant, S. S., Prochnik, S. E., Vallon, O., Harris, E. H., Karpowicz, S. J., Witman, G. B., Terry, A., Salamov, A., Fritz-Laylin, L. K. & Maréchal-Drouard, L. (2007) The *Chlamydomonas* genome reveals the evolution of key animal and plant functions. *Science*, 318(5848), 245-250.

Pearce, D. A. (2008) Climate change and the microbiology of the Antarctic peninsula region. *Science progress*, 91(2), 203-217

Appendix A: Supplementary information for chapter 4

Variations of algal communities cause darkening of a Greenland glacier.

Lutz, S., Anesio, A. M., Villar, S. E. J. & Benning, L. G.

Published in *FEMS microbiology ecology*, 89(2), 402-414 (2014)

Methods

Field sampling

Twenty-four snow, ice and water samples were collected. For inorganic aqueous analyses samples were collected either in sterile 50 mL centrifuge tubes or sterile sample bags. The snow/ice samples were melted at room temperature over a ~ 6 hour period and all samples were filtered through single use 0.2 uM cellulose-acetate syringe filters. For cation analyses by inductively coupled plasma mass spectrometry (ICP-MS), samples were directly filtered into acid-washed (HCl) and pre-acidified (Aristar grade HNO_3) Nalgene HDPE bottles, while for anion analyses by ion chromatography (IC), samples were stored un-acidified in 15 mL centrifuge tubes.

For dissolved organic and inorganic carbon (DOC and DIC, respectively) and organic particulate analysis, samples were collected in 250 mL glass jars that had been ashed at 450 °C. After melting at room temperature these samples were filtered through ashed 0.7 µm glass fibre filters (GFF) directly into either pre-acidified (for DOC, 100µl Aristar grade HNO_3) or non-acidified (for DIC) 40 mL, amber glass vials with Teflon® seals (Supelco). The filters containing particulates were folded into quarters and preserved cold and in ashed aluminium foil for pigment analysis. From these solution samples particulates for XRD, FTIR and Raman analysis were also collected by filtering through 0.2 µm polycarbonate filters. Finally, for imaging and cell counts using light microscopy (LM) as well as for scanning and transmission electron microscopy (SEM, TEM) melted but unconcentrated samples were preserved in 2.5% glutaraldehyde. Samples were returned to Leeds either frozen in liquid nitrogen in a cryo-shipper or in an ice-box at ~ 4 ˚C.

Field measurements

To evaluate community activity and the proportion of autotrophy *vs.* heterotrophy, respiration experiments were carried out by measuring O_2 concentrations using different substrates (red snow, biofilms, ice algae and cryoconites). For this a large volume of each sample was collected in sterile sampling bags and slowly (~ 3-4 h) thawed on-site. For each sample type, melted but homogenous subsamples were transferred into 50 mL glass bottles that had been each rinsed multiple times with

the respective sample. The bottles were completely filled up, initial (time zero) O_2 concentrations measured and subsequently air-tightly sealed with ground glass stoppers. O_2 concentrations were measured with a O_2 meter (Hach HQ30d). Per sample three bottles were wrapped in light impermeable, white plastic to measure net community O_2 respiration, while three bottles each were left unwrapped to measure O_2 production and respiration. The bottles were left for up to two days on the glacial surface and final O_2 concentrations were measured after 24 or 48 h. Net O_2 production was calculated by the difference between wrapped and unwrapped bottles. At each measurement point the temperature, was simultaneously measured with the O_2 meter and temperature corrections (ref) were applied.

Analyses of returned samples

Aqueous samples

Nutrients (NO_2^-, NO_3^-, Cl^-, SO_4^{2-}) were analysed in filtered samples by ion chromatography (IC) on a Dionex DX 600 system with an autosampler, an IonPac AS16 analytical column with an AG16 guard column, an eluent gradient of 0-15 mM KOH and an ED50 conductivity detector. Injection volume was 25 uL and flow rate was set to 0.35 mL min^{-1}. For NO_2^- analysis the UV detector was set to 211 nm. Error of measurement was <5%. Major, minor and trace elements were measured by inductively coupled plasma mass spectrometry (ICP-MS) on an Agilent 7500ce with collision cell Octopole Reaction System (ORS) technology (ICP-MS facility, University of Portsmouth). Analytical errors for both IC and ICP-MS are below 5%.

Dissolved organic and inorganic carbon (DOC and DIC, respectively) were analysed on a Shimadzu TOC analyser (University of Plymouth). Due to an error in sample handling all DOC and DIC became contaminated and the analyses gave unrealistically high values and were therefore not used.

Solid analyses

Cell morphologies and organic and inorganic debris distributions were imaged by light microscopy and scanning and transmission electron microscopy (LM, SEM and TEM). For SEM imaging of cell morphologies and distribution of organic and inorganic debris an ethanol exchange series (30, 50, 70, 90, 100%; 30 min per step)

was prepared on samples that had been preserved in 2.5 % glutaraldehyde. A droplet of the fixed and exchanged sample was dispersed on an Al stub, air-dried and coated with 3 nm of Pt. Images were acquired on a Phillips Environmental Scanning Electron Microscope (E-SEM) at an accelerating voltage of 10 kV and a working distance of 10-12 mm and a LEO 1530 Field-Emission Gun SEM (FEG-SEM) at an accelerating voltage of 3 kV and working distance of 3-4 mm. For TEM, microtomed sections of the fixed and ethanol exchanged samples were prepared and resulting grids were imaged on a JEOL 1200-TEM at an accelerating voltage of 80 keV.

Functional groups distributions were determined on bulk, dried samples by Fourier transform infrared (FTIR) using an A2 Technology Microlab Portable mid-IR spectrometer with a Diamond internal
reflection cell (DATR), with spectra acquired in the mid-infrared range (650- 4000 cm-1). From the bulk spectra, the peak area ratios of the main functional groups representing the *lipids* (CH_2 and CH_3 stretching modes between 3050 and 2800 cm^{-1}), and *proteins* (amide I and II bands at 1700-1500 cm^{-1}) to those of the *carbohydrates* (C-O-C, C-O-P, P-O-P ring vibrations between 1204-815 cm^{-1}) were evaluated. Raman analyses were performed on a Renishaw InVia Raman spectrometer with two lasers at 514 nm and 785 nm excitation wavelengths, an attached microscope with a 50x magnification objective and a resolution of 4 cm^{-1}. Raman spectra were collected on singe algal cells or individual mineral grains with the aim to cross-confirm organic compound specificity and mineral composition.

The mineralogical composition of each sample was determined by X-ray diffraction (XRD) with dried and ground samples analysed on a Bruker D8 Advance diffractometer. XRD spectra were recorded from 2-75°2Θ using a copper diffraction source and a run time of 12 min per sample.

To determine the carotenoid and chlorophyll contents in the snow algae samples, high pressure liquid chromatography (HPLC) and a modified carotenoid/chlorophyll specific extraction protocol (after Remias and Lutz (2007) was used. Cells were disrupted by shock freezing in liquid nitrogen for 10 min followed by grinding in a Teflon® mortar and pestle. The resulting powder was re-suspended in 1 mL of dimethylformamide (DMF) and 1.0 mm glass beads and horizontally shaken on a laboratory shaker (MoBio Vortex Genie 2) at maximum

speed (3000 rpm) for 10 min followed by centrifugation for 5 min 10 000 rpm. The supernatant was separated from the debris by filtering through a 0.45 µm Teflon® filter and the filtrate was mixed with methanol (25 vol %). Extracted samples were analysed immediately on an Agilent Technologies 1200 Infinity HPLC instrument with a gradient pump, an autosampler, a variable wavelength detector and ODS Hypersil column (250x4.6 mm; 5 um particle size). Two solvents were used: solvent A consisted of a mixture of acetonitrile/water/methanol/hexane/tris buffer at ratios of 80:7:3:1:1 while solvent B was a mix of methanol and hexane at a ratio of 5:1. The HPLC was run at a flow rate of 1 mL min^{-1} and with an injection volume of 25 µL. Spectra were recorded from 200 to 800 nm and chromatograms were quantified at 450 nm for carotenoids and 660 nm for chlorophyll a and b. Run time was 60 min and the protocol required a 15 minute run with 100% of solvent A followed by a linear gradient from 100 % solvent A to 100% solvent B between 32 and 45 min and finally with 15 minutes of column re-equilibration through a 5 min linear gradient from solvent B back to 100% solvent to A, followed by a further column conditioning with 100 % solvent A for 10 min. Various commercially available standards (Sigma, Carotenature) and published retention times were used for peak identification. Chromatogram peak areas were calculated and the carotenoid data is reported as normalized to the peak area of chlorophyll a. The error of measurements for the HPLC was <5%.

Details of all microbial activity measurements

Red snow, biofilm and grey ice samples all showed positive values with + 194 ugC L^{-1} day^{-1} for red snow, between +182 and +480 ugC L^{-1} day^{-1} for the different grey ice samples and with the highest values (+ 682 ugC L^{-1} day^{-1}) for the biofilm sample. Only the cryoconites showed overall negative rates with one exemption (-1601/-283.75/-27.5/+156 ugC L^{-1}). The positive values for the snow and ice algae samples indicates accumulation of organic matter in all surface glacial habitats, except for the cryoconites which most likely were dominated by a heterotrophic community at the time of sampling,

Table A.1: Albedo measurements across the 1 km^2 area shown in Figure 4.1 with coordinates and 10 measurements/site; the five up and down values represent five incident and five reflected radiation measurements at each point.

Category	Measure-Ment no.	24 H	UTM	Up #1	Down #1	U/ D #1	Up #2	Down #2	U/D #2	Up #3	Down #3	U/D #3	Up #4	Down #4	U/D #4	Up #5	Down #5	U/D #5	Average
Clean	ALB-19	0552166	7285960	142	106	75	142	105	74	142	111	78	142	110	77	144	102	71	75
Snow	ALB-20	0552166	7285960	141	108	77	142	108	76	146	108	74	145	106	73	144	106	74	75
	ALB-21	0552166	7285960	139	105	76	140	102	73	141	103	73	141	104	74	141	104	74	74
	ALB-66	0552141	7285611	320	242	76	329	240	73	315	240	76	315	240	76	311	237	76	75
	ALB-69	0552141	7285611	312	233	75	315	236	75	338	231	68	313	231	74	310	234	75	73
	ALB-70	0552141	7285611	317	210	66	299	210	70	298	209	70	304	212	70	299	208	70	69
	ALB-83	0552201	7285775	278	193	69	276	191	69	268	189	71	268	185	69	262	184	70	70
	ALB-84	0552201	7285775	243	201	83	241	200	83	262	199	76	253	200	79	250	202	81	80
	MIT-3	0551579	7285535	268	228	85	266	224	84	272	232	85	279	233	84	258	211	82	84
Average																			**75 ± 5**
Green	ALB-25	0552071	7286234	110	50	45	112	49	44	112	48	43	112	50	45	114	50	44	44
snow	MIT-11	0551435	7285308	197	81	41	214	81	38	212	84	40	234	96	41				40
	MIT-22	0551778	7286368	330	158	48	337	155	46	317	153	48	290	139	48	317	145	46	47
Average																			**44 ± 4**
Light	ALB-16	0552166	7285960	150	107	71	149	108	72	149	107	72	148	105	71	147	106	72	72
Red	ALB-17	0552166	7285960	144	102	71	146	107	73	147	104	71	149	108	72	149	106	71	72
Snow	ALB-18	0552166	7285960	147	107	73	147	106	72	149	105	70	149	106	71	148	105	71	71
	ALB-48	0551681	7285613	319	264	83	351	265	75	335	265	79	325	265	82	329	262	80	80
	ALB-49	0551681	7285613	309	260	84	313	258	82	305	255	84	307	258	84	309	255	83	83
	ALB-51	0551690	7285639	302	130	43	340	130	38	318	130	41	318	132	42	331	132	40	41

	ALB-53	0551690	7285639	324	220	68	323	220	68	321	224	70	324	222	69	319	222	70	69
	ALB-54	0551690	7285639	317	261	82	315	260	83	328	258	79	323	255	79	321	259	81	81
	ALB-55	0551690	7285639	317	281	89	311	281	90	329	283	86	334	281	84	354	284	80	86
	ALB-58	0551716	7285652	314	199	63	313	198	63	330	192	58	324	190	59	321	192	60	61
	ALB-59	0551716	7285652	328	235	72	328	234	71	327	234	72	331	236	71	325	235	72	72
	ALB-60	0551716	7285652	312	258	83	304	215	71	311	256	82	310	258	83	317	258	81	80
	ALB-74	0552318	7285716	292	205	70	283	206	73	267	205	77	302	203	67	297	205	69	71
	ALB-75	0552318	7285716	278	175	63	285	175	61	280	173	62	280	170	61	267	169	63	62
	ALB-79	0552292	7285836	271	149	55	276	150	54	274	151	55	268	150	56	262	150	57	56
	ALB-81	0552201	7285775	273	193	71	268	200	75	289	200	69	287	203	71	285	203	71	71
	ALB-90	0551766	7285796	86	40	47	86	41	48	87	41	47	85	41	48	86	41	48	47
	ALB-112	0552166	7285960	139	101	73	140	99	71	141	99	70	141	99	70	142	100	70	71
	ALB-113	0552166	7285960	142	96	68	142	97	68	141	96	68	143	97	68	143	100	70	68
	ALB-131	0552131	7286079	129	90	70	128	91	71	129	88	68	130	88	68	127	89	70	69
	ALB-132	0552131	7286079	128	88	69	129	96	74	130	97	75	129	96	74	129	96	74	73
	ALB-133	0552131	7286079	131	96	73	130	94	72	132	93	70	134	96	72	135	95	70	72
	ALB-134	0552131	7286079	133	86	65	129	88	68	132	86	65	131	86	66	134	86	64	66
	ALB-135	0552131	7286079	140	90	64	139	94	68	140	93	66	143	96	67	144	96	67	66
	MIT-17	0552441	7285291	339	200	59	362	204	56	354	199	56	345	197	57				57
Average																			**69 ± 11**
Very	ALB-23	0552071	7286234	165	109	66	172	109	63	172	110	64	171	110	64	171	109	64	64
Red	ALB-24	0552071	7286234	165	88	53	161	87	54	155	87	56	158	87	55	157	87	55	55
Snow	ALB-56	0551716	7285652	331	161	49	335	161	48	347	162	47	326	160	49	334	163	49	48
	ALB-92	0551972	7285813	109	48	44	111	49	44	111	50	45	112	50	45	113	50	44	44

	MIT-15	0552463	7285438	322	183	57	324	188	58	333	186	56	324	180	56	325	184	57	57
	MIT-19	0551778	7286368	320	123	38	334	130	39	345	134	39	332	135	41				39
Average																			**49 ± 8**
Clean ice	ALB-1	0551878	7285946	183	108	59	184	107	58	183	106	58	182	104	57	184	109	59	58
	ALB-2	0551878	7285946	171	90	53	175	90	51	170	90	53	171	90	53	174	90	52	52
	ALB-3	0551878	7285946	186	102	55	185	101	55	186	101	54	186	103	55	186	104	56	55
	ALB-35	0551703	7285413	316	185	59	310	181	58	313	183	58	325	183	56	327	185	57	58
	ALB-42	0551752	7285525	331	143	43	337	144	43	340	144	42	339	146	43	332	146	44	43
	ALB-47	0551681	7285613	315	204	65	335	202	60	349	197	56	338	200	59	334	203	61	60
	ALB-50	0551681	7285613	334	191	57	335	189	56	347	186	54	361	185	51	338	186	55	55
	ALB-62	0552059	7285700	379	222	59	318	219	69	304	219	72	309	217	70	313	215	69	68
	ALB-67	0552141	7285611	314	184	59	311	185	59	323	184	57	307	182	59	313	185	59	59
	ALB-68	0552141	7285611	311	208	67	318	209	66	340	205	60	318	209	66	303	207	68	65
	ALB-71	0552318	7285716	300	185	62	303	180	59	294	179	61	292	178	61	296	179	60	61
	ALB-72	0552318	7285716	279	204	73	287	198	69	288	200	69	277	200	72	291	199	68	70
	ALB-76	0552292	7285836	286	180	63	271	175	65	275	175	64	280	177	63	276	176	64	64
	ALB-77	0552292	7285836	285	192	67	289	193	67	304	190	63	301	191	63	289	194	67	65
	ALB-78	0552292	7285836	295	176	60	283	176	62	281	179	64	283	180	64	284	178	63	62
	ALB-80	0552292	7285836	292	183	63	281	183	65	292	184	63	310	184	59	295	182	62	62
	ALB-95	0551972	7285813	120	53	44	120	53	44	121	54	45	122	53	43	122	54	44	44
	ALB-98	0552035	7286025	141	70	50	143	71	50	143	70	49	143	70	49	141	68	48	49
	ALB-107	0551878	7285946	136	57	42	140	57	41	140	58	41	141	58	41	139	57	41	41
	MIT-14	0552441	7285291	320	228	71	352	215	61	340	210	62							65
Average																			**58 ± 8**

Light	ALB-4	0551878	7285946	199	83	42	200	84	42	190	83	44	191	80	42	196	77	39	42
Grey	ALB-5	0551878	7285946	195	100	51	190	100	53	194	101	52	201	103	51	201	107	53	52
Ice	ALB-6	0551878	7285946	207	97	47	218	99	45	221	101	46	225	101	45	224	104	46	46
	ALB-37	0551762	7285494	322	161	50	304	161	53	304	163	54	308	163	53	308	160	52	52
	ALB-38	0551762	7285494	319	179	56	323	180	56	302	182	60	303	176	58	305	179	59	58
	ALB-39	0551762	7285494	306	153	50	318	152	48	313	150	48	311	149	48	324	151	47	48
	ALB-40	0551762	7285494	312	175	56	322	174	54	338	174	51	341	171	50	331	170	51	53
	ALB-41	0551752	7285525	333	180	54	334	181	54	340	179	53	342	180	53	331	179	54	54
	ALB-46	0551681	7285613	308	127	41	324	126	39	331	127	38	319	127	40	331	127	38	39
	ALB-52	0551690	7285639	340	186	55	350	182	52	347	188	54	338	187	55	337	184	55	54
	ALB-64	0552059	7285700	304	171	56	303	174	57	296	174	59	298	178	60	307	168	55	57
	ALB-86	0551766	7285796	84	43	51	84	43	51	84	43	51	85	43	51	84	43	51	51
	ALB-89	0551766	7285796	90	41	46	90	41	46	90	40	44	91	40	44	91	40	44	45
	ALB-93	0551972	7285813	115	63	55	117	63	54	117	63	54	117	64	55	117	63	54	54
	ALB-97	0552035	7286025	142	62	44	145	62	43	145	62	43	144	63	44	143	62	43	43
	ALB-99	0552035	7286025	145	67	46	143	67	47	143	68	48	144	68	47	145	68	47	47
	ALB-114	0552166	7285960	135	71	53	137	72	53	138	73	53	139	74	53	135	72	53	53
	ALB-118	0552266	7286120	138	67	49	139	66	47	136	66	49	135	68	50	139	65	47	48
Average																			**50 ± 5**
Medium	ALB-7	0551878	7285946	225	59	26	225	57	25	215	55	26	217	57	26	217	58	27	26
Grey	ALB-8	0551878	7285946	246	65	26	230	60	26	208	55	26	200	53	27	206	52	25	26
Ice	ALB-9	0551878	7285946	209	65	31	208	63	30	204	64	31	203	64	32	205	63	31	31
	ALB-43	0551752	7285525	322	148	46	341	153	45	343	148	43	312	151	48	319	150	47	46
	ALB-57	0551716	7285652	321	125	39	324	124	38	336	124	37	346	126	36	320	126	39	38

	ALB-82	0552201	7285775	290	156	54	290	152	52	279	155	56	289	154	53	186	156	84	60
	ALB-111	0552166	7285960	137	56	41	138	57	41	139	57	41	138	55	40	139	56	40	41
	ALB-115	0552166	7285960	137	63	46	139	63	45	138	63	46	138	62	45	137	62	45	45
	ALB-116	0552266	7286120	141	38	27	140	39	28	140	39	28	140	40	29	141	39	28	28
	ALB-117	0552266	7286120	137	47	34	139	46	33	138	46	33	139	46	33	138	46	33	33
	ALB-119	0552266	7286120	141	48	34	134	49	37	139	49	35	138	49	36	140	50	36	35
	ALB-120	0552266	7286120	137	67	49	136	70	51	138	66	48	138	67	49	136	69	51	49
	ALB-121	0552107	7286218	129	33	26	130	33	25	129	33	26	129	34	26	131	33	25	26
	ALB-123	0552107	7286218	129	40	31	131	40	31	129	39	30	131	40	31	129	39	30	31
	ALB-124	0552107	7286218	131	34	26	136	36	26	142	34	24	133	34	26	133	34	26	25
	ALB-127	0552025	7286134	132	32	24	128	33	26	132	31	23	128	32	25	130	31	24	24
	ALB-129	0552025	7286134	134	37	28	133	37	28	132	37	28	132	37	28	131	37	28	28
	ALB-130	0552025	7286134	138	32	23	132	32	24	131	32	24	130	31	24	131	31	24	24
	ALB-125	0552107	7286218	136	43	32	138	43	31	137	42	31	136	42	31	137	42	31	31
	MIT-16	0552463	7285438	331	126	38	343	127	37	328	128	39	314	127	40	323	128	40	39
	MIT-23	0551651	7285404	335	127	38	336	130	39	338	129	38	337	130	39	329	131	40	39
Average																			**35 ± 10**
Very	ALB-10	0551878	7285946	207	18	9	207	17	8	209	18	9	210	18	9	202	17	8	9
Grey	ALB-11	0551878	7285946	209	23	11	207	26	13	219	24	11	213	24	11	217	25	12	11
Ice	ALB-12	0551878	7285946	221	21	10	210	21	10	219	21	10	216	21	10	220	22	10	10
	ALB-36	0551762	7285494	291	102	35	312	105	34	304	104	34	295	104	35	304	103	34	34
	ALB-44	0551752	7285525	319	126	39	344	146	42	334	124	37	346	125	36	341	125	37	38
	ALB-45	0551752	7285525	343	99	29	345	99	29	342	99	29	329	100	30	330	100	30	29
	ALB-65	0552059	7285700	312	129	41	323	129	40	317	130	41	318	131	41	305	128	42	41

	ALB-85	0552201	7285775	271	102	38	248	104	42	258	102	40	240	103	43	259	103	40	40
	ALB-87	0551766	7285796	87	36	41	88	36	41	88	35	40	88	35	40	88	35	40	40
	ALB-94	0551972	7285813	118	31	26	119	31	26	120	31	26	121	32	26	122	32	26	26
	ALB-96	0552035	7286025	148	55	37	143	54	38	144	55	38	143	56	39	144	55	38	38
	ALB-100	0552035	7286025	146	46	32	147	46	31	147	46	31	147	47	32	146	47	32	32
	ALB-101	0551921	7286055	136	12	9	137	12	9	137	12	9	140	12	9	140	12	9	9
	ALB-102	0551921	7286055	138	42	30	137	43	31	134	42	31	136	42	31	138	41	30	31
	ALB-103	0551921	7286055	136	15	11	136	15	11	134	15	11	136	15	11	138	16	12	11
	ALB-105	0551921	7286055	138	57	41	139	57	41	139	56	40	139	55	40	139	56	40	40
	ALB-106	0551878	7285946	140	44	31	141	44	31	141	44	31	140	44	31	141	44	31	31
	ALB-108	0551878	7285946	144	50	35	144	49	34	144	50	35	141	51	36	143	52	36	35
	ALB-109	0551878	7285946	143	31	22	146	30	21	146	30	21	148	30	20	146	30	21	21
	ALB-126	0552025	7286134	127	17	13	126	17	13	125	17	14	127	18	14	129	16	12	13
	ALB-128	0552025	7286134	129	15	12	131	16	12	131	15	11	132	15	11	129	14	11	12
Average																			**26 ± 12**
Light	ALB-29	0551597	7285532	155	56	36	164	56	34	167	56	34	167	56	34	167	56	34	34
Biofilm	ALB-30	0551597	7285532	160	57	36	163	58	36	164	57	35	165	57	35	165	56	34	35
	ALB-31	0551597	7285532	166	62	37	165	62	38	164	63	38	164	64	39	164	64	39	38
Average																			**36 ± 2**
Dense	ALB-32	0551597	7285532	175	39	22	175	39	22	175	39	22	173	40	23	169	40	24	23
biofilm	ALB-33	0551597	7285532	206	26	13	202	27	13	209	26	12	202	26	13	207	26	13	13
	ALB-34	0551597	7285532	205	42	20	214	42	20	213	44	21	219	43	20	223	43	19	20
	MIT-18	0552463	7285438	326	75	23	315	72	23	313	71	23	352	78	22	326	76	23	23
	MIT-24	0551705	7285631	295	58	20	279	58	21	297	56	19	279	55	20	282	54	19	20

Average																		**20 ± 4**
Cryo-	ALB-13	0551878	7285946	206	20	10	211	21	10	212	21	10	208	21	10	208	21	10	10
Conite	ALB-14	0551878	7285946	185	20	11	183	18	10	184	19	10	185	19	10	187	19	10	10
	ALB-15	0551878	7285946	178	35	20	179	35	20	170	36	21	169	33	20	169	30	18	20
	ALB-61	0552059	7285700	325	30	9	329	31	9	328	32	10	312	30	10	328	30	9	9
	ALB-63	0552059	7285700	318	120	38	325	120	37	317	118	37	319	122	38	325	119	37	37
	ALB-73	0552318	7285716	294	185	63	283	184	65	301	184	61	303	185	61	297	186	63	63
	ALB-88	0551766	7285796	87	23	26	85	23	27	85	24	28	85	23	27	84	22	26	27
	ALB-91	0551972	7285813	108	23	21	110	23	21	105	21	20	106	21	20	104	21	20	20
	ALB-104	0551921	7286055	135	23	17	134	23	17	137	23	17	136	23	17	137	23	17	17
	ALB-110	0551878	7285946	143	24	17	144	25	17	142	25	18	148	25	17	148	25	17	17
	ALB-122	0552107	7286218	127	18	14	128	19	15	125	19	15	127	18	14	127	18	14	15
	MIT-21	0551741	7285782	328	82	25	312	91	29	329	91	28	337	94	28				27
Average																			**23 ± 15**
Runoff	ALB-26	0551597	7285532	190	55	29	180	54	30	183	54	30	185	54	29	184	53	29	29
	ALB-27	0551597	7285532	171	44	26	162	43	27	170	44	26	168	43	26	159	43	27	26
	ALB-28	0551597	7285532	173	57	33	174	57	33	171	56	33	165	58	35	169	58	34	34
Average																			**30 ± 4**

Table A.2: Aqueous chemical analyses of anions and cations by IC and ICP-MS in all samples.

Sample no.	$NO_3^{-\#}$	$NO_2^{-\#}$	$Cl^{-\#}$	$SO_4^{2-\#}$	B*	Na*	Mg*	Al*	Si*	P*	K*	Ca*	Cr*	Mn*	Fe*	Co*	Ni*	Cu*	Zn*	Sr*	Cd*	Ba*	Pb*
MIT-2	104	ND	131	LOD	2	86	4	1	4	0	20	19	0	0	2	0	0	0	2	0	0	4	0
MIT-3	LOD	ND	94	LOD	1	93	4	1	5	0	6	14	0	0	2	0	0	0	1	0	0	1	0
MIT-4	LOD	ND	157	LOD	1	100	5	3	17	1	48	17	0	1	5	0	0	0	2	0	0	2	0
MIT-5	LOD	ND	118	LOD	0	80	10	2	7	0	15	20	0	1	2	0	0	0	2	0	0	1	0
MIT-6	LOD	ND	97	LOD	1	215	38	5	43	10	354	22	0	1	13	0	0	0	2	0	0	1	0
MIT-7	53	ND	458	393	0	134	7	3	24	6	212	19	0	1	6	0	0	0	1	0	0	1	0
MIT-8	66	ND	225	165	5	207	28	5	97	11	115	30	0	5	7	0	0	1	15	0	0	2	0
MIT-9	LOD	ND	24	LOD	0	22	21	7	15	10	42	39	0	2	21	0	0	0	1	1	0	8	0
MIT-10	LOD	ND	129	LOD	0	75	10	1	9	1	12	13	0	2	3	0	0	0	1	0	0	2	0
MIT-11	LOD	ND	65	LOD	0	69	28	5	26	0	43	23	0	1	22	0	1	1	3	0	0	1	0
MIT-12	LOD	ND	744	302	0	498	4	3	16	1	72	11	0	0	4	0	0	0	1	0	0	1	0
MIT-13	LOD	ND	408	LOD	0	113	2	3	12	0	12	10	0	0	4	0	0	0	1	0	0	1	0
MIT-14	489	ND	12	LOD	0	4	2	1	11	0	6	10	0	0	4	0	0	0	3	0	0	2	0
MIT-15	LOD	ND	181	106	0	111	8	5	19	7	88	14	0	0	7	0	0	0	2	0	0	1	0
MIT-16	LOD	ND	24	LOD	0	13	5	3	8	0	36	13	0	0	12	0	0	0	0	0	0	1	0
MIT-17	LOD	ND	126	107	0	75	5	7	15	2	43	16	0	0	14	0	0	1	2	0	0	1	0
MIT-18	LOD	ND	407	LOD	0	232	18	4	26	1	251	48	0	0	5	0	0	0	6	0	0	1	0
MIT-19	LOD	ND	291	LOD	0	148	3	3	22	0	29	18	0	1	4	0	0	0	3	0	0	3	0

MIT-20	LOD	ND	107	LOD	0	68	27	5	25	0	42	21	0	1	22	0	1	1	3	0	0	1	0
MIT-21	LOD	ND	131	108	0	58	29	9	37	2	26	20	0	1	8	0	0	0	1	1	0	1	0
MIT-22	LOD	ND	336	LOD	0	211	19	6	36	0	36	15	0	3	24	0	0	1	2	0	0	2	0
MIT-23	LOD	ND	13	LOD	0	15	8	8	23	6	41	18	0	1	15	0	0	2	2	0	0	1	0
MIT-24	134	ND	229	LOD	0	207	19	9	34	3	199	22	0	2	50	0	0	1	4	0	0	2	0

all values in ppb; determined by $^{\#}$IC, *ICP-MS; Limit of detection (LOD) for IC: NO_3^- = 51 ppb, Cl^- = 36 ppb, SO_4^{2-} = 102 ppb, for ICP-MS: < 1 ppb) ND = not detectable;

Raman spectroscopy

Individual spherical red or green snow algae and filamentous ice algae as well as mineral grains, all identified with the microscope attached to the Raman system were analyses either at 514 nm or at 785 nm. Chlorophyll was detected in the red and green snow algae samples primarily with the near-infrared Raman laser. Most of the carotenoids detected showed the typical C=C stretching band at 1519 ± 3 cm^{-1} (Fig S2). For red snow algae cysts, three different peak regions for carotenoids were identified: 1517-1522 cm^{-1}, 1508-1512 cm^{-1} and 1525-1527 cm^{-1}. The main carotenoid in green snow algae cells also appeared around 1519 cm^{-1} but additionally a carotenoid band at 1530 cm^{-1} was detected. The filamentous ice algae cells showed Raman bands at five regions but all were rather weak as the cells were very small and thin: 1525-1524 cm^{-1}, 1520 cm^{-1}, 1515-1516 cm^{-1},1513 - 1508 cm^{-1} and 1528 cm^{-1}. However, based on the Raman analyses an unambiguous identification and assignment of bands to specific carotenoids could not be done (de Oliveira et al., 2010) and thus below in Table A.3) the organic bands are identified only as compound 1 to 7. In addition, many mineral phases were identified and are listed below in Table A.4.

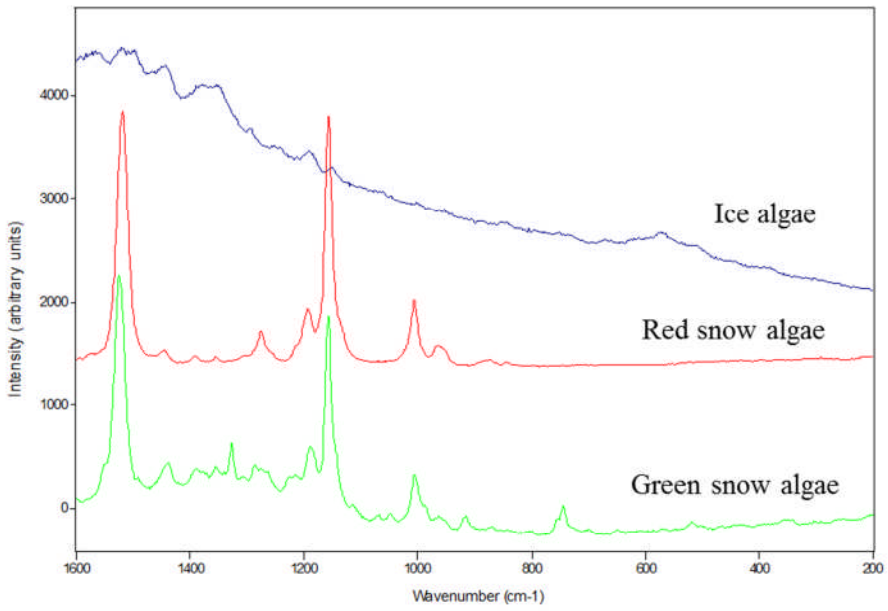

Figure A.1: Raman spectra of three different cell types: ice algae (blue), red mature snow algae (red) and young green snow algae (green).

Table A.3: Raman spectroscopy analyses of minerals and black carbon in the three samples (in bold shown main peak assignments).

Inorganic compounds	Wavenumbers (cm^{-1})	Sample type
Haematite	640, 410, **292**, 225	Red snow
Limonite	550, **391**, 297, 245, 202	Red snow
Iron oxide	686, 460, 335, 261	Grey ice
Feldspar	**508**, **480**	Red snow
Microcline	**513**, **474**, 437, 355, 284, 154	Red snow
Zircon	**1005**, 973, 437, **355**	Red snow
Quartz	**463**, 205	Red snow
Black carbon	**1618**, **1330**	Red snow, grey ice, biofilm
Garnet	1043 **916**, 861, 635, 556, 502, 480, **350**, 209	Red snow
(Ortho-) Pyroxene	**1000**, **674**, 654, **335**, 229	Red snow

Table A.4: Raman spectroscopy analyses of organic compounds (in bold shown main peak assignments).

Organic compounds	Wavenumbers (cm^{-1})	Sample category/cell type
Compound 1	**1615, 1567, 1447, 1378, 1359, 1300, 1192, 84**9, 750, **574, 513**	Biofilm/ice algae
Compound 2	**1624, 1571**, 1533, **1506, 1452, 1387, 1350, 1301, 1255, 1199, 850, 579, 511**	Grey ice/snow algae
Compound 3	**1622, 1568, 1509, 1448, 1382, 1359, 1300, 1265, 1194, 853, 576, 513**	Grey ice/snow algae
Compound 4	1670, 1500, 1410, 1280, 1260, 1222	Red snow/snow algae
Compound 5	1444, 1357, 1274, 511	Red snow/snow algae
Compound 6	1677, 1601, 1585, 1567, 1558, 1483, 1432, 1426, 1399, 1364, 1305, 1292, 1184, 1118, 1063, 1018, 991, 907, 803, 780, 700, 657, 599	Red snow/snow algae
Compound 7	1617, 1325, 1292, 1263	Red snow/snow algae

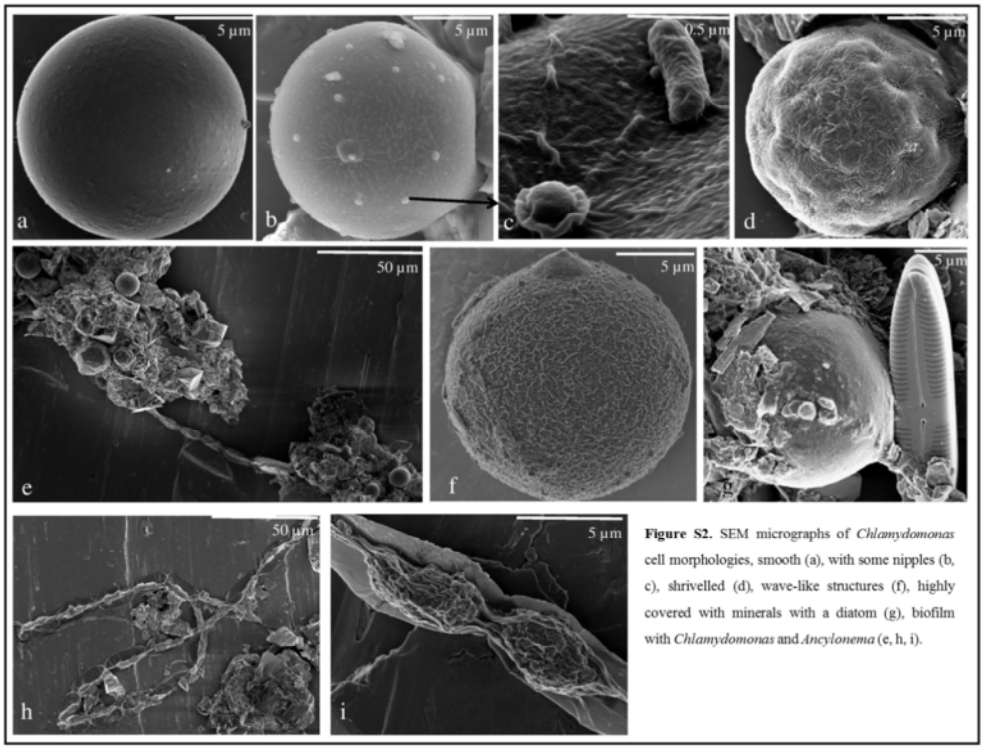

Figure A.2: SEM micrographs of *Chlamydomonas* cell morphologies, smooth (a), with some nipples (b,c), shrivelled (d), wave-like structures (f), highly covered with minerals with a diatom (g), biofilm with *Chlamydomonas* and *Ancylonema* (e, h, i).

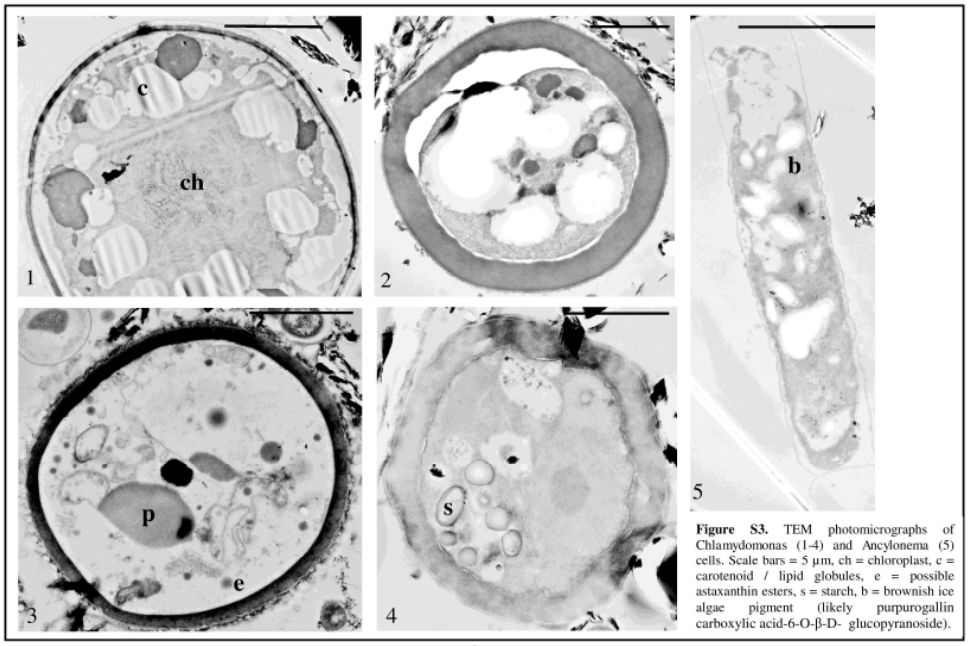

Figure A.3: TEM photomicrographs of Chlamydomonas (1-4) and Ancylonema (5) cells. Scale bars = 5 µm, ch = chloroplast, c = carotenoid/lipid globules, e = possible astaxanthin esters, s = starch, b = brownish ice algae pigment (likely purpurogallin carboxylic acid-6-O-β-D-glucopyranoside).

Appendix B: Supplementary information for chapter 5

Microbial diversity on Icelandic glaciers and ice caps.

Lutz, S., Anesio, A. M., Edwards, A. & Benning, L. G.

Published in *Frontiers in microbiology*, 6, 307 (2015)

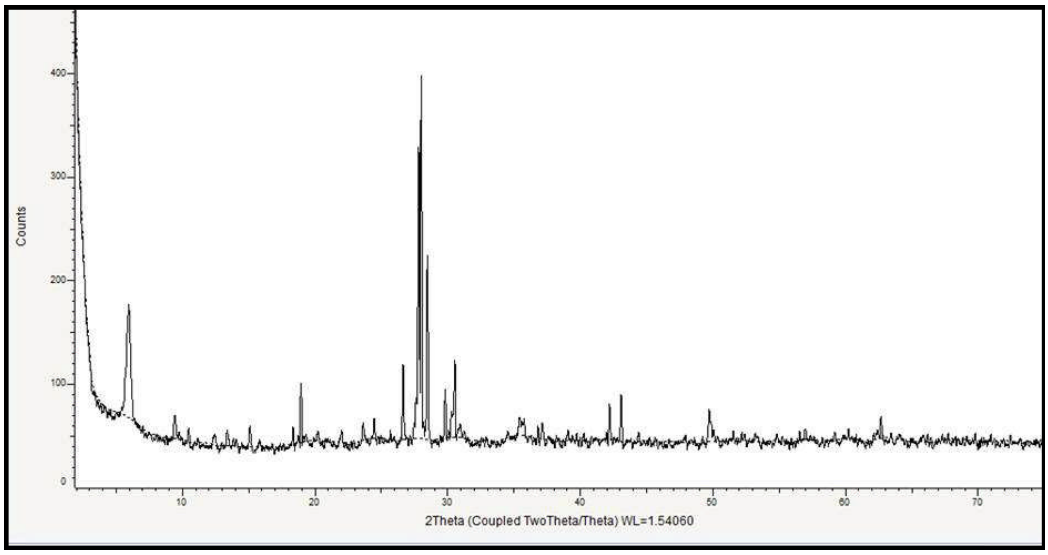

Figure B.1: XRD pattern of one representative sample (ICE-13_15, Vatnajökull) and typical for all Iceland samples showing the main mineral components quartz, feldspars, pyroxene and olivine and minor contributions from clays, basaltic glass and hematite.

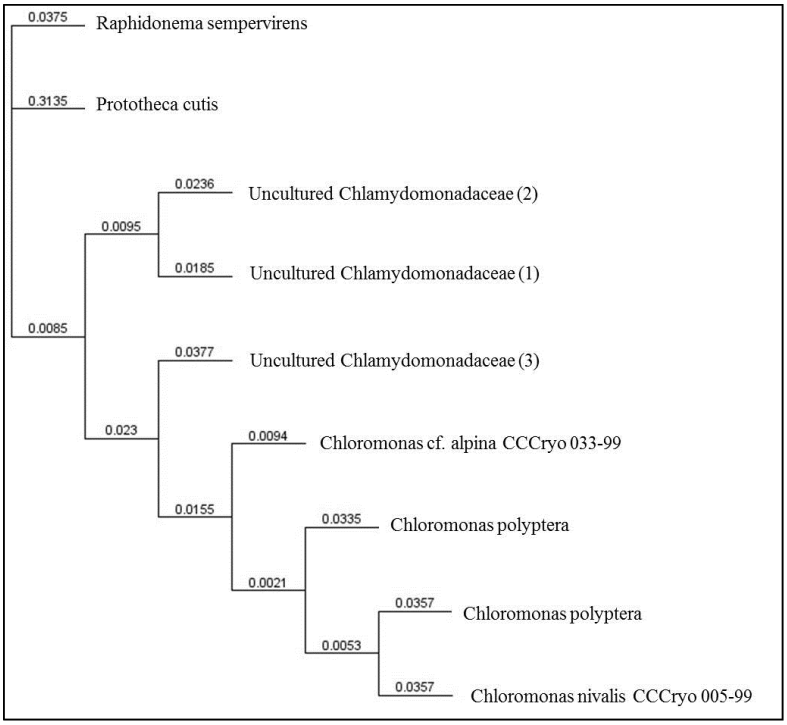

Figure B.2: Phylogenetic tree of main algal species showing the inferred evolutionary relationships between the main algal species in our samples. Based on their 18S rRNA sequences they are closely related (89-92% similarity) to other *Chloromonas* species found.

Table B.1: Fatty acid composition of red snow samples. Fatty acid compounds are reported as percentage of total fatty acids. b=branched, A = Alkane.

Compound	C14:0	C15 b	C15:0	C16:4	C15 b	C16:1	C16:1	C16:1	C16:0	C18:3	C18:4	C18:2	C18:3	C18:1	C18:1	C21 A	C18:0	C20:5	C23 A	C20:0	C21:0	C22:0	C26 A	C27 A	C24:0
ICE-12_2	0	0	0	0	0	8	0	0	20	0	0	7	7	46	12	0	0	0	0	0	0	0	0	0	0
ICE-12_3	0	0	0	0	0	8	0	0	18	0	0	5	4	47	5	0	10	0	0	2	0	0	0	0	0
ICE-12_5	0	0	0	0	0	0	3	0	16	0	0	0	0	18	0	7	57	0	0	0	0	0	0	0	0
ICE-12_6	2	0	0	0	0	2	0	0	18	0	0	5	3	50	2	0	18	0	0	0	0	0	0	0	0
ICE-12_7	3	0	2	0	0	4	0	0	14	0	4	27	0	43	0	0	3	0	0	0	0	0	0	0	0
ICE-13_1	0	6	6	0	0	16	0	0	16	0	0	6	3	8	5	0	17	0	0	0	0	0	0	0	0
ICE-13_2	1	0	0	0	0	12	0	0	19	0	0	11	6	8	6	1	12	0	1	2	0	3	0	2	2
ICE-13_4	0	0	0	0	0	0	0	0	94	0	0	0	0	6	0	0	0	0	0	0	0	0	0	0	0
ICE-13_5	5	0	0	0	0	8	0	0	25	0	2	12	12	9	0	0	16	0	0	3	0	4	0	0	0
ICE-13_6	3	0	0	0	0	2	0	0	21	2	4	10	13	13	0	7	12	1	2	3	0	3	0	0	0
ICE-13_8	2	0	0	0	0	0	0	0	42	0	0	0	0	0	0	0	56	0	0	0	0	0	0	0	0
ICE-13_9	0	0	0	0	0	0	0	0	38	0	0	9	0	16	0	0	38	0	0	0	0	0	0	0	0
ICE-13_12	0	0	0	5	0	5	0	0	22	0	4	6	16	20	0	0	12	4	0	0	0	3	0	0	3
ICE-13_14	3	0	0	0	0	5	0	0	26	0	0	14	29	0	0	0	11	1	0	3	0	4	0	0	2
ICE-13_15	2	0	0	0	0	0	0	0	26	0	0	4	5	16	0	3	17	0	4	5	0	6	1	4	4
ICE-13_16	4	0	0	0	0	2	0	0	24	2	5	14	13	15	0	0	10	2	0	2	2	2	0	0	2
ICE-13_18	2	0	0	0	0	4	0	0	25	0	0	9	6	16	0	0	30	0	0	2	1	3	0	0	2
ICE-13_19	2	0	0	0	0	2	0	0	33	0	0	3	3	5	0	0	49	0	0	2	0	2	0	0	0
ICE-13_21	1	0	0	6	1	1	0	1	27	0	0	7	16	21	0	0	9	0	0	3	0	4	0	0	2
ICE-13_24	8	0	0	0	0	2	0	0	28	0	0	7	7	16	0	2	12	0	2	4	0	6	0	1	3

Table B.2: Counts of OTUs matching eukaryotes, algae (*Chloroplastida*) and bacteria, clustered at 99%, 97% and 95% similarities after removal of singletons.

	99 %	**97 %**	**95 %**
All eukaryotes	4,170	2,811	1,901
Chloroplastida	807	567	395
Bacteria	1,591	1,733	1,500

Table B.3: Distribution of OTUs clustered at 99%, 97% and 95% similarities aligned and assigned to eukaryotes. Values are the relative abundance of the taxa in percentage of total sequences and table shows taxa with >0.1% abundance.

	Drangajokull ICE12.2.3			Laugafell ICE12.4			Hofsjokull ICE12.6.7			Vatnajokull ICE13.14.15			Langjokull ICE13.16.18			Langjokull ICE13.19		
OTU similarity	**99%**	**97%**	**95%**	**99%**	**97%**	**95%**	**99%**	**97%**	**95%**	**99%**	**97%**	**95%**	**99%**	**97%**	**95%**	**99%**	**97%**	**95%**
Archaeplastida; Chloroplastida	32.3	45.3	46.3	32.6	35.9	30.6	63.9	60.6	56.3	59.9	56.6	57.3	2.6	9.7	10.2	1.8	4.5	5.3
Opisthokonta; Fungi	29.8	27.0	23.4	54.7	53.5	46.8	17.9	19.7	18.3	39.7	41.4	41.7	97.4	89.9	89.1	98.2	94.9	94.7
SAR; Alveolata	0.2	0.1	0.1	11.6	6.3	5.9	1.6	2.6	2.6	0.0	0.0	0.0	0.0	0.0	0.0	0.0	0.0	0.0
SAR; Rhizaria	37.7	27.6	30.2	1.2	4.2	16.7	16.4	16.5	21.7	0.0	1.5	0.4	0.0	0.2	0.6	0.0	0.7	0.0
SAR; Stramenopiles	0.0	0.0	0.0	0.0	0.0	0.0	0.2	0.6	1.1	0.4	0.6	0.5	0.0	0.2	0.1	0.0	0.0	0.0
Zeuk77; uncultured eukaryote	0.0	0.0	0.0	0.0	0.0	0.0	0.0	0.0	0.0	0.0	0.0	0.0	0.0	0.0	0.0	0.0	0.0	0.0

	Snaefellsjokull ICE13.21.24			Eyafjallajokull ICE13.4.5.6			Mýrdalsjokull ICE13.8.9			Eyafjallajokull ICE14.1			Eyafjallajokull ICE14.2			Eyafjallajokull ICE14.3		
OTU similarity	**99%**	**97%**	**95%**	**99%**	**97%**	**95%**	**99%**	**97%**	**95%**	**99%**	**97%**	**95%**	**99%**	**97%**	**95%**	**99%**	**97%**	**95%**
Archaeplastida; Chloroplastida	8.1	7.8	5.5	35.9	29.8	27.5	21.4	19.7	20.3	21.1	17.3	16.4	66.0	57.9	55.4	43.9	35.4	33.2
Opisthokonta; Fungi	91.9	87.4	87.9	63.4	67.0	70.0	78.6	78.7	76.6	12.2	12.1	12.0	10.5	12.0	11.5	4.7	6.6	7.7
SAR; Alveolata	0.0	0.0	0.2	0.0	0.0	0.0	0.0	0.0	0.0	19.6	16.3	15.6	1.5	1.8	1.9	4.2	3.7	3.6
SAR; Rhizaria	0.0	4.8	6.4	0.0	2.0	0.5	0.0	1.6	3.1	0.0	0.0	0.5	0.0	0.0	1.1	0.0	0.0	0.3
SAR; Stramenopiles	0.0	0.0	0.0	0.7	1.1	2.0	0.0	0.0	0.0	46.3	54.3	55.4	21.5	28.1	29.7	47.0	53.9	54.7
Zeuk77; uncultured eukaryote	0.0	0.0	0.0	0.0	0.0	0.0	0.0	0.0	0.0	0.8	0.0	0.1	0.4	0.2	0.3	0.2	0.4	0.5

Table B.4: Distribution of OTUs clustered at 99%, 97% and 95% similarities aligned and assigned to algal sequences (*Chloroplastida*). Values are the relative abundance of the taxa in percentage of total sequences and table shows taxa with >0.05% abundance.

	Drangajökull ICE12.2.3			Laugafell ICE12.4			Hofsjökull ICE12.6.7			Vatnajökull ICE13.14.15			Langjökull ICE13.16.18			Langjökull ICE13.19		
OTU similarity	**99%**	**97%**	**95%**	**99%**	**97%**	**95%**	**99%**	**97%**	**95%**	**99%**	**97%**	**95%**	**99%**	**97%**	**95%**	**99%**	**97%**	**95%**
Chlorophyceae; Chloromonas cf. alpina CCCryo 033-99	0.0	0.2	0.5	0.0	1.7	2.6	0.5	0.8	1.0	0.0	0.0	1.5	3.4	2.2	2.7	0.0	0.0	0.0
Chlorophyceae; Chloromonas nivalis CCCryo 005-99	3.2	14.9	1.4	0.0	6.7	6.5	0.0	0.2	0.3	0.0	0.0	0.0	0.0	0.0	0.0	0.0	0.0	2.6
Chlorophyceae; Chloromonas polyptera	32.8	27.8	43.3	21.1	23.3	29.9	4.5	5.1	4.8	25.0	14.3	13.6	33.3	31.1	32.7	52.4	36.1	28.2
Chlorophyceae; Chloromonas tughillensis	2.5	4.6	5.7	0.0	1.7	1.3	0.0	0.0	0.0	0.0	0.0	0.0	0.0	0.0	0.0	0.0	0.0	0.0
Chlorophyceae; uncultured Chlamydomonadaceae	8.9	1.4	0.0	7.9	3.3	0.0	0.0	0.0	0.0	6.3	0.0	0.0	0.0	0.0	0.0	4.8	0.0	0.0
Chlorophyceae; uncultured Chlamydomonadaceae	33.4	34.5	32.3	36.8	43.3	37.7	0.5	0.5	0.4	0.0	2.0	1.5	0.0	0.7	0.7	0.0	5.6	5.1
Chlorophyceae; uncultured Chlamydomonadaceae	0.6	0.0	0.0	0.0	0.0	0.0	0.0	0.0	0.0	0.0	0.0	0.0	0.0	0.0	0.0	0.0	0.0	0.0
Trebouxiophyceae; Chloroidium	0.0	0.0	0.0	0.0	0.0	0.0	0.0	0.0	0.0	0.0	0.0	0.0	0.0	0.0	0.0	0.0	0.0	0.0
Trebouxiophyceae; Coccomyxa	0.0	0.0	0.0	0.0	0.0	0.0	0.0	0.0	0.0	0.0	0.0	4.5	0.0	0.0	0.0	0.0	0.0	0.0
Trebouxiophyceae; Prototheca cutis	0.0	0.0	0.0	0.0	0.0	1.3	0.0	0.2	0.8	0.0	0.0	0.0	62.1	65.2	63.3	42.9	58.3	64.1
Trebouxiophyceae; Raphidonema nivale CCCryo 130-01	0.0	0.0	0.0	0.0	0.0	0.0	0.0	0.0	0.0	0.0	0.0	0.0	0.0	0.0	0.0	0.0	0.0	0.0
Trebouxiophyceae; Raphidonema pyrenoidifera	0.0	0.0	0.0	0.0	0.0	0.0	0.0	0.0	0.0	0.0	0.0	0.0	0.0	0.0	0.0	0.0	0.0	0.0
Trebouxiophyceae; Raphidonema sempervirens	18.5	16.6	17.0	34.2	20.0	20.8	94.6	93.3	92.7	68.8	53.1	45.5	1.1	0.7	0.7	0.0	0.0	0.0
Trebouxiophyceae; Trebouxia usneae	0.0	0.0	0.0	0.0	0.0	0.0	0.0	0.0	0.0	0.0	0.0	15.2	0.0	0.0	0.0	0.0	0.0	0.0
Trebouxiophyceae; uncultured	0.0	0.0	0.0	0.0	0.0	0.0	0.0	0.0	0.0	0.0	30.6	18.2	0.0	0.0	0.0	0.0	0.0	0.0

Table B.4 continued.

	Snaefellsjökull ICE13.21.24			Eyafjallajökull ICE13.4.5.6			Mýrdalsjökull ICE13.8.9			Eyafjallajökull ICE14.1			Eyafjallajökull ICE14.2			Eyafjallajökull ICE14.3		
OTU similarity	**99%**	**97%**	**95%**	**99%**	**97%**	**95%**	**99%**	**97%**	**95%**	**99%**	**97%**	**95%**	**99%**	**97%**	**95%**	**99%**	**97%**	**95%**
Chlorophyceae; Chloromonas cf. alpina CCCryo 033-99	0.0	0.0	0.0	0.0	16.7	12.1	0.0	0.0	0.0	0.1	0.1	0.0	0.0	0.0	0.0	0.1	0.1	0.0
Chlorophyceae; Chloromonas nivalis CCCryo 005-99	0.0	0.0	0.0	0.0	0.0	3.0	0.0	0.0	12.5	1.2	1.0	0.0	0.0	0.0	0.0	0.0	0.0	0.0
Chlorophyceae; Chloromonas polyptera	58.8	75.9	63.6	40.0	41.7	15.2	71.4	71.4	50.0	4.7	6.5	7.9	0.8	0.9	0.9	3.1	3.6	4.0
Chlorophyceae; Chloromonas tughillensis	0.0	0.0	0.0	0.0	0.0	0.0	0.0	0.0	0.0	0.0	0.0	0.0	0.0	0.0	0.0	0.0	0.0	0.0
Chlorophyceae; uncultured Chlamydomonadaceae	5.9	0.0	0.0	0.0	0.0	0.0	14.3	14.3	0.0	0.3	0.0	0.0	0.0	0.0	0.0	0.0	0.0	0.0
Chlorophyceae; uncultured Chlamydomonadaceae	23.5	20.7	21.2	20.0	8.3	3.0	14.3	14.3	37.5	0.2	0.8	1.1	0.0	0.1	0.1	0.0	0.0	0.2
Chlorophyceae; uncultured Chlamydomonadaceae	0.0	0.0	0.0	0.0	0.0	0.0	0.0	0.0	0.0	0.3	0.1	0.0	0.0	0.0	0.0	0.2	0.2	0.0
Trebouxiophyceae; Chloroidium	0.0	0.0	6.1	0.0	0.0	21.2	0.0	0.0	0.0	0.0	0.0	0.0	0.0	0.0	0.0	0.0	0.0	0.0
Trebouxiophyceae; Coccomyxa	0.0	0.0	0.0	0.0	0.0	27.3	0.0	0.0	0.0	0.0	0.0	0.0	0.0	0.0	0.0	0.0	0.0	0.0
Trebouxiophyceae; Prototheca cutis	5.9	0.0	6.1	0.0	0.0	0.0	0.0	0.0	0.0	0.0	0.1	0.1	0.0	0.1	0.2	0.1	0.2	0.4
Trebouxiophyceae; Raphidonema nivale CCCryo 130-01	0.0	0.0	0.0	0.0	0.0	0.0	0.0	0.0	0.0	0.0	0.5	0.0	0.0	0.4	0.0	0.0	0.5	0.0
Trebouxiophyceae; Raphidonema pyrenoidifera	0.0	0.0	0.0	0.0	0.0	0.0	0.0	0.0	0.0	0.0	0.0	0.0	0.0	0.0	0.1	0.0	0.0	0.1
Trebouxiophyceae; Raphidonema sempervirens	5.9	3.4	3.0	40.0	33.3	12.1	0.0	0.0	0.0	93.2	90.9	90.1	99.2	98.5	97.0	96.5	95.4	92.2
Trebouxiophyceae; Trebouxia usneae	0.0	0.0	0.0	0.0	0.0	0.0	0.0	0.0	0.0	0.0	0.0	0.0	0.0	0.0	0.0	0.0	0.0	0.0
Trebouxiophyceae; uncultured	0.0	0.0	0.0	0.0	0.0	3.0	0.0	0.0	0.0	0.0	0.0	0.0	0.0	0.0	0.0	0.0	0.0	0.0

Table B.5: Distribution of OTUs clustered at 99%, 97% and 95% similarities aligned and assigned to bacterial sequences. Values are the relative abundance of the taxa in percentage of total sequences and table shows taxa with >0.01% abundance.

	Drangajökull ICE12.2.3			Laugafell ICE12.4			Hofsjökull ICE12.6.7			Vatnajökull ICE13.14.15			Langjökull ICE13.16.18			Langjökull ICE13.19		
OTU similarity	**99%**	**97%**	**95%**	**99%**	**97%**	**95%**	**99%**	**97%**	**95%**	**99%**	**97%**	**95%**	**99%**	**97%**	**95%**	**99%**	**97%**	**95%**
Acidobacteria; Acidobacteriia	0.6	0.4	0.3	0.0	0.0	0.0	0.0	0.1	0.2	0.0	0.0	0.2	0.0	0.2	0.0	0.0	0.0	0.0
Actinobacteria; Actinobacteria	10.7	6.0	5.6	0.8	2.6	2.8	1.2	0.9	1.4	0.0	0.3	1.4	3.6	4.1	3.4	26.4	15.9	14.6
Bacteroidetes; Cytophagia	0.2	0.1	0.0	10.0	5.4	4.8	1.2	1.4	1.1	0.0	2.3	1.8	0.0	0.0	0.4	0.0	0.7	0.6
Bacteroidetes; Flavobacteriia	0.0	0.0	0.1	0.0	0.0	0.0	0.0	0.0	0.0	0.0	0.0	0.0	0.0	0.0	0.0	0.0	0.0	0.0
Bacteroidetes; Sphingobacteriia	23.6	18.8	18.3	0.0	0.0	0.0	50.1	32.2	29.3	0.0	0.0	0.0	0.9	0.2	0.2	0.5	0.7	0.9
Bacteroidetes; Saprospirae	8.0	24.1	26.6	49.2	28.5	26.8	29.5	38.4	37.1	0.0	0.0	0.0	1.8	1.4	1.3	2.0	3.8	4.8
Chlorobi; Ignavibacteria	8.0	0.0	0.0	0.0	0.0	0.0	0.0	0.0	0.0	0.0	0.0	0.0	0.0	0.0	0.0	0.0	0.0	0.0
Cyanobacteria;	0.0	0.0	0.0	0.0	0.0	0.0	0.0	0.0	0.0	0.0	2.7	11.7	0.0	0.0	0.5	0.0	0.0	0.3
Cyanobacteria; Nostocophycideae	0.0	0.0	0.0	0.0	0.2	0.2	0.0	0.0	0.0	57.1	30.8	14.6	0.0	0.0	0.0	0.0	0.0	0.0
Cyanobacteria; Oscillatoriophycideae	0.0	0.0	0.0	0.0	0.0	0.2	0.0	0.0	0.0	21.4	9.0	16.2	0.9	0.5	0.5	0.0	0.0	0.0
Cyanobacteria; Synechococcophycideae	0.0	0.5	0.4	0.8	0.5	0.6	0.0	0.0	0.0	0.0	3.7	5.9	0.0	0.0	0.2	0.0	0.0	0.2
Firmicutes; Bacilli	0.0	0.0	0.0	0.0	0.0	0.0	0.0	0.0	0.0	0.0	0.0	0.0	0.0	0.0	0.0	0.0	0.1	0.1
Gemmatimonadetes; Gemmatimonadetes	0.2	0.1	0.1	0.0	0.5	0.7	0.0	0.0	0.0	0.0	0.0	0.0	0.0	0.0	0.0	0.0	0.1	0.1
Proteobacteria; Alphaproteobacteria	46.4	42.0	41.4	0.8	5.4	8.1	6.2	6.6	7.5	21.4	49.5	44.6	3.6	11.6	12.1	3.4	5.1	6.0
Proteobacteria; Betaproteobacteria	1.6	4.9	4.1	38.3	56.2	55.1	11.5	20.1	22.9	0.0	0.3	0.9	86.5	80.3	79.3	66.0	71.9	71.1
Proteobacteria; Gammaproteobacteria	0.6	1.3	1.1	0.0	0.0	0.2	0.3	0.1	0.3	0.0	0.0	1.4	2.7	1.8	2.2	1.8	1.6	1.4
Bacteria; WPS-2	0.2	0.9	0.9	0.0	0.0	0.0	0.0	0.0	0.0	0.0	0.3	0.2	0.0	0.0	0.0	0.0	0.0	0.0

Table B.5 continued.

	Snaefellsjökull ICE13.21.24			Eyafjallajökull ICE13.4.5.6			Mýrdalsjökull ICE13.8.9			Eyafjallajökull ICE14.1			Eyafjallajökull ICE14.2			Eyafjallajökull ICE14.3		
OTU similarity	**99%**	**97%**	**95%**	**99%**	**97%**	**95%**	**99%**	**97%**	**95%**	**99%**	**97%**	**95%**	**99%**	**97%**	**95%**	**99%**	**97%**	**95%**
Acidobacteria; Acidobacteriia	0.0	0.5	0.5	5.5	8.6	2.4	0.0	0.0	0.0	0.0	0.0	0.0	0.0	0.0	0.0	0.0	0.0	0.0
Actinobacteria; Actinobacteria	0.0	0.0	0.1	3.6	1.0	0.4	0.0	8.0	4.1	0.5	0.8	0.9	0.4	0.5	0.6	0.2	0.6	0.6
Bacteroidetes; Cytophagia	0.0	0.1	0.7	0.0	5.4	2.1	0.0	12.0	8.2	0.2	0.1	0.1	0.5	0.7	0.7	2.0	1.7	1.7
Bacteroidetes; Flavobacteriia	0.0	0.0	0.0	0.0	0.0	0.0	50.0	0.0	2.0	0.0	0.0	0.0	0.0	0.0	0.0	0.0	0.0	0.0
Bacteroidetes; Sphingobacteriia	0.0	0.0	0.0	1.8	0.6	0.5	50.0	4.0	4.1	7.1	5.3	5.1	1.1	0.8	0.8	10.5	8.1	7.7
Bacteroidetes; Saprospirae	0.0	0.0	0.1	0.0	0.2	0.1	0.0	4.0	6.1	56.0	45.5	43.1	31.2	28.0	27.2	33.5	29.7	28.6
Chlorobi; Ignavibacteria	0.0	0.0	0.0	0.0	0.0	0.0	0.0	12.0	6.1	0.0	0.0	0.0	0.0	0.0	0.0	0.0	0.0	0.0
Cyanobacteria;	0.0	0.0	0.1	0.0	4.1	56.6	0.0	0.0	18.4	0.0	0.0	0.2	0.0	0.0	0.2	0.0	0.0	0.1
Cyanobacteria; Nostocophycideae	1.0	1.5	0.1	14.5	13.7	2.8	0.0	0.0	0.0	0.0	0.0	0.0	0.0	0.0	0.0	0.0	0.0	0.0
Cyanobacteria; Oscillatoriophycideae	0.0	0.0	1.0	23.6	4.3	3.8	0.0	0.0	0.0	0.0	0.0	0.0	0.0	0.0	0.0	0.0	0.0	0.0
Cyanobacteria; Synechococcophycideae	0.0	0.0	0.5	0.0	0.3	1.2	0.0	0.0	0.0	0.0	0.0	0.0	0.0	0.0	0.0	0.0	0.0	0.0
Firmicutes; Bacilli	0.0	0.0	0.0	0.0	0.0	0.0	0.0	8.0	6.1	0.0	0.0	0.0	0.0	0.0	0.0	0.0	0.0	0.0
Gemmatimonadetes; Gemmatimonadetes	0.0	0.0	0.0	0.0	0.0	0.0	0.0	0.0	0.0	0.0	0.0	0.0	0.0	0.0	0.0	0.0	0.0	0.0
Proteobacteria; Alphaproteobacteria	0.0	2.7	2.9	10.9	42.6	17.9	0.0	20.0	22.4	14.0	15.6	15.6	3.6	4.5	4.9	30.3	31.2	31.4
Proteobacteria; Betaproteobacteria	99.0	95.1	92.8	40.0	16.2	8.1	0.0	24.0	12.2	22.2	32.6	34.6	63.0	65.4	65.5	23.4	28.7	29.7
Proteobacteria; Gammaproteobacteria	0.0	0.1	0.9	0.0	0.3	2.7	0.0	0.0	6.1	0.0	0.0	0.0	0.1	0.1	0.1	0.1	0.1	0.1
Bacteria; WPS-2	0.0	0.1	0.1	0.0	2.1	0.8	0.0	0.0	0.0	0.0	0.0	0.0	0.0	0.0	0.0	0.0	0.0	0.0

Table B.6: Distribution of OTUs clustered at 99%, 97% and 95% similarities aligned and assigned to archaeal sequences. Values are the relative abundance of the taxa in percentage of total sequences.

	Laugafell			Hofsjökull			Vatnajökull			Langjökull			Langjökull		
	ICE12.4			ICE12.6.7			ICE13.14.15			ICE13.16.18			ICE13.16.19		
OTU similarity	**99%**	**97%**	**95%**	**99%**	**97%**	**95%**	**99%**	**97%**	**95%**	**99%**	**97%**	**95%**	**99%**	**97%**	**95%**
Crenarchaeota; MBGA	0.2	0.0	1.7	0.0	0.0	0.0	0.0	0.0	0.0	0.0	0.0	2.1	1.3	0.0	0.1
Crenarchaeota; Thaumarchaeota; Cenarchaeales; Cenarchaeaceae	0.6	2.8	3.3	0.0	0.7	1.8	1.4	7.7	8.6	0.3	1.1	1.5	0.0	2.4	3.3
Crenarchaeota; Thaumarchaeota; Cenarchaeales; SAGMA-X	0.0	0.0	0.1	0.0	0.0	0.0	0.0	0.0	0.0	0.0	0.5	0.0	0.0	0.0	1.6
Crenarchaeota; Thaumarchaeota; Nitrososphaerales; Nitrososphaeraceae	99.3	96.5	91.7	33.3	27.6	29.4	98.6	92.0	91.3	99.7	98.1	92.3	98.7	97.6	94.2
Euryarchaeota; Methanobacteria; Methanobacteriales; MSBL1	0.0	0.0	0.0	0.0	0.0	0.0	0.0	0.0	0.0	0.0	0.0	0.0	0.0	0.0	0.0
Euryarchaeota; Methanomicrobia; Methanosarcinales; Methanosarcinaceae	0.0	0.0	0.0	66.7	71.6	68.9	0.0	0.0	0.0	0.0	0.0	0.0	0.0	0.0	0.0

	Snaefellsjökull			Eyafjallajökull			Eyafjallajökull			Eyafjallajökull		
	ICE13.21.24			ICE14.1			ICE14.2			ICE14.3		
OTU similarity	**99%**	**97%**	**95%**	**99%**	**97%**	**95%**	**99%**	**97%**	**95%**	**99%**	**97%**	**95%**
Crenarchaeota; MBGA	0.0	0.2	0.4	0.0	0.0	0.0	0.0	0.0	0.0	0.0	0.0	0.0
Crenarchaeota; Thaumarchaeota; Cenarchaeales; Cenarchaeaceae	0.6	4.2	6.0	0.0	0.0	0.9	0.0	0.0	2.1	0.0	0.0	4.9
Crenarchaeota; Thaumarchaeota; Cenarchaeales; SAGMA-X	0.0	0.0	0.0	0.0	0.0	0.0	15.4	18.1	17.5	0.0	0.0	0.0
Crenarchaeota; Thaumarchaeota; Nitrososphaerales; Nitrososphaeraceae	99.4	95.6	93.1	99.9	100.0	99.0	72.3	78.6	77.2	99.9	99.9	95.8
Euryarchaeota; Methanobacteria; Methanobacteriales; MSBL1	0.0	0.0	0.0	0.0	0.0	0.0	0.0	0.0	0.0	0.0	0.0	0.0
Euryarchaeota; Methanomicrobia; Methanosarcinales; Methanosarcinaceae	0.0	0.0	0.0	0.0	0.0	0.0	0.0	3.2	3.2	0.0	0.0	0.0

Table B.7: Output of the PHREEQC geochemical modelling shown for one representative sample (ICE-13_15, Vatnajökull).

Phase	SI	1=SUPERSATURATED; 0=UNDERSATURATED	log IAP	log KT	Formula
Albite	-9.3	0	-5.97	3.33	NaAlSi3O8
Albite_high	-10.79	0	-5.97	4.82	NaAlSi3O8
Albite_low	-9.3	0	-5.97	3.33	NaAlSi3O8
Analcime	-8.28	0	-1.1	7.18	Na.96Al.96Si2.04O6:H2O
Anorthite	-16.31	0	14.92	31.23	CaAl2(SiO4)2
Beidellite-Mg	-3.6	0	4.26	7.87	Mg.165Al2.33Si3.67O10(OH)2
Beidellite-Na	-4.34	0	3.47	7.81	Na.33Al2.33Si3.67O10(OH)2
Boehmite	0.74	1	10.1	9.37	AlO2H
Brucite	-12.36	0	5.73	18.09	Mg(OH)2
Ca-Al_Pyroxene	-21.23	0	20.43	41.66	CaAl2SiO6
Chalcedony	-1.19	0	-5.51	-4.32	SiO2
Clinochlore-14A	-44.5	0	32.32	76.82	Mg5Al2Si3O10(OH)8
Clinochlore-7A	-48.09	0	32.32	80.41	Mg5Al2Si3O10(OH)8
Cristobalite(alpha)	-1.51	0	-5.51	-4	SiO2
Cristobalite(beta)	-2.03	0	-5.51	-3.49	SiO2
Diaspore	1.18	1	10.1	8.92	AlHO2
Diopside	-22.5	0	0.44	22.93	CaMgSi2O6
Enstatite	-12.35	0	0.22	12.57	MgSiO3
Fayalite	-17.01	0	4.45	21.46	Fe2SiO4
Fe(OH)2	-10.45	0	4.98	15.44	Fe(OH)2
Fe(OH)3	-5.59	0	1.41	7	Fe(OH)3
FeO	-10.25	0	4.98	15.23	FeO
Forsterite	-25.13	0	5.95	31.08	Mg2SiO4
Gibbsite	0.73	1	10.1	9.38	Al(OH)3
Goethite	-0.12	0	1.41	1.53	FeOOH

Hedenbergite	-21.74	0	-0.31	21.43	CaFe(SiO3)2
Hematite	0.67	1	2.82	2.15	Fe2O3
Hercynite	-9.17	0	25.19	34.36	FeAl2O4
Kaolinite	0.13	1	9.19	9.06	Al2Si2O5(OH)4
Laumontite	-12.38	0	3.9	16.27	CaAl2Si4O12:4H2O
Lawsonite	-11.04	0	14.92	25.96	CaAl2Si2O7(OH)2:H2O
Magnetite	-6.1	0	7.8	13.9	Fe3O4
Monticellite	-26.69	0	5.95	32.64	CaMgSiO4
Montmor-Ca	-6.08	0	-2.33	3.74	Ca.165Mg.33Al1.67Si4O10(OH)2
Montmor-Mg	-6.01	0	-2.34	3.67	Mg.495Al1.67Si4O10(OH)2
Montmor-Na	-6.75	0	-3.13	3.62	Na.33Mg.33Al1.67Si4O10(OH)2
Mordenite	-10.66	0	-16.56	-5.9	Ca.2895Na.361Al.94Si5.06O12:3.468H2O
Mordenite-dehy	-27.42	0	-16.56	10.86	Ca.2895Na.361Al.94Si5.06O12
Nontronite-Ca	-1.81	0	-13.13	-11.31	Ca.165Fe2Al.33Si3.67H2O12
Nontronite-H	-1.68	0	-14.07	-12.39	H.33Fe2Al.33Si3.67H2O12
Nontronite-Mg	-1.82	0	-13.13	-11.3	Mg.165Fe2Al.33Si3.67H2O12
Nontronite-Na	-2.56	0	-13.92	-11.36	Na.33Fe2Al.33Si3.67H2O12
Periclase	-18.01	0	5.73	23.74	MgO
Pyrophyllite	-3.54	0	-1.84	1.71	Al2Si4O10(OH)2
Quartz	-0.9	0	-5.51	-4.62	SiO2
SiO2(am)	-2.4	0	-5.51	-3.11	SiO2

Appendix C: Supplementary information for chapter 6

Integrated ‘omics’, targeted metabolite and single-cell analyses of Arctic snow algae functionality and adaptability.

Lutz, S., Anesio, A. M., Field, K. & Benning, L. G.

Published in *Frontiers in microbiology*, 6, 1323 (2015)

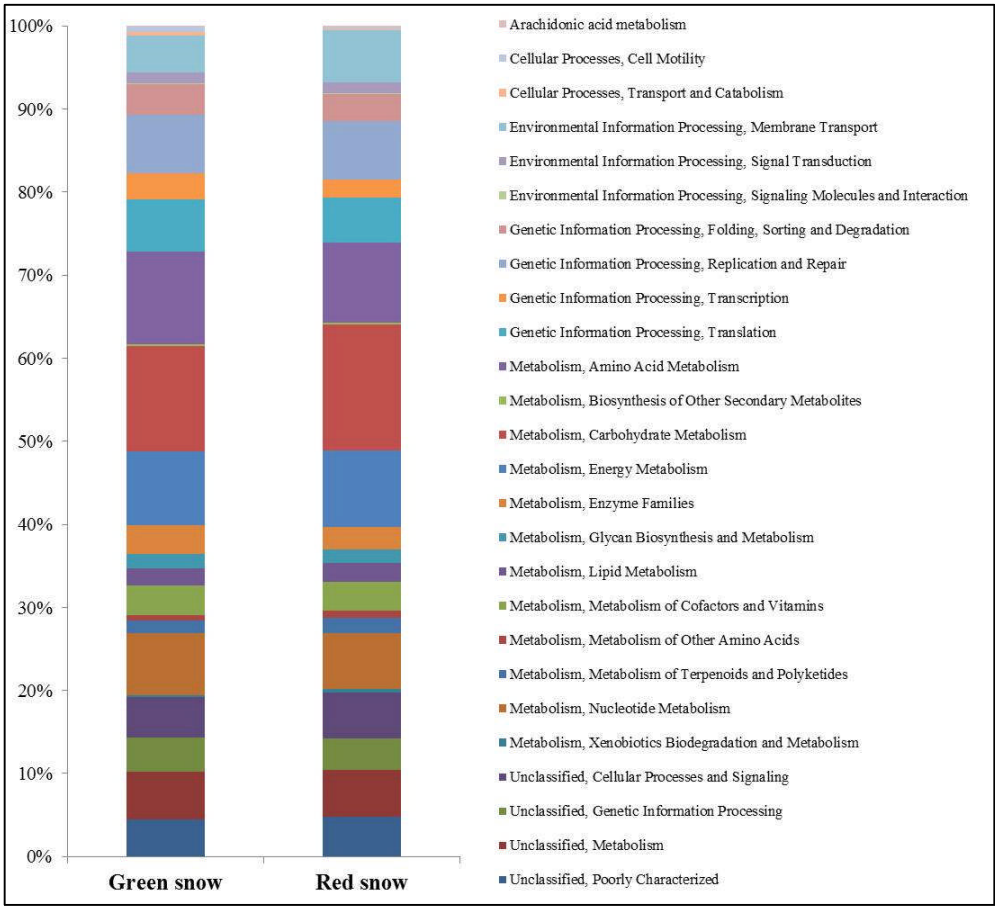

Figure C.1: Metagenomes showing proportions of main gene families in green and red snow. No major differences at this sequencing depth.

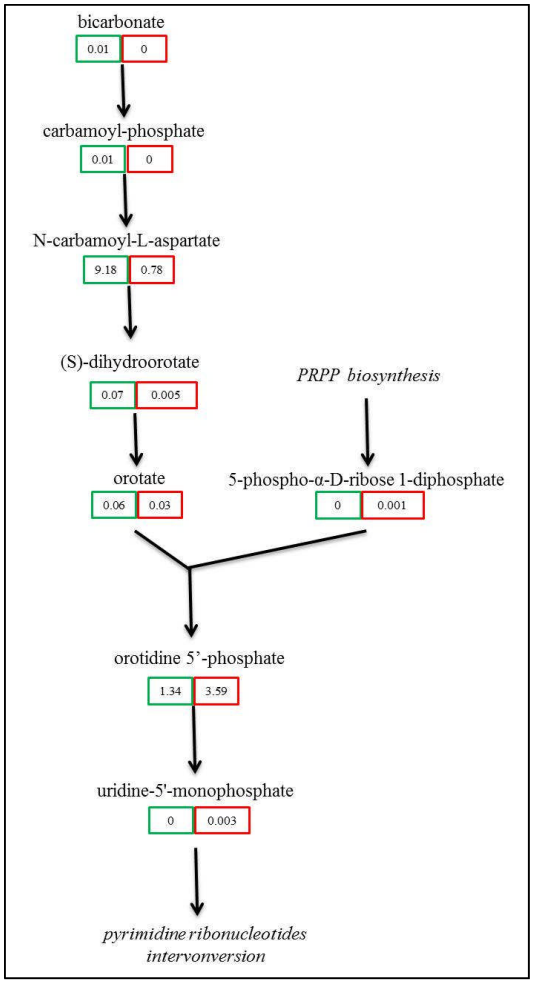

Figure C.2: Metabolomics data mapped on uridine monophosphate (UMP) biosynthesis pathway. Numbers represent relative abundance (in %) of metabolites for green (green boxes) and red (red boxes) snow.

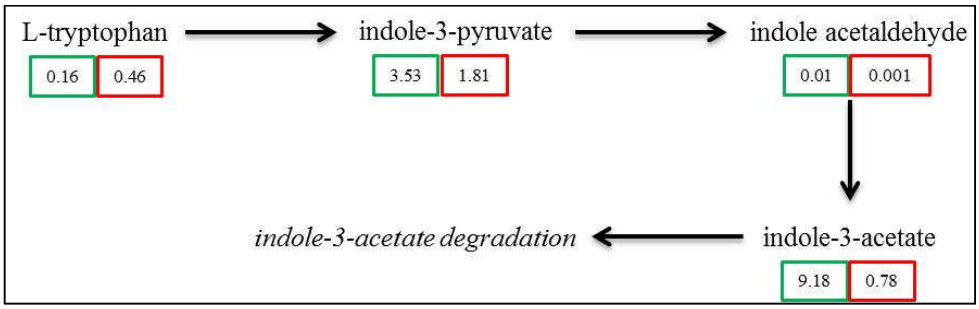

Figure C.3: Metabolomics data mapped on tryptophan degradation pathway. Numbers represent relative abundance (in %) of metabolites for green (green boxes) and red (red boxes) snow.

Table C.1: Distribution of 97% clustered OTUs aligned and assigned to *Archaeplastida* (green algae). Values are the relative abundance of the taxa in percentage of total sequences and table shows taxa with OTUs of a minimum total observation count of 0.1%.

	Green snow	**Red snow**
***Chlamydomonas cf. proboscigera* CCCryo 217-05**	0.57	0.00
***Chloromonas cf. alpina* CCCryo 033-99 (AF514403)**	0.09	5.02
***Chloromonas cf. platystigma* CCCryo 020-99**	0.03	1.64
***Chloromonas nivalis (*AF514409)**	0.24	48.24
***Chloromonas polyptera (*JQ790556)**	0.06	13.13
Chloromonas tughillensis	0.06	1.50
Microglena sp.* (polar subclade *Chlamydomonas*) (EF537906*)	98.52	0.09
***Raphidonema sempervirens* (AJ309939)**	0.33	3.61
Uncultured *Chlamydomonadaceae* (1)	0.00	3.00
Uncultured *Chlamydomonadaceae* (2) (GU117577)	0.09	23.68

Table C.2: Distribution of 97% clustered OTUs aligned and assigned to known bacterial classes (bold) and the orders, families and genera therein (indented), where possible ("__" = lack of assignment depth). Values are the relative abundance of the taxa in percentage of total sequences and taxa with >0.01% abundance are shown.

Taxon	Green snow	Red snow
Actinobacteria, Actinobacteria	0.08	1.03
Actinomycetales; Sporichthyaceae; __	0.08	1.03
Bacteriodetes, Cytophagia	3.61	0.88
Cytophagales, Cytophagaceae, Flectobacillus	3.61	0.88
Bacteriodetes, Flavobacteria	76.84	0.00
Flavobacteriales, Flavobacteriaceae, Flavobacterium	76.84	0.00
Bacteriodetes, Saprospirae	2.80	86.93
Saprospirales, Chitinophagaceae, __	2.80	86.93
Chlorobi, Ignavibacteria	2.00	1.62
Ignavibacteriales, Ignavibacteriaceae, __	2.00	1.62
Proteobacteria, Alphaproteobacteria	4.25	0.37
__, __, __	2.88	0.37
BD7-3, __, __	0.96	0.00
Rickettsiales, Pelagibacteraceae, __	0.40	0.00
Proteobacteria, Betaproteobacteria	10.42	9.18
Burkholderiales, __, __	0.16	2.86
Burkholderiales, Comamonadaceae, __	1.60	0.00
Burkholderiales, Comamonadaceae, Methylibium	0.32	0.81
Burkholderiales, Comamonadaceae, Paucibacter	0.16	1.47
Burkholderiales, Comamonadaceae, Polaromonas	0.00	0.44
Burkholderiales, Comamonadaceae, Rhodoferax	0.32	2.42
Burkholderiales, Comamonadaceae, Rubrivivax	0.40	0.00
Burkholderiales, Oxalobacteraceae, __	0.80	0.00
Burkholderiales, Oxalobacteraceae, Janthinobacterium	0.40	0.00
Gallionellales, Gallionellaceae, Gallionella	5.53	1.10
Rhodocyclales, Rhodocyclaceae, __	0.72	0.07

Table C.3: Distribution of 97% clustered OTUs aligned and assigned to archaea.

Taxon	Green snow	Red snow
Thaumarchaeota, Cenarchaeaceae	0.03	25.63
Thaumarchaeota, Nitrososphaeraceae	99.93	74.34

Table C.4: Relative abundance of functional categories for the annotated genes in the metagenomes of green and red snow with relevant sub-categories (underlined) and KEGG orthology (KO) identifiers. Gene categories that were also represented in the metabolomes are in bold (see also Table 6.4).

Level 1, Level 2	**Level 3**	**Level 4**	**Green snow [%]**	**Red snow [%]**	**KO**
Cellular Processes, Cell Motility			0.61	0.18	
Cellular Processes, Transport and Catabolism			0.41	0.16	
Environmental Information Processing, Membrane Transport			4.44	6.26	
Environmental Information Processing, Signal Transduction			1.26	1.25	
Environmental Information Processing, Signaling Molecules and Interaction			0.18	0.08	
Genetic Information Processing, Folding, Sorting and Degradation			3.68	3.33	
Genetic Information Processing, Replication and Repair			7.01	7.03	
Genetic Information Processing, Transcription			3.07	2.10	
Genetic Information Processing, Translation			6.26	5.48	
Metabolism, Amino Acid Metabolism			11.21	9.58	
	Alanine, aspartate and glutamate metabolism		0.43	0.42	
	Amino acid related enzymes		2.43	2.23	
	Arginine and proline metabolism		0.91	0.87	
	Cysteine and methionine metabolism		0.83	0.96	
	Glycine, serine and threonine metabolism		1.37	1.21	
	Histidine metabolism		0.85	0.48	
	Lysine biosynthesis		0.53	0.52	
	Lysine degradation		1.04	0.26	
	Phenylalanine metabolism		0.15	0.22	

	Phenylalanine, tyrosine and tryptophan biosynthesis		0.62	0.69	
	Tryptophan metabolism		0.28	0.16	
		L-tryptophan aminotransferase	0	0	K16903
		indolepyruvate decarboxylase	0	0	K04103
		indole-3-acetaldehyde	0	0	K11817
	Tyrosine metabolism		0.46	0.31	
	Valine, leucine and isoleucine biosynthesis		0.92	0.85	
	Valine, leucine and isoleucine degradation		0.40	0.40	
Metabolism, Biosynthesis of Other Secondary Metabolites			0.19	0.24	
	Flavonoid biosynthesis		0.06	0.02	
		5-amino-6-(5-phospho-D-ribitylamino) uracil phosphatase			
Metabolism, Carbohydrate Metabolism			12.68	15.15	
	Amino sugar and nucleotide sugar metabolism		0.82	1.14	
	Ascorbate and aldarate metabolism		0.04	0.08	
	Butanoate metabolism		0.85	0.97	
	C5-Branched dibasic acid metabolism		0.10	0.14	
	Citrate cycle (TCA cycle)		1.67	1.76	
	Fructose and mannose metabolism		0.80	1.00	
		mannitol dehydrogenase	0	0	K00045
		mannitol-1-phosphatase			
		mannitol-1-phosphate dehydrogenase	0	0	K00009
		pyrophosphate-dependent phosphofructokinase	0	0	K00895
		fructokinase	0.02	0.01	K00847

	Galactose metabolism	0.60	0.69
	Glycolysis / Gluconeogenesis	2.36	2.40
	Glyoxylate and dicarboxylate metabolism	1.19	1.43
	Inositol phosphate metabolism	0.21	0.11
	Pentose and glucuronate interconversions	0.30	0.90
	Pentose phosphate pathway	0.70	0.99
	Propanoate metabolism	0.88	0.96
	Pyruvate metabolism	1.21	1.51
	Starch and sucrose metabolism	0.97	1.07
Metabolism, Energy Metabolism		8.85	9.23
	Carbon fixation in photosynthetic organisms	0.21	0.18
	Carbon fixation pathways in prokaryotes	0.16	0.23
	Methane metabolism	0.70	1.02
	Nitrogen metabolism	1.55	1.61
	Oxidative phosphorylation	3.82	4.17
	Photosynthesis	2.16	1.42
	Photosynthesis - antenna proteins	0.01	0.00
	Photosynthesis proteins	0.00	0.01
	Sulfur metabolism	0.23	0.59
Metabolism, Enzyme Families		3.42	2.70
Metabolism, Glycan Biosynthesis and Metabolism		1.76	1.64
Metabolism, Lipid Metabolism		2.07	2.29
	Biosynthesis of unsaturated fatty acids	0.16	0.11
	Fatty acid biosynthesis	0.71	0.66

	Fatty acid metabolism		0.30	0.32	
	Glycerolipid metabolism		0.20	0.17	
	Glycerophospholipid metabolism		0.33	0.39	
	Linoleic acid metabolism		0.07	0.05	
	Lipid biosynthesis proteins		0.07	0.13	
	Primary bile acid biosynthesis		0.00	0.01	
	Sphingolipid metabolism		0.04	0.18	
	Steroid biosynthesis		0.03	0.00	
	Steroid hormone biosynthesis		0.01	0.02	
Arachidonic acid metabolism			0.14	0.24	
Metabolism, Metabolism of Cofactors and Vitamins			3.47	3.44	
	Riboflavin metabolism		0.20	0.26	
Metabolism, Metabolism of Other Amino Acids			0.75	0.84	
Metabolism, Metabolism of Terpenoids and Polyketides			1.48	1.82	
	Carotenoid biosynthesis		0.14	0.09	
		zeta-carotene desaturase	0.0047	0.0000	K00514
		15-cis-phytoene desaturase	0.0047	0.0000	K02293
		beta-carotene hydroxylase	0.0375	0.0057	K02294
		lycopene beta-cyclase	0.0141	0.0000	K06443
		prolycopene isomerase	0.0141	0.0000	K09835
		phytoene desaturase	0.0609	0.0738	K10027
		diapolycopene oxygenase	0.0000	0.0057	K10210
Metabolism, Nucleotide Metabolism			7.43	6.76	
	Purine metabolism		5.86	5.24	

	Pyrimidine metabolism		1.56	1.52	
		carbamoyl-phosphate synthase	0	0	K01954
		aspartate carbamoyltransferase	0	0	K00608
		dihydroorotase	0.18	0.11	K01465
		dihydroorotase dehydrogenase	0	0	K00254
		orotate phosphoribosyltransferase	0.03	0.02	K00762
		orotidine-5'-phosphate decarboxylase	0.04	0.03	K01591
Metabolism, Xenobiotics Biodegradation and Metabolism			0.28	0.44	
Unclassified, Cellular Processes and Signaling			4.80	5.51	
Unclassified, Genetic Information Processing			4.14	3.75	
Unclassified, Metabolism			5.70	5.70	
Unclassified, Poorly Characterized			4.46	4.74	

Table C.5: Comparison of main pathways in metabolomes and metagenomes of green and red snow.

	Metabolomics [%]		**Metagenomics [%]**	
	Green snow	Red snow	Green snow	Red snow
purine metabolism	30.0	62.8	5.9	5.2
pyrimidine metabolism	1.5	3.6	1.6	1.5
tryptophan metabolism	12.9	3.0	0.3	0.2
mannitol cycle	0.4	0.8	0.8	1.0
sphingolipid metabolism	4.5	12.9	0.0	0.2

Table C.6: Number of raw and processed sequences for amplicons and metagenomes.

	Green snow		**Red snow**	
	raw sequences	after QC	raw sequences	after QC
Eukaryotes	7552	4334	8292	4595
assigned to algae		3685		3131
Bacteria	7568	3100	15665	4011
Archaea	162714	154711	65697	57661
Metagenomes	504879	343339	261005	184871

Appendix D: Supplementary information for chapter 7

Algae Melt Arctic Glaciers: The Biogeography and Function of Snow Microbiomes.

Lutz, S., Anesio, A. M., Raiswell, R., Edwards, A., Newton, R.J., Gill, F. & Benning, L. G.

In review with *Nature Communications*.

Statement on sample exclusion

All samples for DNA and aqueous analyses were collected and analysed in the same exact way for all samples from Greenland, Iceland, Svalbard and Sweden.

However, pigment and fatty acid data is only shown for all samples from Svalbard and Sweden. For Greenland and Iceland these data have previously been published(Lutz et al, 2015; Lutz et al, 2014) and have been excluded from comparison here for different reasons. The pigment and fatty acid data in Greenland has been quantified in a slightly different way. The pigments were normalized to Chlorophyll a, whereas in all other study area they were quantified with the appropriate pigment standards. The fatty acid components were analysed by GC-MS, whereas all samples from Svalbard and Sweden were also quantified by flame ionization detection. The pigment and fatty acid data from Iceland was excluded from comparison since we found a large amount of moss (identified by microscopy and DNA sequences) in our samples that could not be separated from the algae before pigment and fatty acid extraction, and therefore likely 'skewed' the data.

Statement on primer choice

Primers targeting the 18S rRNA gene were chosen because there are more sequences in the databases for green algae than for rbcL or ITS. Before sequencing, we carried out an *in-silico* investigation including 18S rNRA sequences from 122 snow and permafrost algae in order to make sure that the chosen primers are suitable for a vast number of green algae and that there is enough variability in the chosen region (v4-v5) to distinguish between species.

Previous studies (Potvin & Lovejoy, 2009) have found that one primer pair is not sufficient to recover all eukaryotic groups in one sample. However, we chose our primer pair based on one group we were specifically targeting, *i.e.*, the green algae. We do not claim to have equally recovered all other groups among the micro-eukaryotes such as fungi or the "SAR"-group. Furthermore, they found that libraries derived from different primer pairs grouped together for individual samples with no significant differences. Based on our *in silico* test of 122 snow and permafrost algae and the rarefaction curves, we are fairly confident that the choice of our primer pair has resulted in a good coverage of the algal diversity.

Table D.1: Overview of samples, locations, coordinates and field measurements for red snow algae samples collected from Svalbard (SVA), Northern Sweden (TAR), Greenland (MIT) and Iceland (ICE). Only a few samples from Greenland and Iceland have been included in this study for the pan-Arctic comparison and many more data from other snow and ice habitat samples can be found in previous publications(Lutz et al, 2015; Lutz et al, 2014).

Sample ID	Location	Collection date	GPS location [UTM]	Elev. [m a.s.l.]	pH	Snow temp. [°C]	PAR [W/m²]	UV-A [W/m²]	UV-B [W/m²]	Albedo
Svalbard, Norway										
SVA-13_2	Vestre Brøggerbreen	20/07/2013	33H 0433169 E, 8759838 N	265	7.03	0	48			0.63
SVA-13_4	Vestre Brøggerbreen	20/07/2013	33H 0432976 E, 8760004 N	254	6.10	0	39			0.67
SVA-13_10	Midre Lovénbreen	21/07/2013	33H 0436410 E, 8757512 N	299	6.65	0	54	7.49	3.99	0.76
SVA-13_20	Austre Brøggerbreen	24/07/2013	33X 0429286 E, 8761458 N	209	6.38		91			0.60
SVA-13_23	Austre Brøggerbreen	24/07/2013	33X 0429448 E, 8761568 N	227	6.27		75			0.63
SVA-13_31	Austre Brøggerbreen	24/07/2013	33X 0430139 E, 8761706 N	146	8.07		70			0.62
SVA-13_33	Pedersenbreen	27/07/2013	33X 0441747 E, 8756068 N	320			22	24.7	1.07	0.55
SVA-13_36	Pedersenbreen	27/07/2013	33X 0441609 E, 8756682 N	262			115			0.55
SVA-13_43	Austre Lovénbreen	03/08/2013	33X 0439635 E, 8756676 N	413	6.3	0.1	182	19.6	0.66	0.66
SVA-13_48	Austre Lovénbreen	03/08/2013	33X 0438286 E, 8756948 N	345			36			0.60
SVA-13_54	Feiringsbreen	05/08/2013	33X 0446691 E, 8773282 N	401	5.68		88	11.8	0.35	0.51
SVA-13_65	Midre Lovénbreen	05/08/2013	33X 0436693 E, 8759332 N	151			108			0.49
Tarfala, Sweden										
TAR-13_1	Storglaciären	01/07/2013	34W 0398931 E, 7533637 N	1268	6.98	0	52	8.05	0.08	0.56
TAR-13_5	Storglaciären	01/07/2013	34W 0399260 E, 7534131 N	1221	5.56	0	30			0.66
TAR-13_8	Storglaciären	03/07/2013	34W 0397551 E, 7534187 N	1412	7.23	0.1	97			0.72
TAR-13_17	Rabot	05/07/2013	34W 0394929 E, 7534801 N	1350	6.13	0	112	16.5	1.05	0.75
TAR-13_21	Rabot	05/07/2013	34W 0394160 E, 7535197 N	1282	5.45	0	122			0.73
TAR-13_24	Rabot	05/07/2013	34W 0393074 E, 7534485 N	1165			95			0.54
TAR-13_27	Liljetopsrännan	06/07/2013	34W 0398423 E, 7533989 N	1119	5.41	0.2	54	11.1	0.4	0.65
TAR-13_28	Liljetopsrännan	06/07/2013	34W 0398656 E, 7536883 N	1209	6.35	0	51			0.56
TAR-13_30	SE-Kasskasatjåkkå	07/07/2013	34W 0399446 E, 7537111 N	1374	0.45	0.3	123	19.4	2.78	0.77
TAR-13_32	SE-Kasskasatjåkkå	07/07/2013	34W 0399458 E, 7536982 N	1318	5.78	0	108			0.57
TAR-13_35	Storglaciären	09/07/2013	34W 0398849 E, 7534337 N	1308	5.41	0	88			0.76
TAR-13_36	Permanent snow field	09/07/2013	34W 0399453 E, 7534692 N	1167	5.68	0	85			0.65
TAR-13_37	Permanent snow field	09/07/2013	34W 0399376 E, 7534942 N	1163	5.73	0.4	82			0.62
TAR-13_39	Permanent snow field	10/07/2013	34W 0400256 E, 7535905 N	1318			199	18.4	3.86	0.66
TAR-13_41	Björling	11/07/2013	34W 0395764 E, 7532198 N	1295	5.44	0	127	20.3	4.49	0.66
TAR-13_42	Björling	11/07/2013	34W 0396623 E, 7531127 N	1156	6.1	0.3	100			0.57
TAR-14_1	Storglaciären	04/07/2014	34W 0398031 E, 7533618 N	1268	7.4	0.1				
TAR-14_4	Storglaciären	07/07/2014	34W 0398886 E, 7533623 N	1277	7.35	0.1				
TAR-14_5	Storglaciären	07/07/2014	34H 0399085 E, 7533632 N	1247	7.78	0.3				
TAR-14_6	Storglaciären	07/07/2014	34H 0393734 E, 7535101 N	1226	6.17	0.1				

TAR-14_7	Rabot	09/07/2014	34W 0394036 E, 7535053 N	1326	8.13	0.1				
TAR-14_10	Liljetopsrännan	10/07/2014	34W 0398650 E, 7536880 N	1215	7.51	0.1				
TAR-14_11	SE-Kasskasatjåkkå	10/07/2014	34W 0399438 E, 7537029 N	1340	7.14	0.1				
Mittivakkat, Greenland										
MIT-12_7	Mittivakkat	10/07/2012	24H 0551567 E, 7285460 N	155	5.67	0	204	28.1	1.13	
MIT-12_19	Mittivakkat	17/07/2012	24H 0551778 E, 7286368 N	150	4.68	0.73	345	46.2	1.54	39
Iceland										
ICE-12_3	Drangajökull	27/07/2012	27W 0442125 E, 7334250 N	196	6.15					
ICE-12_4	Laugafell	29/07/2012	27W 0632892 E, 7222179 N	908	4.96		237	21.2	1.24	42

Table D.2: Distribution of 97% clustered OTUs aligned and assigned to known bacterial species. Values are the relative abundance of the taxa in percentage of total sequences and figure shows taxa with >0.01% abundance. It is important to note that values are rounded to one digit; therefore the abundance of a taxon with a value of 0 in one sample can range between 0 and 0.04%.

Phylum	***Acidobacteria***		***Actinobacteria***		***Bacteriodetes***				***Chlorobi***	***Chloroflexi***		
Class	**Acidobacteriia**	***Solibacteres***	***Acidimicrobiia***	***Actinobacteria***	***Cytophagia***	***Flavobacteriia***	***Sphingobacteriia***	***Saprospirae***	***Ignavibacteria***	***Anaerolineae***	***C0119***	***Ktedonobacteria***
SVA-13_4	0	0	0	0.5	37.4	0	0.3	51.2	0	0	0	0
SVA-13_10	17	0	0	0	9	0	0	3	0	0	0	0
SVA-13_20	0	0	0	0	10.6	0	1.5	45.2	1.8	0	0	0
SVA-13_23	0	0	0	0.3	6.3	4.6	0	1	0	0	0	0
SVA-13_31	0	0	0	4.2	11.6	0.4	0	44.9	0	0	0	0
SVA-13_33	0.4	0	0	2.1	3.9	0	2.8	26.8	0	0	0	0
SVA-13_36	3.4	0	0	8.4	39	0.5	0.8	1.6	0	0	0	0
SVA-13_43	0.8	0	0	0.8	12.5	0	0.4	67.3	0	0	0	0
SVA-13_48	0	0	0	0.6	44.5	0.6	0	19.1	0	0	0	0
SVA-13_54	0.2	0	0	15.7	3.4	0.5	34.6	3.6	0	0	0	0
SVA-13_65	0.4	0	0	0.2	5.9	1	0.3	3.7	0	0.1	0	0
TAR-13_1	0	0	0	0.1	3.6	0	91.1	1.9	0	0	0	0
TAR-13_8	0.4	0	0	0	0	0	89.3	0	0.4	0	0	0
TAR-13_17	0.2	0	0	0	0.8	0	90.7	0.1	0	0	0	0
TAR-13_21	0	0	0	0	1	0	75.7	22.3	0	0	0	0
TAR-13_27	0	0	0	0	0.5	0	71.4	0.5	5.1	0	0	0
TAR-13_28	4.7	0	0	0	0	0	12.5	0	0	0	0	0
TAR-13_30	0.2	0	0	0	3.8	0	81.6	3.2	0.2	0	0	0
TAR-13_35	0.8	0	0	0.1	4.1	0.9	63	4.3	0	0	0	0
TAR-13_41	0	0	0	0.1	0.5	0	82.1	15.8	0.3	0	0	0
TAR-14_1	1.1	0	0	4.3	1.2	0	46.3	11.2	0	0	0	0
TAR-14_4	10.7	0.3	0	0	0	0	0.2	0	0	0.1	0	0
TAR-14_5	16.7	0.2	0	0	15	0	1.3	0	0	0	0	0
TAR-14_6	0.1	0	0	0.1	1.9	0.1	81.3	2.4	0	0	0	0
TAR-14_7	17.2	0.3	0	0	0	0.1	1.7	0	0	0	0	0
TAR-14_10	17.1	0.7	0	0.1	7.3	0	45.8	1	0	0	0	0
TAR-14_11	4.6	0.5	0	0.4	13.6	0	51.8	6.3	0	0	0	0
TAR-14_12	3.1	0	0	0.3	2.2	0	59.3	0	0	0	0	0
MIT-12_7	1.2	0	0	0.3	4.8	0	33.2	12.4	0	0	0	0
MIT-12_19	0	0	0	1.1	2.9	0	14.6	10.8	0	0	0	0
ICE-12_3	0.4	0	0	6.0	0.1	0	18.8	24.1	0	0	0	0
ICE-12_4	0	0	0	2.6	5.4	0	0	28.5	0	0	0	0

Table D.2 continued.

Phylum	*Cyanobacteria*				*Fibrobacteres*	*Firmicutes*	*Gemmatimonadetes*	*Proteobacteria*				*TM7-3*	*WPS-2*	*Thermi*
Class	**Cyano-bacteria**	**Nostoco-phycideae**	**Oscillatorio-phycideae**	**Synechococco-phycideae**	**Fibrobacteria**	**Clostridia**	**Gemmatimonadetes**	**Alphaproteo-bacteria**	**Betaproteo-bacteria**	**Deltaproteo-bacteria**	**Gammaproteo-bacteria**	**TM7-3**	**WPS-2**	**Deinococci**
SVA-13_4	0	0.3	0	0.5	0	0	0	0	9.5	0	0.3	0	0	0
SVA-13_10	0	1	17	20	0	2	0	8	22	0	0	0	1	0
SVA-13_20	0	0.6	1.2	1.5	0	0	0	0	30.2	0	7.6	0	0	0
SVA-13_23	0.3	2.9	0.1	77.3	0	1.3	0	0.7	4.9	0	0.3	0	0	0
SVA-13_31	0	1.8	0.4	10.2	0	0	0	1.1	25.6	0	0	0	0	0
SVA-13_33	0	0.2	0	0.6	0	0.2	0	2.1	60.8	0	0	0	0	0
SVA-13_36	0	0	0	8.2	0	0	0	12	24.3	0.1	0	0.1	0	1.4
SVA-13_43	0	0	0	0	0	0	0	0.8	17.5	0	0	0	0	0
SVA-13_44	0	0	0	0.1	0	0	0	0.8	49.4	0	0	0	0	0
SVA-13_47	0	0	0	43.6	0	0	0.1	11.3	0.6	0.2	0	0.3	3.3	0
SVA-13_48	0	0	0	4.2	0	0	0	0.6	30.4	0	0	0	0	0
SVA-13_54	0	0.2	0	18.5	0	0	0	4.8	18.4	0	0.2	0	0	0
SVA-13_65	0	0.2	0	24.2	0	0.1	0	0.9	62.6	0	0.4	0	0.1	0
TAR-13_1	0.1	0	0	0.1	0	0	0	0.1	2.1	0	1	0	0	0
TAR-13_8	0.8	3.1	3.3	0	0	0	0	2.3	0.4	0	0	0	0.1	0
TAR-13_17	0.2	4.8	1.4	0.1	0	0	0	1.3	0.4	0	0	0	0	0
TAR-13_21	0.1	0	0	0.1	0	0	0	0.1	0.3	0	0.2	0	0	0
TAR-13_27	0	4.3	0.8	0.5	0	0	0	6.6	0.3	0	10	0	0	0
TAR-13_28	1.6	20.3	4.7	6.3	0	0	0	50	0	0	0	0	0	0
TAR-13_30	0.7	1.1	0.9	0.1	0	0	0	1.1	7	0	0.2	0	0	0
TAR-13_35	0	3	0.4	20.6	0	0.2	0	1	1.3	0	0.4	0	0	0
TAR-13_41	0	0.2	0.2	0.2	0	0	0	0.5	0.1	0	0	0	0	0
TAR-14_1	0	0.4	0.4	1.8	0	0	0	18.7	14.4	0	0.2	0	0	0
TAR-14_4	0.6	38.6	30	5	0	0	0	13.9	0.5	0	0	0	0	0
TAR-14_5	3	12.7	15.5	1.9	0	0	0	32.2	1.3	0	0	0	0.2	0
TAR-14_6	0	0.1	0.1	10.2	0	0	0	2.1	1.1	0	0.5	0	0	0
TAR-14_7	3.1	42.8	2.5	1.8	0	0	0	26.1	4.4	0	0	0	0.1	0
TAR-14_10	0.2	0.7	0.3	0.5	0	0	0	8.8	16.9	0	0.4	0	0.2	0
TAR-14_11	0	0.1	0.2	0.1	0	0	0	4.4	4.2	0	13.8	0	0.2	0
TAR-14_12	0	0.6	0	16.7	0	0	0	17	0.3	0	0.6	0	0	0
MIT-12_7	0	0.6	0.3	0	0	0	0	1.2	45.3	0	0.6	0	0	0
MIT-12_19	0	50.2	7	2.5	0	0	0	8.2	2.7	0	0	0	0	0
ICE-12_3	0	0	0	0.5	0	0	0.1	42.0	4.9	0	1.3	0	0.9	0
ICE-12_4	0	0.2	0	0.5	0	0	0.5	5.4	56.2	0	0	0	0	0

Table D.3: Distribution of 97% clustered OTUs aligned and assigned to eukaryotes. Values are the relative abundance of the taxa in percentage of total sequences. It is important to note that values are rounded to one digit; therefore the abundance of a taxon with a value of 0 in one sample can range between 0 and 0.04%.

Taxon	*Amoebozoa*	*Archaeplastida*	*Centrohelida*	*Kathablepharidae*	*Opisthokonta*	*RT5iin25*	*SAR*	*Zeuk77*
SVA-13_2	0	68.0	0	0	31.5	0	0.5	0
SVA-13_4	0	83.3	0	0	4.0	0	12.7	0.0
SVA-13_10	0	74.5	0	0	24.7	0	0.7	0
SVA-13_20	0	81.8	0	0	12.9	0	5.3	0
SVA-13_23	0.0	63.3	0	0	32.5	0	2.9	0
SVA-13_31	0.0	82.4	0	0	9.1	0	7.9	0
SVA-13_33	0	58.0	0	0	26.8	0	14.2	1.0
SVA-13_36	0	42.0	0	0	38.4	0	19.0	0.1
SVA-13_43	0	56.6	0	0	24.4	0	17.5	1.5
SVA-13_48	0.1	82.5	0	0	12.9	0	4.2	0
SVA-13_54	0	62.3	0	0	33.8	0	3.8	0
SVA-13_65	0	67.8	0	0	20.8	0	9.3	0
TAR-13_1	0	64.1	0	0	32.1	0	3.8	0
TAR-13_8	0	44.7	0	0	47.9	0	7.4	0
TAR-13_17	0	27.1	0	0	72.6	0	0.3	0
TAR-13_21	0	68.0	0	0	23.4	0	8.5	0.1
TAR-13_27	0	29.5	0	0	68.3	0	1.8	0
TAR-13_28	0	76.4	0	0	23.2	0	0.4	0
TAR-13_30	0	38.1	0	0	61.0	0	1.0	0
TAR-13_35	0	72.8	0	0	19.6	0	6.7	0
TAR-13_39	0	88.0	0	0	11.0	0	1.0	0
TAR-13_41	0	75.0	0	0	19.8	0	5.2	0
TAR-14_1	0.2	38.1	0	0	50.9	0	10.4	0
TAR-14_4	0	14.2	0	0	69.9	0	15.3	0
TAR-14_5	0	32.6	0	0	58.5	0	8.6	0
TAR-14_6	0.1	37.2	0	0	51.1	0	9.7	0
TAR-14_7	0	47.6	0	0	48.4	0	1.4	0
TAR-14_10	0	26.0	0	0	71.8	0	1.4	0
TAR-14_11	0	18.2	0	0	77.2	0	3.8	0

TAR-14_12	0	68.8	0	0	21.1	0	9.5	0.2
MIT-12_7	0	47.4	0	0	22.9	0	29.7	0
MIT-12_19	0	53.0	0	0	25.8	0	21.2	0
ICE-12_3	0	45.3	0	0	23.2	0	30.7	0.1
ICE-12_4	0	19.8	0	0	29.0	0	49.6	1.6

Table D.4: Distribution of 97% clustered OTUs aligned and assigned to *Archaeplastida* (green algae). Values are the relative abundance of the taxa in percentage of total sequences and table shows taxa with OTUs of a minimum total observation count of 0.1%. It is important to note that values are rounded to one digit; therefore the abundance of a taxon with a value of 0 in one sample can range between 0 and 0.04%.

Species:	***Ancylo-nema nordens-kioeldii***	***Chloro-monas cf. alpina* AF514403**	***Chlamydo-monas cf. proboscigera***	***Chloro-monas nivalis* AF514409**	***Chloro-monas polyptera* JQ790556**	***Chloro-monas spec. CCCryo 273-06***	***Chloro-monas tughillensis***	***Microglena polar subclade Chlamydo-Monas* EF537906**	***Prototheca cutis***	***Raphido-nema semper-virens* AJ309939**	***Trebouxia usneae***	**Uncultured *Chlamydo-monadaceae* (a) GU117577**	**Uncultured *Chlamydo-monadaceae* (b) GU117576**	**Uncultured *Chlamydo-monadaceae* (c) GU117575**
SVA-13_2	0	0.1	0	1.8	22.5	0	0	0	0	0	0.2	72.3	3	0.2
SVA-13_4	0	0.8	0	0.7	0.9	0	0.9	0.1	0	0	0	87.8	8.8	0
SVA-13_10	0	0	0	0.2	5.3	0	0	0	0	0	0	83.8	10.7	0.1
SVA-13_20	0	0	0	14	8.8	0	0.4	0	0	1.7	0	65	10.1	0
SVA-13_23	0	0	0	0.6	6.5	0	0	0	0	0.2	0	89.9	2.6	0.1
SVA-13_31	0	0	0	2.7	5.8	0	0	0	0.3	0.5	0	88.9	1.8	0
SVA-13_33	0	1.9	0	9.3	10.8	0.3	0	0	0	5.1	0	65.2	7.6	0
SVA-13_36	8.6	0.3	0.1	1.3	16.5	0	0.1	0	0.3	3.6	0	65.9	3.2	0.1
SVA-13_43	0	0.9	0	2.8	10.3	0	0.3	0.1	0	35.5	0	45.8	4.2	0.1
SVA-13_48	0	1.4	0	2.8	12.4	0	0	0	0.1	21.3	0	59.3	2.1	0.5
SVA-13_54	0	0	0	0.6	1.5	0.1	0	0	0	2.3	0	93.3	2.1	0
SVA-13_65	0.1	0.2	1.2	0	14.3	0	0	0	0.1	0.5	0	81.8	1.8	0.1
TAR-13_1	0	0	0	1.2	12.2	0	1.3	0	0	0	0.1	76.1	8.9	0
TAR-13_8	0	5.7	0	4.6	52.6	0	0.1	0	0.1	0.1	0	33.4	3.3	0
TAR-13_17	0	0.2	0	0.4	9	0	0	0	0	14.1	0	67.7	8.6	0
TAR-13_21	0	0.1	0	12.6	6.1	0	1.3	0	0	0	0	72.1	7.6	0.1
TAR-13_27	0	0	0	8.8	17	0	0.1	0	0.1	1.7	0.1	69.0	3.2	0
TAR-13_28	0	0	0	1.1	17.6	0	0	0	0	0.3	0	74.5	6.5	0
TAR-13_30	0	0	0	2	1	0	0.3	0.6	0	1.9	0.1	87.7	6.4	0
TAR-13_35	0	12.9	0	7.2	26.9	0	0.9	0	0.4	0	0.1	32.1	0.7	18.9
TAR-13_39	0	0	0	5.2	6.4	0	0.1	0	0	0	0	75.3	13	0
TAR-13_41	0	0	0	8.3	5.4	0	2.7	0	0	0.1	0	71.8	11.6	0
TAR-14_1	0	0.3	0	0.7	23.2	0	0.1	0	16.8	0.7	0.2	54.8	1.9	1.4
TAR-14_4	0	1	0	3.3	10.1	0	0.4	0	0.5	1	12.2	68.9	2.4	0.1
TAR-14_5	0	0.1	0	2.7	4.9	0	0.2	0	0.2	0.1	5.1	84.1	2.7	0
TAR-14_6	0	0	0	0	8.1	0	0	0	4.4	0.5	0	85.1	2	0
TAR-14_7	0	22.7	0	0	53.1	0	0	0	1.5	0.4	10	7.9	0.4	4
TAR-14_10	0.2	0	0	9.4	14.4	0	0.1	0	0.3	1.2	0.9	71.1	2.4	0
TAR-14_11	0.2	0	0	5.1	21.1	0	0	0	0.2	3.6	8.5	59.8	1.5	0
TAR-14_12	0	0	0	3.8	5.7	0	0	0	0	20.5	1.2	67.3	1.3	0.2

MIT-12_7	0	0	0	17.8	12.5	0	1	0	0	0	0	63.2	5.6	0
MIT-12_19	0	0.2	0	8.2	23.2	0	0.4	0	0	2.5	0.1	61.1	4.3	0
ICE-12_3	0	0.2	0	14.9	27.8	0	4.6	0	0	16.6	0	34.5	1.4	0
ICE-12_4	0	1.7	0	6.7	23.3	0	1.7	0	0	20.0	0	43.3	3.3	0

Table D.5: Distribution of 97% clustered OTUs aligned and assigned to archaea. It is important to note that values are rounded to one digit; therefore the abundance of a taxon with a value of 0 in one sample can range between 0 and 0.04%.

Phylum	***Crenarchaeota***					***Euryarchaeota***			
Class **Order**	***MBGA***	***MBGA;*** ***NRP-J***	***MCG;*** ***pGrfC26***	***Thaumarchaeota;*** ***Cenarchaeales***	***Thaumarchaeota;*** ***Nitrososphaerales***	***Methanobacteria;*** ***Methanobacteriales***	***Methanomicrobia;*** ***Methanomicrobiales***	***Methanomicrobia;*** ***Methanosarcinales***	***Thermoplasmata;*** ***E2***
SVA-13_2	0	0	0	0.3	99.7	0.0	0	0	0
SVA-13_23	0	0	0	0.5	99.4	0.2	0	0	0
SVA-13_31	0	0	0	0.0	99.4	0.6	0	0	0
SVA-13_36	0	0	0	3.6	92.9	2.4	0	0	1.2
SVA-13_48	0	0	0	5.0	16.8	78.2	0	0	0
SVA-13_54	0	0	0	13.2	74.5	8.5	0	0	3.8
SVA-13_65	0	0	0	14.3	42.9	28.6	14.3	0	0
TAR-13_8	0	0	0	4.9	86.2	2.0	1.2	0	5.7
TAR-14_1	0	0	0	0.1	100.0	0	0	0	0
TAR-14_4	0	0	0	0.6	99.4	0	0	0	0.0
TAR-14_5	0	0	0	2.2	97.8	0	0	0	0
TAR-14_6	0	0	0	0	0	0	0	90.0	10.0
ICE-12_3	0	0	0	2.8	96.5	0	0	0	0
ICE-12_4	0	0	0	0.7	27.6	0	0	71.6	0

Table D.6: Number of sequences before and after quality control, assigned to taxa and with respective Shannon diversity indices for eukaryotes, algae and bacteria. Shannon indices for archaea have not been calculated due to the very low species diversity.

	Eukaryotes			Algae		Bacteria				Archaea		
	Raw seqs	Seqs after QC	Shannon	Seqs assigned to algae	Shannon	Raw seqs	Seqs after QC	Seqs assigned to bacteria	Shannon	Raw seqs	Seqs after QC	Seqs assigned to archaea
SVA-13_2	6135	5148	3.34	3500	2.34	98*	4*	1*		60965	54688	53817
SVA-13_4	6979	3937	4.56	3280	3.41	7509	1421	770	6.16			
SVA-13_10	13448	6583	4.24	4904	3.52	29728	3511	334	6.69			
SVA-13_20	7130	3952	5.20	3226	4.08	12881	2344	987	7.00			
SVA-13_23	5373	4485	2.93	2832	1.74	8352	4008	1850	5.36	1695	732	657
SVA-13_31	12752	10621	3.07	8743	1.79	5040	2341	598	5.52		43331	42417
SVA-13_33	7678	3008	6.22	1727	4.40	9129	1911	1041	6.86			
SVA-13_36	23283	16789	5.28	7056	2.93	11503	6109	2573	4.26	2318	921	272
SVA-13_43	16457	5447	7.24	3059	5.43	5473	988	627	6.60			
SVA-13_48	6294	5123	3.96	4184	2.93	2838	1183	556	4.83	2665	722	410
SVA-13_54	23068	16698	3.89	10391	1.68	3777	1519	812	4.84	39830	34942	34121
SVA-13_65	7362	5408	4.17	3667	2.42	13545	7349	4245	4.25	1267	295	68
TAR-13_1	9632	4770	5.29	3058	4.23	21581	6431	5087	4.39			
TAR-13_8	77757	26947	5.85	12012	4.64	12368	3661	1051	4.39	2059	926	310
TAR-13_17	8767	4863	4.85	1318	4.68	16240	5850	3632	4.36			
TAR-13_21	9330	4354	5.25	2920	3.89	10946	3997	3169	5.45			
TAR-13_27	19416	15725	2.55	4639	3.04	16105	2297	630	5.87			
TAR-13_28	9402	5344	4.39	4082	3.56	15312	2525	227	6.28			
TAR-13_30	6493	3042	4.56	1133	2.91	10571	2327	1558	5.27			
TAR-13_35	7274	5474	4.91	3987	3.61	4562	2424	1437	4.04			
TAR-13_39	11667	6810	4.25	5992	3.41	15247	3447	0*				
TAR-13_41	7606	3715	4.83	2785	3.73	17534	5305	3651	4.99			
TAR-14_1	12436	9069	5.12	3454	3.34	3009	1705	1356	4.00	148712	146362	145547
TAR-14_4	10393	7341	5.40	1013	2.93	8647	5419	3922	5.55	1023027	886676	879402
TAR-14_5	4251	3254	3.99	1059	1.86	1974	1064	724	5.86	1020	590	520
TAR-14_6	7573	5312	3.93	1976	2.03	9112	4794	3868	2.25	587	414	109
TAR-14_7	2038	1265	5.71	586	3.76	6318	3729	2055	6.04			
TAR-14_10	6037	4720	3.68	1218	2.50	5809	3158	2412	5.32			
TAR-14_11	4899	3453	5.47	614	3.42	4453	2404	1893	4.76			
TAR-14_12	7387	5701	4.29	3909	2.54	1892	979	425	4.30			
MIT-12_7	5375	869	6.15	412	4.11	21459	1712	988	6.45			
MIT-12_19	6007	2342	6.12	1240	4.44	6503	1979	963	5.92			
ICE-12_3	5474	2013	5.55	1509	4.50	6383	2333	1602	5.13	9206	1443	4*
ICE-12_4	1908	597	6.02	359	4.47	2533	818	444	5.27	18323	6294	540

* removed from analysis due to low sequence numbers

Table D.7: Snow algal cell counts for the Svalbard (SVA), Sweden (TAR) and Greenland (MIT) samples, average diameter of the cells in each sample and inferred cell volume (assuming a spherical cell shape) and biomass (cell counts x volume). No cell counts for the Iceland samples.

Sample ID	Cell counts [mL^{-1}]	Diameter [µm]	Volume [$µm^3$]	Biomass [$mm^3 L^{-1}$]
SVA-13_2	28125 ± 4419	6.4 ± 2.0	137	4
SVA-13_4	15104 ± 2210	12.0 ± 3.4	904	14
SVA-13_10	8750 ± 11110	15.8 ± 4.4	2064	18
SVA-13_20	32292 ± 24307	n.d.	n.d.	n.d.
SVA-13_23	61875 ± 6187	n.d.	n.d.	n.d.
SVA-13_31	75000 ± 35355	n.d.	n.d.	n.d.
SVA-13_33	6875 ± 2652	12.0 ± 2.5	904	6
SVA-13_36	n.d.	12.1 ± 3.4	n.d.	n.d.
SVA-13_43	9191 ± 4864	20.0 ± 7.6	4187	38
SVA-13_48	23438 ± 6629	n.d	n.d	n.d
SVA-13_54	43750 ± 6629	13.0 ± 4.7	1150	50
SVA-13_65	27344 ± 16573	18.0 ± 6.3	3052	83
TAR-13_1	31250 ± 22097	14.3 ± 4.1	1530	36
TAR-13_5	23438 ± 11049	n.d	n.d	n.d
TAR-13_8	3438 ± 1326	15.0 ± 5.0	1766	3
TAR-13_17	26787	n.d.	n.d.	n.d.
TAR-13_21	6757 ± 2389	18.2 ± 3.9	3155	15
TAR-13_27	16667 ± 10312	19.0 ± 3.9	3590	36
TAR-13_28	n.d.	16.0 ± 2.7	n.d.	n.d.
TAR-13_32	29785 ± 7596	13.9 ± 3.1	1405	35
TAR-13_36	6875.	17.1 ± 3.1	2617	18
TAR-13_39	15625 ± 4419	18.6 ± 5.1	3368	2
TAR-13_41	41146 ± 6629	21.5 ± 4.4	5201	14
TAR-13_42	31250 ± 5682	12.5 ± 3.0	1022	36
MIT-12_7	25800	n.d.	n.d.	n.d.
MIT-12_19	5900	n.d.	n.d.	n.d.

n.d. = not determined

Table D.8: Fatty acid composition of the Svalbard (SVA) and Northern Sweden (TAR) samples as they contained sufficient particulate material for analysis. Fatty acid compounds are reported as percentage of total fatty acids. Most prominent fatty acids are reported as well as total saturated (SFA), total monounsaturated (MUFA) and total polyunsaturated (PUFA) fatty acids. b=branched, A = Alkane.

Although the sample preparation method, i.e. the filtration step, could potentially allow the extraction of fatty acids from non-algal sources, e.g. bacteria, the suite of fatty acids recovered from both Svalbard and Northern Sweden is characteristic of snow algae, with high abundance of monounsaturated and polyunsaturated C18 fatty acids and C16:0 and C16:4 fatty acids (Spijkerman et al, 2012). Site TAR-13-1 has the only occurrence of a branched C15 fatty acid, which has not been reported from snow algae but is typical of bacteria, including Sphingobacteria (Prasad et al, 2013). This is consistent with the dominance of Sphingobacteria OTUs (91.1 % of total bacterial sequences) at this site (Table D.4). The absence of putative bacterial fatty acids at other sites likely reflects lower abundance relative to algal taxa.

Sample ID	C14:0	C15:0	C15 b	C16:0	C16:1	C16:3	C16:4	C18:0	C18:1	C18:2	C18:3	C18:4	C20:0	C21 A	C22:0	C23 A	C24:0	C27 A	SFA	MUFA	PUFA
SVA-13_2	0	0	0	25	0	2	12	5	16	9	15	10	3	0	2	0	0	0	34	16	49
SVA-13_4	2	0	0	25	1	2	13	3	15	5	20	9	3	0	1	0	0	0	35	16	50
SVA-13_10	0	0	0	28	0	0	12	8	2	7	31	9	1	0	0	0	0	0	37	2	59
SVA-13_20	0	0	0	23	2	2	15	4	13	7	27	7	0	0	0	0	0	0	27	14	59
SVA-13_23	3	0	0	23	2	2	15	3	12	6	27	7	0	0	0	0	0	0	29	14	57
SVA-13_31	0	0	0	24	4	2	12	4	15	9	22	9	0	0	0	0	0	0	27	19	53
SVA-13_33	0	0	0	23	7	1	6	6	15	10	18	5	2	0	1	1	0	0	32	23	40
SVA-13_36	1	0	0	30	2	1	7	5	15	8	14	6	2	1	2	0	0	2	40	17	37
SVA-13_43	1	0	0	20	3	2	8	4	17	8	14	3	4	1	2	0	1	0	32	20	36
SVA-13_48	0	0	0	20	3	2	12	3	13	10	21	9	0	0	0	0	0	0	24	16	54
SVA-13_54	2	0	0	27	1	4	14	2	14	8	18	8	1	0	0	0	0	0	32	15	52
TAR-13_1	2	0	1	45	4	5	35	0	0	0	0	0	2	0	1	0	0	0	50	4	40
TAR-13_5	3	0	0	26	0	0	19	3	15	1	31	0	0	0	0	0	0	0	32	15	52
TAR-13_8	3	0	0	0	3	4	0	6	19	3	37	7	4	0	3	2	2	4	18	22	51
TAR-13_21	0	1	0	31	2	2	8	2	13	4	20	13	0	0	1	0	1	0	37	15	48
TAR-13_27	0	0	0	42	0	1	7	5	12	4	11	3	4	0	3	1	2	2	56	12	26
TAR-13_28	0	0	0	25	1	2	13	5	12	10	16	15	1	0	0	0	0	0	32	13	56
TAR-13_30	0	0	0	39	0	0	4	14	8	6	6	4	5	1	3	1	2	2	62	8	19
TAR-13_32	0	0	0	22	2	2	16	4	13	7	21	12	0	0	0	0	0	0	26	15	58
TAR-13_35	0	0	0	34	0	2	9	17	10	5	14	3	2	0	2	0	0	0	55	10	31
TAR-13_37	0	0	0	21	0	2	15	6	12	0	28	14	0	0	0	0	0	0	26	12	60
TAR-13_39	0	0	0	26	1	2	13	3	12	7	20	10	1	0	1	0	0	1	31	13	53
TAR-13_41	0	0	0	24	2	2	9	7	13	9	18	8	2	0	2	0	0	2	34	16	46
TAR-13_42	0	0	0	21	1	3	17	4	13	5	22	12	1	0	0	0	0	0	26	15	58

Table D.9: Pigment composition of samples from Svalbard (SVA) and Northern Sweden (TAR) as they contained sufficient particulate material for analysis. Individual pigments were quantified in ug/L and are reported as total chlorophylls, total primary carotenoids and total secondary carotenoids in % of total pigments. Chl a = chlorophyll a, Chl b = chlorophyll b, Neo = Neoxanthin, Vio = Violaxanthin, Ant = Antheraxanthin, Lut = Lutein, Zea = Zeaxanthin, β-car = β-carotene, Ast=Astaxanthin.

Sample ID	Chl a	Chl b	Neo	Vio	Ant	Lut	Zea	b-car	trans-Ast	cis-Ast	trans- Ast mono esters	cis-Ast mono esters	total Ast di esters	total chloro-phylls [%]	total primary carotenoids [%]	total secondary carotenoids [%]
SVA-13-2	3682	3132	215	147	0	1155	0	15	2976	115	62922	6457	1523	8	3	89
SVA-13-4	3359	2873	114	175	0	1133	0	81	2664	116	38758	4397	1776	11	4	85
SVA-13_10	882	748	25	10	0	351	0	853	1002	15	5164	362	76	17	14	69
SVA-13_20	1200	980	100	36	6	573	0	3193	3090	194	17661	1906	2316	7	13	80
SVA-13_23	1703	1141	239	290	107	1080	0	1059	4648	372	17305	1916	2779	9	9	82
SVA-13_31	327	266	308	468	0	1116	0	51	3927	164	1448	21	178	7	23	69
SVA-13_33	534	426	33	26	0	355	0	237	1251	64	3248	201	540	14	10	77
SVA-13_36	376	230	93	98	0	155	0	501	1456	86	9142	877	1318	4	6	90
SVA-13_43	672	757	56	113	0	577	0	298	868	9	4332	432	1873	14	11	75
SVA-13_54	450	507	472	624	0	1525	0	240	9272	904	5640	546	745	5	14	82
TAR-13_1	3253	2712	117	328	0	1499	9	1025	1867	101	28521	3562	4005	8	4	88
TAR-13_5	6068	5167	354	670	351	2449	88	957	3546	266	48066	6860	6299	8	4	88
TAR-13_8	3084	3212	315	1149	73	2574	14	728	3658	225	21286	2508	6384	9	7	84
TAR-13_17	2153	1605	402	721	0	1637	0	1136	3292	122	16014	3063	3949	7	8	85
TAR-13_21	1323	1266	315	374	0	1384	0	390	2386	158	13318	1449	2447	7	6	87
TAR-13_27	478	373	0	0	0	241	0	50	398	0	3145	286	404	10	3	87
TAR-13_28	672	417	597	381	0	563	0	88	1886	115	11182	1113	959	4	5	91
TAR-13_30	495	328	0	-31	0	89	0	0	243	0	3035	164	202	11	1	89
TAR-13_32	2490	2203	304	823	69	2021	7	459	2078	59	20966	2608	2913	8	6	86
TAR-13_35	2319	1578	50	162	0	691	0	402	963	14	10994	1557	2416	11	5	84
TAR-13_36	492	310	157	154	0	628	0	107	1599	92	6407	551	981	4	6	90
TAR-13_37	1655	1328	47	59	0	638	0	102	1351	57	5628	749	1229	15	5	79
TAR-13_41	541	426	747	565	48	1180	0	640	2764	222	8401	884	1766	4	12	85
TAR-13_42	7724	8730	1007	1391	111	5052	8	778	5032	205	29339	3554	4411	16	9	75
TAR-14_1	1414	632	0	0	0	318	0	0	938	0	21910	2344	639	6	24	71
TAR-14_4	369	0	0	0	0		0	0	76	0	693	0	0	32	0	68
TAR-14_5	2864	1391	0	0	0	528	22	0	207	0	2418	304	47	55	7	38
TAR-14_6	14924	10007	822	752	312	4414	0	0	17256	662	141903	13779	3548	12	4	84
TAR-14_7	4458	2533	59	0	29	963	6	0	330	0	4565	391	0	52	9	39
TAR-14_10	594	0	0	0	0	49	0	0	238	0	6358	663	133	7	2	90
TAR-14_11	332	0	0	0	0		0	0	0	0	102	0	0	76	0	24
TAR-14_12	4238	2694	16	25	0	1013	4	0	1751	170	45152	5915	1015	11	2	86

Table D.10: Aqueous geochemical data for dissolved organic carbon (DOC), nutrients (PO_4^{3-}, NO_3^-, SO_4^{2-}) and trace metals (Al to Zn) in the filtered red snow samples from Svalbard (SVA), Northern Sweden (TAR), Greenland (MIT) and Iceland (ICE).

Sample ID	DOC	PO_4^{3-}	NO_3^-	SO_4^{2-}	Cl^-	Al	Ba	Bi	Ca	Cd	Co	Cr	Cu	Fe	K	Mg	Mn	Na	Ni	Pb	S	Si	Sr	Zn
SVA-13-2	31	0.19	1043	<	344	0.4	<	<	100	<	<	<	<	0.5	14	44	1.7	228	<	<	12	<	0.2	0.9
SVA-13-4	39	0.14	288	<	381	0.9	0.3	<	94	<	<	<	<	0.9	59	46	1.7	248	<	0.0	14	<	0.3	1.3
SVA-13_10	17	0.05	1862	<	242	1.1	0.3	<	64	<	<	0.1	<	2.1	19	12	1.3	139	<	0.0	17	<	0.2	1.2
SVA-13_20	41	0.04	7010	160	545	2.1	0.2	<	180	0.0	<	<	<	2.8	56	70	2.0	376	<	0.0	34	<	0.7	0.7
SVA-13_23	36	0.08	<	<	332	1.7	0.8	<	955	<	<	0.1	0.2	1.6	65	396	3.1	250	0.1	0.0	48	16	0.9	4.5
SVA-13_31	51	0.14	<	<	321	2.0	0.5	<	2020	<	<	<	<	2.0	68	687	3.4	244	0.1	0.0	17	<	2.1	0.6
SVA-13_33	18	0.02	895	<	342	1.1	0.5	<	69	<	0.2	<	0.3	1.1	27	12	9.5	243	0.1	0.0	<	15	0.4	0.4
SVA-13_36	20	0.05	999	<	354	2.1	0.2	<	34	<	<	<	0.2	4.3	45	15	1.9	259	<	0.2	<	<	0.2	0.7
SVA-13_43	60	1.21	<	<	136	1.4	5.6	<	212	<	0.2	<	0.2	2.1	27	65	13.0	90	0.3	0.1	50	<	0.6	0.9
SVA-13_48	40	6.08	<	<	297	2.3	6.3	<	639	<	0.1	<	0.1	2.9	64	94	6.1	172	0.2	0.0	30	17	0.9	0.4
SVA-13_54	38	0.51	<	<	158	1.3	6.0	<	188	<	<	<	<	1.3	31	53	0.7	97	<	0.0	61	<	0.4	1.0
SVA-13_65	39	0.71	<	<	254	0.2	6.7	<	22	<	<	<	<	1.6	20	7	0.5	179	<	0.1	20	<	0.4	0.5
TAR-13_1	107	0.26	<	<	102	1.0	<	<	2	<	<	<	<	0.4	47	2	0.1	75	<	<	12	11	<	0.4
TAR-13_5	170	0.08	<	<	<	1.1	<	<	2	<	<	<	<	0.3	31	1	0.0	40	<	<	15	12	<	0.2
TAR-13_8	198	0.05	<	<	<	1.6	<	<	<	<	<	<	<	2.1	97	4	0.2	42	<	0.0	<	24	<	0.9
TAR-13_17	75	0.08	<	<	48	1.3	<	<	5	<	<	<	<	0.9	34	2	0.1	16	<	0.0	<	31	<	0.8
TAR-13_21	246	0.10	<	<	173	3.4	0.1	<	14	<	<	<	0.1	3.3	28	3	0.2	132	<	0.0	<	<	<	0.5
TAR-13_24	n.d.	n.d.	<	<	75	n.d.	n.d.	n.d.	n.d.	n.d.	n.d.	n.d.	n.d.	n.d.	n.d.	n.d.	n.d.	n.d.	n.d.	n.d.	n.d.	n.d.	n.d.	n.d.
TAR-13_27	n.d.	n.d.	157	<	<	0.8	5.4	<	6	<	<	<	<	2.1	12	1	0.1	45	<	0.0	<	29	0.2	0.7
TAR-13_28	n.d.	n.d.	<	<	<	n.d.	n.d.	n.d.	n.d.	n.d.	n.d.	n.d.	n.d.	n.d.	n.d.	n.d.	n.d.	n.d.	n.d.	n.d.	n.d.	n.d.	n.d.	n.d.
TAR-13_30	n.d.	n.d.	<	<	90	2.6	5.9	<	127	0.2	<	<	0.5	2.7	66	5	0.2	298	0.5	0.1	<	11	0.4	6.8
TAR-13_32	n.d.	n.d.	<	<	<	0.4	5.6	<	4	<	<	<	<	0.9	18	2	0.1	22	<	<	<	<	0.2	0.5
TAR-13_35	n.d.	n.d.	256	<	<	1.1	6.1	<	12	<	<	<	<	0.3	32	3	0.2	45	<	0.0	<	<	0.2	1.0
TAR-13_36	n.d.	n.d.	<	<	<	1.1	6.0	<	7	<	<	<	<	1.2	38	3	0.1	31	<	0.0	<	<	0.3	0.4
TAR-13_37	303	0.07	17	147	310	2.6	1.1	<	55	<	<	<	0.4	2.1	52	10	0.3	190	0.2	0.1	<	13	0.2	2.7
TAR-13_39	n.d.	n.d.	<	<	83	0.8	7.1	<	2	<	<	<	<	0.5	20	1	0.0	76	<	0.0	<	<	0.2	0.2
TAR-13_41	305	3.18	2351	149	554	7.6	1.8	<	191	<	0.1	<	1.3	2.7	303	11	0.9	414	0.7	0.2	67	16	0.5	12.9
TAR-13_42	107	0.48	1240	<	<	3.5	0.2	<	43	<	<	<	0.2	1.9	94	5	0.4	44	<	0.0	<	<	0.2	4.8
MIT-12_7	n.d.	n.d.	53	393	458	3.0	1.0		19	0	0	0	0	6	212	7	1	134	0	0	n.d.	24	0	1
MIT-12_19	n.d.	n.d.	<	<	291	3.0	3.0		18	0	0	0	0	4	29	3	1	148	0	0	n.d.	22	0	3
ICE-12_3	n.d.	n.d.	0	0	114	17	7	22	0	0	1	1	17	38	11	0	99	0	-1	0	n.d.	40	0	25
ICE-12_4	n.d.	n.d.	0	181	275	4	13	26	0	0	0	0	3	44	13	1	234	0	-3	0	n.d.	483	0	30

All values except DOC and PO_4^{3-} are given in ppb; NO^{3-}, SO_4^{2-} and Cl^- all determined by IC, all others analysed by ICP-MS; limit of detection (LOC,<) for IC: NO_3^- = 96 ppb, Cl^- = 72 ppb, SO_4^{2-} = 121 ppb, LOD's for ICP-MS: Al, Ba, Co, Cr, Cu, Fe, Mg, Ni, Si, Sr, Zn = 0.1 ppb; Bi, Cd, Mn, Pb = 0.01 ppb; Ca, Na = 1 ppb; K,P,S = 10 ppb; n.d. = not determined.

Table D.11: Total particulate carbon (TC), total nitrogen (TN), total phosphorus (TP) and total sulphur (TS) (all based on % of dry weight of solid sample) as well as the organic nitrogen and carbon isotope values from the analysed particulates in the Northern Sweden (TAR) and Svalbard (SVA) samples that contained sufficient particulate material for analyses; listed are also the solid C/N (Redfield: 6.6), C/P (Redfield: 106) and N/P (Redfield: 16) ratios calculated from the TC, TN and TP values. Iceland and Greenland samples did not contain enough particulate material for analyses.

Sample ID	Total C [%]	Total N [%]	Total P [%]	Total S [%]	C/N	C/P	N/P	$\delta^{15}N$ [‰]	$\delta^{13}C$ [‰]
SVA-13-2	3.69	0.26	0.06	0.16	14.44	59.17	4.10	-8.86	n.d.
SVA-13-4	3.05	0.21	0.06	0.11	14.89	51.17	3.44	-6.37	n.d.
SVA-13_10	1.45	0.11	0.06	0.18	12.92	23.64	1.83	-6.92	n.d.
SVA-13_20	1.87	0.19	0.15	0.07	10.02	12.44	1.24	0.27	-26.06
SVA-13_23	7.40	0.45	0.09	0.12	16.57	86.52	5.22	-3.52	-28.42
SVA-13_31	8.85	0.50	0.08	0.14	17.70	111.16	6.28	-2.35	-27.80
SVA-13_33	2.98	0.21	0.06	0.06	13.93	47.03	3.38	-5.18	-25.00
SVA-13_36	6.27	0.36	0.06	0.10	17.59	107.07	6.09	-5.37	n.d.
SVA-13_43	2.73	0.15	0.04	0.10	18.70	62.63	3.35	-2.60	-27.95
SVA-13_48	4.90	0.23	0.06	0.12	21.06	79.54	3.78	-6.13	-28.18
SVA-13_54	17.38	1.02	n.d.	0.12	17.11	n.d.	n.d.	-4.66	-29.43
SVA-13_65	4.53	0.27	0.06	0.10	16.51	74.75	4.53	-5.52	-29.23
TAR-13_1	4.15	0.25	0.05	0.02	16.59	84.41	5.09	-4.94	-25.01
TAR-13_5	30.04	1.84	n.d.	0.11	16.32	n.d.	n.d.	n.d.	-28.73
TAR-13_8	12.90	0.78	n.d.	0.06	16.64	n.d.	n.d.	-1.10	n.d.
TAR-13_17	19.68	1.11	n.d.	0.10	17.71	n.d.	n.d.	0.37	-26.59
TAR-13_21	8.79	0.41	0.04	0.07	21.60	220.17	10.19	-4.19	-21.80
TAR-13_24	8.61	0.47	0.05	0.08	18.17	165.77	9.12	-5.11	-25.32
TAR-13_27	8.41	0.33	0.08	0.06	25.70	112.09	4.36	-4.76	-27.74
TAR-13_28	12.91	0.57	0.07	0.07	22.63	176.06	7.78	-5.49	-24.63
TAR-13_30	11.05	0.28	0.04	0.06	39.41	287.09	7.28	-3.29	-24.86
TAR-13_32	5.07	0.34	0.07	0.05	15.02	75.07	5.00	-5.96	-26.61
TAR-13_35	9.72	0.46	0.07	0.08	21.02	148.70	7.07	-4.54	n.d.
TAR-13_36	25.30	0.90	0.07	0.09	28.07	369.73	13.17	-4.95	n.d.
TAR-13_37	9.04	0.39	0.07	0.06	23.09	129.79	5.62	-5.40	n.d.
TAR-13_41	9.61	0.50	0.03	0.07	19.13	275.76	14.42	-6.15	n.d.
TAR-13_42	11.46	0.55	0.06	0.09	20.76	191.61	9.23	-4.73	n.d.

n.d. = not determined

Table D.12: Geology and mineralogical composition of the Svalbard, Northern Sweden, Greenland and Iceland samples derived from X-ray diffraction analysis.

Location	Geology	Main minerals
Svalbard	Metamorphic and sedimentary rocks	quartz, plagioclase, pyroxene, mica, chlorite, muscovite; Austre Brøggerbreen and Feiringbreen: calcite, dolomite
Northern Sweden	Metamorphic rocks (gneisses, amphibolites)	quartz, plagioclase, hornblende, minor contributions from biotite, mica and chlorite
Greenland	Metamorphic (gneisses) and igneous rocks (gabbro-anorthosite intrusions)	quartz, plagioclase, smectite, mica, hornblende and chlorite
Iceland	Igneous rocks (basalt)	quartz, plagioclase, pyroxene, minor contributions from clays, basaltic glass and hematite

Table D.13: Distribution of 97% clustered OTUs aligned and assigned to the "SAR"-group (*stramenopiles*, *alveolata*, *rhizaria*) and taxa within the *stramenopiles*. Values are the relative abundance of the taxa in percentage of total. The "SAR"-group was screened for other other pigmented micro-eukaryotes, *i.e*., the *Chrysophyceae*. In nearly all samples the relative abundance of *Chryosphyceae* was below 0.1% and therefore they are considered negligible in terms of contribution to albedo.

	Alveolata	***Rhizaria***	***Stramenopiles***
SVA-13_2	0.2	0.3	0
SVA-13_4	1.6	11.0	0.0
SVA-13_10	0.2	0.5	0.1
SVA-13_20	0.3	5.1	0
SVA-13_23	0.0	2.9	0
SVA-13_31	0.1	5.2	2.6
SVA-13_33	6.6	7.4	0.1
SVA-13_36	4.6	14.3	0.1
SVA-13_43	7.2	10.3	0
SVA-13_48	0.0	3.4	0.7
SVA-13_54	0.8	2.4	0.1
SVA-13_65	0.5	5.0	3.8
TAR-13_1	0.1	3.7	0
TAR-13_8	1.4	6.0	0
TAR-13_17	0.1	0.3	0
TAR-13_21	0.4	7.9	0.2
TAR-13_27	0.0	1.8	0.0
TAR-13_28	0.0	0.4	0
TAR-13_30	0.0	1.0	0
TAR-13_35	4.8	1.9	0.0
TAR-13_39	0.1	1.0	0
TAR-13_41	0.1	5.2	0
TAR-14_1	0.0	10.3	0.1
TAR-14_4	0.0	15.2	0.0
TAR-14_5	0.1	8.5	0.1
TAR-14_6	0.1	9.7	0
TAR-14_7	0	1.43	0
TAR-14_10	0.1	1.2	0.1
TAR-14_11	0.5	3.2	0.2
TAR-14_12	0.8	1.7	7.0
MIT-12_7	1.7	28.0	0
MIT-12_19	0.8	20.4	0
ICE-12_3	0.5	30.11	0.1
ICE-12_4	6.4	42.46	0.8

Table D.13 continued.

	Stramenopiles									
	CCI40	*Chrysophyceae*						*Peronosporomycetes*	*Synurales*	*Xanthophyceae*
		CCMP1899, Chrysophyceae sp. I76	*CCMP1899, Ochromonas*	*CCMP1899*	*Chromulinales, LG31-02*	*Chrysocapsales, Hydrurus*	*Ochromonadales, Paraphysomonas*	*Phytophthora, Halophytophthora*	*Synura, Synura uvella*	*Tribonematales, Botrydiopsis*
SVA-13_2	0	0	0	0	0	0	0	0	0	0
SVA-13_4	0	0	0	0	0	0	0	0.03	0	0
SVA-13_10	0	0	0.02	0.03	0	0	0	0	0	0
SVA-13_20	0	0	0	0	0	0	0	0	0	0
SVA-13_23	0	0	0	0	0	0	0	0	0	0
SVA-13_31	0	0.01	0.05	2.46	0.06	0	0	0	0	0
SVA-13_33	0.03	0	0	0.03	0	0	0	0	0	0
SVA-13_36	0	0	0	0.01	0	0	0.02	0	0	0.01
SVA-13_43	0	0	0	0	0	0	0	0	0	0
SVA-13_48	0	0.02	0	0.7	0.02	0	0	0	0	0
SVA-13_54	0	0	0	0.08	0	0	0	0	0	0.05
SVA-13_65	0	0.02	0.06	3.74	0	0	0	0	0	0
TAR-13_1	0	0	0	0	0	0	0	0	0	0
TAR-13_8	0	0	0	0	0	0	0	0	0	0
TAR-13_17	0	0	0	0	0	0	0	0	0	0
TAR-13_21	0	0	0	0	0	0	0	0.23	0	0
TAR-13_27	0	0	0	0	0	0.02	0	0	0	0
TAR-13_28	0	0	0	0	0	0	0	0	0	0
TAR-13_30	0	0	0	0	0	0	0	0	0	0
TAR-13_35	0	0	0	0	0	0.02	0	0	0	0

TAR-13_39	0	0	0	0	0	0	0	0	0	0
TAR-13_41	0	0	0	0	0	0	0	0	0	0
TAR-14_1	0	0	0	0	0	0.02	0	0	0	0
TAR-14_4	0	0	0	0	0	0.01	0	0	0	0
TAR-14_5	0	0	0	0	0	0.06	0	0	0	0
TAR-14_6	0	0	0	0	0	0	0	0	0	0
TAR-14_7	0	0	0	0	0	0	0	0	0	0
TAR-14_10	0	0	0	0	0	0.13	0	0	0	0
TAR-14_11	0	0	0	0	0	0.12	0	0	0.03	0
TAR-14_12	0.07	0	0	0	0	6.79	0	0	0.11	0
MIT-12_7	0	0	0	0	0	0	0	0	0	0
MIT-12_19	0	0	0	0	0	0	0	0	0	0
ICE-12_3	0	0	0	0	0	0.11	0	0	0	0
ICE-12_4	0	0	0	0	0.40	0.20	0	0	0	0.20

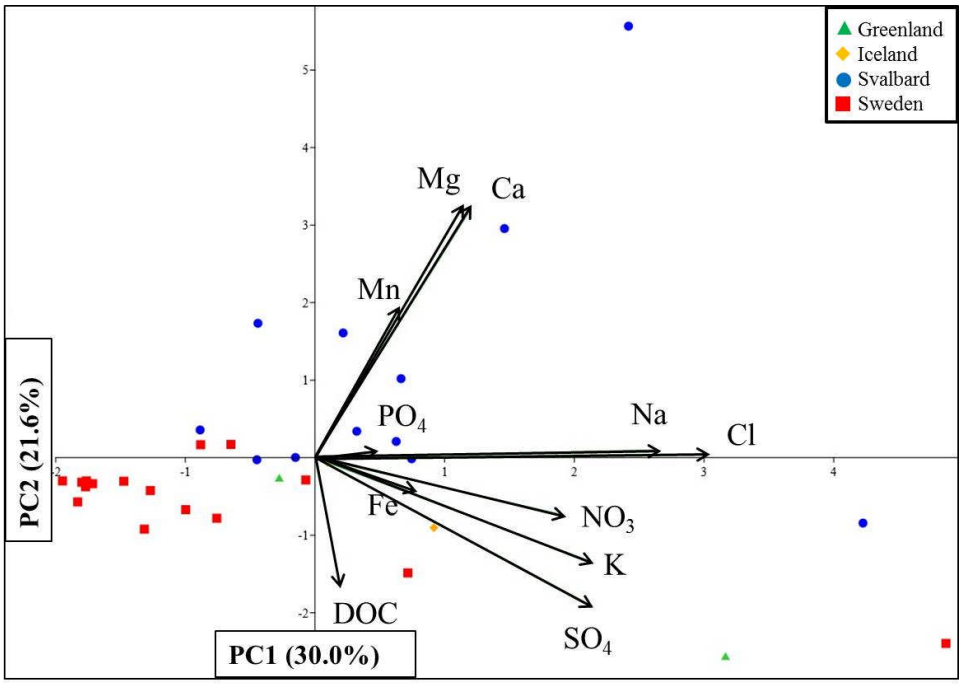

Figure D.1: PCA of aqueous geochemical parameters revealing differences between locations. Samples cluster according to locations with Arctic Sweden showing a trend in higher DOC concentrations whereas higher Ca, Cl, Mg, Mn, and Na concentrations are matching the Svalbard samples.

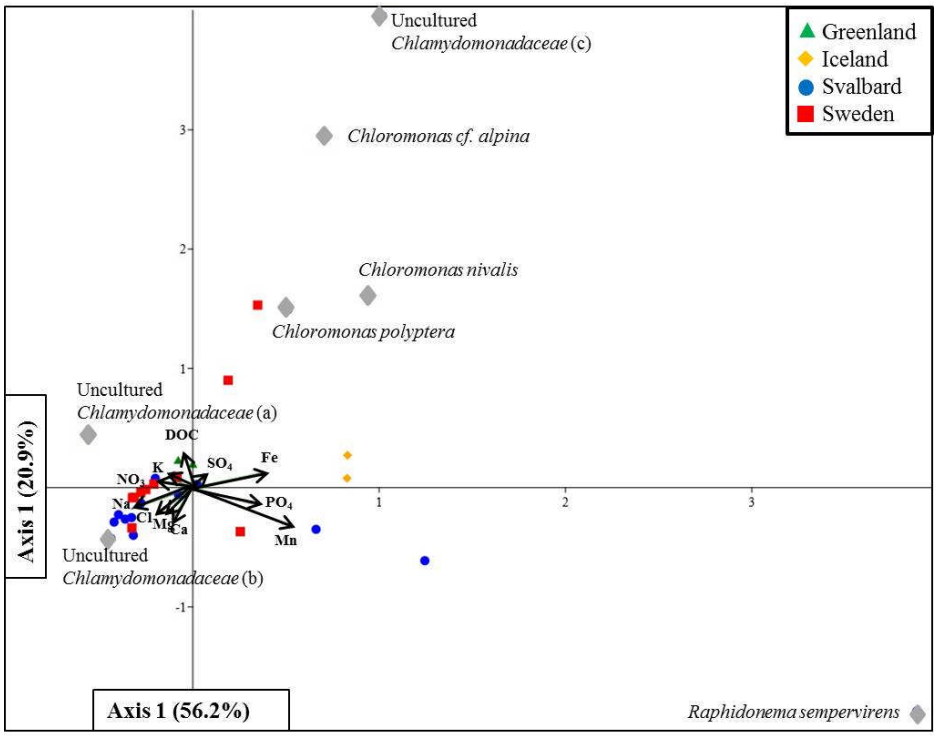

Figure D.2: CCA for algal species (grey diamonds) and geochemistry (arrows) showing no clustering of samples and no trends for any of the samples or species with the analysed aqueous geochemical parameters.

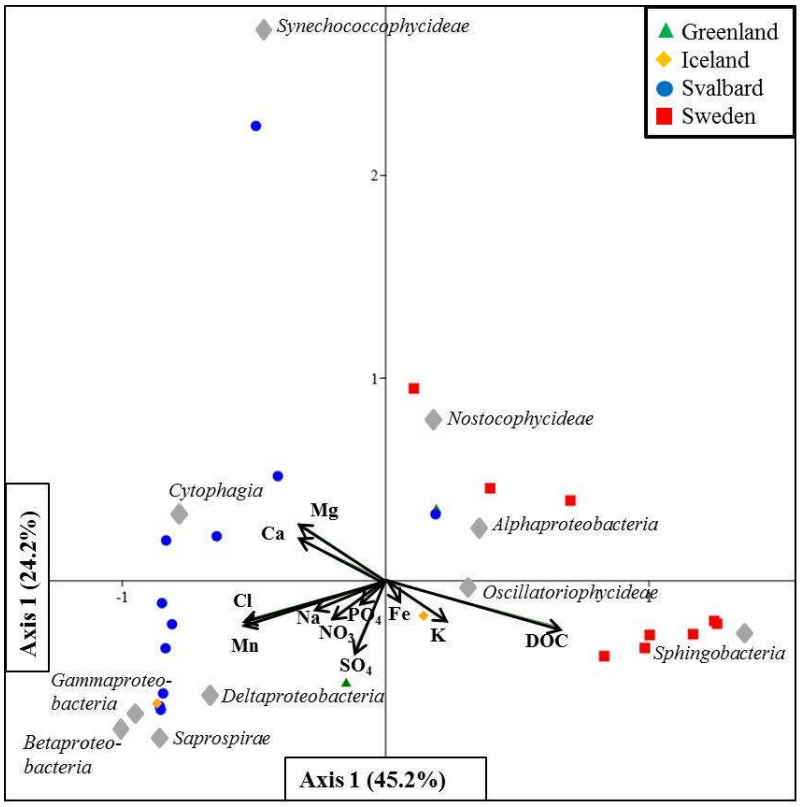

Figure D.3: CCA for bacterial classes (grey diamonds) and geochemistry (arrows) showing a clustering of samples according to locations and a positive correlation between *Sphingobacteria* and DOC.

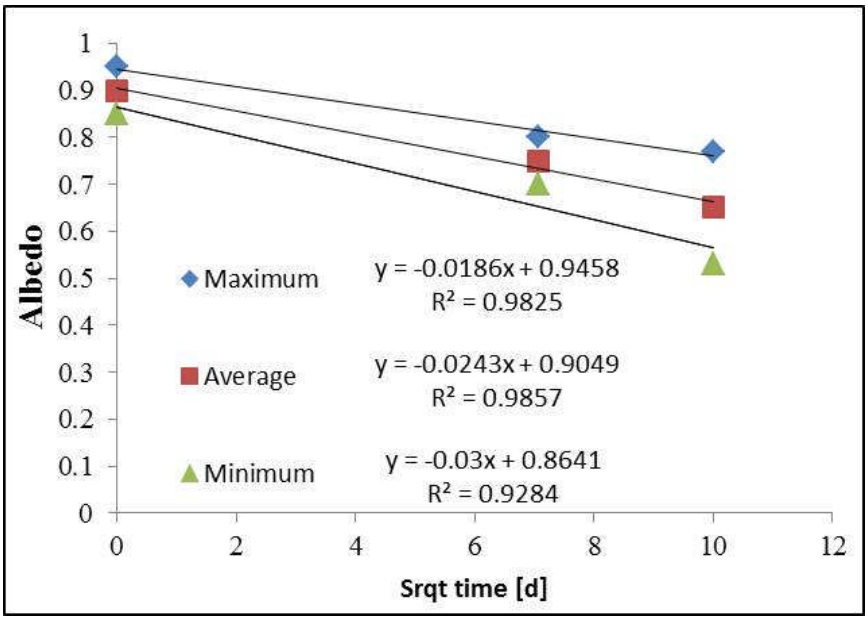

Figure D.4: Sensitivity analysis for albedo model with equations for maximum, average and minimum values for dry clean snow, wet clean snow and red snow (Table 7.2). The full sensitivity analysis is provided in the methods section at the end of the manuscript.

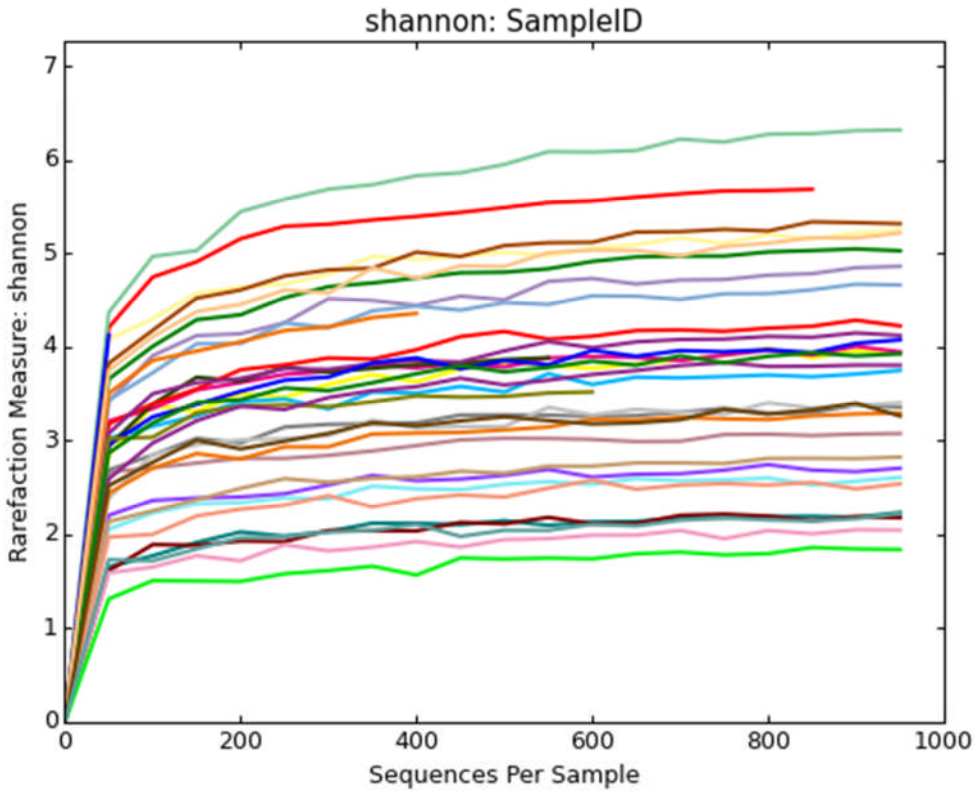

Figure D.5: Rarefaction curves for all samples (algal sequences) suggesting a good coverage of the algal diversity. Samples were rarefied to the smallest library size and alpha diversity was estimated using Shannon indices.

References

Lutz, S., Anesio, A. M., Edwards, A. & Benning, L. G. (2015) Microbial diversity on Icelandic glaciers and ice caps. *Frontiers in microbiology*, 6, 307.

Lutz, S., Anesio, A. M., Villar, S. E. J. & Benning, L. G. (2014) Variations of algal communities cause darkening of a Greenland glacier. *FEMS microbiology ecology*, 89(2), 402-414.

Potvin, M. & Lovejoy, C. (2009) PCR-Based Diversity Estimates of Artificial and Environmental 18S rRNA Gene Libraries. *Journal of Eukaryotic Microbiology*, 56(2), 174-181.

Prasad, S., Manasa, B. P., Buddhi, S., Pratibha, M. S., Begum, Z., Bandi, S., Tirunagari, P. & Shivaji, S. (2013) Arcticibacter svalbardensis gen. nov., sp. nov., of the family Sphingobacteriaceae in the phylum Bacteroidetes, isolated from Arctic soil. *International Journal of Systematic and Evolutionary Microbiology*, 63(Pt 5), 1627-1632.

Spijkerman, E., Wacker, A., Weithoff, G. & Leya, T. (2012) Elemental and fatty acid composition of snow algae in Arctic habitats. *Frontiers in microbiology*, 3, 380.

Appendix E: Supplementary information for chapter 8

Linking microbial diversity and functionality of Arctic glacial surface habitats.

Lutz, S., Anesio, A. M., Edwards, A, Newton, R. J. & Benning, L. G.

In preparation for submission to the *ISME Journal.*

Material and Methods

Field measurements

At each sampling point prior to sampling, the snow temperature (upper few cm), pH and conductivity were measured *in-situ* using a multi-meter (Hanna instruments, HI 98129). For all snow and runoff samples, pH and conductivity were measured after allowing the multi-meter to equilibrate in the upper 2-3 cm of the sampling site. For ice samples this was achieved by melting a few ice chips prior to measurements. Furthermore, at each site, irradiation was measured using a radiometer with specific sensors for photosynthetic active radiation (PAR) and ultraviolet radiation (UV-A and UV-B) (SolarLight PMA2100). Albedo was calculated by taking the ratio of reflected to incident radiation (400-700 nm range) and measuring the values always in the same position to the sun. Measurements were carried out with the sensors held at 30 cm above the snow surface (field of view 160º, effective measurement area 0.5 m^2) and by first pointing the sensor upwards (incident radiation) and then towards the snow/ice surface (reflected radiation). Five measurements for incident and reflected radiation were acquired each. The error of the measurement (standard deviation) was below 10 %.

Field sampling strategy

Based on visual observations several distinct microbial glacial surface habitats that were considered to be highly representative of the whole glacial surface were defined as follows: clean snow (white snow with no visual presence of particles), green snow (light to dark green colouration, often deep penetration of the snowpack), red snow (red colouration with all shades from orange to pink with variable densities of particles and only within the surface layer), biofilms (wet snow at snow-ice melting interfaces), clean ice (white ice with no visual presence of particles), grey ice (light grey to dark grey colouration and variable densities of particles), cryoconite holes (1-50 cm large rounded or elongated and variably deep holes filled with sediment), and glacial runoff (melt rivers and channels). In each of these habitats (except for glacial runoff where only one sample was collected) various samples were collected for microbial, mineralogical and geochemical analyses.

Field sample preservation and handling

For inorganic aqueous analyses samples were collected either in sterile 50 mL centrifuge tubes or sterile sample bags. The snow/ice samples were melted at room temperature over a ~ 6 hour period and all samples were filtered through single use 0.2 uM cellulose-acetate syringe filters. For cation analyses by inductively coupled plasma mass spectrometry (ICP-MS), samples were directly filtered into acid-washed (HCl) and pre-acidified (Aristar grade HNO_3) Nalgene HDPE bottles, while for anion analyses by ion chromatography (IC), samples were stored un-acidified in 15 mL centrifuge tubes.

For dissolved organic carbon (DOC) and organic particulate analysis, samples were collected in 250 mL glass jars that had been ashed at 450 °C. for > 4 h. After melting at room temperature these samples were filtered through ashed 0.7 µm glass fibre filters (GFF) directly into pre-acidified (100µl Aristar grade HNO_3) 40 mL, amber glass vials with Teflon® seals (Supelco). The filters containing particulates were folded into quarters and preserved cold and in ashed aluminium foil for pigment and fatty acid analyses.

From these samples particulates for X-ray diffraction (XRD) and Fourier transform infrared spectroscopy (FTIR) were also collected by filtering through 0.2 µm polycarbonate filters. Samples were returned to Leeds either frozen in liquid nitrogen in a cryo-shipper or in an ice-box at ~ 4 ˚C.

Aqueous organic (DOC) and inorganic analyses

Nutrients (NO_3^-, Cl^-, SO_4^{2-}) were analysed in filtered samples by ion chromatography (IC) on a Dionex DX 600 system with an autosampler, an IonPac AS16 analytical column with an AG16 guard column, an eluent gradient of 0-15 mM KOH and an ED50 conductivity detector. Injection volume was 25 µL and flow rate was set to 0.35 mL min^{-1}. The precision of the analysis was 5% and the limits of detection (LOD) were the following: NO_3^- = 96 ppb, Cl^- = 72 ppb, SO_4^{2-} = 121 ppb.

Major, minor and trace elements were measured by inductively coupled plasma mass spectrometry (ICP-MS) on an Agilent 7500ce with collision cell Octopole Reaction System (ORS) technology (ICP-MS facility, University of Portsmouth). The precision of the analysis was 3% and LODs were the following: Al, Ba, Co, Cr, Cu, Fe, Mg, Ni, Si, Sr, Zn = 0.1 ppb; Bi, Cd, Mn, Pb = 0.01 ppb; Ca, Na = 1 ppb; K,P,S = 10 ppb**.**

Dissolved organic carbon (DOC) was analysed on a Shimadzu TOC analyser (University of Plymouth). PO_4 was analysed by segmented flow-injection analyses (AutoAnalyser3, Seal Analytical).

Total carbon, total nitrogen, total sulphur, total phosphate and carbon and nitrogen isotopes

Particulates in the samples were analysed for $\delta^{15}N$ and $\delta^{13}C$ by a Vario Pyro Cube elemental analyser (Elementar Inc) coupled to an Isoprime mass spectrometer. Samples were combusted in tin capsules at 1150 °C and gases were separated using temperature controlled adsorption/desorption columns. Carbon analyses were calibrated with in-house C4-sucrose and urea standards assigned values of -11.93‰ and -46.83‰ respectively via calibration with the international standards LSVEC (-46.479‰), CH7 (-31.83‰), CH6 (-10.45‰), and CO-1 (+2.48‰). Nitrogen isotope values were calibrated using the international standards USGS-25 and USGS-26 with assigned values of -30.4‰ and +53.7‰ respectively. Total carbon (TC), total nitrogen (TN), and total sulphur (TS) were derived from the thermal conductivity detector in the elemental analyser and calibrated using a sulphanilamide standard. Particulate phosphorus was extracted by ashing of the samples at 550°C for 2 h and incubating in 1 M HCl for 16 h according to extraction step V in Ruttenberg et al.(2009).

Mineralogy

The mineralogical composition of each sample was determined by X-ray diffraction (XRD) with dried and ground samples analysed on a Bruker D8 Advance diffractometer. XRD spectra were recorded from 2-75°2Θ using a copper diffraction source and a run time of 12 min per sample. Spectra were analysed in DIFFRAC.EVA (Bruker, V.3.0).

Fourier transform infrared spectroscopy

Functional groups distributions were determined on bulk, dried samples by Fourier transform infrared (FTIR) using an A2 Technology Microlab Portable mid-IR spectrometer with a Diamond internal reflection cell (DATR), with spectra acquired in the mid-infrared range (650- 4000 cm-1). From the bulk spectra, the peak area ratios of the main functional groups representing the lipids (CH_2 and CH_3 stretching modes between 3050 and 2800 cm^{-1}), and proteins (amide I and II bands

at 1700-1500 cm^{-1}) to those of the carbohydrates (C-O-C, C-O-P, P-O-P ring vibrations between 1204-815 cm^{-1}) were evaluated in Omnic (Thermos Scientific, V.5.1).

Pigment analysis

To determine the carotenoid and chlorophyll contents in the samples, high pressure liquid chromatography (HPLC) and a modified carotenoid/chlorophyll specific extraction protocol (Remias and Lutz 2007) were used. Cells were disrupted by shock freezing in liquid nitrogen for 10 min followed by grinding using a Teflon® mortar and pestle. The resulting powder was re-suspended in 1 mL of dimethylformamide (DMF) and 1.0 mm glass beads and horizontally shaken on a laboratory shaker (MoBio Vortex Genie 2) at maximum speed (3000 rpm) for 10 min followed by centrifugation for 5 min at 10 000 rpm. The supernatant was separated from the debris by filtering through a 0.45 µm Teflon® filter and the filtrate was mixed with methanol (25 vol %). Extracted samples were analysed immediately on an Agilent Technologies 1200 Infinity HPLC instrument with a gradient pump, an autosampler, a variable wavelength detector and ODS Hypersil column (250x4.6 mm; 5 um particle size). Two solvents were used: solvent A consisted of a mixture of acetonitrile/water/methanol/hexane/tris buffer at ratios of 80:7:3:1:1 while solvent B was a mix of methanol and hexane at a ratio of 5:1. The HPLC was run at a flow rate of 1 mL min^{-1} and with an injection volume of 25 µL. Spectra were recorded from 200 to 800 nm and chromatograms were quantified at 450 nm for carotenoids and 660 nm for chlorophyll a and b. Run time was 60 min and the protocol required a 15 minute run with 100% of solvent A followed by a linear gradient from 100 % solvent A to 100% solvent B between 32 and 45 min and finally with 15 minutes of column re-equilibration through a 5 min linear gradient from solvent B back to 100% solvent to A, followed by a further column conditioning with 100 % solvent A for 10 min. The following commercially available standards were used for peak identification: chlorophyll a, chlorophyll b (Sigma), violaxanthin, neoxanthin, antheraxanthin, lutein, β-carotene, trans-astaxanthin, and cis-astaxanthin (Carotenature). Chromatogram peak areas were calculated and the carotenoid data is reported as normalized to the peak area of chlorophyll a. The precision of the analysis was 5%.

Fatty acids analysis

Fatty acids were extracted according to the method described by Wacker & Martin-Creuzberg (2007). Briefly, 20 ng of internal standard (tricosanoic acid methyl ester) were added to each sample, before ultrasonic extraction using dichloromethane:methanol (2:1 v:v), followed by centrifugation to remove particulates and evaporation of solvent from the supernatant. Fatty acids were transesterified by adding methanolic HCl to the dried extract and heating at 60˚ C for 20 minutes. After cooling, fatty acid methyl esters were extracted in isohexane, solvent was removed under nitrogen and the sample resuspended in isohexane for analysis

Analysis of fatty acid methyl esters was carried out using a Trace 1300 gas chromatograph with flame ionisation detector (Thermo Scientific, Hemel Hempstead, UK), equipped with a non-polar-fused silica capillary column (CPSil-5CB, 50m x 0.32mm x 0.12 mm, Agilent Technologies, USA). Samples (1µl) were injected in splitless mode, with the injector maintained at 200˚C. Carrier gas was helium, with a constant flow rate of 1.5 ml/min. The following temperature programme was used: initial temperature 40 °C, rising to 140 °C at 20 °C min^{-1}, then rising to 240 °C at 4 ° min^{-1}, holding at 240 °C for 5 min. Fatty acid methyl esters were identified by comparison of retention time with those of reference compounds (Supelco, USA) and by gas chromatography/mass spectrometry. Gas chromatography/mass spectrometry was carried out using the gas chromatograph and column previously described, with identical operating conditions, coupled to an ISQ mass spectrometer (Thermo Scientific, Hemel Hempstead, UK). The transfer line and the ion source were maintained at 300˚C. The emission current was set to 50mA and the electron energy to 70 eV. The analyser was set to scan at m/z 50–650 with a scan cycle time of 0.6 s. The precision of the analysis was 5%.

DNA analysis

Total DNA was extracted using the PowerSoil® DNA Isolation kit (MoBio Laboratories). 16S rRNA genes were amplified using bacterial primers 27F (5'-AGAGTTTGATCMTGGCTCAG) and 357R (5'-CTGCTGCCTYCCGTA) (tagged with the Ion Torrent adapter sequences and MID barcode) spanning the V1-V2 hypervariable regions. 18S rRNA genes were amplified using the eukaryotic primers 528F (5′-GCGGTAATTCCAGCTCCAA) and 706R (5'-AATCCRAGAATTTCACCTCT) (Cheung et al., 2010) (tagged with the Ion

Torrent adapter sequences and MID barcode) spanning the V4-V5 hypervariable region. Polymerase chain reactions (PCR) were performed using Platinum® PCR SuperMix High Fidelity according to manufacturer's protocols. Initial denaturation at 95 ºC for 5 min was followed by 30 cycles of denaturation at 95 ºC for 30 s, annealing at 60 ºC for 30 s and elongation at 72 ºC for 30 s. Final elongation was at 72 ºC for 7 min. Archaeal 16S rRNA genes were amplified following a nested PCR approach. The first PCR reaction was carried out using primers 20F and 915R. Initial denaturation at 95 ºC for 5 min was followed by 35 cycles of denaturation at 95 ºC for 30 s, annealing at 62 ºC for 30 s and elongation at 72 ºC for 180 s. Final elongation was at 72 ºC for 10 min. The PCR product was used as template for the second PCR reaction with primers 21F (5'-TCCGGTTGATCCYGCCGG) and 519R (5'- GWATTACCGCGGCKGCTG) (tagged with the Ion Torrent adapter sequences and MID barcode) spanning the V1-V2 hypervariable region. Initial denaturation at 95 ºC for 5 min was followed by 30 cycles of denaturation at 95 ºC for 30 s, annealing at 60 ºC for 30 s and elongation at 72 ºC for 30 s. Final elongation was at 72 ºC for 7 min. All PCRs were carried out in triplicates to reduce amplification bias and in reaction volumes of 1 x 25 µl and 2 x 12.5 µl. All pre-amplification steps were done in a laminar flow hood with DNA-free certified plastic ware and filter tips. The pooled amplicons were purified with AMPure XP beads (Agencourt©) with a bead to DNA ratio of 0.6 to remove nucleotides, salts and primers and analyzed on the Agilent 2100 Bioanalyser (Agilent Technologies) with the High Sensitivity DNA kit (Agilent Technologies) and quality, size and concentration were determined. Sequencing was performed on an Ion Torrent Personal Genome Machine using the Ion Xpress™ Template Kit and the Ion 314™ or Ion 316™ chips following manufacturer's protocols. The raw sequence data was processed in QIIME (Caporaso et al., 2010). Barcodes and adapter sequences were removed from each sequence. Filtering of sequences was performed using an average cutoff of Q20 over a 350 bp range. Reads shorter than 200 bp were removed. OTUs were picked *de novo* using a threshold of 99%, 97% and 95% identity. Taxonomic identities were assigned for representative sequences of each OTU using the reference databases Greengenes for bacteria and archaea. The Silva database (DeSantis et al., 2006; extended with additional 223 sequences of cryophilic algae kindly provided by Dr. Thomas Leya from the CCCryo - Culture Collection of Cryophilic Algae, Fraunhofer IZI-BB) was used for eukaryotes. Data were aligned using PyNAST and a 0.80 confidence threshold. Singletons were excluded from the analysis. For bacterial sequence matching, plant plastids were

removed from the data set prior to further analysis. For eukaryotic sequence matching *Chloroplastida* were pulled out of the data set and stored in a separate OTU table. In order to focus upon algal diversity, sequences matching *Embryophyta* (e.g., moss, fern) were removed from the data set. For archaea, sequences matching bacteria were removed. Finally, for diversity analyses samples were rarefied to the smallest sequence number and Shannon indices were calculated in QIIME. A matrix of each OTU table representing relative abundance was imported into Past3 (Hammer et al., 2012) for multivariate statistical analyses (principal component analysis, PCA). Representative sequences of the major algal species found in all samples were imported into Geneious (7.1.3., Biomatters) for phylogenetic tree building based on neighbor-joining.

References

Remias D, Lutz C (2007). Characterisation of esterified secondary carotenoids and of their isomers in green algae: a HPLC approach. *Algological Studies* **124:** 85-94.

Ruttenberg K, Ogawa N, Tamburini F, Briggs R, Colasacco N, Joyce E (2009). Improved, high-throughput approach for phosphorus speciation in natural sediments via the SEDEX sequential extraction method. *Limnology and Oceanography: Methods* **7:** 319-333.

Wacker A, Martin-Creuzburg D (2007). Allocation of essential lipids in Daphnia magna during exposure to poor food quality. *Functional Ecology* 21: 738-747.

Table E.1: Overview of sample numbers, locations, coordinates and field measurements

Sample ID	Glacier	Habitat	Collection date	GPS location [UTM]	Elevation [m a.s.l.]	pH	Snow temp. [°C]	PAR [W/m²]	UV-A [W/m²]	UV-B [W/m²]	Albedo [%]
Svalbard, Norway (SVA)											
SVA-13_1	Vestre Brøggerbreen	Green snow	20/07/2013	33H 0433185 E, 8759758 N	257	7.00	0.0	36	6.8	3.37	31
SVA-13_2	Vestre Brøggerbreen	Red snow	20/07/2013	33H 0433169 E, 8759838 N	265	7.03	0.0	48			63
SVA-13_3	Vestre Brøggerbreen	Clean snow	20/07/2013	33H 0433169 E, 8759838 N	265	7.32	0.0	43			72
SVA-13_4	Vestre Brøggerbreen	Red snow	20/07/2013	33H 0432976 E, 8760004 N	254	6.10	0.0	39			67
SVA-13_5	Vestre Brøggerbreen	Cryoconite hole	20/07/2013	33H 0432098 E, 8760034 N	196			35			24
SVA-13_6	Vestre Brøggerbreen	Clean ice	20/07/2013	33H 0432098 E, 8760034 N	196			41			59
SVA-13_7	Vestre Brøggerbreen	Dirty ice	20/07/2013	33H 0432098 E, 8760034 N	196			41			42
SVA-13_8	Vestre Brøggerbreen	Dirty ice	20/07/2013	33H 0432098 E, 8760034 N	196			31			48
SVA-13_10	Midre Lovénbreen	Red snow	21/07/2013	33H 0436410 E, 8757512 N	299	6.65	0.0	54	7.5	3.99	76
SVA-13_12	Midre Lovénbreen	Clean snow	21/07/2013	33H 0436410 E, 8757512 N	299	7.30	0.0	61			76
SVA-13_16	Midre Lovénbreen	Cryoconite hole	21/07/2013	33H 0436414 E, 8758244 N	267			50			36
SVA-13_17	Midre Lovénbreen	Clean ice	21/07/2013	33H 0436414 E, 8758244 N	267			54			61
SVA-13_18	Midre Lovénbreen	Dirty ice	21/07/2013	33H 0436402 E, 8758208 N	276			80			41
SVA-13_19	Midre Lovénbreen	Dirty ice	21/07/2013	33X 0436467 E, 8759176 N	172			81			35
SVA-13_20	Austre Brøggerbreen	Red snow	24/07/2013	33X 0429286 E, 8761458 N	209	6.38		91			60
SVA-13_21	Austre Brøggerbreen	Green snow	24/07/2013	33X 0429228 E, 8761426 N	232	6.56		86	12.5	3.25	26
SVA-13_22	Austre Brøggerbreen	Clean snow	24/07/2013	33X 0429286 E, 8761458 N	209	6.29		77			76
SVA-13_23	Austre Brøggerbreen	Red snow	24/07/2013	33X 0429448 E, 8761568 N	227	6.27		75			63
SVA-13_24	Austre Brøggerbreen	Green snow	24/07/2013	33X 0429448 E, 8761568 N	227			75			45
SVA-13_25	Austre Brøggerbreen	Dirty ice	24/07/2013	33X 0430467 E, 8762386 N	91			64			37
SVA-13_26	Austre Brøggerbreen	Dirty ice	24/07/2013	33X 0430087 E, 8761810 N	144			79			39
SVA-13_27	Austre Brøggerbreen	Cryoconite hole	24/07/2013	33X 0430087 E, 8761810 N	144	6.36		83			22
SVA-13_29	Austre Brøggerbreen	Clean ice	24/07/2013	33X 0430087 E, 8761810 N	144			82			59
SVA-13_31	Austre Brøggerbreen	Red snow	24/07/2013	33X 0430139 E, 8761706 N	146	8.07		70			62
SVA-13_33	Pedersenbreen	Red snow	27/07/2013	33X 0441747 E, 8756068 N	320			22	24.7	1.07	55
SVA-13_35	Pedersenbreen	Clean snow	27/07/2013	33X 0441747 E, 8756068 N	320			25			64
SVA-13_36	Pedersenbreen	Red snow	27/07/2013	33X 0441609 E, 8756682 N	262			115			55

SVA-13_37	Pedersenbreen	Cryoconite hole	27/07/2013	33X 0441593 E, 8756844 N	237			94				26
SVA-13_38	Pedersenbreen	Dirty ice	27/07/2013	33X 0441593 E, 8756844 N	237			147				44
SVA-13_39	Pedersenbreen	Clean ice	27/07/2013	33X 0441593 E, 8756844 N	237			273				61
SVA-13_40	Pedersenbreen	Dirty ice	27/07/2013	33X 0441898 E, 8757712 N	115			48				37
SVA-13_43	Austre Lovénbreen	Red snow	03/08/2013	33X 0439635 E, 8756676 N	413	6.3	0.1	182	19.6	0.66		66
SVA-13_44	Austre Lovénbreen	Green snow	03/08/2013	33X 0439635 E, 8756676 N	413			212				26
SVA-13_45	Austre Lovénbreen	Clean snow	03/08/2013	33X 0439635 E, 8756676 N	413			224				71
SVA-13_47	Austre Lovénbreen	Dirty ice	03/08/2013	33X 0439077 E, 8756528 N	383	5.17		170				55
SVA-13_48	Austre Lovénbreen	Red snow	03/08/2013	33X 0438286 E, 8756948 N	345			36				60
SVA-13_49	Austre Lovénbreen	Clean ice	03/08/2013	33X 0438640 E, 8757616 N	287			73				56
SVA-13_50	Austre Lovénbreen	Dirty ice	03/08/2013	33X 0438640 E, 8757616 N	287			107				37
SVA-13_51	Austre Lovénbreen	Cryoconite hole	03/08/2013	33X 0438658 E, 8757902 N	252	5.94	0.0	191				37
SVA-13_54	Feiringbreen	Red snow	05/08/2013	33X 0446691 E, 8773282 N	401	5.68		88	11.8	0.35		51
SVA-13_55	Feiringbreen	Clean snow	05/08/2013	33X 0446691 E, 8773282 N	401			66				74
SVA-13_56	Feiringbreen	Biofilm	05/08/2013	33X 0446574 E, 8772968 N	367							
SVA-13_60	Feiringbreen	Clean ice	05/08/2013	33X 0445766 E, 8772392 N	262			62				55
SVA-13_61	Feiringbreen	Cryoconite hole	05/08/2013	33X 0445766 E, 8772392 N	262	5.23		47				43
SVA-13_62	Feiringbreen	Dirty ice	05/08/2013	33X 0445766 E, 8772392 N	262	5.14		47				45
SVA-13_63	Feiringbreen	Dirty ice	05/08/2013	33X 0445766 E, 8772392 N	262			63				47
SVA-13_65	Midre Lovénbreen	Red snow	05/08/2013	33X 0436693 E, 8759332 N	151			108				49
Tarfala, Sweden (TAR)												
TAR-13_1	Storglaciären	Red snow	01/07/2013	34W 0398931 E, 7533637 N	1268	6.98	0.0	52	8.1	0.08		56
TAR-13_2	Storglaciären	Green snow	01/07/2013	34W 0399035 E, 7533630 N	1258	5.81	0.0	32	6.3	0.15		32
TAR-13_3	Storglaciären	Green snow	01/07/2013	34W 0399035 E, 7533630 N	1258	4.85	0.0	26.5				18
TAR-13_4	Storglaciären	Green snow	01/07/2013	34W 0398948 E, 7534177 N	1291	5.78	0.0	61.1				34
TAR-13_5	Storglaciären	Red snow	01/07/2013	34W 0399260 E, 7534131 N	1221	5.56	0.0	29.8				66
TAR-13_8	Storglaciären	Red snow	03/07/2013	34W 0397551 E, 7534187 N	1412	7.23	0.1	97				72
TAR-13_9	Storglaciären	Clean snow	03/07/2013	34W 0397551 E, 7534187 N	1412	7.55	0.0	83.9				78
TAR-13_10	Storglaciären	Biofilm	03/07/2013	34W 0397494 E, 7534083 N	1419			142				30
TAR-13_11	Storglaciären	Biofilm	03/07/2013	34W 0397705 E, 7533762 N	1383	5.87	0.0	81				34
TAR-13_12	Storglaciären	Clean ice	03/07/2013	34W 0397705 E, 7533762 N	1383	5.93	0.0	84				56

TAR-13_13	Storglaciären	Dirty ice	03/07/2013	34W 0398556 E, 7534166 N	1436	5.55	0.0	55			42
TAR-13_14	Storglaciären	Dirty ice	03/07/2013	34W 0398727 E, 7533953 N	1320	5.34	0.0	72			33
TAR-13_16	Storglaciären	Green snow	03/07/2013	34W 0399301 E, 7534133 N	1203	5.48	0.0	80			31
TAR-13_17	Rabot	Red snow	05/07/2013	34W 0394929 E, 7534801 N	1350	6.13	0.0	112	16.5	1.05	75
TAR-13_18	Rabot	Clean snow	05/07/2013	34W 0394929 E, 7534801 N	1350	6.38	0.0	114			84
TAR-13_19	Rabot	Biofilm	05/07/2013	34W 0394909 E, 7534939 N	1357	6.34	0.0	124			33
TAR-13_21	Rabot	Red snow	05/07/2013	34W 0394160 E, 7535197 N	1282	5.45	0.0	122			73
TAR-13_22	Rabot	Dirty ice	05/07/2013	34W 0392291 E, 7534683 N	1193	5.69	0.0	80			37
TAR-13_24	Rabot	Red snow	05/07/2013	34W 0393074 E, 7534485 N	1165			95			54
TAR-13_27	Liljetopsrännan	Red snow	06/07/2013	34W 0398423 E, 7533989 N	1119	5.41	0.2	54	11.1	0.40	65
TAR-13_28	Liljetopsrännan	Red snow	06/07/2013	34W 0398656 E, 7536883 N	1209	6.35	0.0	51			56
TAR-13_30	SE-Kasskasatjåkkå	Red snow	07/07/2013	34W 0399446 E, 7537111 N	1374	0.45	0.3	123	19.4	2.78	77
TAR-13_31	SE-Kasskasatjåkkå	Clean snow	07/07/2013	34W 0399446 E, 7537111 N	1374	5.80	0.0	178			64
TAR-13_32	SE-Kasskasatjåkkå	Red snow	07/07/2013	34W 0399458 E, 7536982 N	1318	5.78	0.0	108			57
TAR-13_33	SE-Kasskasatjåkkå	Green snow	07/07/2013	34W 0399820 E, 7536730 N	1247	5.83	0.0	113			28
TAR-13_34	Storglaciären	Cryoconite hole	09/07/2013	34W 0398607 E, 7534297 N	1338	5.6	0.4				
TAR-13_35	Storglaciären	Red snow	09/07/2013	34W 0398849 E, 7534337 N	1308	5.41	0.0	88			76
TAR-13_36	Permanent snow field	Red snow	09/07/2013	34W 0399453 E, 7534692 N	1167	5.68	0.0	85			65
TAR-13_37	Permanent snow field	Red snow	09/07/2013	34W 0399376 E, 7534942 N	1163	5.73	0.4	82			62
TAR-13_39	Permanent snow field	Red snow	10/07/2013	34W 0400256 E, 7535905 N	1318			199	18.4	3.86	66
TAR-13_40	Permanent snow field	Clean snow	10/07/2013	34W 0400256 E, 7535905 N	1318	6.28		158			77
TAR-13_41	Björling	Red snow	11/07/2013	34W 0395764 E, 7532198 N	1295	5.44	0.0	127	20.3	4.49	66
TAR-13_42	Björling	Red snow	11/07/2013	34W 0396623 E, 7531127 N	1156	6.1	0.3	100			57
TAR-14_1	Storglaciären	Red snow	04/07/2014	34W 0398031 E, 7533618 N	1268	7.4	0.1				
TAR-14_2	Storglaciären	Green snow	04/07/2014	34W 0399302 E, 7534091 N	1216		0.1				
TAR-14_3	SE-Kasskasatjåkkå	Green snow	05/07/2014	34W 0399093 E, 7534138 N	1249	7.3	0.1				
TAR-14_4	Storglaciären	Green snow	07/07/2014	34W 0398886 E, 7533623 N	1277	7.35	0.1				
TAR-14_5	Storglaciären	Red snow	07/07/2014	34H 0399085 E, 7533632 N	1247	7.78	0.3				
TAR-14_6	Storglaciären	Red snow	07/07/2014	34H 0393734 E, 7535101 N	1226	6.17	0.1				
TAR-14_7	Rabot	Green snow	09/07/2014	34W 0394036 E, 7535053 N	1326	8.13	0.1				
TAR-14_8	Rabot	Green snow	09/07/2014	34W 0392829 E, 7534726 N	1088		0.1				
TAR-14_9	Rabot	Green snow	09/07/2014	34W 0399578 E, 7536800 N	1249						

TAR-14_10	Liljetopsrännan	Red snow	10/07/2014	34W 0398650 E, 7536880 N	1215	7.51	0.1
TAR-14_11	SE-Kasskasatjåkkå	Red snow	10/07/2014	34W 0399438 E, 7537029 N	1340	7.14	0.1
TAR-14_12	Permanent snow field	Red snow	10/07/2014	34W 0400194 E, 7535878 N	1318	8.16	0.1

• Temperature was also measured at each site and in most cases it was 0.0 ^{o}C; only in a few snow samples did we measure 0.1 or 0.2 ^{o}C.

Table E.2: Distribution of 97% clustered OTUs aligned and assigned to *Archaeplastida* (green algae) taxa separated by habitat and locations. Values are the relative abundance of the taxa in percentage of total sequences and table shows taxa with OTUs of a minimum total observation count of 0.1%. It is important to note that values are rounded to one digit; therefore the abundance of a taxon with a value of 0 in one sample can range between 0 and 0.04%. The clean snow and clean ice habitats did not contain enough particulates for DNA analyses.

Species	***Ancylonema nordenskiöldii***	***Chloromonas cf. alpina* AF514403**	***Chlamydomonas cf. proboscigera***	***Chloromonas polyptera* JQ790556**	***Chloromonas sp.* CCCryo 273-06**	***Chloromonas nivalis* AF514409**	***Chloromonas tughillensis***
Sample ID							
Green snow							
SVA-13_1	0	0.1	1.6	0.4	0.1	0	0
SVA-13_21	0	1.2	0.1	1	31.4	0	0.1
SVA-13_44	0	4.7	0	8.8	0	0.7	0
Average SVA	**0**	**2.0 ± 2.4**	**0.6± 0.9**	**3.4 ± 4.7**	**10.5 ± 18.1**	**0.2 ± 0.4**	**0.0 ± 0.1**
TAR-13_2	0	8.6	0	21.5	0	0.4	0
TAR-13_3	8.5	16.5	0.2	17	0	0.3	0
TAR-13_4	0.2	22.3	0.1	18	0.9	0.8	0.1
TAR-13_16	0	5.1	0	30.1	0	32	6.5
TAR-13_33	0	3.7	0	52.5	0	14.9	4.1
TAR-14_2	0	0.2	0	45	0	20.5	2.1
TAR-14_3	0.1	0.6	0.1	35.2	0	20.1	1
TAR-14_4	0	1	0	10.1	0	3.3	0.4
TAR-14_7	0	22.7	0	53.1	0	0	0
TAR-14_8	0	0.3	0	90.6	0	0	0
TAR-14_9	0	1.9	0	38.1	0	1.9	0.1
Average TAR	**0.8 ± 2.6**	**7.5 ± 8.8**	**0.0 ± 0.1**	**37.4 ± 22.8**	**0.1 ± 0.3**	**8.6 ± 11.3**	**1.3 ± 2.1**
Red snow							
SVA-13_2	0	0.1	0	22.5	0	1.8	0
SVA-13_4	0	0.8	0	0.9	0	0.8	0.9

SVA-13_10	0	0	0	5.3	0	0.2	0
SVA-13_20	0	0	0	8.8	0	14	0.4
SVA-13_23	0	0	0	6.6	0	0.6	0
SVA-13_31	0	0	0	5.8	0	2.7	0
SVA-13_33	0	1.9	0	10.8	0.3	9.3	0
SVA-13_36	8.6	0.3	0.1	16.5	0	1.3	0.1
SVA-13_43	0	0.9	0	10.3	0	2.8	0.3
SVA-13_48	0	1.4	0	12.4	0	2.8	0
SVA-13_54	0	0	0	1.5	0.1	0.6	0
SVA-13_65	0.1	0.2	1.2	14.3	0	0	0
Average SVA	**0.7 ± 2.5**	**0.5 ± 0.6**	**0.1 ± 0.3**	**9.6 ± 6.3**	**0.0 ± 0.1**	**3.1 ± 4.2**	**0.1 ± 0.3**
TAR-13_1	0	0.1	0	12.3	0	1.2	1.3
TAR-13_8	0	5.7	0	52.6	0	4.6	0.1
TAR-13_17	0	0.2	0	9	0	0.4	0
TAR-13_21	0	0.1	0	6.1	0	12.6	1.3
TAR-13_27	0	0	0	17	0	8.8	0.1
TAR-13_28	0	0	0	17.6	0	1.1	0
TAR-13_30	0	0	0	1	0	2	0.3
TAR-13_35	0	12.9	0	26.9	0	7.2	0.9
TAR-13_39	0	0	0	6.4	0	5.2	0.1
TAR-13_41	0	0	0	5.4	0	8.4	2.7
TAR-14_1	0	0.3	0	23.2	0	0.7	0.1
TAR-14_5	0	0.1	0	4.9	0	2.7	0.2
TAR-14_6	0	0	0	8.1	0	0	0
TAR-14_10	0.2	0	0	14.4	0	9.4	0.1
TAR-14_11	0.2	0	0	21.1	0	5.1	0
TAR-14_12	0	0	0	5.7	0	3.8	0
Average TAR	**0.0 ± 0.1**	**1.2 ± 3.4**	**0**	**14.5 ± 12.6**	**0**	**4.6 ± 3.8**	**0.5 ± 0.7**

Biofilms							
SVA-13_56	0	8.3	0	33.9	0.5	15.1	0.1
TAR-13_10	0	6.2	0	53.2	0	5.5	0.1
TAR-13_11	0	11.9	0	41.1	0	0.2	0
TAR-13_19	0	6.6	0	72.5	0	6.9	5.4
Average TAR	**0**	**8.2 ± 3.2**	**0**	**55.6 ± 15.8**	**0**	**4.2 ± 3.5**	**1.8 ± 3.1**
Dirty ice							
SVA-13_7	0	0	0	7.5	0	0	0.2
SVA-13_8	9.4	0.1	0.1	31.5	0	0.1	0
SVA-13_18	0	1.6	0	4.6	0	0	0
SVA-13_19	65.1	0.8	0	0.8	0	0	0
SVA-13_26	0	0	0.6	15.4	0	0	0
SVA-13_38	0	0.4	31.3	5.9	0	0	0.4
SVA-13_47	0	0.4	0	3.6	0.2	0.4	0
SVA-13_50	41.6	0.9	1.8	4.9	0.1	0.1	0
SVA-13_62	30.1	1.4	0	6.9	0	0	0
Average SVA	**16.2 ± 23.9**	**0.6 ± 0.6**	**3.8 ± 10.3**	**9.0 ± 9.3**	**0.0 ± 0.1**	**0.1 ± 0.1**	**0.1 ± 0.1**
TAR-13_13	0	0.9	0	6.1	0	0.3	0
Cryoconite holes							
SVA-13_5	1.3	0	0	3.8	0	2.1	0
SVA-13_16	3.8	0	0	1	0	0	0
SVA-13_27	2.1	0	0	1.1	0	0	0
SVA-13_37	4.1	0	0	3.7	0	2.3	0
SVA-13_51	54.1	0.1	0.3	0.6	0	0.2	0
SVA-13_61	3.8	0	0	1.3	0.3	0	0
Average SVA	**11.5 ± 20.9**	**0**	**0.1 ± 0.1**	**1.9 ± 1.4**	**0.1 ± 0.1**	**0.8 ± 1.1**	**0**

TAR-13_34	6.2	1.5	0.2	1.5	1.9	0.2	0

Table E.2 continued.

Species **Sample ID**	***Microglena sp.* EF537906**	***Prototheca cutis***	***Trebouxia usneae***	***Raphidonema sempervirens* AJ309939**	**Uncultured *Chlamydo-monadaceae* (1) GU117577**	**Uncultured *Chlamydo-monadaceae* (2)**	**Uncultured *Chlamydo-monadaceae* (3)**
Green snow							
SVA-13_1	0.6	0	0	93.4	3.4	0.5	0
SVA-13_21	60.1	0	0	2.7	3	0.3	0
SVA-13_44	0	0	0	68.9	16.3	0.8	0
Average SVA	**20.2 ± 34.5**	**0**	**0**	**55.0± 46.9**	**7.6 ± 7.6**	**0.5 ± 0.3**	**0**
TAR-13_2	0	0	0	11.9	53.2	4.5	0
TAR-13_3	0	8.3	0	35.7	8.5	0.2	5
TAR-13_4	0	37.8	0	6.1	4.1	0.2	9.6
TAR-13_16	0	0	0.2	1.4	23.1	1.4	0.4
TAR-13_33	0	12	0	0	11.6	0	1.2
TAR-14_2	0	2.1	0.1	1.7	27.6	0.7	0.1
TAR-14_3	0	0.8	0	3.6	37.7	0.9	0.1
TAR-14_4	0	0.5	12.2	1	68.9	2.4	0.1
TAR-14_7	0	1.5	10	0.4	7.9	0.4	4
TAR-14_8	0	1.5	0.8	0.3	5.4	0.5	0.7
TAR-14_9	0	8.4	0.2	0.1	47.1	1.9	0.4
Average TAR	**0**	**6.6 ± 11.1**	**2.1 ± 4.5**	**5.7** ± 10.6	**26.8 ± 22.2**	**1.2 ± 1.3**	**2.0 ± 3.1**

Red snow							
SVA-13_2	0	0	0.2	0	72.3	3	0.2
SVA-13_4	0.1	0	0	0	87.8	8.8	0
SVA-13_10	0	0	0	0	83.8	10.7	0.1
SVA-13_20	0	0	0	1.7	65.0	10.1	0
SVA-13_23	0	0	0	0.2	89.9	2.6	0.1
SVA-13_31	0	0.3	0	0.5	88.9	1.8	0
SVA-13_33	0	0	0	5.1	65.2	7.6	0
SVA-13_36	0	0.3	0	3.6	65.9	3.2	0.1
SVA-13_43	0.1	0	0	35.5	45.8	4.2	0.1
SVA-13_48	0	0.1	0	21.3	59.3	2.1	0.5
SVA-13_54	0	0	0	2.3	93.3	2.1	0
SVA-13_65	0	0.1	0	0.5	81.8	1.8	0.1
Average SVA	**0**	**0.1± 0.1**	**0.0 ± 0.1**	**5.9 ± 11.1**	**74.9 ± 14.8**	**4.8 ± 3.4**	**0.1 ± 0.1**
TAR-13_1	0	0	0.1	0	76.2	8.9	0.1
TAR-13_8	0	0.1	0	0.1	33.5	3.3	0
TAR-13_17	0	0	0	14.2	67.7	8.6	0
TAR-13_21	0	0	0.1	0.1	72.1	7.6	0.1
TAR-13_27	0	0.1	0.1	1.7	69	3.2	0
TAR-13_28	0	0	0	0.3	74.5	6.5	0
TAR-13_30	0.6	0	0.1	1.9	87.7	6.4	0
TAR-13_35	0	0.4	0.1	0	32.1	0.7	18.9
TAR-13_39	0	0	0	0	75.3	13	0
TAR-13_41	0	0	0	0.1	71.8	11.6	0.1
TAR-14_1	0	16.8	0.2	0.7	54.8	1.9	1.4
TAR-14_5	0	0.2	5.1	0.1	84.1	2.7	0
TAR-14_6	0	4.4	0	0.5	85.1	2	0

TAR-14_10	0	0.3	0.9	1.2	71.1	2.4	0
TAR-14_11	0	0.2	8.5	3.6	59.8	1.5	0
TAR-14_12	0	0	1.2	20.5	67.3	1.3	0.2
Average TAR	**0.0 ± 0.2**	**1.4 ± 4.2**	**1.0 ± 2.4**	**2.8 ± 5.9**	**67.6 ± 16.0**	**5.1 ± 3.9**	**1.3 ± 4.7**
Biofilms							
SVA-13_56	0	0	0.1	2.2	38.2	1.5	0.1
TAR-13_10	0	0	0	0	31.7	3.3	0.1
TAR-13_11	0	4.4	0	27.5	3.9	0.3	10.7
TAR-13_19	0	0	0	0.3	7.5	0.9	0
Average TAR	**0**	**1.5 ± 2.5**	**0**	**9.3 ± 15.8**	**14.4 ± 15.1**	**1.5 ± 1.6**	**3.6 ± 6.1**
Dirty ice							
SVA-13_7	0	0	0	62	28.1	2.2	0
SVA-13_8	0.1	0	0.1	49.2	7.1	0.1	2.4
SVA-13_18	0.3	0	0	31.3	58.7	3.3	0.3
SVA-13_19	0	0	0	7.9	20.6	0	4.8
SVA-13_26	0	0	0	40.1	42	1.9	0
SVA-13_38	0.8	0	0	18.8	38.3	3.9	0.4
SVA-13_47	0.4	0	0	78.3	14.1	2.4	0.2
SVA-13_50	0	0	0	37.7	12.7	0.3	0.1
SVA-13_62	1.4	0	0	12.3	42.5	0	5.5
Average SVA	**0.3 ± 0.5**	**0**	**0**	**37.5 ± 23.2**	**29.3 ± 17.2**	**1.6 ± 1.5**	**1.5 ± 2.2**
TAR-13_13	0.9	0	0	87.5	4.3	0	0
SVA-13_5	0	0	0.2	52	38.4	2.3	0
SVA-13_16	0	0	0	41.2	54.1	0	0

SVA-13_27	0	0	0	35.3	60.7	0.8	0
SVA-13_37	0	0.2	0.2	16.3	71.7	1.6	0
SVA-13_51	0	0	0	18	26.1	0.2	0.3
SVA-13_61	0	0	0	3.3	91	0.5	0
Average SVA	**0**	**0.0 ± 0.1**	**0.1 ± 0.1**	**27.7 ± 18.2**	**57.0 ± 23.2**	**0.9 ± 0.9**	**0.1 ± 0.1**
TAR-13_34	0	0.1	0	83.6	4.6	0	0.1

Table E.3: Distribution of 97% clustered OTUs aligned and assigned to eukaryote taxa separated by habitat and locations. Values are the relative abundance of the taxa in percentage of total sequences. It is important to note that values are rounded to one digit; therefore the abundance of a taxon with a value of 0 in one sample can range between 0 and 0.04%. The clean snow and clean ice habitats did not contain enough particulates for DNA analyses.

Sample ID	Amoebozoa	Archaeplastida	Centrohelida	Kathablepharidae	Opisthokonta	RT5iin25	SAR	Zeuk77
Green snow								
SVA-13_1	0	64.8	0	0	1.2	0	33.9	0.1
SVA-13_21	0	87.6	0	0	0.7	0	11.3	0.4
SVA-13_44	0	44.7	0	0	38.3	0	15.7	1.3
Average SVA	**0**	**65.7 ± 21.5**	**0**	**0**	**21.6 ± 22.4**	**0**	**20.3 ± 12.0**	**0.6 ± 0.6**
TAR-13_2	0	21.6	0	0	22.4	0	34.9	21.1
TAR-13_3	0	53	0	0	30.7	0	15.9	0
TAR-13_4	0.2	57.1	0	0	37	0	5	0
TAR-13_16	0	37.2	0	0	25.1	0	36.1	1.6
TAR-13_33	0.2	51.4	0	0	19.2	0	24.2	2.4
TAR-14_2	0	56.4	0	0	25.3	0	14	2.8
TAR-14_3	0	46.3	0	0	31.9	0	18.7	1.6
TAR-14_4	0	14.2	0	0	69.9	0	15.3	0
TAR-14_7	0	47.6	0	0	48.4	0	1.4	0
TAR-14_8	0	47.4	0	0	49.9	0	2.3	0
TAR-14_9	0	42	0	0	42.6	0	13.1	2.3
Average TAR	**0.0 ± 0.1**	**43.1 ± 13.9**	**0**	**0**	**36.6 ± 15.1**	**0**	**16.4 ± 11.7**	**2.9 ± 6.1**
Red snow								
SVA-13_2	0	68.0	0	0	31.5	0	0.5	0
SVA-13_4	0	83.3	0	0	4.0	0	12.7	0
SVA-13_10	0	74.5	0	0	24.7	0	0.7	0
SVA-13_20	0	81.8	0	0	12.9	0	5.3	0

SVA-13_23	0	63.3	0	0	32.5	0	2.9	0
SVA-13_31	0	82.4	0	0	9.1	0	7.9	0
SVA-13_33	0	58.0	0	0	26.8	0	14.2	1
SVA-13_36	0	42.0	0	0	38.4	0	19	0.1
SVA-13_43	0	56.6	0	0	24.4	0	17.5	1.5
SVA-13_48	0.1	82.5	0	0	12.9	0	4.2	0
SVA-13_54	0	62.3	0	0	33.8	0	3.8	0
SVA-13_65	0	67.8	0	0	20.8	0	9.3	0
Average SVA	**0**	**68.5 ± 12.9**	**0**	**0**	**22.7 ± 10.9**	**0**	**8.2 ± 6.4**	**0.2 ± 0.5**
TAR-13_1	0	64.1	0	0	32.1	0	3.8	0
TAR-13_8	0	44.7	0	0	47.9	0	7.4	0
TAR-13_17	0	27.1	0	0	72.6	0	0.3	0
TAR-13_21	0	68.0	0	0	23.4	0	8.5	0.1
TAR-13_27	0	29.5	0	0	68.3	0	1.8	0
TAR-13_28	0	76.4	0	0	23.2	0	0.4	0
TAR-13_30	0	38.1	0	0	61.0	0	1.0	0
TAR-13_35	0	72.8	0	0	19.6	0	6.7	0
TAR-13_39	0	88	0	0	11.0	0	1.0	0
TAR-13_41	0	75	0	0	19.8	0	5.2	0
TAR-14_1	0.2	38.1	0	0	50.9	0	10.4	0
TAR-14_5	0	32.6	0	0	58.5	0	8.6	0
TAR-14_6	0.1	37.2	0	0	51.1	0	9.7	0
TAR-14_10	0	26	0	0	71.8	0	1.4	0
TAR-14_11	0	18.2	0	0	77.2	0	3.8	0
TAR-14_12	0	68.8	0	0	21.1	0	9.5	0.2
Average TAR	**0.0 ± 0.1**	**50.3 ± 22.3**	**0**	**0**	**44.3 ± 22.6**	**0**	**5.0 ± 3.7**	**0.0 ± 0.1**

Biofilms								
SVA-13_56	0	48.9	0	0	27.5	0	20.6	1.8
TAR-13_10	0	46.1	0	0	50	0	3.9	0
TAR-13_11	0	56.1	0	0	25.2	0	18.0	0
TAR-13_19	0	36.8	0	0	60.4	0	2.7	0
Average TAR	**0**	**46.3 ± 9.7**	**0**	**0**	**45.2 ± 18.1**	**0**	**8.2 ± 8.5**	**0**
Dirty ice								
SVA-13_7	0.2	47.5	0	0	14.6	4.6	32.0	1.1
SVA-13_8	0	34.9	0	0	17.1	0	47.3	0.1
SVA-13_18	0	60.7	0	0	30.7	0	8.6	0
SVA-13_26	0	53.2	0	0	18.1	0	28.7	0
SVA-13_38	0.1	53.2	0	0	9.0	0	36.9	0.9
SVA-13_47	0	33.8	0	0	33.9	0	32	0.3
SVA-13_50	0	68.4	0	0	20.1	0	8.4	0
SVA-13_62	0	35.6	0	0	50.8	0	13.1	0.5
Average SVA	**0.0 ± 0.1**	**48.4 ± 12.9**	**0**	**0**	**24.3 ± 13.5**	**0.6 ± 1.6**	**25.9 ± 14.3**	**0.4 ± 0.4**
TAR-13_13	0	57.7	0	0	38	0	4.3	0
Cryoconite holes								
SVA-13_5	0.1	48.2	0	0	23.2	0	24	0.4
SVA-13_16	0.3	10.7	0	0	66.4	0	20.3	0
SVA-13_27	0.1	13.5	0	0	75.6	0	7.8	0.1
SVA-13_37	0.1	38	0	0	39.6	0	17.9	0.2
SVA-13_51	0.1	22.9	0	0	47.8	0	26.4	0
SVA-13_61	0.2	9.7	0	0.1	79.9	0	7.9	0
Average SVA	**0.2 ± 0.1**	**23.8 ± 16.0**	**0**	**0**	**55.4 ± 22.2**	**0**	**17.4 ± 7.9**	**0.1 ± 0.2**
TAR-13_34	0	47.6	0	0	10.9	0	41.2	0

Table E.4: Distribution of 97% clustered OTUs aligned and assigned to known bacterial taxa separated by habitat and locations. Values are the relative abundance of the taxa in percentage of total sequences and figure shows taxa with >0.01% abundance. It is important to note that values are rounded to one digit; therefore the abundance of a taxon with a value of 0.0 in one sample can range between 0 and 0.04%. The clean snow and clean ice habitats did not contain enough particulates for DNA analyses

Phyla	***Acidobacteria***		***Actinobacteria***		***Bacteriodetes***				***Chlorobi***	***Chloroflexi***		
Class	*Acidobacteriia*	*Solibacteres*	*Acidimicrobiia*	*Actinobacteria*	*Cytophagia*	*Flavobacteriia*	*Sphingobacteriia*	*Saprospirae*	*Ignavibacteria*	*Anaerolineae*	*C0119*	*Ktedonobacteria*
Green snow												
SVA-13_1	9	0	0	0	8	0.1	12.3	6.2	0	0	0	0
SVA-13_21	0	0	0	0	3.2	10.7	7.2	1.4	0	0	0	0
SVA-13_44	0.1	0	0	1.7	2.2	5.8	0.2	39.6	0	0	0	0
Average SVA	**3.0 ± 5.2**	**0**	**0**	**0.6 ± 0.1**	**4.5 ± 3.1**	**5.5 ± 5.3**	**6.6 ± 6.1**	**15.7 ± 20.8**	**0**	**0**	**0**	**0**
TAR-13_2	0	0	0	0.1	0.4	0	18.1	42.1	0	0	0	0
TAR-13_3	0.3	0.3	0	1.8	0.2	0.3	47.3	4.3	0	0	0	0
TAR-13_4	0.8	0.1	0	0.1	0.8	0	33.6	1.6	0	0	0	0
TAR-13_16	0	0	0	0.3	0.9	0	23.7	26.9	0.1	0	0	0
TAR-13_33	0	0	0	1.7	1.3	0.1	31.4	14	0	0	0	0
TAR-14_2	0.1	0	0	1.2	6.9	0.1	4.6	18.9	0	0	0	0
TAR-14_3	0.3	0.2	0	2.2	1.6	0.2	12.3	15.5	0	0	0	0
TAR-14_4	10.7	0.3	0	0	0	0	0.2	0	0	0.1	0	0
TAR-14_7	17.2	0.3	0	0	0	0.1	1.7	0	0	0	0	0
TAR-14_8	4.8	0	0	1.4	1.3	0	48.5	0.3	0	0	0	0
TAR-14_9	1.7	0	0	0	1.7	0	6.7	10	0	0	0	0
Average TAR	**3.3 ± 5.7**	**0.1 ± 0.1**	**0**	**0.8 ± 0.9**	**1.4 ± 1.9**	**0.1 ± 0.1**	**20.7 ± 17.6**	**12.1 ± 13.4**	**0**	**0**	**0**	**0**
Red snow												
SVA-13_4	0	0	0	0.5	37.4	0	0.3	51.2	0	0	0	0
SVA-13_10	17	0	0	0	9	0	0	3	0	0	0	0

SVA-13_20	0	0	0	0	10.6	0	1.5	45.2	1.8	0	0	0
SVA-13_23	0	0	0	0.3	6.3	4.6	0	1	0	0	0	0
SVA-13_31	0	0	0	4.2	11.6	0.4	0	44.9	0	0	0	0
SVA-13_33	0.4	0	0	2.1	3.9	0	2.8	26.8	0	0	0	0
SVA-13_36	3.4	0	0	8.4	39	0.5	0.8	1.6	0	0	0	0
SVA-13_43	0.8	0	0	0.8	12.5	0	0.4	67.3	0	0	0	0
SVA-13_48	0	0	0	0.6	44.5	0.6	0	19.1	0	0	0	0
SVA-13_54	0.2	0	0	15.7	3.4	0.5	34.6	3.6	0	0	0	0
SVA-13_65	0.4	0	0	0.2	5.9	1	0.3	3.7	0	0.1	0	0
Average SVA	**2.0 ± 5.1**	**0**	**0**	**3.0 ± 4.9**	**16.7** ± 15.5	**0.7 ± 1.3**	**3.7 ± 10.3**	**24.3 ± 24.1**	**0.2 ± 0.5**	**0**	**0**	**0**
TAR-13_1	0	0	0	0.1	3.6	0	91.1	1.9	0	0	0	0
TAR-13_8	0.4	0	0	0	0	0	89.3	0	0.4	0	0	0
TAR-13_17	0.2	0	0	0	0.8	0	90.7	0.1	0	0	0	0
TAR-13_21	0	0	0	0	1	0	75.7	22.3	0	0	0	0
TAR-13_27	0	0	0	0	0.5	0	71.4	0.5	5.1	0	0	0
TAR-13_28	4.7	0	0	0	0	0	12.5	0	0	0	0	0
TAR-13_30	0.2	0	0	0	3.8	0	81.6	3.2	0.2	0	0	0
TAR-13_35	0.8	0	0	0.1	4.1	0.9	63	4.3	0	0	0	0
TAR-13_41	0	0	0	0.1	0.5	0	82.1	15.8	0.3	0	0	0
TAR-14_1	1.1	0	0	4.3	1.2	0	46.3	11.2	0	0	0	0
TAR-14_5	16.7	0.2	0	0	15	0	1.3	0	0	0	0	0
TAR-14_6	0.1	0	0	0.1	1.9	0.1	81.3	2.4	0	0	0	0
TAR-14_10	17.1	0.7	0	0.1	7.3	0	45.8	1	0	0	0	0
TAR-14_11	4.6	0.5	0	0.4	13.6	0	51.8	6.3	0	0	0	0
TAR-14_12	3.1	0	0	0.3	2.2	0	59.3	0	0	0	0	0
Average TAR	**3.3 ± 5.8**	**0.1 ± 0.2**	**0**	**0.4 ± 1.1**	**3.7 ± 4.7**	**0.1 ± 0.2**	**62.9 ± 27.5**	**4.6 ± 6.7**	**0.4 ± 1.3**	**0**	**0**	**0**
Biofilms												

SVA-13_56	0	0	0	7.6	9.5	5.4	2.8	14.2	0	0	0	0
TAR-13_10	0	0	0	0	0.2	0	92.1	1.9	0	0	0	0
TAR-13_11	0.1	0	0	3.8	0.7	0	66.8	2.8	0	0	0	0
TAR-13_19	0	0	0	0	1	0	97.8	0.8	0	0	0	0
Average TAR	**0.0 ± 0.1**	**0**	**0**	**1.3 ± 2.2**	**0.6 ± 0.4**	**0**	**85.6 ± 16.5**	**1.8 ± 1.0**	**0**	**0**	**0**	**0**
Dirty ice												
SVA-13_7	0.2	0	0	0.4	2.9	30.8	4.4	0.5	0	0	0	0
SVA-13_8	1.6	0.2	0.1	7	0.2	0	1.7	2.6	0	1.1	0	0.2
SVA-13_18	8.7	0	0	2.1	37.6	0.2	2.1	1.1	0	0	0	0
SVA-13_19	5	0.2	0	8	0.5	0	4.2	0.3	0	0.3	0	0
SVA-13_26	0.2	0.2	0	5.1	1.3	0.2	4.2	5.9	0	0	0	0
SVA-13_38	2.9	0.4	0	3.6	1	0.2	7.1	8.9	0	0.1	0	0
SVA-13_47	22.8	0.1	0	1.9	4.1	0.2	9.5	1.7	0	0	0	0
SVA-13_50	3.2	0	0	15.9	4.7	0	2.9	2.7	0	0	0	0
SVA-13_62	1	0.1	0	1.6	8.3	0.4	8.3	1.7	0	0	0	0
Average SVA	**5.1 ± 7.2**	**0.1 ± 0.1**	**0**	**5.1 ± 4.8**	**6.7 ± 11.9**	**3.6 ± 10.2**	**4.9 ± 2.8**	**2.8 ± 2.8**	**0**	**0.2 ± 0.4**	**0**	**0.0 ± 0.1**
TAR-13_13	7.3	0	0	0.3	8.1	0.2	10.4	18.5	0	0	0	0
TAR-13_14	38.9	0	0	0	0	0	11.1	0	0	0	0	0
Average TAR	**23.1 ± 22.3**	**0**	**0**	**0.2 ± 0.2**	**4.1 ± 5.7**	**0.1 ± 0.1**	**10.8 ± 0.5**	**9.3 ±13.1**	**0**	**0**	**0**	**0**
Cryoconite holes												
SVA-13_5	1.3	0.4	0.3	0.7	0.3	0.5	0.5	4.8	0	7.4	0	0.5
SVA-13_16	0.5	0.2	0	1.4	0.1	0	0.7	6.2	0	4.7	0	0.1
SVA-13_27	0.2	0.6	0	1.6	0.1	0.1	1.3	5.5	0	3.7	0	0
SVA-13_37	1.1	0.1	0	1.3	0	0	1.1	0.9	0	4.3	0	0
SVA-13_51	0.6	0.1	0	1.1	0	0	0.8	2.7	0	3.4	0	0
SVA-13_61	1.3	0.4	0	2.4	0.3	0	2.7	29.4	0	13.4	1.5	0

Average SVA	**0.8 ± 0.5**	**0.3 ± 0.2**	**0.1 ± 0.1**	**1.4 ± 0.6**	**0.1 ±0.1**	**0.1 ± 0.2**	**1.2 ± 0.8**	**8.3 ± 10.5**	**0**	**6.2 ± 3.8**	**0.3 ±0.6**	**0.1 ± 0.2**
TAR-13_34	7	0.2	0.1	2.3	0.6	0	2.5	0	0	0	0	0

Table E.4: continued

Phyla	***Cyanobacteria***				***Fibrobacteres***	***Firmicutes***	***Gemmati-monadetes***	***Proteobacteria***				***TM7-3***	***WPS-2***	***Thermi***
Class	*Cyano-bacteria*	*Nostoco-phycideae*	*Oscillatorio-phycideae*	*Synechococco-phycideae*	*Fibrobacteria*	*Clostridia*	*Gemmati-monadetes*	*Alphaproteo-bacteria*	*Betaproteo-bacteria*	*Deltaproteo-bacteria*	*Gammaproteo-bacteria*	*TM7-3*	*WPS-2*	*Deino-cocci*
Green snow														
SVA-13_1	0	0	0	0.3	0	0	0	57.1	5	0.1	0.1	0.1	1.8	0
SVA-13_21	0	0	0	0.2	0	0	0	0.6	76.5	0.1	0.1	0	0	0
SVA-13_44	0	0	0	0.1	0	0	0	0.8	49.4	0	0	0	0	0
Average SVA	**0**	**0**	**0**	**0.2 ± 0.1**	**0**	**0**	**0**	**19.5 ± 32.6**	**43.6 ± 36.1**	**0.1 ± 0.1**	**0.1 ± 0.1**	**0.0 ± 0.1**	**0.6 ±1.0**	**0**
TAR-13_2	0	0	0	0	0	0	0	0.8	38.5	0	0	0	0	0
TAR-13_3	0	0.8	0	1.8	0	0	0	7.8	34.7	0	0.5	0	0.1	0
TAR-13_4	0	0.1	0	0	0	0	0	14.1	48.6	0	0.3	0	0	0
TAR-13_16	0	0	0	0	0	0	0	2	46.2	0	0	0	0	0
TAR-13_33	0	0	0	0.3	0	0	0	10.1	41	0	0	0	0	0
TAR-14_2	0	0.4	0.1	3	0	0	0	3	61.2	0	0.5	0	0	0
TAR-14_3	0	0.1	0	3.5	0	0.1	0.1	4.4	59.1	0	0.4	0	0.1	0
TAR-14_4	0.6	38.6	30	5	0	0	0	13.9	0.5	0	0	0	0	0
TAR-14_7	3.1	42.8	2.5	1.8	0	0	0	26.1	4.4	0	0	0	0.1	0
TAR-14_8	0.2	0	0.9	0.7	0	0	0	1.6	31.2	0	9	0	0.1	0
TAR-14_9	0	1.7	0	1.7	0	0	0	0	76.7	0	0	0	0	0
Average TAR	**0.4 ± 0.9**	**7.7 ± 16.4**	**3.0 ± 9.0**	**1.6 ± 1.7**	**0**	**0**	**0**	**7.6 ± 8.0**	**40.2 ± 22.8**	**0**	**1.0 ± 2.7**	**0**	**0.0 ± 0.1**	**0**

Red snow														
SVA-13_4	0	0.3	0	0.5	0	0	0	0	9.5	0	0.3	0	0	0
SVA-13_10	0	1	17	20	0	2	0	8	22	0	0	0	1	0
SVA-13_20	0	0.6	1.2	1.5	0	0	0	0	30.2	0	7.6	0	0	0
SVA-13_23	0.3	2.9	0.1	77.3	0	1.3	0	0.7	4.9	0	0.3	0	0	0
SVA-13_31	0	1.8	0.4	10.2	0	0	0	1.1	25.6	0	0	0	0	0
SVA-13_33	0	0.2	0	0.6	0	0.2	0	2.1	60.8	0	0	0	0	0
SVA-13_36	0	0	0	8.2	0	0	0	12	24.3	0.1	0	0.1	0	1.4
SVA-13_43	0	0	0	0	0	0	0	0.8	17.5	0	0	0	0	0
SVA-13_48	0	0	0	4.2	0	0	0	0.6	30.4	0	0	0	0	0
SVA-13_54	0	0.2	0	18.5	0	0	0	4.8	18.4	0	0.2	0	0	0
SVA-13_65	0	0.2	0	24.2	0	0.1	0	0.9	62.6	0	0.4	0	0.1	0
Average SVA	**0.0 ± 0.1**	**0.7 ± 0.9**	**1.7 ± 5.1**	**15.0 ± 22.4**	**0**	**0.3 ± 0.7**	**0**	**2.8 ± 3.9**	**27.8 ± 18.5**	**01**	**0.8 ± 2.3**	**0**	**0.1 ± 0.3**	**0.1 ± 0.4**
TAR-13_1	0.1	0	0	0.1	0	0	0	0.1	2.1	0	1	0	0	0
TAR-13_8	0.8	3.1	3.3	0	0	0	0	2.3	0.4	0	0	0	0.1	0
TAR-13_17	0.2	4.8	1.4	0.1	0	0	0	1.3	0.4	0	0	0	0	0
TAR-13_21	0.1	0	0	0.1	0	0	0	0.1	0.3	0	0.2	0	0	0
TAR-13_27	0	4.3	0.8	0.5	0	0	0	6.6	0.3	0	10	0	0	0
TAR-13_28	1.6	20.3	4.7	6.3	0	0	0	50	0	0	0	0	0	0
TAR-13_30	0.7	1.1	0.9	0.1	0	0	0	1.1	7	0	0.2	0	0	0
TAR-13_35	0	3	0.4	20.6	0	0.2	0	1	1.3	0	0.4	0	0	0
TAR-13_41	0	0.2	0.2	0.2	0	0	0	0.5	0.1	0	0	0	0	0
TAR-14_1	0	0.4	0.4	1.8	0	0	0	18.7	14.4	0	0.2	0	0	0
TAR-14_5	3	12.7	15.5	1.9	0	0	0	32.2	1.3	0	0	0	0.2	0
TAR-14_6	0	0.1	0.1	10.2	0	0	0	2.1	1.1	0	0.5	0	0	0
TAR-14_10	0.2	0.7	0.3	0.5	0	0	0	8.8	16.9	0	0.4	0	0.2	0
TAR-14_11	0	0.1	0.2	0.1	0	0	0	4.4	4.2	0	13.8	0	0.2	0
TAR-14_12	0	0.6	0	16.7	0	0	0	17	0.3	0	0.6	0	0	0

Average TAR	**0.4 ± 0.8**	**3.4 ± 5.7**	**1.9 ± 4.0**	**3.9 ± 6.7**	**0**	**0.0 ± 0.1**	**0**	**9.7 ± 14.4**	**3.3 ± 5.4**	**0**	**1.8 ± 4.2**	**0**	**0.0 ± 0.1**	**0**
Biofilms														
SVA-13_56	0	0	0	6.4	0	0	0	6.2	47.8	0	0	0	0	0
TAR-13_10	0	0.1	0.1	0	0	0	0	1.5	4.1	0	0	0	0	0
TAR-13_11	0	0.1	0.1	0.9	0	0	0	9.1	15	0	0.4	0	0	0
TAR-13_19	0	0	0	0	0	0	0	0.4	0	0	0	0	0	0
Average TAR	**0**	**0.1 ± 0.1**	**0.1 ± 0.1**	**0.3 ± 0.5**	**0**	**0**	**0**	**3.7 ± 4.7**	**6.4 ± 7.8**	**0**	**0.1 ± 0.2**	**0**	**0**	**0**
Dirty ice														
SVA-13_7	0	0	0.5	12.6	0	0	0	3.7	17.7	0.1	26.2	0.1	0.1	0
SVA-13_8	0	0	0	75.5	0	0	0.1	6.4	0.6	0.1	0	0.1	2.3	0
SVA-13_18	0	0	0	2.8	0	0	0	43.8	1.4	0.2	0	0	0	0
SVA-13_19	0	0	0	68.7	0	0.1	0	11.3	0.2	0.1	0	0.1	0.7	0.1
SVA-13_26	0	2.3	0	29.7	0	0	0.1	34.8	11.9	1.8	0	2.1	0	0
SVA-13_38	0	0.1	0.1	22	0	0	0.4	17.9	28.7	1.5	0	3	2.1	0
SVA-13_47	0	0	0	43.6	0	0	0.1	11.3	0.6	0.2	0	0.3	3.3	0
SVA-13_50	0	0	0	42.4	0	0	0	19.5	7.3	0.2	0	1.1	0	0.1
SVA-13_62	0	0.5	0	11.5	0	0	0	44.1	20.8	0.7	0.3	0.3	0.5	0
Average SVA	**0**	**0.3 ± 0.8**	**0.1 ± 0.2**	**34.3 ± 25.5**	**0**	**0**	**0.1 ± 0.1**	**21.4 ± 15.6**	**9.9 ± 10.5**	**0.5 ± 0.7**	**2.9 ± 8.7**	**0.8 ± 1.1**	**1.0 ± 1.2**	**0**
TAR-13_13	0	0	0	0.6	0	0	0	35.7	17.4	0.2	0	0	1.4	0
TAR-13_14	0	0	0	5.6	0	0	0	38.9	5.6	0	0	0	0	0
Average TAR	**0**	**0**	**0**	**3.1± 3.5**	**0**	**0**	**0**	**37.3 ± 2.3**	**11.5 ± 8.3**	**0.1 ± 0.1**	**0**	**0**	**0.7 ± 1.0**	**0**
Cryoconite holes														
SVA-13_5	0	0	0.1	69.2	6.7	0	0.5	3.8	0.5	0.3	0	0	2.3	0
SVA-13_16	0	0	0.3	79.8	0.3	0	0	2.9	0.7	0.7	0	0	1.5	0
SVA-13_27	0	0.2	0.3	71.9	0.5	0	1	5.2	7.4	0.2	0	0	0.2	0

SVA-13_37	0	0	0.2	88.2	0	0	0	2.1	0.1	0	0	0	0.4	0
SVA-13_51	0	0	0	88.5	0	0	0	1.9	0.1	0	0	0	0.4	0
SVA-13_61	0	0.1	0	31.4	0	0	0	10.2	3.5	0.2	0	0.1	3	0
Average SVA	**0**	**0.1 ± 0.1**	**0.2 ± 0.1**	**71.5 ± 21.2**	**1.3 ± 2.7**	**0**	**0.3 ± 0.4**	**4.4 ± 3.1**	**2.1 ±2.9**	**0.2 ±0.3**	**0**	**0**	**1.3 ± 1.2**	**0**
TAR-13_34	0	0	0	0.2	0	7.4	0	8.1	18.7	0	51.5	0.1	1.4	0

Table E.5: Distribution of 97% clustered OTUs aligned and assigned to archaea separated by habitat and locations. It is important to note that values are rounded to one digit; therefore the abundance of a taxon with a value of 0 in one sample can range between 0 and 0.04%. The clean snow and clean ice habitats did not contain enough particulates for DNA analyses.

	Crenarchaeota					***Euryarchaeota***			
	MBGA	*MBGA; NRP-J*	*MCG; pGrfC26*	*Thaumarchaeota; Cenarchaeales*	*Thaumarchaeota; Nitrososphaerales*	*Methanobacteria; Methanobacteriales*	*Methanomicrobia; Methanomicrobiales*	*Methanomicrobia; Methanosarcinales*	*Thermoplasmata; E2*
Green snow									
SVA-13_1	0	0	0	1.7	98.3	**0**	**0**	**0**	**0**
SVA-13_21	0	0	0	1.9	97.8	0.2	0	0	0.1
Average SVA	**0**	**0**	**0**	**1.8 ± 0.1**	**98.1 ± 0.4**	**0.1 ± 0.1**	**0**	**0**	**0.1 0.1**
TAR-13_4	0	0.2	0	0.2	3.4	76	0	9.3	11
TAR-13_33	2.8	0.1	0	83	7	0.1	0.1	0	6.9
TAR-14_2	0	0	0	0.1	0.6	0	0	99.3	0
TAR-14_3	0	0	0	99.7	0.1	0	0	0	0.2
TAR-14_4	0	0	0	0.6	99.4	0	0	0	0
TAR-14_8	0	0	0	98.9	1.1	0	0	0	0
TAR-14_9	0	0	1.9	87.7	9	0	0	0.1	1.2
Average TAR	**0.4 ± 1.1**	**0.0 ± 0.1**	**0.3 ±**0.7	**52.9 ± 49.5**	**17.2 ± 36.4**	**10.9 ± 28.7**	**0**	**15.5 ± 37.1**	**2.8 ± 4.4**
Red snow									
SVA-13_2	0	0	0	0.3	99.7	0	0	0	0
SVA-13_23	0	0	0	0.5	99.4	0.2	0	0	0
SVA-13_31	0	0	0	0	99.4	0.6	0	0	0
SVA-13_36	0	0	0	3.6	92.9	2.4	0	0	1.2
SVA-13_48	0	0	0	5	16.8	78.2	0	0	0

SVA-13_54	0	0	0	13.2	74.5	8.5	0	0	3.8
SVA-13_65	0	0	0	14.3	42.9	28.6	14.3	0	0
Average SVA	**0**	**0**	**0**	**5.3 ± 6.1**	**75.1 ± 33.0**	**16.9 ± 28.9**	**2.0 ± 5.4**	**0**	**0.7 ± 1.4**
TAR-13_8	0	0	0	4.9	86.2	2	1.2	0	5.7
TAR-14_1	0	0	0	0.1	100	0	0	0	0
TAR-14_5	0	0	0	2.2	97.8	0	0	0	0
TAR-14_6	0	0	0	0	0	0	0	90	10
Average TAR	**0**	**0**	**0**	**1.8 ± 2.3**	**71.0 ± 47.7**	**0.5 ± 1.0**	**0.3 ± 0.6**	**22.5 ± 45.0**	**3.9 ± 4.9**
Biofilms									
SVA-13_56	0	0	0	48.7	51.3	0	0	0	0
TAR-13_10	0	0	0	3.2	91.6	5.3	0	0	0
TAR-13_11	0	0.1	0	99.1	0.2	0	0	0	0.6
Average TAR	**0**	**0.1 ± 0.1**	**0**	**51.2 ± 67.8**	**45.9 ± 64.6**	**2.7 ± 3.7**	**0**	**0**	**0.3 ± 0.4**
Dirty ice									
SVA-13_8	0	0	0	0	100	0	0	0	0
SVA-13_19	0	0	3.1	0	53.1	0	0	0	43.9
SVA-13_50	0	0	0	6.3	40.5	46.8	0	0	6.3
Average SVA	**0**	**0**	**1.0 ± 1.8**	**2.1 ± 3.6**	**64.5 ± 31.4**	**15.6 ± 27.0**	**0**	**0**	**16.7 ± 23.7**
TAR-13_14	0	0	0	4.9	80.6	12.6	0	0	1.9
Cryoconite holes									
SVA-13_5	0	0	3.5	1.8	36.8	7	0	5.3	45.6

SVA-13_16	0	0	0	0	99.9	0.1	0	0	0
SVA-13_27	2.2	0	0	28.1	64.5	4.2	0.3	0	0.6
SVA-13_37	0	0	0	2.8	97.2	0	0	0	0
SVA-13_51	0	0	0	0	0	0	26.9	0	73
SVA-13_61	1.5	0	0	30.9	47.1	16.2	0	0	4.4
Average SVA	**0.6 ± 1.0**	**0**	**0.6 ± 1.4**	**10.6 ± 14.7**	**57.6 ± 38.1**	**4.6 ± 6.4**	**4.5 ± 11.0**	**0.9 ± 2.2**	**20.6 ± 31.2**

Table E.6: Number of sequences before and after quality control, assigned to taxa and with respective diversity indices (Shannon, Simpson).

	Eukaryotes				Algae			Bacteria					Archaea	
Sample ID	**Raw seqs**	**Seqs after QC**	**Shannon**	**Simpson**	**Seqs assigned to algae**	**Shannon**	**Simpson**	**Raw seqs**	**Seqs after QC**	**Seqs assigned to bacteria**	**Shannon**	**Simpson**	**Raw seqs**	**Seqs after QC**
Green snow														
SVA-13_1	2912	2634	6.09	0.94	1078	4.45	0.85	15036	3013	1841	5.23	0.92	85586	71255
SVA-13_21	14590	6238	5.53	0.9	5460	4.68	0.87	16095	4621	3092	5.69	0.93	55972	45789
SVA-13_44	7775	2900	6.04	0.95	1295	4.86	0.9	11369	2817	1838	6.83	0.98		
TAR-13_2	10765	2454	6.87	0.98	743	4.88	0.9	14136	5417	4010	6.25	0.97		
TAR-13_3	17796	11388	6.04	0.96	6031	4.15	0.88	3595	2040	1458	4.34	0.84		
TAR-13_4	19323	13597	5.34	0.93	7765	3.32	0.81	4654	2514	2258	4.44	0.89	4528	1396
TAR-13_16	8022	2183	7.17	0.98	809	5.22	0.94	7453	3842	2097	4.21	0.97	5229	265
TAR-13_33	1389	947	5.8	0.95	487	5.1	0.92	3095	1576	1282	4.71	0.9	72767	64246
TAR-14_2	6064	4332	5.43	0.94	2441	3.52	0.82	5513	2976	2253	5.57	0.94	30663	19720
TAR-14_3	6799	5052	5.28	0.94	2341	3.35	0.8	6142	3215	2506	5.25	0.92	127172	114214
TAR-14_4	10393	7341	5.4	0.93	1013	2.93	0.7	8647	5419	3922	5.55	0.94	1023027	886676
TAR-14_7	2038	1265	5.71	0.95	586	3.76	0.85	6318	3729	2055	6.04	0.96		
TAR-14_8	22201	16264	3.86	0.82	7700	2.08	0.47	7456	3602	1426	3.42	0.78	1548	530
TAR-14_9	7479	5575	4.92	0.9	2336	3.55	0.8	263	107	80	6.34	0.92	94145	82445
Red snow														
SVA-13_2	6135	5148	3.34	0.76	3500	2.34	0.57	98*	4*	1*			60965	54688
SVA-13_4	6979	3937	4.56	0.8	3280	3.41	0.7	7509	1421	770	6.16	0.97		40
SVA-13_10	13448	6583	4.24	0.81	4904	3.52	0.73	29728	3511	334	6.69	0.99		

SVA-13_20	7130	3952	5.2	0.88	3226	4.08	0.81	12881	2344	987	7.00	0.99		
SVA-13_23	5373	4485	2.93	0.68	2832	1.74	0.39	8352	4008	1850	5.36	0.94	1695	732
SVA-13_31	12752	10621	3.07	0.6	8743	1.79	0.4	5040	2341	598	5.52	0.95		43331
SVA-13_33	7678	3008	6.22	0.94	1727	4.4	0.84	9129	1911	1041	6.86	0.98		
SVA-13_36	23283	16789	5.28	0.91	7056	2.93	0.67	11503	6109	2573	4.26	0.86	2318	921
SVA-13_43	16457	5447	7.24	0.98	3059	5.43	0.93	5473	988	627	6.60	0.98		
SVA-13_48	6294	5123	3.96	0.8	4184	2.93	0.7	2838	1183	556	4.83	0.91	2665	722
SVA-13_54	23068	16698	3.89	0.73	10391	1.68	0.36	3777	1519	812	4.84	0.9	39830	34942
SVA-13_65	7362	5408	4.17	0.77	3667	2.42	0.55	13545	7349	4245	4.25	0.8	1267	295
TAR-13_1	9632	4770	5.29	0.91	3058	4.23	0.81	21581	6431	5087	4.39	0.85		
TAR-13_8	77757	26947	5.85	0.96	12012	4.64	0.9	12368	3661	1051	4.39	0.84	2059	926
TAR-13_17		4863	4.85	0.88	1318	4.68	0.86	16240	5850	3632	4.36	0.83		
TAR-13_21	9330	4354	5.25	0.89	2920	3.89	0.79	10946	3997	3169	5.45	0.92		
TAR-13_27	19416	15725	2.55	0.59	4639	3.04	0.68	16105	2297	630	5.87	0.96		
TAR-13_28	9402	5344	4.39	0.84	4082	3.56	0.73	15312	2525	227	6.28	0.94		
TAR-13_30	6493	3042	4.56	0.86	1133	2.91	0.61	10571	2327	1558	5.27	0.98	1871	371
TAR-13_35	7274	5474	4.91	0.92	3987	3.61	0.85	4562	2424	1437	4.04	0.77		
TAR-13_39	11667	6810	4.25	0.79	5992	3.41	0.72	15247	3447					
TAR-13_41	7606	3715	4.83	0.86	2785	3.73	0.77	17534	5305	3651	4.99	0.91		
TAR-14_1	12436	9069	5.12	0.92	3454	3.34	0.76	3009	1705	1356	4.00	0.83	148712	146362
TAR-14_5	4251	3254	3.99	0.8	1059	1.86	0.42	1974	1064	724	5.86	0.97	1020	590
TAR-14_6	7573	5312	3.93	0.8	1976	2.03	0.46	9112	4794	3868	2.25	0.48	587	414
TAR-14_10	6037	4720	3.68	0.75	1218	2.5	0.6	5809	3158	2412	5.32	0.91		
TAR-14_11	4899	3453	5.47	0.93	614	3.42	0.77	4453	2404	1893	4.76	0.87		

TAR-14_12	7387	5701	4.29	0.83	3909	2.54	0.65	1892	979	425	4.30	0.82		
Biofilms														
SVA-13_56	8929	6986	4.88	0.92	3412	3.78	0.84	9055	5154	3570	6.04	0.97	177818	150612
TAR-13_10	14460	5679	5.63	0.95	2604	4.54	0.9	26266	10369	8418	4.25	0.83	2852	473
TAR-13_11	24975	16236	5.52	0.94	9112	3.75	0.85	10536	6442	1893	3.62	0.71	558037	467198
TAR-13_19	9524	4315	5.18	0.93	1585	4.97	0.91	4408	2502	1621	6.63	0.84		
Dirty ice														
SVA-13_7	2201	1790	6.73	0.97	931	5.12	0.92	18431	5685	3999	6.36	0.97		
SVA-13_8	9012	6619	4.96	0.92	2313	4.03	0.85	5506	3193	2738	3.59	0.71	2481	716
SVA-13_18	2833	938	5.59	0.93	569	4.37	0.85	7824	1468	671	5.28	0.94		
SVA-13_19	1980	1189	4.08	0.8	152			137044	74279	60321	3.36	0.72	2214	562
SVA-13_26	3340	536	6.77	0.97	285	5.03	0.92	16847	2833	1750	6.92	0.99		
SVA-13_38	4410	1205	6.61	0.97	634	5.3	0.94	13137	2866	1676	6.88	0.99		
SVA-13_47	7694	2784	7.28	0.98	942	4.71	0.87	13273	6486	3359	6.16	0.97		
SVA-13_50	3912	2525	5.11	0.94	1726	3.84	0.88	9188	5116	1736	4.85	0.91	761	385
SVA-13_62	7900	970	6.87	0.97	344	6.07	0.97	16249	2635	1658	6.24	0.97		
TAR-13_13	15845	1228	6.3	0.95	706	5	0.89	20891	3256	1126	6.25	0.98		
TAR-13_14	280	93			3*			14006	6574	24*			2924	596
Cryoconite holes														
SVA-13_5	2450	1707	5.08	0.93	823	3.04	0.78	9897	5263	5087	3.99	0.78	2307	1102
SVA-13_16	6223	3874	5.5	0.92	416	2.57	0.74	9096	5195	4670	2.96	0.62	19551	13644

SVA-13_27	5344	3445	4.23	0.85	461	2.52	0.66	11963	6675	5846	3.85	0.75	3869	1185
SVA-13_37	3158	2075	5.65	0.93	788	2.92	0.67	10262	6041	5692	2.33	0.51	36724	28732
SVA-13_51	9796	7221	5.53	0.95	1653	2.53	0.71	18289	11166	10434	2.28	0.49	66266	78352
SVA-13_61	8588	5913	4.18	0.79	583	2.58	0.6	19110	10769	9207	4.53	0.9	3133	1055
TAR-13_34	18043	13464	3.9	0.8	6405	1.87	0.44	5001	2983	2531	4.35	0.85		

* removed from analysis due to low sequence numbers (sequences < 100)

Table E.7: Dissolved organic carbon (DOC), nutrients and other inorganic aqueous chemical data for Svalbard (SVA-) and Arctic Sweden (TAR-) samples separated into habitats.

Sample ID	DOC [µM]	PO_4^{3-} [µM]	NO_3^-	SO_4^{2-}	Cl^-	Al	Ba	Bi	Ca	Cd	Co	Cr	Cu	Fe	K	Mg	Mn	Na	Ni	P	Pb	S	Si	Sr	Zn
Clean snow																									
SVA-13-3	24	0.31	<	<	678	0.5	0.3	<	26	<	<	<	<	0.3	12	5	2.2	494	<	<	<	<	<	<	1.3
SVA-13_12	42	0.27	6026	<	191	0.7	<	<	15	<	<	<	<	0.5	<	5	0.1	129	<	<	<	16	<	<	1.3
SVA-13_22	125	0.05	263	<	494	1.1	<	<	23	<	<	0.2	<	1.4	39	12	0.2	370	<	<	<	12	<	0.1	2
SVA-13_35	19	0.08	1040	<	449																				
SVA-13_45	18	1.29	<	<	139	0.2	5.5	<	3	<	<	<	<	0.1	<	2	0.4	94	<	<	<	22	<	0.2	1.8
SVA-13_55	15	5.73	<	<	269	0.2	6.1	<	14	<	<	<	<	<	<	4	0.1	182	<	<	<	62	<	0.2	0.7
TAR-13_9	129	0.07	573	<	<	0.5	<	<	6	<	<	<	<	0.3	18	2	<	27	<	<	<	<	<	<	1.4
TAR-13_18	56	0.05	<	<	<	0.5	<	<	<	<	<	<	<	0.3	<	1	<	12	<	<	<	<	11	<	1
TAR-13_31			<	167	<	0.4	6.3	<	<	<	<	<	<	1.3	<	1	<	43	<	<	<	<	11	0.2	0.6
TAR-13_40			<	<	123	0.4	5.7	<	14	<	<	<	<	<	24	1	<	86	<	<	<	<	<	0.2	1.4
Green snow																									
SVA-13-1	35	0.07	<	152	478	1.8	1.4	<	166	<	<	<	<	1.4	77	52	6.2	328	<	<	<	<	35	0.4	0.6
SVA-13_21	99	0.55	<	103	302	7.5	0.7	<	410	<	<	0.2	0.2	4.6	97	176	1.3	251	0.3	<	<	32	32	0.7	1.2
SVA-13_24	92	0.12	<	169	492	1	0.3	<	1260	<	<	<	<	0.4	130	341	0.5	353	<	28.2	<	74	<	1.4	1.8
SVA-13_44	45	1.29	<	<	126	1.8	7.3	<	317	<	0.5	<	0.3	1.7	92	78	40.9	93	0.6	<	0.1	44	11	0.7	0.5
TAR-13_2	210	0.11	<	<	148	3.5	0.5	<	10	<	0.2	<	1.4	1.8	56	3	1.8	271	0.2	<	<	25	22	0.1	0.6
TAR-13_3	87	0.41	<	<	<	2.5	0.5	<	79	<	0.2	<	0.7	3	37	13	1.3	9	0.2	<	<	<	32	0.4	0.9
TAR-13_4	154	0.24	<	<	<	2.8	0.4	<	47	<	<	<	0.5	4.3	66	7	0.6	20	0.1	<	<	<	48	0.2	1.2
TAR-13_16	93	0.5	230		74	1.8	0.3	<	26	<	0.2	<	0.5	5.3	36	4	1.1	40	<	<	<	<	18	0.2	0.8
TAR-13_33			<	<	<	1	5.7	<	24	<	0.4	<	0.3	10.5	<	4	2.8	46	<	<	<	<	16	0.4	0.2

Red snow																								
SVA-13-2	31	0.19	1043	<	344	0.4	<	<	100	<	<	<	<	0.5	14	44	1.7	228	<	<	<	12	<	0.2	0.9
SVA-13-4	39	0.14	288	<	381	0.9	0.3	<	94	<	<	<	<	0.9	59	46	1.7	248	<	<	0	14	<	0.3	1.3
SVA-13_10	17	0.05	1862	<	242	1.1	0.3	<	64	<	<	0.1	<	2.1	19	12	1.3	139	<	<	0	17	<	0.2	1.2
SVA-13_20	41	0.04	7010	160	545	2.1	0.2	<	180	0	<	<	<	2.8	56	70	2	376	<	<	0	34	<	0.7	0.7
SVA-13_23	36	0.08	<	<	332	1.7	0.8	<	955	<	<	0.1	0.2	1.6	65	396	3.1	250	0.1	<	0	48	16	0.9	4.5
SVA-13_31	51	0.14	<	<	321	2	0.5	<	2020	<	<	<	<	2	68	687	3.4	244	0.1	<	0	17	<	2.1	0.6
SVA-13_33	18	0.02	895	<	342	1.1	0.5	<	69	<	0.2	<	0.3	1.1	27	12	9.5	243	0.1	<	0	<	15	0.4	0.4
SVA-13_36	20	0.05	999	<	354	2.1	0.2	<	34	<	<	<	0.2	4.3	45	15	1.9	259	<	<	0.2	<	<	0.2	0.7
SVA-13_43	60	1.21	<	<	136	1.4	5.6	<	212	<	0.2	<	0.2	2.1	27	65	13	90	0.3	<	0.1	50	<	0.6	0.9
SVA-13_48	40	6.08	<	<	297	2.3	6.3	<	639	<	0.1	<	0.1	2.9	64	94	6.1	172	0.2	<	0	30	17	0.9	0.4
SVA-13_54	38	0.51	<	<	158	1.3	6	<	188	<	<	<	<	1.3	31	53	0.7	97	<	<	0	61	<	0.4	1
SVA-13_65	39	0.71	<	<	254	0.2	6.7	<	22	<	<	<	<	1.6	20	7	0.5	179	<	<	0.1	20	<	0.4	0.5
TAR-13_1	107	0.26	<	<	102	1	<	<	2	<	<	<	<	0.4	47	2	0.1	75	<	<	<	12	11	<	0.4
TAR-13_5	170	0.08	<	<	<	1.1	<	<	2	<	<	<	<	0.3	31	1	0	40	<	<	<	15	12	<	0.2
TAR-13_8	198	0.05	<	<	<	1.6	<	<	<	<	<	<	<	2.1	97	4	0.2	42	<	<	0	<	24	<	0.9
TAR-13_17	75	0.08	<	<	48	1.3	<	<	5	<	<	<	<	0.9	34	2	0.1	16	<	<	0	<	31	<	0.8
TAR-13_21	246	0.1	<	<	173	3.4	0.1	<	14	<	<	<	0.1	3.3	28	3	0.2	132	<	<	0	<	<	<	0.5
TAR-13_24			<	<	75																				
TAR-13_27			157	<	<	0.8	5.4	<	6	<	<	<	<	2.1	12	1	0.1	45	<	<	0	<	29	0.2	0.7
TAR-13_28			<	<	<																				
TAR-13_30			<	<	90	2.6	5.9	<	127	0.2	<	<	0.5	2.7	66	5	0.2	298	0.5	74.5	0.1	<	11	0.4	6.8
TAR-13_32			<	<	<	0.4	5.6	<	4	<	<	<	<	0.9	18	2	0.1	22	<	<	<	<	<	0.2	0.5
TAR-13_35			256	<	<	1.1	6.1	<	12	<	<	<	<	0.3	32	3	0.2	45	<	<	0	<	<	0.2	1
TAR-13_36			<	<	<	1.1	6	<	7	<	<	<	<	1.2	38	3	0.1	31	<	<	0	<	<	0.3	0.4
TAR-13_37	303	0.07	17	147	310	2.6	1.1	<	55	<	<	<	0.4	2.1	52	10	0.3	190	0.2	<	0.1	<	13	0.2	2.7
TAR-13_39			<	<	83	0.8	7.1	<	2	<	<	<	<	0.5	20	1	0	76	<	<	0	<	<	0.2	0.2

TAR-13_41	305	3.18	2351	149	554	7.6	1.8	<	191	<	0.1	<	1.3	2.7	303	11	0.9	414	0.7	<	0.2	67	16	0.5	12.9
TAR-13_42	107	0.48	1240	<	<	3.5	0.2	<	43	<	<	<	0.2	1.9	94	5	0.4	44	<	<	0	<	<	0.2	4.8
Biofilms																									
SVA-13_56	73	2.22	<	<	275	4.3	7	<	647	0	<	<	0.2	4.4	120	96	0.6	157	<	14.7	0.1	125	<	1	0.9
TAR-13_10	166	0.06	<	<	76	3.1	<	<	15	<	<	<	<	2	148	8	0.2	44	<	<	0.1	12	25	0.2	0.9
TAR-13_11	1142	2.13	133	<	<	24.2	1.1	<	266	0.1	0.6	0.5	3.9	23.8	1030	62	2.9	62	1.6	332	0.8	134	273	1.7	4.1
TAR-13_19	760	1.28	<	<	<	4.3	<	<	18	<	<	<	0.1	4.3	478	12	0.4	35	<	<	0.1	37	31	0.4	1.9
Clean ice																									
SVA-13-6	29	0.27	430	<	115	1	<	<	41	<	<	0.2	<	0.5	31	10	0.8	75	0.3	<	0	20	<	0.1	2.6
SVA-13_17	22	0.18	444	<	<	1.1	<	<	25	0	<	<	0.1	1.5	36	3	0.3	11	0.2	<	0	12	<	<	1.7
SVA-13_29	46	0.12	99	<	<	1.2	0.2	0.1	99	<	<	<	<	0.7	24	7	0.2	53	0.5	<	0.1	32	<	0.2	3.7
SVA-13_39	23	0.04	<	<	211	0.4	5.8	<	7	<	<	<	<	1.9	<	3	0.3	53	<	<	0.1	69	<	0.2	0.8
SVA-13_49	13	1.17	115	<	125	0.2	5.8	<	4	<	<	<	<	8.1	<	3	0.3	47	0.1	<	0	<	<	0.2	1
SVA-13_60	66	0.72	<	<	<	5.4	5.8	0	10	<	<	<	<	2.4	<	3	0.3	8	0.2	<	<	41	<	0.2	3.1
TAR-13_12	51	0.15	<	<	<	1.2	0.2	<	44	<	<	<	0.5	5.3	<	4	0.7	17	<	<	<	<	32	0.2	1.1
Dirty ice																									
SVA-13-7	32	1.8	<	<	127	19.2	1.7	<	1540	0	<	0.1	0.2	22.7	52	804	7.8	96	0.1	<	0	22	22	0.9	0.5
SVA-13-8	22	0.11	1363	<	263	2.5	0.5	<	34	<	<	<	<	2.3	11	18	4.2	171	0.2	<	<	<	<	0.2	0.9
SVA-13_18	25	0.09	928	<	164	1.7	0.1	<	18	<	<	0.2	<	6.2	33	9	1.1	106	<	<	0.3	<	<	0.1	1.7
SVA-13_19	34	0.09	<	<	<	5.3	0.3	<	15	<	<	<	<	7.5	29	6	1.5	24	<	<	1.3	16	12	0.2	1.8
SVA-13_25	33	0.05	5883	<	<	2.4	0.2	<	188	<	<	<	<	8	69	75	1	77	0.2	<	0.4	13	<	0.3	1.3
SVA-13_26	48	0.05	<	<	109	7.7	0.4	<	558	<	<	<	<	4.1	18	246	2.9	108	0.2	<	0.3	33	31	1.1	1.6
SVA-13_38	33	0.08	<	<	89	2.7	0.2	<	23	<	<	<	<	14.4	24	14	0.9	50	<	<	1.1	<	<	0.2	0.5
SVA-13_40	29	0.12	<	<	<	2	5.7	<	52	<	<	<	<	6	26	11	1.4	14	<	<	0	<	17	0.3	0.6
SVA-13_47	30	3.4	<	<	417	0.5	6.8	<	8	<	<	<	<	2.1	12	11	0.6	230	<	<	0.1	170	11	0.3	0.8

SVA-13_50	37	1.2	<	178	512	5.7	6.9	<	165	<	0.2	<	0.2	7.9	64	84	8.5	334	0.2	<	0.2	32	19	0.8	1.2
SVA-13_62	116	1.43	<	<	<	1.4	5.8	<	62	<	<	<	<	4.4	<	20	0.8	19	<	<	0.2	49	<	0.3	0.3
SVA-13_63	40	0.94	<	158	80	3	7.8	<	114	<	<	<	<	8.3	86	17	0.6	54	<	<	0.4	132	<	0.5	2.8
TAR-13_13	194	0.05	<	<	149	16.1	0.2	<	43	<	<	<	<	169	57	18	0.8	159	<	<	4.7	15	24	0.3	1.8
TAR-13_14	103	0.04	4048	<	76	7.1	0.7	<	30	<	<	<	<	149	73	11	0.6	74	<	<	2.7	<	<	0.2	7.6
TAR-13_22	190	0.08	<	<	<	12.9	<	<	8	<	<	<	0.1	44.2	<	1	0.2	15	<	<	2.1	<	30	<	0.4
Cryoconite holes																									
SVA-13-5	63	0.06	<	131	247	11.8	1	<	448	0	0.3	0.1	0.4	13.4	146	282	13	282	0.2	24.2	0.2	79	130	1.7	3.5
SVA-13_16	22	0.07	<	140	95	5.6	0.7	<	209	<	0.1	0.2	0.1	5.6	41	107	6.1	65	0.1	<	0.4	47	56	0.8	2.4
SVA-13_27	42	0.05	<	127	99	1.1	<	<	100	<	<	<	<	0.4	<	43	0.4	162	<	<	0.1	48	<	0.3	1.1
SVA-13_37	20	0.05	5005	152	261	2.2	0.6	<	96	<	<	<	0.2	4.2	87	71	2.6	226	<	<	0.5	45	42	0.9	1.7
SVA-13_51	27	1.24	<	139	271	4.5	7.8	<	56	0	0.1	<	0.2	5	58	34	4.6	229	0.1	<	0.4	43	50	0.8	1.9
SVA-13_61	37	0.99	<	155	<	1.2	5.8	<	119	<	<	<	<	1.4	20	45	1.2	27	<	<	0.4	70	25	0.8	0.7
TAR-13_34	54	0.09	<	141	<	4.9	1.6	0	3	0	<	<	0.6	8.4	33	4	0.5	40	0.2	15.1	0.8	32	25	0.2	0.5

All values except DOC and PO_4^{3-} are given in ppb; NO^{3-}, SO_4^{2-} and Cl^- all determined by IC, all others analysed by ICP-MS; limit of detection (LOD) for IC: NO_3^- = 96 ppb, Cl^- = 72 ppb, SO_4^{2-} = 121 ppb, LOD's for ICP-MS: Al, Ba, Co, Cr, Cu, Fe, Mg, Ni, Si, Sr, Zn = 0.1 ppb; Bi, Cd, Mn, Pb = 0.01 ppb; Ca, Na = 1 ppb; K,P,S = 10 ppb; no value indicates no measurement available for the respective sample.

Table E.8: Total carbon (TC), total nitrogen (TN), total phosphorus (TP) and total sulphur (TS) values reported as % of dry weight of sample with the corresponding C/N, C/P and N/P ratios as well as $\delta^{15}N$ and $\delta^{13}C$ isotopes; samples are separated by habitat and location and the averages for each habitat and location are also shown. Samples that did not contain enough particulate material for analyses are shown as n.s. (no sample). For the Sweden (TAR) samples pollen counts are also included since they have likely contributed to higher TC and therefore C/N and C/P values.

Sample ID	Total C [%]	Total N [%]	Total P [%]	Total S [%]	C/N	C/P	N/P	$d^{15}N$ [‰]	$d^{13}C$ [‰]	Pollen [ml^{-1}]
Green snow										
SVA-13_1	1.5	0.21	0.05	0.06	7	32	4	-4.98	-29.28	
SVA-13_21	1	0.14	0.07	0.07	7	15	2	-2.10	-38.97	
SVA-13_44	2.8	0.13	0.09	0.09	21	32	2	-2.81	-27.14	
Average SVA	**1.8 ± 0.9**	**0.16 ± 0.04**	**0.07 ± 0.02**	**0.07 ± 0.02**	**12 ± 8**	**26 ± 10**	**3 ± 1**	**-3.30 ± 1.50**	**-31.80 ± 6.30**	
TAR-13_2	2.2	0.27	0.05	0.02	8	40	5	-5.74	-26.71	n.s.
TAR-13_3	1.8	0.2	0.1	0.02	9	19	2	-1.66	-26.55	7813
TAR-13_4	0.5	0.08	n.s.	0.02	6	n.s.	n.s.	2.32	-28.95	n.s.
TAR-13_16	1.5	0.14	0.06	0.03	11	26	2	-6.19	-26.8	3125
TAR-13_33	1.2	0.09	0.07	0.04	13	16	1	-4.6	-25.94	2604
Average TAR	**1.4 ± 0.6**	**0.16 ± 0.08**	**0.07 ± 0.02**	**0.03 ± 0.01**	**9 ± 3**	**25 ± 11**	**3 ± 2**	**-3.17 ± 3.54**	**-26.99 ± 1.15**	
Red snow										
SVA-13_2	3.7	0.26	0.06	0.16	14	59	4	-8.86	n.s.	
SVA-13_4	3.1	0.21	0.06	0.11	15	51	3	-6.37	n.s.	
SVA-13_10	1.5	0.11	0.06	0.18	13	24	2	-6.92	n.s.	
SVA-13_20	1.9	0.19	0.15	0.07	10	12	1	0.27	-26.06	
SVA-13_31	8.9	0.50	0.08	0.14	18	111	6	-2.35	-27.8	
SVA-13_33	3	0.21	0.06	0.06	14	47	3	-5.18	-25	
SVA-13_36	6.3	0.36	0.06	0.1	18	107	6	-5.37	n.s.	
SVA-13_43	2.7	0.15	0.04	0.1	19	63	3	-2.6	-27.95	
SVA-13_48	4.9	0.23	0.06	0.12	21	80	4	-6.13	-28.18	

SVA-13_54	17.4	1.02	n.s.	0.12	17			-4.66	-29.43	
SVA-13_65	4.5	0.27	0.06	0.1	17	75	5	-5.52	-29.23	
Average SVA	**5.3 ± 4.5**	**0.32 ± 0.26**	**0.07 ± 0.03**	**0.11 ± 0.04**	**16 ± 3**	**63 ± 32**	**4 ± 2**	**-4.88 ± 2.50**	**-27.66 ± 1.61**	
TAR-13_1	4.1	0.25	0.05	0.02	17	84	5	-4.94	-25.01	7813
TAR-13_5	30.0	1.84	n.s.	0.11	16	n.s.	n.s.	n.s.	-28.73	0
TAR-13_8	12.9	0.78	n.s.	0.06	17	n.s.	n.s.	-1.1	n.s.	1250
TAR-13_17	19.7	1.11	n.s.	0.1	18			0.37	-26.59	893
TAR-13_21	8.8	0.41	0.04	0.07	22	220	10	-4.19	-21.8	422
TAR-13_24	8.6	0.47	0.05	0.08	18	166	9	-5.11	-25.32	n.s.
TAR-13_27	8.4	0.33	0.08	0.06	26	112	4	-4.76	-27.74	16667
TAR-13_28	12.9	0.57	0.07	0.07	23	176	8	-5.49	-24.63	521
TAR-13_30	11.0	0.28	0.04	0.06	39	287	7	-3.29	-24.86	1339
TAR-13_32	5.1	0.34	0.07	0.05	15	75	5	-5.96	-26.61	4395
TAR-13_35	9.7	0.46	0.07	0.08	21	149	7	-4.54	n.s.	1042
TAR-13_36	25.3	0.9	0.07	0.09	28	370	13	-4.95	n.s.	0
TAR-13_37	9.0	0.39	0.07	0.06	23	130	6	-5.4	n.s.	0
TAR-13_41	9.6	0.5	0.03	0.07	19	276	14	-6.15	n.s.	7292
TAR-13_42	11.5	0.55	0.06	0.09	21	192	9	-4.73	n.s.	446
Average TAR	**12.4 ± 7.2**	**0.61 ± 0.42**	**0.06 ± 0.02**	**0.07 ± 0.02**	**22 ± 6**	**186 ± 89**	**8 ± 3**	**-4.30 ± 1.84**	**-25.70 ± 2.02**	
Biofilms										
SVA-13_56	7.8	0.81	0.13	0.09	10	60	6	4.24	-27.38	
TAR-13_10	26.1	1.56	0.13	0.12	17	205	12	-3.77	-27.42	29688
TAR-13_11	17.3	1.69	n.s.	0.18	10	n.s.	n.s.	-4.07	-30.03	156
TAR-13_19	27.7	1.9	n.s.	0.17	15	n.s.	n.s.	-5.02	-29.5	21875
Average TAR	**23.7 ± 5.6**	**1.72 ± 0.17**	**0.13**	**0.16 ± 0.03**	**14 ± 4**	**205**	**12**	**-4.29 ± 0.65**	**-28.98 ± 1.38**	
Dirty ice										

SVA-13_7	0.9	0.09	0.06	0.05	10	17	2	-2.14		
SVA-13_8	1.4	0.13	0.03	0.06	11	42	4	-2.78	-25.21	
SVA-13_18	1.3	0.14	0.06	0.05	9	24	3	-5.54	-26.88	
SVA-13_19	2.1	0.17	0.05	0.06	13	45	4	-4.01	-25.93	
SVA-13_25	7.4	0.03	0.03	0.06	217	277	1	9.84	-25.9	
SVA-13_26	2.5	0.22	0.07	0.07	12	36	3	-1.49	-25.41	
SVA-13_38	1.9	0.18	0.05	0.07	10	40	4	-2.89	-26.46	
SVA-13_40	1.3	0.09	0.05	0.06	14	26	2	-2.5	-26.21	
SVA-13_47	2.5	0.25	0.05	0.1	10	54	5	-5.51	-27.37	
SVA-13_50	0.9	0.06	0.05	0.08	14	19	1	-0.29	-26.27	
SVA-13_62	2.3	0.21	0.04	0.05	11	65	6	-1.31	-26.33	
SVA-13_63	3.2	0.27	n.s.	0.06	12	n.s.	n.s.	-1.46	-26.7	
Average SVA	**2.3 ± 1.8**	**0.15 ± 0.08**	**0.05 ± 0.01**	**0.06 ± 0.01**	**29 ± 56**	**59 ± 74**	**3 ± 2**	**-1.67 ± 3.97**	**-26.24 ± 0.63**	
TAR-13_13	16.3	1.49	n.s.	0.12	11	n.s.	n.s.	-1.47	n.s.	1250
TAR-13_14	8.7	0.77	0.08	0.07	11	115	10	-2.62	-25.8	0
TAR-13_22	3.8	0.29	0.06	0.04	13	58	4	-2.45	-25.88	1875
Average TAR	**9.6 ± 6.3**	**0.85 ± 0.60**	**0.07 ± 0.01**	**0.08 ± 0.04**	**12 ± 1**	**87 ± 40**	**7 ± 4**	**-2.18 ± 0.62**	**-25.84 ± 0.06**	
Cryoconite holes										
SVA-13_5	1.0	0.11	0.04	0.06	9	27	3	-2.92	-25.14	
SVA-13_16	1.5	0.16	0.03	0.06	10	44	4	-3.47	-25.53	
SVA-13_27	2.2	0.2	0.04	0.06	11	50	5	-0.92	-25.54	
SVA-13_61	3.2	0.31	0.04	0.06	10	81	8	-1.27	-25.74	
Average SVA	**2.0 ± 1.0**	**0.20 ± 0.09**	**0.04 ± 0.01**	**0.06 ± 0.00**	**10 ± 1**	**51 ± 23**	**5 ± 2**	**-2.15 ± 1.24**	**-25.49 ± 0.25**	
TAR-13_34	10.4	0.65	0.06	0.12	16	168	10	-3.49	-25.96	n.s.

Table E.9: Bulk functional group distribution from the FTIR analyses of samples that contained enough particulate material, again separated by habitat and location and reported with averages. Main functional groups representing the lipids (CH_2 and CH_3 stretching modes between 3050 and 2800 cm^{-1}), proteins (amide I and II bands between 1700-1500 cm^{-1}) and carbohydrates (C-O-C, C-O-P, P-O-P ring vibrations between 1204-815 cm^{-1}) are reported as percentage of total functional groups.

Sample ID	lipids [%]	proteins [%]	carbohydrates [%]
Green snow			
SVA-13_1	0.2	3.3	96.4
SVA-13_21	0.2	1.5	98.3
SVA-13_44	0.2	2.1	97.7
Average SVA	**0.2 ± 0.0**	**2.3 ± 0.9**	**97.5 ± 1.0**
TAR-13_3	1.1	5.1	93.8
TAR-13_4	12.4	23.3	64.3
TAR-13_16	0.2	5.3	94.5
Average TAR	**4.6 ± 6.8**	**11.2 ± 10.5**	**84.2 ± 17.2**
Red snow			
SVA-13_2	1.8	4.2	94.1
SVA-13_4	1.1	3	95.9
SVA-13_10	0.9	2.1	97
SVA-13_20	3.2	5.3	91.5
SVA-13_31	4.7	6	89.3
SVA-13_33	0.9	3.7	95.4
SVA-13_36	3	5.6	91.4
SVA-13_43	1.7	10.7	87.5
SVA-13_48	3.7	6.5	89.8
SVA-13_54	7.9	12.6	79.5
SVA-13_65	1.3	3.3	95.4
Average SVA	**2.7 ± 2.1**	**5.7 ± 3.3**	**91.5 ± 5.0**
TAR-13_1	6	11.4	82.6
TAR-13_8	7.9	17	75.2
TAR-13_17	7.1	13.7	79.2
TAR-13_21	5.4	19.5	75.1
TAR-13_24	3.7	10.2	86.1
TAR-13_27	4.8	8.9	86.3
TAR-13_28	11.4	19.3	69.2
TAR-13_30	4.5	8.8	86.6
TAR-13_35	9.3	17.6	73.1
TAR-13_36	12.8	17.5	69.7
TAR-13_37	9.7	13	77.2
TAR-13_41	10.2	15	74.7
TAR-13_42	12.4	19.8	67.8
Average TAR	**8.1 ± 3.1**	**14.7 ± 4.0**	**77.1 ± 6.6**
Biofilms			
SVA-13_56	3.9	15.3	80.8
TAR-13_10	9.8	15	75.3
TAR-13_11	3.8	10.4	85.8
TAR-13_19	8.9	16	75.1
Average TAR	**6.6 ± 3.2**	**14.2 ± 2.6**	**79.3 ± 5.1**
Dirty ice			
SVA-13_7	0	0.3	99.6
SVA-13_8	0.2	1.8	98
SVA-13_18	0.3	1.8	97.9
SVA-13_19	0.5	2.2	97.3
SVA-13_26	0.2	1.6	98.2

SVA-13_38	0.7	3.4	95.9
SVA-13_40	0.3	1.5	98.2
SVA-13_47	0.8	7.6	91.6
SVA-13_50	0.2	6.7	93.1
SVA-13_62	0.7	5.8	93.5
SVA-13_63	1.0	4.2	94.7
Average SVA	**0.4 ± 0.3**	**3.4 ± 2.4**	**96.2 ± 2.6**
TAR-13_13	3.3	9.8	86.8
TAR-13_14	4	9.7	86.4
TAR-13_22	0.9	5.3	93.8
Average TAR	**2.7 ± 1.6**	**8.3 ± 2.6**	**89.0 ± 4.2**

Table E.10: Dominant fatty acid compounds present in the samples separated by habitats and locations and reported as % of total fatty acid content with B designating the Branched and A the Alkane compounds. Total saturated (SFA), total monounsaturated (MUFA) and total polyunsaturated (PUFA) fatty acids are also reported in grey columns.

Sample ID	C14:0	C15:0	C15 B	C16:0	C16:1	C16:3	C16:4	C17 B	C18:0	C18:1	C18:2	C18:3	C18:4	C20:0	C21:0	C21 A	C22:0	C23 A	C24:0	C27 A	SFA	MUFA	PUFA
Green snow																							
SVA-13_1	10	0	0	17	18	0	5	0	2	21	4	0	5	0	1	0	0	0	0	0	30	39	14
SVA-13_21	3	0	0	17	15	2	13	0	0	14	6	21	5	0	0	0	0	0	0	0	21	29	47
SVA-13_24	14	0	0	7	1	0	2	0	5	5	5	4	17	0	9	0	0	0	0	0	34	6	28
SVA-13_44	0	0	0	19	7	2	4	0	4	16	9	14	4	4	0	2	2	1	1	2	30	23	32
Average SVA																					**29 ± 6**	**24 ± 14**	**30 ± 14**
TAR-13_2	0	0	0	23	23	0	7	0	4	13	4	11	6	2	0	0	2	1	1	2	32	36	28
TAR-13_3	2	0	0	32	10	1	6	0	4	26	0	5	4	2	0	0	2	1	0	2	42	36	17
TAR-13_4	10	0	0	24	27	2	7	0	4	12	9	0	3	2	0	0	2	0	0	0	41	39	20
TAR-13_16	0	0	0	24	13	1	6	0	7	20	5	13	4	2	0	0	0	0	0	0	34	33	29
TAR-13_33	2	0	0	30	13	0	5	0	6	16	4	13	2	3	0	0	3	0	0	0	44	29	25
Average TAR																					**39 ± 5**	**35 ± 4**	**24 ± 5**
Red snow																							
SVA-13_2	0	0	0	25	0	2	12	0	5	16	9	15	10	3	0	0	2	0	0	0	34	16	49
SVA-13_4	2	0	0	25	1	2	13	0	3	15	5	20	9	3	0	0	1	0	0	0	35	16	50
SVA-13_10	0	0	0	28	0	0	12	0	8	2	7	31	9	1	0	0	0	0	0	0	37	2	59
SVA-13_20	0	0	0	23	2	2	15	0	4	13	7	27	7	0	0	0	0	0	0	0	27	14	59
SVA-13_23	3	0	0	23	2	2	15	0	3	12	6	27	7	0	0	0	0	0	0	0	29	14	57
SVA-13_31	0	0	0	24	4	2	12	0	4	15	9	22	9	0	0	0	0	0	0	0	27	19	53
SVA-13_33	0	0	0	23	7	1	6	0	6	15	10	18	5	2	0	0	1	1	0	0	32	23	40
SVA-13_36	1	0	0	30	2	1	7	0	5	15	8	14	6	2	0	1	2	0	0	2	40	17	37

SVA-13_43	1	0	0	20	3	2	8	0	4	17	8	14	3	4	0	1	2	0	1	0	32	20	36
SVA-13_48	0	0	0	20	3	2	12	0	3	13	10	21	9	0	0	0	0	0	0	0	24	16	54
SVA-13_54	2	0	0	27	1	4	14	0	2	14	8	18	8	1	0	0	0	0	0	0	32	15	52
Average SVA																					**32 ± 5**	**16 ± 5**	**50 ± 8**
TAR-13_1	2	0	1	45	4	5	35	0	0	0	0	0	0	2	0	0	1	0	0	0	50	4	40
TAR-13_5	3	0	0	26	0	0	19	0	3	15	1	31	0	0	0	0	0	0	0	0	32	15	52
TAR-13_8	3	0	0	0	3	4	0	0	6	19	3	37	7	4	0	0	3	2	2	4	18	22	51
TAR-13_21	0	1	0	31	2	2	8	0	2	13	4	20	13	0	0	0	1	0	1	0	37	15	48
TAR-13_27	0	0	0	42	0	1	7	0	5	12	4	11	3	4	0	0	3	1	2	2	56	12	26
TAR-13_28	0	0	0	25	1	2	13	0	5	12	10	16	15	1	0	0	0	0	0	0	32	13	56
TAR-13_30	0	0	0	39	0	0	4	0	14	8	6	6	4	5	0	1	3	1	2	2	62	8	19
TAR-13_32	0	0	0	22	2	2	16	0	4	13	7	21	12	0	0	0	0	0	0	0	26	15	58
TAR-13_35	0	0	0	34	0	2	9	0	17	10	5	14	3	2	0	0	2	0	0	0	55	10	31
TAR-13_37	0	0	0	21	0	2	15	0	6	12	0	28	14	0	0	0	0	0	0	0	26	12	60
TAR-13_39	0	0	0	26	1	2	13	0	3	12	7	20	10	1	0	0	1	0	0	1	31	13	53
TAR-13_41	0	0	0	24	2	2	9	0	7	13	9	18	8	2	0	0	2	0	0	2	34	16	46
TAR-13_42	0	0	0	21	1	3	17	0	4	13	5	22	12	1	0	0	0	0	0	0	26	15	58
Average TAR																					**37 ± 14**	**13 ± 4**	**46 ± 13**
Biofilms																							
SVA-13_56	3	1	1	15	16	2	8	0	2	20	5	17	4	0	0	0	0	0	0	0	22	37	37
TAR-13_10	2	0	0	30	3	2	6	0	5	15	5	13	5	3	0	0	3	2	2	4	45	18	30
TAR-13_11	13	0	0	26	4	2	5	0	3	16	4	0	11	1	2	0	1	0	0	0	46	20	22
TAR-13_19	3	0	0	36	2	2	8	0	5	18	0	20	3	3	0	0	1	0	0	0	47	20	33
Average TAR																					**46 ± 1**	**19 ± 1**	**28 ± 6**
Dirty ice																							
SVA-13_7	3	2	5	20	9	5	2	1	8	16	7	15	0	2	3	0	1	1	0	0	38	25	29

SVA-13_8	2	3	8	23	9	2	1	3	3	15	6	12	2	1	0	2	2	3	0	2	34	24	23
SVA-13_18	2	3	8	36	4	0	0	0	14	13	6	10	4	0	0	0	0	0	0	0	55	17	20
SVA-13_19	3	6	19	39	14	3	4	4	0	0	0	0	7	0	0	0	0	0	0	0	48	14	15
SVA-13_25	2	0	2	30	7	3	2	0	21	10	8	13	2	0	0	0	0	0	0	0	53	17	28
SVA-13_26	1	2	10	24	7	0	2	2	4	14	8	20	3	0	0	0	1	0	1	0	33	22	33
SVA-13_38	2	2	10	26	5	2	3	2	2	10	8	17	6	0	0	1	1	2	0	0	34	15	36
SVA-13_40	2	2	4	34	6	2	3	2	8	16	8	8	5	1	0	0	0	0	0	0	47	22	24
SVA-13_47	3	7	7	22	8	2	2	5	3	11	4	12	0	2	0	2	2	3	1	1	40	19	20
SVA-13_50	3	2	3	33	7	1	3	2	4	15	4	13	4	2	0	0	2	0	1	0	47	22	25
SVA-13_62	2	3	6	22	8	2	0	3	2	13	7	11	2	1	0	3	2	4	3	2	35	21	23
SVA-13_63	2	2	3	27	6	2	3	2	2	12	9	17	8	0	0	0	1	2	1	0	36	18	39
Average SVA																					**42 ± 8**	**20 ± 4**	**26 ± 7**
TAR-13_13	0	1	0	30	3	3	9	0	2	11	2	25	14	0	0	0	0	0	0	0	33	13	52
TAR-13_22	0	1	0	30	2	2	7	0	2	11	7	23	13	0	0	0	1	0	0	0	34	13	53
Average TAR																					**34 ± 1**	**13 ± 0**	**53 ± 1**
<u>Cryoconite holes</u>																							
SVA-13_5	2	3	6	20	11	3	1	2	3	12	6	17	3	2	1	2	2	2	1	0	34	23	30
SVA-13_16	2	3	15	19	10	1	0	2	4	8	8	13	0	2	0	2	2	3	2	2	34	18	23
SVA-13_27	2	2	20	19	8	0	0	2	3	11	19	12	0	0	0	0	0	2	2	0	26	18	31
SVA-13_37	1	3	20	19	7	2	0	3	3	9	13	16	0	1	0	1	1	1	0	0	28	16	31
SVA-13_51	0	3	16	24	6	0	0	2	5	11	8	18	2	0	0	0	2	2	0	0	34	17	28
SVA-13_61	5	3	8	23	12	2	0	2	6	10	5	16	0	0	0	2	2	2	1	0	40	22	23
Average SVA																					**33 ± 5**	**19 ± 3**	**28 ± 4**
TAR-13_34	3	3	0	24	4	0	0	2	7	6	0	1	0	5	2	5	9	10	7	10	60	10	1

Table E.11: Pigment composition of samples that contained enough particulate material for analysis and separated by habitats and locations. Individual pigments were quantified in ug/L and grey columns show total chlorophylls, total primary carotenoids and total secondary carotenoids in % of total pigments. Chl a = chlorophyll a, Chl b = chlorophyll b, Neo = Neoxanthin, Vio = Violaxanthin, Ant = Antheraxanthin, Lut = Lutein, Zea = Zeaxanthin, β-car = β-carotene, Ast=Astaxanthin.

Sample ID	Chl a	Chl b	Neo	Vio	Ant	Lut	Zea	β-car	trans-Ast	cis-Ast	trans- Ast mono esters	cis-Ast mono esters	total Ast di esters	total chlorophylls [%]	total primary carotenoids [%]	total secondary carotenoids [%]
Clean snow																
SVA-13_3	159	60									305	0	0	42	0	58
SVA-13_12	361	141						24	144		3733	164	164	11	1	89
SVA-13_22	279	114									412	0	0	49	0	51
SVA-13_35	88										0	0	0	100	0	0
Average SVA														**51 ± 37**	**0 ± 1**	**50 ± 37**
TAR-13_9	911	828		12		212		3	70		2077	92	33	27	4	69
TAR-13_18	410	176				40			27		614	59	0	29	2	69
TAR-13_40	2985	2230	162	105	90	997		2274	2574	160	34045	4424	9802	5	4	91
Average TAR														**20 ± 13**	**3 ± 1**	**76 ± 13**
Green snow																
SVA-13_1	489	391				32			64		181	0	0	76	3	21
SVA-13_21	495	730				223					58	0	0	81	15	4
SVA-13_24	4254	158		1236	133	4	58	62	2079		936	17	0	49	17	34
SVA-13_44	88			62		329			242		0	0	0	12	54	34
Average SVA														**55 ± 32**	**22 ± 22**	**23 ± 14**
TAR-13_2		60							23		0	0	0	72	0	28
TAR-13_3	890	766	449	1490	356	2766	102		325		247	0	113	21	67	12
TAR-13_4	305	301	23	130		428			162		6	0	0	45	43	13
TAR-13_16	1105	837		45		245			140		1509	45	0	35	5	59
TAR-13_33	723	560				137			124		87	0	0	75	8	17
TAR-14_2	2280	1391	14	77		506			902		17713	2336	0	12	22	67

TAR-14_3	444	408							33		2284	205	52	20	19	60
TAR-14_4	369								76		693	0	0	32	0	68
TAR-14_7	4458	2533	59		29	963	6		330		4565	391	0	52	9	39
TAR-14_8	15518	15150	913	2649	1200	6747	534		11752	791	155232	23059	3208	13	5	82
TAR-14_9	7644	5221	283	274	357	1513			4383	448	118162	13976	3038	8	3	89
Average TAR														**35 ± 24**	**16 ± 21**	**49 ± 28**
Red snow																
SVA-13_2	3682	3132	215	147		1155		15	2976	115	62922	6457	1523	8	3	89
SVA-13_4	3359	2873	114	175		1133		81	2664	116	38758	4397	1776	11	4	85
SVA-13_10	882	748	25	10		351		853	1002	15	5164	362	76	17	14	69
SVA-13_20	1200	980	100	36	6	573		3193	3090	194	17661	1906	2316	7	13	80
SVA-13_31	327	266	308	468		1116		51	3927	164	1448	21	178	7	23	69
SVA-13_33	534	426	33	26		355		237	1251	64	3248	201	540	14	10	77
SVA-13_36	376	230	93	98		155		501	1456	86	9142	877	1318	4	6	90
SVA-13_43	672	757	56	113		577		298	868	9	4332	432	1873	14	11	75
SVA-13_54	450	507	472	624		1525		240	9272	904	5640	546	745	5	14	82
Average SVA														**10 ± 5**	**11 ± 6**	**80 ± 8**
TAR-13_1	3253	2712	117	328		1499	9	1025	1867	101	28521	3562	4005	8	4	88
TAR-13_5	6068	5167	354	670	351	2449	88	957	3546	266	48066	6860	6299	8	4	88
TAR-13_8	3084	3212	315	1149	73	2574	14	728	3658	225	21286	2508	6384	9	7	84
TAR-13_17	2153	1605	402	721		1637		1136	3292	122	16014	3063	3949	7	8	85
TAR-13_21	1323	1266	315	374		1384		390	2386	158	13318	1449	2447	7	6	87
TAR-13_27	478	373				241		50	398		3145	286	404	10	3	87
TAR-13_28	672	417	597	381		563		88	1886	115	11182	1113	959	4	5	91
TAR-13_30	495	328		-31		89			243		3035	164	202	11	1	89
TAR-13_32	2490	2203	304	823	69	2021	7	459	2078	59	20966	2608	2913	8	6	86
TAR-13_35	2319	1578	50	162		691		402	963	14	10994	1557	2416	11	5	84
TAR-13_36	492	310	157	154		628		107	1599	92	6407	551	981	4	6	90
TAR-13_37	1655	1328	47	59		638		102	1351	57	5628	749	1229	15	5	79
TAR-13_41	541	426	747	565	48	1180		640	2764	222	8401	884	1766	4	12	85
TAR-13_42	7724	8730	1007	1391	111	5052	8	778	5032	205	29339	3554	4411	16	9	75

TAR-14_1	1414	632				318			938		21910	2344	639	6	24	71
TAR-14_5	2864	1391				528	22		207		2418	304	47	55	7	38
TAR-14_6	14924	10007	822	752	312	4414			17256	662	141903	13779	3548	12	4	84
TAR-14_10	594					49			238		6358	663	133	7	2	90
TAR-14_11	332										102	0	0	76	0	24
TAR-14_12	4238	2694	16	25		1013	4		1751	170	45152	5915	1015	11	2	86
Average TAR														**14 ± 18**	**6 ± 5**	**80 ±**17
Biofilms																
SVA-13_56	311	87		10		69			62		991	50	313	21	4	75
TAR-13_10	436	230	97	102		34		97	124		3023	224	0	9	4	87
TAR-13_11	1541	417		69		98					1103	0	0	45	4	51
TAR-13_19	473	292				3			28		942	47	0	28	0	72
Average TAR														**27 ± 18**	**3 ± 2**	**70 ± 18**
Clean ice																
SVA-13_6	117										0	0	0	100	0	0
SVA-13_17	145				218						6	0	0	39	59	2
SVA-13_29	88										0	0	0	100	0	0
Average SVA														**80 ± 35**	**20 ± 34**	**1 ±** 1
TAR-13_12	339	167									162	0	0	61	0	39
Dirty ice																
SVA-13_7	264	42				10					0	0	0	97	3	0
SVA-13_18	655	346		14	221	131			6		386	0	372	47	17	36
SVA-13_25	159										0	0	0	100	0	0
SVA-13_38	1763	301		1119		171					341	0	0	56	35	9
SVA-13_47	230	19		296							3	0	0	45	54	1
SVA-13_62	681	257		91		198					146	0	550	49	15	36
Average SVA														**66 ±26**	**21 ± 21**	**14 ± 18**
TAR-13_13	1056	882	231	1252	63	2259	21	89			189	0	0	31	63	6
TAR-13_22	1094	721		502		1046		55	82		279	0	0	45	40	16

Average TAR										**38 ± 10**	**51 ± 16**	**11 ± 7**
Cryoconite holes												
SVA-13_5	654	596	148	114	874	71	64	0	0	50	45	5
SVA-13_16	119			498			0	0	0	19	81	0
SVA-13_27	707	87		713	28	151	131	0	0	44	41	15
SVA-13_37	298	31		187			2	0	0	64	36	0
SVA-13_51	657	275		33	107	13	-3	0	0	86	13	1
Average SVA										**53 ± 25**	**43 ± 24**	**4 ± 6**
TAR-13_34							0	0	0			

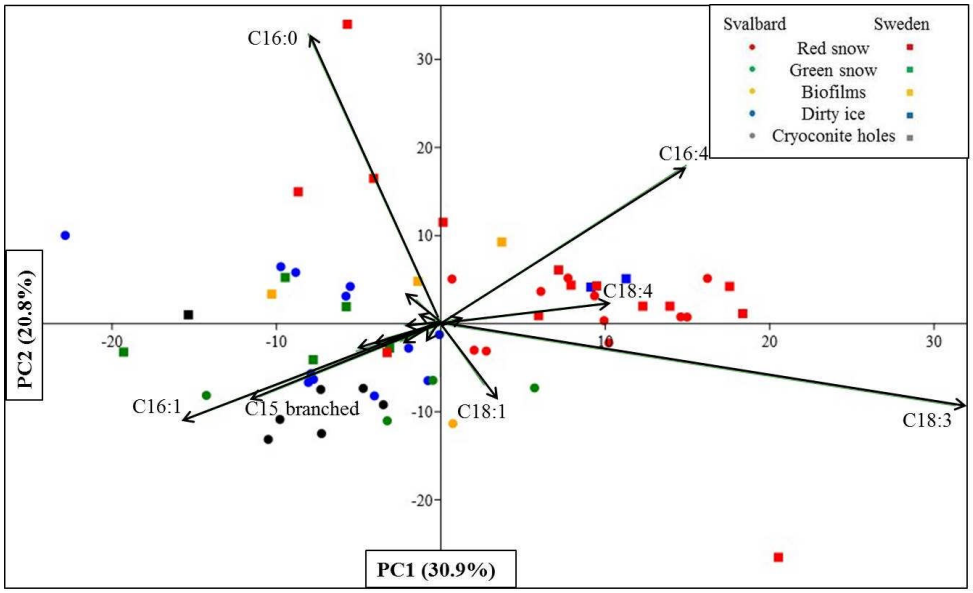

Figure E.1: Principal component analysis of fatty acids in the Svalbard and Arctic Sweden samples revealing distance between samples and showing the main fatty acid compounds causing the separations. Samples cluster according to habitats in all locations.

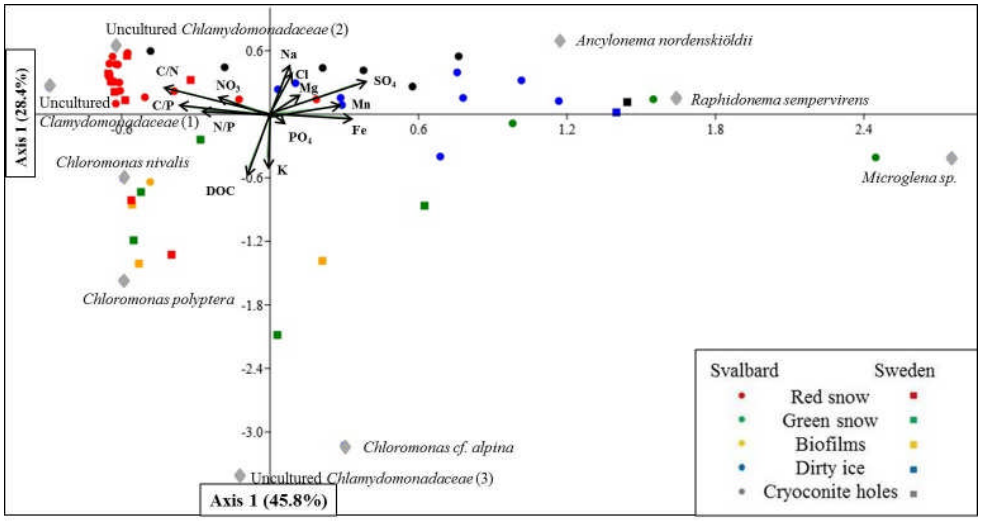

Figure E.2: CCA analysis showing the links between algal species and various relevant geochemical parameters. The two uncultured *Chlamydomonadaceae* (1) and (2) positively correlated with increasing C/N ratios, *Chloromonas polyptera* with DOC and K, *Raphidonema sempervirens* with Fe and Mn, and *Chloromonas cf. alpina* with DOC.

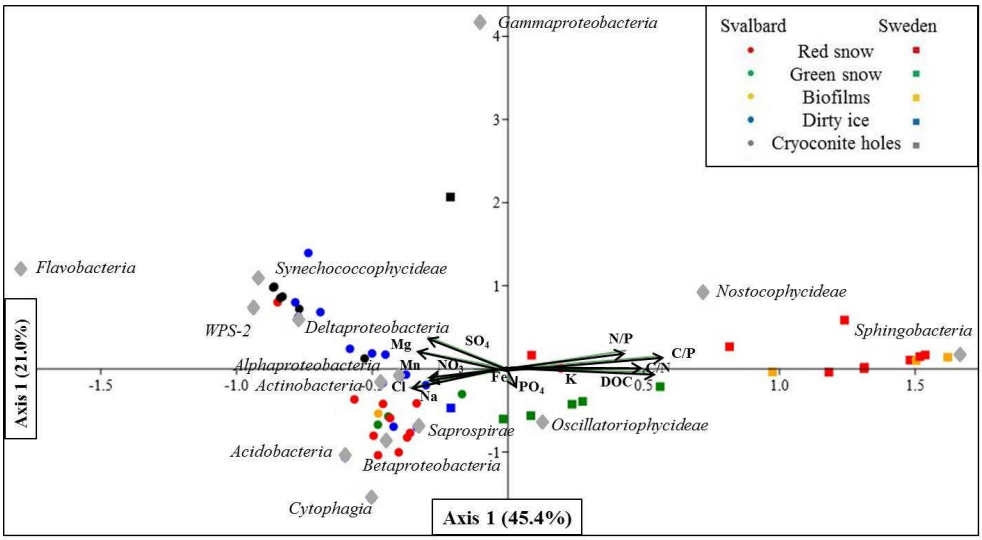

Figure E.3: CCA analysis showing the links between bacterial classes and various relevant geochemical parameters. *Sphingobacteria* positively correlated with DOC, C/N, C/P, N/P and K, and *Synechococcophycideae* with SO_4.

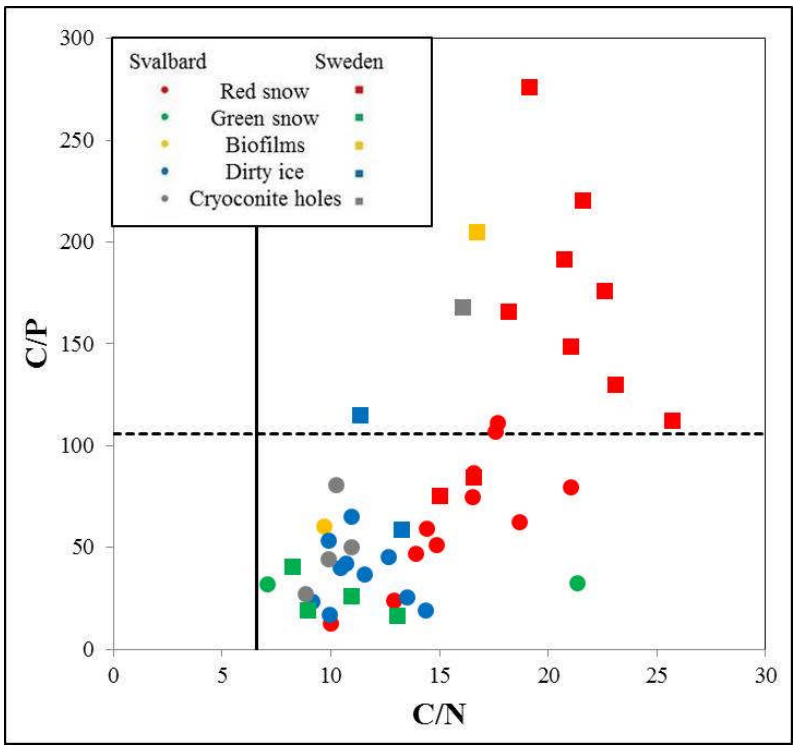

Figure E.4: C/N and C/P ratios for the analysed Svalbard and Arctic Sweden samples. Lines show optimal Redfield ratios (solid line: C/N, dashed line: C/P). Most samples were above the optimal Redfield ratio for C/N but only the samples from the red snow habitats from Arctic Sweden were above the optimal C/P ratio. Samples cluster according to habitats within their respective location.

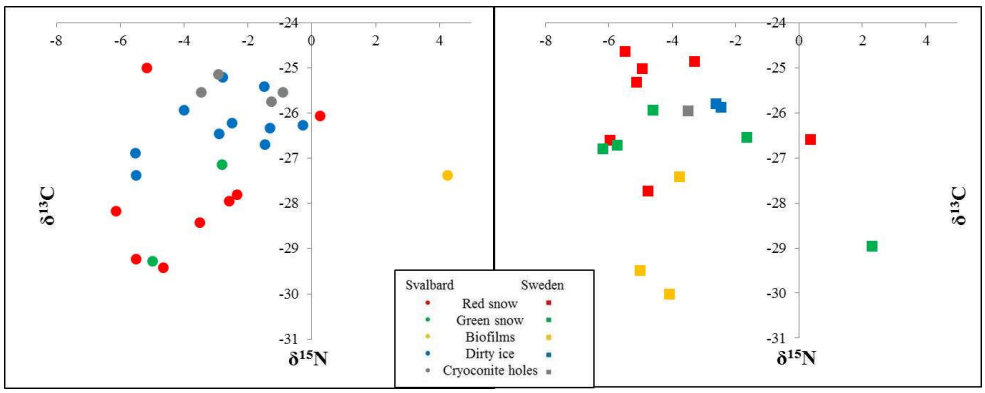

Figure E.5: Carbon and nitrogen isotopes. $\delta^{15}N$ values were predominately negative but show no significant trend ($p>0.05$) for habitats or locations. $\delta^{13}C$ values varied over a narrow range and significant trends ($p=0.004$) were only established for habitats in Svalbard (left) where on average most red snow samples showed more negative values than the grey ice and cryoconite hole samples. No significant trends were observed for samples from Sweden (right).

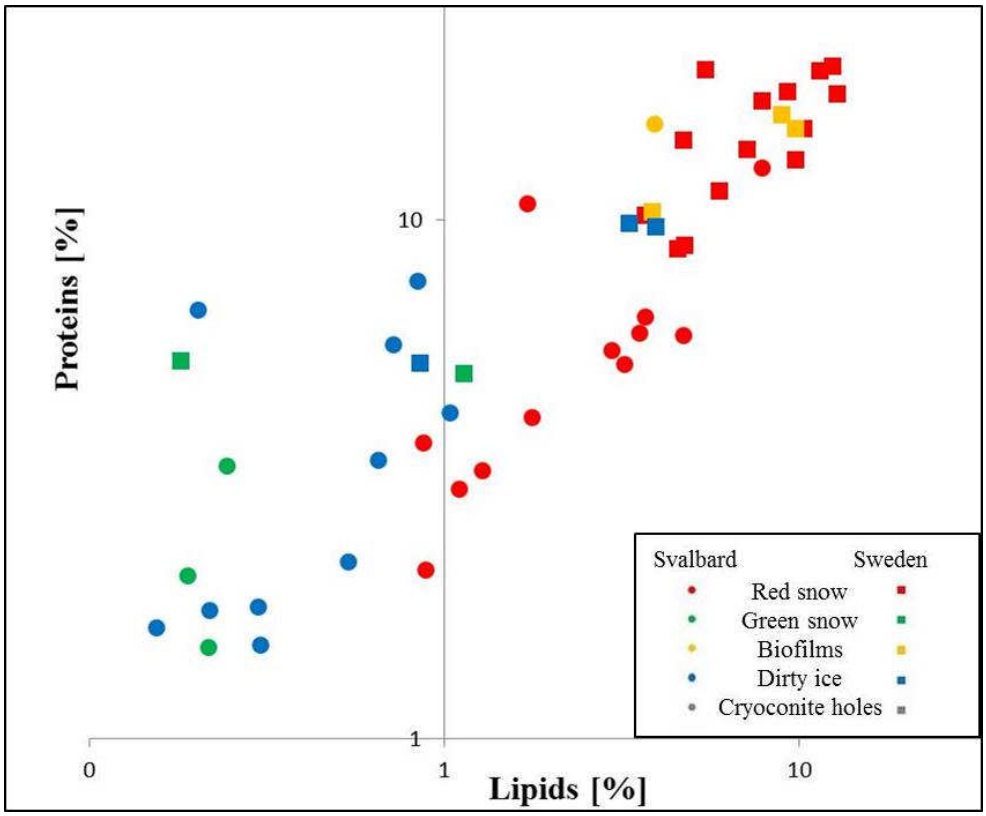

Figure E.6: Relative abundance of functional group corresponding to lipids and proteins showing that samples cluster according to algal habitats. Lipids and proteins show highest values in red snow (specifically in the Arctic Sweden samples), whereas in the Svalbard samples lipids were significantly higher but not proteins.